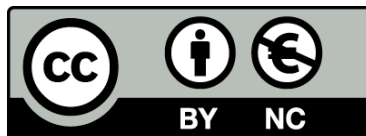




UNIVERSITAT<sub>DE</sub>  
BARCELONA

## Targeting the I<sub>2</sub> Imidazoline Receptors: the neuroprotective role of selective ligands in Alzheimer's Disease

Foteini Vasilopoulou



Aquesta tesi doctoral està subjecta a la llicència **Reconeixement- NoComercial 4.0. Espanya de Creative Commons.**

Esta tesis doctoral está sujeta a la licencia **Reconocimiento - NoComercial 4.0. España de Creative Commons.**

This doctoral thesis is licensed under the **Creative Commons Attribution-NonCommercial 4.0. Spain License.**





UNIVERSITAT DE  
BARCELONA

University of Barcelona  
Faculty of Pharmacy and Food Sciences

**Targeting the I<sub>2</sub> Imidazoline Receptors:  
the neuroprotective role of selective ligands  
in Alzheimer's Disease**

**Foteini Vasilopoulou**

**2021**





UNIVERSITAT DE  
BARCELONA

Department of Pharmacology, Toxicology and  
Therapeutic Chemistry

## DOCTORAL THESIS

PhD program in Biotechnology

# Targeting the I<sub>2</sub> Imidazoline Receptors: the neuroprotective role of selective ligands in Alzheimer's Disease

*Dissertation presented by Foteini Vasilopoulou to apply for the doctorate  
degree by the University of Barcelona*

Director

Prof. Mercè Pallàs

Director

Dr. Christian Griñan

Doctoral Student

Foteini Vasilopoulou

**Foteini Vasilopoulou**  
**2021**



This doctoral thesis has been funded by:



UNIVERSITAT DE  
BARCELONA

Universitat de Barcelona



UNIVERSITAT DE  
BARCELONA

**Fundació Montcelimar**

Fundació Montcelimar  
Universitat de Barcelona



Institut de Neurociències  
UNIVERSITAT DE BARCELONA

Institut de Neurociències  
Universitat de Barcelona



**Generalitat  
de Catalunya**

Generalitat de Catalunya



Ministerio de Ciencia,  
innovación y universidades



Caixa Impulse,  
"La Caixa" Foundation





Those who have a "why" to live,  
can bear almost any "how".  
— Friedrich Nietzsche



# Acknowledgements

Firstly, I would like to express my sincere gratitude to my tutor and supervisor, Dr. Mercè Pallàs, for giving me the opportunity to join her group and work on this project, as well as for her guidance and support that contributed significantly to my professional growth during my PhD degree. Afterwards, I would like to deeply thank my supervisor Dr. Christian Griñan Ferré, for inspiring me at the beginning of this academic stage. His guidance and tutelage provided me with the necessary tools throughout the conduction of this dissertation and formed a major part of my current scientific knowledge.

Moreover, I would like to thank Dr. Carmen Escolano for giving me the opportunity to work on this exciting and promising project, and also my colleagues Sergio and Andrea for contributing substantially to the scientific studies included in this dissertation. I would also like to thank Dr. Jari Koistinaho for hosting me in the Neuroscience Center of the University of Helsinki as well as Dr. Taisia Rolova, Marja and Pinja for the invaluable guidance, help and advice in terms of my short-term visit to their lab.

I would like to express my deep gratitude to my group colleague and special friend Julia CA, for her invaluable support and insightful suggestions, for sharing both good and difficult moments with me and being always available and willing to help whenever necessary. Moreover, I would like to thank Aina for her valuable help and comments and for transmitting positive and encouraging energy in the last stage of my PhD.

I also thank all current and past members of my research group Vanesa, Dolors, Veronica for providing me with help and advice, when necessary, as well as former students of the group, including but not limited to Reab, Albert, Laia, who demonstrated their willingness to help and learn. I would like to offer my special thanks to the department technicians and administration staff, Silvia, Mar and Kim, for their help and support. I would like to extend my sincere thanks to the Animal facilities staff, and especially to Marta and Paula,

for their assistance and useful advice. Ultimately, I thank all my department colleagues Miren, Raul, Leti, Lucía, Xavi, Emma, David, Triana, Oriol, Marina, Roger, Anna for the moments of joy that we share in the lab during these almost five years.

I will be eternally grateful to my «second family», Aleix and Karine, for forming essential part of my professional and personal life in Barcelona, giving me their unlimited support and invaluable advice during this journey. I would also like to thank my lifetime best friends Stella and Maira, who, even kilometres away, supported me both scientifically and emotionally in each and every step of this doctoral thesis. Ultimately, I would like to thank a person of special importance, Giorgos, for his encouragement, sympathy, and patience in the last and crucial part of my PhD, and importantly, for supporting me in writing this document in LaTeX.

My last round of acknowledgements is devoted to my family: my parents Ioannis and Ioanna, and my beloved sister Christina, whose value to me only grows with age. Thank you for supporting and encouraging me to fulfill my dreams and goals during this thesis and throughout my life.

# **Statement of Originality**

With this statement, I hereby declare that the submitted PhD thesis is my own original work and includes material for five scientific articles that have been previously published in international peer-reviewed journals. All the assistance received in preparing this thesis and sources have been acknowledged.

**Foteini Vasilopoulou,**

**July 2021**



# Abstract

The identification of imidazoline receptors (IR) as a novel class of receptors has posed manifold research questions regarding their pharmacological and potential therapeutic properties. Among them, I<sub>2</sub>-IR receptors are widely distributed in the central nervous system (CNS) with predominant localization in glial cells. Remarkably, their activation has been shown to exhibit neuroprotective properties, yet through not fully understood molecular mechanisms. Furthermore, alterations of I<sub>2</sub>-IR density have been detected in patients with different brain disorders, including Alzheimer's Disease (AD), suggesting a potential therapeutic value of I<sub>2</sub>-IR in AD.

The latter suggestion is of special clinical significance since AD is an irreversible neurodegenerative disease and the most common form of dementia that affects millions of people worldwide. The consequences of AD range from detrimental outcomes for both the patients and their caregivers to a wide socioeconomic footprint, and unfortunately, there is still no cure for the disease. At the same time, AD prevalence is rapidly growing due to an increase in life expectancy in developed countries, further highlighting the urgency to identify new targets for halting disease progression and providing effective treatment.

In this context, this doctoral dissertation aims to contribute to the scientific knowledge of I<sub>2</sub>-IR pharmacological possibilities in neurodegenerative diseases with unmet medical needs, such as AD. More concretely, during this thesis, we evaluate the neuroprotective properties of both well-established and structurally novel selective I<sub>2</sub>-IR ligands in late-onset AD (LOAD) and early-onset AD (EOAD) mouse models, with the aim to point out I<sub>2</sub>-IR as a novel potential therapeutic target for AD.

In summary, we demonstrate that chronic treatment with potent and highly selective I<sub>2</sub>-IR ligands prevents cognitive decline and ameliorates behavioural and psychological symptoms of dementia (BPSD) -related phenotypes such as anxiety-, depressive-like

behaviours and social deficits in the AD mouse models used. Furthermore, the prevention of the generalized cognitive downfall of the mice delivered by I<sub>2</sub>-IR treatments is consistent with favourable alterations at a molecular level. Notably, we provide evidence for beneficial effects on the AD classical hallmarks, namely A $\beta$  pathology and tau hyperphosphorylation, as well as mitigation of neuroinflammation and oxidative damage, processes with a pivotal role in AD initiation and progression. Remarkably, we detected alterations in Ca<sup>2+</sup> related key enzymes induced by selective I<sub>2</sub>-IR treatment, providing insights into processes involved in the mechanism of neuroprotective action of I<sub>2</sub>-IR ligands. Ultimately, in our hands, I<sub>2</sub>-IR treatment exerted greater beneficial effects than donepezil under the neurodegenerative process. We conclude that I<sub>2</sub>-IR modulation by selective ligands can be a novel therapeutic strategy for AD therapy.



# Resumen

La identificación de los receptores imidazolínicos (IR) como una nueva clase de receptores ha planteado múltiples cuestiones sobre sus propiedades farmacológicas potenciales y terapéuticas. Los receptores I<sub>2</sub>-IR están ampliamente distribuidos en el sistema nervioso central con una localización predominante en las células gliales. Se ha demostrado que su activación tiene propiedades neuroprotectoras, aunque los mecanismos moleculares por los cuales se produce no se no son totalmente conocidos. Además, en pacientes con diferentes trastornos cerebrales, incluida la enfermedad de Alzheimer (EA) se han detectado alteraciones en la densidad de I<sub>2</sub>-IR, lo que sugiere un valor terapéutico potencial de los I<sub>2</sub>-IR en la EA.

Esta última sugerencia es de especial importancia clínica, ya que la EA es una enfermedad neurodegenerativa irreversible además de ser la forma más común de demencia, que afecta a millones de personas en todo el mundo. Las consecuencias de la EA abarcan desde los efectos perjudiciales tanto para los pacientes como para sus cuidadores hasta un impacto socioeconómico y, por desgracia, aún no existe cura para la enfermedad. Al mismo tiempo, la prevalencia de la EA está creciendo rápidamente debido al aumento de la esperanza de vida en los países desarrollados, lo que pone de manifiesto la urgencia de identificar nuevas dianas terapéuticas para detener la progresión de la enfermedad y proporcionar un tratamiento eficaz.

En este contexto, esta tesis doctoral pretende contribuir al conocimiento científico de las posibilidades farmacológicas de los I<sub>2</sub>-IR en enfermedades neurodegenerativas con necesidades médicas no cubiertas, como la EA. Más concretamente, durante esta tesis, evaluamos las propiedades neuroprotectoras de ligandos selectivos de los I<sub>2</sub>-IR, que están bien caracterizados además de ser estructuralmente novedosos, en modelos de ratón de EA de inicio tardío y de inicio temprano, con el objetivo de proponer a los I<sub>2</sub>-IR como una

nueva diana terapéutica para la EA.

En resumen, demostramos que el tratamiento crónico con ligandos potentes y altamente selectivos para los I<sub>2</sub>-IR previene el deterioro cognitivo y mejora los fenotipos relacionados con los síntomas conductuales y psicológicos de la demencia, como los comportamientos ansiosos y depresivos además de los déficits sociales en los modelos de ratón de EA utilizados. Además, la prevención del declive cognitivo generalizado de los ratones tratados con los diferentes ligandos I<sub>2</sub>-IR es coherente con los cambios positivos a nivel molecular. En particular, aportamos pruebas de los efectos beneficiosos sobre las principales características de la EA como la patología A $\beta$  y la hiperfosforilación de Tau, además de la mitigación de la neuroinflamación y el daño oxidativo, procesos con un papel fundamental en el inicio y la progresión de la EA. Notablemente, hemos detectado alteraciones en las enzimas clave relacionadas con la señalización de Ca<sup>2+</sup> inducidas por el tratamiento con ligandos selectivos de los I<sub>2</sub>-IR, lo que proporciona información sobre los procesos implicados en el mecanismo de acción neuroprotectora. Finalmente, el tratamiento con ligandos I<sub>2</sub>-IR ejerció mayores efectos beneficiosos que el donepezilo en el proceso neurodegenerativo. Concluimos, por lo tanto, que la modulación del I<sub>2</sub>-IR mediante ligandos selectivos puede ser una estrategia terapéutica novedosa para la EA.

# Thesis Structure

The present doctoral dissertation is presented in the following chapters:

**Chapter 1 - Introduction** provides background knowledge and summarises the existing research of the topic in which this thesis is framed, i.e., the Imidazoline Receptor System, with a special focus on the I<sub>2</sub> Imidazoline Receptors, and the Alzheimer's Disease.

**Chapter 2 - Objectives** contains the general aim and central problems that were addressed during the development of this dissertation and at the beginning of each scientific work.

**Chapter 3 - Methods and Results** is divided into five sections, each one of which is based on a separate scientific investigation, already published in international peer-review journals. In the aforementioned sections we provide evidence regarding the beneficial effects observed after treatment with structurally novel, as well as with already established selective I<sub>2</sub> Imidazoline Receptor ligands on: (a) cognition, (b) behaviour and (c) molecular pathways in two well-established mouse models of neurodegeneration and Alzheimer's Disease.

**Chapter 4 - Discussion** provides an in-depth interpretation of the results obtained throughout the dissertation, seeking emergent patterns among findings and comparing them with the evidence already described in the literature.

**Chapter 5 - Conclusions** is a set of concluding statements based on the findings collected from the five different investigations.

The **Annex** contains the following: (a) unpublished results, collected during this thesis by the author and other members of the same research group, that provide additional information and extend the discussion of the results. (b) publications in which the author substantially participated during the thesis preparation period, the results of which are also discussed yet are not considered part of the main content.

Below we list the five scientific papers that form the research output of the present dissertation:

### **Publication 1**

Griñán-Ferré C\*, **Vasilopoulou F\***, Abás S, Rodríguez-Arévalo S, Bagán A, Sureda FX, Pérez B, Callado LF, García-Sevilla JA, García-Fuster MJ, Escolano C, Pallàs M. (2019). Behavioral and Cognitive Improvement Induced by Novel Imidazoline I<sub>2</sub> Receptor Ligands in Female SAMP8 Mice. *Neurotherapeutics*. 16(2):416-431. doi: <https://doi.org/10.1007/s13311-018-00681-5>. \* Equal contribution

### **Publication 2**

**Vasilopoulou F**, Bagan A, Rodriguez-Arevalo S, Escolano C, Griñán-Ferré C, Pallàs M. (2020). Amelioration of BPSD-Like Phenotype and Cognitive Decline in SAMP8 Mice Model Accompanied by Molecular Changes after Treatment with I<sub>2</sub>-Imidazoline Receptor Ligand MCR5. *Pharmaceutics*. 12(5):475. doi: <https://doi.org/10.3390/pharmaceutics12050475>.

### **Publication 3**

**Vasilopoulou F**, Griñán-Ferré C, Rodríguez-Arévalo S, Bagán A, Abás S, Escolano C, Pallàs M. (2021). I<sub>2</sub> imidazoline receptor modulation protects aged SAMP8 mice against cognitive decline by suppressing the calcineurin pathway. *Geroscience*. 43(2):965-983. doi: <https://doi.org/doi:10.1007/s11357-020-00281-2>

### **Publication 4**

**Vasilopoulou F**, Rodríguez-Arévalo S, Bagán A, Escolano C, Griñán-Ferré C, Pallàs M. (2021). Disease-modifying treatment with I<sub>2</sub>imidazoline receptor ligand LSL60101 in an Alzheimer's disease mouse model: a comparative study with donepezil. *British Journal of Pharmacology*. 178(15):3017-3033. doi: <https://doi.org/10.1111/bph.15478>

### **Publication 5**

**Vasilopoulou F**, Escolano C, Pallàs M, Griñán-Ferré C. (2021). Microarray analysis reveals inflammatory transcriptomic changes after LSL60101 treatment in 5XFAD mice model. *Genes*. 12(9):1315. doi: <https://doi.org/10.3390/genes12091315>

Furthermore, two additional scientific papers have been published during the period of the thesis as a result of the author's participation in other studies carried out by members of the same research group. The content of these publications has not been included in the main document since the author contributed as a collaborator instead of leading the investigation.

- Abás S, Rodríguez-Arévalo S, Bagán A, Griñán-Ferré C, **Vasilopoulou F**, Brocos-Mosquera I, Muguruza C, Pérez B, Molins E, Luque FJ, Pérez-Lozano P, de Jonghe S, Daelemans D, Naesens L, Brea J, Loza MI, Hernández-Hernández E, García-Sevilla JA, García-Fuster MJ, Radan M, Djikic T, Nikolic K, Pallàs M, Callado LF, Escolano C. (2020). Bicyclic  $\alpha$ -Iminophosphonates as High Affinity Imidazoline I<sub>2</sub> Receptor Ligands for Alzheimer's Disease. *Journal of Medicinal Chemistry*. 2020 63(7):3610-3633. doi: <https://doi.org/10.1021/acs.jmedchem.9b02080>
- Rodríguez-Arévalo S, Bagán A, Griñán-Ferré C, **Vasilopoulou F**, Pallàs M, Brocos-Mosquera I, Callado LF, Loza MI, Martínez AL, Brea A, Pérez B, Molins E, Jonghe S, Daelemans D, Radan, Djikic T, Nikolic K, Hernández-Hernández E, Julia García-Fuster M, García-Sevilla JA, Escolano C. (2021). Benzofuranyl-2-imidazoles as imidazoline I<sub>2</sub> receptor ligands for Alzheimer's disease. *European Journal of Medicinal Chemistry*.doi: <https://doi.org/10.1016/j.ejmech.2021.113540>



# Abbreviations

**5-HT:** 5-Hydroxytryptamine

**AChE:** Acetylcholinesterase

**AD:** Alzheimer's Disease

**ALDH2:** Aldehyde dehydrogenase

**APOE:** Apolipoprotein E

**APP:** Amyloid Precursor Protein

**AR:** Adrenergic receptors

**ATP:** Adenosine triphosphate

**A $\beta$ :** Amyloid  $\beta$

**BAD:** Bcl-2 associated death protein

**BBB:** Blood-brain barrier

**Bcl-2:** B-cell lymphoma protein 2

**BDNF:** Brain-derived neurotrophic factor

**BPSD:** Behavioural and psychological symptoms of dementia

**CAMK:** Calcium calmodulin kinase

**CaN:** Calcineurin

**CAT:** Catalase

**CCL:** CC-Motif Chemokine Ligand

**CDK5:** Cyclin-dependent kinase 5

**CDS:** Clonidine-displacing substance

**CDS:** clonidine-displacing substance

**CNS:** Central Nervous System

**COX-2:** Cyclooxygenase-2

**CREB:** cAMP response element-binding protein

**CXCL-10:** Chemokine C-X-C motif ligand 10

**DARPP-32:** Dopamine- and cAMP-regulated phosphoprotein 32 kDa

**EAAT:** excitatory amino acid transporter  
**EMA:** European Medicines Agency  
**EOAD:** Early-onset Alzheimer's Disease  
**ERK:** Extracellular signal-regulated protein kinase  
**FADD:** Fas associated protein with death domain  
**FDA:** Food and Drug Administration  
**GFAP:** Glial fibrillary acidic protein  
**GPX:** Glutathione peroxidase  
**GSK3 $\beta$ :** Glycogen synthase kinase-3 beta  
**HD:** Huntington's Disease  
**HMOX1:** Heme oxygenase-1  
**HPA:** Hypothalamic-pituitary adrenal  
**I<sub>1</sub>-IR:** I<sub>1</sub> Imidazoline receptors  
**I<sub>2</sub>-IR:** I<sub>2</sub> Imidazoline receptors  
**I<sub>3</sub>-IR:** I<sub>3</sub> Imidazoline receptors  
**IDE:** Insulin-degrading enzyme  
**IFN- $\gamma$ :** Interferon gamma  
**ILs:** Interleukins  
**iNOS:** Inducible NOS  
**iPSCs:** Induced pluripotent stem cells  
**IR:** Imidazoline Receptors  
**IRAS:** IR antisera-selected  
**IRBP:** Imidazoline binding protein  
**JNK1/2:** c-Jun N-terminal kinase 1/2  
**LOAD:** Late-Onset AD  
**LTP:** Long term potentiation  
**MAO:** Monoamine oxidase  
**MAPK:** Mitogen-activated protein kinase  
**mRNA:** Messenger RNA  
**mTOR:** Mammalian target of rapamycin  
**mTORC1:** Mammalian target of rapamycin complex 1  
**NADPH:** Nicotinamide adenine dinucleotide phosphatase  
**NEP:** Neprilysin  
**NFAT:** Nuclear factor of activated T cells  
**NF- $\kappa$ B:** Nuclear factor- $\kappa$ B  
**NFTs:** Neurofibrillary tangles  
**NGF:** Nerve growth factor  
**NMDA:** N-methyl-D-aspartate  
**NOS:** Nitric oxide synthase



**Nrf2:** Nuclear factor erythroid-2 related factor  
**NSAID:** Nonsteroidal anti-inflammatory drugs  
**NT:** Neurotrophin  
**OS:** Oxidative stress  
**p70S6K:** p70 S6 kinase  
**p75NTR:** Neurotrophin receptor p75  
**PAC:** para-aminoclonidine  
**PD:** Parkinson's Disease  
**PET:** Positron Emission Tomography  
**PI3K:** Phosphoinositide 3-kinase  
**PKA:** Protein kinase A  
**PP1:** Protein phosphatase 1  
**PSD95:** Post-synaptic density protein 95  
**PSEN:** Presenilin  
**RNS:** Reactive nitrogen Species  
**ROS:** Reactive oxygen species  
**SAM:** Senescence-accelerated mouse  
**SAMP:** Senescence-accelerated mouse prone  
**SAMP8:** Senescence-accelerated mouse prone 8  
**SAMR:** Senescence-accelerated mouse resistant  
**sAPP $\alpha$ :** Soluble amyloid precursor protein alpha  
**sAPP $\beta$ :** Soluble amyloid precursor protein beta  
**Ser:** Serine  
**SOD:** Superoxide dismutase  
**SYN:** Synaptophysin  
**TGF $\beta$ :** Transforming growth factor beta  
**Th:** Threonine  
**TNF- $\alpha$ :** Tumor necrosis factor alpha  
**TREM2:** Triggering Receptor Expressed on myeloid cells 2  
**Trk:** Tyrosin kinase  
**Tyr:** Tyrosine  
**WT:** wildtype <sup>1</sup>

---

<sup>1</sup>The abbreviations throughout Chapter 3 (Methods and Results) may vary. Each publication contains separate abbreviations section according to the guidelines of the journal.

# Contents

<b>Acknowledgements</b>	<b>ix</b>
<b>Statement of Originality</b>	<b>xi</b>
<b>Abstract (English/Spanish)</b>	<b>xiii</b>
<b>Thesis Structure</b>	<b>xvii</b>
<b>Abbreviations</b>	<b>xxi</b>
<b>1 Introduction</b>	<b>1</b>
1.1 Imidazoline Receptor System . . . . .	1
1.1.1 Discovery, History and Classification . . . . .	1
1.2 I <sub>2</sub> Imidazoline Receptors . . . . .	5
1.2.1 Identification of I <sub>2</sub> Imidazoline Receptors in the brain . . . . .	5
1.2.2 Cellular localisation of I <sub>2</sub> Imidazoline Receptors in brain . . . . .	6
1.2.3 Subcellular distribution of I <sub>2</sub> Imidazoline Receptors . . . . .	6
1.3 I <sub>2</sub> Imidazoline Receptor ligands . . . . .	8
1.3.1 Endogenous Imidazoline Receptor ligands . . . . .	8
1.3.2 Synthetic I <sub>2</sub> Imidazoline Receptor ligands . . . . .	9
1.3.3 Structurally novel I <sub>2</sub> Imidazoline Receptor ligands . . . . .	10
1.4 Neuropharmacology of I <sub>2</sub> Imidazoline Receptor ligands . . . . .	12
1.4.1 Putative neuroprotective effects . . . . .	12
1.4.2 Other CNS pharmacological effects . . . . .	14
1.5 I <sub>2</sub> Imidazoline Receptors in Brain Disorders . . . . .	14
1.5.1 I <sub>2</sub> Imidazoline Receptors and neurodegenerative diseases . . . . .	14
1.5.2 I <sub>2</sub> Imidazoline Receptors and depression . . . . .	15
1.6 Brain ageing and neurodegeneration . . . . .	17
1.7 Alzheimer's Disease . . . . .	19
1.7.1 Background . . . . .	19
1.7.2 Clinical symptoms . . . . .	20
1.7.3 Risk factors and classification . . . . .	20

1.8	Neuropathology of Alzheimer's Disease . . . . .	21
1.8.1	Macroscopic features of Alzheimer's Disease brain . . . . .	21
1.8.2	Classical hallmarks of Alzheimer's Disease . . . . .	22
1.8.3	Neuroinflammation in Alzheimer's Disease . . . . .	26
1.8.4	Oxidative stress and mitochondrial dysfunction in Alzheimer's Disease . . . . .	27
1.8.5	Dysregulation of calcium homeostasis in Alzheimer's disease . . . . .	29
1.8.6	Neuronal and synaptic loss in Alzheimer's Disease . . . . .	32
1.9	Treatment of Alzheimer's Disease . . . . .	33
1.9.1	Current approved treatments . . . . .	33
1.9.2	Emerging disease-modifying therapies in clinical trials . . . . .	34
1.10	Alzheimer's Disease Mouse Models . . . . .	35
1.10.1	5XFAD mouse model for early-onset familial Alzheimer's Disease . . . . .	35
1.10.2	SAMP8 mouse model for ageing, neurodegeneration, and sporadic Alzheimer's Disease . . . . .	36
<b>2</b>	<b>Objectives</b>	<b>41</b>
<b>3</b>	<b>Methods and Results</b>	<b>43</b>
3.1	<b>Publication 1:</b> Behavioral and cognitive improvement induced by novel imidazoline I <sub>2</sub> receptor ligands in female SAMP8 mice . . . . .	45
3.2	<b>Publication 2:</b> Amelioration of BPSD-like phenotype and cognitive decline in SAMP8 mice model accompanied by molecular changes after treatment with I <sub>2</sub> -imidazoline receptor ligand MCR5 . . . . .	77
3.3	<b>Publication 3:</b> I <sub>2</sub> imidazoline receptor modulation protects aged SAMP8 mice against cognitive decline by suppressing the calcineurin pathway . . . . .	107
3.4	<b>Publication 4:</b> Disease-modifying treatment with I <sub>2</sub> imidazoline receptor ligand LSL60101 in an Alzheimer's disease mouse model: A Comparative study with donepezil. . . . .	139
3.5	<b>Publication 5:</b> Microarray analysis revealed inflammatory transcriptomics changes after LSL60101 treatment in 5XFAD mice model. . . . .	177
<b>4</b>	<b>Discussion</b>	<b>201</b>
4.1	Effects of treatment with I <sub>2</sub> -IR ligands on memory loss and BPSD present in AD . . . . .	202
4.1.1	Cognitive symptoms . . . . .	202
4.1.2	Non-cognitive symptoms . . . . .	204
4.2	Effects of I <sub>2</sub> -IR ligands on histological and molecular AD hallmarks . . . . .	205

---

4.2.1	$A\beta$ pathology . . . . .	205
4.2.2	Tau hyperphosphorylation . . . . .	207
4.3	Effects of $I_2$ -IR ligands on neuroinflammation . . . . .	208
4.4	Changes in oxidative stress process induced by $I_2$ -IR ligands . . . . .	211
4.5	Alterations in $Ca^{2+}$ signaling after treatment with $I_2$ -IR ligands . . . . .	213
4.6	Effects on neuronal and synaptic loss delivered by $I_2$ -IR ligands . . . . .	214
4.6.1	Apoptotic factors . . . . .	214
4.6.2	Synaptic plasticity . . . . .	215
4.7	Combination treatment of $I_2$ -IR ligand with AChE Inhibitor . . . . .	216
4.8	Final Considerations . . . . .	218
<b>5</b>	<b>Conclusions</b>	<b>221</b>
	<b>Bibliography</b>	<b>223</b>
	<b>A. ANNEX</b>	<b>271</b>
A.1	Preliminary evaluation of the effect of $I_2$ Imidazoline Receptor ligands in human APP Swedish mutated iPSC-derived astrocytes from Alzheimer's disease patients . . . . .	273
A.2	Evaluation of MAO inhibitory activity and NMDA antagonistic activity of selective $I_2$ -IR compounds MCR5 and MCR9 . . . . .	279
A.3	Bicyclic $\alpha$ -Iminophosphonates as High Affinity Imidazoline $I_2$ Receptor ligands for Alzheimer's Disease. . . . .	283
A.4	Benzofuranyl-2-imidazoles as Imidazoline $I_2$ Receptor ligands for Alzheimer's disease . . . . .	309

# List of Figures

1	Chemical Structures of Imidazoline, Imidazole, Guanidine, Clonidine, Idazoxan . . . . .	3
2	Schematic classification of IR and major IR-associated pharmacological target effects. . . . .	4
3	Schematic distribution, cellular and subcellular localisation of I <sub>2</sub> -IR in the brain. . . . .	8
4	Chemical structures of the proposed endogenous ligands candidates. . . . .	9
5	Chemical structures of known I <sub>2</sub> -IR ligands. . . . .	10
6	Chemical structures of novel I <sub>2</sub> -IR ligands . . . . .	11
7	Hallmarks of Ageing, present in neurogenerative diseases. . . . .	19
8	Macroscopic features of AD brains (Source: Alzheimer’s Association) . . . . .	22
9	Scheme of APP processing pathways and formation of extracellular A $\beta$ plaques. . . . .	23
10	Process of tau hyperphosphorylation mediated by major tau kinases such as CDK5, GSK3 $\beta$ , ERK1/2. . . . .	25
11	Inflammatory process in glial cells- triggered by and triggering AD features such as A $\beta$ plaque formation, NFTs and ROS generation, leading synergistically to neuronal loss. . . . .	27
12	Generation of ROS and RNS in mitochondria promotes neurodegenerative processes; a malicious cycle is created that eventually result in cell death. . . . .	29
13	Schematic of Ca <sup>2+</sup> dysregulation in AD. A $\beta$ plaques, NFTs as well as inflammatory mediators and ROS released by glial cells trigger Ca <sup>2+</sup> influx which subsequently initiate signaling cascades involved in synaptic loss, neuroinflammation and apoptosis. . . . .	31
14	AD characteristics of SAMP8 and 5XFAD animal models and approximate age of appearance. . . . .	39
15	Schematic representation of the beneficial effects of novel and well-established I <sub>2</sub> -IR ligands on central AD pathological processes after treatment in SAMP8 and 5XFAD mouse models of AD, delivering neuroprotection and protecting the mice against generalized cognitive downfall and BPSD. . . . .	219



# List of Tables

1	Key findings in chronological order that suggested the existence of non-adrenergic receptors for imidazoline compounds. . . . .	2
2	I <sub>2</sub> -IR and $\alpha_2$ -AR affinities (pKi) of established and novel I <sub>2</sub> -IR ligands in membranes from postmortem human frontal cortex. Competition experiments against [ <sup>3</sup> H]-2-BFI were biphasic for most of the compounds. . . .	11
3	Alterations of I <sub>2</sub> -IR density and IR immunoreactivity in brain tissue from patients with brain disorders. PM binding and immunodetection experiments were performed in tissue membranes. . . . .	16

---

The figures and tables of the included publications are not listed.





# Chapter 1

## Introduction

### 1.1 Imidazoline Receptor System

#### 1.1.1 Discovery, History and Classification

Imidazoline receptors (IR), also called imidazoline binding sites, are a family of heterogeneous entities with a high affinity for compounds bearing an imidazoline ring [(a five-atom ring, two of which are nitrogen atoms, (Fig. 1)] (Bousquet et al., 1984). The concept of the IR system was introduced decades ago, following extensive research documenting their relationship and, finally, their distinction from the adrenergic receptors (AR), and in particular, the subtype  $\alpha_2$  ( $\alpha_2$ -AR). The  $\alpha_2$ -AR are involved in the negative feedback control of the release of the sympathetic system neurotransmitter noradrenaline and also recognise imidazoline-related compounds (Langer et al., 1977). However, a significant part of the biomedical community is still unfamiliar with the IR system, and this may be partially due to its limited mention in scientific sources of the major pharmacological targets and receptors (Alexander et al., 2011). Nevertheless, at present, there is an emerging research interest in the IR owing to a large body of evidence demonstrating the promising pharmacological and therapeutic potential of IR ligands in several pathological conditions.

In the 1960s, the discovery of clonidine, later described as an  $\alpha_2$ -AR agonist, marked the first step in the emerging field of IR research (Stähle, 2000). Clonidine, a chemical compound that contains an imidazoline ring (Fig. 1), although initially developed for the treatment of rhinorrhoea, was shown to exert hypotensive and bradycardic effects due to its action in the central nervous system (CNS) by inhibiting the sympathetic tone (J.M. Armstrong & Boura, 1973; Klupp et al., 1970; Kobinger, 1967; Kobinger & Walland, 1967, 1972b, 1972a). Clonidine's hypotensive effect was initially attributed to its  $\alpha_2$ -AR

properties, given that  $\alpha_2$ -AR antagonists (e.g., yohimbine, piperoxan) blocked this effect (Greenberg et al., 1976; Rouot & Snyder, 1979; Schmitt & Fénard, 1973). However, several subsequent findings indicated that the  $\alpha_2$ -AR mechanism hypothesis of clonidine's action was not sufficient to completely explain its hypotensive effect; therefore, it was suggested that clonidine and imidazoline related compounds might act through specific sites (non-adrenergic) that recognise imidazoline/imidazole-containing ligands.

This was formalised by Bousquet et al. in 1984, who first proposed the “sites preferring the imidazoline structure” and introduced the concept of non-adrenergic receptors for imidazoline compounds (Bousquet et al., 1984) while the, now used by the scientific community, denomination “imidazoline receptors” was introduced in 1987 (Ernsberger et al., 1987). Most of the studies published during the 1980s and early 1990s regarding the IR, described not only the physiologic and pharmacologic features of these new molecular entities but also their distinction from  $\alpha_2$ -AR, some of which are reported in Table 1 .

**Table 1:** Key findings in chronological order that suggested the existence of non-adrenergic receptors for imidazoline compounds.

YEAR	FINDINGS
1976	Clonidine's hypotensive effect was effectively blocked by an imidazole-containing histamine H <sub>2</sub> receptor antagonist (cimetidine) without actions on $\alpha_2$ -AR (Karppanen et al., 1976).
1977	Lack of cross-desensitisation between structurally dissimilar $\alpha$ -AR agonists (imidazolines, phenylethylamines, catecholamines) was reported ( Ruffolo et al., 1977).
1981	Nucleus reticularis lateralis (NRL) (small nucleus which contains sympathetic neurons, acting as a vasopressor centre) was considered a primary site of hypotensive action for clonidine, which permitted a pharmacological distinction from $\alpha_2$ -AR compounds action in latter experiments (Bousquet et al., 1981).
1983	Differences in the nature of binding to $\alpha_2$ -AR receptors between compounds with imidazoline structure or phenylethylamine structure were reported (Ruffolo et al., 1983).
1984	Structure-activity relationship studies using phenylethylamine-based chemical compounds (e.g. $\alpha$ -methylnoradrenaline), highly selective for $\alpha_2$ -AR, did not lower the blood pressure after microinjection into the NRL in contrast to the imidazoline compounds (Bousquet et al., 1984).
1987-1994	A significant percentage of the specific [ <sup>3</sup> H]-clonidine or [ <sup>3</sup> H]-para-aminoclonidine (PAC) high-affinity binding was not displaced by catecholamines (e.g. adrenaline, norepinephrine, dopamine) in brain tissue (Bricca et al., 1988, 1989, 1993, 1994; Ernsberger et al., 1987).
2001	Administration of clonidine induced hypotensive effects in engineered mice without functional $\alpha_2$ -AR, suggesting that exclusive action on the imidazoline receptors is enough to induce a hypotensive action (Bruban et al., 2001, 2002).

In the early 1990s, the radioligand [ $^3\text{H}$ ]-idazoxan, an imidazoline and antagonist for  $\alpha_2$ -AR, was shown to recognise non-adrenergic binding sites different from those labelled by the non-imidazoline  $\alpha_2$ -AR antagonist [ $^3\text{H}$ ]-rauwolscine in autoradiographic distributions studies (Boyajian et al., 1987; De Vos et al., 1991; Mallard et al., 1992). More importantly, it was revealed later that the non-adrenergic binding sites labelled by [ $^3\text{H}$ ]-idazoxan were different from those labelled by [ $^3\text{H}$ ]-para-aminoclonidine (PAC) (analogue of clonidine used as a tool to label non-adrenergic sites), and their pharmacological properties were also different (Wikberg, 1989; Wikberg & Uhlén, 1990). These findings suggested the existence of different categories of non-adrenergic binding sites. Ultimately, it was shown that clonidine and idazoxan could bind to both sites categories albeit with different affinities, leading to the subdivision of the IR into two principal subtypes: the  $\text{I}_1$  Imidazoline receptors ( $\text{I}_1$ -IR), which represent the non-adrenergic clonidine-preferring subtype and the  $\text{I}_2$  Imidazoline receptors ( $\text{I}_2$ -IR) being the non-adrenergic idazoxan-preferring subtype (Regunathan & Reis, 1996).

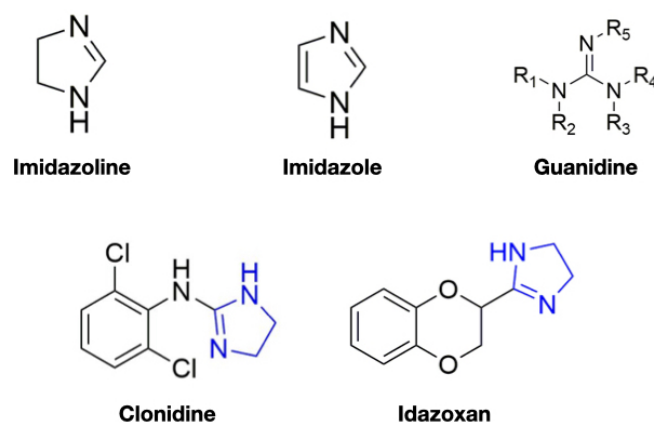


**Figure 1:** Chemical Structures of Imidazoline, Imidazole, Guanidine, Clonidine, Idazoxan

To date, the IR have been classified into three subtypes based on biochemical, functional and ligand binding characterisations. Below, we highlight their main properties and distinguishing features (Fig.2).

- The  $\text{I}_1$ -IR display high affinity for the imidazoline-containing clonidine, its analogue PAC and related compounds (e.g. moxonidine, rilmenidine, efaroxan) (Molderings et al., 1993).  $\text{I}_1$ -IR have been shown to mediate the hypotensive effects of clonidine and clonidine-like drugs; thus, they are involved in blood pressure control and hypertension (Ernsberger & Haxhiu, 1997; G. Head & Mayorov, 2008).  $\text{I}_1$ -IR ligands such as moxonidine and rilmenidine are clinically used to treat hypertension (Fenton et al., 2006; Kawecka-Jaszcz et al., 2006; Sica, 2007).
- The  $\text{I}_2$ -IR display high affinity for the imidazoline-containing idazoxan and related

$I_2$ -IR compounds (see section 1.3) and guanidines (Fig. 1) (Miralles et al., 1993). Of note, the  $I_2$ -IR were further sub-divided into  $I_{2A}$  and  $I_{2B}$  according to their high or low affinity for amiloride (a guanidinium-derivative), respectively, presenting different pharmacological profiles (Diamant et al., 1992; Escribá et al., 1996; Miralles et al., 1993; Olmos, Alemany, et al., 1999).  $I_2$ -IR are involved in various centrally mediated pharmacological effects related to analgesia (Diaz et al., 1997; J. X. Li & Zhang, 2011), hyperphagia (Jackson et al., 1991; Polidori et al., 2000), hypothermia (Thorn et al., 2012), depression (Halaris & Piletz, 2003; Holt, 2003) and neuroprotection, on the latter of which focuses the present doctoral dissertation (see section 1.4.1).

- Finally, some **atypical IR**, whose pharmacological properties do not correspond to any of the previous subtypes, have been identified in pancreatic  $\beta$ -cells and designated as  $I_3$  Imidazoline receptors ( **$I_3$ -IR**).  $I_3$ -IR have been involved in insulin secretion (Chan et al., 1994; Y. Li et al., 2015).

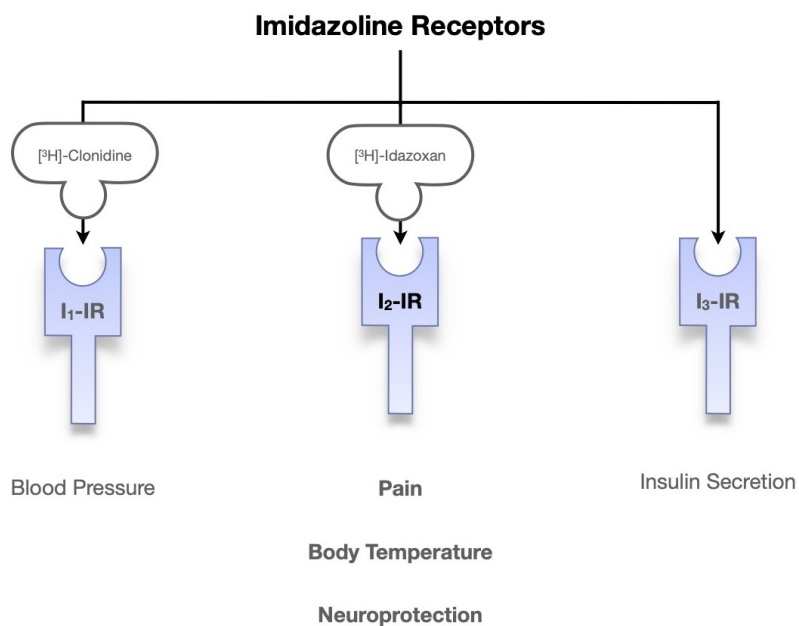


**Figure 2:** Schematic classification of IR and major IR-associated pharmacological target effects.

## 1.2 I<sub>2</sub> Imidazoline Receptors

As mentioned, the I<sub>2</sub>-IR, also called idazoxan-preferring subtype, display high affinity for [<sup>3</sup>H]-idazoxan radioligand and lower affinity for [<sup>3</sup>H]-clonidine (Regunathan & Reis, 1996). Unfortunately, I<sub>2</sub>-IR have not been cloned yet, and their structures remain unidentified. For this reason, knowledge of the I<sub>2</sub>-IR field has been primarily based on studies using mixed antagonists for I<sub>2</sub>-IR and  $\alpha_2$ -AR, such as the I<sub>2</sub>-IR prototype idazoxan (similar affinities for I<sub>2</sub>-IR and  $\alpha_2$ -AR) (Table 2) and later more selective I<sub>2</sub>-IR ligands. In fact, although idazoxan is not a selective I<sub>2</sub>-IR ligand, it has been an invaluable tool for the discrimination, localisation, characterisation and functionality of the I<sub>2</sub>-IR in the early research stages. Thus, ligand binding studies in membranes isolated from different tissues and species, autoradiographic and immunodetection studies have established the I<sub>2</sub>-IR distribution provided information concerning the kinetics of binding and recognition of the subclasses. I<sub>2</sub>-IR have been identified in many organs and tissues (brain, kidney, liver, colon, placenta, prostate, urethra, adrenal medulla, carotid bodies) and cell types (astrocytes, glial cells platelets, pancreatic cells, vascular smooth muscle cells) (Regunathan & Reis, 1996).

### 1.2.1 Identification of I<sub>2</sub> Imidazoline Receptors in the brain

I<sub>2</sub>-IR were initially labelled by the radioligands [<sup>3</sup>H]-idazoxan and later by its analogue [<sup>3</sup>H]-2-BFI (selective I<sub>2</sub>-IR ligand, see section 1.3.3) in human and rodent brains, and rapidly it became evident that they constitute a highly heterogeneous group of multiple proteins (Boyajian et al., 1987; De Vos et al., 1991; Lione et al., 1998; Mallard et al., 1992; Miralles et al., 1993). Early immunological studies further contributed to ascribing the IR nature to distinct proteins in human and rodent brains. These studies primarily used a polyclonal antiserum named imidazoline receptor binding protein (IRBP), raised in rabbits against a 70 kDa protein purified from bovine adrenal chromaffin cell membranes by idazoxan or clonidine affinity chromatography (H. Wang et al., 1992, 1993). In brain tissues, the anti-IRBP antibody recognised multiple protein bands (human brains: 30, 47, 60, 66 kDa; rat brains: 30, 45, 66 and 85 kDa; mouse brains: 20, 57, 66 and 85 kDa; rabbit brains: 30, 57, 66, 85), thus pointing out the heterogeneity of IR proteins as well as a differential expression among species (Escribá et al., 1994, 1996; Olmos, Alemany, et al., 1999). It must nevertheless be emphasised that the anti-IRBP antibody used in those studies was not able to distinguish between I<sub>1</sub>-IR and I<sub>2</sub>-IR.

Unlike I<sub>2</sub>-IR, I<sub>1</sub>-IR candidate proteins (molecular weight about 167 kDa), namely human IR antisera-selected (IRAS) protein (Piletz, Ivanov, et al., 2000) and its mouse homolog nischarin (Alahari et al., 2000) were cloned and suggested to represent functional I<sub>1</sub>-IR, precursor proteins of IR entities or subunits of complex structures responsible for binding

imidazoline compounds (Piletz et al., 1999, 2003; Piletz, Ivanov, et al., 2000; Sun et al., 2007). Hence, in a more recent study, Keller and Garcia-Sevilla (2015) using the three antibodies anti-IRBP ( $I_1/I_2$ -IR), anti-NISH ( $I_1$ -IR) and anti-nischarin ( $I_1$ -IR) immunodetected, characterised and compared the expression of IR in mouse and human brains. Regarding the  $I_2$ -IR, with the antibodies used, immunoreactive proteins approximately of 30, 45, 66 kDa were related to the  $I_2$ -IR type. This was supported by the fact that treatments with  $I_2$ -IR selective ligands but not with  $I_1$ -IR ligands modulated these contents in the mouse brain cortex (Keller & García-Sevilla, 2015) and was in agreement with previous literature, which demonstrated that the 29/30 and 45 kDa IR proteins expression correlated with  $I_2$ -IR labelled by [ $^3$ H]-idazoxan densities suggesting these proteins to be the main binding entities (Escribá et al., 1996; J. A. García-Sevilla, Sastre, et al., 1995; Sastre et al., 1996).

### 1.2.2 Cellular localisation of $I_2$ Imidazoline Receptors in brain

At a cellular level, the  $I_2$ -IR are expressed in both neurons and glia cells in the CNS (Keller & García-Sevilla, 2015; Regunathan et al., 1993). Although early binding studies with [ $^3$ H]-Idazoxan showed that  $I_2$ -IR were expressed in rat cortical astrocytes (the primary type of glial cells), but not in cortical neurons (Regunathan et al., 1993), it was demonstrated later that  $I_2$ -IR are also found in neurons albeit in a lower density (Garcia-Sevilla & Ferrer-Alcon, 2003; Keller & García-Sevilla, 2015; Ruggiero et al., 1995, 1998) (Fig.3). Interestingly, incubation of rat cortical astrocytes with [ $^3$ H]-idazoxan was also shown to increase the mRNA of glial fibrillary acidic protein (GFAP), a marker of astrocytes activation (Regunathan et al., 1993). Similarly, astrocytic hyperplasia and upregulation of GFAP expression were observed in rat brains after chronic treatment with  $I_2$ -IR drugs, which more importantly went in parallel with  $I_2$ -sites density (J. A. García-Sevilla, Alemany, et al., 1995; Olmos et al., 1994). This evidence not only supported the primary localisation of  $I_2$ -IR in astrocytes but also postulated a close relationship of  $I_2$ -IR with glia modulation (see also section 1.4.1).

### 1.2.3 Subcellular distribution of $I_2$ Imidazoline Receptors

At a subcellular level,  $I_2$ -IR are localised in the cell membrane and predominately in the outer membrane of mitochondria of various rabbit, bovine and human tissues, including the brain (Limon et al., 1992; Regunathan & Reis, 1996; Tesson et al., 1991, 1992; Tesson & Parini, 1991). In this context, biochemical and pharmacological studies suggested a possible structural and functional correlation between  $I_2$ -IR and monoamine oxidases (MAO), two mitochondrial enzymes (MAO-A, MAO-B) involved in the oxidate deamination of neurotransmitters and exogenous amines; however, the nature of their relationship was debated for decades.

Early studies demonstrated a significant correlation between I<sub>2</sub>-IR and MAO-B expression in the human brain (Sastre & García-Sevilla, 1993), suggesting their co-expression although discounting a direct interaction of I<sub>2</sub>-IR ligands (e.g. idazoxan) with the active centre of both isoenzymes of MAO (J. A. García-Sevilla, Sastre, et al., 1995; Olmos et al., 1993; Sastre & García-Sevilla, 1993). Albeit several studies postulated that the I<sub>2</sub>-IR are located in MAO (Parini et al., 1996; Raddatz et al., 1997; Remaury et al., 1998, 1999) lines of evidence supported the existence of various I<sub>2</sub>-IR that are distinct from MAO isoenzymes (Ballesteros et al., 2000; Escribá et al., 1996; Olmos, Alemany, et al., 1996; Ozaita et al., 1997; Sastre & García-Sevilla, 1997). For example, MAO isoenzymes and IR proteins were shown to have different molecular weights (29/30 and 45 kDa for IR proteins versus 63 and 59 kDa for MAO-A and MAO-B isoforms, respectively) (Escribá et al., 1996, 1999) and notably, I<sub>2</sub>-IR binding was reported in MAO knockout mice (Anderson, Seif, et al., 2006; Remaury et al., 2000).

At the same time, chronic treatments with MAO inhibitors (e.g. phenelzine) were associated with downregulation of brain I<sub>2</sub>-IR, implying a relationship between I<sub>2</sub>-IR and MAO, although this was suggested to occur through an indirect mechanism (Alemany et al., 1995; Escribá et al., 1996; Olmos et al., 1993). Interestingly, I<sub>2</sub>-IR ligands were shown to inhibit MAO-A and/or MAO-B *in vitro* and *in vivo*, and in some cases to elevate monoamine levels (Carpéné et al., 1995; F. Ferrari et al., 2011; Ozaita et al., 1997; Raasch et al., 1999; Sastre-Coll et al., 1999; Ugedo et al., 1999). Furthermore, the fact that the nature of the inhibition was shown to vary (competitive for MAO-A; competitive, non-competitive or through mixed mechanisms for MAO-B) suggested that I<sub>2</sub>-IR on MAO represent allosteric regulatory sites that are able to modulate MAO activity through an allosteric inhibitory mechanism. (McDonald et al., 2010; Parini et al., 1996; Paterson et al., 2007; Tesson et al., 1995). Nevertheless, the fact that I<sub>2</sub>-IR radioligands saturate their receptors at low nanomolar concentrations while for MAO inhibition are required millimolar concentrations is enigmatic (Olmos, Alemany, et al., 1999; Ozaita et al., 1997). Ultimately, more recent studies demonstrated that radiolabelling of I<sub>2</sub>-IR in rhesus monkeys and human brains was not blocked by MAO inhibitors (Parker et al., 2014; Tyacke et al., 2018) or that MAO inhibitors blocked only the labelling of a subpopulation of I<sub>2</sub>-IR in human brains (A. Kumar et al., 2021).

Taken together, to date, there is little doubt that several I<sub>2</sub>-IR are related to MAO enzymes through the presence of an I<sub>2</sub>-IR population situated away from the active/substrate site, which has important implications on the enzyme's activity; however, MAO cannot account for all I<sub>2</sub>-IR. More importantly, Kimura et al. (2009) reported the identity of the 45 kDa imidazoline protein to be brain creatine kinase and that I<sub>2</sub>-IR are expressed within the enzyme, further confirming the existence of I<sub>2</sub>-IR unrelated to MAO and the heterogeneous

nature of I<sub>2</sub>-IR (Kimura et al., 2009) (Fig.3).

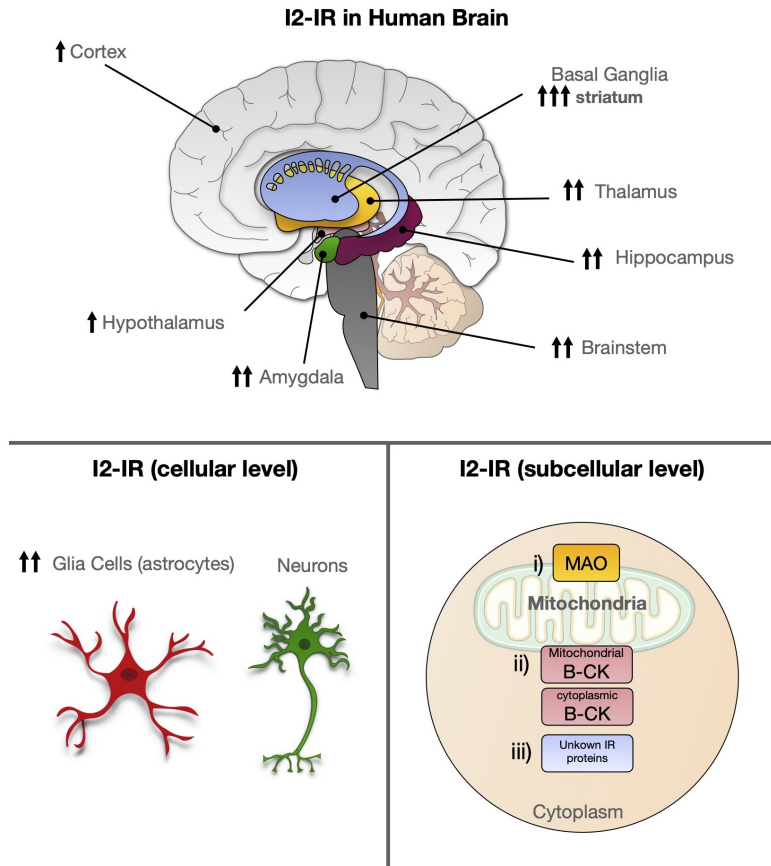


**Figure 3:** Schematic distribution, cellular and subcellular localisation of I<sub>2</sub>-IR in the brain.

## 1.3 I<sub>2</sub> Imidazoline Receptor ligands

### 1.3.1 Endogenous Imidazoline Receptor ligands

Extensive research in the imidazoline field has been performed to identify the endogenous ligands. The putative candidates are the clonidine-displacing substance (CDS), agmatine, Imidazole-4 Acetic Acid-Ribotide (IAA-RP) and harmane (Fig. 4). In 1984, the substance CDS was purified from the mammalian brain and launched the endogenous ligands research (Atlas & Burstein, 1984). CDS was shown to displace [<sup>3</sup>H]-clonidine binding to α<sub>2</sub>-AR and labelled ligands from I<sub>1</sub>-IR and I<sub>2</sub>-IR (Coupry et al., 1990; Ernsberger et al., 1988). Two of the active constituents of CDS were reported to be the β-carbolines harmane, and harmalan which display affinity at I<sub>1</sub>-IR and I<sub>2</sub>-IR (Husbands et al., 2001; Parker et al., 2004), and harmane additionally was shown to bind to I<sub>3</sub>-IR (Morgan et al., 2003). Interestingly, harmane was reported to control blood pressure through I<sub>1</sub>-IR (Musgrave and Badoer, 2000), to inhibit MAO-A with evidence suggesting this to occur through I<sub>2</sub>-IR (Anderson, Tyacke, et al., 2006; Lallies et al., 1999; MacInnes & Handley, 2002),



and to be involved in I<sub>3</sub>-IR-mediated insulin release (Morgan et al., 2003); however, so far, a neurotransmitter role for harmaine has not been assigned (Bousquet et al., 2020). In 2004, Prell et al. proposed IAA-RP as a neurotransmitter acting via IR, present in the brain and neurons and detectable in CDS extracts. IAA-RP increased blood pressure and induced synaptic depression (Bozdagi et al., 2011; Prell et al., 2004). These effects were suggested to involve I<sub>1</sub>-IR and/or I<sub>3</sub>-IR activation, suggesting IAA-RP to be an important candidate as an endogenous ligand for IR (Bousquet et al., 2020). In 1994, agmatine was first proposed as an endogenous ligand for IR (G. Li et al., 1994) and an endogenous neurotransmitter within the CNS (Reis & Regunathan, 1999, 2000), which agreed with its anatomical distribution within the brain (Raasch et al., 1995). Agmatine has been shown to bind both to  $\alpha$ -AR and IR (I<sub>1</sub>-IR and I<sub>2</sub>-IR) with low affinity (Hudson et al., Reis & Regunathan, 2000), and the IR involvement was reported to account for several of agmatine's effects (G. A. Head & Mayorov, 2006; Piletz et al., 2013). Besides, agmatine has several molecular targets other than IR, such as N-methyl-D-aspartate (NMDA) receptors, 5-hydroxytryptamine (5-HT) or serotonin 5-HT<sub>2A</sub> and 5-HT<sub>3</sub> receptors, nitric oxide synthase (NOS), among others (Berkels et al., 2004; Piletz et al., 2013). As a result, it is still unclear whether all the biological effects produced are attributed to IR modulation (G. A. Head & Mayorov, 2006). However, agmatine is presumed as the endogenous ligand for IR over the other proposed substances (Hudson, 2015; Piletz et al., 2013).

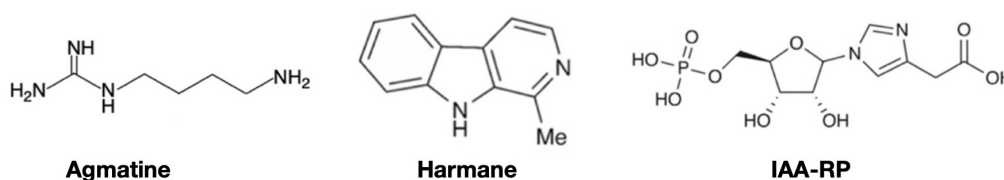


**Figure 4:** Chemical structures of the proposed endogenous ligands candidates.

### 1.3.2 Synthetic I<sub>2</sub> Imidazoline Receptor ligands

As mentioned, idazoxan was the first I<sub>2</sub>-IR ligand used for the characterisation of I<sub>2</sub>-IR; however, idazoxan also binds to  $\alpha_2$ -AR (Michel & Insel, 1989) and 5-HT<sub>1A</sub> (Lladó et al., 1996). Consequently, given the complex nature of the imidazoline system, the development of selective I<sub>2</sub>-IR ligands became a pressing need for the understanding of I<sub>2</sub>-IR. In efforts to chemically modify the structure of idazoxan, several selective I<sub>2</sub>-IR ligands were synthesised over the past decades. All these ligands share a common characteristic: the imidazoline moiety (except two that bare an imidazole structure instead) and display variable affinity and selectivity for IR/ $\alpha_2$ -AR or I<sub>1</sub>-IR/I<sub>2</sub>-IR (Table 2). These include: **LSL61122**; **valdemossine** or **tracizoline** (2-styryl-2-imidazoline), **LSL60101** [2-(2-benzofuranyl)imidazole], **2-BFI** [2-(2-benzofuranyl)-2-imidazoline] and its quinoline analogue **BU224** [2-(4,5-dihydroimidazol-2-yl) quinoline hydrochloride], the

irreversible ligand **BU99006** [5-isothiocyanato-2-benzofuranyl-2-imidazoline], **CR4056** and the radiolabelled [ $^{11}\text{C}$ ]-**BU99008** and [ $^3\text{H}$ ]-**BU99008** (Fig. 5). These  $\text{I}_2$ -IR ligands have been used extensively for the characterisation of  $\text{I}_2$ -IR and/or the assessment of functional and pharmacological effects mediated by the  $\text{I}_2$ -IR system, and notably, the compounds CR4056, [ $^{11}\text{C}$ ]-BU99008 and [ $^3\text{H}$ ]-BU99008 have been recently used in human studies as well (Comi et al., 2017; A. Kumar et al., 2021; Rovati et al., 2020; Tyacke et al., 2018).

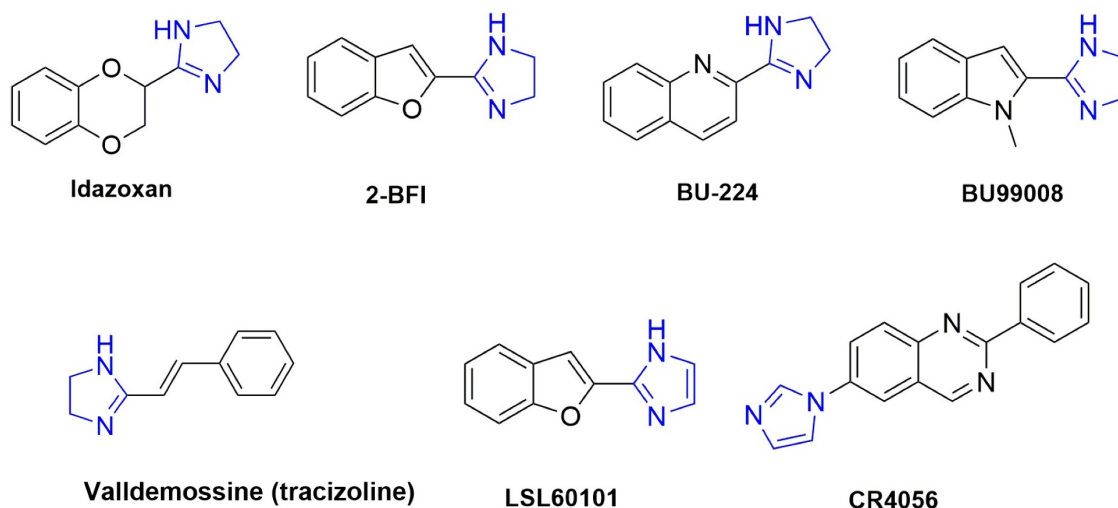


**Figure 5:** Chemical structures of known  $\text{I}_2$ -IR ligands.

### 1.3.3 Structurally novel $\text{I}_2$ Imidazoline Receptor ligands

It is important to note that structurally, the above-listed imidazoline ligands, widely used for the characterisation of IR, present a restricted variation being all imidazoline (or imidazole) compounds substituted at the 2-position with distinct heterocycles (except for agmatine and agmatine-like aliphatic guanidines). It was then hypothesised that structure modifications beyond the 2-position substitution could lead to  $\text{I}_2$ -IR ligands with an improved affinity and selectivity for the  $\text{I}_2$ -IR over the  $\text{I}_1$ -IR and  $\alpha_2$ -AR, and thus enhanced pharmacological properties and/or limited side effects resulted from  $\alpha_2$ -AR binding. This hypothesis was addressed by Abas et al., (2017) and gave rise to a different series of compounds pertaining to a chemical family named (2-imidazolin-4-yl) phosphonates (Abás et al., 2017). This new family present 2 different series of compounds, both substituted in position 1 and 4 (in contrast to previously known 2-substituted  $\text{I}_2$ -IR ligands), bearing also or not, an extra phenyl. Through competition binding studies against selective  $\text{I}_2$ -IR radioligand ([ $^3\text{H}$ ]-2BFI) or selective  $\alpha_2$ -AR radioligand ( $^3\text{H}$ ]-RX821002), it was shown that the structurally new compounds presented higher affinity for  $\text{I}_2$ -IR and/or higher  $\text{I}_2/\alpha_2$  selectivity when compared to idazoxan (Table 2). Among them, 2 compounds emerged as promising ones: the **MCR5** [diethyl (1-(3-chloro-4- fluorobenzyl)-5,5-dimethyl-4-phenyl- 4,5-dihydro-1H- midazole-

4-yl)phosphonate] presenting an outstanding affinity for I<sub>2</sub>-IR and **MCR9** (replacement of the phosphonate ester in position 4 by a methyl ester) [methyl 1-(3-chloro-4-fluorobenzyl)-5,5-dimethyl-4-phenyl-4,5-dihydro-1H-imidazole-4-carboxylate] with a 4-fold increase in selectivity over the α<sub>2</sub>-AR (Abás et al., 2017). The promising results from a chemical point of view led to the synthesis of compounds pertaining to the bicyclic α- iminophosphonates family. Among them, **B06** diethyl (1RS, 3aSR, 6aSR)-5-(3-chloro-4-fluorophenyl)-4,6-dioxo-1-phenyl-1,3a,4,5,6,6a-hexahydropyrrolo[3,4-c]pyrrole-1-phosphonate displayed an outstanding affinity for the I<sub>2</sub>-IR and excellent selectivity index regarding I<sub>1</sub>-IR and α<sub>2</sub>-AR (Table 2) (Abás et al., 2020) (Annex A.3). All the above evidence points out **MCR5**, **MCR9** and **B06** to be appropriate I<sub>2</sub>-IR candidates for unravelling the biological and pharmacological actions of I<sub>2</sub>-IR (Fig. 6).

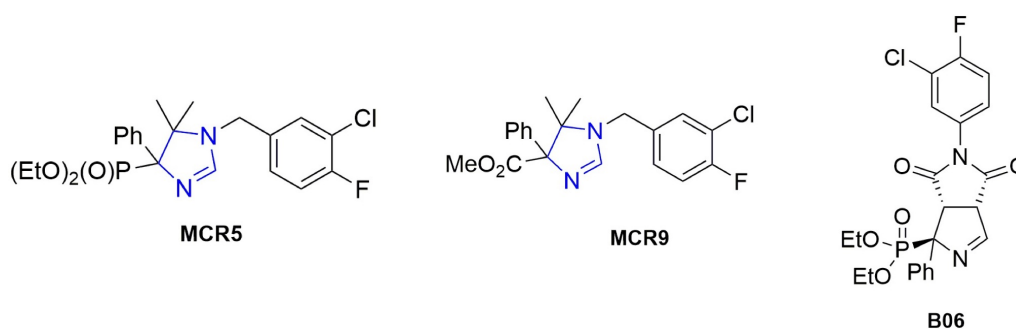


**Figure 6:** Chemical structures of novel I<sub>2</sub>-IR ligands

**Table 2:** I<sub>2</sub>-IR and α<sub>2</sub>-AR affinities (pKi) of established and novel I<sub>2</sub>-IR ligands in membranes from postmortem human frontal cortex. Competition experiments against [<sup>3</sup>H]-2-BFI were biphasic for most of the compounds.

Compound	[ <sup>3</sup> H]-2-BFI I <sub>2</sub> pKi one site	[ <sup>3</sup> H]-2-BFI I <sub>2</sub> pKi two sites		[ <sup>3</sup> H]-RX821002 α <sub>2</sub>	Selectivity I <sub>2</sub> /α <sub>2</sub>
<b>Idazoxan</b>	7.41 ± 0.63	7.87 ± 0.74	5.76 ± 0.57	7.92 ± 0.07	-
<b>2-BFI</b>	8.31 ± 0.13	9.08 ± 0.22	7.15 ± 0.31	4.58 ± 0.22	5370
<b>CR4056</b>	5.95 ± 0.11	7.72 ± 0.31	5.45 ± 0.15	2.65 ± 1.24	1995
<b>LSL60101</b>	6.67 ± 0.09	8.17 ± 0.19	6.02 ± 0.10	3.18 ± 0.17	3090
<b>BU99008</b>	7.05 ± 0.17	6.89 ± 0.21	3.82 ± 0.30	4.37 ± 0.17	479
<b>Tracizoline</b>	7.58 ± 0.12	8.48 ± 0.51	6.48 ± 0.32	4.33 ± 0.22	1778
<b>MCR5</b>	9.42 ± 0.16	N/A	N/A	6.76 ± 0.22	457
<b>MCR9</b>	8.85 ± 0.21	N/A	N/A	5.58 ± 0.14	1862
<b>B06</b>	8.56 ± 0.32	8.61 ± 0.28	4.29 ± 0.20	6.27 ± 0.56	195

## 1.4 Neuropharmacology of I<sub>2</sub> Imidazoline Receptor ligands

The up-to-date approaches for identifying the I<sub>2</sub>-IR proteins suggested their existence as a heterogeneous population and confirmed their differential expression among species and tissues. This is of special significance since this heterogeneity can often be translated into differences in pharmacological effects induced by I<sub>2</sub>-IR ligands *in vivo* and *in vitro*. Nevertheless, albeit I<sub>2</sub>-IR are considered more a heterogeneous group of proteins rather than classic receptors, I<sub>2</sub>-IR binding of I<sub>2</sub>-IR drugs has been shown to exert common pharmacological effects in the CNS associated with neuroprotection hypothermia, analgesia, and discriminative stimulus effects.

### 1.4.1 Putative neuroprotective effects

By definition, neuroprotection refers to the “relative preservation of neuronal structure and/or function”, and it is an action that aims to prevent acute neuronal damage or chronic neurodegeneration (Wiendl et al., 2015). Several studies have evaluated the neuroprotective effect of well-established I<sub>2</sub>-IR ligands by influencing cellular and molecular mechanisms that lead to neuronal damage and death, such as inflammation, calcium (Ca<sup>2+</sup>) dysregulation, oxidative damage and apoptosis.

I<sub>2</sub>-IR ligands appear to modulate the inflammation response by altering astrocytic reactivity (GFAP upregulation or downregulation) (Casanovas et al., 2000; J. A. García-Sevilla, Alemany, et al., 1995; Olmos et al., 1994; Siemian et al., 2018) attenuating microglial activation and decreasing the pro-inflammatory cytokine secretion in *in vitro* and *in vivo* experimental models of CNS disorders, including pain (Feinstein et al., 1999; Ni et al., 2019; Regunathan et al., 1999; Siemian et al., 2018; Y.-B. Zhu et al., 2015). Similarly, agmatine has been shown to exert anti-inflammatory properties (Abe et al., 2000; Ahn et al., 2012). Of note, glia modulation by I<sub>2</sub>-IR ligands is consistent with the primary localisation of I<sub>2</sub>-IR in glial cells. Moreover, an association of I<sub>2</sub>-IR modulation with neuroinflammatory response has also been suggested to result from their close relationship to MAO-B activation, given that reactive astroglia increases MAO-B levels (Quintana et al., 2005; Wilson et al., 2019). Thus, it has been postulated that regulation of neuroinflammation by I<sub>2</sub>-IR ligands may account for the mediated neuroprotective effects.

The neuroprotective action of certain I<sub>2</sub>-IR ligands has been associated with their ability to modulate NMDA type glutamate receptor activity (DeGregorio-Rocasolano et al., 1999; Olmos, DeGregorio-Rocasolano, et al., 1999; Olmos, Ribera, et al., 1996), a Ca<sup>2+</sup> channel which over-stimulation leads to intracellular Ca<sup>2+</sup> overloading, excitotoxicity and

eventually neuronal death (Dong et al., 2009). In particular, I<sub>2</sub>-IR ligands such as 2-BFI, idazoxan and the endogenous ligand agmatine have been shown to inhibit NMDA-mediated glutamate toxicity and/or intracellular Ca<sup>2+</sup> influx *in vitro* and *in vivo* (Han et al., 2013; Jiang et al., 2010; Yang & Reis, 1999). Thus, given that dysregulated Ca<sup>2+</sup> homeostasis as an increase in intracellular Ca<sup>2+</sup> concentration is present in the neurodegenerative process, Ca<sup>2+</sup> influx regulation, which can be delivered by NMDA inhibition, has been proposed as a mechanism whereby the I<sub>2</sub>-IR ligands confer neuroprotection. In this context, it is important to note that I<sub>2</sub>-IR localisation on mitochondrial membranes, which are linked to Ca<sup>2+</sup> mobilisation, could further indicate that alterations in Ca<sup>2+</sup> intracellular concentration may be involved in I<sub>2</sub>-IR mediated neuroprotection.

Interestingly, I<sub>2</sub>-IR ligands have been demonstrated to inhibit apoptosis, one of the main mechanisms of neuronal death (Yakovlev & Faden, 2004), and this effect is considered to account at least in part for the I<sub>2</sub>-IR mediated neuroprotection. For example, various I<sub>2</sub>-IR drugs have been shown to down-regulate the content of pro-apoptotic factors and upregulate survival anti-apoptotic ones in rat brain cortex (Garau et al., 2013). Likewise, I<sub>2</sub>-IR ligand 2-BFI decreased the levels of caspase-3, a crucial mediator of apoptosis, and inhibited apoptosis by stabilising the mitochondrial membrane potential in cultured rat cortical astrocytes (J. Tian et al., 2018). Furthermore, an anti-apoptotic action has also been assigned to agmatine in *in vitro* and *in vivo* experimental models of neurodegeneration (Hooshmandi et al., 2019; Moosavi et al., 2014). Ultimately, other mechanisms have also been involved in the neuroprotective effects of I<sub>2</sub>-IR drugs, including but not limited to oxidative damage mitigation *in vitro* and *in vivo* and lysosomal membrane stabilisation in astrocytes (D.-H. Choi et al., 2018; S.-H. Choi et al., 2002; Guerra de Souza et al., 2018; J.-S. Tian et al., 2017).

At last, I<sub>2</sub>-IR modulation by I<sub>2</sub>-IR ligands has linked to body temperature regulation (Thorn et al., 2012). Indeed, hypothermia (body temperature decrease) has been associated with neuroprotection and appears to be a common dose- and time-dependent effect mediated by I<sub>2</sub>-IR ligands. Thus, the I<sub>2</sub>-IR neuroprotective effects have been partially attributed to hypothermic induced effects. Interestingly, studies that reported hypothermic effects of I<sub>2</sub>-IR ligands showed an almost full reversion of the effect by pre-treatment with idazoxan, but not by other I<sub>1</sub>-IR or  $\alpha_2$ -AR (Thorn et al., 2012). Therefore, it has been suggested that body temperature assessment under I<sub>2</sub>-IR treatment can be indicative of imidazoline drugs nature (e.g. I<sub>1</sub>/I<sub>2</sub>-IR ligands, agonistic/antagonistic properties), especially in the early steps of the development of novel I<sub>2</sub>-IR ligands (Abás et al., 2017).

## 1.4.2 Other CNS pharmacological effects

The I<sub>2</sub>-IR have been established as a promising target for the development of analgesics against chronic pain. Preclinical studies have demonstrated that I<sub>2</sub>-IR ligands such as 2-BFI, tracizoline, LSL60101 as well as the endogenous ligand agmatine are effective for chronic inflammatory and neuropathic pain in several rodent models (J. X. Li & Zhang, 2011; J.-X. Li et al., 2014; Thorn et al., 2017). Of note, the selective I<sub>2</sub>-IR ligand CR4056 recently completed a Phase II clinical trial for the treatment of chronic inflammatory pain conditions (F. Ferrari et al., 2011; Rovati et al., 2020). Moreover, the I<sub>2</sub>-IR ligands were shown to potentiate the opioid analgesic effects and decrease adverse effects related to opioid use (e.g. antinociceptive tolerance); thus, I<sub>2</sub>-IR drugs were further suggested as promising therapeutic co-adjuvants in the management of chronic pain with opiate drugs (Boronat et al., 1998; F. Ferrari et al., 2011; Siemian et al., 2016; Thorn et al., 2011, 2015, 2016). Additionally, the I<sub>2</sub>-IR ligands are capable of producing discriminative stimulus effects, in such way suggesting or confirming that: i) I<sub>2</sub>-IR ligands share similar pharmacological mechanisms (Qiu et al., 2014, 2015) ii) I<sub>2</sub>-IR are closely related to MAO-A, which modulation possibly contributes to discriminative stimulus effects (Jordan et al., 1996; MacInnes & Handley, 2002), and iii) more than one I<sub>2</sub>-IR (several I<sub>2</sub>-IR proteins) exist at which I<sub>2</sub>-IR ligands such as idazoxan may act differently, for example, either as antagonists or agonists.

## 1.5 I<sub>2</sub> Imidazoline Receptors in Brain Disorders

As already mentioned, the I<sub>2</sub>-IR identification and their cellular and subcellular distribution in the brain have been well established over the years, providing the basis for the investigation of their biological and pharmacological properties. In fact, the early assessment of the I<sub>2</sub>-IR critical role in glial modulation and their intimate relationship with MAO enzymes prompted several groups in the 1990s to investigate the putative I<sub>2</sub>-IR involvement in brain diseases associated with these pathophysiological features, such as neurodegenerative and neuropsychiatric diseases (J. García-Sevilla et al., 1995; J. A. García-Sevilla et al., 1999).

### 1.5.1 I<sub>2</sub> Imidazoline Receptors and neurodegenerative diseases

Early studies demonstrated altered I<sub>2</sub>-IR densities in neurodegenerative diseases, including Alzheimer's Disease (AD), Parkinson's Disease (PD) and Huntington's Disease (HD) (Table 3). Moreover, series of preclinical studies have demonstrated the efficacy of I<sub>2</sub>-IR modulation against ischemic stroke (Gustafson et al., 1990; Han et al., 2013; Maiese et al., 1992), autoimmune encephalomyelitis (Gilad et al., 1996; F. Li et al., 2012; P. Wang et al., 2011; Y.-B. Zhu et al., 2015), focal cerebral ischemia (Han et al., 2009, 2010, 2012; Zhang

et al., 2018), traumatic brain injury (Ni et al., 2019). Therefore, this evidence suggests that I<sub>2</sub>-IR distribution and modulation may be associated with neurodegeneration.

Particularly in AD, the most common age-related neurodegenerative disease (described in detail in Section 1.7), increased density of I<sub>2</sub>-IR labelled by [<sup>3</sup>H]-idazoxan and immunoreactivity of IR proteins (29, 30, 45 kDa bands) were detected in post-mortem patients' brains compared to healthy controls (J. A. García-Sevilla et al., 1998; Ruiz et al., 1993). Accordingly, I<sub>2</sub>-IR labelled by [<sup>3</sup>H]-idazoxan showed a positive correlation with age in studies with elderly samples (Sastre & García-Sevilla, 1993). In parallel, α<sub>2</sub>-AR density was decreased both in aged individuals and the AD samples, further indicating the independence between α<sub>2</sub>-AR and I<sub>2</sub>-IR and, more importantly, their involvement in age-related disorders such as AD (Ruiz et al., 1993). Interestingly, changes in expression of I<sub>2</sub>-IR were also associated with increased astrocytic activation in neurodegenerative disorders. Recent studies using the I<sub>2</sub>-IR radioligand [<sup>3</sup>H]-BU99008 to evaluate astroglia pathology in neurodegenerative brains confirmed an altered expression of I<sub>2</sub>-IR in different brain regions (AD (increased): frontal cortex, hippocampus; early PD (increased) cortical areas and the brainstem; moderate/advanced PD (decreased): cortical, subcortical areas) (A. Kumar et al., 2021; Wilson et al., 2019) (Table 3). Interestingly, in AD post-mortem brains, [<sup>3</sup>H]-BU99008 was shown not only to detect I<sub>2</sub>-IR by visualising reactive astrogliosis but also to present a multiple affinity binding site model, highlighting the heterogeneity of I<sub>2</sub>-IR in the AD brain (A. Kumar et al., 2021). These findings, taking as well into account that both glia reactivity (increased GFAP) and MAO system alterations in play a pivotal role in the neurodegenerative process (K. Li et al., 2019; Naoi et al., 2012), point out the potential of selective I<sub>2</sub>-IR ligands to mediate neuroprotective and potentially therapeutic effects under neurodegenerative processes such as AD.

### 1.5.2 I<sub>2</sub> Imidazoline Receptors and depression

Alterations in the brain densities of IR (both I<sub>1</sub>-IR and I<sub>2</sub>-IR) have also been associated with neuropsychiatric disorders (Table 3). Moreover, IR have been shown to influence the actions of the antidepressants involved in the pathophysiology of depression (J. A. García-Sevilla et al., 1996; Piletz et al., 2008; Piletz et al., 1994). Chronic antidepressant treatment (e.g. fluoxetine, citalopram, imipramine, desipramine) and treatment with MAO inhibiting antidepressant drugs (e.g. phenelzine, clorgyline) were shown to normalise this IR dysregulation (Alemany et al., 1995; Piletz et al., 2008; H. Zhu et al., 1997). Focusing on the I<sub>2</sub>-IR, the latter findings are not surprising given the association of I<sub>2</sub>-IR with the MAO enzyme protein and together have suggested that treatment with selective I<sub>2</sub>-IR ligands could be relevant in the treatment of depression.

Indeed, based on this evidence, numerous studies evaluated the potential antidepressant

**Table 3:** Alterations of I<sub>2</sub>-IR density and IR immunoreactivity in brain tissue from patients with brain disorders. PM binding and immunodetection experiments were performed in tissue membranes.

Disease	Type Of Study	Detection	Brain Tissue	I <sub>2</sub> -IR Density	References
<b>Ageing</b>	PM Binding/age	[ <sup>3</sup> H]-Idazoxan	FCx	<b>Increased</b>	Sastre & García-Sevilla, 1993
	Immunoreactivity/age	<b>29/30, 45 kDa IR</b>	FCx	<b>Increased</b>	J. A. García-Sevilla, Sastre, et al., 1995
<b>Alzheimer's Disease</b>	PM Binding	[ <sup>3</sup> H]-Idazoxan	PFCx	<b>Increased</b>	Ruiz et al., 1993
	Immunoreactivity	<b>29/30, 45 kDa IR</b>	FCx	<b>Increased</b>	J. A. García-Sevilla et al., 1998
	PM Binding	[ <sup>3</sup> H]-BU99008	Cx, Hip	<b>Increased</b>	A. Kumar et al., 2021
<b>Parkinson's Disease</b>	PM Binding	[ <sup>3</sup> H]-Idazoxan	Cx	<b>Unaltered</b>	Gargalidis-Moudanos et al., 1997
	PM Binding	[ <sup>3</sup> H]-2BFI	Cx, Putamen	<b>Unaltered</b>	Reynolds et al., 1996
	In vivo imaging (E)	[ <sup>11</sup> C]-BU99008	Cx, brainstem	<b>Increased</b>	Wilson et al., 2019
	In vivo imaging (M/A)	[ <sup>11</sup> C]-BU99008	Cx	<b>Decreased</b>	Wilson et al., 2019
<b>Huntington's Disease</b>	PM Binding	[ <sup>3</sup> H]-2BFI	Putamen	<b>Decreased</b>	Reynolds et al., 1996
<b>Depression</b>	PM Binding	[ <sup>3</sup> H]-Idazoxan	FCx	<b>Increased</b>	Meana et al., 1993
	PM Binding	[ <sup>3</sup> H]-idazoxan	FCx	<b>Decreased</b>	Sastre & García-Sevilla, 1997
	Immunoreactivity	<b>29-30 kDa IR</b>	FCx	<b>Decreased</b>	Sastre & García-Sevilla, 1997
	Immunoreactivity	<b>45 kDa IR</b>	FCx	<b>Increased</b>	Sastre & García-Sevilla, 1997
	Immunoreactivity	<b>40-50 kDa IR</b>	Hip	<b>Decreased</b>	Piletz, Zhu, et al., 2000

PM (Post- Mortem), Cx (Cortex), FCx (Frontal Cortex), PFCx (Prefrontal Cortex), Hip (Hippocampus), E (Early), M (Moderate), A (Advanced)

effects of I<sub>2</sub>-IR ligands *in vivo*. I<sub>2</sub>-IR ligands 2-BFI, BU224, CR4056 treatments induced antidepressant-like effects in murine behavioural models (Finn et al., 2003; Siemian et al., 2019; Tonello et al., 2012). In the same studies, 2-BFI effect was blocked by pre-treatment with I<sub>2</sub>-IR ligand idazoxan, suggesting the involvement of I<sub>2</sub>-IR, while BU224 reported effect was additionally linked to hypothalamic-pituitary adrenal (HPA) axis and central monoaminergic activity, including serotonergic 5-HT system alterations (Finn et al., 2003; Tonello et al., 2012). Of note, other studies reported a lack of antidepressant effects after treatments with I<sub>2</sub>-IR ligands such as LSL60101 and 2-BFI in rodent models (Hernández-Hernández et al., 2021; Siemian et al., 2019). Ultimately, several studies evaluated the antidepressant effect of agmatine *in vivo* (Z.-D. Chen et al., 2018; Y. F. Li et al., 2003; Zomkowski et al., 2002). Although some attributed agmatine's antidepressant effect to interaction with NMDA receptors, L-arginine-nitric oxide pathway and  $\alpha_2$ -AR, more recent studies suggested the involvement of I<sub>2</sub>-IR, among others (Kotagale et al., 2020; Kotagale et al., 2013). Overall, albeit several possible explanations concerning the implicated mechanisms of such effects have been reported, the exact molecular mechanism remains to be elucidated. However, it can be concluded that I<sub>2</sub>-IR may be potential targets for the therapeutic effects of antidepressants.



## 1.6 Brain ageing and neurodegeneration

Ageing is a highly complex inevitable process characterised by a steady decline in physiological functions that lead to physical changes and cognitive impairment, identifiable in individual organisms (Deary et al., 2009; Niccoli & Partridge, 2012). During brain ageing, multiple molecular, cellular, structural, and functional alterations occur, which result in dysregulation of several biological systems from their homeostatic state and may set the stage for age-related diseases. The ageing process is fundamental to neurodegeneration, since together with genetic and environmental factors, it contributes to the formation of neurodegenerative diseases AD, PD, HD, amyotrophic lateral sclerosis, frontotemporal dementia and spinocerebellar ataxias (Duncan, 2011; Hou et al., 2019). In fact, ageing is considered the primary risk factor for these diseases. However, there are crucial differences between the alterations in the normal-ageing brain and neurodegenerative brains (e.g. neurodegenerative brain shows significant neuronal death) (Godin et al., 2018). Thus, it is still unknown whether the observed ageing-related alterations represent lesser aspects of brain ageing that do not considerably affect function or whether they are harbingers (precursors) of neurodegeneration and disease.

The basic biological mechanisms that underlie human ageing are associated with the nine so-called hallmarks of ageing processes (Hou et al., 2019; López-Otín et al., 2013). These widely used in the scientific community hallmarks are classified into primary, antagonistic and integrative hallmarks and may serve as a link between ageing and neurodegeneration since they appear to be also present in the neurodegenerative process (Fig. 7). The primary hallmarks of ageing consist of genomic instability, telomere attrition, epigenetic alterations, and loss of proteostasis. DNA damage (e.g. bulky adducts, basic sites, DNA single-strand breaks and deletion), as well as defects in repairing processes (e.g. mutations in repairing mechanisms), result in genomic instability and activation of signalling cascades, which all together promote cellular senescence and inflammation, and eventually exacerbate ageing-related neurodegeneration (Jeppesen et al., 2011). Telomere attrition, mostly associated with telomere shortening, occurs during cell division and, unless prevented, leads to accelerated ageing and neurodegeneration (López-Otín et al., 2013). Moreover, epigenetic modifications, including methylation and acetylation of DNA, among others, result in altered chromatin activity and function, with implications in age-related pathologies (Bradley-Whitman & Lovell, 2013). Interestingly, it has been proposed that genetic and epigenetic studies could provide a better understanding of the molecular links between ageing and neurodegeneration (Wyss-Coray, 2016). Ultimately, loss of proteostasis (defects in proteasome regulation, autophagy process ubiquitination and lysosomal system), responsible for maintaining protein synthesis and degradation balance, may lead to protein misfolding, aggregation and deposition. (López-Otín et al., 2013; Tanaka & Matsuda,

2014). All these characteristics are present and, in some cases, (e.g. amyloid  $\beta$  ( $A\beta$ ) aggregates in AD, huntingtin with tandem glutamine repeats in HD,  $\alpha$ -synuclein in PD etc.) are considered causative of many neurodegenerative diseases.

The antagonistic hallmarks of ageing represent compensatory responses to the primary damage that eventually can become damaging themselves. These hallmarks include mitochondrial dysfunction characterised by excessive reactive oxygen species (ROS) production and alterations in mitochondria-associated processes, including lipid biosynthesis, calcium signalling, and cell apoptosis, which, notably, play a key role in the development of neurodegenerative diseases (Filosto et al., 2011; Johri & Beal, 2012). In addition, cell senescence, another antagonistic hallmark, is activated for cell survival maintenance (Kültz, 2005); however, cellular senescence due to DNA damage, telomere attrition, inflammation, autophagy process and mitochondrial dysfunction because of ageing exacerbates age-related brain impairments and leads to neuron degeneration (Barzilai, 2010; Rubinsztein et al., 2011; Wiley et al., 2016). At last, antagonistic hallmarks also include altered nutrient sensing and metabolic deregulation, which has been linked with ageing and the neurodegenerative process (Babbar & Sheikh, 2013; López-Otín et al., 2013).

The integrative hallmarks of ageing include alterations in immune function and intercellular communication, as well as stem cell functional loss. Genetic, transcriptomic and proteomic studies indicate that inflammatory changes constitute primary aspects of brain ageing and neurodegeneration (Wyss-Coray, 2016). Age-associated chronic neuroinflammatory response (persistent activation of microglia, sustained elevation of pro-inflammatory mediators) is present in the aged brain and associated with age-related neurodegenerative diseases (Amor & Woodroffe, 2014). Lastly, stem cell exhaustion is caused by several of the aforementioned processes (e.g. DNA damage and repair, proteostasis mitochondrial dysfunction, cell senescence etc.), which declines during ageing (Oh et al., 2014).

Therefore, the observation that pathways that modulate longevity and the ageing process also affect the development of various age-related neurodegenerative diseases suggests that brain ageing may form a continuum with neurodegeneration. However, the mechanisms that underlie the transition from normal to pathological ageing remains a central issue (Yankner et al., 2008). In this context, it has been proposed that the declines in homeostatic quality controls that occur in healthy ageing (e.g. DNA damage, mitochondrial dysfunction, energy metabolism dysregulation, autophagy defects, unfolded protein stress etc) can make the ageing brain susceptible to neurodegenerative stimuli that in turn, when present, can worsen these declines leading to numerous forms of neurodegeneration with unique pathologies compared to normal brain ageing.

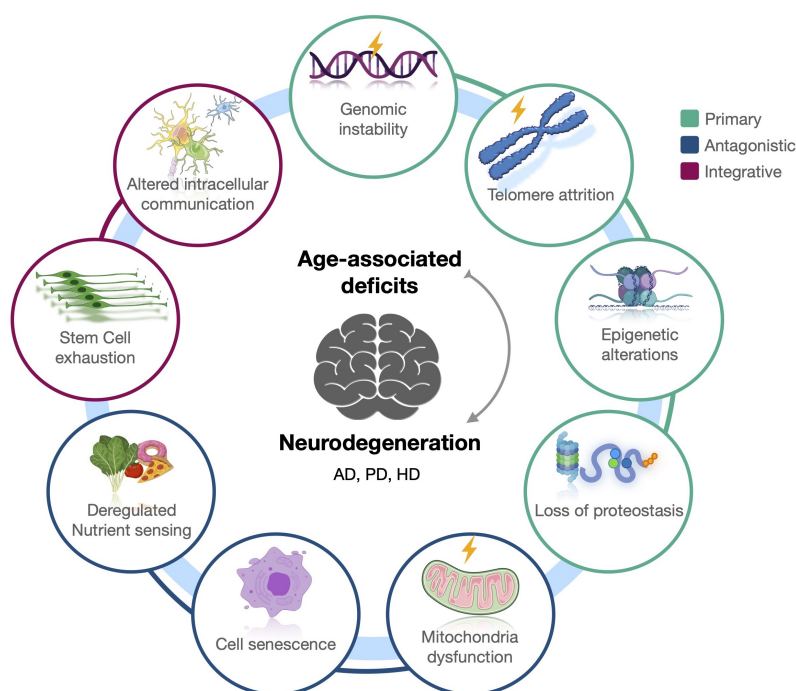


**Figure 7:** Hallmarks of Ageing, present in neurodegenerative diseases.

## 1.7 Alzheimer's Disease

### 1.7.1 Background

Of all age-related syndromes, perhaps none is more strongly associated with ageing than dementia. Alois Alzheimer first described AD in 1907. In 1901, Alois Alzheimer examined a middle-aged woman who presented memory deficits and progressive cognitive decline, including spatial orientation and suspicion. After her death, distinct morphological characteristics, now known as  $A\beta$  plaques and intracellular neurofibrillary tangles (NTFs) were detected in an autopsy of the brain. This form of dementia was subsequently named Alzheimer's disease (Hippius & Neundörfer, 2003; Möller & Graeber, 1998). AD is the most common neurodegenerative disease and currently the leading cause of dementia in the elderly. Alzheimer's Disease International estimated that over 50 million people with dementia worldwide in 2020, and this number is projected to rise to 82 million in 2030 and 152 million by 2050. AD accounts for 60%-80% of all dementia cases, and it is currently considered one of the leading causes of death and disability among the elderly, with immense social costs and severe consequences on the quality of life of both patients and caregivers ('2021 Alzheimer's Disease Facts and Figures', 2021)

### 1.7.2 Clinical symptoms

Clinically, dementia, including AD, manifests as a widespread deterioration and loss of cognitive function and memory, sufficient to lead to occupational and social function impairment. The pathology is initially characterised by mild cognitive impairment, with prominent memory disturbance appearing early and gradually progresses to severe memory loss, learning deficits and disorientation (Hugo & Ganguli, 2014).

As the severity of the disease increases, dementia patients frequently present non-cognitive neuropsychiatric symptoms, which have also been accepted as behavioural and psychological symptoms of dementia (BPSD). BPSD include behavioural symptoms such as aggression, screaming, agitation, and psychological symptoms such as depressive mood, anxiety, mood hallucinations (Shinosaki et al., 2000). Altogether have an impact on the patient's social functioning (Chakraborty et al., 2019; Finkel et al., 1996). Among BPSD, depression frequently occurs in AD patients leading to higher and faster decline and mortality, and it has been associated with a state of "accelerated ageing" affecting the brain and other systems (Kessing, 2012); however, it is still unclear whether AD-related depression is a symptom or an independent risk factor and a prodrome for AD (Byers et al., 2012; Ownby et al., 2006). Overall, BPSD are major AD components resulting in suffering, premature institutionalisation, increased costs of care, and significant loss of quality of life for the patients and their family and caregivers (Baharudin et al., 2019).

### 1.7.3 Risk factors and classification

The origin of the disease is not known. However, it might be influenced by various factors, including demographic (e.g. age, education, gender), genetic, epigenetic, medical (e.g. cardiovascular disease, obesity, traumatic brain injury, immune system dysfunction, mitochondrial dysfunction), psychiatric (e.g. depression, early stress) and due to infection (A. Armstrong, 2019). In addition, environmental and lifestyle factors such as physical exercise, stress, sleep disturbances, high-fat diets, alcohol abuse, and high blood pressure have also been shown to modify the risk for AD development (A. Armstrong, 2019; Reitz & Mayeux, 2014). Interestingly, in terms of treatable medical conditions and lifestyle choices, several of the identified risk factors are considered modifiable (Edwards III et al., 2019). It was recently estimated that 35 of lifetime risk for AD is modifiable, over 58 to 79 of risk due to genetics. (Livingston et al., 2017; Sierksma et al., 2020). However, it is important to note that the genetics can provide justifications for only a small percentage of the cases and cannot fully explain the aetiology of the rest of the cases. In this context, epigenetic mechanisms appear to serve a critical role mediating the interaction between environmental and genetic factors and provide valuable insights in the pathogenesis of AD (Daniilidou et al., 2011).

Among all reported risk factors for AD, advanced age and genetics currently serve as the basis for the AD classification. By the age of the onset, AD can be classified into sporadic or late-onset AD (LOAD) and familial early-onset AD (EOAD) cases. LOAD appears at the age of 65 and accounts for 95% of the AD cases, while EOAD appears before the age of 65 and accounts for less than 5% of the AD cases (Masters et al., 2015). On the one hand, in sporadic LOAD, age is the greatest risk factor, while its appearance is also linked to a complex interaction between genetic and other intrinsic and environmental factors. Inheritance of the  $\epsilon 4$  allele of apolipoprotein E (APOE) is considered the most important genetic risk factor (isoform APOE  $\epsilon 4$  allele confers for a high AD risk) for LOAD (Van Cauwenberghe et al., 2016). On the other hand, familial EOAD has a mainly genetic background, and it is linked to dominantly inherited mutations in the genes that encode amyloid precursor protein (APP), presenilin (PSEN) 1 and PSEN2. These mutations predominantly lead to an overproduction of  $A\beta$  and are considered causative for EOAD development (Cacace et al., 2016; Campion et al., 1999). Nevertheless, the clinical phenotype and neuropathology between LOAD and EOAD are generally indistinguishable, and the most significant difference is the age of onset and the fact that EOAD progresses more rapidly (Selkoe & Podlisny, 2002).

## 1.8 Neuropathology of Alzheimer's Disease

### 1.8.1 Macroscopic features of Alzheimer's Disease brain

At a macroscopic level, AD brain is characterised by significant atrophy in selective brain regions involved in cognitive function (hippocampus, entorhinal and frontal cortices). The macroscopic features include a typical symmetric pattern of cortical atrophy, which affects predominately the medial temporal lobes. Brain atrophy is accompanied by enlargement of the frontal and temporal horns of the lateral ventricles, while medial temporal atrophy has been shown to affect the amygdala and the hippocampus (DeTure & Dickson, 2019). In addition, the AD affected individuals present decreased brain weight. Moreover, the AD brain is characterised by loss of neuromelanin pigmentation in the locus coeruleus. Among BPSD, depression is characterized by structural brain alterations in the frontal, temporal and occipital lobes and its neuropathology is mainly associated with the frontal-subcortical limbic circuits in AD as well as alterations in hippocampus linked to prefrontal cortex damage (Y. Chen et al., 2021). Although the above-mentioned stereotypic macroscopic features are not specific for AD, they are considered supportive and suggestive of the pathology (Fig.8) (Dickerson, Bakkour, et al., 2009; Dickerson et al., 2011; Dickerson, Feczko, et al., 2009; Perl, 2010). Nonetheless, the definitive diagnosis of AD can only be made by examining the post-mortem brain tissue based on the presence of microscopic characteristics, which are considered the hallmarks of the disease (DeTure & Dickson,

2019).

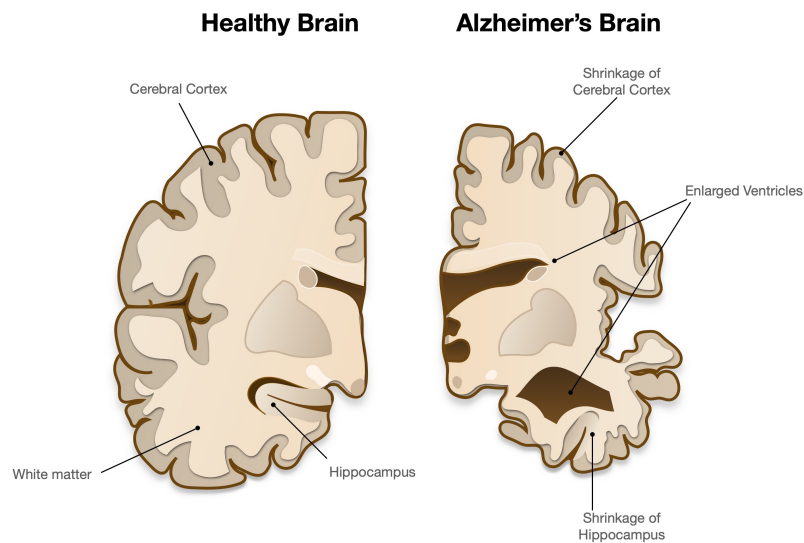


**Figure 8:** Macroscopic features of AD brains (Source: Alzheimer's Association)

## 1.8.2 Classical hallmarks of Alzheimer's Disease

The pathological hallmarks of AD and clues as to its aetiology can be observed only at the microscopic level and consist of extracellular plaques formed by  $A\beta$  peptides and intracellular NFTs comprised of hyperphosphorylated tau (p-tau) protein, that eventually lead to loss of neuron and synapses (Bloom, 2014). Therefore, based on the presence of  $A\beta$  plaques and NFTs in AD brains, the  $A\beta$  cascade hypothesis and the tau hypothesis, respectively, have been the mainstream explanations for the pathogenesis of AD.

### Abnormal amyloid $\beta$ accumulation and impaired clearance

$A\beta$  plaques are extracellular deposits consisting mainly of  $A\beta$  peptide (36 to 43 amino acid peptide). Plaques accumulate mainly in the hippocampus and, during the course of the disease, spread to the cortex and other brain regions, and symptoms of dementia arise as a clinical manifestation of the resulting severe brain atrophy. The  $A\beta$  cascade hypothesis, which postulates that deposition of  $A\beta$  protein is the causative agent of AD, is still widely accepted as a central process of AD (Selkoe et al., 2016).

$A\beta$  is generated by the proteolytic cleavage of the APP, a transmembrane protein expressed in many tissues, including the brain, with unknown function. The extracellular part of APP is shed from the cell surface, either by  $\alpha$ -secretase (ADAM10) or by  $\beta$ -secretase (BACE1), generating extracellular soluble N-terminal fragments soluble APP alpha (sAPP $\alpha$ ) or beta (sAPP $\beta$ ) respectively. The  $\alpha$ -secretase activity on APP occurs within the  $A\beta$  sequence; hence it prevents  $A\beta$  formation by generating a non-amyloidogenic carboxy-terminal

fragment of APP (C83). On the other hand, APP cleavage by  $\beta$ -secretase gives rise to an amyloidogenic carboxy-terminal fragment (C99), which is subsequently cleaved by  $\gamma$ -secretase complex [consisting of PSENs, nicastrin, anterior pharynx defective 1, and PSEN enhancer 2] and results in  $A\beta$  generation.  $A\beta$  monomers polymerise, generating first soluble oligomers and then larger insoluble fragments (major species  $A\beta_{40}$ ,  $A\beta_{42}$ ), which precipitate as amyloid fibrils. In this context, the differential APP cleavage follows either a non-amyloidogenic pathway (regulated by  $\alpha$ -secretase) or an amyloidogenic pathway which leads to  $A\beta$  generation ( $\beta$ -,  $\gamma$ - secretase) (O'Brien & Wong, 2011) (Fig.9). Abnormalities of the APP molecule that renders it more amyloidogenic or defects of normal APP processing (this appears to be the case in infrequent genetic forms of AD) results in an abnormally increased production of  $A\beta$  protein, which in turn drives excessive  $A\beta$  accumulation and aggregation, and eventually plaque formation (Chow et al., 2010).

Apart from  $A\beta$  synthesis, impaired  $A\beta$  clearance or degradation is also critical in accumulating  $A\beta$  (Yoon & Jo, 2012). Several mechanisms are involved in this process, including non-enzymatic and enzymatic pathways. The enzymatic ones involve proteases, called  $A\beta$  degrading enzymes, such as neprilysin (NEP), insulin-degrading enzyme (IDE), matrix metalloproteinase -9 and carboxypeptidase II. Conversely, non-enzymatic clearance is mediated by microglia or astrocytic phagocytosis (the main innate immune cells), interstitial fluid drainage, and transport across the blood vessels walls into the circulation (Yoon & Jo, 2012). Ultimately, it appears that there is a strong association between AD genetics and  $A\beta$  plaque formation since all high penetrance AD genetic risk alleles (i.e. APOE  $\epsilon 4$ , APP mutations, PSEN1 and PSEN2 mutations and Down syndrome) have been shown to influence  $A\beta$  deposition and plaque formation (Tang & Gershon, 2003).

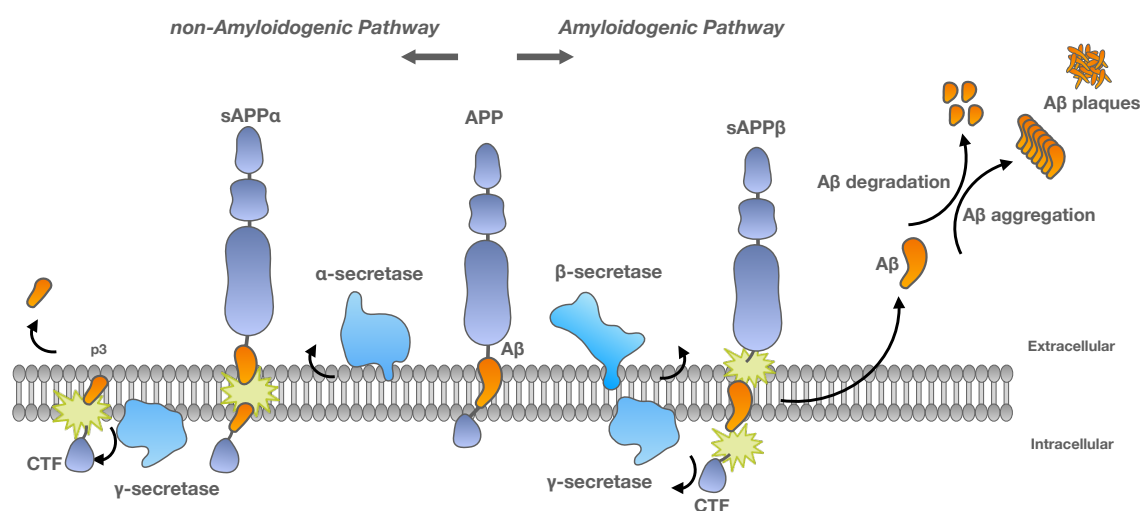


**Figure 9:** Scheme of APP processing pathways and formation of extracellular  $A\beta$  plaques.

## Hyperphosphorylation of tau protein

NFTs, composed of p-tau protein, constitute another major pathological feature of AD (Bloom, 2014). The deposition of NFTs occur within the neocortex, hippocampus and other cognition-related subcortical structures and the number of NFTs correlates with the severity of dementia in AD (Arriagada et al., 1992). Tau protein, under normal conditions, is involved in microtubule assembly and stabilisation in neurons, and it is vital for neuronal functions and axonal transport (Weingarten et al., 1975). Pathological modification of tau results in tau detachment from microtubules, synaptic loss, neuronal dysfunction, and tau aggregation (Fig.10). Post-translation regulation of tau may occur through phosphorylation of its serine (Ser) or threonine (Th) residues (Martin et al., 2011; Zaplatić et al., 2019). Given that hyperphosphorylation of tau is common to all diseases with NFTs it is considered necessary for toxicity. Tau can be phosphorylated in different sites, and there are several protein kinases and phosphatases responsible for its phosphorylation, such as glycogen synthase kinase-3 beta ( $GSK3\beta$ ) (Mandelkowitz et al., 1992) cyclin-dependent kinase 5 (CDK5) (Baumann et al., 1993) calcium calmodulin kinase (CAMK), mitogen-activated protein kinase (MAPK) (Billingsley & Kincaid, 1997).

- **GSK3 $\beta$** :  $GSK3\beta$  is a proline-directed Ser/Th kinase and constitutes one of the major kinases that phosphorylate tau at many sites. Its activity is regulated by phosphorylation at Ser9 (inhibition of  $GSK3\beta$ ) and phosphorylation at Tyr216 (activation of  $GSK3\beta$ ) (Q. M. Wang et al., 1994). Activation of phosphoinositide 3-kinase (PI3K) pathway inhibits  $GSK3\beta$  by phosphorylation at Ser9 by AKT, decreasing its activity with a net result being a decrease in tau phosphorylation (van Weeren et al., 1998).  $Ca^{2+}$  has also been reported to regulate  $GSK3\beta$  activity (an increase in intracellular  $Ca^{2+}$  results in a prolonged increase in  $GSK3$ -dependent tau phosphorylation. In this context, activation of  $GSK3\beta$  and subsequent promotion of tau aggregation also occurs by  $Ca^{2+}$ -dependent enzymes through dephosphorylation at Ser9 (W.-Y. Kim et al., 2009) (see also section 1.8.5).
- **CDK5**: CDK5 is a member of the cyclin kinase family. The activity of CDK5 is regulated by its binding with neuron-specific activation proteins, including p35 and p25. Cleavage of p35 to the more stable proteolytic fragment p25 is increased in the AD brain, leading to subsequent upregulation of CDK5 activity (Tseng et al., 2002). The p25 protein generation from p35 precursor can occur by the  $Ca^{2+}$ -dependent protease calpain, and indeed, it has been shown that calpains are upregulated in the AD brain (Ferreira, 2012; Lee et al., 2000). Aberrant activation of CDK5 is capable of phosphorylating tau at several epitopes of relevance to AD such as Ser202, Th181, Th231 and Ser396/404, and its activity involves several kinases (Noble et al., 2003).



- **ERK<sup>1/2</sup>**: In the MAPK family, the extracellular signal-regulated protein kinases (ERKs), including p44 ERK1 and p42 ERK2, and PK40 ERK, have been involved in tau hyperphosphorylation (Drewes et al., 1992). The activated ERK<sup>1/2</sup>, as the downstream kinases of Raf and MEK<sup>1/2</sup> (Kolch, 2000) has been shown to phosphorylate many substrates, being cytoskeleton proteins like tau among them (T. Li et al., 2018). In particular, *in vitro* results demonstrated ERKs associated phosphorylation of tau at Ser199, Ser202, Th205 and Ser404 (Cai et al., 2012). Interestingly, ERK dysregulation and subsequent tau phosphorylation have been reported to result from ROS (Haque et al., 2019; G. Perry et al., 1999).

Additionally, increasing evidence suggests that A $\beta$  can trigger tau aggregation. For example, A $\beta$  peptide has been shown to induce tau phosphorylation *in vitro* (Busciglio et al., 1995; A. Ferrari et al., 2003; Zheng et al., 2002) and enhance tau tangle formation in mutant tau mice (Götz et al., 2001; Lewis et al., 2001); however, the responsible signalling pathways still need to be elucidated. Interestingly, A $\beta$  has been reported to activate GSK3 $\beta$  *in vitro* and in transgenic AD models (Takashima et al., 1996; Terwel et al., 2008). Interestingly, PSEN1 mutations have been involved in the inhibition of PI3K/AKT signalling, promoting GSK3 and tau phosphorylation (Baki et al., 2004). Additionally, A $\beta$  has been shown to induce tau hyperphosphorylation via the CDK5 pathway (Town et al., 2002). Another possible connection between A $\beta$  and tau phosphorylation has been reported to be A $\beta$ -induced Ca<sup>2+</sup> through NMDA receptors and subsequent activation of CAMKK and ERK<sup>1/2</sup> (Danysz & Parsons, 2012). Collectively, deposition of p-tau insoluble polymers in the neuronal body and NFTs formation lead to neurofibrillary degeneration.

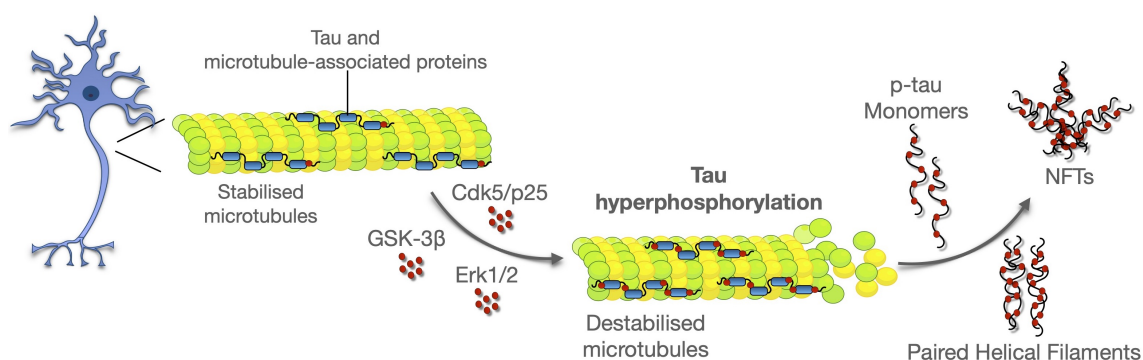


**Figure 10:** Process of tau hyperphosphorylation mediated by major tau kinases such as CDK5, GSK3 $\beta$ , ERK<sup>1/2</sup>.

### 1.8.3 Neuroinflammation in Alzheimer's Disease

In the context of neurodegeneration, neuroinflammation, which generally refers to an inflammatory response within the CNS, tends to be a chronic process that fails to resolve by itself (Heneka et al., 2014; Lucas et al., 2006). Neuroinflammation is considered an early characteristic of neurodegeneration and AD, with discrete components contributory to AD pathology, while emerging genetic and clinical evidence suggests that might also be a vital component in the initiation of AD (Fu et al., 2019; Hensley, 2010; Podtelezchnikov et al., 2011).

The innate immune cells involved in this process are primarily microglia and astrocytes (Fig.11). Microglia physiologically exerts a surveillance function with an important role in neuronal apoptosis and synaptic plasticity, among others (Deverman & Patterson, 2009; Wu et al., 2015). Once triggered by pathological factors like neuronal death or protein aggregates, microglia initiates an innate immune response by producing pro-inflammatory cytokines such as tumor necrosis factor-alpha (TNF- $\alpha$ ), interleukins (ILs) [(e.g. IL-1 $\beta$ , IL-6, IL-18) and chemokines [(e.g. C-C Motif Chemokine Ligand (CCL) 1, CCL5, chemokine C-X-C motif ligand 10 (CXCL10)] (Du et al., 2017; S. U. Kim & Vellis, 2005). Microglia activation is a complex process; under different circumstances, it can represent a pro-inflammatory phenotype characterised by increased pro-inflammatory cytokines (M1 state, detrimental phenotype) or an anti-inflammatory phenotype characterised by secretion of anti-inflammatory cytokines, such as IL-4, IL-10 and transforming growth factor-beta (TGF $\beta$ ) (M2 state, protective phenotype) or a surveillance state (M0) (Orihuela et al., 2016). In the ageing CNS, microglia is characterised by functional impairments and senescence, leading to sustained activation and enhanced sensitivity to further insults (a phenomenon termed priming), which may partially contribute to neurodegenerative diseases pathogenesis (V. H. Perry & Teeling, 2013).

Similarly, astrocytes regulate homeostasis, synaptic plasticity and provide neuroprotection under normal circumstances, whereas astrocytes respond through reactive gliosis upon pathological insults. Reactive astrocytes characterised by upregulation of GFAP release cytokines, ILs, and nitric oxide, among others, hence exacerbating neuroinflammatory response (K. Li et al., 2019; Rossi & Volterra, 2009).

In AD, both A $\beta$  and tau oligomers have been shown to induce abnormal glial (astrocytic and microglial) activation leading to neuronal dysfunction and death, while according to the amyloid cascade-inflammation hypothesis, microglial activation acts as a bridge between A $\beta$  plaques and NFTs (Leng & Edison, 2021; Serrano-Pozo et al., 2011) (Fig.11). Notably, both astrocytes and microglia activations are involved in A $\beta$  clearance mechanisms and are associated with the expression of extracellular A $\beta$  degrading proteases.

Additionally, microglia mediate clearing pathways through phagocytosis. In this context, increased cytokine levels may impair microglia phagocytic capacity and downregulate  $A\beta$  phagocytosis receptors such as myeloid-lineage gene Triggering receptor expressed on myeloid cells 2 (TREM2) (Nizami et al., 2019). Interestingly, rare polymorphisms in TREM2 have been associated with an increased risk of developing AD, constituting further evidence of a direct relationship between altered immune function and AD pathogenesis (Guerreiro et al., 2013; Jonsson et al., 2013).

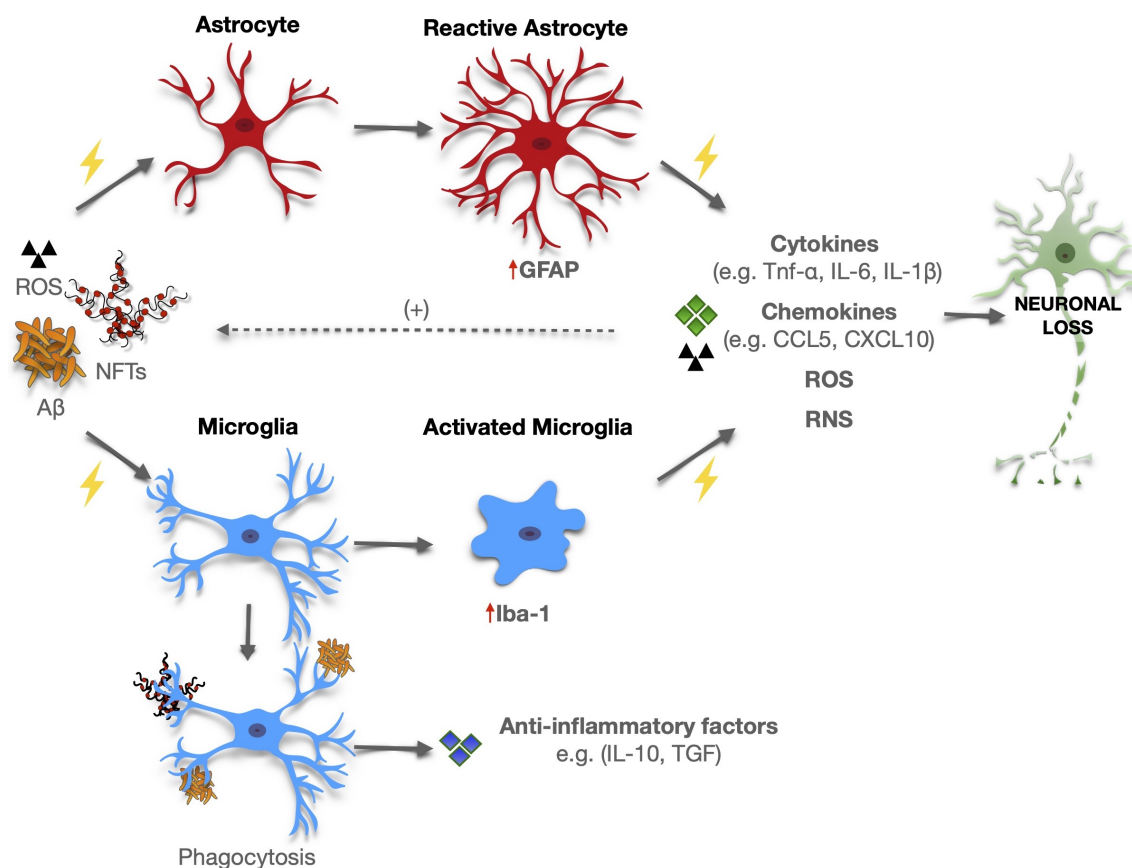


**Figure 11:** Inflammatory process in glial cells- triggered by and triggering AD features such as  $A\beta$  plaque formation, NFTs and ROS generation, leading synergistically to neuronal loss.

### 1.8.4 Oxidative stress and mitochondrial dysfunction in Alzheimer's Disease

Oxidative stress (OS), characterised by overproduction of ROS, is thought to play a crucial role in AD, which accelerates the pathology, being at the same time one of the earliest events in AD pathogenesis (Zhao & Zhao, 2013). OS is a process that refers to an imbalance between the generation of reactive oxygen/nitrogen species (ROS/RNS) and the antioxidant defence. Among multiple sources of ROS, including endoplasmic reticulum (ER), peroxisomes, NADPH oxidases family and enzymes such MAO, mitochondria are the

main cellular generators of ROS and RNS (Fig.12). In the mitochondrial inner membrane, inefficient electron transport through the mitochondrial respiratory complexes can lead to reduced ATP synthesis and an initial superoxide anions formation ( $O_2^-$ ) which further reacts and generates other types of ROS [e.g. hydrogen peroxide ( $H_2O_2$ ), hydroxyl radicals (OH) and hydroxyl ions ( $OH^-$ )] and RNS [e.g. peroxynitrite, nitrogen ( $ONOO^-$ ) dioxide ( $\cdot NO_2$ )] (Koopman et al., 2010). ROS and RNS generation can also occur under astrocytes and microglia activation (Pawate et al., 2004). Under normal conditions, antioxidant enzymes such as superoxide dismutase (SOD), glutathione peroxidase (GPX) and catalase (CAT), among others, mediate ROS levels by acting as radical scavengers. An additional antioxidant mechanism involves the activation of the nuclear factor erythroid-2-related factor (Nrf2), which, when translocated to the nucleus, activates the transcription of genes related to antioxidant defence such as glutathione S transferase, SOD, GPX, heme oxygenase-1 (HMOX1), NADPH: quinone oxidoreductase-1. However, increased ROS and RNS, as well as impaired antioxidant defence, mediate lipid, protein, DNA and RNA oxidation and glycooxidation (Uttara et al., 2009). The products of these reactions have been shown to have detrimental effects, being in most cases indicative of oxidative damage (Yu, 1994).

The processes that ultimately cause the redox imbalance in AD are still unclear; however, their close relationship is well documented. Increased OS is a major sign of aged brain, suggesting that insufficient protection against ROS production during ageing can be an important factor in AD progression and one of the possible triggering causes of the disease. In fact, in the ageing brain, OS imbalance could result in functional and organelle (e.g. mitochondria) deficits that in turn would lead to synaptic loss and cell death and eventually to the manifestation of clinical symptoms of AD (Tönnies & Trushina, 2017).

Furthermore, both major AD hallmarks  $A\beta$  and p-tau, have been shown to result in ROS formation, mitochondria dysfunction and ultimately apoptosis (Cheignon et al., 2018; Moreira et al., 2009). In fact, OS has been shown to be one of the first consequences under  $A\beta$  and tau proteins accumulation *in vivo* and *in vitro* (Butterfield & Lauderback, 2002; Uddin & Kabir, 2019). Interestingly, an inverse relationship between AD and OS has also been suggested, since OS has been demonstrated to induce  $A\beta$  overproduction and accumulation (L. Chen et al., 2008; Oda et al., 2010; Tamagno et al., 2002) as well as to assist in the polymerisation and phosphorylation of tau (Gamblin et al., 2000; Melov et al., 2007). Therefore, it seems that a malicious cycle is created that stimulates the progression of the disease (Fig.12). Furthermore, ROS overproduction has been implicated in explanations for the disease mechanisms, other than the  $A\beta$  cascade hypothesis, related to mitochondrial dysfunction. In this context, the mitochondrial cascade hypothesis states that in sporadic, late-onset AD, the age-associated loss of mitochondrial function

resulting in ROS production affects the expression and processing of APP initiating A $\beta$  accumulation as well as tau pathology, contributing to the early stages of AD prior to the onset of clinical symptoms (Swerdlow et al., 2010). Ultimately, OS association with AD is further supported by evidence indicating a relationship between the risk gene factor APOE4 and OS. In fact, in the hippocampus of AD patients, APOE4 was associated with higher OS and reduced antioxidant enzyme activity (Cioffi et al., 2019).

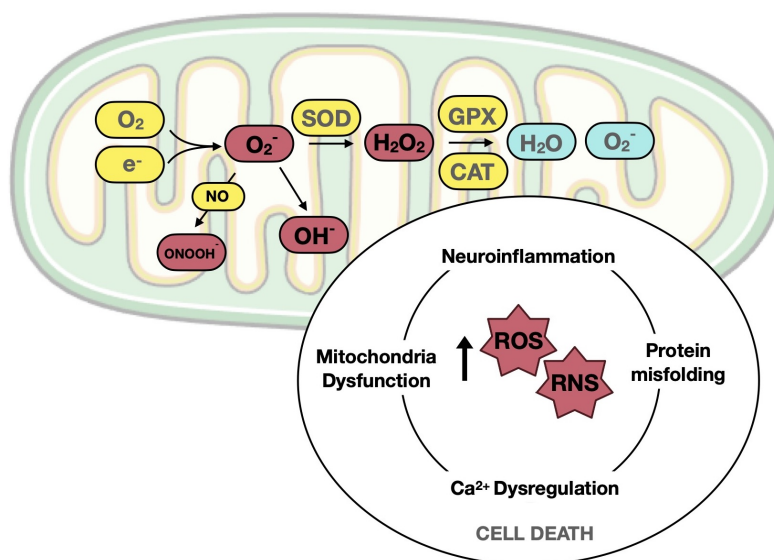


**Figure 12:** Generation of ROS and RNS in mitochondria promotes neurodegenerative processes; a malicious cycle is created that eventually result in cell death.

### 1.8.5 Dysregulation of calcium homeostasis in Alzheimer's disease

Along with the causative hypotheses other than A $\beta$  pathology and tau,  $Ca^{2+}$  dysregulation possesses an important role in AD pathogenesis. In fact, ageing has been linked to  $Ca^{2+}$  dysregulation, and this age-related  $Ca^{2+}$  disruption may also contribute to  $Ca^{2+}$  dysregulation in AD and consequently to synaptic deficits and AD hallmarks accumulation (Tong et al., 2018).

$Ca^{2+}$  signalling is involved in multiple physiological activities, including neurite growth, differentiation, synaptic transmission, plasticity learning and memory, as well as in pathological conditions including apoptosis, autophagy deficits, necrosis and degeneration (Kawamoto et al., 2012; Pinton et al., 2008). Generally,  $Ca^{2+}$  signals are generated by  $Ca^{2+}$  from intracellular stores in the endoplasmic reticulum (ER) and mitochondria or by an influx of  $Ca^{2+}$  from the extracellular environment. In AD,  $Ca^{2+}$  signals are produced in response to various stimuli, including A $\beta$  aggregates, NFTs, inflammatory mediators and ROS (Bojarski et al., 2008; Esteras et al., 2021; Sama & Norris, 2013). For example, A $\beta$  aggregates can disrupt  $Ca^{2+}$  signalling in several ways as it can trigger  $Ca^{2+}$  release from

ER stores through the corresponding receptors (Inositol triphosphate receptor, InsP3R and Ryanodine) and allow  $\text{Ca}^{2+}$  influx, rendering neurons vulnerable to apoptosis. Moreover, inappropriate levels of  $\text{Ca}^{2+}$  influx into the cytoplasm through NMDA receptors can contribute to neuronal loss through excitotoxicity (Ndountse & Chan, 2009) (Fig. 13).

Due to the increased  $\text{Ca}^{2+}$  influx,  $\text{Ca}^{2+}$ -buffer and  $\text{Ca}^{2+}$ -sensitive proteins (e.g. calmodulin) are altered, leading to activation of signalling cascades of phosphorylation, mediated primarily by CAMKs, and dephosphorylation by phosphatases (Marambaud et al., 2009). In this context, calcineurin (CaN), a  $\text{Ca}^{2+}$ -sensitive Ser/Th phosphatase also known as protein phosphatase protein 2B, is significant in AD pathological events. Elevated  $\text{Ca}^{2+}$  intracellular levels have been reported to lead to CaN increase and subsequent hyperactivity on downstream proteins and transcriptional factors associated with neuroinflammation such as a nuclear factor of activated T cells (NFAT), and synaptic plasticity and memory impairment such as cAMP response element-binding protein (CREB) (Reese & Tagliatela, 2011).

NFAT transcription factor shuttles to and from the nucleus depending on the phosphorylation status, which is altered in response to changes in  $\text{Ca}^{2+}$  intracellular levels and regulates the expression of genes upon immune cell activation. In the hippocampus of AD patients, an accumulation of nuclear NFAT has been reported, which can be likely attributed to aberrant CaN signalling (Abdul et al., 2009, 2010).

Transcriptional factor CREB is involved in pathways and mechanisms activated during the process of memory formation. When phosphorylated through CAMKs cascade, cAMP-protein kinase A (PKA) pathway and MAPK pathway, among others, phosphorylated CREB (p-CREB) regulates the expression of memory-associated genes such as brain-derived neurotrophic factor (BDNF). Hyperactivated CaN has been shown to decrease CREB phosphorylation via disinhibition of protein phosphatase 1 (PP1) (Groth et al., 2003; Hagiwara et al., 1992). In the signalling cascade downstream of PKA to CREB activation, dopamine- and cAMP-regulated phosphoprotein 32 kDa (DARPP-32) is one of the key molecules involved in the activation state of PKA-CREB (Svenningsson et al., 2004). Phosphorylated DARPP-32 (p-DARPP32) at Th75 by CDK5 inhibits PKA and subsequently CREB phosphorylation. In contrast, phosphorylation of DARPP-32 at Th34 by PKA has been shown to inhibit PP1 and increase CREB phosphorylation (Hemmings et al., 1990). Of note, apart from mediating disinhibition of PP1, CaN also dephosphorylates p-DARPP32 at Th34 (inactivation), thus promoting CREB dephosphorylation indirectly (Nishi et al., 2002). To sum up, disruption of  $\text{Ca}^{2+}$  homeostasis and kinases/phosphatase dysregulation results in reduced CREB activation and may underlie the impaired memory- and learning-associated activation of CREB in AD. The list of CaN substrates also includes

Bcl-2 associated death protein (BAD) which regulates apoptotic cell death, as well as GSK3 $\beta$ , which, as already mentioned, is implicated in tau hyperphosphorylation (Reese & Tagliatela, 2011) (Fig. 13). Overall, it becomes clear that Ca<sup>2+</sup> homeostasis dysregulation plays an essential role in orchestrating the dynamic of the neuropathology of AD and associated memory loss and cognitive function; however, it is still controversial whether these alterations are secondary to neurodegeneration or underlie the disease pathogenesis.

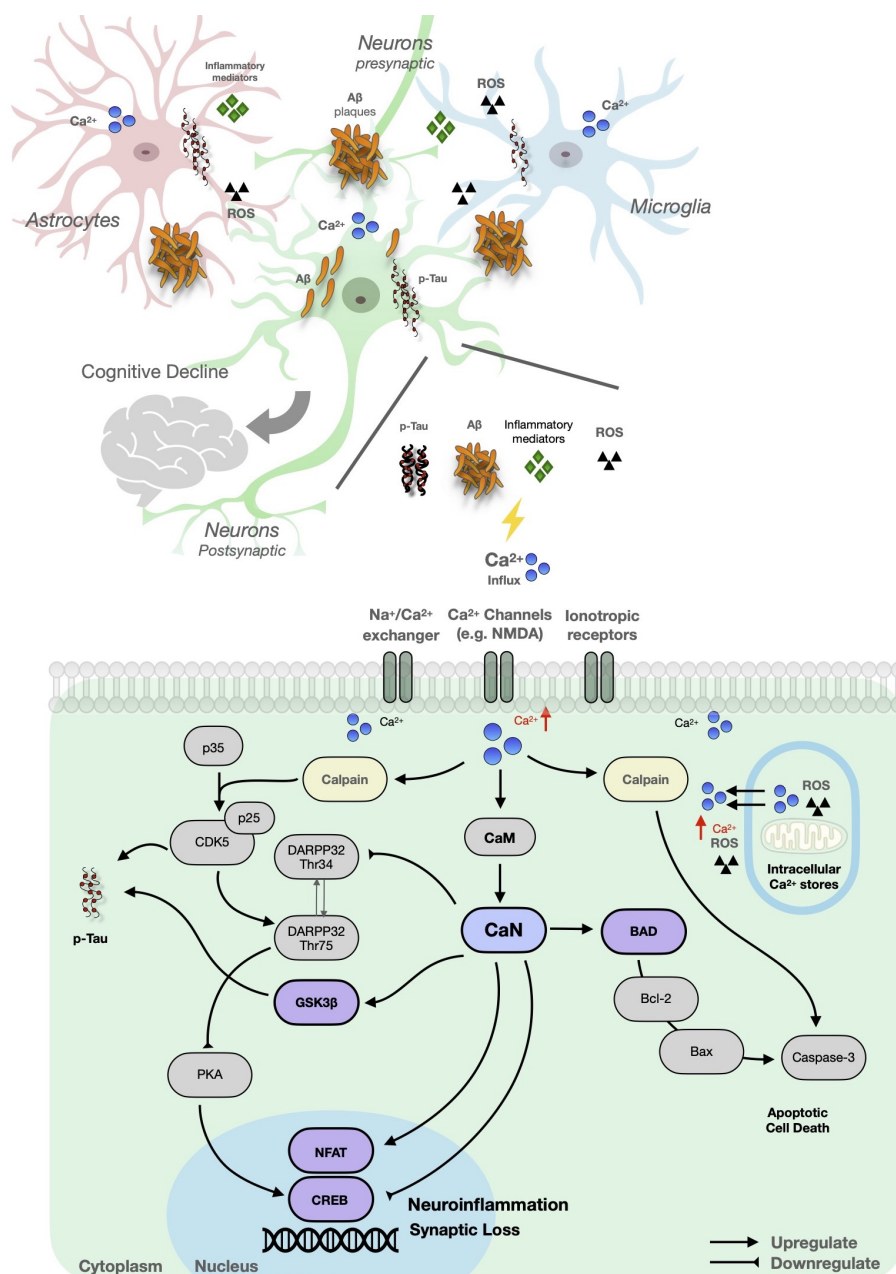


**Figure 13:** Schematic of Ca<sup>2+</sup> dysregulation in AD. A $\beta$  plaques, NFTs as well as inflammatory mediators and ROS released by glial cells trigger Ca<sup>2+</sup> influx which subsequently initiate signaling cascades involved in synaptic loss, neuroinflammation and apoptosis.

### 1.8.6 Neuronal and synaptic loss in Alzheimer's Disease

Neurodegeneration drives synaptic and neuronal death, which are the most prominent AD features at the functional level, linked to early signs of cognitive decline (Kashyap et al., 2019; Spires-Jones & Hyman, 2014; Terry et al., 1981). Neuronal loss affects predominately the basal forebrain cholinergic neurons, their projections to the hippocampus and cerebral cortex, and is the main pathological substrate of cortical atrophy that correlate with the severity of memory decline (Giannakopoulos et al., 2003). Likewise, loss or damage of the synapses, the essential parts of neurons that form the requisites connection of the neuronal networks that underlie cognition, correlates most strongly with cognitive decline in AD. AD-associated alterations in both presynaptic proteins (e.g. synaptophysin, synaptobrevin, SNAP 25, synaptotagmin, syntaxin, rab3a, synapsin), and postsynaptic proteins (e.g. postsynaptic density protein 95 (PSD95), drebrin) have been reported and are widespread in brain regions, including the hippocampus, frontal temporal and parietal lobes (Counts et al., 2006; Marksteiner et al., 2002; Scheff et al., 2014; Tannenberg et al., 2006).

Cell death can be divided into necrosis and apoptosis. Apoptosis plays a pivotal role in AD-associated neuronal cell death. Apoptosis occurs either through an intrinsic pathway, also known as the mitochondrial pathway or through a death receptor-mediated/extrinsic apoptotic pathway, which both converge to the activation of caspases and eventually lead to DNA fragmentation and cell death. Some of the most critical apoptotic mediators forming members of the B-cell lymphoma protein 2 (Bcl-2) family, such as Bax, Bcl-2, Bcl-xL, and caspases 2,3 8, 9 are involved in this process (Obulesu and Lakshmi 2014). Moreover,  $Ca^{2+}$ -dependent proteases calpains have been implicated in the apoptotic pathway by processing several members of the Bcl-2 family (Raynaud and Marcilhac 2006). In AD, a distorted expression of apoptotic and anti-apoptotic proteins has been observed. Although the mechanism progression to neuronal apoptosis is unclear, pathological features of AD, including  $A\beta$  peptides,  $Ca^{2+}$  dysregulation, OS and neuroinflammation, has been shown to trigger the initiation of apoptotic cell death (Bamberger & Landreth, 2002; Calissano et al., 2009; Tönnies & Trushina, 2017) (Fig. 13).

Neurotrophins are considered important for neuronal survival, maintenance and regeneration (Huang & Reichardt, 2001). The family of neurotrophins consist of nerve growth factor (NGF), BDNF, Neurotrophin (NT) 3 and NT4 which functions are mediated by the pan-neurotrophin receptor p75 (p75NTR) and tyrosine kinase (Trk) receptors. Among them, NGF promotes and maintains synaptic contact with hippocampal and cortical neurons, while BDNF possesses a pivotal role in the survival and function of hippocampal cortical cholinergic and dopaminergic neurons (Alderson et al., 1990; Ghosh et al., 1994; Hyman et al., 1991; Lindholm et al., 1996). BDNF is a key molecule in synaptic plasticity,



long term potentiation (LTP) and memory formation (Lu et al., 2008). In AD brains, decreases in either NGF, BDNF levels or their binding to the correspondent receptors contribute to cholinergic atrophy, deficits in LTP and impaired synaptic plasticity, which explain the subsequent cognitive deficits and memory impairments observed in early-stage AD (Allen et al., 2011, 2013). Of note, the importance of BDNF in AD is associated not only with the cognitive symptoms of the disease but also with the non-cognitive ones such as depression (Karege et al., 2002). BDNF expression is trophic for serotonergic neurons (Mamounas et al., 1995), which are affected in AD, being likely responsible for the depressive symptoms and, as a result, a potential target for BPSD management.

## 1.9 Treatment of Alzheimer's Disease

### 1.9.1 Current approved treatments

Current AD drugs including acetylcholinesterase (AChE) inhibitors [donepezil (Aricept®), rivastigmine (Exelon®) and galantamine (Razadyne®)] and an NMDA receptor antagonist [memantine (Ebixa®)] address only symptoms of AD. AChE inhibitors were developed to facilitate cholinergic neurotransmission by inhibiting AChE, an enzyme responsible for synaptic recycling of acetylcholine in grey matter (Čolović et al., 2013). AChE inhibitors are prescribed to patients with mild to moderate AD, and they are currently considered the standard and first-line treatment for AD. The benefit of the AChE inhibitors on cognition are modest (Lleó, 2007; Xu et al., 2021). Memantine, approved by European Medicines Agency (EMA) in 2002 and by Food and Drug Administration (FDA) in 2003 is an uncompetitive low-affinity NMDA receptor antagonist involved in the mitigation of glutamate-induced excitotoxicity (Parsons et al., 2007). Memantine is used for patients with moderate to severe AD. Additionally, memantine has been shown to deliver beneficial effects on BPSD (Maidment et al., 2008). Combination therapy of memantine with AChE inhibitors has been studied with mixed results, supporting either a moderate benefit on cognition without differences in adverse effects or no additional cognitive effect (Farlow et al., 2010; Feldman et al., 2006; Howard et al., 2012; Tariot et al., 2004). The above-mentioned approved drugs cannot cure the disease or reverse its progression. Recently, FDA has granted accelerated approval to aducanumab, a monoclonal antibody that lowers  $A\beta$  levels. Aducanumab is the first drug approved by FDA since 2003 for AD treatment and the first approved disease-modifying treatment in the history of AD; however, there is controversy with respect to its approval due to lack of strong evidence concerning its beneficial effects on cognition (Mullard, 2021).

The management of BPSD, i.e. comorbid depression in AD consists of the use of serotonin reuptake inhibitors (e.g. fluoxetine, citalopram, sertraline, paroxetine), as well as

combined selective noradrenaline and serotonin inhibitors (e.g. mirtazapine, venlafaxine, duloxetine and bupropion) (Ballard & Corbett, 2010; F. Wang et al., 2016; Zec & Burkett, 2008). For the management of psychotic symptoms of agitation/aggression in AD patients, antipsychotics and atypical agents (e.g. olanzapine, risperidone, quetiapine) are used while treatment with benzodiazepines aims to reduce agitation and anxiety in AD patients. However, the use of these drugs for BPSD management has been associated with the appearance of adverse effects and even worsening of cognitive impairment (Devanand & Schultz, 2011; Tampi et al., 2016).

### 1.9.2 Emerging disease-modifying therapies in clinical trials

Most of the agents that are currently in AD clinical trials are disease-modifying agents (82,5% of the total number of drugs in trial), which aim to alter AD biology by targeting its pathological mechanisms and features and hence, to deliver neuroprotection. In contrast, the 10,3% of the under development agents target cognitive enhancement while the 7,1% of drugs target the neuropsychiatric and behavioral symptoms of AD (Cummings et al., 2021). Disease-modifying agents that target the  $A\beta$  pathology, including monoclonal antibodies (e.g. Gantenerumab, solenazumab, lecanemab) and a small molecule which ameliorates  $A\beta$  pathology through inflammatory-associated effects (Azeliragon) are currently in phase 3 clinical trials. In contrast, several BACE inhibitors were shown to be toxic or futile thereby, clinical trials were discontinued. Similarly, inhibitors of  $\gamma$ -secretase were proven to be unsuccessful due to side effects; however,  $\gamma$ -secretase modulators are in development. Likewise, several agents that target tau, are currently in AD trials and other tauopathies trials, including monoclonal antibodies, which aim to tau removal and propagation prevention and several small molecules that inhibit tau synthesis and aggregation. Among them, a tau protein aggregation inhibitor (TRx0237) is currently in phase 3 clinical trial. In addition, agents with neuroprotective or anti-inflammatory mechanisms, MAO inhibitors, molecules addressing oxidative damage, proteolysis, metabolism as well as growth factors, and hormones are being studied. Several epigenetic regulators are also in trial being one agent [Lamivudine (3CT)] currently in phase 2 clinical trial. Other under development agents aim to improve the neuropsychiatric symptoms presented in AD patients. Among them, several target agitation symptoms in AD such as brexpiprazole, a D2 receptor partial agonist/serotonin-dopamine modulator, escitalopram a selective serotonin reuptake inhibitor, and mirtazapine, an  $\alpha_2$ -AR antagonist, being in phase 3 clinical trials (Cummings et al., 2021).

## 1.10 Alzheimer's Disease Mouse Models

In the preclinical research in AD pathogenesis and development of potential therapeutics, several animal models have been generated, including fruit fly, Zebrafish, worms, mouse, rabbit, dog, and non-human primates (Van Dam & De Deyn, 2011). More recent models incorporate newer technologies such as genomics and stem cell biology, including human induced pluripotent stem cells (iPSCs) that contribute even more powerfully in developing effective vaccines, drugs, and medical devices (Penney et al., 2020). Among the animal models, the mouse is the most popular model in the neuroscience umbrella. In the AD field, rodent models have been primarily used in the last decades to evaluate the efficacy of new agents in preclinical studies and to study the underlying molecular mechanisms of AD. AD mouse models can be classified into transgenic and non-transgenic models. The former ones consist of single or multi transgenic models harbouring human mutations in  $A\beta$ -related genes (APP, PSENs), and/or other genes related to AD markers like tau or models carrying APOE mutations. The non-transgenic models include models of ageing, and models produced by injections in the brain, e.g.  $A\beta$  injection or tau (Van Dam & De Deyn, 2011).

It is important to note that even the existing AD mouse models present histopathological features and symptoms of AD being invaluable in the AD research field, none of them alone recapitulates all aspects of the multifactorial disease; hence a combination of both transgenic and non-transgenic models in preclinical studies could overcome limitations of the different models.

### 1.10.1 5XFAD mouse model for early-onset familial Alzheimer's Disease

The 5XFAD mouse model is a widely used AD mouse model originally designed to investigate APP and  $A\beta$  related pathology. The 5XFAD is a double transgenic APP/PSEN1 model that co-expresses five AD mutations. The model was generated by introducing human APP Swedish (K670N)/Florida(1716V)/London(V717I) mutations and PSEN1 M146L and L286V mutations into APP (695) and PSEN1 cDNAs via site-directed mutagenesis (Oakley et al., 2006).

APP Swedish mutation increases  $A\beta$  production while APP Florida, London, and PSEN1 mutations result in higher  $A\beta_{42}$  levels in comparison to  $A\beta_{40}$ . As a result, 5XFAD mice express high  $A\beta_{42}$  levels and present early amyloid deposition and  $A\beta$  plaque formation, starting at the 2 months, increasing with age and reaching massive levels by 6 months (Oakley et al., 2006; Richard et al., 2015). In 5XFAD brains, the  $A\beta$  plaques first appear in cortex and subiculum, while in later stages, plaques spread to other brain areas, including

hippocampus. Given the close relationship between  $A\beta$  pathology and neuroinflammation, 5XFAD mice present neuroinflammatory characteristics, particularly astrogliosis and microgliosis, which start at 2 months old and increase with age in parallel with  $A\beta$  deposition. By 9 months, 5XFAD mice are characterised by severe gliosis in cortex and hippocampus (Giannoni et al., 2016; Oakley et al., 2006).

Although initial studies did not detect any tau-related pathology in 5XFAD mice, to date, more and more studies demonstrate the presence of p-tau aggregates in the 5XFAD cortex and hippocampus. In particular, at ages ranging from 2 to 6 months, the 5XFAD mice present increased tau phosphorylation in different tau epitopes such as Ser396, Ser202 and Th205. Moreover, age-related increased tau phosphorylation appears to be accompanied by increased GSK3 $\beta$  activity (Cho et al., 2020; Kanno et al., 2014; Shin et al., 2021; Shukla et al., 2013). 5XFAD mice also exhibit neuron loss and age-dependent synaptic degeneration indicated by a reduction of synaptic markers (Buskila et al., 2013; Oakley et al., 2006). By the age of 12 months 5XFAD mice present an approximately 40% loss of layer V pyramidal neurons (Jawhar et al., 2012). The neuronal degeneration was reported to be potentially attributed to increased intraneuronal  $A\beta$  that occur before the start of amyloid deposition in 5XFAD mice (Oakley et al., 2006). Notably, the 5XFAD model is one of the few currently available AD mouse models known to develop neuron loss. Cognitive deficits and behavioural alterations accompany the accelerated severe AD-like pathology exhibited by 5XFAD mice as assessed in several behavioural paradigms. The model is characterised by impaired spatial working memory starting at the age of 3-4 months of age, and behaviours akin to BPSD in AD patients such as anxiety disturbances, reduced social investigation and signs of aggression when compared to their wildtype (WT) littermates (Jawhar et al., 2012; Kosel et al., 2019) (Fig. 14).

Overall, the 5XFAD model presents rapid onset AD-like amyloid pathology, gliosis, and neurodegeneration, accompanied by memory deficits. As a result, it constitutes a valuable animal model in the AD field, pivotal for molecular studies and drug evaluation for AD.

### **1.10.2 SAMP8 mouse model for ageing, neurodegeneration, and sporadic Alzheimer's Disease**

The senescence-accelerated mouse prone 8 (SAMP8) model has drawn attention in gerontological research of dementia, especially in AD research, since it presents many of the behavioural and histopathological indicators of AD, triggered by a combination of age-related events and unknown risk factors. Thus, the SAMP8 model has been proposed as a neurodegeneration model to study sporadic LOAD related to ageing (Akiguchi et al., 2017; Pallàs, 2012).

The senescence-accelerated mouse (SAM) strains are inbred strains characterised by stable homozygosity and pathologic phenotypes and were established in 1973, by professor Takeda, through phenotypic selection (senescence scores, lifespan, pathological phenotypes) from an AKR/J mice pool (Flood & Morley, 1998; Takeda, 1999; Takeda et al., 1991, 1997). In particular, selective breeding, using sister-brother mating through subsequent generations, gave rise to several sublines of SAM prone (SAMP) mice, which are characterised by age-associated disease phenotypes (lifespan: 10-12 months, median survival time: 9.7), and SAM resistant (SAMR) mice which present typical ageing characteristics (lifespan: 19-21 months, median survival time 16.3). In total, there are 9 SAMP lines and 3 SAMR sublines. Among SAMP lines, the SAMP8 is characterised by progressive age-related cognitive decline and emotional alterations, which represent the model's main phenotypic characteristics. In addition, accelerated senescence in SAMP8 manifests as reduced lifespan, lordosis, hair loss, skin ageing, heart ageing, hearing loss, and reduced physical activity, characteristics similar to the ones presented by aged humans, in contrast to SAMR1 strain, which shows a normal ageing pattern (Takeda, 1999).

#### **AD-like cognitive and emotional alterations in SAMP8 mice**

First Miyamoto et al. (Miyamoto et al., 1986) and then several studies reported an age-related cognitive decline in SAMP8 mice, translated into memory and learning deficits in several behavioural tasks. SAMP8 mice develop an early-onset age-related decline in spatial learning and memory in hippocampal-dependent tasks such as Morris water maze test and other mazes. SAMP8 impairment in spatial memory can be detected as early as 4-month-old (or earlier depending on the task) and increases with age (Pallas et al., 2008). SAMP8 mice also exhibit impairments in different avoidance tasks compared to SAMR1 mice (Flood & Morley, 1998; Miyamoto, 2004). Ultimately, SAMP8 mice exhibit cortex-dependent declarative memory deficits, evaluated by object recognition memory tests (Pallas et al., 2008; Takeda, 1999).

In SAMP8 mice, cognitive decline is accompanied by non-cognitive symptoms, and in particular age-related emotional alterations that occur in SAMP8 as young as 4 months old. These include anxiety disturbances manifested as either reduced or increased anxiety-like behaviour depending on the sex, age and experimental conditions (G.-H. Chen et al., 2007; Miyamoto et al., 1992; Yanai & Endo, 2016). Moreover, SAMP8 mice exhibit depressive-like behaviour and increased aggression compared to SAMR1 mice (Maes et al., 2020; Pérez-Cáceres et al., 2013). Of note, these emotional changes in SAMP8 have been associated with learning tasks impairments (Miyamoto, 1997); (unpublished data). Ultimately, SAMP8 strains are characterised by circadian rhythm abnormalities (McAuley et al., 2004). Overall, these emotional changes could substantially mimic the AD-like non-cognitive symptoms, namely the BPSD, further reinforcing the utility of the SAMP8

model in AD research.

### **AD-like pathological features in SAMP8 mice**

Age-related neuropathologic characteristics identified in SAMP8 brains include neuron and dendrite spine loss, cholinergic deficits in the forebrain, degeneration of dopamine neurons (substantia nigra) and noradrenaline neurons (in locus coeruleus), and synaptic dysfunction (Akiguchi et al., 2017; Karasawa et al., 1997; Kawamata et al., 1998). Additionally, SAMP8 brains show a model-unique spongiosis as well as characteristic age-related increased permeability of blood-brain barrier (BBB) (Vorbrodt et al., 1995) more evident in 12-month-old SAMP8 mice compared to SAMR1.

Age-associated abnormal glial responses have been detected in SAMP8 mice. In particular, SAMP8 brains present severe astrogliosis characterised by significant age-related increases in GFAP expression (García-Matas et al., 2008; Wu et al., 2005) mostly in the hippocampus and reactive microgliosis detected in the hippocampus and cerebral cortex, which also increases with age (Akiguchi et al., 2017). Moreover, the strain in whole shows increased expression of inflammatory markers compared to SAMR1, while this neuroinflammaging profile correlates with earlier cognitive impairment and the neurodegeneration process (Griñan-Ferré et al., 2016). In addition, oxidative damage in SAMP8 is well-documented (Morley et al., 2012; Pallas et al., 2008; Sato, Kurokawa, et al., 1996; Sato, Oda, et al., 1996); from 6-12 months, oxidative stress in SAMP8 brains is markedly increased and accompanied by altered expression of genes and activity of enzymes associated with ROS and antioxidant defence (Butterfield et al., 1997; Kurokawa et al., 2001; Sureda et al., 2006). Indeed, OS has been considered the main mechanism that leads to accelerated senescence that characterises the SAMP sublines (Hosokawa, 2002; Mori et al., 1998). OS has also been associated with relatively early mitochondrial dysfunction, which is shown in SAMP8 brains compared to SAMR1 mice (Nishikawa et al., 1998) (Fig.14).

Several studies in SAMP8 mice reported age-dependent  $A\beta$  deposition and impaired  $A\beta$  clearance. In fact, SAMP8 brains show overproduction of APP jointly with increased cortical and hippocampal APP mRNA expression (V. B. Kumar et al., 2000, 2001; Morley et al., 2000) as well as increased  $A\beta$  levels compared to SAMR1, detected by a polyclonal antibody to  $A\beta$ 1-42 and  $A\beta$ 1-40, (Fukunari et al., 1994; Takemura et al., 1993). Moreover, SAMP8 showed increased levels of enzymes involved in  $A\beta$  generation, e.g. BACE1, PSEN 1 and PSEN2 (Griñan-Ferré et al., 2016; V. B. Kumar et al., 2009; Wei et al., 1999) as well as decreased  $A\beta$ -degradation enzymes such as IDE and NEP. Of note, evidence strongly suggests that alterations in  $A\beta$  dynamics contribute to cognitive decline in SAMP8 (Banks et al., 2007; Butterfield & Poon, 2005). Likewise, tau hyperphosphorylation (e.g. Ser396 and Ser404 sites of tau) is detected in the cortex and the hippocampus of SAMP8

mice as early as 5 months of age (Pallas et al., 2008). In addition, several enzymes involved in tau hyperphosphorylation have been altered consistently in SAMP8 brains. For example, increased CDK5 and activated GSK3 $\beta$  levels were reported in SAMP8 brains (Canudas et al., 2005; Liu et al., 2020), as well as altered Ca<sup>2+</sup> dependent enzymes (e.g. CAMKII) (Armbrecht et al., 1999). The latter findings are further supported by the fact that SAMP8 mice also presented Ca<sup>2+</sup> dysregulation. Overall, the presence of cognitive and non-cognitive symptoms accompanied by alterations in several AD-like pathologies and processes involved in age-related cognitive decline reinforce the utility of the model not only as a robust model of ageing but also as a valuable model for age-related LOAD (Fig.14)

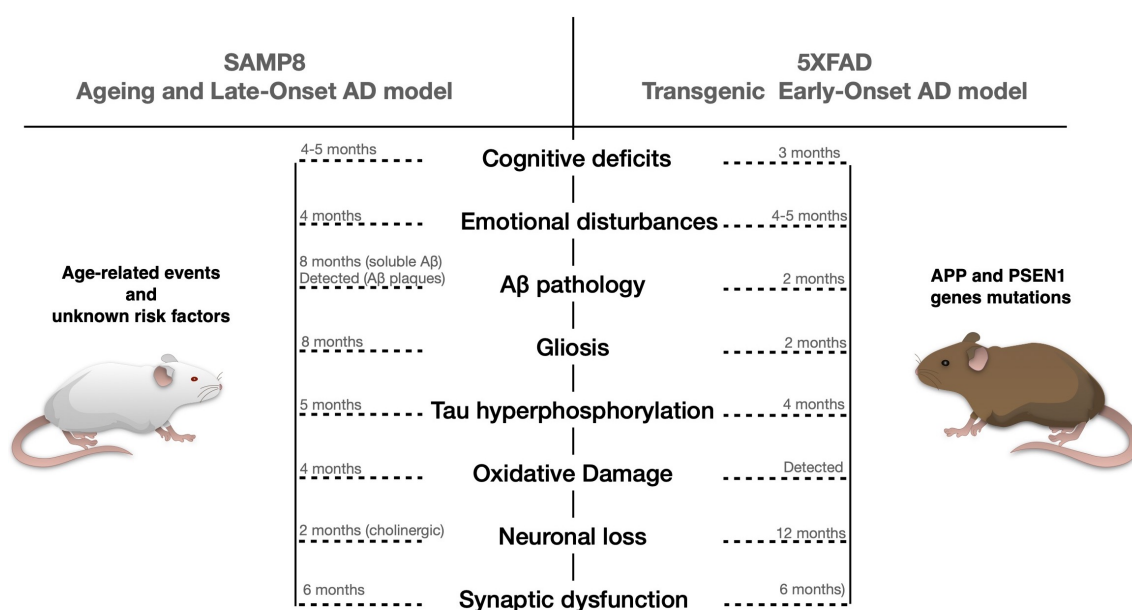


**Figure 14:** AD characteristics of SAMP8 and 5XFAD animal models and approximate age of appearance.





# Chapter 2

## Objectives

With the rapid growth in the proportions of the older population worldwide, cognitive decline and dementia are becoming an increasing burden. At present, there are not successful pharmacological treatments for modifying the progression of AD, and therefore the identification of new pharmacological targets for effective treatment is an active area of research.

I<sub>2</sub>-IR has been identified as one of the promising biological targets that deserve further investigation to permit researchers to build a complete map of their pharmacological possibilities. Dysregulation of I<sub>2</sub>-IR have been associated with ageing and neurodegenerative diseases, while I<sub>2</sub>-IR activation has been shown to exert neuroprotection. This evidence suggests that selective I<sub>2</sub>-IR ligands could contribute to the delay of neurodegeneration. However, their potential therapeutic value in AD is still underexplored.

In this context, the general aim of the present doctoral thesis has been to foster scientific knowledge regarding the pharmacological modulation of the I<sub>2</sub>-IR under neurodegenerative processes by assessing the pharmacological effects delivered by selective I<sub>2</sub>-IR ligands in *in vivo* models of LOAD and EOAD.

In order to pursue this aim, several specific objectives have been established:

- 1. Evaluate the neuroprotective effect of the novel I<sub>2</sub>-IR ligands MCR5, MCR9 in aged 12-month-old female SAMP8 mice.**
  - To determine the effects of **MCR5, MCR9** on cognitive decline and behavior.
  - To investigate molecular alterations in major pathophysiological pathways of AD (APP processing and tau hyperphosphorylation, neuroinflammation and

OS) after I<sub>2</sub>-IR treatment.

**2. Assess the effect of the novel I<sub>2</sub>-IR ligand MCR5 on cognitive and non-cognitive symptoms of AD presented by 10-month-old male SAMP8.**

- To evaluate the effect of **MCR5** on cognitive and psychological symptoms of dementia.
- To investigate a possible involvement of **MCR5** treatment in serotonergic system, as well as alterations in molecular pathways related to neurotrophic factors, synaptic plasticity and neuroinflammation after I<sub>2</sub>-IR treatment.

**3. Delineate the molecular mechanisms involved in the neuroprotective effect of I<sub>2</sub>-IR by evaluating the novel improved I<sub>2</sub>-IR ligand B06, in 12-month-old SAMP8 female mice.**

- To evaluate the cognitive and behavioural status of aged SAMP8 mice after **B06** treatment.
- To determine the effect of chronic **B06** treatment on age-related and AD neurodegenerative processes.
- To identify key neurodegenerative mechanisms modulated by I<sub>2</sub>-IR ligands *in vivo*.

**4. Validate the I<sub>2</sub>-IR as a pharmacological target for AD treatment by assessing the disease-modifying effect of the I<sub>2</sub>-IR ligand LSL60101 alone and in combination with the AChE inhibitor donepezil using 7-month-old female 5XFAD mice.**

- To assess the cognitive and behavioural changes after treatment with **LSL60101**, donepezil and co-treatment.
- To explore the **LSL60101**, donepezil and combination treatment effects on advanced AD pathology marked by severe amyloidosis, tau hyperphosphorylation and gliosis.
- To unravel the effect of **LSL60101** on inflammatory response by identifying alterations in the gene expression of several inflammatory mediators in 5XFAD and WT mice after chronic treatment.

# **Chapter 3**

## **Methods and Results**



### **3.1 Publication 1**

#### **Behavioral and cognitive improvement induced by novel imidazoline I<sub>2</sub> receptor ligands in female SAMP8 mice**

Adapted from: Griñán-Ferré C\*, **Vasilopoulou F\***, Abás S, Rodríguez-Arévalo S, Bagán A, Sureda FX, Pérez B, Callado LF, García-Sevilla JA, García-Fuster MJ, Escolano C, Pallàs M, *Neurotherapeutics*. 2019 Apr;16(2):416-431.

doi: <https://doi.org/10.1007/s13311-018-00681-5>.

## SUMMARY

AD, the most common age-related neurodegenerative disease and main cause of dementia in the elderly, remains an unmet medical need as the life expectancy increases, especially provided that the scientific community still lacks an effective cure. Thus, the identification of new targets is essential to reverse the cognitive decline and halt the progression of the disease. In the CNS, I<sub>2</sub>-IR have been found to increase with age and more importantly, a dysregulation of the receptors has been linked to neurodegeneration and brain disorders. Thus, we hypothesize that modulation of I<sub>2</sub>-IR by high-affinity selective I<sub>2</sub>-IR ligands could lead to beneficial outcomes by contributing to the delay of neurodegeneration.

Here, we evaluated for the first time *in vivo*, the effect of structurally novel I<sub>2</sub>-IR ligands, **MCR5** and **MCR9**, on the behavioral alterations, cognitive decline and neurodegenerative molecular processes presented by aged SAMP8 mice after oral administration. To this end, behavioral tests (Novel object recognition test, Open Field, Elevated Plus Maze test) were performed, as well as cellular and biochemical assessment of AD associated parameters in SAMP8 brains.

I<sub>2</sub>-IR ligands were able to deliver a beneficial effect on cognition and anxiety-like behavior in 12-months old female SAMP8. Changes in synaptic markers such as PSD95 and synaptophysin and in apoptotic factors such as caspase-3, Bcl-2, Bax were consistent with the behavioral results obtained. Accordingly, I<sub>2</sub>-IR treatment attenuated neuroinflammation in SAMP8 brains by decreasing GFAP protein levels and inflammatory markers gene expression. A beneficial effect on OS levels was also determined after treatment. Ultimately, I<sub>2</sub>-IR treatment ameliorated the APP processing and A $\beta$  degradation, as well as diminished tau hyperphosphorylation, which we found to be accompanied by alterations in signaling pathways involved in this process.

Collectively, we demonstrated the neuroprotective role of these new I<sub>2</sub>-IR ligands in a mouse model of brain aging and neurodegeneration and this evidence suggest the potential of I<sub>2</sub>-IR as therapeutic targets in brain disorders and age-related neurodegenerative diseases such as AD.

## Behavioral and cognitive improvement induced by novel imidazoline I<sub>2</sub> receptor ligands in female SAMP8 mice

Christian Griñán-Ferré,<sup>1#</sup> Foteini Vasilopoulou,<sup>1#</sup> Sònia Abás,<sup>2</sup> Sergio Rodríguez-Arévalo,<sup>2</sup> Andrea Bagán,<sup>2</sup> Francesc X. Sureda,<sup>3</sup> Belén Pérez,<sup>4</sup> Luis F. Callado,<sup>5,6</sup> Jesús A. García-Sevilla,<sup>7</sup> M. Julia García-Fuster,<sup>7</sup> Carmen Escolano,<sup>2</sup> and Mercè Pallàs<sup>1</sup>

<sup>1</sup>Pharmacology Section. Department of Pharmacology, Toxicology and Medicinal Chemistry, Faculty of Pharmacy and Food Sciences, and Institut de Neurociències, University of Barcelona, Av. Joan XXIII, 27-31, 08028 Barcelona, Spain.

<sup>2</sup>Laboratory of Medicinal Chemistry (Associated Unit to CSIC), Department of Pharmacology, Toxicology and Medicinal Chemistry, Faculty of Pharmacy and Food Sciences, and Institute of Biomedicine (IBUB), University of Barcelona, Av. Joan XXIII, 27-31, 08028 Barcelona, Spain.

<sup>3</sup>Pharmacology Unit, Faculty of Medicine and Health Sciences, University of Rovira and Virgili, C./St. Llorenç 21, 43201 Reus, Tarragona, Spain.

<sup>4</sup>Departament of Pharmacology, Therapeutic and Toxicology, Autonomous University of Barcelona E-08193, Spain.

<sup>5</sup>Department of Pharmacology, University of the Basque Country, UPV/EHU, E-48940 Leioa, Bizkaia, Spain.

<sup>6</sup>Centro de Investigación Biomédica en Red de Salud Mental, CIBERSAM, Leioa, Spain. <sup>7</sup>Laboratory of Neuropharmacology, IUNICS and IdISBa, University of the Balearic Islands (UIB), Cra. Vallde-mossa km 7.5, 07122 Palma de Mallorca, Spain.

#Equal Contribution

**Keywords:** Imidazoline I<sub>2</sub> receptors, (2-imidazolin-4-yl)phosphonates, behavior, cognition, neurodegeneration, neuroprotection, aging.

### ABSTRACT

As populations increase their life expectancy, age-related neurodegenerative disorders such as Alzheimer's disease have become more common. I<sub>2</sub>-Imidazoline receptors (I<sub>2</sub>-IR) are widely distributed in the central nervous system, and dysregulation of I<sub>2</sub>-IR in patients with neurodegenerative diseases has been reported, suggesting their implication in cognitive impairment. This evidence indicates that high-affinity selective I<sub>2</sub>-IR ligands potentially contribute to the delay of neurodegeneration. *In vivo* studies in the female senescence accelerated mouse-prone 8 mice have shown that treatment with I<sub>2</sub>-IR ligands, **MCR5** and **MCR9**, produce beneficial effects in behavior and cognition. Changes in molecular pathways implicated in oxidative stress, inflammation, synaptic plasticity, and apoptotic cell death were also studied. Furthermore, treatments with these I<sub>2</sub>-IR ligands

diminished the amyloid precursor protein processing pathway and increased  $A\beta$  degrading enzymes in the hippocampus of SAMP8 mice. These results collectively demonstrate the neuroprotective role of these new  $I_2$ -IR ligands in a mouse model of brain aging through specific pathways and suggest their potential as therapeutic agents in brain disorders and age-related neurodegenerative diseases.

### 3.1.1 INTRODUCTION

Imidazoline receptors (non-adrenergic receptors for imidazolines) [1] have been identified as a promising biological target that deserves further investigation using multidisciplinary approaches to build a comprehensive understanding of their pharmacological possibilities. To date, three main imidazoline receptors,  $I_1$ -,  $I_2$ - and  $I_3$ -IR, have been identified as binding sites that recognize different radiolabeled ligands involving different locations and physiological functions [2-4]. The pharmacological characterization of  $I_1$ -IR is understood the best, and they are used in the antihypertensive drugs moxonidine [5] or rilmenidine [6]. To date,  $I_2$ -IR have not been structurally described, although García-Sevilla's group has defined distinct binding proteins corresponding to subgroups of  $I_2$ -IR sites [7].  $I_2$ -IR are involved in analgesia [8] glial tumors [9], inflammation [10] and a plethora of brain disorders, such as Alzheimer's Disease (AD) [11,12], Parkinson's disease (PD) [13], and different psychiatric disorders [14-16]. The efficacy of the analgesic CR4056 in osteoarthritis has advanced this compound in the first-in-class  $I_2$ -IR ligand to achieve phase II clinical trials [17].  $I_2$ -IR are widely distributed in the CNS, binds imidazoline-based compounds [18, 19], such as idazoxan or valldemossine [20], and have been associated with the catalytic site of monoamine oxidase enzyme (MAO) [21]. A neuroprotective role for  $I_2$ -IR was described through the pharmacological activities observed for their ligands [22]. Idazoxan reduced neuron damage in the hippocampus after global ischemia in the rat brain [23] and agmatine, identified as the endogenous  $I_2$ -IR ligand [24], has demonstrated modulatory actions in several neurotransmitters that produce neuroprotection both *in vitro* and in rodent models [25]. The compelling evidence has demonstrated that other selective  $I_2$ -IR ligands (Figure 1) provide benefits such as being neuroprotective against cerebral ischemia *in vivo* [26, 27], inducing beneficial effects in several models of chronic opioid therapy, leading to neuroprotection by direct blocking of N-methyl-D-aspartate receptor (NMDA) mediated intracellular  $[Ca^{2+}]$  influx [28], or provoking morphological/biochemical changes in astroglia that are neuroprotective after neonatal axotomy [22].

At a cellular level,  $I_2$ -IR are situated in the outer membrane of the mitochondria in astrocytes [29], and a direct physiological function of glial  $I_2$ -imidazoline preferring sites that regulate the level of the astrocyte marker glial fibrillary acidic protein (*Gfap*)



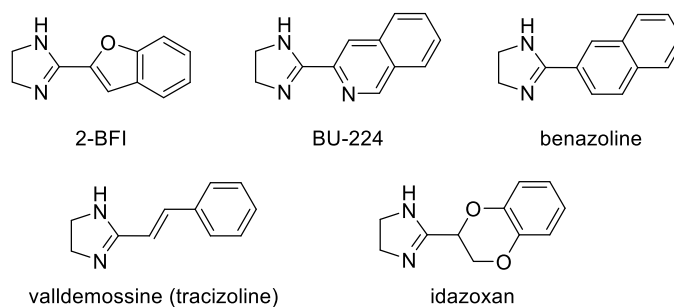


**Figure 1:** Representative I<sub>2</sub>-IR ligands.

has been proposed [30]. In addition, astrogliosis is a pathophysiological trend in brain neurodegeneration as in AD [31]. The density of I<sub>2</sub>-IR is markedly increased in the brains of patients with AD [13], and in gliosis associated with brain injury [32].

The pharmacological characterization of these receptors relies on the discovery of selective I<sub>2</sub>-IR ligands devoid of a high affinity for I<sub>1</sub>-IR and  $\alpha_2$ -adrenoceptors. The reported I<sub>2</sub>-IR ligands are structurally restricted, featuring rigid substituted pattern imidazolines, and most of which are not entirely selective and thus interact with  $\alpha$ -adrenoceptors [19], which causes side effects [33]. Our chemistry program aimed to find new selective I<sub>2</sub>-IR ligands to increase the arsenal of pharmacological tools to exploit the therapeutic potential of I<sub>2</sub>-IR in neuroprotection.

We have recently synthesized a series of new chemical scaffolds, 2-imidazolin-4-yl) phosphonates [34], by an isocyanide-based multicomponent reaction under microwave irradiation to avoid using solvents. The experimental synthetic conditions fulfill the principles of green chemistry, giving access to novel compounds with high selectivity and affinity for I<sub>2</sub>-IR. Among them, we tested **MCR5** [diethyl (1-(3-chloro-4-fluorobenzyl)-5,5-dimethyl-4-phenyl-4,5-dihydro-1H-imidazol-4-yl)phosphonate] in previous work to demonstrate its neuroprotective and analgesic effects, and it showed promising results in models of brain damage [35]. In particular, mechanisms of neuroprotection related to regulating apoptotic pathways or inhibiting p35 cleavage mediated by this new active compound have been found. In the present work, we explored the behavioral and cognitive status, including molecular changes associated with age and neurodegenerative processes, presented by SAMP8 mice when treated with the new highly selective I<sub>2</sub>-IR ligands **MCR5** and **MCR9** [methyl 1-(3-chloro-4-fluorobenzyl)-5,5-dimethyl-4-phenyl-4,5-dihydro-1H-imidazole-4-carboxylate] (Figure 2). SAMP8 is a naturally occurring mouse strain that displays a phenotype of accelerated aging with cognitive decline, as observed in AD, and is widely used as a feasible rodent model of cognitive dysfunction [36]. To the best of our knowledge, this manuscript reports the first study that includes cognitive and behavioral parameters of novel I<sub>2</sub>-IR ligands in a well-characterized animal model for studying brain

aging and neurodegeneration.

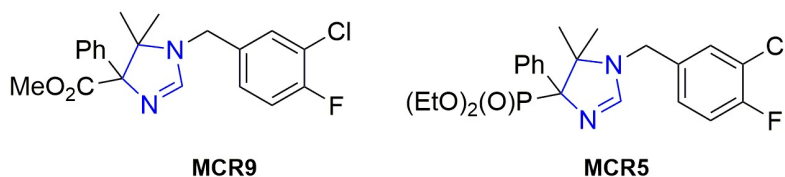


**Figure 2:** Structure of I<sub>2</sub>-IR ligands **MCR5** and **MCR9**.

### 3.1.2 MATERIALS AND METHODS

#### Synthesis of I<sub>2</sub>-IR ligands **MCR5** and **MCR9**

The compounds were prepared using our previously optimized conditions [34]. I<sub>2</sub>-IR pK<sub>i</sub> for **MCR5** and **MCR9** were determined as 9.42±0.16 nM and 8.85±0.21 nM, respectively, showing that both compounds also had high selectivity against α<sub>2</sub> adrenergic receptors (457 and 1862, respectively) [35].

#### The blood-brain barrier (BBB) determination method

The *in vitro* permeability (Pe) of the novel compounds through a lipid extract of the porcine brain was determined using a mixture of PBS/EtOH 70:30. The concentration of drugs was determined using a UV/VIS (250-500 nm) plate reader. Assay validation was carried out by comparing the experimental and reported permeability values of 14 commercial drugs (see supporting information), which provided a good linear correlation:  $Pe(\text{exp}) = 1.003Pe(\text{lit}) - 0.783$  ( $R^2 = 0.93$ ). Using this equation and the limits established by Di et al. [37] for BBB permeation, the following ranges of permeability were established:  $Pe(10^{-6}\text{cm} \cdot \text{s}^{-1}) > 5.18$  for compounds with high BBB permeation (CNS+);  $Pe(10^{-6}\text{cm} \cdot \text{s}^{-1}) < 2.06$  for compounds with low BBB permeation (CNS-); and  $5.18 > Pe(10^{-6}\text{cm} \cdot \text{s}^{-1}) > 2.06$  for compounds with uncertain BBB permeation (CNS±).

#### Measurements of hypothermic effects

For this study, 25 adult male CD-1 mice (30-40 g) bred in the animal facility at the University of the Balearic Islands were used. Mice were housed in standard cages under defined environmental conditions (22°C, 70% humidity, and a 12-h light/dark cycle, lights on at 8:00 AM) and with free access to a standard diet and tap water. Experimental procedures followed the ARRIVE [38] and standard ethical guidelines (European Communities Council Directive 86/609/EEC and Guidelines for the Care and Use of Mammals in Neuroscience and Behavioral Research, National Research Council 2003) and were approved by the Local Bioethics Committee (UIB-CAIB). All efforts were made to minimize the

number of mice used and their suffering.

Mice were handled and weighed by the same person for 2 days so they could habituate to the experimenter before any experimental procedures were initiated. For the acute treatment, mice received a single dose of **MCR9** (20 mg/kg, i.p., n=6) or vehicle (a mixture of equal parts of DMSO and saline, i.p., n=7). For the repeated treatment, mice were daily treated with **MCR9** (20 mg/kg, i.p., n=6) or vehicle (a mixture of equal parts of DMSO and saline, i.p., n=6) for 5 consecutive days. The hypothermic effect of compound **MCR9** was evaluated by measuring rectal temperature before any drug treatment (basal value) and 1 h after drug injection by a rectal probe connected to a digital thermometer (compact LCD thermometer, SA880-1M, RS, Corby, UK). Mice were sacrificed immediately after the last measurement of rectal temperature.

### **SAMP8 mouse *in vivo* experiments**

SAMP8 female mice (n=26) (12 months old) were used to carry out cognitive and molecular analyses. We divided these animals randomly into three groups: SAMP8 Control (SP8-Ct, n=10) and SAMP8 treated with I<sub>2</sub>-IR ligands (**MCR5**, n=8 and **MCR9**, n=8). Animals had free access to food and water and were kept under standard temperature conditions (22±2°C) and a 12-h light/dark cycle (300 lux/0 lux). **MCR5** and **MCR9** (5 mg/Kg/day) were dissolved in 1,8% 2-hydroxypropyl- $\beta$ -cyclodextrin and administered through drinking water for 4 weeks. Water consumption was controlled each week, and I<sub>2</sub>-IR ligand concentrations were adjusted accordingly to reach the optimal dose. Studies and procedures involving mice brain dissection and subcellular fractionation were performed by the ARRIVE [38] and international guidelines for the care and use of laboratory animals (see above) and approved by the Ethics Committee for Animal Experimentation at the University of Barcelona.

### **Open field (OFT), elevated plus maze (EPM), and novel object recognition test (NORT)**

The OFT apparatus was a white polywood box (50x50x25 cm). The floor was divided into two areas defined as center zone and peripheral zone (15 cm between the center zone and the wall). Behavior was scored with SMART® ver.3.0 software, and each trial was recorded for later analysis using a camera situated above the apparatus. Twenty-six mice (n=8-10 per group) were placed at the center and allowed to explore the box for 5 min. Afterward, the mice were returned to their home cages and the OFT apparatus was cleaned with 70% EtOH. The parameters scored included center staying duration, rears, defecations, and the distance traveled, calculated as the sum of total distance traveled in 5 min.

The EPM apparatus consists of opened arms and closed arms, crossed in the middle perpendicularly to each other, and a central platform (5×5cm) constructed of dark and white plywood (30×5×15 cm). To initiate the test session, 26 mice (n=8-10 per group) were placed on the central platform, facing an open arm, and allowed to explore the apparatus for 5 min. After the 5-min test, mice were returned to their home cages, and the EPM apparatus was cleaned with 70% EtOH and allowed to dry between tests. Behavior was scored with SMART® ver.3.0 software, and each trial was recorded for later analysis using a camera fixed to the ceiling at a height of 2.1 m and situated above the apparatus. The parameters recorded included time spent on opened arms, time spent on closed arms, time spent in the center zone, rears, defecation and urination.

The NORT protocol employed was a modification of that of Ennaceur and Delacour [39]. In brief, 26 mice (n=8-10 per group) were placed in a 90°, two-arm, 25-cm-long, 20-cm-high, 5-cm-wide black maze. The walls could be removed for easy cleaning. Light intensity in mid-field was 30 lux. Before performing the test, the mice were individually habituated to the apparatus for 10 min for 3 days. On day 4, the animals were submitted to a 10-min acquisition trial (first trial), during which they were placed in the maze in the presence of two identical, novel objects (A+A or B+B) at the end of each arm. A 10-min retention trial (second trial) was carried out 2 h and 24 h later, with one of the two objects changed. During these second trials, mice behavior was recorded with a camera. The time with the new object (TN) and the time with the old object (TO) were measured. A discrimination index (DI) was defined as  $(TN-TO)/(TN+TO)$ . The maze and the objects were cleaned with 96% EtOH after each test to eliminate olfactory cues.

### **Brain processing**

Mice were euthanized by cervical dislocation 1 day after the behavioral and cognitive tests finished. Brains were immediately removed from the skull. The hippocampus of each mouse was then isolated and frozen in powdered dry ice. Each hippocampus was maintained at -80°C for further use. Tissue samples were homogenized in lysis buffer containing phosphatase and protease inhibitors (Cocktail II, Sigma-Aldrich). Total protein levels were obtained, and the Bradford method was used to determine protein concentration. **Protein levels determination by western blot (WB)** For WB, aliquots of 15  $\mu$ g of hippocampal protein were used. Protein samples from 15 mice (n=5 per group) were separated by SDS-PAGE (8%-12%) and transferred onto PVDF membranes (Millipore). Afterward, membranes were blocked in 5% non-fat milk in 0,1% Tween20 TBS (TBS-T) for 1 h at room temperature, followed by overnight incubation at 4°C with the primary antibodies listed in Table 1 (Supporting Information). Membranes were washed and incubated with secondary antibodies for 1 h at room temperature. Immunoreactive proteins were viewed

with a chemiluminescence-based detection kit, following the manufacturer's protocol (ECL Kit; Millipore) and digital images were acquired using a ChemiDoc XRS+ System (BioRad). Semi-quantitative analyses were carried out using ImageLab software (BioRad), and results were expressed in arbitrary units, considering control protein levels as 100%. Protein loading was routinely monitored by immunodetection of glyceraldehyde-3-phosphate dehydrogenase (GAPDH).

### **Determination of OS in the hippocampus**

Hydrogen peroxide (H<sub>2</sub>O<sub>2</sub>) from 12 mice (n=4 per group) was measured in hippocampal tissue protein extracts obtained as described above. It was used as an indicator of OS and was quantified using a hydrogen peroxide assay kit (Sigma-Aldrich, St. Louis, MI) according to the manufacturer's instructions.

### **RNA extraction and gene expression determination**

Total RNA isolation was carried out using the TRIzol® reagent according to manufacturer's instructions. The yield, purity, and quality of RNA were determined spectrophotometrically with a NanoDrop™ ND-1000 (Thermo Scientific) apparatus and an Agilent 2100B Bioanalyzer (Agilent Technologies). RNAs with 260/280 ratios and RIN higher than 1.9 and 7.5, respectively, were selected. Reverse Transcription-Polymerase Chain Reaction (RT-PCR) was performed as follows: 2 µg of mRNA was reverse-transcribed using the high capacity cDNA reverse transcription kit (Applied Biosystems). Real-time quantitative PCR (qPCR) was employed to quantify the mRNA expression of OS genes heme oxygenase (de-cycling) 1 (*Hmox1*), aldehyde oxidase 1 (*Aox1*), cyclooxygenase 2 (*Cox2*), inflammatory genes interleukin 6 (*Il-6*), interleukin 1 beta (*Il-1β*), tumor necrosis factor alpha (*Tnf-α*), amyloid processing gene disintegrin, and metalloproteinase domain-containing protein 10 (*Adam10*) and amyloid degradation gene neprilysin (*NEP*). The primers are listed in Table 2 (Supporting Information).

SYBR® Green real-time PCR was performed in a Step One Plus Detection System (Applied-Biosystems) employing SYBR® Green PCR Master Mix (Applied-Biosystems). Each reaction mixture contained 7.5 µL of cDNA (a 2-µg concentration), 0.75 µL of each primer (a 100-nM concentration, each), and 7.5 µL of SYBR® Green PCR Master Mix (2X).

TaqMan-based real-time PCR (Applied Biosystems) was also performed in a Step One Plus Detection System (Applied-Biosystems). Each 20 µL of TaqMan reaction contained 9 µL of cDNA (25 ng), 1 µL 20X probe of TaqMan Gene Expression Assays and 10 µL of 2X TaqMan Universal PCR Master Mix.

Data were analyzed using the comparative cycle threshold (Ct) method ( $\Delta\Delta Ct$ ), where the housekeeping gene level was used to normalize differences in sample loading and preparation. Normalization of expression levels was performed with actin for SYBR® green-based real-time PCR results and Tbp for TaqMan-based real-time PCR. Each sample (n=4-5 per group) was analyzed in duplicate, and the results represent the n-fold difference of the transcript levels among different groups.

### Statistical analysis

The statistical analyses were conducted using GraphPad Prism ver. 6 statistical software. Data were expressed as the mean  $\pm$  standard error of the mean (SEM). Means were compared with one-way analysis of variance (ANOVA) and Tukey's post hoc test or two-tailed Student's t-test when necessary. Statistical significance was considered when p values were  $<0.05$ . Statistical outliers were performed out with Grubbs' test and were removed from the analysis.

## 3.1.3 RESULTS

### BBB permeation assay for I<sub>2</sub>-IR ligands MCR5 and MCR9

The tested compounds **MCR5** and **MCR9** had Pe values of  $13.5\pm 0.9$  and  $26.9\pm 1.7$ , respectively, well above the threshold for high BBB permeation, so they were predicted to be able to cross the BBB and reach their biological target in the CNS. Supplementary information on results analysis can be found in the supporting material (Table 3).

### Hypothermic effects of MCR9 in mice

Selective I<sub>2</sub>-IR ligands induce hypothermia in rodents [4]. In particular, the hypothermic effect of compound **MCR5** in mice was evaluated in a recent study from our research group (results for compound 2c in ref 35) [35]. Similar to **MCR5**, **MCR9** induced mild hypothermia as assessed by a moderate reduction ( $-2.3^{\circ}\text{C}$ ) in rectal temperature 1 h after injection at the tested dose of 20 mg/kg in adult CD-1 mice and as compared with vehicle-treated controls (Figure 3a, day 1). While repeated (5 days) administration (20 mg/kg) revealed persistent the hypothermic effects of **MCR9** from days 1 to 4 (range from  $-2.3$  to  $-3.2^{\circ}\text{C}$ ), on day 5 no significant change was observed in body temperature ( $-1.8^{\circ}\text{C}$  change) as compared with vehicle-treated controls (Figure 3b).

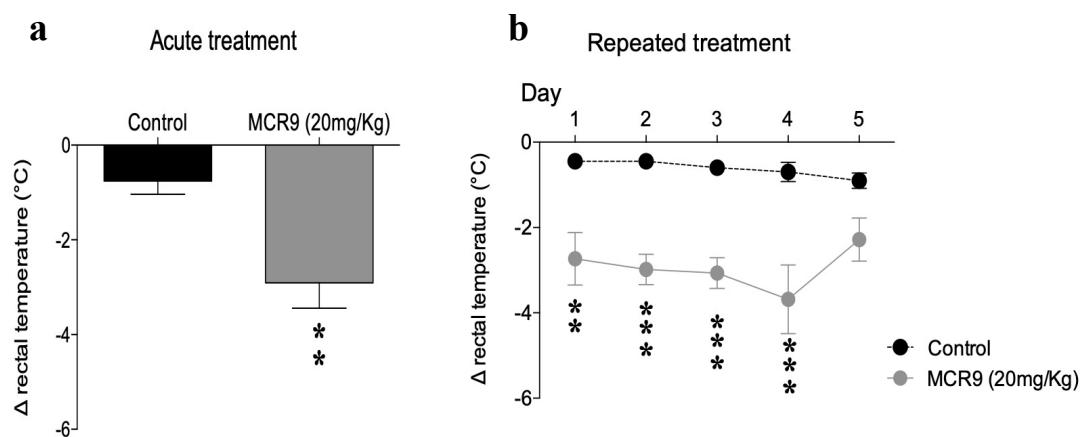


**Figure 3: Acute and repeated measurement of the hypothermic effect of compound MCR9 in mice.** (a) Effect of acute treatment with **MCR9** (20mg/kg, i.p.) on rectal body temperature in mice. Columns are means  $\pm$  SEM of the difference ( $\Delta$ , 1h - basal value) in body temperature ( $^{\circ}$ C) for **MCR9**-treated mice compared to vehicle-treated Control mice. Data were analyzed using Student t-test. \*\* $p < 0.01$ . (b) Effect of repeated (5 days) treatments with **MCR9** (20mg/kg, i.p., closed circles) on rectal body temperature in mice. Circles are means  $\pm$  SEM of the difference ( $\Delta$ , 1h - basal value) in body temperature ( $^{\circ}$ C) for **MCR9**-treated mice compared to vehicle-treated Controls. Data were analyzed by using repeated measures ANOVA followed by Sidak's multiple comparison test. \*\* $p < 0.01$ , \*\*\* $p < 0.001$ ; (n=6-7 animals per group).

### Beneficial effects on behavior and cognition induced by MCR5 and MCR9 in SAMP8 mice

Results obtained in OFT demonstrated that both compounds increased locomotor activity and time spent in the center zone (Figure 4a and b). Furthermore, a significant increment in the vertical activity, quantified by the number of total rears, was observed in mice treated with **MCR5** or **MCR9** in OFT and the EPM (Figure 4c and f). EPM data indicated a reduction in anxiety-like behavior by a significant decrease in time spent in closed arms for treated animals compared with controls (Figure 4e). These results are supported by a preference for opened arms, although not significant, for **MCR5** (Figure 4d). Moreover, a significant increase in the DI indicates an improved performance in recognition of the new object in the NORT between **MCR5**- and **MCR9**-treated SAMP8 mice compared with the control group. A robust effect in short (2 h) and long-term (24 h) memory was found for the two tested compounds (Figure 4g and h).

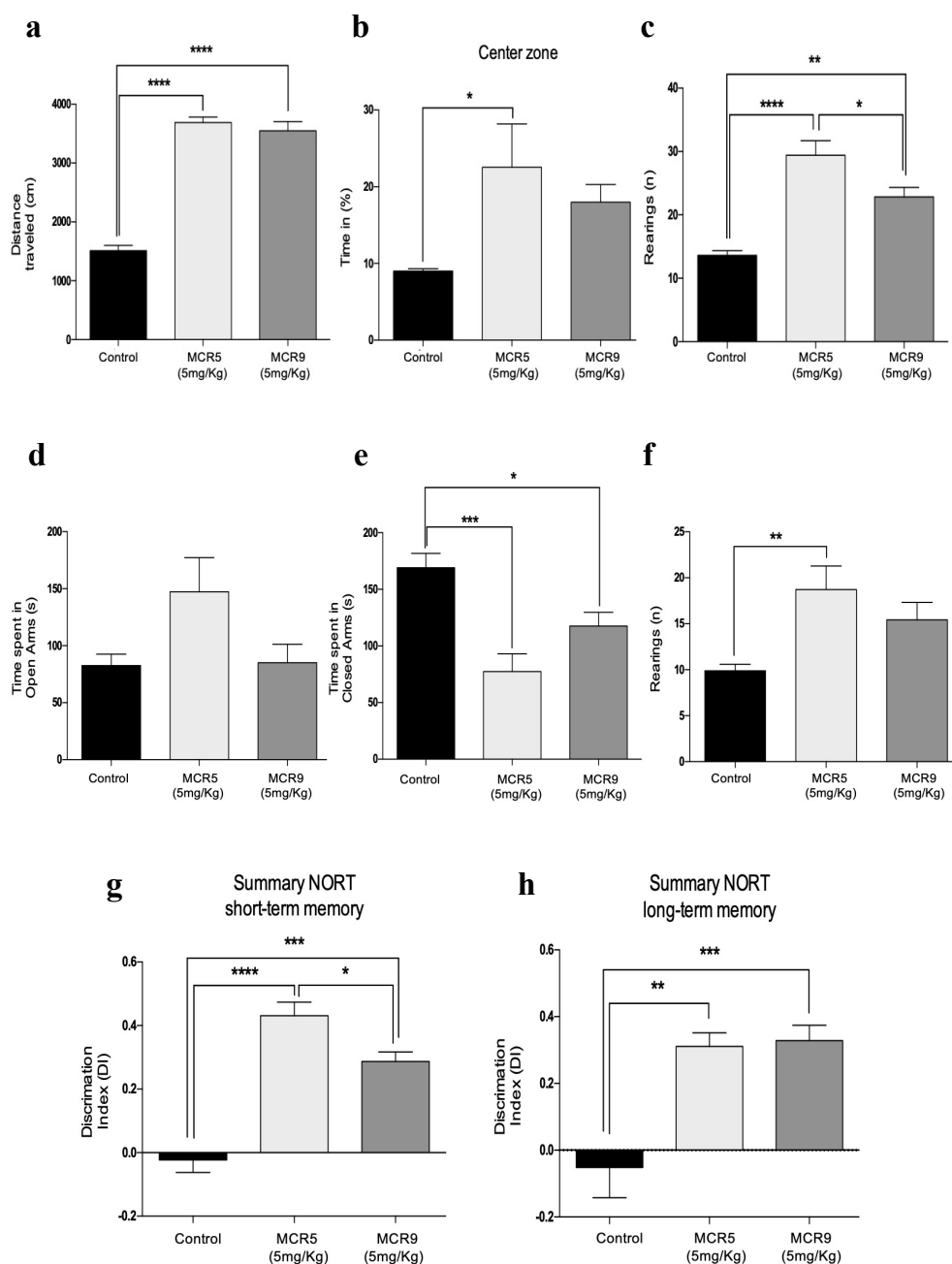


**Figure 4: Behavioral and cognitive improvement in SAMP8 12-month-old treated mice with both  $I_2$ -IR ligands.** (a) A significant increase in the distance travelled in the open field test in  $I_2$ -IR ligands treated groups in comparison with the Control group. (b) A significant increase in the percentage of time in the center zone of the opened field test in **MCR5** treated group compared to the Control group, and no significant difference between **MCR9** and the Control group. (c) A significant increase in the number of total rears of the opened field test among groups. (d) The time spent in the opened arms of the EPM did not differ among groups. (e) A significant increase in the time spent in the closed arms among Control group in comparison with treated groups. (f) A significant increase in the number of total rears of the EPM in **MCR5** group in comparison with Control group. (Continued)



**Figure 4:** (Continued) (g) The results of the NORT in the short-term memory 2h revealed a significant increase in both I<sub>2</sub>-IR ligands treated groups in comparison with the Control group as well as a significant reduction in the DI of **MCR9** group compared to **MCR5** group, and (h) a significant increase in the DI of the long-term memory 24h in both I<sub>2</sub>-IR ligands treated groups compared to the Control group. Data expressed as means  $\pm$  SEM (n=8-10 animals per group) and analyzed using a One-way ANOVA followed by Tukey's post hoc test for multiple comparisons. \*p<0.05, \*\*p<0.01, \*\*\*p<0.001 and \*\*\*\*p<0.0001.

### **OS and inflammatory markers reduced by MCR5 and MCR9 in SAMP8 mice**

OS and neuroinflammation are thought to be key risk factors in the development of neurodegeneration. The hydrogen peroxide levels in the hippocampus were significantly reduced in brains of mice treated with either **MCR5** or **MCR9** compared with the control group (Figure 5a). Of note, superoxide dismutase 1 (SOD1) protein levels in treated mice were reduced by **MCR5** but not by **MCR9** (Figure 5b). Moreover, *Hmox1* gene expression, an important key enzyme in cellular antioxidant-defense, was also significantly increased with both **MCR5** and **MCR9** (Figure 5d). Other OS markers, such as *Aox1* or *Cox2*, were not significantly altered (Figure 5d). Regarding the inflammation markers, no changes were observed in *Il-6* gene expression for tested compounds, but a significant decrease in *Il-1 $\beta$*  and *Tnf- $\alpha$*  for **MCR5** treated SAMP8 mice was found (Figure 5e). Moreover, a significant diminution in GFAP protein levels was determined, reinforcing the prevention of inflammatory processes by **MCR5** and **MCR9** (Figure 5c).

### **Changes in synaptic markers and apoptotic factors induced by MCR5 and MCR9 in SAMP8 mice**

**MCR5**, but not **MCR9**, induced an increase in postsynaptic density protein 95 (PSD95) protein levels (Figure 6a). Protein levels for synaptophysin (SYN), a presynaptic protein, showed a slight increase for both compounds, although it did not reach significance (Figure 6b). To determine the implication of proteolytic processes in the **MCR5** and **MCR9** compounds, we found reduced levels of calpain (data not shown) with a significant diminution in 150  $\alpha$ -spectrin breakdown fragment (SPBD) (Figure 6c). Furthermore, **MCR9** and **MCR5** reduced caspase-3 activity in SAMP8 mouse hippocampi, because of the diminution of caspase-3 protein levels and 120 SPBD fragments, which reached significance for **MCR9** (Figure 6c and d). Moreover, B-cell lymphoma 2 (Bcl-2) levels were diminished, and Bcl-2-associated X (Bax), a key protein in the apoptotic cascade, was reduced by **MCR5** (Figure 6e and f), supporting a possible implication of I<sub>2</sub>-IR in apoptosis processes.

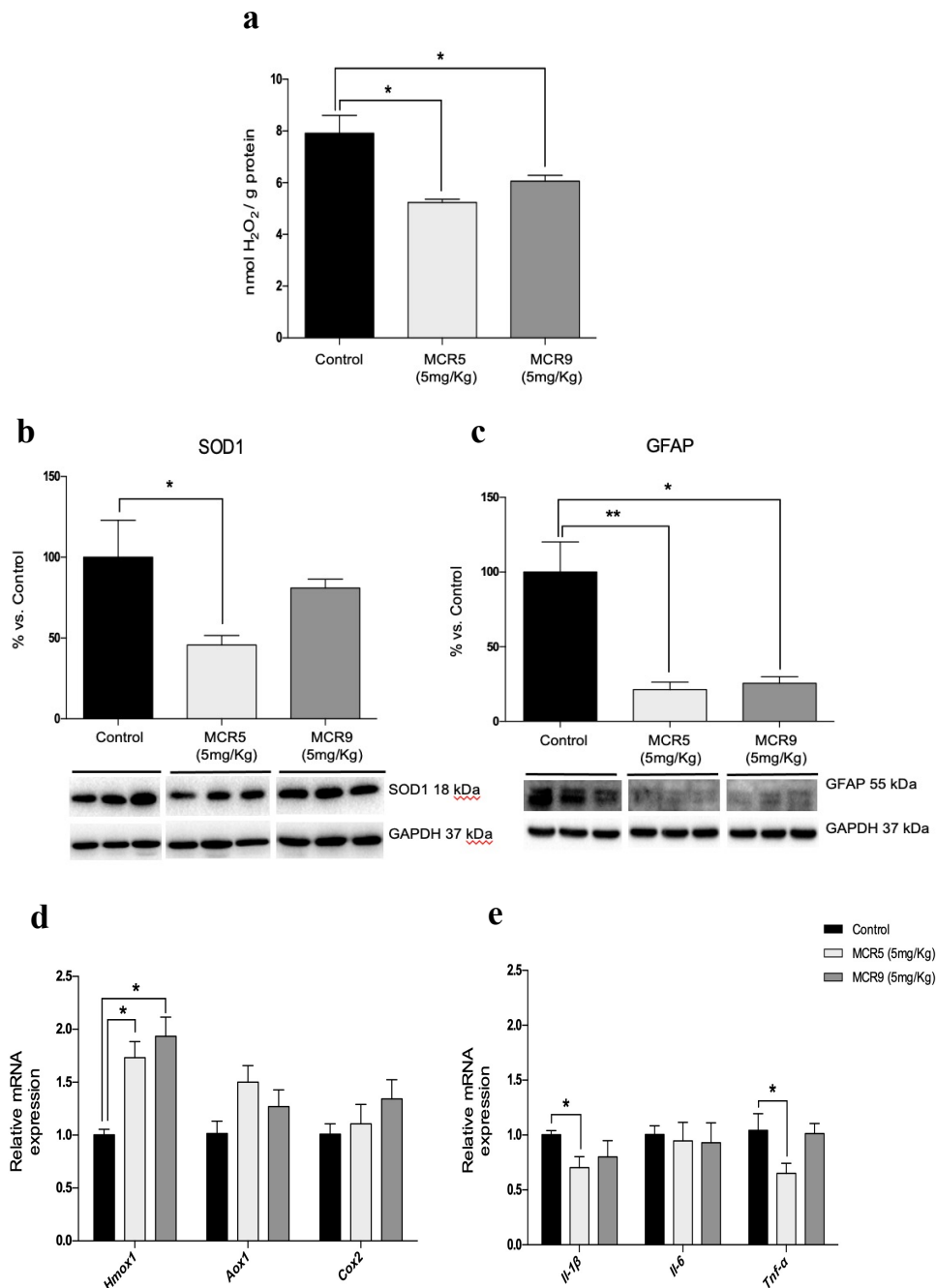


**Figure 5: Reduced OS and inflammatory markers in SAMP8 12-month-old treated mice with both I<sub>2</sub>-IR ligands.** (a) There was a significant reduction in hydrogen peroxide concentration in both I<sub>2</sub>-IR ligands treated groups in comparison with the Control group in homogenates of the hippocampus tissue. (b) A significant reduction in protein levels of SOD1 in **MCR5** group compared to the Control group and no difference between **MCR9** and Control group. (c) A significant reduction in protein levels of Gfap in **MCR5** and **MCR9** in comparison with the Control group. (d) Gene expression of antioxidant enzymes in the mice hippocampus. A significant increase in *Hmox1* gene expression, but not for *Aox1* and *Cox2*, among both I<sub>2</sub>-IR ligands and Control group. (e) Significant reduction in gene expression of *Il-1β* and *Tnf-α* in **MCR5** group in comparison with the Control group, and a tendency to reduce in **MCR9** group for the same genes. However, *Il-6* gene expression did not differ among groups. Values in bar graphs are adjusted to 100% for protein level of the Control group. Gene expression levels were determined by real-time PCR. Data expressed as means ± SEM (n=4-5 animals per group) and analyzed using a One-way ANOVA followed by Tukey's post hoc test for multiple comparisons. \*p<0.05.

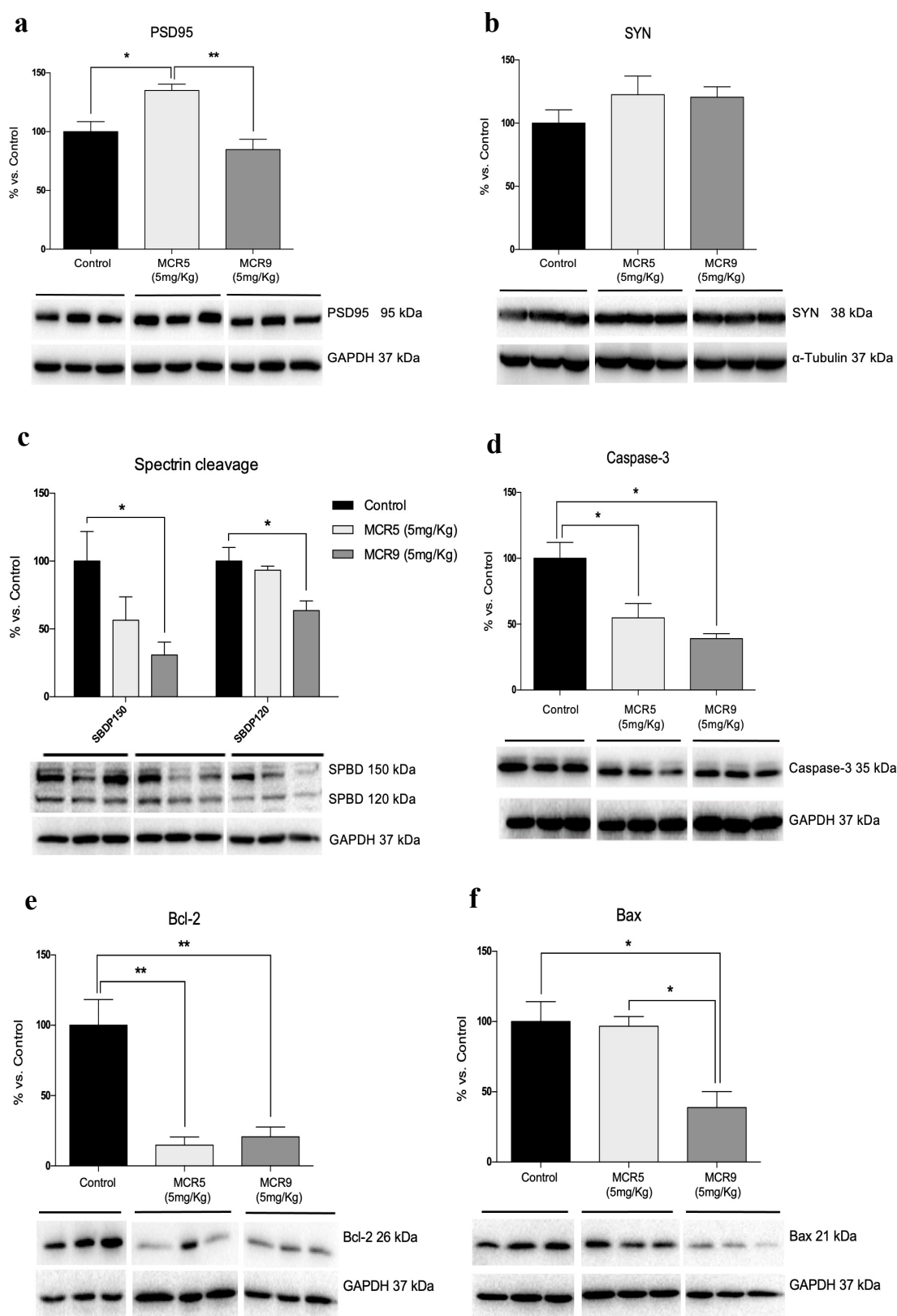


**Figure 6: Changes in synaptic markers and apoptotic factors in 12-month-old treated SAMP8 mice with both  $I_2$ -IR ligands.** (a) A significant increase in protein levels of PSD95 in MCR5 group in comparison with the other two groups. (b) A tendency to increase in protein levels of SYN in both  $I_2$ -IR ligands treated groups in comparison with the Control group.

**Figure 6:** (Continued) (c) There was a tendency to reduce in the spectrin fragment SPBD 150, and a significant reduction in the spectrin fragment SPBD 120 in **MCR9** group in comparison with the Control group. (d) A significant reduction in Caspase-3 protein levels in both I<sub>2</sub>-IR ligands group in comparison with the Control group. (e) A significant reduction in Bcl-2 protein levels in both I<sub>2</sub>-IR ligands group in comparison with the Control group. (f) A significant reduction in Bax protein levels among the **MCR9** group and the other groups. Values in bar graphs are adjusted to 100% for protein level of the Control group. Representative WB for each protein in the hippocampus mice was showed. Data expressed as means  $\pm$  SEM (n=5 animals per group) and analyzed using a One-way ANOVA followed by Tukey's post hoc test for multiple comparisons. \*p<0.05, \*\*p<0.001.

### **Changes in mitogen-activated protein kinase (MAPK) signaling pathways reduced hyperphosphorylation of Tau induced by MCR5 and MCR9 in SAMP8 mice**

Key proteins associated with molecular pathways disturbed in brain disorders and neurodegeneration were evaluated by WB. Interestingly, **MCR5**, but not **MCR9**, increased the p-AKT/AKT ratio (protein kinase B) (Figure 7a). Accordingly, higher levels of inactivated glycogen synthase kinase 3 beta (GSK3 $\beta$ ), phosphorylated in Ser9, were determined (Figure 7b). Extracellular signal-regulated kinase (ERK $\frac{1}{2}$ ) inhibition by **MCR5** and **MCR9** was demonstrated by a reduction of the p-ERK $\frac{1}{2}$  ratio (Figure 7c). Furthermore, cyclin-dependent kinases 5 (CDK5) measured by the p-CDK5/CDK5 and p25/p35 ratios were also reduced (Figure 7d and e). Taking into account the results obtained on kinases CDK5, GSK3 $\beta$ , AKT, and ERK $\frac{1}{2}$ , we studied Tau hyperphosphorylation levels in the hippocampi of SAMP8 mice. A significant reduction in Tau phosphorylation in treated SAMP8 mice was found, specifically for the Ser404 phosphorylation site, whereas the Ser396 phosphorylation site was reduced without reaching significance (Figure 7f).

### **Changes in APP processing and A $\beta$ degradation induced by MCR5 and MCR9 in SAMP8 mice**

We found a significant increase in sAPP $\alpha$  protein levels in **MCR9** treated SAMP8 mice (Figure 8a) and a significant reduction in sAPP $\beta$  protein levels in **MCR5** treated SAMP8 mice (Figure 8b). Furthermore, a significant increase in gene expression for *Adam10*, an  $\alpha$ -secretase that cleaves APP and *NEP*, an A $\beta$  degrading enzyme (Figure 8c and d) was observed in both treated mice groups compared with that in non-treated animals.

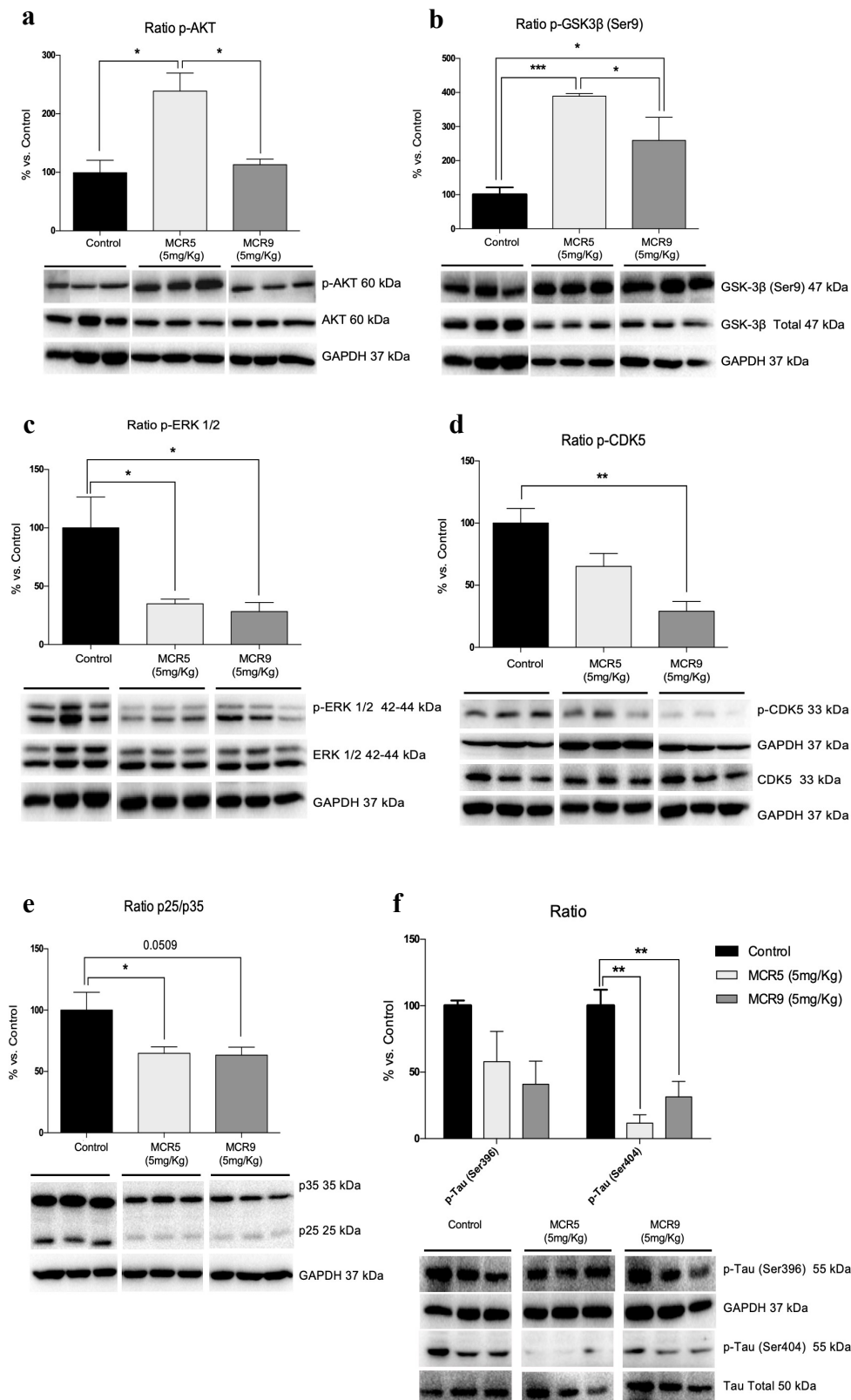


**Figure 7: Changes in kinase signaling pathways reduced hyperphosphorylation of Tau in 12-month-old SAMP8 mice treated with both I<sub>2</sub>-IR ligands.**(a) A significant increase in the p-AKT ratio in the MCR5 group compared with the other two groups. (Continued)

**Figure 7:** (Continued) (b) A significant increase in inactive p-GSK3 $\beta$  (Ser9) protein levels in both I<sub>2</sub>-IR ligand treated groups compared with the Control group. (c) A significant reduction in p-ERK1/2 in both I<sub>2</sub>-IR ligand treated groups compared with the Control group. (d) Changes in the p-CDK5/CDK5 ratio induced by **MCR5** and **MCR9** treatment. (e) Changes in the p25/p35 ratio in the **MCR5** and **MCR9** groups compared with the Control group. Representative WB are shown. (f) A reduction in p-Tau (Ser396), as well as a significant reduction in p-tau (Ser404) in both I<sub>2</sub>-IR ligand treated groups compared with the Control group. Values in bar graphs are adjusted to 100% for protein level of the Control group. Data are expressed as means  $\pm$  SEM (n=5 animals per group) and analyzed using one-way ANOVA followed by Tukey's post hoc test for multiple comparisons. \*p<0.05, \*\*p<0.01, \*\*\*p<0.001.

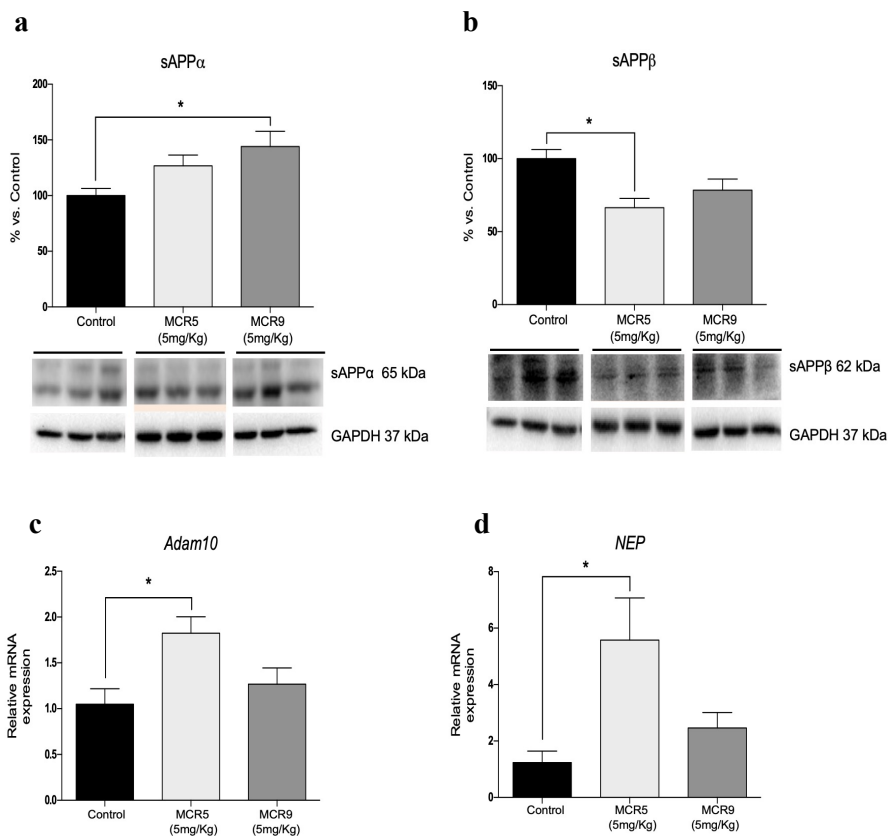


**Figure 8: Changes in APP processing and A $\beta$  degradation enzymes in SAMP8 12-month-old treated with both I<sub>2</sub>-IR ligands.** Representative WB of the APP, and its fragments. (a) Significant increase in sAPP $\alpha$  protein levels in **MCR9** group compared to the Control group, and no significant difference between **MCR5** and the Control group. (b) Significant reduction in sAPP $\beta$  in protein levels in **MCR5** group compared to the Control group, and no significant difference between **MCR9** and the Control group. (c) Significant increase in gene expression of *Adam10* in **MCR5** group compared to the Control group, and no significant difference in **MCR9** group. (d) There was a significant increase in gene expression of *NEP* in **MCR5** group compared to the Control group, and no significant difference in **MCR9** group. Values in bar graphs were adjusted to 100% for protein level of the Control group. Gene expression levels were determined by real-time PCR. Data expressed as means  $\pm$  SEM (n=4-5 animals per group) and analysed using a One-way ANOVA followed by Tukey's post hoc test for multiple comparisons. \*p<0.05.

### 3.1.4 DISCUSSION

I<sub>2</sub>-IR are related to several physiological and pathological processes, including those of the CNS, such as pain [8], neuropathic pain [40], seizures [41, 42], and neurodegenerative diseases such as AD [14, 43]. Our lab has a research line on developing new high affinity and selectivity I<sub>2</sub>-IR ligands, maintaining the imidazoline scaffold and incorporating several substituents in the imidazoline ring. Some of these were previously tested for their neuroprotective role [35].

Given the enormous potential of I<sub>2</sub>-IR and their implications in brain disorders and neurodegenerative diseases such as AD, we set out to explore whether **MCR5** and **MCR9**, two members of a structurally new family of I<sub>2</sub>-IR ligands, might improve the behavioral and cognitive status in SAMP8 model mice. The main chemical structural differences were a phosphonate substituent on the imidazoline ring for **MCR5** in contrast with an ester group for **MCR9** (Figure 2).

Published results from our lab demonstrated that **MCR5** presented a pKi for the I<sub>2</sub>-IR of 9.42±0.16 and high selectivity when compared with the  $\alpha$ 2 receptor affinity [35]. Likewise, **MCR9** is a high-affinity I<sub>2</sub>-IR ligand (pKi 8.85±0.21) but with a higher selectivity against  $\alpha$ 2 receptors. Both **MCR5** and **MCR9** were predicted to be able to cross the BBB, an important drug characteristic when action is expected in the CNS.

Previous studies have evaluated the effects of selective I<sub>2</sub>-IR ligands on inducing hypothermia in rodents [e.g., idazoxan or BU224] [44]. Accordingly, **MCR5** can induce hypothermia in mice, and showed a neuroprotective role in kainate-induced seizures, modifying levels of a Fas-associated protein with death domain (FADD) receptor [35]. While acute **MCR5** (5 and 20 mg/kg) induced mild hypothermia, repeated (20 mg/kg, 5 days) administration of **MCR5** revealed significantly attenuated hypothermic effects from day 2, which indicated the induction of tolerance to the hypothermic effects of the drug [35]. For **MCR9**, repeated (20 mg/kg, 5 days) administration revealed persistent hypothermic effects up to day 4. These results suggest that the slow induction of tolerance to the hypothermic effects caused by **MCR9** might be started following 5 days of drug administration, although a more extended treatment paradigm might be needed for confirmation.

The hypothermic effects exerted by **MCR5** and **MCR9** might be relevant to induce neuroprotection because it was previously proposed for some of the neuroprotective effects induced by the I<sub>2</sub>-IR selective ligand idazoxan. Several experiments have ascertained a possible role for hypothermia in mediating neuroprotection. For example, small drops in temperature exerted neuroprotection in cerebral ischemia [45] and are typically used in the clinic to improve the neurological outcome under various pathological conditions (e.g.,

stroke, brain injury). Although the mechanisms explaining the neuroprotective effects mediated by hypothermia are not well understood, some researchers have suggested that they might be related to the inhibition of glutamate release [46].

SAMP8 mice have been studied as a non-transgenic murine mouse model of accelerated senescence and late-onset AD. These mice exhibit cognitive and emotional disturbances, probably due to the early development of pathological brain hallmarks, such as OS, inflammation, and activation of neuronal death pathways, which mainly affect the cerebral cortex and hippocampus [47, 48]. To date, this rodent model has not been used to test I<sub>2</sub>-IR ligands. Thus, this work is the first investigation of the effects of the improvement of cognitive impairment and behavior in this mouse model after treatment with I<sub>2</sub>-IR ligands.

Behavioral and cognitive effects were investigated through three well-established tests in SAMP8 mice: the OFT, which is an experiment used to assay general locomotor activity and anxiety in rodents [49]; the EPM, one of the most widely used tests for measuring anxiety-like behavior [50]; and the NORT, as a standard measure of cognition (for short- and long-term memory) [51].

The OFT and EPM parameters indicated a reduction in cognitive impairment through showing improved locomotor activity jointly with an anti-anxiousness effect. Likewise, the NORT results demonstrated an improvement in cognitive and short- and long-term learning capabilities in hippocampal memory processes. Therefore, all the assessed parameters showed robust beneficial effects on cognition and behavior after **MCR5** and **MCR9** treatment in SAMP8 mice.

The results in cognitive and behavioral effects were supported by a cellular and biochemical assessment of characteristic parameters related to cognitive decline and AD. The compelling evidence demonstrated a neuroprotective role for I<sub>2</sub>-IR. The neuroprotective role can be related to OS and inflammation [52] by measuring OS indicators and inflammation markers in SAMP8 mouse brain tissue treated with the I<sub>2</sub>-IR ligands, **MCR5** and **MCR9**. Results showed significant reduced hydrogen peroxide levels in hippocampal tissue and increased *Hmox1* gene expression in treated **MCR5** and **MCR9** SAMP8 mice, but not in other sensors for OS, such as *Aox1* or *Cox2*. SOD1 protein levels were reduced by **MCR5** but not by **MCR9**. Regarding inflammation markers, no changes were observed in *Il-6* gene expression for tested compounds, but a significant decrease in *Il-1 $\beta$*  and *Tnf- $\alpha$*  for **MCR5** treated SAMP8 mice was found. In addition, reduced astrogliosis was found in treated animals, corroborating a reduced inflammatory environment in hippocampi of **MCR5** and **MCR9** treated SAMP8 mice. Altogether these results showed a relatively weak influence in OS and inflammation mechanisms by I<sub>2</sub>-IR ligands in SAMP8 mice [53-57]. However, a role for those two pathological conditions related to I<sub>2</sub>-IR ligand



interaction cannot be discarded because **MCR5** elicited beneficial effects despite the old age of the SAMP8 mice. Aged SAMP8 mice present lower inflammation and OS due to being at the endpoint of the senescence process [56, 57]. Therefore, it can be challenging to determine drug effects on these processes in aged SAMP8 mice.

**MCR5** and **MCR9** effects on key molecular markers for synapsis and apoptosis were studied to unravel the prevention of cognitive decline by I<sub>2</sub>-IR ligands in SAMP8 mice, which is characterized by alterations in those processes. In consonance with better cognitive performance, the compounds tested increased synaptic markers such as SYN and PSD95, indicating a neuroprotective role for **MCR5** and **MCR9**.

There are several cellular and molecular pathways related to better synaptic performance, including proteolytic and phosphorylation activities or apoptotic processes. Regarding proteolytic processes, calpain is an intracellular protease that cleaves the CDK5 activator p35 to a p25 fragment. **MCR5** and **MCR9** diminished calpain levels and its activity with a reduced 150 SPBD fragment. Moreover, a significant reduction in p25 protein levels was found in treated SAMP8 mice. A decrease in p25 can also influence CDK5 activity, as implicated in Tau phosphorylation [58, 59]. These results indicate that CDK5 phosphorylation activity should be diminished after I<sub>2</sub>-IR ligand treatment, corroborating results obtained previously for **MCR5** in a kainate model of neuronal damage [60].

Caspase 3 mediated apoptosis was also addressed. A significant reduction of caspase 3 activity and diminution of Bax protein were found in **MCR9** treated SAMP8 mice. Because Bax is described as a pro-apoptotic protein, its diminution indicates a possible protective role for I<sub>2</sub>-IR ligands in neurons [61]. By contrast, reduced levels of Bcl-2, considered an anti-apoptotic protein, deserve further studies. Several authors have indicated that when Bax is reduced, Bcl-2 is less necessary for blocking Bax dimer to form the mitochondrial pore; in this situation cells reduce the Bcl-2 levels as a control mechanism [62].

An increase in p-AKT was induced by the I<sub>2</sub>-IR ligands, whereas a decrease in ERK<sup>1/2</sup> activation was observed. p-AKT inactivated GSK3 $\beta$ , a key kinase involved in the process of Tau hyperphosphorylation, by phosphorylation in Ser9. To this point, **MCR5** and **MCR9** treated SAMP8 mice showed an increase of Ser9 phosphorylated GSK3 $\beta$  and reduced Tau hyperphosphorylation.

ERK<sup>1/2</sup> inhibition (that reduction of p42/p44) by **MCR5** and **MCR9** can contribute to the beneficial effect elicited by I<sub>2</sub>-IR on synaptic markers and Tau phosphorylation processes. ERK<sup>1/2</sup> belongs to a subfamily of MAPKs and plays diverse roles in the CNS, such as neuronal survival or death, synaptic plasticity, and learning and memory through phosphorylation of regulatory enzymes and kinases [63, 64]. Although crucial for neuronal

survival, there is some evidence that prolonged activation of the ERK pathway can induce a deleterious effect to the cell [65, 66]. Interestingly, long-lasting ERK activation in neurons has been demonstrated in neurodegenerative diseases such as AD [67, 68] and PD [69]. Here, the inhibition of this kinase participates in post-translational modifications in cytoskeletal proteins such as Tau, ameliorating the neuronal network functioning, as demonstrated with an increase in synaptic markers.

The relationship among MAPKs, such as ERK $\frac{1}{2}$ , [70] and PI3K, such as AKT, and imidazoline receptors is well defined [71, 72]. In this respect, it has been described that either ERK or AKT can be associated with the multifunctional Fas/FADD complex [73, 74]. Apoptosis is an important contributor to neurodegeneration [75], and in this regard, the FADD protein has been suggested as a putative biomarker for pathological processes associated with the course of clinical dementia [76]. It has been reported that total FADD has a central role in promoting apoptosis [77, 78] and its phosphorylation at Ser191/194 mediates non-apoptotic actions such as cell growth and differentiation [79]. In our previous work, we demonstrated that **MCR5** modified FADD phosphorylation (i.e., it increased the p-FADD/FADD ratio) in a kainate-treated rat model [35]. These results could explain the modulation of proteins from the apoptotic pathway mentioned before (e.g., a diminution in caspase 3 activation and significant changes in Bcl-2 and Bax), which seems to favor anti-apoptotic actions mediated through I<sub>2</sub>-receptors, and especially by **MCR5**.

Tau hyperphosphorylation is a histological trend in many neurodegenerative diseases characterized by cognitive decline, including AD. Therefore we studied APP processing pathways. Aberrant APP processing is a hallmark of cognitive decline diseases [80]. To assess the capacity of the tested compounds to modify this pathological hallmark, we evaluated APP fragments, specifically, sAPP $\alpha$  and sAPP $\beta$ . Despite neither APP fragment reaching significance in either I<sub>2</sub>-IR ligand treated SAMP8 mice group, we found a clear tendency, which indicates the non-amyloidogenic pathway preference. Moreover, sAPP $\alpha$  is described as a neuroprotective, neurotrophic and cell excitable regulator with synaptic plasticity [81]. *Adam10* [82] and *NEP* [83] gene expression were higher in **MCR5** and **MCR9** treated mice groups than in non-treated animals. In sum, I<sub>2</sub>-IR ligands foster a diminution in the amyloidogenic pathway and higher degradation of  $\beta$ -amyloid in the SAMP8 mice model.

In conclusion, the effectiveness of the two new I<sub>2</sub>-IR ligands in an *in vivo* female model for cognitive decline was demonstrated in this study. SAMP8 model mice are gated to neurodegenerative processes, such as AD, and our research has shown that **MCR5** and **MCR9** can open new therapeutic avenues against these pathological conditions that currently have unmet medical needs. Although different authors have previously indicated

the relationship between I<sub>2</sub>-IR and cognitive decline, this study is the first experimental evidence that demonstrates the possibility of using this receptor as a target for cognitive impairment. Here, we demonstrate that this strategy could represent a future approach to treating devastating conditions such as AD.

**Author contributions:** C. G.-F. and F. V. contributed equally. C. G.-F., C. E., L. F. C. and M. P. designed the study. B. P. performed the PAMPA-BBB permeation experiments. C. G.-F. and F. V. carried out the behavior and cognition studies and cellular parameters determination (OS and inflammation markers, synaptic markers and apoptotic factors, and hyperphosphorylation of Tau). J. A. G.-S. and M. J. G.-F. performed the hypothermic studies. S. A., S. R.-A. and A. B. synthesized and purified the I<sub>2</sub>-IR ligands. C. G.-F., L. F. C., F. X. S., J. A. G.-S., M. J. G.-F., C. E. and M. P. contributed to writing the manuscript. All authors have read and approved the final version of the manuscript.

**Acknowledgements:** This study was supported by Ministerio de Economía y Competitividad of Spain (SAF2016-33307 and SAF2014-55903-R) and the Basque Government (IT616/13). C. G.-F., F. V., F. X. S., C. E. and M. P. belong to 2017SGR106 (AGAUR, Catalonia). J. A. G.-S. is a member emeritus of the Institut d'Estudis Catalans (Barcelona, Catalonia). Financial support was provided for F. V. (University of Barcelona, APIF\_2017), S. R.-A. (Generalitat de Catalunya, 2018FI\_B\_00227) and A. B. (Institute of Biomedicine UB\_2018).

**Abbreviations:** AD, Alzheimer's disease; Adam10, A disintegrin and metalloproteinase domain-containing protein 10; ANOVA, one-way analysis of variance; APP, amyloid precursor protein; Aox1, aldehyde oxidase 1; AKT, protein kinase B; Bcl-2, B-cell lymphoma 2; Bax, Bcl-2-associated X; BBB, blood-brain barrier; CDK5, cyclin-dependent kinase 5; CNS, central nervous system; Cox2, cyclooxygenase 2; Ct, cycle threshold; DI, discrimination index; EPM, elevated plus maze; ERK, extracellular signal-regulated kinase; GAPDH, glyceraldehyde-3-phosphate dehydrogenase; FADD, Fas-associated protein with death domain; Gfap, glial fibrillary acidic protein; GSK3 $\beta$ , glycogen synthase kinase 3 beta; Hmox1, heme oxygenase (decycling) 1; I<sub>2</sub>-IR, I<sub>2</sub>-Imidazoline receptors; Il-1 $\beta$ , interleukin 1 beta; Il-6, interleukin 6; MAO, monoamine oxidases; MAPK, mitogen-activated protein kinase; NEP, neprilysin; NMDA, N-methyl-D-aspartate; NORT, novel object recognition test; OFT, open field test; OS, oxidative stress; PCR, polymerase chain reaction; PD, Parkinson's disease; Pe, permeability; PI3K, phosphatidylinositol-4,5-bisphosphate 3-kinase; PSD95, postsynaptic density protein 95; SAMP8, senescence accelerated mouse prone 8; SPBD, spectrin breakdown; SEM, standard error of the mean; SOD1, superoxide dismutase 1; SYN, synaptophysin; TBP, tata-binding protein; TN, time with new object; Tnf- $\alpha$ , tumor necrosis factor alpha; TO, time with old object; WB, western blot.

## REFERENCES

- [1] Bousquet P, Feldman J, Schwarts J. Central cardiovascular effects of alpha-adrenergic drugs: differences between catecholamines and imidazolines. *J. Pharmacol. Exp. Ther.* 1984;230:232-236.
- [2] Head GA, Mayorov DN. Imidazoline receptors, novel agents and therapeutic potential. *Cardio-vasc. Hematol Agents Med. Chem.* 2006;4:17-32.
- [3] Lowry JA, Brown JT. Significance of the imidazoline receptors in toxicology. *Clin. Toxicol.* 2014;52:454-469. [4] Li, JK. Imidazoline I<sub>2</sub> receptors: An update. *Pharmacol. Ther.* 2017;178:48-56.
- [5] Fenton, C, Keating, G M, Lyseng-Williamson KA. Moxonidine: a review of its use in essential hypertension. *Drugs* 2006;6:477-496.
- [6] Reid JL. Rilmenidine: A clinical overview. *Am. J. Hypertens.* 2000;13:106S-111S.
- [7] Olmos G, Alemany R, Boronat MA, García-Sevilla JA. Pharmacologic and molecular discrimination of I<sub>2</sub>-imidazoline receptor subtypes. *Ann. N. Y. Acad. Sci.* 1999;881:144-160.
- [8] Li JX, Zhang Y. Imidazoline I<sub>2</sub> receptors: target for new analgesics? *Eur. J. Pharmacol.* 2011;658:49-56.
- [9] Callado LF, Martín-Gomez JI, Ruiz J, Garibi J, and Meana JJ. Imidazoline I<sub>2</sub> receptors density increases with the malignancy of human gliomas. *J. Neurol., Neurosurg. Psychiatry* 2004;75:785-787.
- [10] Regunathan S, Feinstein DL, Reis DJ. Anti-proliferative and anti-inflammatory actions of imidazoline agents. Are imidazoline receptors involved? *Ann. N. Y. Acad. Sci.* 1999;881:410-419.
- [11] Ruíz J, Martín I, Callado LF, Meana JJ, Barturen F, García-Sevilla JA. Non-adrenoreceptor [3H]idazoxan binding sites (I<sub>2</sub>-imidazoline sites) are increased in postmortem brain from patients with Alzheimer's disease. *Neurosci. Lett.* 1993;160:109-112.
- [12] García-Sevilla JA, Escribá PV, Walzer C, Bouras C, Guimón J. Imidazoline receptor proteins in brains of patients with Alzheimer's disease. *Neurosci. Lett.* 1998;247:95-98.
- [13] Gargalidis-Moudanos C, Pizzinat N, Javoy-Agid F, Remaury A, Parini A. I<sub>2</sub>-imidazoline binding sites and monoamine oxidase activity in human postmortem brain from patients with Parkinson's disease. *Neurochem. Int.* 1997;30:31-36.
- [14] Meana JJ, Barturen, F, Martín I, García-Sevilla JA. Evidence of increased non-adrenoreceptor [3H]idazoxan binding sites in the frontal cortex of depressed suicide victims. *Biol. Psychiatry* 1993;34:498-501.
- [15] García-Sevilla JA, Escribá PV, Sastre, et al. Immunodetection and quantitation of imidazoline receptor proteins in platelets of patients with major depression and in brains of suicide victims. *Arch. Gen. Psychiatry* 1996;53:803-810.
- [16] Smith KL, Jessop DS, Finn DP. Modulation of stress by imidazoline binding sites: implications for psychiatric disorders. *Stress* 2009;12:97-114.
- [17] Comi E, Lanza M, Ferrari F, Mauri V, Caselli G, Rovati LC. Efficacy of CR4056, a first-in-class

imidazoline-2 analgesic drug, in comparison with naproxen in two rat models of osteoarthritis. *J. Pain Res.* 2017;10:1033-1043.

[18] Regunathan S, Reis DJ. Imidazoline receptors and their endogenous ligands. *Ann. Rev. Pharmacol. Toxicol.* 1996;36:511-544.

[19] Dardonville C, Rozas I. Imidazoline binding sites and their ligands: an overview of the different chemical structures. *Med. Res. Rev.* 2004;24:639-661.

[20] Boronat MA, Olmos G, García-Sevilla JA. Attenuation of tolerance to opioid-induced antinociception and protection against morphine-induced decrease of neurofilament proteins by idazoxan and other I<sub>2</sub>-imidazoline ligands. *Br. J. Pharmacol.* 1998;125:175-185.

[21] McDonald GR, Olivieri A, Ramsay RR, Holt A. On the formation and nature of the imidazoline I<sub>2</sub> binding site on human monoamine oxidase B. *Pharmacol. Res.* 2010;62:475-488. [22] Casanovas A, Olmos G, Ribera J, Boronat MA, Esquerda JE, García-Sevilla JA. Induction of reactive astrogliosis and prevention of motoneuron cell death by the I<sub>2</sub>-imidazoline receptor ligand LSL 60101. *Br. J. Pharmacol.* 2000;130:1767-1776.

[23] Gustafson I, Westerberg E, Wieloch T. Protection against ischemia-induced neuronal damage by the  $\alpha$ 2-adrenoceptor antagonist idazoxan: influence of time of administration and possible mechanisms of action. *J. Cereb. Blood Flow Metab.* 1990;10:885-894.

[24] Qiu WW, Zheng RY. Neuroprotective effects of receptor imidazoline 2 and its endogenous ligand agmatine. *Neurosci. Bull.* 2006;22:187-191.

[25] Gilad GM, Gilad VH. Accelerated functional recovery and neuroprotection by agmatine after spinal cord ischemia in rats. *Neurosci. Lett.* 2000;296:97-100.

[26] Han Z, Xiao MJ, Shao B, Zheng RY, Yang GY, Jin K. Attenuation of ischemia induced rat brain injury by 2-(2-benzofuranyl)-2-imidazoline, a high selectivity ligand for imidazoline I(2) receptors. *Neurol. Res.* 2009;31:390-395.

[27] Maiese K, Pek L, Berger SB, Reis DJ. Reduction in focal cerebral ischemia by agents acting at imidazole receptors. *J. Cereb. Blood Flow Metab.* 1992;12:53-63.

[28] Jiang SX, Zheng RY, Zheng JQ, Li XL, Han Z, Hou ST. Reversible inhibition of intracellular calcium influx through NMDA receptors by imidazoline (I)<sub>2</sub> receptor antagonists. *Eur. J. Pharmacol.* 2010;629:12-19.

[29] Ruggiero DA, Regunathan S, Wang H, Milner TA, Reis DJ. Immunocytochemical localization of an imidazoline receptor protein in the central nervous system. *Brain Res.* 1998;780:270-293.

[30] Olmos G, Alemany R, Escriba PV, García-Sevilla JA. The effects of chronic imidazoline drug treatment on glial fibrillary acidic protein concentrations in rat brain. *Br. J. Pharmacol.* 1994;111:997-1002.

[31] Rodríguez-Arellano JJ, Parpura V, Zorec R, Verkhratsky, A. Astrocytes in physiological aging and Alzheimer's disease. *Neuroscience* 2016;323:170-182.

[32] Martín-Gómez JJ, Ruíz J, Barrondo S, Callado, LF, Meana JJ. Opposite changes in Imidazoline I<sub>2</sub> receptors and  $\alpha$ 2-adrenoceptors density in rat frontal cortex after induced gliosis. *Life Sci.*

2005;78:205-209.

[33] Sica DA. Alpha 1-adrenergic blockers: current usage considerations. *J. Clin. Hypertens. (Greenwich)* 2005;7:757-762.

[34] Abás S, Estarellas C, Luque FJ, Escolano C. Easy access to (2-imidazolin-4-yl)phosphonates by a microwave assisted multicomponent reaction. *Tetrahedron* 2015;71:2872-2881. [35] Abás S, Erdozain AM, Keller B et al. Neuroprotective effects of a structurally new family of high affinity imidazoline I<sub>2</sub> receptors ligands. *ACS Chem. Neurosci.* 2017;8:737-742.

[36] Morley JE, Farr SA, Kumar VB, Armbrecht HJ. The SAMP8 mouse: a model to develop therapeutic interventions for Alzheimer's disease. *Curr. Pharm. Des.* 2012;18:1123-1130.

[37] Di L, Kerns EH, Fan K, McConnell OJ, Carter G. T. High throughput artificial membrane permeability assay for blood-brain barrier. *Eur. J. Med. Chem.* 2003;38:223-232.

[38] McGrath JC, Lilley E. Implementing guidelines on reporting research using animals (ARRIVE etc.): new requirements for publication in *BJP. Br. J. Pharmacol.* 2015;172:3189-3193.

[39] Ennaceur A, Delacour J. (1988) A new one-trial test for neurobiological studies of memory in rats. 1: Behavioral data. *Behav. Brain Res.* 1998;31:47-59.

[40] Ferrari F, Fiorentino S, Mennuni L, Garofalo P, Letari O, Mandelli S, Giordani A, Lanza M, Caselli G. Analgesic efficacy of CR4056, a novel imidazoline-2 receptor ligand, in rat models of inflammatory and neuropathic pain. 2011;4:111-125.

[41] Jackson HC, Ripley TL, Dickinson SL, Nutt DJ. Anticonvulsant activity of the imidazoline 6,7-benzodiazoxan. *Epilepsy Res.* 1991;9(2):121-126.

[42] Min JW, Peng BW, He X, Zhang Y, Li JX. Gender difference in epileptogenic effects of 2-BFI and BU224 in mice. *Eur J Pharmacol.* 2013;718(1-3):81-86.

[43] Keller B, García-Sevilla JA. Immunodetection and subcellular distribution of imidazoline receptor proteins with three antibodies in mouse and human brains: Effects of treatments with I<sub>1</sub>- and I<sub>2</sub>-imidazoline drugs. *J Psychopharmacol.* 2015;29(9):996-1012.

[44] Thorn DA, An XF, Zhang Y, Pignini M, Li, JX. Characterization of the hypothermic effects of imidazoline I<sub>2</sub> receptor agonist in rats. *Br. J. Pharmacol.* 2009;166:1936-1945.

[45] Craven JA, Conway EL. Effects of alpha 2-adrenoceptor antagonists and imidazoline 2-receptor ligands on neuronal damage in global ischemia in the rat. *Clin. Exp. Pharmacol. Physiol.* 1997;24:204-207.

[46] Illevich UM, Zornow MH, Choi KT, Scheller M, Strnat MA. Effects of hypothermic metabolic suppression on hippocampal glutamate concentrations after transient global cerebral ischemia. *Anesth. Analg.* 1994;78:905-911.

[47] Takeda T. Senescence-accelerated mouse (SAM) with special references to neurodegeneration models, SAMP8 and SAMP10 mice. *Neurochem. Res.* 2009;34:639-659.

[48] Pallàs M. Senescence-accelerated mice P8: a tool to study brain aging and Alzheimer's disease in a mouse model. *ISRN Cell Biol.* 2012:1-12.

- [49] Archer J. Tests for emotionality in rats and mice: A review. *Anim. Behav.* 1973;21:205-235.
- [50] Dawson GR, Tricklebank MD. Use of the elevated plus maze in the search for novel anxiolytic agents. *Trends Pharmacol. Sci.* 1995;16:33-36.
- [51] Antunes M, Biala G. The novel object recognition memory: neurobiology, test procedure, and its modifications. *Cogn. Process.* 2012;13:93-110.
- [52] Gao H-M, Zhou H, Hong JS. Oxidative Stress, Neuroinflammation, and Neurodegeneration. In: Peterson P. K., Toborek M. (Eds) *Neuroinflammation and Neurodegeneration*, 2014; pp. 81-104, Springer, New York, NY.
- [53] Fujibayashi Y, Yamamoto S, Waki A, Konishi J, Yonekura Y. Increased mitochondrial DNA deletion in the brain of SAMP8, a mouse model for spontaneous oxidative stress brain. *Neurosci. Lett.* 1998;254:109-112.
- [54] Sureda FX, Gutierrez-Cuesta J, Romeu M, Mulero M, Canudas AM, Camins A, Mallol J, Pallàs M. Changes in oxidative stress parameters and neurodegeneration markers in the brain of the senescence-accelerated mice SAMP-8. *Exp. Gerontol.* 2006;41:360-367.
- [55] Gutierrez-Cuesta J, Sureda FX, Romeu M, Canudas AM, Caballero B, Coto-Montes A, Camins A, Pallàs M. Chronic administration of melatonin reduces cerebral injury biomarkers in SAMP8. *J. Pineal Res.* 2007;42:394-402.
- [56] Griñán-Ferré C, Palomera-Avalos V, Puigoriol-Illamola D, Camins A, Porquet D, Plà V, Aguado F, Pallàs M. Behaviour and cognitive changes correlated with hippocampal neuroinflammation and neuronal markers in SAMP8, a model of accelerated senescence. *Exp. Gerontol.* 2016;80:57-69.
- [57] Griñán-Ferré C, Puigoriol-Illamola D, Palomera-Ávalos, V. et al. Environmental enrichment modified epigenetic mechanisms in SAMP8 mouse hippocampus by reducing oxidative stress and inflammation and achieving neuroprotection. *Front. Aging Neurosci.* 2016;8:1-12.
- [58] Gao L, Tian S, Gao H, Xu Y. Hypoxia increases Abeta-induced tau phosphorylation by calpain and promotes behavioral consequences in AD transgenic mice. *J. Mol. Neurosci.* 2013;51:138-147.
- [59] Kimura T, Ishiguro K, Hisanaga S. Physiological and pathological phosphorylation of tau by Cdk5. *Front. Mol. Neurosci.* 2014;7:1-10.
- [60] Keller B, García-Sevilla JA. Regulation of hippocampal Fas receptor and death-inducing signaling complex after kainic acid treatment in mice. *Prog. Neuropsychopharmacol. Biol. Psychiatry.* 2015;3:63:54-62.
- [61] Cheng EH, Wei MD, Weiler S, Flavell RA, Mak TW, Lindster T, Korsmeyer SJ. BCL-2, BCL-X(L) sequester BH3 domain-only molecules preventing BAX- and BAK-mediated mitochondrial apoptosis. *Mol. Cell.* 2001;8:705-711.
- [62] Martin LJ. Mitochondrial and Cell Death Mechanisms in Neurodegenerative Diseases. *Pharmaceuticals.* 2010;3:839-915. [63] Sweatt JD. The neuronal MAP kinase cascade: a biochemical signal integration system subserving synaptic plasticity and memory. *J Neurochem.* 2001;76:1-10.
- [64] Hardingham GE, Bading H. Synaptic versus extrasynaptic NMDA receptor signalling: implications for neurodegenerative disorders. *Nat. Rev. Neurosci.* 2010;11:682-696.

- [65] Imajo M, Tsuchiya Y, Nishida E. Regulatory mechanisms and functions of MAP Kinase signalling pathways. *IUBMB Life* 2006;58:312-317.
- [66] Cruz. CD, Cruz F. The ERK 1 and 2 pathway in the nervous system: from basic aspects to possible clinical applications in pain and visceral dysfunction. *Curr. Neuropharmacol.* 2007;5:244-252.
- [67] Hyman BT, Elvhage TE, Reiter J. Extracellular signal regulated kinases. Localization of protein and mRNA in the human hippocampal formation in Alzheimer's disease. *Am. J. Pathol.* 1994;144:565-572.
- [68] Russo C, Dolcini V, Salis S, Venezia V, Zambrano N, Russo, T, Schettini G. Signal transduction through tyrosine-phosphorylated C-terminal fragments of amyloid precursor protein via an enhanced interaction with Shc/Grb2 adaptor proteins in reactive astrocytes of Alzheimer's disease brain. *J. Biol. Chem.* 2002; 277: 35282-35288.
- [69] Kulich SM, Chu, CT. Sustained extracellular signal-regulated kinase activation by 6-hydroxy-dopamine: implications for Parkinson's disease. *J. Neurochem.* 2001;77:1058-1066.
- [70] Montolio M, Gregori-Puigjané E, Pineda D, Mestres J, Navarro P. Identification of small molecule inhibitors of amyloid  $\beta$ -induced neuronal apoptosis acting through the imidazoline I<sub>2</sub> receptor. *J. Med. Chem.* 2012;55(22):9838-46.
- [71] Zhang F, Ding T, Yu L, Zhong Y, Dai H, Yan M. Dexmedetomidine protects against oxygen-glucose deprivation-induced injury through the I<sub>2</sub> imidazoline receptor-PI3K/AKT pathway in rat C6 glioma cells. *J Pharm Pharmacol.* 2012;64(1):120-7.
- [72] Xuanfei L, Hao C, Zhujun Y, Yanming L, Jianping. Imidazoline I<sub>2</sub> receptor inhibitor idazoxan regulates the progression of hepatic fibrosis via Akt-Nrf2-Smad2/3 signaling pathway. *Oncotarget.* 2017;8(13):21015-21030.
- [73] García-Fuster, MJ, Miralles, A, and García-Sevilla, JA. Effects of opiate drugs on Fas-Associated Protein with Death Domain (FADD) and effector caspases in the rat brain: Regulation by the ERK1/2 MAP kinase pathway. *Neuropsychopharmacology* 2007;32:399-411.
- [74] Ramos-Miguel A, García-Fuster MJ, Callado LF, La Harpe R, Meana JJ, García-Sevilla JA. Phosphorylation of FADD (Fas-associated death domain protein) at serine 194 is increased in the prefrontal cortex of opiate abusers: relation to mitogen activated protein kinase, phosphoprotein enriched in astrocytes of 15 kDa, and Akt signaling pathways involved in neuroplasticity. *Neuroscience* 2009;161:23-38.
- [75] Papaliagkas V, Anogianaki A, Anogianakis G, Ilonidis G. The proteins and the mechanisms of apoptosis: A mini-review of the fundamentals. *Hippokratia* 2007;11:108-113.
- [76] Ramos-Miguel A, García-Sevilla JA, Barr A. et al. Decreased cortical FADD protein is associated with clinical dementia and cognitive decline in an elderly community sample. *Mol. Neurodegener.* 2017;12:26.
- [77] Chinnaiyan AM, O'Rourke K, Tewari M, Dixit VM. FADD, a novel death domain-containing protein, interacts with the death domain Fas and initiates apoptosis. *Cell.* 1997;81:505-512.



- [78] Scott FL, Stec B, Pop C, et al. The Fas-FADD death domain complex structure unravels signalling by receptor clustering. *Nature* 2009; 457:1019-1022.
- [79] Alappat EC, Feig C, Boyerinas B. et al. Phosphorylation of FADD at serine 194 by CKI $\alpha$  regulates its nonapoptotic activities. *Mol. Cell.* 2005;19:321-332.
- [80] O'Brien RJ, Wong PC. Amyloid precursor protein processing and Alzheimer's disease. *Annu. Rev. Neurosci.* 2011;34:185-204.
- [81] Gralle M, Botelho MG, Wouters FS. Neuroprotective secreted amyloid precursor protein acts by disrupting amyloid precursor protein dimers. *J. Biol. Chem.* 2016; 284:15016-15025.
- [82] Lichtenthaler SF. Alpha-secretase cleavage of the amyloid precursor protein: proteolysis regulated by signaling pathways and protein trafficking. *Curr. Alzheimer Res.* 2012;9:165-177.
- [83] El-Amouri SS, Zhu H, Yu J, Marr R, Verma IM, Kindy MS. Neprilysin: An Enzyme Candidate to Slow the Progression of Alzheimer's Disease. *Am. J. Pathol.*2008;172:1342-1354.

## SUPPLEMENTARY MATERIAL

**Table 1:** Antibodies used in Western blot studies.

Antibody	Host	Source/Catalog	WB dilution
PSD95	Rabbit	Abcam/ab18258	1:1000
Synaptophysin (SYN)	Rabbit	Dako/CloneSY38	1:2000
Caspase-3	Rabbit	BD Transduction Laboratories/C31720	1:1000
Bax	Rabbit	Cell Signaling/#2772	1:1000
Bcl-2	Rabbit	Cell Signaling/#2870	1:1000
Spectrin	Mouse	Millipore/MAB1622	1:1000
GSK3- $\beta$	Rabbit	Cell Signaling/#9315	1:1000
p-GSK3- $\beta$ (Ser9)	Rabbit	Cell Signaling/#9336	1:1000
AKT	Rabbit	Cell Signaling/#9272	1:1000
p-AKT (Ser473)	Rabbit	Cell Signaling/#D9E	1:1000
CREB	Rabbit	Cell Signaling/#48H2	1:1000
p-CREB (Ser133)	Rabbit	Cell Signaling/#87G3	1:1000
SOD1	Sheep	Calbiochem/574597	1:1000
sAPP $\beta$	Rabbit	Covance/SIG-39138-050	1:1000
sAPP $\alpha$	Rabbit	Covance/SIG-39139	1:1000
ERK $\frac{1}{2}$	Rabbit	Cell Signaling/#9102	1:1000
p-ERK $\frac{1}{2}$ (Thr202/Tyr204)	Rabbit	Cell Signaling/#9101	1:1000
CDK5	Rabbit	SantaCruz Biotech/sc-173	1:1000
p-CDK5	Rabbit	Abcam/ab63550	1:1000
GAPDH	Mouse	Millipore/MAB374	1:2000
p-Tau Ser396	Rabbit	Invitrogen/44752G	1:1000
p-Tau Ser404	Rabbit	Invitrogen/44758G	1:1000
Tau total	Goat	Santa cruz/sc-1995	1:1000
Rabbit-anti-sheep HRP conjugated		Abcam/ab97130	1:2000
Goat-anti-mouse HRP conjugated		Biorad/#170-5047	1:2000
Donkey-anti-goat HRP conjugated		Santa Cruz/sc-2020	1:2000
Goat-anti-rabbit HRP conjugated		Cell Signaling/#7074	1:2000
GAPDH	Mouse	Millipore/MAB374	1:5000
Actin	Mouse	Sigma-Aldrich/A5441	1:2500
Goat-anti-mouse HRP conjugated		Biorad/170-5047	1:5000
Goat-anti-rabbit HRP conjugated		Biorad/170-6515	1:5000
Donkey-anti-goat HRP conjugated		Santa Cruz/sc-2020	1:5000

**Table 2:** Primers and probes used in qPCR.

Target	Product size (bp)	Forward primer (5'-3')	Reverse primer (5'-3')
<i>Aox1</i>	286	CATAGGCGGCCAGGAACATT	TCCTCGTTCCAGAATGCAGC
<i>Cox2</i>	126	TGACCCCCAAGGCTCAAATA	CCCAGGTCCTCGCTTATGATC
<i>Il-1<math>\beta</math></i>	179	ACAGAATATCAACCAACAAGTGATATTCTC	GATTCTTTCCTTTGAGGCCCA
<i>Il-6</i>	189	ATCCAGTTGCCTTCTTGGGACTGA	TAAGCCTCCGACTTGTGAAGTGGT
<i>Tnf-<math>\alpha</math></i>	157	TCGGGGTGATCGGTCCCCAA	TGGTTTGCTACGACGTGGGCT
<i>Gfap</i>	125	CCTTCTGACACGGATTTGGT	ACATCGAGATCGCCACCTAC
<i>Adam10</i>	125	GGAAGAAATGCAAGCTGAA	CTGTACAGCAGGGTCTTGTAC
<i>NEP</i>	196	TTGGGAGACCTGGCGGAAAC	CATTCTTGGACCCTCACCCC
<i>Actin</i>	190	CAACGAGCGGTTCCGAT	GCCACAGGTTCCATACCCA

#### Taqman Probes

Target	Product size (bp)	Reference
<i>Hmox1</i>	69	Mm00516005_m1
<i>Tbp</i>	93	Mm00446971_m1

#### Parallel Artificial Membrane Permeation Assays- Blood-Brain Barrier (PAMPA-BBB)

To evaluate the brain penetration of the different compounds, a parallel artificial membrane permeation assay for blood-brain barrier was used, following the method described by Di et al.(2003). The *in vitro* permeability ( $Pe$ ) of fourteen commercial drugs through lipid extract of porcine brain membrane together with the test compounds were determined. Commercial drugs and assayed compounds were tested using a mixture of PBS:ETOH (70:30). Assay validation was made by comparing the experimental permeability with the reported values of the commercial drugs by bibliography and lineal correlation between experimental and reported permeability of the fourteen commercial drugs using the parallel artificial membrane permeation assay was evaluated ( $y=1,5481x-1,0128$ ;  $R^2=0,9405$ ). From this equation and taking into account the limits established by Di et al. for BBB permeation, we established the ranges of permeability as compounds of high BBB permeation (CNS+): $Pe(10^{-6}cm \cdot s^{-1}) > 5.179$  compounds of low BBB permeation(CNS-): $Pe(10^{-6}cm \cdot s^{-1}) > 2.083$  and compounds of uncertain BBB permeation(CNS $\pm$ ): $5,179 > Pe(10^{-6}cm \cdot s^{-1}) > 2.083$

Table 3 shows permeability results from the different commercial and assayed compounds (three different experiments in triplicate) and predictive penetration in the CNS.

**Table 3:** Permeability [ $Pe(10^{-6} \text{cm} \cdot \text{s}^{-1})$ ] in the PAMPA-BBB assay of 14 commercial drugs and tested compounds and predictive penetration in the CNS.

Compound	Bibliography value(a)	Experimental value(b) (n=3) $\pm$ S.D.	CNS Prediction
Verapamil	16,0	26,4 $\pm$ 0,5	
Testosterone	17,0	24,9 $\pm$ 0,4	
Costicosterone	5,1	6,7 $\pm$ 0,1	
Clonidine	5,3	6,5 $\pm$ 0,05	
Ofloxacin	0,8	0,99 $\pm$ 0,04	
Lomefloxacin	0,0	0,7 $\pm$ 0,04	
Progesterone	9,3	16,8 $\pm$ 0,0,3	
Promazine	8,8	13,8 $\pm$ 0,3	
Imipramine	13,0	12,3 $\pm$ 0,1	
Hydrocortisone	1,9	1,4 $\pm$ 0,05	
Piroxicam	2,5	1,9 $\pm$ 0,02	
Desipramine	12,0	17,8 $\pm$ 0,1	
Cimetidine	0,0	0,7 $\pm$ 0,03	
Norfloxacin	0,1	0,9 $\pm$ 0,02	
<b>MCR5</b>		13,5 $\pm$ 0,9	CNS+
<b>MCR9</b>		26,9 $\pm$ 1,7	CNS+

a) Taken from Di et al. (2003).

b) Values obtained by the authors

Di, L.; Kerns, E. H.; Fan, K.; McConnell, O. J.; CarTer, G. T. High throughput artificial membrane permeability assay for blood-brain barrier. *Eur. J. Med.Chem.* 2003, 38, 223-232.

\*Poor dissolution

## 3.2 Publication 2

### **Amelioration of BPSD-like phenotype and cognitive decline in SAMP8 mice model accompanied by molecular changes after treatment with I<sub>2</sub>-imidazoline receptor ligand MCR5**

Adapted from: **Vasilopoulou F**, Bagan A, Rodriguez-Arevalo S, Escolano C, Griñán-Ferré C, Pallàs M, *Pharmaceutics*. 2020 May 23;12(5):475.  
doi: <https://doi.org/10.3390/pharmaceutics12050475>.

## SUMMARY

Together with the cognitive symptoms, BPSD, including depressive and fear-anxiety-like behaviour constitute distressing major components of the disease, that affect the quality of life of both patients and their caregivers. I<sub>2</sub>-IR density has been shown altered in neuropsychiatric disorders including depressive syndromes, as well as in neurodegenerative diseases and AD. Thus, this work aimed to evaluate the effect of I<sub>2</sub>-IR ligand MCR5 on cognitive and non-cognitive symptoms exhibited by SAMP8 model of dementia and neurodegeneration. After oral administration of the I<sub>2</sub>-IR ligand MCR5 (5mg/kg for four weeks) in 10-month-old SAMP8 male mice, cognitive and BPSD status of the mice were evaluated by performing different behavioral tasks (Novel Object recognition test, Tail Suspension Test, Forced Swimming Test, Elevated Plus Maze, Open Field). Alterations in molecular pathways underlying depression, anxiety phenotype and memory loss after I<sub>2</sub>-IR treatment were assessed by molecular techniques.

I<sub>2</sub>-IR treatment with MCR5 attenuated depressive-like behavior and fear-anxiety-like behavior exhibited by SAMP8 male mice compared to sex and age matched SAMR1, delivering improvement as well in spatial and recognition memory. These beneficial effects were not attributed to interaction of the I<sub>2</sub>-IR ligand with serotonergic system since MCR5 neither displaced specific ligands 5-HT receptors nor altered their gene expression. Instead, MCR5 treatment enhanced AKT/mTOR/GSK3 $\beta$  pathways by increasing their protein levels in SAMP8 brains. Moreover, an increase in PKA and CREB levels was detected which was consistent with changes in NMDAR phosphorylation state, decrease in CDK5 and DARPP32 levels. MCR5 treatment reduced pro-inflammatory markers in SAMP8 brains with a parallel increase in PSD95 and amelioration of TrkB and NGFR signalling indicating that neuroinflammatory attenuation and synaptic plasticity increase could explain the cognitive and BPSD improvement.

Collectively, the results of this study highlight and increase the potential of highly selective I<sub>2</sub>-IR ligands as therapeutic agents in brain disorders associated with cognitive decline and age-related BPSD.

## Amelioration of BPSD-like phenotype and cognitive decline in SAMP8 mice model accompanied by molecular changes after treatment with I<sub>2</sub>-imidazoline receptor ligand MCR5

Foteini Vasilopoulou,<sup>1</sup> Andrea Bagán,<sup>2</sup> Sergio Rodríguez-Arévalo,<sup>2</sup> Carmen Escolano,<sup>2</sup> Christian Griñán-Ferré,<sup>1</sup> Mercè Pallàs<sup>1</sup>

<sup>1</sup>*Pharmacology Section. Department of Pharmacology, Toxicology and Medicinal Chemistry, Faculty of Pharmacy and Food Sciences, and Institut de Neurociències, University of Barcelona, Av. Joan XXIII, 27-31, 08028 Barcelona, Spain.*

<sup>2</sup>*Laboratory of Medicinal Chemistry (Associated Unit to CSIC), Department of Pharmacology, Toxicology and Medicinal Chemistry, Faculty of Pharmacy and Food Sciences, and Institute of Biomedicine (IBUB), University of Barcelona, Av. Joan XXIII, 27-31, 08028 Barcelona, Spain.*

**Keywords:** I<sub>2</sub>-imidazoline receptors; BPSD; BDNF; neuroinflammation; age.

### ABSTRACT

Behavioural and Psychological Symptoms of Dementia (BPSD), including fear-anxiety- and depressive-like behaviour, are present in Alzheimer's disease (AD), together with memory decline. I<sub>2</sub>-imidazoline receptors (I<sub>2</sub>-IRs) have been associated with neuropsychiatric and neurodegenerative disorders, further, I<sub>2</sub>-IR ligands have demonstrated a neuroprotective role in the central nervous system (CNS). In this study, we assessed the effect of the I<sub>2</sub>-IR ligand MCR5 on both cognitive and non-cognitive symptoms in the Senescence accelerated mice prone 8 (SAMP8) mouse model. Oral administration of I<sub>2</sub>-IR ligand MCR5 (5mg/kg/day for four weeks) in 10-month SAMP8 mice ameliorated both BPSD-like phenotype and cognitive decline by attenuating depressive-like behaviour, reducing fear-anxiety-like behaviour and improving cognitive performance using different tasks. Interaction of I<sub>2</sub>-IR ligand MCR5 with serotonergic system did not account for behavioral or cognitive improvement, although changes in molecular pathways underlying depression and anxiety phenotype were observed. MCR5 increased levels of p-AKT, phosphorylated Glycogen synthase kinase 3  $\beta$  (GSK3 $\beta$ ) at Ser9 and phosphorylated mammalian target of rapamycin complex 1 (mTORC1) levels in SAMP8 treated mice compared to SAMP8 control. Moreover, MCR5 treatment altered NMDA2B phosphorylation, and decreased the protein levels of phosphorylated Cyclin-Dependent Kinase 5 (p-CDK5) and dopamine- and cAMP-regulated phosphoprotein of Mr 32 kDa phosphorylated at Thr75 (p-DARPP32), with a parallel increase in PKA and p-CREB levels. Consistent with these changes MCR5 attenuated neuroinflammation by decreasing expression of pro-inflammatory markers such as Tumor necrosis factor-alpha (Tnf- $\alpha$ ), Interleukin 1 $\beta$  (Il-1 $\beta$ ), Interleukin 6 (Il-6), and promoted synaptic plasticity by increasing levels of Postsynaptic density protein 95 (PSD95)

as well as ameliorating Tropomyosin-related kinase B (TrkB) and Nerve growth factor receptor (NGFR) signalling. Collectively, these results increase the potential of highly selective I<sub>2</sub>-IR ligands as therapeutic agents in age-related BPSD and cognitive alterations.

### 3.2.1 INTRODUCTION

Nowadays, the global population of the elderly is increasing in parallel to the diagnosis of neurodegenerative diseases (ND) and psychiatric disorders. Thus, ageing is the main factor associated with ND, such as Alzheimer's disease (AD), which is the leading cause of dementia [1]. So far, the AD research has mainly focused on cognitive impairment and typical AD hallmarks, although no effective treatments are able to reduce or halt the progression of the disease [2].

On the other hand, non-cognitive symptoms are becoming increasingly important due to their prevalence, generating several dysfunctions and representing one of the most troublesome domains of treating dementia [3]. These non-cognitive symptoms that patients suffer, commonly referred to as "Behavioral and psychological symptoms of dementia" (BPSD), mainly include aberrant motor behaviour, hallucinations, aggressive and anxiety behaviour and depression, among others [4]. The importance of BPSD is increasing due to several of them can be treated effectively, while the mechanisms are still poorly understood. In AD, the patients present BPSD since the early stages [5], which, as the disease is progressing, tend to increase their frequency. BPSD are the cause of higher morbidity and poor quality of life for patients and caregivers [6]. Approximately between 40% and 60% of AD patients experience anxiety and depressive symptoms [7]. Therefore, these symptoms are associated with cognitive impairment, increasing the risk of persistence for mild cognitive impairment (MCI) and dementia, being both the most common psychiatric syndromes [8, 9].

The biogenic monoamine 5-hydroxytryptamine (5-HT), or serotonin, has been tied to cognitive decline and multiple other BPSD domains [10, 11], while it is well-known that loss in serotonin transporters and changes in synaptic proteins can fire mechanisms linked to depression by alteration of specific cerebral circuits [12]. Several studies support that the mechanisms underlying the complex manifestations of anxiety and depressive illness involve dysregulation of brain-derived neurotrophic factor (BDNF) [13, 14] and N-methyl-d-aspartate receptor (NMDAR) [15], promoting disturbances in cellular signalling and neuronal plasticity. Among cellular pathways affected in the pathophysiology of depression, we can name the mammalian target of rapamycin (mTOR), mitogen-activated protein kinases (MAPK) or glycogen synthase kinase 3 (GSK-3) is discussed.

I<sub>2</sub>-Imidazoline receptors (I<sub>2</sub>-IRs) have been progressively attracting scientific interest as a



promising biological target, which modulation could result in potential therapeutic effects. Several preclinical studies describe I<sub>2</sub>-IRs involvement in neurological diseases such as AD, Parkinson's disease (PD) and multiple psychiatric disorders [16–18]. I<sub>2</sub>-IRs have been associated with anxiety and depressive behaviours [16, 19]. In preclinical models of mood disorders, several I<sub>2</sub>-IR ligands exerted beneficial effects on non-cognitive symptoms [20, 21]. Interestingly, agmatine, the endogenous I<sub>2</sub>-IR ligand [22], has a modulatory effect on anxiety and depression [23, 24]. Specifically, those studies that had utilized allegedly  $\alpha_2$ -selective imidazoline radioligands, i.e., [<sup>3</sup>H]-clonidine, could be reinterpreted in terms of the increased number of those receptors in depression. Although the molecular identity of the I<sub>2</sub> binding site remains unknown, an I<sub>2</sub> binding site has been reported to be encoded by monoamine oxidase genes (both MAO-A and MAO-B), suggesting a novel explanation for the antidepressant efficacy of idazoxan, a prototypic I<sub>2</sub>-IR ligand. We have previously described, MCR5 diethyl [(1-(3-chloro-4-fluorobenzyl)-5,5-dimethyl-4-phenyl-4,5-dihydro-1H-imidazol-4-yl)phosphonate] (Fig 1A) as an I<sub>2</sub>-IR highly selective compound over  $\alpha_2$ -adrenoreceptors and high affinity for the I<sub>2</sub>-IR [25], characterized by neuroprotective abilities in models of cognitive decline and AD [26, 27].

The senescence-accelerated mouse prone 8 (SAMP8) is an accelerated ageing model, established through phenotypic selection from a common genetic pool of AKR/J-strain of mice [28–30]. Besides the age-related cognitive decline that mainly characterizes the SAMP8 model, this strain also displays anxiety- and depressive-like behaviour in comparison to their senescence-acceleration resistant counterparts, SAMR1 mice [28]. In particular, the SAMP8 mouse presents alterations in the serotonergic system and BDNF expression, calcium signalling pathways and increased neuroinflammation that lead to the development of BPSD and in particular depressive-like behaviour [31]. Collectively, therefore it is believed that this rodent model is appropriate for studying depressive-like behaviour in an aged population with cognitive impairment.

In the present study, we assessed the cognitive and non-cognitive effects, especially anxiety- and antidepressant-like effects as the main BPSD behaviours of the I<sub>2</sub>-IR ligand MCR5 diethyl [(1-(3-chloro-4-fluorobenzyl)-5,5-dimethyl-4-phenyl-4,5-dihydro-1H-imidazol-4-yl)phosphonate] *in vivo*, providing as well the evidence referred to induced molecular changes that could explain such effects, using the SAMP8 mice model. As aforementioned, MCR5 tested in previous works of our group, presented neuroprotective and analgesic effects, showed promising results in models of brain damage [26] and prevented cognitive decline in SAMP8 aged female mice, including molecular changes associated with age and neurodegenerative processes [27]. Thus, we studied some molecular pathways related to neurodegeneration and neuropsychiatric disorders that are characteristic of age-related behavioural and cognitive abnormalities of SAMP8.

### 3.1.3 METHODS

#### Animals

SAMR1 (n=11) and SAMP8 (n=25) male mice (10-month-old) were used to perform behavioural and molecular analyses. The animals were divided randomly into three groups: SAMR1 Control (SR1-Ct) (n=11), SAMP8 Control (SP8-Ct) (n=11) and SAMP8 treated with I<sub>2</sub>-IR ligand MCR5 (5mg/Kg) (SP8-MCR5) (n=14). Animals had free access to food and water and were kept under standard temperature conditions (22±2°C) and a 12-h light/dark cycle (300 lux/0 lux). Control groups received water plus vehicle (1.8% 2-hydroxypropyl-β-cyclodextrin). MCR5 (5 mg/Kg/day) was dissolved in vehicle and administered through drinking water for 4 weeks. Water consumption was controlled each week, and I<sub>2</sub>-IR ligand concentrations in water were adjusted accordingly to reach the optimal dose.

All experimental procedures involving animals followed the standard ethical guidelines of European Communities Council Directive 86/609/EEC and by the Institutional Animal Care and Use Committee of the University of Barcelona (670/14/8102, approved at 11/14/2014) and by Generalitat de Catalunya (10291, approved 1/28/2018).

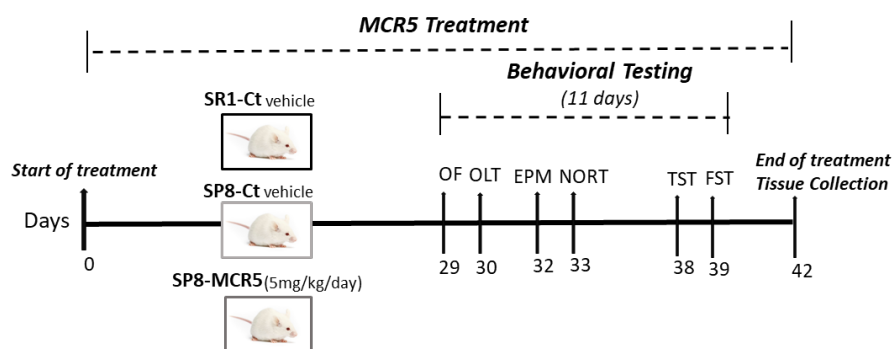


**Figure 1:** Scheme of experimental design.

#### Evaluation of anxiety- and depressive-like behaviour as well as cognitive performance

##### *Tail suspension test (TST)*

Briefly, to evaluate the potential anti-depressant effect of MCR5 in mice. Animals were suspended by their tails leads to an immobile posture using adhesive tape and hung approximately 30 cm above the table. The fragments, 17 cm each, of tape, were cut and an imprint 2 cm, on each fragment, was placed from one end. The task lasts for 6 min, and the duration of immobility was evaluated manually. Passively hanging was considered as immobility. The total time of mobility was subtracted from the 6 min of task time and was

declared as the immobility time [32, 33].

#### *Forced Swimming Test (FST)*

The cylindrical tank (10 cm internal diameter, 50 cm high) filled with water (10 cm height) at 22–25 °C required for mice forced to swim for 6 min. The mice behaviour to avoid the aversive situation was recorded during this time. The session was videotaped, and the time that each mice remain mobile was entirely analyzed. The total time of mobility was subtracted from the 6 min of task time and was called as the immobility time. The mice were considered as immobile when they keep floating, doing only those movements necessary to maintain their heads out of the water [34].

#### *Elevated Plus Maze (EPM)*

The anxiety-related behaviour was assessed by elevated plus maze (EPM) [35]. The apparatus consisted of two open arms (30×5×15 cm), and two enclosed arms (30×5×15 cm) positioned 40 cm above the ground. The junction of four arms formed a central square platform (5×5 cm). Each mouse was located on the central platform facing and was allowed to move freely for 5 min. The behaviour parameters evaluated were the number of entries in the open arms and the percentage of time spent in the open and closed arms, among others, scored with SMART® vers.3.0 software. In addition, the anxiety index was calculated as follows: Anxiety Index =  $1 - \frac{([\text{Open arm time}/\text{Test duration}] + [\text{Open arms entries}/\text{Total number of entries}])}{2}$  [36]. The tests were recorded using a camera attached to the roof and located above the apparatus.

#### *Open Field Test (OFT)*

In brief, the OFT was performed using a wall-enclosed area as previously described [37]. The ground was divided into two defined as the center and peripheral areas. Behaviour was evaluated with SMART® ver.3.0 software, and each test was recorded for later evaluation using a camera located above the apparatus. Mice were located at the center and allowed to explore the white polywood box (50×50×25cm) for 5 minutes. Then, the animals were returned to their home cages, and the OFT apparatus was cleaned with 70% ethanol (EtOH). The parameters measured included center time duration, rearings, defecations, and the locomotor activity, calculated as the sum of global distance moved in the arena for 5 minutes.

### *Novel Object Recognition Test (NORT)*

In brief, mice were located in a 90°, two-arm, 25x20x5 cm black maze. The walls could be removed for easy cleaning. Before the memory phase, a 3-day-habituation was performed in which the mice were located individually in the apparatus for 10 min. On day 4, the familiarization phase took place, in which the animals were placed in the maze in the presence of two identical, novel objects (A+A) or (B+B) located at the end of each corner arm. During this 10-min acquisition trial, the mice were allowed to explore the two identical objects. After 2 h and 24 h from that trial, the animals were submitted to a 10-min retention trial in which one of the two objects was replaced by a novel object. The behaviour of the mice was recorded during the 2 h and 24 h retention trials using a camera attached to the roof and located above the apparatus. The time spent exploring the new object (TN) and the time spent exploring the old one (TO) were evaluated manually and the discrimination index (DI) was calculated as  $(TN-TO)/(TN+TO)$  [38]. To avoid olfactory cues, 70% EtOH was used to clean the arms and objects after test.

### *Object Location Test (OLT)*

The test was performed in a cage (50 × 50 × 25 cm), in which three walls were white except one that was black and lasted 3 days. On day 1, mice were familiarized to the arena for 10-min. On day 2, two identical objects (A+A) were located in front of the black wall, and the mice were freely allowed to explore both objects for 10 min (Trial 1 - training phase). On day 3, after a retention period of 24 h mice were returned to the testing arena for another 10 min (Trial 2 – testing phase) with one object moved to a different position (opposite direction toward the black wall) and were allowed to explore. The trials were recorded, and the object exploration time was measured manually. The time sniffing the object in the old position (PO) and the time exploring the object in the new position (TN) were evaluated. The DI defined as  $(PN-TO)/(PN+PO)$  was determined as an indicator of the cognitive performance [39]. For the elimination of olfactory cues, 70% EtOH was used to clean the testing arena after each trial.

## **Determination of transporters, receptors and alterations in molecular pathways**

### *In Vitro Pharmacology: Binding Assays*

The purpose of this study was to test MCR5 in Binding assays by using Eurofins radioligand assays. Briefly, binding for receptors 5-HT1A, 5-HT1B, 5-HT2A, 5-HT2B, ion channel 5-HT3 and 5-HT transporter (SERT) was studied using radioactively labelled ligands specific for each target in human recombinant cell lines (For details see Table S6). MCR5 was tested at 10  $\mu$ M. MCR5 interaction was calculated as a % inhibition of the binding

of a radioactively labelled ligand specific for each target. Percentages were calculated as follow: percent inhibition of control specific binding =  $100 - [(measured\ specific\ binding / control\ specific\ binding) * 100]$ . Results showing an inhibition or stimulation higher than 50% are considered to represent significant effects of the test compounds.

*Tissue preparation for biochemical analysis* Euthanized mice by cervical dislocation 3 days after the behavioural and cognitive tests were finished. Brains were immediately dissected out from the skull. The hippocampus of each animal was separated, snap frozen in dry ice and kept at  $-80^{\circ}\text{C}$ .

For Western Blot (WB) and immunodetection, hippocampus samples were thawed and mixed in lysis buffer containing phosphatase and protease inhibitors (Cocktail II, Sigma-Aldrich). Once mixed, samples were maintained on ice for 30min. Samples were centrifugated at  $10,000\times g$  for 30 minutes at  $4^{\circ}\text{C}$ , and the supernatants were collected and saved at  $-80^{\circ}\text{C}$ . Total protein amounts were obtained, and the Bradford method was used to determine protein concentration.

For ELISA evaluation, samples were processed following the instructions provided by the kit manufacturer (Biosensis). In brief, hippocampus samples were thawed and mixed through sonication at  $4^{\circ}\text{C}$  in 200 volumes of RIPA buffer (50 mM Tris-HCl, 150 mM NaCl, 1% (v/v) NP-40 and 0.5% (w/v) sodium deoxycholate, pH=7,5–8) containing a protease and phosphatase inhibitor cocktail. Once mixed, samples were maintained on ice for 30min. Sample sonication and cooling with ice were performed. Samples were centrifuged at  $14,000\times g$  for 30min at  $4^{\circ}\text{C}$ , and the supernatants were obtained and maintained at  $-80^{\circ}\text{C}$ . Protein amount was quantified through the Bradford method.

#### *Protein levels determination by Western blot*

For WB, aliquots of 15  $\mu\text{g}$  of hippocampal protein were used. Protein samples were isolated by Sodium dodecyl sulphate-Polyacrylamide gel electrophoresis SDS-PAGE (8-15%) and transferred onto PVDF membranes (Millipore). The membranes were blocked in 5% non-fat milk or 5% bovine serum albumin (BSA) in Tris-buffered saline (TBS) solution with 0.1% Tween 20 (TBS-T) during 1 h at room temperature. Next, the membranes were incubated overnight at  $4^{\circ}\text{C}$  containing the primary antibodies listed in Table S1. The antibodies were dissolved in TBS-T with 5% BSA or 5% non-fat milk.

Membranes were cleaned and incubated with the secondary antibodies for 1 h at room temperature. Immunoreactive proteins were detected with a chemiluminescence-based detection kit, following the manufacturer's protocol (ECL Kit, Millipore). Digital images were collected using a ChemiDoc XRS+ System (BioRad). Semi-quantitative analyses of

the band intensities were carried out using ImageLab software (BioRad), and results were expressed in arbitrary units (AU). Values were normalized to Glyceraldehyde-3-phosphate dehydrogenase (GAPDH) or  $\beta$ -Actin.

#### *Determination of proBDNF and mBDNF levels in the hippocampus*

The hippocampal determination of pro-Brain-derived neurotrophic factor (proBDNF) and mature-Brain-derived neurotrophic factor (mBDNF) protein levels was made according to the instructions of the ELISA kit (Biosensis). 2.3.5. RNA extraction and gene expression determination RNA isolation from hippocampal samples was performed using the TRIzol® reagent according to the manufacturer's protocols (Bioline Reagent). The yield, purity and quality of RNA were determined with a NanoDrop™ND-1000 (Thermo Scientific) apparatus and an Agilent 2100B Bioanalyzer (Agilent Technologies). RNAs with 260/280 ratios and RIN higher than 1.9 and 7.5, respectively, were collected. Reverse Transcription-Polymerase Chain Reaction (RT-PCR) was performed as follows: 2  $\mu$ g of messenger RNA (mRNA) was reverse-transcribed using the high capacity cDNA reverse transcription kit (Applied Biosystems). Real-time quantitative PCR (qPCR) was employed to quantify the mRNA expression of the genes evaluated listed in Table S2. SYBR® Green real-time PCR was performed using a Step One Plus Detection System (Applied-Biosystems) employing SYBR® Green PCR Master Mix (Applied-Biosystems). Each reaction mixture contained 6.75  $\mu$ L of complementary DNA (cDNA) (2 $\mu$ g concentration), 0.75  $\mu$ L of each primer (100nM concentration), and 6.75  $\mu$ L of SYBR® Green PCR Master Mix (2X).

Data were measured using the comparative cycle threshold (Ct) method ( $\Delta\Delta$ Ct), where the housekeeping gene expression  $\beta$ -Actin was used to normalize differences in sample loading and preparation. Each sample was evaluated per duplicate, and the results represent the n-fold difference of the gene expression among groups.

#### **Data acquisition and statistical analysis**

Data are expressed as mean  $\pm$  standard error of the mean (SEM). Statistical analyses were performed using One-Way analysis of variance (ANOVA) with the Tukey's as a post hoc tests or two-tail Student's t-test if it was necessary through GraphPad Prism ver. 8 for Mac (GraphPad Software). Statistical differences were considered significant when values of p were  $< 0.05$ . Statistical outliers were discriminated using Grubbs' test and were removed from the analysis.

### 3.2.3 RESULTS

#### **I<sub>2</sub>-IR ligand MCR5 reduced cognitive loss in SAMP8 male mice**

NORT and OLT revealed robust impairment in working, and spatial memory in SAMP8 control in comparison with age and sex mated SAMR1 control (Figs 2B-D). Remarkably, after treatment with MCR5, a significant increase in the discrimination index (DI) was obtained both in the NORT short-term memory test (Fig 2B) and the NORT long-term memory test in treated SAMP8 compared to the SAMP8 control group (Fig 2C). Moreover, DI for treated SAMP8 group was closer to DI delivered by SAMR1, indicating a neuro-protective effect for MCR5. Similarly, in OLT, I<sub>2</sub>-IR treatment significantly improved spatial memory in treated SAMP8 compared to the SAMP8 control group by increasing the DI, further demonstrating the beneficial effect of MCR5 on cognitive loss associated to age in SAMP8 mice (Fig 2D). The summary data of the NORT and OLT are presented in Supplementary Table S3.

#### **I<sub>2</sub>-IR ligand MCR5 improved emotional parameters associated with fear- anxiety- and depressive-like behaviours in SAMP8 male mice**

To evaluate the anti-depressant like effect of MCR5, we assessed the TST and FST. By one hand, an increase in both immobility and floating time was obtained from the TST and FST respectively between SAMR1 and SAMP8 control groups (Figs 3A-F), corroborating the depressive-like behaviour described in SAMP8 mice. On the other hand, MCR5 treatment induced a significant decrease in time of immobility and/or floating in treated SAMP8 when compared to SAMP8 control. Therefore, in both widely used tests for the study of depression-like behaviour, we were able to observe that MCR5 treatment reversed the depressive-like signs that SAMP8 mice exhibit, driving them to a similar behaviour to SAMR1. Behavioural and emotional changes after MCR5 treatment were evaluated by EPM and OFT. Regarding the EPM, although there were found no differences in the anxiety-like phenotype between the SAMR1 control group and SAMP8 control group, MCR5 treatment induced an anxiolytic effect on SAMP8 mice in comparison with both control groups (Fig 3G). Additional parameters measured in the EPM are presented in Supplementary Table S4. The OFT demonstrated that SAMP8 control group exhibited increased fear, presenting decreased time spent in center as well as vertical activity or rearings (Figs 3H-I). Strikingly, MCR5 treatment induced an anxiolytic effect on SAMP8 mice in comparison with the SAMP8 control group (Figs 3H-I). Furthermore, according to the results obtained in the OFT paradigm, locomotor activity was improved in SAMP8 treated group (Fig 3J). Additional parameters and statistical scores obtained in the OFT are depicted in Supplementary Table S5. Thus, results obtained in both EPM and OFT demonstrated changes in fear-anxiety-like behaviour and locomotor activity after treatment

with MCR5.

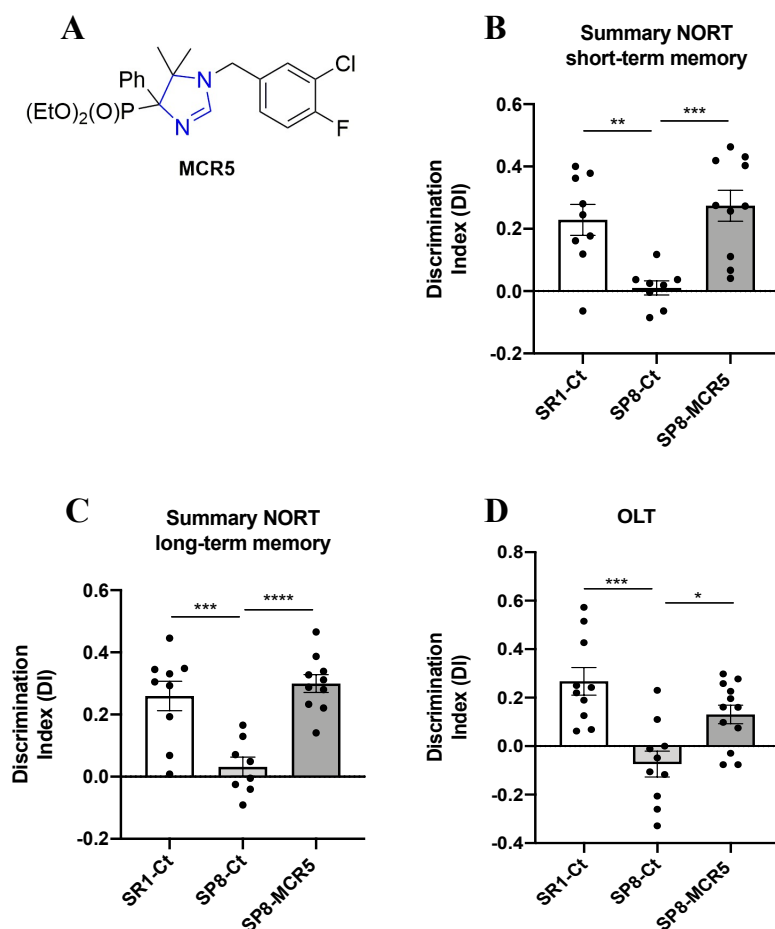


**Figure 2:** Structure of I<sub>2</sub>-IR ligand MCR5 (A). Results of Novel object recognition test (NORT), and Object location test (OLT) in male mice at 10-month-old SR1 and SP8 Ct mice groups and SP8 treated with I<sub>2</sub>-IR ligand MCR5 (5mg/Kg) mice group. For NORT: Summary of Discrimination Index (DI) from short-term memory (B), and summary of DI from long-term memory (C). For OLT: Summary of DI (D). Values represented are mean ± Standard error of the mean (SEM); n = 36 (SR1-Ct n = 11; SP8-Ct n = 11; SP8-MCR5 n = 14). \*p<0.05; \*\*p<0.01; \*\*\*p<0.001; \*\*\*\*p<0.0001.

### Interaction of I<sub>2</sub>-IR ligand MCR5 with serotonin receptors and transporter

Provided that the serotonergic system is implicated in depressive behaviour, it was worth paying attention to the effect of MCR5 on serotonin receptors and transporter. Binding studies with 10 μM MCR5 to the 5-HT receptors and 5-HT transporter were performed by Eurofins (<https://www.eurofinsdiscoveryservices.com/>). The experiment was performed following Eurofins validation Standard Operating Procedure. The compound binding was calculated as a % inhibition of the binding of each radioactively labelled ligand specific for its target. Results indicated that MCR5 did not display a specific capacity to displace specific ligands for 5-HT1A, 5-HT1B, 5-HT2A, 5-HT2B, ion channel 5-HT3 and 5-HT transporter (Table S6). Moreover, we studied the gene expression of 5-HT1A, 5-HT1B



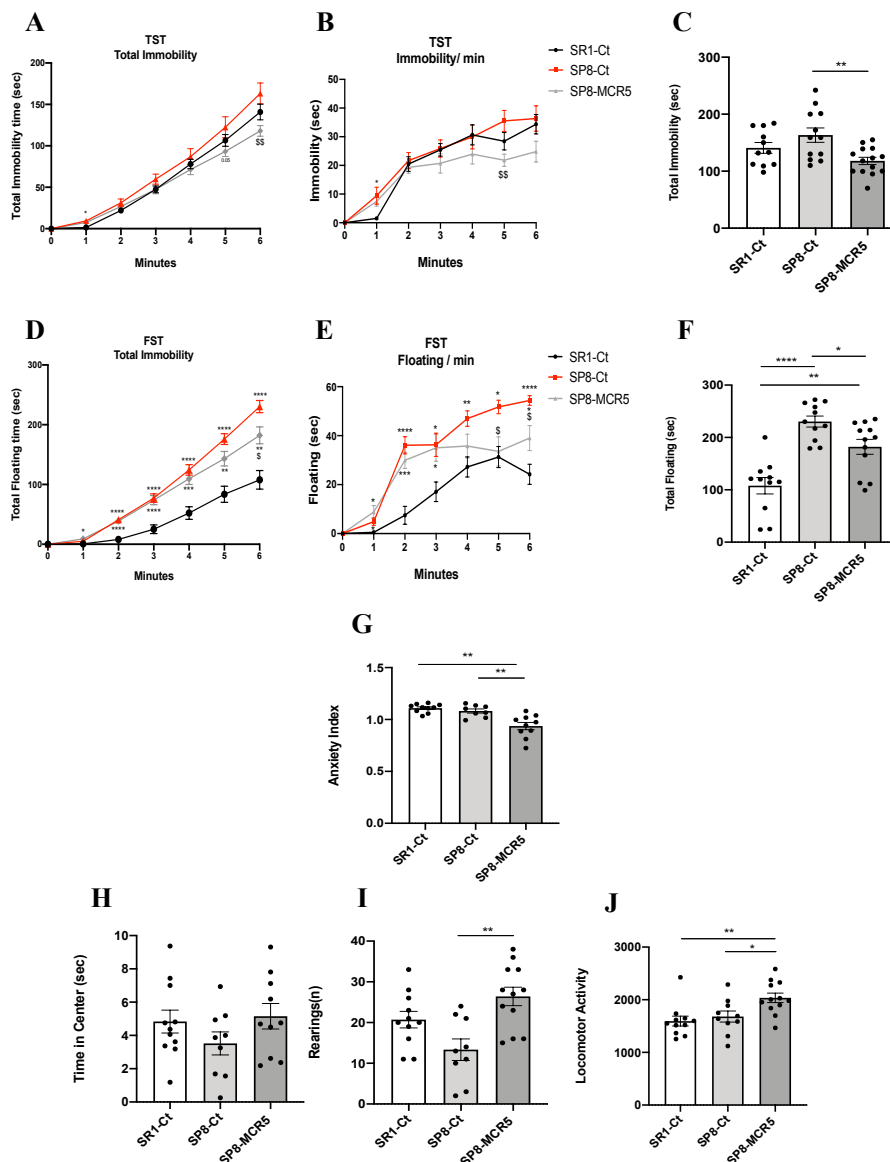


**Figure 3:** Results of Tail suspension test (TST), Forced swimming test (FST), Elevated plus maze (EPM), and Open field test (OFT) in male mice at 10-month-old SR1 and SP8 Ct mice groups and SP8 treated with I<sub>2</sub>-IR ligand MCR5 (5mg/Kg) mice group. For TST: total immobility curve (A), immobility/min (B), and total immobility (C). For FST: total immobility curve (D), floating/min (E), and total floating (F). For EPM: anxiety index (G). For OFT: time in the center (H), rearings (I), and locomotor activity (J). Values represented are mean  $\pm$  Standard error of the mean (SEM); n = 36 (SR1-Ct n = 11; SP8-Ct n = 11; SP8-MCR5 n = 14). \*p<0.05; \*\*p<0.01; \*\*\*p<0.001; \*\*\*\*p<0.0001.

and 5-HT<sub>2A</sub> receptors. As described, SAMP8 only presented a significant reduction in gene expression of 5-HT<sub>1A</sub> and 5-HT<sub>2A</sub> receptors compared to the SAMR1 control group (Fig 4A). Interestingly, treatment with MCR5 was only able to produce slight restoration of 5-HT<sub>2A</sub> gene expression in SAMP8 (Fig 4A). Likewise, protein levels of SERT were unchanged between SAMR1 and SAMP8 control groups, and the MCR5 treatment did not alter the transporter's protein levels (Figs 4B-C).

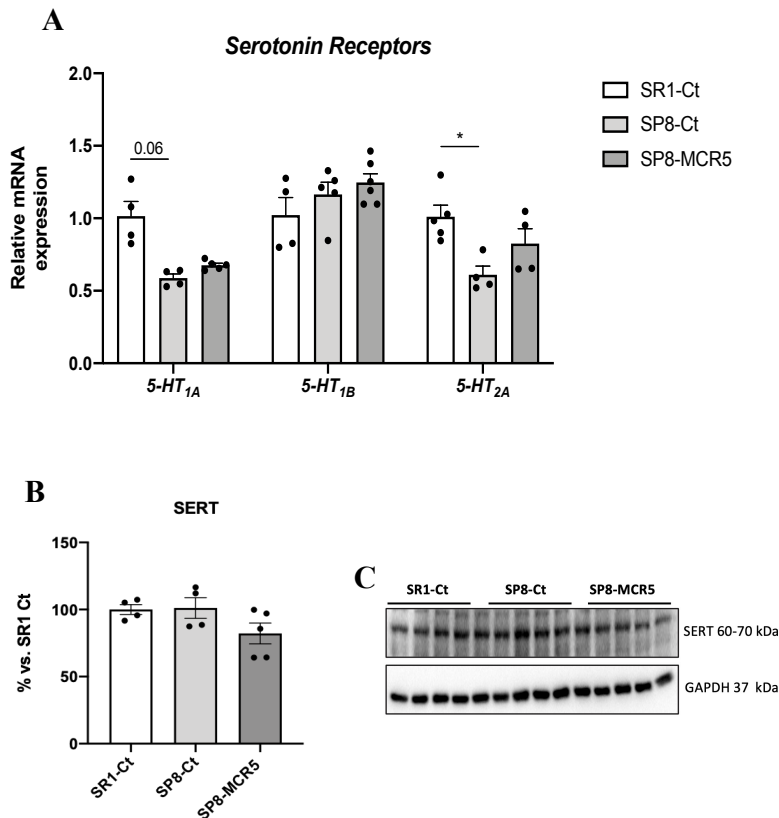


**Figure 4:** Representative gene expression for *5-HT1A*, *5-HT1B*, and *5-HT2A* (A). Representative Western Blot and quantification for SERT (B-C). Gene expression levels were determined by real-time PCR. Values in bar graphs are adjusted to 100% for protein levels of the control SAMR1 (SR1-Ct). Values are the mean  $\pm$  Standard error of the mean (SEM); (n = 4-6 for each group). \*p<0.05.

### MCR5 enhanced AKT/mTOR/GSK3 $\beta$ pathways promoting a reduction of pro-inflammatory cytokines in SAMP8 male mice

Critical proteins linked to molecular pathways that are altered in the pathology of depression associated with neuronal inflammation were evaluated. WB analysis showed a significant decrease in p-AKT/AKT ratio (protein kinase B) in SAMP8 control in comparison with the SAMR1 control group. MCR5 administration to SAMP8 promoted a significant increase in p-AKT/AKT ratio compared to SAMP8 control (Figs 5A and 5H). We observed a slight but not significant increase in Phosphatidylinositol 3,4,5-trisphosphate 3-phosphatase (PTEN) protein levels in SAMP8 mice in comparison with SAMR1. Conversely, we found a significant diminution in PTEN levels in SAMP8 treated mice compared to the SAMP8 control group (Figs 5B and 5H). Accordingly, protein levels of GSK3 $\beta$  phosphorylated in Ser9 (p-GSK3 $\beta$ (Ser9)) were significantly increased after MCR5 treatment in SAMP8 mice. No significant changes between SAMR1 control and SAMP8 control were determined for this kinase (Figs 5C and 5H). On the other hand, p-mTOR/mTOR ratio was unaltered among the three experimental groups. (Figs 5D and 5I). Interestingly, MCR5 increased

in a significant way p-TORC1/TORC1 ratio in SAMP8 treated mice compared to both control groups (Figs 4E and 4H). Lastly, albeit did not reach significance, a tendency to increase p-p70S6K/p70S6K ratio after I<sub>2</sub>-IR ligand treatment compared to both control groups, was observed (Figs 5F and 5H).

Considering the results obtained on these pathways, we studied pro-inflammatory cytokines markers in the hippocampus of SAMR1 and SAMP8 mice. Significantly increased gene expression of *Il-1β* and *Il-6* in SAMP8 control in comparison with SAMR1 mice was determined, confirming the inflammatory phenotype related to anxiety- and depressive-like behaviours presented by SAMP8 (Fig 5H). A significant reduction of *Tnf-α* gene expression in MCR5 treated SAMP8 mice group compared to both control groups was found (Fig 5I). By last, a tendency to reduce *Il-1β* and *Il-6* gene expression in MCR5 treated SAMP8 mice group compared to the SAMP8 control group, restoring levels to those of SAMR1 control strain was found (Fig 5I). Jointly with the decrease in the proinflammatory cytokines, an increase in the anti-inflammatory cytokine ratio, TGF-1β monomer/dimer was induced by MCR5 in SAMP8 treated mice (Figs 5H and 5G).

#### **Changes in PKA/CREB and NMDAR/CDK5/DARPP32 signalling cascades after treatment with I<sub>2</sub>-IR ligand MCR5 in SAMP8 male mice**

A significant increase in PKA protein levels was found after MCR5 treatment in SAMP8 compared to untreated SAMP8 control, which expressed slightly lower levels of the mentioned kinase in comparison with SAMR1 control (Figs 6A and 6G). Accordingly, we found a diminished p-CREB/CREB ratio in SAMP8 mice group compared to SAMR1 mice group, and MCR5 treatment restored the ratio in SAMP8 treated mice to SAMR1 levels (Figs 6B and 6G). A significant increase in the p-NMDA2B/NMDA2B ratio between the SAMR1 control, and SAMP8 control was observed (Figs 6C and 6G), and MCR5 increased p-NMDA2B/NMDA2B ratio in treated SAMP8 mice in comparison with the SAMP8 control. Moreover, we determined a significant reduction in the p-CDK5/CDK5 ratio between SAMR1 control and SAMP8 control (Figs 6D and 6G). Besides, a significant reduction in the p-CDK5/CDK5 ratio in SAMP8 treated mice group in comparison with the SAMP8 control mice was found. Conversely, we found reduced p-DARPP32 (Thr75)/DARPP32 ratio in the SAMR1 control group and SAMP8 treated group compared to the SAMP8 control, being significant only in the SAMP8 treated group (Figs 6E and 6G). Finally, we found significantly higher levels of ratio p-Erk<sub>1/2</sub>/Erk<sub>1/2</sub> were determined in SAMP8 control mice when compared to SAMR1 control, whereas MCR5 restored p-Erk<sub>1/2</sub>/Erk<sub>1/2</sub> to SAMR1 levels (Figs 6F and 6G).

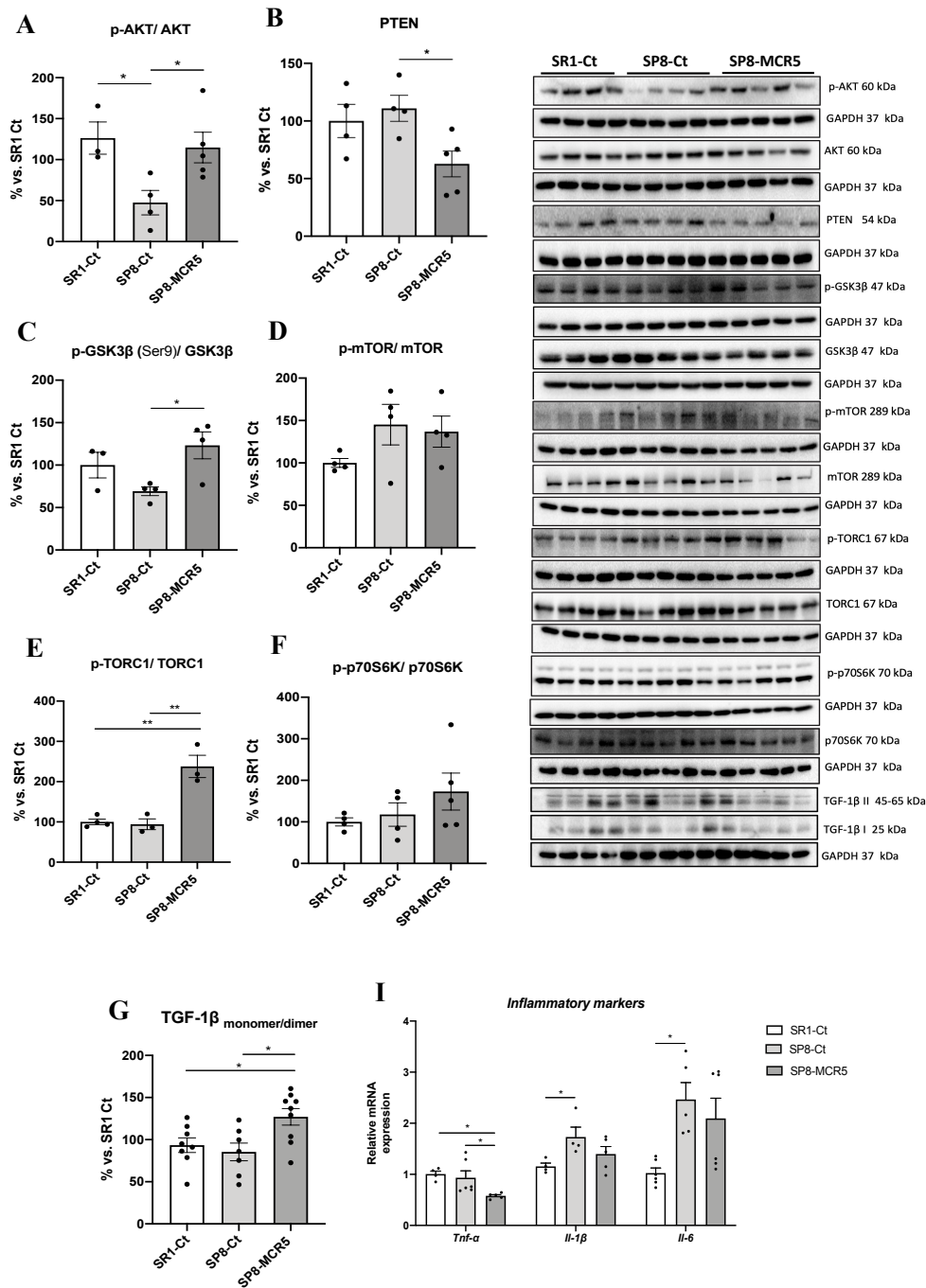


**Figure 5:** Representative Western blots and quantifications for the ratio of p-AKT/AKT, PTEN, ratio p-GSK3β(Ser9)/GSK3β, ratio p-mTOR/mTOR, ratio p-TORC1/TORC1, p-p70S6K/p70S6K, and TGF-1β monomer/dimer (A-H). Values in bar graphs are adjusted to 100% for protein levels of the control SAMR1 (SR1-Ct). Representative gene expression for *Tnf-α*, *Il-1β*, and *Il-6* (I). Gene expression levels were determined by real-time PCR. Values are the mean ± Standard error of the mean (SEM); (n = 4-6 for each group). \*p<0.05; \*\*p<0.01.

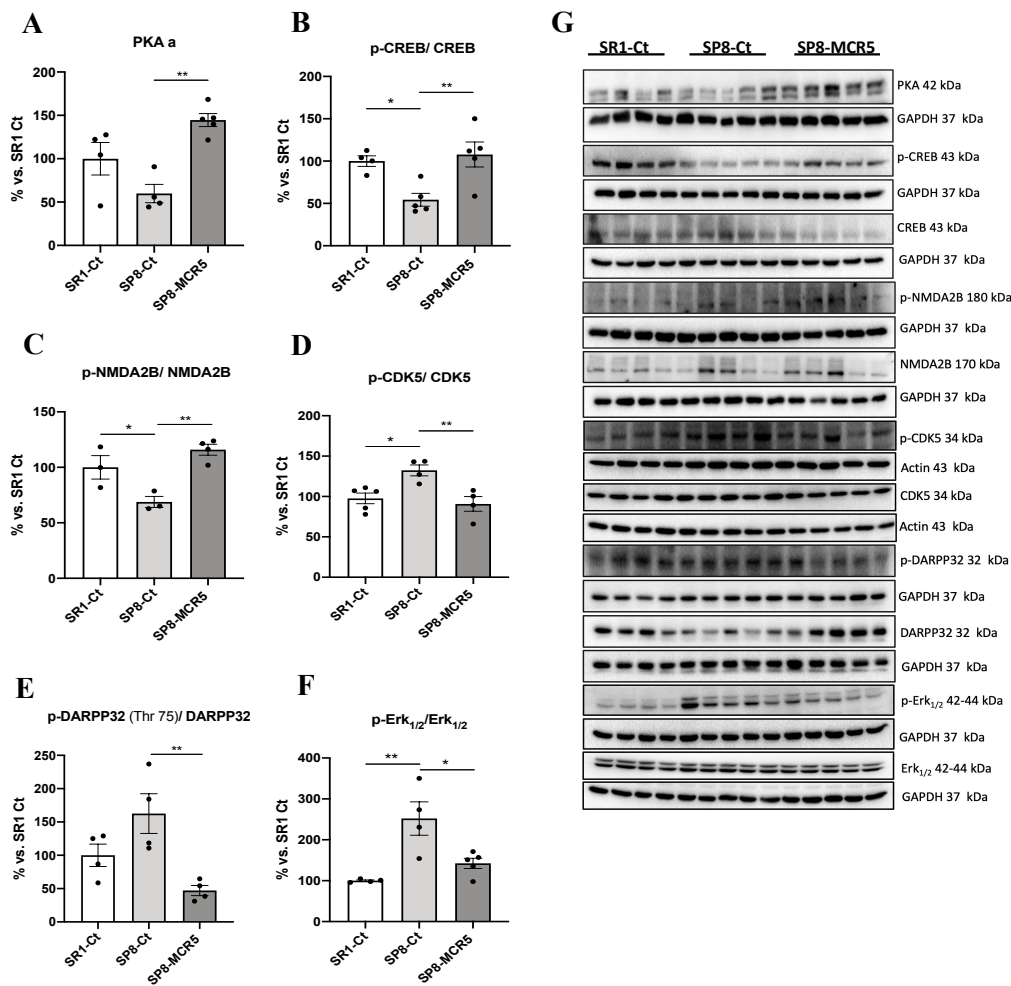


**Figure 6:** Representative Western blots and quantifications for PKA a, the ratio p-NMDA2B/NMDA2B, ratio p-DARPP32(Thr75)/DARPP32, ratio p-CDK5/CDK5, ratio p-CREB/CREB and p-Erk<sub>1/2</sub>/Erk<sub>1/2</sub> (A-G). Values in bar graphs are adjusted to 100% for protein levels of the control SAMR1 (SR1-Ct). Values represented are mean  $\pm$  Standard error of the mean (SEM); (n=4-6 for each group). \* $p < 0.05$ ; \*\* $p < 0.01$ .

### Effects of I<sub>2</sub>-IR ligand MCR5 on BDNF/TrkB/NGFR(p75) signalling pathway after treatment with MCR5

An increase in proBDNF protein levels in both SAMP8 groups in comparison with the SAMR1 control group is observed, albeit no significant differences were found (Fig 7A). Likewise, no changes in the mBDNF protein levels among experimental groups were found (Fig 7B). Pursuing BDNF molecular pathways, TrkB levels were also evaluated. Ratio TrkB-truncated (TL)/Full Length (FL) was slightly higher in the SAMP8 group compared to the SAMR1 group and was significantly reduced after MCR5 treatment (Fig 7C and 7F). According to these findings, a significant increase in nerve growth factor receptor (NGFR) protein levels in MCR5 treated SAMP8 in comparison with SAMP8 mice was found. Besides, a significant increase in NGFR protein levels in SAMR1 mice compared to

the SAMP8 control was determined (Figs 7D and 7G). By last, we also extend the analysis of the Postsynaptic density 95 (PSD95) protein levels, a synaptic plasticity marker, which is regulated by BDNF/TrkB signalling and AKT/mTOR/ GSK3 $\beta$ . Noteworthy, we found higher levels in SAMP8 treated with MCR5 than in control mice groups (Figs 7F and 7G).

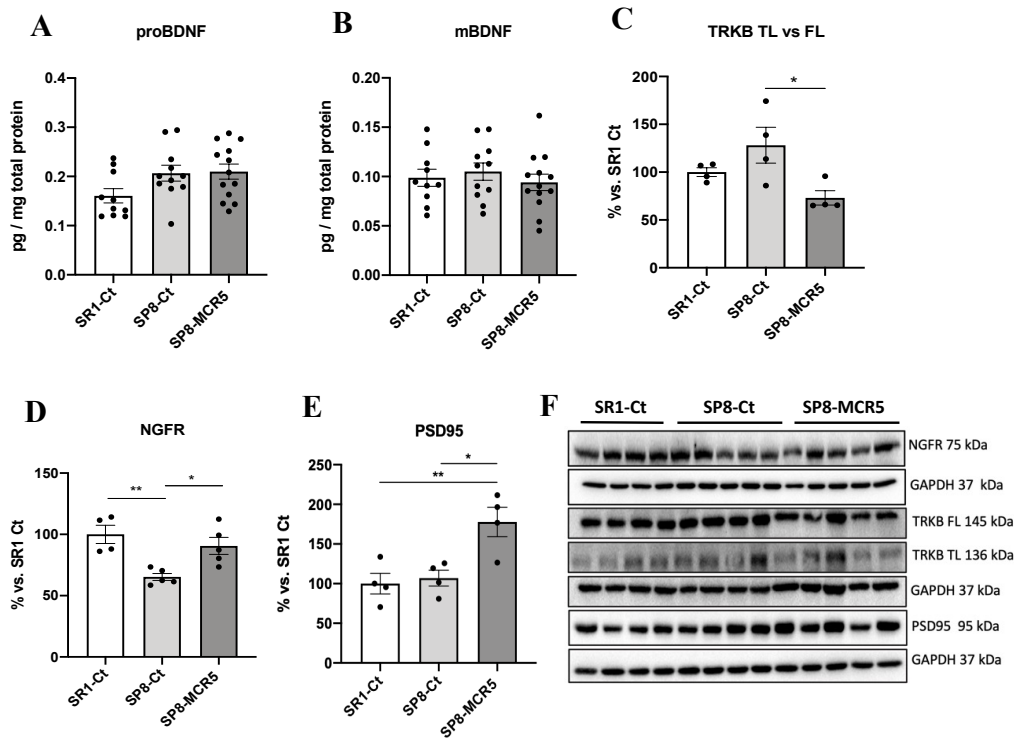


**Figure 7:** Protein levels of proBDNF (A), and mBDNF (B). Representative Western Blot and quantifications for ratio TrkB-TL vs TrkB-FL, NGFR, and PSD95 (C-F). Values represented are mean  $\pm$  Standard error of the mean (SEM); (n = 4-13 for each group). \*p<0.05; \*\*p<0.01.

### 3.2.4 DISCUSSION

Besides neurodegeneration, AD has been associated with increased incidents of neuropsychiatric disorders in humans, such as anxiety and depression, among other BPSD. New research has to be performed to face this collateral complication of AD because current therapies for both AD and BPSD are not completely effective and safe. On the one hand, some AD drugs can develop BPSD signs as adverse effects, i.e., memantine. On the other hand, BPSD drugs exacerbate cognitive impairment [7].

As aforementioned, I<sub>2</sub>-IR are associated with the pathogenesis of several brain disorders [40, 41] and neurodegenerative diseases such as AD [18]. Furthermore, I<sub>2</sub>-IR ligand MCR5 demonstrated neuroprotective effects under different interventions and rodent models [26, 27, 42]. In line with these results, MCR5 treatment improved cognitive decline presented by older SAMP8 male mice, including working and spatial memory by using NORT and

OLT, respectively. The behavioural tests applied demonstrated that older SAMP8 presented, in whole, anxiety- and depressive-like behaviours, as well as fearful behaviour, with less locomotion and rears, avoiding the OF center zone. In the present study, we showed a substantial improvement in BSPD and cognitive performance, demonstrating anti-anxiety- and anti-depressant-like effects after treatment with MCR5 in older SAMP8. Therefore, to our knowledge, this is the first study in which both changes have been demonstrated in AD mice for an I<sub>2</sub>-IR ligand.

Those non-cognitive and cognitive modifications promoted by MCR5 were accompanied by changes in some molecular pathways associated with ND process presented in these brain disorders. Previously it has been demonstrated that serotonin receptor densities such as 5-HT<sub>2A</sub> did not suffer changes with age in SAMR1 compared to SAMP8 mice, whereas SERT increases at 9 months of age [31]. Regarding the serotonergic system, here, we did not observe any significant change in gene expression of serotonin receptors and SERT protein levels after MCR5 treatment. Additionally, MCR5 did not bind to these membrane structures, allowing discarding an antidepressant effect mediated by inhibition of SERT or by interaction with 5-HT receptors.

It is important to note that, although the dopamine and serotonin pathways are the major targets for neuropsychiatric drugs, new mechanisms have been described, including mechanisms related to the neurodegenerative process presented in AD [43]. Indeed, it is well-demonstrated that I<sub>2</sub>-IR neuroprotective effects are mediated by pleiotropic mechanisms.

Accumulating evidence suggests that the pathology of main brain disorders is associated with neuronal inflammation [44, 45]. It has been described that AKT/GSK3/mTOR signalling is involved in the immune cell activation, downregulating pro-inflammatory cytokines such as TNF- $\alpha$ , IL-1 $\beta$ , IL-6, and IFN- $\gamma$  and upregulating the anti-inflammatory cytokines [43, 46]. In addition, recent studies have demonstrated that both dopamine and serotonin exert part of their actions by modulating the activity of this pathway [47]. In this study, we reported that the I<sub>2</sub>-IR ligand treatment modified levels of AKT/GSK3/mTOR key proteins that might explain in part the reduction in the gene expression of the pro-inflammatory cytokine such as *Tnf- $\alpha$* , *Il-1 $\beta$*  and *Il-6*. Conjointly with increased pro-inflammatory markers, a deficit of anti-inflammatory markers such as TGF-1 $\beta$  has been reported, contributing to inflammaging and cognitive impairment both in AD and other brain disorders such as depression [48, 49]. I<sub>2</sub>-IR ligand treatment also increased levels of active TGF-1 $\beta$ . TGF-1 $\beta$ , besides Smad-mediated pathways, activates Smad-independent pathways, including the PIK3/AKT [50], further supporting the alterations observed in this pathway after I<sub>2</sub>-IR treatment.

Phosphorylation of AKT protein has been shown to promote neuroprotection against cell death, increasing cell survival [51]. On the one hand, we found increased levels of p-AKT in treated SAMP8 mice in comparison to the SAMP8 control, reaching the healthy mice group, SAMR1. On the other hand, PTEN a protein that regulates AKT kinase activity was downregulated in SAMP8 treated mice. In line with our findings, fluoxetine upregulates the expression of the p-AKT [52]. Of note, SAMP8 mice showed a higher level of activated GSK3 $\beta$  in comparison with SAMR1 [53, 54]. Moreover, some antidepressant drugs or atypical antipsychotics such as lithium regulate GSK3 by inhibiting its activity in the brain [55, 56]. Changes in GSK3 $\beta$  activity described in SAMP8 mice reinforces the depressive-like behaviour showed. Interestingly, I<sub>2</sub>-IR treatment was able to decrease the GSK3 $\beta$  activity, giving clues for the possible pathway modulated through this receptor leading on anxiety and depression as well as improvement in cognition observed after MCR5 treatment. It can be kept in mind that inhibition of GSK3 $\beta$  may result in a reduction in tau hyperphosphorylation leading to the reduction in neurofibrillary tangles, then neuronal dysfunction accordingly with previous results demonstrating a neuroprotective role for MCR5 [42]. Moreover, dysregulation of mTOR signalling and concretely mTORC1, has been described under chronic restrain stress and administration of escitalopram and paroxetine prevented these changes [57]. Likewise, ketamine has been reported to activate mTOR and downstream constituents such as p70S6K resulting in increased levels of postsynaptic density proteins such as PSD95, GluR1, synapsin I [58]. In this study, we demonstrated that MCR5 treatment significantly increased ratio p-mTORC1 in SAMP8 mice in parallel with an increase in PSD95 levels, which can further explain the improvement of both cognitive and non-cognitive signs presented by SAMP8 mice.

Other signaling cascades altered after MCR5 treatment included NMDAR/CDK5/DARPP32 and PKA/CREB signaling. MCR5 inhibited NMDAR/CDK5/DARPP32 in treated SAMP8. Based on our findings, we suggest that MCR5 might exert anti-depressant-like and neuroprotective effects through this signaling pathway. DARPP32 modulates the dopamine pathway [59] and is, therefore, a key regulator for the pathogenesis of several neuropsychiatric disorders [60]. Here, we found a significant reduction of p-CDK5 and p-DARPP32 (Thr75) in SAMP8 treated with I<sub>2</sub>-IR ligand, implicating this pathway in the beneficial role of MCR5 in SAMP8 neuropathology. Moreover, phosphorylation of DARPP-32 in Thr75 by p-CDK5, in turn, inhibits PKA and thereby reduces the efficacy of dopamine signalling [61].

Interestingly, consistent with the reported decreased levels of p-DARPP32 in Thr75, increased PKA levels were determined in SAMP8 mice treated with I<sub>2</sub>-IR ligand MCR5. Indeed, we also found that MCR5 treatment induced the activation of the PKA/CREB signalling cascade, increasing protein levels of both PKA and p-CREB. Of interest, several



studies demonstrated that activation of PKA/CREB pathway in the hippocampus leads to neuroprotective effects not only by upregulating BDNF protein levels, but also reducing neuroinflammation in several brain disorders such as anxiety, in an early episode of depression and AD [62]. This evidence is coincident with the diminution of pro-inflammatory cytokines such as *Tnf- $\alpha$* , *Il-1 $\beta$*  and *Il-6* found after MCR5 administration. Given its implication in CREB phosphorylation, we also investigated the levels of p-Erk<sub>1/2</sub>. Surprisingly, its levels were found increased in SAMP8 control mice and significantly decreased in the SAMP8 treated mice. However, increased ERK<sub>1/2</sub> activation has been reported in socially defeated animals, and Erk<sub>1/2</sub> mediated increase in inflammatory markers is established [63–65]. In the present study, a reduction of Erk<sub>1/2</sub> activation induced by MCR5 treatment is also consistent with the decreased pro-inflammatory markers observed.

Given that downregulation of BDNF function has been demonstrated in the brains of patients with neurodegenerative or neuropsychiatric disorders, evaluation of the BDNF levels and TrkB signalling in the hippocampus after MCR5 treatment was relevant [13, 14]. Indeed, one cause for the reduced BDNF levels is due to BDNF/TrkB signalling dysfunction mediated by endogenous small molecules, driving to changes associated with the above-mentioned pathways [66, 67]. In our hands, MCR5 treatment did not produce any change in proBDNF and mBDNF protein levels. However, MCR5 ameliorated BDNF/TrkB signalling, promoting TrkB-FL protein levels. BDNF also binds to nerve growth factor receptor (NGFR), also known as p75 neurotrophin receptor (p75NTR), albeit with a low-affinity [68, 69]. MCR5 was also able to increase the levels of NGFR. These changes, jointly with the increase of the synaptic marker PSD95 levels that was demonstrated in SAMP8 mice after I<sub>2</sub>-IR ligand treatment, revealed that MCR5 promoted synaptic function, which is reported.

Altogether, these results demonstrated that MCR5 also plays a neuroprotective role against neurodegeneration induced through pathways associated with anxiety and depression, pointing out an alternative target for slowing down the disease progression (Fig 8).

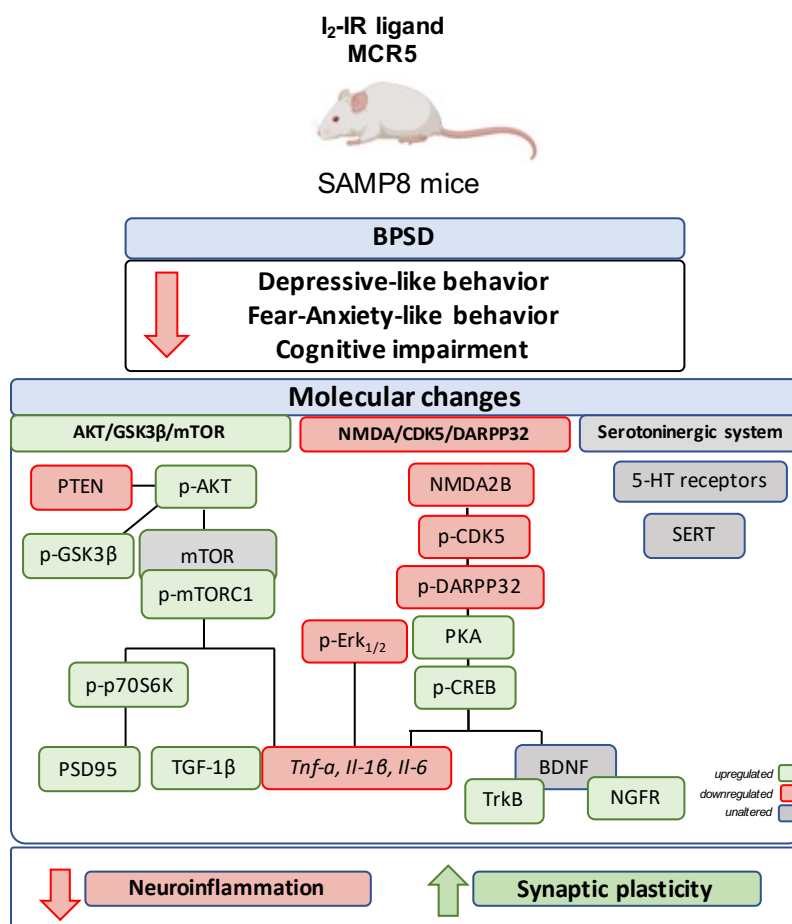


**Figure 8:** Cartoon illustrating a summary of behavioural, cognitive and molecular effects after MCR5 treatment in SAMP8 mice.

**Author contributions:** F.V. carried out the experimental intervention and performed behaviour experiments. F.V. performed WB analysis and RT-PCR experiments. C.G.-F, and M.P. analysed the data and drafted the manuscript. A.B. and SR synthesized and purified MCR5. C.E. designed and supervised MCR5 synthesis. C.G.-F and M.P. designed the experiments and supervised the study. F.V., C.G.-F, A.B., S.R.-A., C.E. and M.P. contributed to the writing the manuscript. All authors read and approved the final version of the manuscript.

**Conflict of interest:** The authors claim no financial conflicts of interests.

**Funding:** This research was funded by the Ministerio de Economía y Competitividad of Spain (SAF2016-3307). The project leading to these results has received funding from “la Caixa” Foundation (ID 100010434) under agreement CI18-00002. C.G.-F, F. V., C. E., S. R.-A., A. B. and M. P. belong to 2017SGR106 (Generalitat de Catalunya). J Financial support was provided for F. V. (University of Barcelona, APIF\_2017), S. R.-A. (Generalitat de Catalunya, 2018FI\_B\_00227), A. B. (Institute of Biomedicine UB\_2018)

## REFERENCES

- [1] Cummings, J. L.; Morstorf, T.; Zhong, K. Alzheimer's Disease Drug-Development Pipeline: Few Candidates, Frequent Failures. *Alzheimers. Res. Ther.*, 2014, 6 (4), 37.
- [2] Cummings, J.; Lee, G.; Ritter, A.; Zhong, K. Alzheimer's Disease Drug Development Pipeline: 2018. *Alzheimer's Dement. Transl. Res. Clin. Interv.*, 2018, 4, 195–214.
- [3] Griñan-Ferré, C.; Puigoriol-Illamola, D.; Palomera-ávalos, V.; Pérez-Cáceres, D.; Companys-Aleman, J.; Camins, A.; Ortuño-Sahagún, D.; Teresa Rodrigo, M.; Pallàs, M. Environmental Enrichment Modified Epigenetic Mechanisms in SAMP8 Mouse Hippocampus by Reducing Oxidative Stress and Inflammation and Achieving Neuroprotection. *Front. Aging Neurosci.*, 2016, 8 (OCT).<https://doi.org/10.3389/fnagi.2016.00241>.
- [4] Cerejeira, J.; Lagarto, L.; Mukaetova-Ladinska, E. Behavioral and Psychological Symptoms of Dementia. *Front. Neurol.*, 2012, 3, 73.
- [5] Reisberg, B.; Borenstein, J.; Salob, S. P.; Ferris, S. H. Behavioral Symptoms in Alzheimer's Disease: Phenomenology and Treatment. *J. Clin. Psychiatry*, 1987.
- [6] Kar, N. Behavioral and Psychological Symptoms of Dementia and Their Management. *Indian J. Psychiatry*, 2009, 51 (Suppl1), S77.
- [7] Kołaczkowski, M.; Mierzejewski, P.; Bienkowski, P.; Wesołowska, A.; Newman-Tancredi, A. Antipsychotic, Antidepressant, and Cognitive-Impairment Properties of Antipsychotics: Rat Profile and Implications for Behavioral and Psychological Symptoms of Dementia. *Naunyn-Schmiedeberg's Arch. Pharmacol.*, 2014, 387 (6), 545–557.
- [8] Leyhe, T.; Reynolds III, C. F.; Melcher, T.; Linnemann, C.; Klöppel, S.; Blennow, K.; Zetterberg, H.; Dubois, B.; Lista, S.; Hampel, H. A Common Challenge in Older Adults: Classification, Overlap, and Therapy of Depression and Dementia. *Alzheimer's Dement.*, 2017, 13 (1), 59–71.
- [9] Mega, M. S.; Cummings, J. L.; Fiorello, T.; Gornbein, J. The Spectrum of Behavioral Changes in Alzheimer's Disease. *Neurology*, 1996, 46 (1), 130–135.
- [10] Dillon, C.; Serrano, C. M.; Castro, D.; Leguizamón, P. P.; Heisecke, S. L.; Taragano, F. E. Behavioral Symptoms Related to Cognitive Impairment. *Neuropsychiatr. Dis. Treat.*, 2013, 9, 1443.
- [11] Lanctôt, K. L.; Herrmann, N.; Mazzotta, P. Role of Serotonin in the Behavioral and Psychological Symptoms of Dementia. *J. Neuropsychiatry Clin. Neurosci.*, 2001, 13 (1), 5–21.
- [12] Lohoff, F. W. Overview of the Genetics of Major Depressive Disorder. *Curr. Psychiatry Rep.*, 2010, 12 (6), 539–546.
- [13] Castrén, E.; Rantamäki, T. The Role of BDNF and Its Receptors in Depression and Antidepressant Drug Action: Reactivation of Developmental Plasticity. *Dev. Neurobiol.*, 2010, 70 (5), 289–297.
- [14] Serafini, G. Neuroplasticity and Major Depression, the Role of Modern Antidepressant Drugs. *World J. psychiatry*, 2012, 2 (3), 49.

- [15] Autry, A. E.; Adachi, M.; Nosyreva, E.; Na, E. S.; Los, M. F.; Cheng, P.; Kavalali, E. T.; Monteggia, L. M. NMDA Receptor Blockade at Rest Triggers Rapid Behavioural Antidepressant Responses. *Nature*, 2011, 475 (7354), 91–95.
- [16] García-Sevilla, J. A.; Escriba, P. V.; Sastre, M.; Walzer, C.; Busquets, X.; Jaquet, G.; Reis, D. J.; Guimon, J. Immunodetection and Quantitation of Imidazoline Receptor Proteins in Platelets of Patients with Major Depression and in Brains of Suicide Victims. *Arch. Gen. Psychiatry*, 1996, 53 (9), 803–810.
- [17] Gargalidis-Moudanos, C.; Pizzinat, N.; Javoy-Agid, F.; Remaury, A.; Parini, A. I<sub>2</sub>-Imidazoline Binding Sites and Monoamine Oxidase Activity in Human Postmortem Brain from Patients with Parkinson's Disease. *Neurochem. Int.*, 1997, 30 (1), 31–36.
- [18] Ruiz, J.; Martín, I.; Callado, L. F.; Meana, J. J.; Barturen, F.; Garcia-Sevilla, J. A. Non-Adrenoceptor [3H] Idazoxan Binding Sites (I<sub>2</sub>-Imidazoline Sites) Are Increased in Postmortem Brain from Patients with Alzheimer's Disease. *Neurosci. Lett.*, 1993, 160 (1), 109–112.
- [19] Parini, A.; Moudanos, C. G.; Pizzinat, N.; Lanier, S. M. The Elusive Family of Imidazoline Binding Sites. *Trends Pharmacol. Sci.*, 1996, 17 (1), 13–16.
- [20] Finn, D. P.; Martí, O.; Harbuz, M. S.; Vallès, A.; Belda, X.; Márquez, C.; Jessop, D. S.; Lallies, M. D.; Armario, A.; Nutt, D. J. Behavioral, Neuroendocrine and Neurochemical Effects of the Imidazoline I<sub>2</sub> Receptor Selective Ligand BU224 in Naive Rats and Rats Exposed to the Stress of the Forced Swim Test. *Psychopharmacology (Berl.)*, 2003, 167 (2), 195–202.
- [21] Tonello, R.; Villarinho, J. G.; da Silva Sant'Anna, G.; Tamiozzo, L.; Machado, P.; Trevisan, G.; Martins, M. A. P.; Ferreira, J.; Rubin, M. A. The Potential Antidepressant-like Effect of Imidazoline I<sub>2</sub> Ligand 2-BFI in Mice. *Prog. Neuro-Psychopharmacology Biol. Psychiatry*, 2012, 37 (1), 15–21.
- [22] Li, G.; Regunathan, S.; Barrow, C. J.; Eshraghi, J.; Cooper, R.; Reis, D. J. Agmatine: An Endogenous Clonidine-Displacing Substance in the Brain. *Science (80-. )*, 1994, 263 (5149), 966–969.
- [23] Aricioglu, F.; Altunbas, H. Is Agmatine an Endogenous Anxiolytic/Antidepressant Agent? *Ann. N. Y. Acad. Sci.*, 2003, 1009 (1), 136–140.
- [24] Head, G. A.; Mayorov, D. N. Imidazoline Receptors, Novel Agents and Therapeutic Potential. *Cardiovasc. Hematol. Agents Med. Chem. (Formerly Curr. Med. Chem. Hematol. Agents)*, 2006, 4 (1), 17–32.
- [25] Abas, S.; Estarellas, C.; Luque, F. J.; Escolano, C. Easy Access to (2-Imidazolin-4-Yl) Phosphonates by a Microwave Assisted Multicomponent Reaction. *Tetrahedron*, 2015, 71 (19), 2872–2881.
- [26] Abás, S.; Erdozain, A. M.; Keller, B.; Rodríguez-Arévalo, S.; Callado, L. F.; García-Sevilla, J. A.; Escolano, C. Neuroprotective Effects of a Structurally New Family of High Affinity Imidazoline I<sub>2</sub> Receptor Ligands. *ACS Chem. Neurosci.*, 2017, 8 (4), 737–742.
- [27] Griñán-Ferré, C.; Vasilopoulou, F.; Abás, S.; Rodríguez-Arévalo, S.; Bagán, A.; Sureda, F. X.; Pérez, B.; Callado, L. F.; García-Sevilla, J. A.; García-Fuster, M. J.; et al. Behavioral and Cognitive

Improvement Induced by Novel Imidazoline I<sub>2</sub> Receptor Ligands in Female SAMP8 Mice. *Neurotherapeutics*, 2019, 16 (2). <https://doi.org/10.1007/s13311-018-00681-5>.

[28] Butterfield, D. A.; Poon, H. F. The Senescence-Accelerated Prone Mouse (SAMP8): A Model of Age-Related Cognitive Decline with Relevance to Alterations of the Gene Expression and Protein Abnormalities in Alzheimer's Disease. *Exp. Gerontol.*, 2005, 40 (10), 774–783.

[29] Miyamoto, M. Characteristics of Age-Related Behavioral Changes in Senescence-Accelerated Mouse SAMP8 and SAMP10. *Exp. Gerontol.*, 1997, 32 (1–2), 139–148.

[30] Pallàs, M. Senescence-Accelerated Mice P8: A Tool to Study Brain Aging and Alzheimer's Disease in a Mouse Model. *ISRN Cell Biol.*, 2012, 2012.

[31] Pérez-Cáceres, D.; Rodrigo, M. T.; Pubill, D.; Camins, A.; Camarasa, J.; Escubedo, E.; Pallàs, M. Depression-like Behavior Is Dependent on Age in Male SAMP8 Mice. *Biogerontology*, 2013, 14 (2), 165–176.

[32] Steru, L.; Chermat, R.; Thierry, B.; Simon, P. The Tail Suspension Test: A New Method for Screening Antidepressants in Mice. *Psychopharmacology (Berl.)*, 1985, 85 (3), 367–370.

[33] Can, A.; Dao, D. T.; Terrillion, C. E.; Piantadosi, S. C.; Bhat, S.; Gould, T. D. The Tail Suspension Test. *JoVE (Journal Vis. Exp.)*, 2012, No. 59, e3769.

[34] Porsolt, R. D.; Le Pichon, M.; Jalfre, M. Depression: A New Animal Model Sensitive to Antidepressant Treatments. *Nature*, 1977, 266 (5604), 730–732.

[35] Lister, R. G. The Use of a Plus-Maze to Measure Anxiety in the Mouse. *Psychopharmacology (Berl.)*, 1987, 92 (2), 180–185.

[36] Cohen, H.; Matar, M. A.; Joseph, Z. Animal Models of Post-traumatic Stress Disorder. *Curr. Protoc. Neurosci.*, 2013, 64 (1), 9–45.

[37] Archer, J. Tests for Emotionality in Rats and Mice: A Review. *Anim. Behav.*, 1973, 21 (2), 205–235.

[38] Ennaceur, A.; Delacour, J. A New One-Trial Test for Neurobiological Studies of Memory in Rats. 1: Behavioral Data. *Behav. Brain Res.*, 1988, 31 (1), 47–59.

[39] Griñán-Ferré, C.; Marsal-García, L.; Bellver-Sanchis, A.; Kondengaden, S. M.; Turga, R. C.; Vázquez, S.; Pallàs, M. Pharmacological Inhibition of G9a/GLP Restores Cognition and Reduces Oxidative Stress, Neuroinflammation and  $\beta$ -Amyloid Plaques in an Early-Onset Alzheimer's Disease Mouse Model. *Aging (Albany. NY.)*, 2019, 11 (23). <https://doi.org/10.18632/aging.102558>.

[40] GARCÍA-SEVILLA, J. A.; Escriba, P. V.; Guimon, J. Imidazoline Receptors and Human Brain Disorders. *Ann. N. Y. Acad. Sci.*, 1999, 881 (1), 392–409.

[41] Li, J.-X.; Zhang, Y. Imidazoline I<sub>2</sub> Receptors: Target for New Analgesics? *Eur. J. Pharmacol.*, 2011, 658 (2–3), 49–56.

[42] Abás, S.; Rodríguez-Arévalo, S.; Bagán, A.; Griñán-Ferré, C.; Vasilopoulou, F.; Brocos-Mosquera, I.; Muguruza, C.; Pérez, B.; Molins, E.; Luque, F. J. Bicyclic  $\alpha$ -Iminophosphonates as High Affinity Imidazoline I<sub>2</sub> Receptor Ligands for Alzheimer's Disease. *J. Med. Chem.*, 2020, 63

(7), 3610–3633.

[43] Kitagishi, Y.; Kobayashi, M.; Kikuta, K.; Matsuda, S. Roles of PI3K/AKT/GSK3/MTOR Pathway in Cell Signaling of Mental Illnesses. *Depress. Res. Treat.*, 2012, 2012.

[44] Hashioka, S.; Klegeris, A.; Monji, A.; Kato, T.; Sawada, M.; McGeer, P. L.; Kanba, S. Antidepressants Inhibit Interferon- $\gamma$ -Induced Microglial Production of IL-6 and Nitric Oxide. *Exp. Neurol.*, 2007, 206 (1), 33–42.

[45] Knezevic, D.; Verhoeff, N. P. L. G.; Hafizi, S.; Strafella, A. P.; Graff-Guerrero, A.; Rajji, T.; Pollock, B. G.; Houle, S.; Rusjan, P. M.; Mizrahi, R. Imaging Microglial Activation and Amyloid Burden in Amnesic Mild Cognitive Impairment. *J. Cereb. Blood Flow Metab.*, 2018, 38 (11), 1885–1895.

[46] Haidinger, M.; Poglitsch, M.; Geyeregger, R.; Kasturi, S.; Zeyda, M.; Zlabinger, G. J.; Pulendran, B.; Hörl, W. H.; Säemann, M. D.; Weichhart, T. A Versatile Role of Mammalian Target of Rapamycin in Human Dendritic Cell Function and Differentiation. *J. Immunol.*, 2010, 185 (7), 3919–3931.

[47] Duman, R. S.; Voleti, B. Signaling Pathways Underlying the Pathophysiology and Treatment of Depression: Novel Mechanisms for Rapid-Acting Agents. *Trends Neurosci.*, 2012, 35 (1), 47–56.

[48] Caraci, F.; Battaglia, G.; Busceti, C.; Biagioni, F.; Mastroiacovo, F.; Bosco, P.; Drago, F.; Nicoletti, F.; Sortino, M. A.; Copani, A. TGF- $\beta$ 1 Protects against A $\beta$ -Neurotoxicity via the Phosphatidylinositol-3-Kinase Pathway. *Neurobiol. Dis.*, 2008, 30 (2), 234–242.

[49] Caraci, F.; Spampinato, S. F.; Morgese, M. G.; Tascetta, F.; Salluzzo, M. G.; Giambirtone, M. C.; Caruso, G.; Munafò, A.; Torrisi, S. A.; Leggio, G. M. Neurobiological Links between Depression and AD: The Role of TGF- $\beta$ 1 Signaling as a New Pharmacological Target. *Pharmacol. Res.*, 2018, 130, 374–384.

[50] Derynck, R.; Zhang, Y. E. Smad-Dependent and Smad-Independent Pathways in TGF- $\beta$  Family Signalling. *Nature*, 2003, 425 (6958), 577–584.

[51] Dudek, H.; Datta, S. R.; Franke, T. F.; Birnbaum, M. J.; Yao, R.; Cooper, G. M.; Segal, R. A.; Kaplan, D. R.; Greenberg, M. E. Regulation of Neuronal Survival by the Serine-Threonine Protein Kinase Akt. *Science* (80-. ), 1997, 275 (5300), 661–665.

[52] David, D. J.; Samuels, B. A.; Rainer, Q.; Wang, J.-W.; Marsteller, D.; Mendez, I.; Drew, M.; Craig, D. A.; Guiard, B. P.; Guilloux, J.-P. Neurogenesis-Dependent and-Independent Effects of Fluoxetine in an Animal Model of Anxiety/Depression. *Neuron*, 2009, 62 (4), 479–493.

[53] Canudas, A. M.; Gutierrez-Cuesta, J.; Rodríguez, M. I.; Acuña-Castroviejo, D.; Sureda, F. X.; Camins, A.; Pallàs, M. Hyperphosphorylation of Microtubule-Associated Protein Tau in Senescence-Accelerated Mouse (SAM). *Mech. Ageing Dev.*, 2005, 126 (12), 1300–1304.

[54] Casadesús, G.; Gutierrez-Cuesta, J.; Lee, H.; Jiménez, A.; Tajés, M.; Ortuño-Sahagún, D.; Camins, A.; Smith, M. A.; Pallàs, M. Neuronal Cell Cycle Re-Entry Markers Are Altered in the Senescence Accelerated Mouse P8 (SAMP8). *J. Alzheimer's Dis.*, 2012, 30 (3), 573–583.

[55] Li, X.; Polter, A. Glycogen Synthase Kinase-3 Is an Intermediate Modulator of Serotonin

Neurotransmission. *Front. Mol. Neurosci.*, 2011, 4, 31.

[56] Young, W. Review of Lithium Effects on Brain and Blood. *Cell Transplant.*, 2009, 18 (9), 951–975.

[57] Seo, M. K.; Choi, C. M.; McIntyre, R. S.; Cho, H. Y.; Lee, C. H.; Mansur, R. B.; Lee, Y.; Lee, J.-H.; Kim, Y. H.; Park, S. W. Effects of Escitalopram and Paroxetine on MTORC1 Signaling in the Rat Hippocampus under Chronic Restraint Stress. *BMC Neurosci.*, 2017, 18 (1), 39.

[58] Li, N.; Lee, B.; Liu, R.-J.; Banasr, M.; Dwyer, J. M.; Iwata, M.; Li, X.-Y.; Aghajanian, G.; Duman, R. S. MTOR-Dependent Synapse Formation Underlies the Rapid Antidepressant Effects of NMDA Antagonists. *Science (80-. )*, 2010, 329 (5994), 959–964.

[59] Fienberg, A. A.; Hiroi, N.; Mermelstein, P. G.; Song, W.-J.; Snyder, G. L.; Nishi, A.; Cheramy, A.; O’callaghan, J. P.; Miller, D. B.; Cole, D. G. DARPP-32: Regulator of the Efficacy of Dopaminergic Neurotransmission. *Science (80-. )*, 1998, 281 (5378), 838–842. [60] Nishi, A.; Shuto, T. Potential for Targeting Dopamine/DARPP-32 Signaling in Neuropsychiatric and Neurodegenerative Disorders. *Expert Opin. Ther. Targets*, 2017, 21 (3), 259–272.

[61] Nishi, A.; Bibb, J. A.; Matsuyama, S.; Hamada, M.; Higashi, H.; Nairn, A. C.; Greengard, P. Regulation of DARPP-32 Dephosphorylation at PKA-and Cdk5-sites by NMDA and AMPA Receptors: Distinct Roles of Calcineurin and Protein Phosphatase-2A. *J. Neurochem.*, 2002, 81 (4), 832–841.

[62] Luo, Y.; Kuang, S.; Li, H.; Ran, D.; Yang, J. cAMP/PKA-CREB-BDNF Signaling Pathway in Hippocampus Mediates Cyclooxygenase 2-Induced Learning/Memory Deficits of Rats Subjected to Chronic Unpredictable Mild Stress. *Oncotarget*, 2017, 8 (22), 35558.

[63] Krishnan, V.; Han, M.-H.; Graham, D. L.; Berton, O.; Renthal, W.; Russo, S. J.; LaPlant, Q.; Graham, A.; Lutter, M.; Lagace, D. C. Molecular Adaptations Underlying Susceptibility and Resistance to Social Defeat in Brain Reward Regions. *Cell*, 2007, 131 (2), 391–404.

[64] Patki, G.; Solanki, N.; Atrooz, F.; Allam, F.; Salim, S. Depression, Anxiety-like Behavior and Memory Impairment Are Associated with Increased Oxidative Stress and Inflammation in a Rat Model of Social Stress. *Brain Res.*, 2013, 1539, 73–86.

[65] Shin, J. A.; Lee, K.-E.; Kim, H.-S.; Park, E.-M. Acute Resveratrol Treatment Modulates Multiple Signaling Pathways in the Ischemic Brain. *Neurochem. Res.*, 2012, 37 (12), 2686–2696.

[66] Greenberg, M. E.; Xu, B.; Lu, B.; Hempstead, B. L. New Insights in the Biology of BDNF Synthesis and Release: Implications in CNS Function. *J. Neurosci.*, 2009, 29 (41), 12764–12767.

[67] Minichiello, L. TrkB Signaling Pathways in LTP and Learning. *Nat. Rev. Neurosci.*, 2009, 10 (12), 850–860. [68] Chao, M. V.; Bothwell, M. A.; Ross, A. H.; Koprowski, H.; Lanahan, A. A.; Buck, C. R.; Sehgal, A. Gene Transfer and Molecular Cloning of the Human NGF Receptor. *Science (80-. )*, 1986, 232 (4749), 518–521.

[69] Sandhya, V. K.; Raju, R.; Verma, R.; Advani, J.; Sharma, R.; Radhakrishnan, A.; Nanjappa, V.; Narayana, J.; Somani, B. L.; Mukherjee, K. K. A Network Map of BDNF/TRKB and BDNF/P75NTR Signaling System. *J. Cell Commun. Signal.*, 2013, 7 (4), 301–307.

## SUPPLEMENTARY MATERIAL

**Table S1:** Antibodies used in Western blot studies.

Antibody	Host	Source/Catalog	WB dilution
SERT	Goat	Abcam/ab130130	1:1000
p-AKT (Ser473)	Rabbit	Cell signaling/#D9E	1:1000
AKT	Rabbit	Cell signaling/#9272	1:1000
PTEN	Rabbit	Abcam/ab31392	1:1000
p-GSK3b (Ser9)	Rabbit	Cell signaling/#9336	1:1000
GSK3b	Rabbit	Cell signaling/#9315	1:1000
p-mTOR	Rabbit	Santa Cruz/sc-293089	1:500
mTOR	Rabbit	Novus Biological/nb100-240	1:500
p-TORC1 (Ser 151)	Rabbit	Cell signaling/#3359	1:500
TORC1	Rabbit	Cell signaling/#2501	1:1000
p-p70S6K	Rabbit	Invitrogen/PA5-18093	1:1000
p70S6K	Goat	Invitrogen/44-920G	1:1000
TGF-1 $\beta$	Rabbit	Cell Signaling/3711	1:1000
PKA a	Mouse	Santa Cruz/sc-28315	1:1000
p-NMDRA2B (Tyr1472)	Rabbit	Invitrogen/OPA1-04116	1:1000
NMDAR2B	Mouse	Santa Cruz/sc-365597	1:1000
p-DARPP32 (Thr75)	Rabbit	Cell Signaling/#2301	1:500
DARPP32	Mouse	Santa Cruz/sc-271111	1:1000
p-CDK5	Rabbit	Abcam/ab63550	1:1000
CDK5	Rabbit	Santa Cruz/sc-173	1:1000
p-CREB(Ser133)	Rabbit	Cell signaling/#9198	1:1000
ERK $\frac{1}{2}$	Rabbit	Cell Signaling/#9102	1:1000
p-ERK $\frac{1}{2}$ (Thr202/Tyr204)	Rabbit	Cell Signaling/#9101	1:1000
CREB	Rabbit	Cell signaling/9197	1:1000
TrkB	Rabbit	Santa Cruz/sc-8316	1:1000
NGFR	Mouse	Santa Cruz/sc-271708	1:500
PSD95	Rabbit	Abcam/ab18258	1:1000
GAPDH	Mouse	Millipore/MAB374	1:5000
Actin	Mouse	Sigma-Aldrich/A5441	1:2500
Goat-anti-mouse HRP conjugated		Biorad/170-5047	1:5000
Goat-anti-rabbit HRP conjugated		Biorad/170-6515	1:5000
Donkey-anti-goat HRP conjugated		Santa Cruz/sc-2020	1:5000



**Table S2:** Primers and probes used in qPCR studies.

Target	Product size (bp)	Forward primer (5'-3')	Reverse primer (5'-3')
<i>5-HT1A</i>	293	GGAGCGGGCACCAGCTTCGGAACA	CACTGTCTTCTCTCACGGGCAA
<i>5-HT1B</i>	125	AAGAAACTCATGGCCGCTAGGGAG	GCGTATCAGTTTGTGGAACGCTTG
<i>5-HT2A</i>	172	GGGTACCTCCCACCGACAT	AGGCCACCGGTACCCATAC
<i>Tnf-<math>\alpha</math></i>	157	TCGGGGTGATCGGTCCCAA	TGGTTTGCTACGACGTGGGCT
<i>Il-1b</i>	179	ACAGAATATCAACCAACAAGTGATATTCTC	GATTCTTTTCTTTGAGGCCCA
<i>Il-6</i>	189	ATCCAGTTGCCTTCTTGGGACTGA	TAAGCCTCCGACTTGTGAAGTGGT
<i>b-actin</i>	190	CAACGAGCGGTTCCGAT	GCCACAGGTTCCATACCCA

**Table S3:** Results of Novel object recognition test (NORT), and Object location test (OLT) in male mice at 10-month-old SR1, SP8 Ct mice groups and SP8 treated with I2-IR ligand MCR5 (5mg/Kg) mice group. Summary of Discrimination Index (DI) from short-term memory (2h), summary of DI from long-term memory (24h), and summary of DI from OLT. \* $p < 0.05$ ; \*\* $p < 0.01$ ; \*\*\* $p < 0.001$ ; \*\*\*\* $p < 0.0001$ . vs SR1-Ct.

Summary NORT 2h		
Group	Number of mice	DI (-1,1)
SR1-Ct	11	0.258 $\pm$ 0.034**
SP8-Ct	11	0.010 $\pm$ 0.022
SP8-MCR5	14	0.274 $\pm$ 0.051***
Summary NORT 24h		
Group	Number of mice	DI (-1,1)
SR1-Ct	11	0.260 $\pm$ 0.048***
SP8-Ct	11	0.032 $\pm$ 0.031
SP8-MCR5	14	0.299 $\pm$ 0.029***
Summary OLT		
Group	Number of mice	DI (-1,1)
SR1-Ct	11	0.267 $\pm$ 0.057***
SP8-Ct	11	-0.045 $\pm$ 0.035
SP8-MCR5	14	0.131 $\pm$ 0.039*

**Table S4:** Parameters measured in the Elevate plus maze (EPM). (n): number of events. Results are expressed as a mean  $\pm$  Standard error of the mean (SEM). \* $p < 0.05$ ; \*\* $p < 0.01$ ; \*\*\* $p < 0.001$ ; \*\*\*\* $p < 0.0001$  vs SP8-MCR5 (5mg/Kg) \$ $p < 0.05$ ; \$\$ $p < 0.01$ ; \$\$\$ $p < 0.0001$  vs SR1-Ct.

	SR1-Ct	SP8-Ct	SP8-MCR5 (5mg/Kg)
Anxiety Index	1.11 $\pm$ 0.01**	1.08 $\pm$ 0.02**	0.95 $\pm$ 0.03
Locomotor Activity (cm)	977.42 $\pm$ 39.85	761.56 $\pm$ 42.70 \$\$ *	954.67 $\pm$ 45.07
Time spent in Open Arms (sec)	25.31 $\pm$ 5.96****	43.52 $\pm$ 10.89***	99.02 $\pm$ 9.80
Time Spent in Closed Arms (sec)	20.50 $\pm$ 2.49****	12.50 $\pm$ 1.21\$ *** \$	15.55 $\pm$ 0.92
Entries in Open Arms	13.90 $\pm$ 4.44*	10.75 $\pm$ 1.57*	17.64 $\pm$ 1.94
Rearings (n)	23.90 $\pm$ 1.25	12.25 $\pm$ 1.59** \$\$\$	19.60 $\pm$ 1.24
Groomings (n)	1.30 $\pm$ 0.29 0.09	1.38 $\pm$ 0.18 0.07	0.60 $\pm$ 0.27
Defecations (n)	0.70 $\pm$ 0.38	0.25 $\pm$ 0.16	0.20 $\pm$ 0.13
Urinations (n)	0.00 $\pm$ 0.00	0.0 $\pm$ 0.00	0.0 $\pm$ 0.00

**Table S5:** Parameters measured in the Open Field Test (OFT). (n): number of events. Results are expressed as a mean  $\pm$  Standard error of the mean (SEM). \* $p < 0.05$ ; \*\* $p < 0.01$ ; \*\*\* $p < 0.001$ ; \*\*\*\* $p < 0.0001$  vs SP8-MCR5 (5mg/Kg). \$ $p < 0.05$  vs SR1-Ct

	SR1-Ct	SP8-Ct	SP8-MCR5 (5mg/Kg)
Locomotor activity (cm)	1594.44 $\pm$ 94.34**	1680.77 $\pm$ 104.53*	2036.58 $\pm$ 89.77
Mean Speed(cm/sec)	5.32 $\pm$ 0.31**	5.60 $\pm$ 0.35*	6.62 $\pm$ 0.26
Distance in Center (cm)	38.36 $\pm$ 4.79	32.67 $\pm$ 5.69*	62.95 $\pm$ 10.86
Entries in Center (n)	3.27 $\pm$ 0.33***	4.30 $\pm$ 0.76*	7.33 $\pm$ 0.94
Time in Center (sec)	4.83 $\pm$ 0.69	3.52 $\pm$ 0.70	5.16 $\pm$ 0.77
Rearings (n)	20.73 $\pm$ 2.03	14.45 $\pm$ 2.31**	26.42 $\pm$ 2.27
Groomings (n)	2.40 $\pm$ 0.31	1.18 $\pm$ 0.26 \$	1.75 $\pm$ 0.25
Defecations (n)	1.55 $\pm$ 0.31	1.18 $\pm$ 0.44	0.75 $\pm$ 0.33
Urinations (n)	0.18 $\pm$ 0.18	0.0 $\pm$ 0.00	0.17 $\pm$ 0.11

### **3.3 Publication 3**

**I<sub>2</sub> imidazoline receptor modulation protects aged SAMP8 mice against cognitive decline by suppressing the calcineurin pathway.**

Adapted from: **Vasilopoulou F**, Griñán-Ferré C, Rodríguez-Arévalo S, Bagán A, Abás S, Escolano S, and Pallàs M, *Geroscience*. 2021 Apr;43(2):965-983.

doi: <https://doi.org/doi:10.1007/s11357-020-00281-2>.

## SUMMARY

Brain aging is the greatest risk for the development of age-related syndromes such as dementia and AD, which unfortunately current treatments fail to stop. I<sub>2</sub>-IR density alterations have been associated with aging, neurodegeneration and AD, while I<sub>2</sub>-IR modulation has been shown to mediate neuroprotection. However, the exact molecular mechanisms through which I<sub>2</sub>-IR ligands deliver their effects have not been identified yet, which could be due to the lack of specific selective I<sub>2</sub>-IR ligands. The aim of this work was to test the action of the highly specific and selective I<sub>2</sub>-IR ligand B06 in the SAMP8 mouse model of aging and AD, by going deeper into the molecular mechanisms involved in the I<sub>2</sub>-IR mediated neuroprotection.

Following a four-week oral administration of B06 (5mg/kg/day), control and treated aged SAMP8 mice were submitted to behavioral tasks for cognitive and behavioral evaluation. Assessment of molecular alterations induced by B06 in the hippocampus of the mice was performed by Western Blot, qPCR and IHC.

Treatment with novel specific and highly selective I<sub>2</sub>-IR improved SAMP8 behavior and cognition, reduced AD hallmarks as well as OS, apoptotic and neuroinflammation markers. In particular, we showed that B06 treatment in SAMP8 mice reduced the levels of CaN active form and, accordingly, modified most of the CaN substrates, such as phosphorylated levels of NFAT cytoplasmic 1, BAD, CREB and GSK3 $\beta$ . Consistent with these results B06 increased *Bdnf* gene expression, altered NMDA phosphorylation and attenuated astrogliosis and neuroinflammation by decreasing GFAP reactivity and inflammatory markers gene expression in SAMP8 brains.

In summary, we identified the CaN pathway as a critical component of the beneficial effects provided by I<sub>2</sub>-IR ligand B06 treatment, which collectively affected several molecular pathways involved in neuroprotection and age-related conditions in SAMP8 mice, providing insight into the molecular modifications under I<sub>2</sub>-IR modulation.

## **I<sub>2</sub> imidazoline receptor modulation protects aged SAMP8 mice against cognitive decline by suppressing the calcineurin pathway**

Foteini Vasilopoulou,<sup>1</sup> Christian Griñán-Ferré,<sup>1</sup> Sergio Rodríguez-Arévalo,<sup>2</sup> Andrea Bagán,<sup>2</sup> Carmen Escolano,<sup>2</sup> Mercè Pallàs<sup>1</sup>

<sup>1</sup>*Pharmacology Section. Department of Pharmacology, Toxicology and Medicinal Chemistry, Faculty of Pharmacy and Food Sciences, and Institut de Neurociències, University of Barcelona, Av. Joan XXIII, 27-31, 08028 Barcelona, Spain.*

<sup>2</sup>*Laboratory of Medicinal Chemistry (Associated Unit to CSIC), Department of Pharmacology, Toxicology and Medicinal Chemistry, Faculty of Pharmacy and Food Sciences, and Institute of Biomedicine (IBUB), University of Barcelona, Av. Joan XXIII, 27-31, 08028 Barcelona, Spain.*

**Keywords:** I<sub>2</sub> Imidazoline receptors, aging, behavior, neuroinflammation, NFAT, neuroprotection, Alzheimer's disease.

### **ABSTRACT**

Brain aging and dementia are current problems that must be solved. The levels of imidazoline 2 receptors (I<sub>2</sub>-IRs) are increased in the brain in Alzheimer's disease (AD) and other neurodegenerative diseases. We tested the action of the specific and selective I<sub>2</sub>-IR ligand B06 in a mouse model of accelerated aging and AD, the senescence-accelerated mouse prone 8 (SAMP8) model. Oral administration of B06 for four weeks improved SAMP8 mouse behavior and cognition and reduced AD hallmarks, oxidative stress, and apoptotic and neuroinflammation markers. Likewise, B06 regulated glial excitatory amino acid transporter 2 and N-methyl-D aspartate 2A and 2B receptor subunit protein levels. Calcineurin (CaN) is a phosphatase that controls the phosphorylation levels of cAMP response element-binding (CREB), apoptotic mediator BCL-2-associated agonist of cell death (BAD) and GSK3 $\beta$ , among other molecules. Interestingly, B06 was able to reduce the levels of the CaN active form (CaN A). Likewise, CREB phosphorylation, BAD gene expression, and other factors were modified after B06 treatment. Moreover, phosphorylation of a target of CaN, nuclear factor of activated T-cells, cytoplasmic 1 (NFAT<sub>C1</sub>), was increased in B06-treated mice, impeding the transcription of genes related to neuroinflammation and neural plasticity. In summary, this I<sub>2</sub> imidazoline ligand can exert its beneficial effects on age-related conditions by modulating CaN pathway action and affecting several molecular pathways, playing a neuroprotective role in SAMP8 mice.

### 3.3.1 INTRODUCTION

Aging has become a problem worldwide, since older people are more prone to develop chronic and degenerative diseases. At the brain level, aging affects several molecular pathways that predispose patients to neurodegeneration, causing dementia, cognitive impairment and loss of quality of life. Among dementias, the most prevalent is Alzheimer's disease (AD) (GBD 2016 Neurology Collaborators, 2019). AD has aroused considerable interest because of its strong influence on quality of life among elderly individuals and because of the limited drugs available to combat cognitive loss and neuropsychiatric symptoms.

$\beta$ -Amyloid deposition in senile plaques and tau hyperphosphorylation forming neurofibrillary tangles are specific hallmarks of AD (Serrano-Pozo et al. 2011). However, there are no successful pharmacological treatments that modify the progression of AD, given that acetylcholinesterase inhibitors and memantine fail to stop the progression of dementia (Cummings et al. 2014, Cummings et al. 2018). Apart from the use of approved drugs, several clinical attempts have been made to treat AD progression by using various other strategies, such as immunotherapy against  $\beta$ -amyloid and beta-secretase (BACE) inhibitor administration, but the results have been disappointing (Cummings et al. 2018). These results show that addressing only the " $\beta$ -amyloid cascade hypothesis" cannot fully control the progression of the disease, and this hypothesis also cannot explain the advanced neuronal damage in AD. Therefore, identifying new pharmacological targets for AD treatment is an active area of research.

In most neurodegenerative processes, including AD, neuroinflammation and oxidative stress (OS) are common traits. It is well-accepted that  $Ca^{2+}$  dysfunction is a consequence of homeostatic imbalance in nerve cells that unleashes a string of molecular and cellular processes, including neuroinflammation, OS, changes in neuronal plasticity, differential expression of glutamate and cholinergic receptors, and amyloid pathology (Sompol and Norris. 2018). Together, these processes end with cognitive decline and neurodegeneration. Calcineurin (CaN), also known as protein phosphatase 2B, is a  $Ca^{2+}$ -dependent Ser/Thr phosphatase that is highly abundant in the brain, appearing at high levels in neurons and low levels in glia in healthy adult animals (Kuno et al. 1992). CaN is related to long-term potentiation (LTP) and long-term depression (LTD), and dysregulation of CaN has been linked with cognitive loss in an AD mouse model (Baumgärtel & Mansuye. 2012; Reese LC and Tagliatela G. 2011). Of importance, CaN levels and signaling are increased in the cortex in AD patients (Wu et al. 2010) and in the contexts of other human neurodegenerative pathologies, including Parkinson's disease (PD) (Caraveo et al. 2014), Lewy body aggregation (Martin et al. 2012), and vascular pathology (Pleiss et al. 2016b).

Moreover, CaN activity prevents fear memory formation in the amygdala by dephosphorylating and inhibiting downstream kinases, including AKT and extracellular signal-regulated kinase (ERK) (Lin et al. 2003). N-methyl-D-aspartate receptor (NMDAR) (Wang et al. 2018; Mulkey et al. 1994) and glycogen synthase kinase 3 $\beta$  (GSK3 $\beta$ ) (Watanabe et al. 2015) are some of the key actors in central nervous system function that are controlled by the phosphatase activity of CaN, which in turn is controlled by calcium calmodulin kinase II (CaMKII) and intracellular Ca<sup>2+</sup> levels (Bezprozvanny and Hiersinger.

2013). Nuclear factor of activated T-cells (NFAT) consists of at least two different components, one with nuclear localization and one that is phosphorylated and localized in the cytoplasm (Horsley and Pavlath. 2002). Furthermore, recently, the CaN pathway has been observed to link astrocytic Ca<sup>2+</sup> dysregulation to neuroinflammation, glutamate,  $\beta$ -amyloid accumulation and synaptotoxicity (Sompol and Norris. 2018).

Imidazoline 2 receptors (I<sub>2</sub>-IRs) (Bousquet et al. 2020) are increased in AD brains (Ruiz J et al. 1993; García-Sevilla et al. 1998), and radioactive ligands have been studied as biomarkers for AD and PD progression in patients (Tyacke et al. 2018; Wilson et al. 2019). There is evidence that I<sub>2</sub>-IR ligands reduce neurodegenerative processes, including cognitive decline, neuroinflammation, OS and AD hallmarks, but less is known about the upstream mechanism involved in the beneficial effects of I<sub>2</sub>-IR modulation. Thus, the objective of this work was to delineate the molecular mechanisms involved in the neuroprotective effect of I<sub>2</sub>-IR modulation in a mouse model of AD linked to the aging process, the senescence-accelerated mouse prone 8 (SAMP8) model. To this end, we used a newly synthesized I<sub>2</sub>-IR ligand, diethyl (1RS,3aSR,6aSR)-5-(3-chloro-4-fluorophenyl)-4,6-dioxo-1-phenyl-1,3a,4,5,6,6a-hexahydropyrrolo[3,4-c]pyrrole-1-phosphonate, named B06, which has outstanding affinity and selectivity for I<sub>2</sub>-IRs over  $\alpha_2$  adrenoreceptors (Escolano et al. 2019).

The SAMP8 strain is a nontransgenic mouse strain established through phenotypic selection of the AKR/J mouse strain and is an attractive model with which to study aging processes, especially age-related deterioration of learning and memory, emotional disorders and neurochemical alterations (Takeda et al. 2009, Pallas. 2012). At approximately 5 months of age, the mice begin to undergo an accelerated process of senescence, and the brain aging manifests as severe cognitive decline and neuroinflammation (Akiguchi et al. 2017). It is considered a late-onset AD mouse model characterized by altered amyloid precursor protein (APP) processing and high levels of tau hyperphosphorylation (Canudas et al. 2005; Morley et al., 2012). Moreover, inflammatory and OS markers are present at early ages and during adulthood (Griñán-Ferré et al. 2015, 2016).

### 3.3.2 METHODS

#### *In vivo* studies in mice

Twelve-month-old female SAMP8 mice ( $n = 23$ ) (Envigo, Sant Feliu de Codines, Barcelona, Spain) were used to carry out cognitive and molecular analyses. The animals were randomly allocated into two experimental groups: the SAMP8 control group (control) ( $n=12$ ), which was administered vehicle (2-hydroxypropyl)- $\beta$ -cyclodextrin 1.8% in drinking water, and the SAMP8 group, which was treated with the I<sub>2</sub>-IR ligand B06 (5 mg/kg) ( $n=11$ ). The animals had free access to food and water and were kept under standard temperature conditions ( $22 \pm 2^\circ\text{C}$ ) and 12-hour/12-hour light/dark cycles (300 lux/0 lux). B06 (5 mg/kg/day) was diluted in 1.8% (2-hydroxypropyl)- $\beta$ -cyclodextrin and administered through drinking water. After 4 weeks of treatment, behavioral and cognitive tests, including short- and long-term memory, were performed to study the effects of treatment on learning and memory. Weight and water consumption were controlled each week, and the B06 concentration was adjusted accordingly to reach the optimal dose until euthanasia. The mice were euthanized 3 days after behavioral test completion by cervical dislocation. The brains were immediately removed from the skulls and frozen on powdered dry ice. The samples were stored at  $-80^\circ\text{C}$  until the biochemical experiments.

The studies and procedures for the mouse behavior tests, brain dissection and extractions followed the ARRIVE and standard ethical guidelines (European Communities Council Directive 2010/63/EU and Guidelines for the Care and Use of Mammals in Neuroscience and Behavioral Research, National Research Council 2003) and were approved by Bioethical Committees from the University of Barcelona and the Government of Catalonia. All efforts were made to minimize the number of animals used and their suffering.

#### **Novel object recognition test (NORT)**

Briefly, mice were placed in a  $90^\circ$  two-arm 25-cm-long, 20-cm-high, 5-cm-wide black maze. Before performing the test, the mice were individually habituated to the apparatus for 10 minutes for 3 days. On day 4, the animals were allowed to freely explore in a 10-minute acquisition trial (first trial), for which they were placed in the maze in the presence of two identical objects at the end of each arm (Fig. 1A). After a delay (2 h for short-term memory evaluation and 24 h for long-term evaluation), the animal was allowed to explore the old object and one novel object in each trial (Fig. 1A). The time that the mice spent exploring the novel object (TN) and the time that the mice spent exploring the old object (TO) were measured. A DI was defined as  $(\text{TN}-\text{TO})/(\text{TN}+\text{TO})$ . Exploration of an object was defined as pointing the nose towards the object at a distance  $\leq 2$  cm and/or touching it with the nose. Turning or sitting around the object was not considered



exploration. To avoid object preference biases, the objects were counterbalanced.

### **Open field test (OFT)**

The open field test (OFT) was performed as previously described (Griñán-Ferré et al., 2015) (Fig. 1B). Briefly, mice were placed at the center of and allowed to explore a white plywood box (50x50x25 cm) for 5 minutes. Behavior was scored with SMART® ver. 3.0 software, and each trial was recorded for later analysis. The parameters scored included the center stay duration, number of rearings, number of defecations, and distance traveled.

### **Determination of oxidative stress**

Hydrogen peroxide (H<sub>2</sub>O<sub>2</sub>) was measured as an indicator of OS, and it was quantified using a hydrogen peroxide assay kit (Cat. No. MAK165, Sigma-Aldrich, Saint Louis, Missouri, Estats Units) according to the manufacturer's instructions.

### **Immunodetection experiments**

#### *Brain processing*

Three days after the behavioral and cognitive tests, mice were euthanized for protein extraction and RNA and DNA isolation. After euthanasia, the brains were immediately removed from the skulls, and the hippocampi were dissected, frozen and maintained at -80°C. For an IHC experiment, mice were anesthetized (ketamine 100 mg/kg and xylazine 10 mg/kg, intraperitoneally) and then perfused with 4% paraformaldehyde (PFA) diluted in 0.1 M phosphate buffer solution intracardially. Their brains were removed and postfixed in 4% PFA overnight at 4°C. Afterwards, the solutions were changed to PFA + 15% sucrose. Finally, the brains were frozen on powdered dry ice and stored at -80°C until sectioning.

#### *Protein level determination by Western blotting*

For subcellular fractionation, 150 µL of buffer A (10 mM HEPES pH 7.9, 10 mM KCl, 0.1 mM EDTA pH 8, 0.1 mM EGTA pH 8, 1 mM DTT, 1 mM PMSF, protease inhibitors) was added to each sample, and the mixtures were incubated on ice for 15 min. After this time, the samples were homogenized with a tissue homogenizer, 12.5 µL Igepal 1% was added, and the Eppendorf tubes were vortexed for 15 s. Following 30 s of full-speed centrifugation at 4°C, the supernatants (cytoplasmic fractions) were collected; 80 µL of buffer C (20 mM HEPES pH 7.9, 0.4 M NaCl, 1 mM EDTA pH 8, 0.1 mM EGTA pH 8, 20% glycerol 1 mM DTT, 1 mM PMSF, protease inhibitors) was added to each pellet, and the pellets were incubated under agitation at 4°C for 15 min. Subsequently, the samples were centrifuged for 10 min at full speed at 4°C. The supernatants (nuclear fractions) were collected.

For Western blotting (WB), aliquots of 20  $\mu\text{g}$  of hippocampal protein were used. Protein samples from mice were separated by sodium dodecyl sulfate-polyacrylamide gel electrophoresis (SDS-PAGE) (8-12%) and transferred onto polyvinylidene difluoride (PVDF) membranes (Millipore). Afterwards, the membranes were blocked in 5% nonfat milk in 0.1% Tris-buffered saline with Tween 20 (TBS-T) for 1 hour at room temperature before being incubated overnight at 4°C with the primary antibodies listed in Table 1.

The membranes were washed and incubated with secondary antibodies for 1 hour at room temperature. Immunoreactive proteins were viewed with a chemiluminescence-based detection kit following the manufacturer's protocol (ECL Kit; Millipore, Burlington, Massachusetts, USA), and digital images were acquired using a ChemiDoc XRS+ System (Bio-Rad, Hercules, California, USA). Semiquantitative analyses were carried out using ImageLab software (Bio-Rad), and the results are expressed in arbitrary units (AU), with the control protein levels set as 100%. Protein loading was routinely monitored by immunodetection of glyceraldehyde-3-phosphate dehydrogenase (GAPDH) or  $\beta$ -actin.

#### *Immunofluorescence*

Brain coronal sections of 30  $\mu\text{m}$  were obtained (Leica Microsystems CM 3050S cryostat, Wetzlar, Germany) and kept in a cryoprotectant solution at -20°C until use. Free-floating slices were placed in a 24-well plate and washed with 0.1M PBS. Next, the free-floating sections were blocked with a solution containing 1% (BSA), 0,3% Triton X-100, 0.1M PBS for 20 min at room temperature; washed with PBS 0.1M two times for 5 minutes each; and incubated with the primary antibodies listed in Table 2 overnight at 4°C. On the following day, the coronal slices were washed with 0.1M PBS 0.1M 2 times for 5 minutes each and then incubated with the secondary antibodies listed in Table 2 at room temperature for 1h. Later, the sections were washed two times for 5 min each with 0.1M PBS and were incubated with 5 $\mu\text{M}$  Hoechst staining solution (Sigma-Aldrich, St. Louis, MO) for 5 minutes in the dark at room temperature. Finally, the slices were mounted using Fluoromount-G (EMS, Hatfield, Pennsylvania, USA), and image acquisition was performed with a fluorescence laser microscope (Olympus BX41, Hamburg, Germany) by using x4 and x20 magnification. At least four images from 4 different individuals in each group were analyzed with ImageJ/Fiji software available online from the National Institutes of Health.

#### **RNA extraction and gene expression determination**

Total RNA isolation was carried out using TRIzol® reagent according to the manufacturer's instructions. The yield, purity, and quality of RNA were determined spectrophotometrically with a NanoDrop™ ND-1000 apparatus (Thermo Scientific, Waltham, Massachusetts, USA)

and an Agilent 2100B Bioanalyzer (Agilent Technologies, Santa Clara, California, USA). RNA samples with 260/280 ratios and RINs higher than 1.9 and 7.5, respectively, were selected. Reverse transcription-polymerase chain reaction (RT-PCR) was performed. Briefly, 2  $\mu\text{g}$  of messenger RNA (mRNA) was reverse-transcribed using a high-capacity cDNA reverse transcription kit (Applied Biosystems, Foster City, California, USD).

SYBR® Green real-time PCR was performed on a StepOnePlus Detection System (Applied Biosystems) with SYBR® Green PCR master mix (Applied Biosystems). Each reaction mixture contained 6.75  $\mu\text{L}$  of complementary DNA (cDNA) (with a concentration of 2  $\mu\text{g}$ ), 0.75  $\mu\text{L}$  of each primer (with a concentration of 100 nM), and 6.75  $\mu\text{L}$  of SYBR® Green PCR master mix (2X). TaqMan-based real-time PCR (Applied Biosystems) was also performed in a StepOnePlus Detection System (Applied Biosystems). Each 20  $\mu\text{L}$  TaqMan reaction contained 9  $\mu\text{L}$  of cDNA (25 ng), 1  $\mu\text{L}$  of 20X TaqMan gene expression assay probe and 10  $\mu\text{L}$  of 2X TaqMan universal PCR master mix. The data were analyzed utilizing the comparative cycle threshold (Ct) ( $\Delta\Delta\text{Ct}$ ) method, in which the levels of a housekeeping gene are used to normalize differences in sample loading and preparation. Normalization of expression levels was performed with  $\beta$ -actin for SYBR® Green-based real-time PCR and Gapdh for TaqMan-based real-time PCR. The primer sequences and TaqMan probes used in this study are presented in Table 3. Each sample was analyzed in duplicate, and the results represent the n-fold differences in the transcript levels among different groups.

### Statistical analysis

Statistical analysis was conducted using GraphPad Prism ver. 8 statistical software. The data are expressed as the mean  $\pm$  standard error of the mean (SEM). Means were compared with two-tailed Student's t-test. Statistical significance was considered when p values were  $<0.05$ . Statistical outliers were determined with Grubbs' test and when necessary were removed from the analyses.

## 3.3.3 RESULTS

### Prevention of memory loss and behavioral impairment in SAMP8 mice after I<sub>2</sub>-IR ligand treatment

The NORT demonstrated significant differences between the control and I<sub>2</sub>-IR ligand B06 groups in both short- and long-term evaluations. Significantly higher DI values were obtained for the B06-treated mice than for the control mice at 2 h and 24 h after novel object exposure, indicating a neuroprotective action of B06 against the characteristic SAMP8 mouse memory loss (Figs. 1C-D). In addition, the results regarding locomotor

activity, time spent in the center area and number of rearings, as assessed with the OFT paradigm, revealed significant changes in behavior in the B06 group in comparison with the control group (Figs. 1E-G).

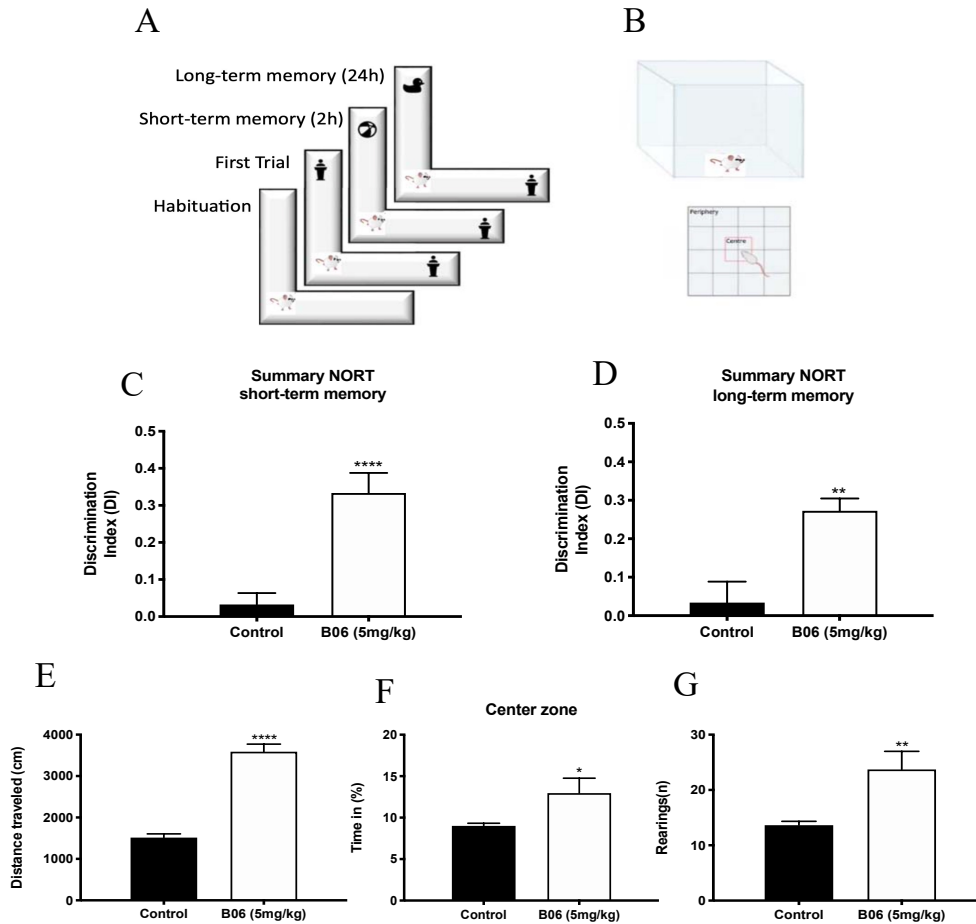


**Figure 1:** Scheme for NORT (A) and OFT (B) experimental paradigms. The I<sub>2</sub>-IR ligand improved the novel object recognition abilities (measured as Discrimination Index, DI) in SAMP8 treated with B06 at 5 mg/Kg/day (B06 5mg/kg) in comparison with the SAMP8 Control both in summary short-term memory (C) and summary long-term memory (D). In the Open Field Test (OFT) 12-month-old SAMP8 treated with B06 at 5 mg/Kg/day (B06 5mg/kg) presented a significant increase in the distance traveled (E), the percentage of time spent in Center zone (F) and the number of Rearings (G). Values represented are mean  $\pm$  Standard error of the mean (SEM); n = 15 (Control n = 8, B06 n = 7); \*p<0.05; \*\*p<0.01; \*\*\*p<0.001; \*\*\*\*p<0.0001 vs. Control.

### AD hallmark modifications in the hippocampi of SAMP8 mice induced by I<sub>2</sub>-IR ligand and treatment

The levels of key proteins involved in APP processing were evaluated. The I<sub>2</sub>-IR ligand B06 promoted significant increases in soluble APP $\alpha$  (sAPP $\alpha$ ) levels but clearly tended to decrease soluble APP $\beta$  (sAPP $\beta$ ) levels (Figs. 2A-B). Accordingly, the gene expression of *Adam10*, a constitutive  $\alpha$ -secretase, increased, indicating a shift to the nonamyloidogenic pathway (Fig. 2C). Moreover, the gene expression of both insulin-degrading enzyme (*Ide*) and neprilysin (*Nep*) was increased after B06 treatment (Fig. 2C). Tau hyperphosphorylation is a characteristic posttranslational modification in aged SAMP8 mice. B06 treatment induced significant decreases in phosphorylation at the Ser404 and Ser396 sites in tau protein (Figs. 3A-B). There are two main kinases implicated in tau hyperphosphorylation: glycogen synthase kinase 3 $\beta$  (GSK3 $\beta$ ) and cyclin-dependent kinase 5 (CDK5). GSK3 $\beta$  phosphorylated at Ser9 is the inactive form of the enzyme and is correlated with reduced tau phosphorylation. As expected, the I<sub>2</sub>-IR ligand B06 increased p-GSK3 $\beta$  (Ser9) levels, indicating that it reduced kinase activity (Fig. 3C). CDK5 is also activated by phosphorylation, and p25, a coactivator, controls its activity. The results showed that the I<sub>2</sub>-IR ligand-treated group presented decreases in the p-CDK5 level and p25/p35 ratio (Figs. 3D-E).

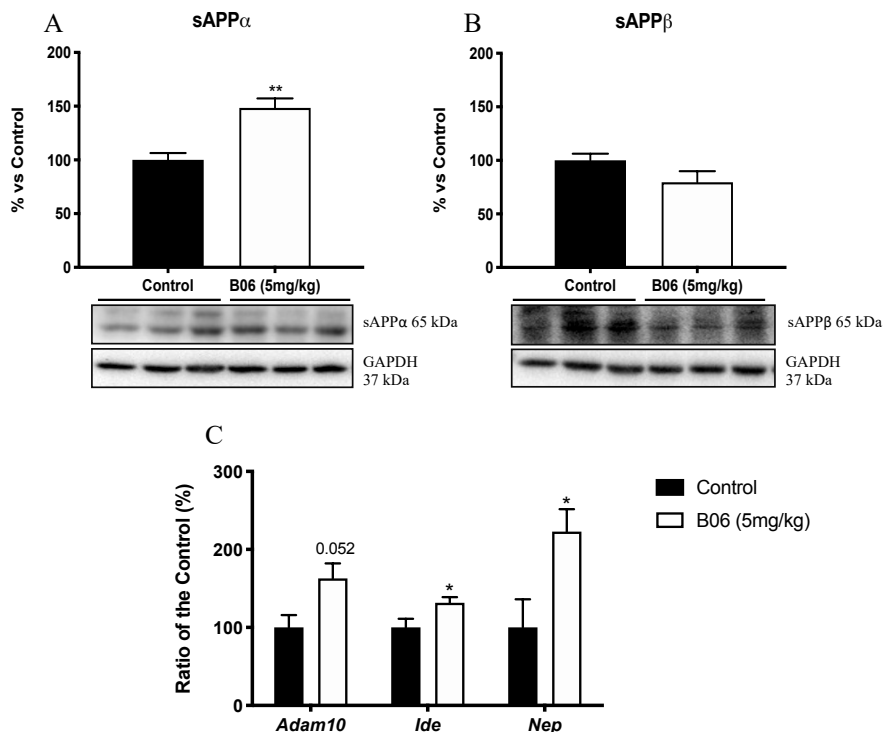


Figure 2: (Caption next page)

**Figure 2:** (Previous page) **Treatment with the I<sub>2</sub>-IR ligand B06 resulted in significant differences in the amyloid processing and A $\beta$  degradation pathway between the 12-month-old control SAMP8 (Control) and the SAMP8 treated with B06 at 5 mg/Kg/day (B06 5mg/kg).** Representative western blot for sAPP $\alpha$  and sAPP $\beta$  protein levels and quantification (A, B). Values in bar graphs were adjusted to 100% for the protein of control SAMP8 (Control). Representative gene expression for *Adam10*, *Ide* and *Nep* (C). Gene expression levels were determined by real-time PCR. Values are the mean  $\pm$  Standard error of the mean (SEM); (n= 3-5 animals per group); \*p<0.05; \*\*p<0.01 vs. Control.

### **I<sub>2</sub>-IR ligand treatment changes synaptic and apoptotic markers in SAMP8 mice**

The I<sub>2</sub>-IR ligand B06 reduced the protein levels of the NMDA 2B receptor, increased those of the form phosphorylated at Tyr1472 and increased those of the NMDA 2A receptor significantly (Figs. 4A-C).

The levels of calcium/calmodulin-dependent protein kinase II (CaMKII), a marker of synaptic plasticity, did not show significant changes, but the levels of the phosphorylated form of cAMP response element-binding protein (CREB) were dramatically increased (Fig. 4D) in the B06 group. Accordingly, the gene expression of the CREB target brain-derived neurotrophic factor (*Bdnf*) was increased in the B06 group (Fig. 4G).

Protein kinase A (PKA) is a master regulator of the activity of CREB, among other transcription factors. B06-treated animals showed increased protein levels of PKA a (the catalytic fragment) (Fig. 4E). We found significant recovery of AKT, also known as protein kinase B, phosphorylation and subsequent activation (Fig. 4F) in the B06 group, indicating a pathway of neuroprotective regulation after B06 treatment.

B-cell lymphoma 2 (BCL-2), Bax, BCL-2-associated agonist of cell death (BAD) and Caspase 3 are key factors in apoptotic signaling in neurons. B06 was able to reduce Caspase 3 and Bcl-2-like protein 4 (Bax) protein levels; surprisingly, it also reduced BCL-2 protein levels (Figs. 5A-C). An increase in p-BAD was also observed (Fig. 5D); however, in this case, phosphorylation of BAD indicated a lack of capacity to form apoptotic pores by dimerizing BAD, which subsequently weakened the proapoptotic role of this factor. Overall, prevention of apoptotic mechanisms followed treatment with the I<sub>2</sub>-IR ligand B06.

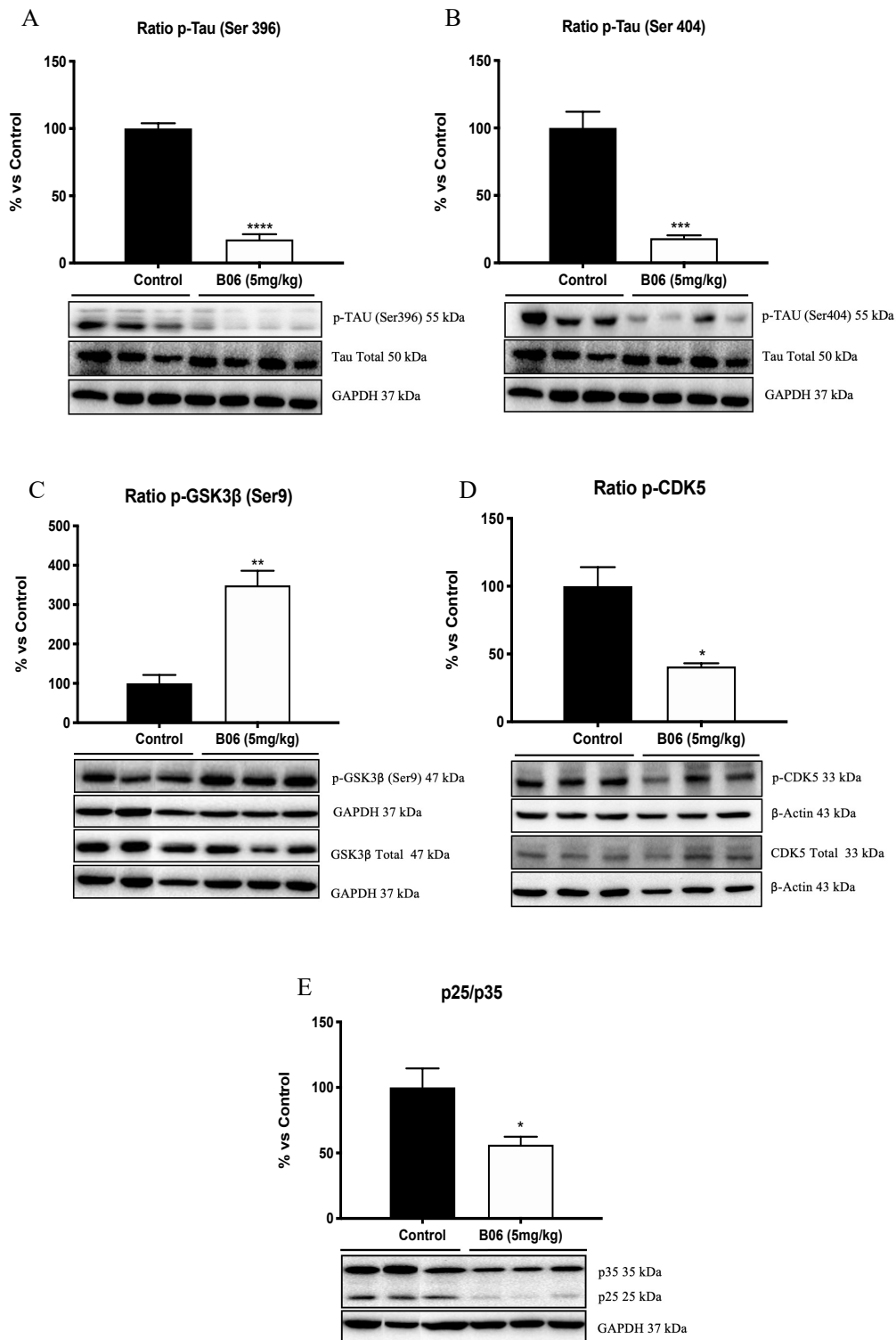


**Figure 3: The I<sub>2</sub>-IR treatment mediated a significant decrease in Tau phosphorylation and the implicated kinases in 12-month-old SAMP8 treated with B06 at 5 mg/Kg/day (B06 5mg/kg) when compared to control SAMP8 (Control). Representative western blot for ratio p-Tau (Ser396 and Ser404), Ratio p-GSK3 $\beta$  (Ser9), Ratio p-CDK5, p25/35 and quantification (A-E). Values in bar graphs were adjusted to 100% for protein of control SAMP8 (Control). Values are the mean  $\pm$  Standard error of the mean (SEM); (n= 3-5 animals per group); \*p<0.05; \*\*p<0.01; \*\*\*p<0.001; \*\*\*\*p<0.0001 vs. Control.**

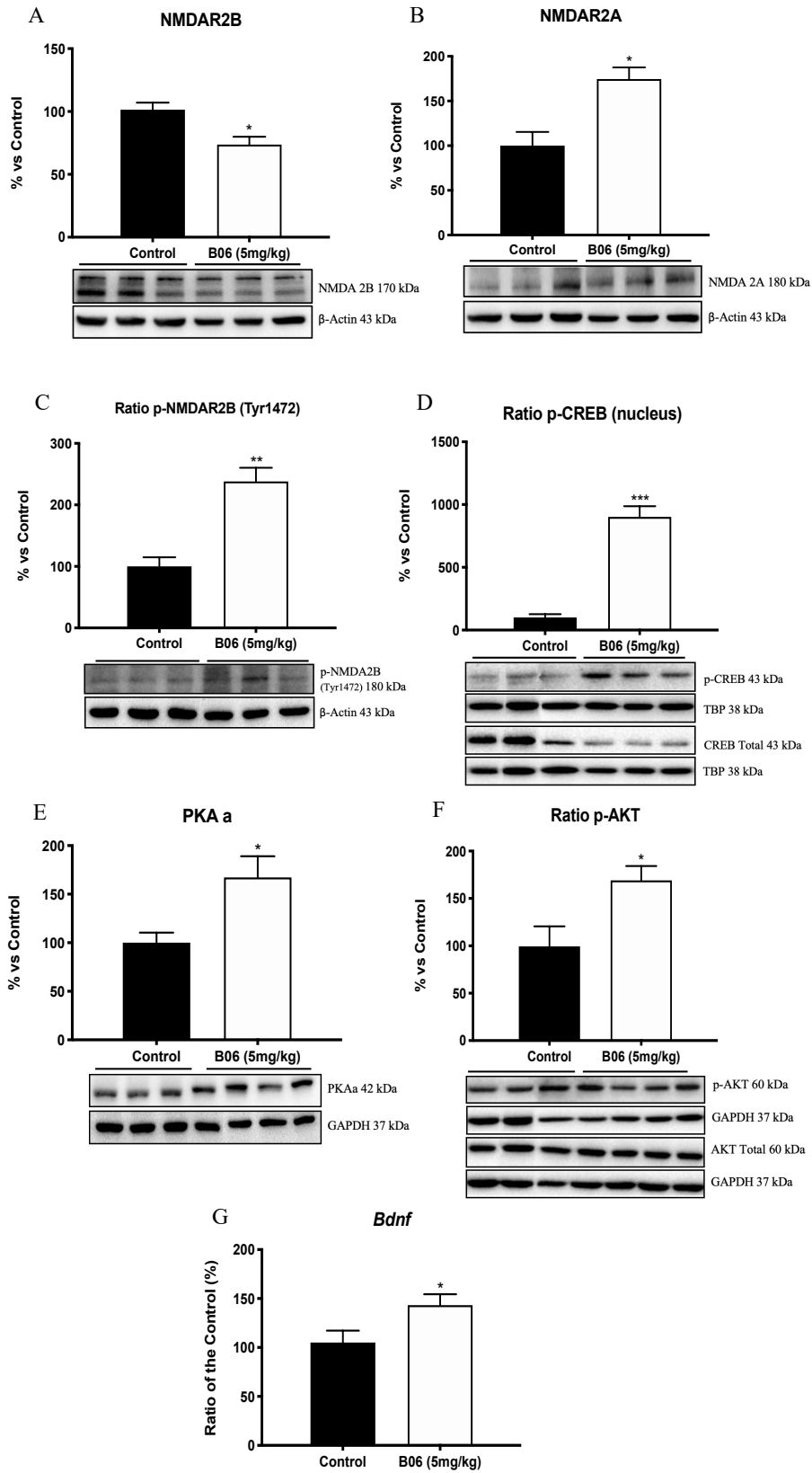
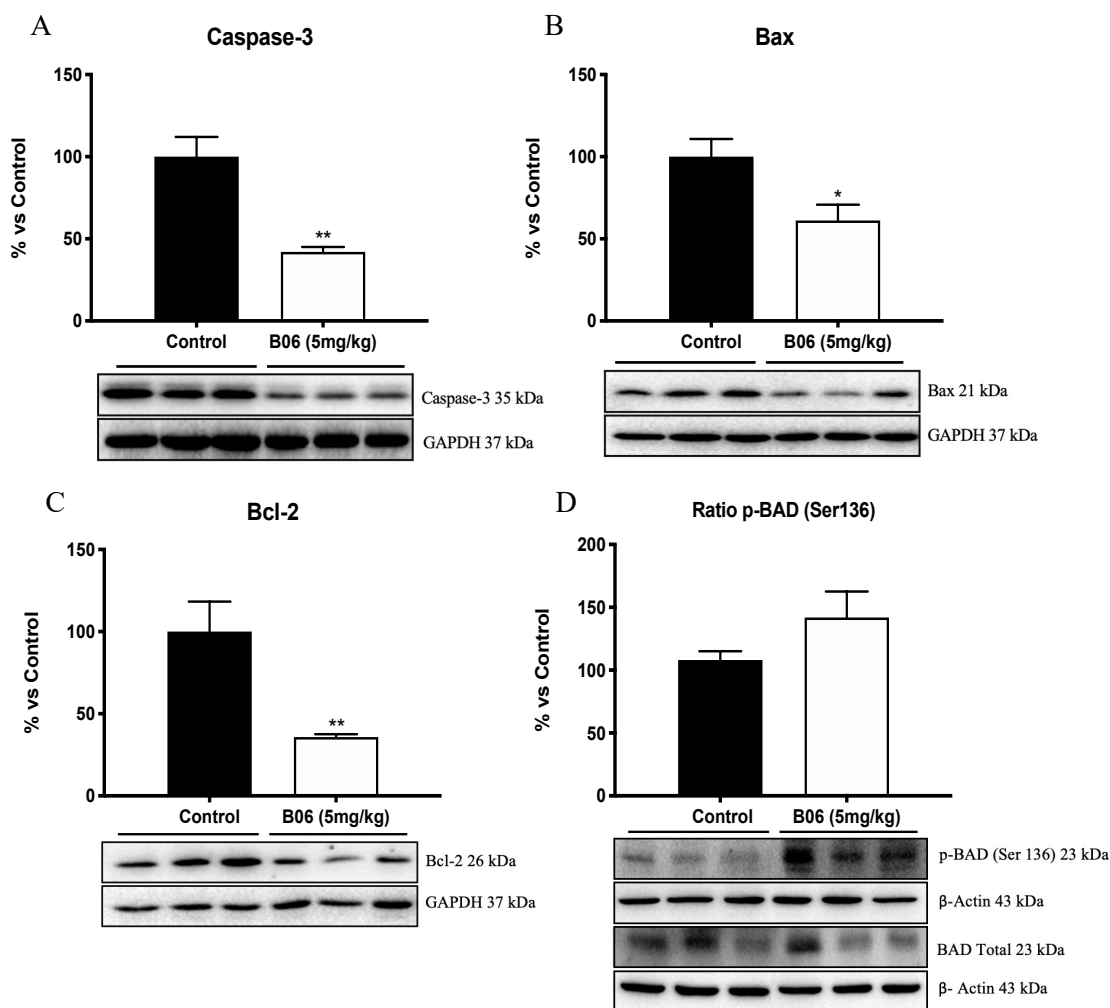


Figure 4: (Caption next page)



**Figure 4:** (Previous page) **Changes in NMDARs, neuronal plasticity and Kinase pathways induced by I<sub>2</sub>-IR ligand B06 in 12-month-old SAMP8 after treatment at 5 mg/Kg/day (B06 5mg/kg) in comparison with 12-month-old control SAMP8 (Control).** Representative western blot for NMDAR2B, NMDAR2A, Ratio p-NMDAR2B (Tyr1472). Ratio p-CREB in nucleus protein levels and quantification (A-D). Representative Western blot for kinases PKA, Ratio p-AKT and quantification (E, F). Values in bar graphs were adjusted to 100% for the protein of control SAMP8 (Control). Representative gene expression for *Bdnf* (G). Gene expression levels were determined by real-time PCR. Values are the mean  $\pm$  Standard error of the mean (SEM); (n= 3-5 animals per group); \*p<0.05; \*\*p<0.01; \*\*\*p<0.001 vs. Control.



**Figure 5:** Treatment with the I<sub>2</sub>-IR ligand B06 suppressed apoptosis by inhibiting the implicated apoptotic factors in 12-month-old SAMP8 treated with B06 at 5 mg/Kg/day (B06 5mg/kg) as compared to control SAMP8 (Control). Representative western blot for caspase-3, Bax, BCL-2, Ratio p-BAD (Ser136) and quantification (A-D). Values in bar graphs were adjusted to 100% for the protein of control SAMP8 (Control). Values are the mean  $\pm$  Standard error of the mean (SEM); (n= 3-5 animals per group); \*p<0.05; \*\*p < 0.01 vs. Control.

**Neuroinflammation and oxidative state changes in SAMP8 mice after I<sub>2</sub>-IR ligand treatment**

GFAP protein levels were highly significantly decreased in the B06 group (Fig. 6A), indicating that astrogliosis and neuroinflammation processes were ameliorated in I<sub>2</sub>-IR ligand B06-treated mice. Astrocytes control glutamatergic signaling through glutamate transporters, and B06 was able to enhance the protein levels of excitatory amino acid transporter (EAAT) 2 (Fig. 6B). The expression of proinflammatory cytokines, such as interleukin 6 (*Il-6*), *Il-18*, *Il-1β*, interferon (*Ifn-γ*), tumor necrosis factor-alpha (*Tnf-α*), and C-X-C motif chemokine ligand 10 (*Cxcl-10*), was decreased after treatment with the I<sub>2</sub>-IR ligand B06 (Fig. 6K), and the decrease reached significance for *Il-6*, *Il-18* and *Il-1β*. H<sub>2</sub>O<sub>2</sub> levels in the hippocampus were significantly diminished in the B06 mouse group, showing that global redox homeostasis was shifted due to the antioxidant role of the I<sub>2</sub>-IR ligand in SAMP8 mice (Fig. 6M). The expression of nuclear factor-erythroid 2-related factor 1 (*Nrf1*), a key gene controlling the oxidative cell environment, was higher in the group treated with the I<sub>2</sub>-IR ligand B06 than in the untreated mouse group (Fig. 6L). In addition, the gene expression of antioxidant machinery enzymes such as hemoxygenase 1 (*Hmox 1*) was increased, whereas that of aldehyde dehydrogenase 2 (*Aldh2*) was reduced, indicating that B06 prevented SAMP8 brain from experiencing an oxidant environment by neutralizing radical oxygen species (ROS) (Fig. 6L). Conversely, a significant increase in the gene expression of inducible nitric oxide synthase (*iNOS*) was found, although this increase could have improved synaptic function (Fig. 6L). Finally, immunostaining quantification of GFAP fluorescence intensity demonstrated that B06 treatment significantly reduced GFAP staining, especially in the dentate gyrus (DG) and CA1 regions (Figs. 6D-J), suggesting a reduction in astrogliosis. Moreover, immunostaining quantification of S100A9 fluorescence intensity showed that B06 treatment reduced S100A9 staining, especially in the CA1 and CA3 regions, but the reductions were not significant (Figs. 6D-J).

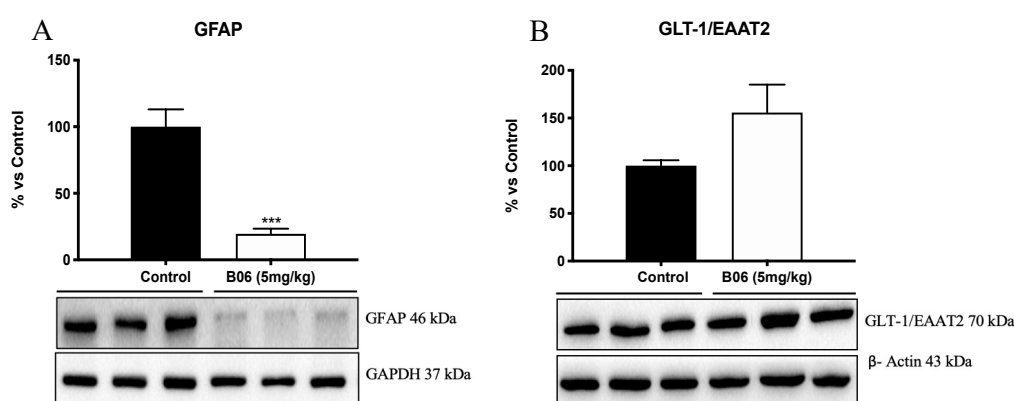
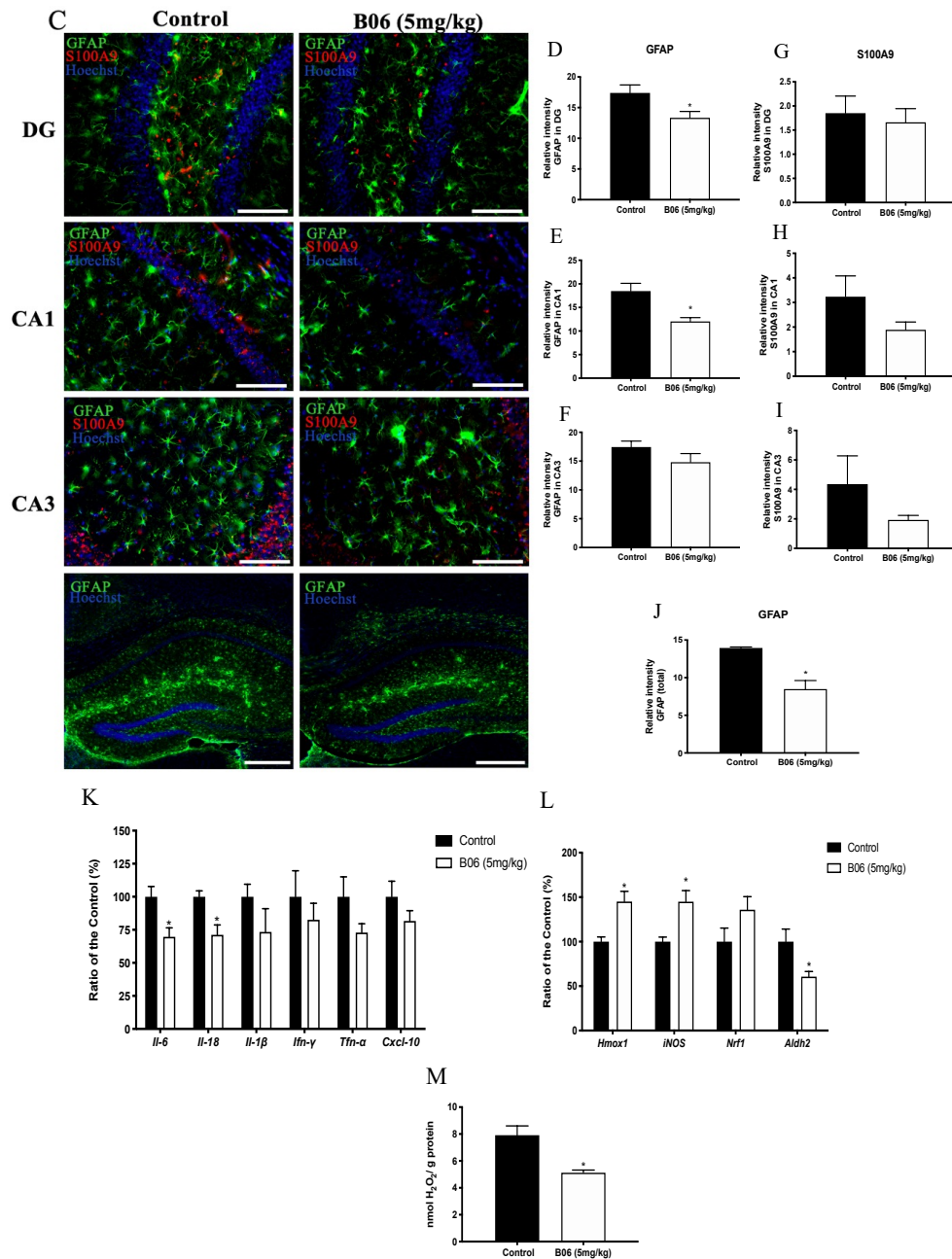


Figure 6: (Continued)



**Figure 6: I<sub>2</sub>-IR ligand, B06, attenuated neuroinflammation and OS state in 12-month-old SAMP8 treated mice at 5 mg/Kg/day (B06 5mg/kg) when compared to the control SAMP8 (Control).** Representative western blot for GFAP, GLT-1/EAAT-2 (A-B). Representative images for GFAP (C) and S100A9 immunostaining (C) and quantifications for GFAP and S100A9 on the bar chart (D-J). Representative gene expression for inflammatory markers such as *Il-6*, *Il-18*, *Il-1β*, *Ifn-γ*, *Tnf-α* and *Cxcl-10* (K) and OS markers such as *Hmox1*, *iNOS*, *Nrf1* and *Aldh2* (L). Quantification of Intracellular H<sub>2</sub>O<sub>2</sub> (μM) (M). Gene expression levels were determined by real-time PCR. Values in bar graphs were adjusted to 100% for the protein of control SAMP8 (Control). DG: Dentate Gyrus. Scale bar for immunohistochemical images is 200 μm. Values are the mean ± Standard error of the mean (SEM); (n = 3-5 animals per group); \*p<0.05; \*\*p<0.001 vs. Control.

### I<sub>2</sub>-IR ligand treatment modifies CaN/NFAT signaling in the SAMP8 mouse hippocampus

In light of the obtained results, we focused on CaN, an upstream protein with phosphatase activity toward CREB or BAD that plays a role in neurodegeneration. The protein levels of CaN A, the active form, were reduced after treatment with the I<sub>2</sub>-IR ligand B06 (Fig. 7A). We also evaluated NFAT<sub>c1</sub>, a different target of CaN. The results showed an increase in the phosphorylated form (Fig. 7B). As a summary of the results, Figure 8 shows the molecular alterations related to cognitive improvement as well as the key role of CaN in controlling the cellular response after treatment with the I<sub>2</sub>-IR ligand B06.

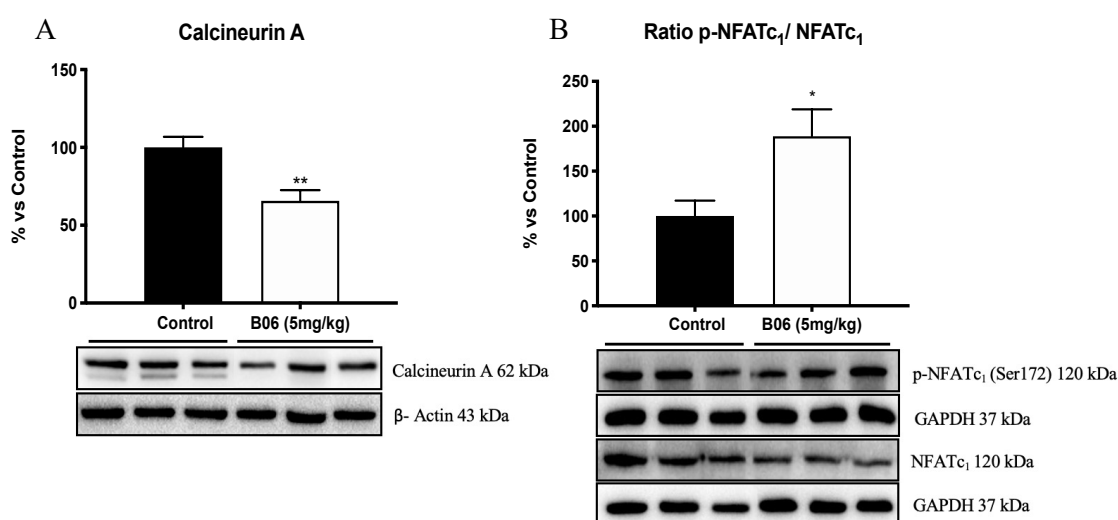


**Figure 7: Modulation of CaN signaling after B06 treatment in 12-month-old SAMP8 treated mice at 5 mg/Kg/day (B06 5mg/kg).** Representative western blot for CaN A, ratio p-NFAT<sub>c1</sub>/NFAT<sub>c1</sub> and quantification (A, B). Values in bar graphs were adjusted to 100% for protein of control SAMP8 (Control). Values are the mean  $\pm$  Standard error of the mean (SEM); (n= 3-5 animals per group); \*p<0.05; \*\*p<0.01 vs. Control.

### 3.3.4 DISCUSSION

Here, we report that treatment with the I<sub>2</sub>-IR ligand B06 in the SAMP8 mouse model, a model of neurodegeneration linked to aging that is considered to recapitulate late-onset AD, has beneficial effects via modulation of the CaN pathway. Imidazoline receptors were described in the nineties, and I<sub>2</sub>-IRs are related to neurodegenerative diseases such as AD (García-Sevilla et al. 1998), Huntington's disease (Reynolds et al. 1996) and PD (Reynolds et al. 1996; Tyacke et al. 2018; Wilson et al. 2019). However, the signal transduction pathway for I<sub>2</sub>-IR remains elusive (Bousquet et al, 2020). Previous reports have indicated putative roles related to monoamine oxidase (MAO) A or B (McDonald et al. 2010) and intracellular calcium concentration control through NMDA receptors or

intracellular calcium stores (Jiang et al. 2010; Zhao Han et al. 2013). Recently, we have demonstrated that ligands for I<sub>2</sub>-IRs are able to prevent neurodegeneration by acting on the apoptotic mechanism (Abas et al. 2017), and decreasing the activity of kinases (CDK5, GSK3 $\beta$ , etc.) (Abas et al. 2016, Griñán-Ferré et al. 2019), leading to the recovery of cognitive capabilities in an AD mouse model (Griñán-Ferré et al. 2019). However, the intrinsic mechanisms that induce these changes are not precisely known.

B06 is a new improved I<sub>2</sub>-IR ligand with a lower K<sub>i</sub> for I<sub>2</sub>-IR than previous ligands and high selectivity for I<sub>2</sub>-IRs over  $\alpha_2$  adrenoceptors (Escolano et al. 2019). The latter characteristic is of the utmost importance for avoidance of undesirable adverse effects on, for example, the vascular system. We have previously reported that administration of B06 to the 5xFAD mouse model, a transgenic representative model of AD, reduces cognitive decline, neuroinflammation, tau hyperphosphorylation and APP processing (Escolano et al. 2019).

In the present work, we demonstrated that the I<sub>2</sub>-IR ligand B06 was able to improve cognition and ameliorate anxiety-like behavior in aged SAMP8 mice. Furthermore, we confirmed that on the molecular level, treatment with B06 reduced the exhibition of AD hallmarks, such as APP processing and tau hyperphosphorylation; inhibited tau kinase (CDK5 and GSK3 $\beta$ ) activation; reduced the gene expression of neuroinflammation markers, such as *Il-6*, *Il-18*, and *Tnf- $\alpha$* , and decreased OS.

When the apoptotic pathway was studied, decreases in Caspase 3, Bax, and BCL-2 levels were found. However, there has been a lack of consistency among I<sub>2</sub>-IR studies regarding the reduction in apoptotic signaling (Garau et al. 2013). Our results are consistent with those of several studies showing that administration of I<sub>2</sub>-IR ligands such as 2-BFI and BU224 can reduce apoptotic marker levels in the rat brain cortex (Li. 2017). Considering that I<sub>2</sub>-IRs have been reported to be involved in key pathways associated with neurodegeneration, we also evaluated several master pathways in B06-treated senescent mice, including those that are under the control of cytosolic calcium, astrocyte activation and synaptic neural plasticity. The localization of I<sub>2</sub>-IRs remains elusive, but several studies have reported astrocytes as a major cell type with I<sub>2</sub>-IR binding sites (Choi et al. 2018). Of note, astrogliosis and activated microglial cells are associated with amyloid processing, indicating that this AD hallmark is a major trigger of gliosis (Vehmas et al. 2003). After B06 treatment, a very significant decrease in the expression of the hippocampal panastrocytic reactive marker GFAP indicated strong control of neuroinflammation and a reduction in astrogliosis that in turn could prevent neuronal function loss. Moreover, S100A9, a Ca<sup>2+</sup>-binding protein with a critical role in modulating the inflammatory response and inducing cytokine release by astrocytes (Wang et al. 2018), was used as

a marker of neuroinflammation mediated by reactive astrocytes. In our study, we found clear reductions in two hippocampal areas, CA1 and CA3, confirming a reduction in the inflammatory state after treatment with B06. Likewise, the expression of the EAAT2 isoform (or Glt 1), a glutamate transporter predominantly located in astrocytes, was increased after treatment with the I<sub>2</sub>-IR ligand B06. EAAT2 is implicated in glutamate clearance and has a leading role in the removal of excess glutamate and other potentially toxic mediators (Furman and Norris. 2014). In line with these findings, our previous results for two other I<sub>2</sub>-IR ligands (Griñán-Ferré et al. 2018) showed the same action regarding astrogliosis. However, in contrast, another study on the I<sub>2</sub>-IR ligand LSL60101 showed induction of reactive astrogliosis in the facial motor nuclei of neonate rats after short-term treatment (Casanovas et al. 2000), suggesting that the effects differ depending on both the physicochemical properties of the I<sub>2</sub>-IR ligand and the experimental model.

Notably, in astrocytes, increased CaN activity can lead to modification of the kinase activity of GSK3 $\beta$  (Watanabe et al. 2015). Calcium entry through NMDA2B receptors enhances the activation of GSK3 $\beta$  through CaN phosphatase activity, and in turn, GSK3 $\beta$  amplifies this phosphatase activity, dephosphorylating CREB (Szatmari et al. 2005; Wang et al. 2018). In addition, the interaction of I<sub>2</sub>-IR ligands with NMDA receptors has been well described (Olmos, De-Gregorio-Rocasolano, et al. 1999; Olmos, Ribera & Garcia-Sevilla. 1996). Thus, our results support the idea that modulation of I<sub>2</sub>-IRs by B06 is able to induce changes in NMDA receptors. We definitively observed changes in NMDA receptor subunit composition and activation. On the one hand, increases in NMDA2A receptor protein levels were observed. On the other hand, decreases in NMDA2B receptor protein levels with increased phosphorylation were observed. These changes are associated with LTP, which may partially explain the improvement in cognition observed in B06-treated SAMP8 mice.

To further elucidate the molecular mechanisms modulated by B06, we examined the negative crosstalk between AKT and GSK3 $\beta$  signaling that participates in synaptic plasticity (Bradley et al. 2012) controlled by CaN phosphatase activity. As mentioned, B06 treatment reduced GSK3 $\beta$  activation by increasing the levels of its inactive form phosphorylated at Ser9, whereas it activated AKT signaling. Because AKT is a recognized prosurvival molecule that participates in neural plasticity, modulation of AKT signaling in animals treated with the I<sub>2</sub>-IR ligand B06 likely contributed to the favorable effects on cognition observed in SAMP8 mice (Zhu et al. 2001; Sun and Nan. 2017).

p-CREB controls the expression of genes related to synaptic disruption and LTP, such as *Bdnf* (Bridi et al. 2017). Neuronal growth and survival require the expression of CREB target genes that control various proteins, including BDNF and its receptor tropomyosin-

related kinase B (TrkB) (Zhang et al. 2012). On the one hand, treatment with the I<sub>2</sub>-IR ligand B06 increased nuclear p-CREB levels and increased *Bdnf* gene expression. On the other hand, B06 increased the levels of PKA, which can drive p-CREB nuclear translocation. Of note, PKA acts as a negative modulator of NFAT<sub>c1</sub>, a transcription factor that regulates the transcription of genes that play crucial roles in axonal outgrowth control (Sheridan et al. 2002). Interestingly, I<sub>2</sub>-IR ligand treatment induced an increase in NFAT<sub>c1</sub> phosphorylation in parallel with decreases in *Il-6*, *Ifn-γ* and *Tnf-α* gene expression. NFAT<sub>c1</sub> and CaN are master regulators that control EAAT2 up- or downregulation (Su et al. 2003). We hypothesize that the observed changes in NFAT<sub>c1</sub> are responsible for the increase in EAAT2 described above.

NFAT<sub>c1</sub> is dephosphorylated by CaN, which enables its nuclear translocation. Continuous NFAT activation and nuclear signaling result in neurodegenerative morphological abnormalities, including neuritic dystrophy, dendritic spine loss and modulation of β-amyloid accumulation. Indeed, NFAT activity stimulates the amyloidogenic pathway (Jin et al. 2012; Sompol et al. 2017), and its inhibition has been found to significantly reduce β-amyloid plaque formation in an AD mouse model (Furman et al. 2012). Therefore, a reduction in nuclear NFAT should have beneficial effects in senescence models, in which overactivation of neurodegenerative pathways is a key cause of cognitive decline (Griñán-Ferré et al. 2015, 2016).

The last finding, closely linked with the findings described above, is the implication of CaN in the beneficial effects of the I<sub>2</sub>-IR ligand B06 in SAMP8 mice. CaN is a multicomponent protein in which CaN A has phosphatase activity regulated by calcium levels (Rusnak F et al. 2010). Calcium dysregulation can be induced by age-related changes, such as OS and inflammation (Furman et al. 2014; Reese and Taglialatela. 2014). Furthermore, inhibition of CaN signaling produces neuroprotection in models of injury and disease (O'Donnell et al. 2016; Xiong et al. 2018), reduces neuroinflammation (Furman and Norris, 2014) and cognitive impairment (Liu et al. 2018), and improves synapse function (Kim et al. 2015). Consistent with these findings, we hypothesized that in SAMP8 mice, which are characterized by neuroinflammation and OS, an imbalance of calcium levels occurs, activating CaN A and inducing neurodegeneration. Specifically, astrocytic CaN is activated under inflammatory conditions and can, for example, activate GSK3β and inactivate AKT, influencing NMDAR-mediated axonal outgrowth (Wang et al. 2018). As stated above, the I<sub>2</sub>-IR ligand B06 reduced CaN A protein levels, and accordingly, we found activation of AKT and strong inactivation of GSK3β.

Regarding the OS observations, CaN can be activated after H<sub>2</sub>O<sub>2</sub> addition to neuronal cultures (Sée and Loeffler. 2001). Likewise, the reductions in OS markers after treatment

with the I<sub>2</sub>-IR ligand B06 could have also contributed to a reduction in CaN activity. These findings correlate with cognitive improvement, increasing neuroprotective signaling and reducing tau hyperphosphorylation. Conversely, CaN A can dephosphorylate tau. However, the balance between tau phosphorylation and dephosphorylation is due to a shift in tau kinase activity (Yu et al. 2008). Hyperactivation of the PP1A domain of CaN A results in dephosphorylation of a few transcription factors, such as CREB (which blocks CREB translocation to the nucleus) and NFAT (which enables NFAT translocation to the nucleus). In both cases, the reduced synaptic and growth gene transcription necessitates plasticity, and the increases in the expression of proinflammatory factors participate in neurodegenerative processes. Moreover, hyperactivation of the phosphatase 2B (PP2B) domain increases BAD dephosphorylation, favoring the action of BAD as a proapoptotic factor (Mukherjee et al. 2010).

In conclusion, the data from our study demonstrate that modulation of I<sub>2</sub>-IRs by B06 reduces neuroinflammation, OS and CaN protein levels in SAMP8 mice. The decreases in CaN protein levels can explain the changes in CREB, NFAT<sub>c1</sub> and BAD phosphorylation levels. In addition, the decreases in CaN levels result in modification of the kinase activity of GSK3 $\beta$  and AKT, among other molecules, leading to reduced tau hyperphosphorylation and preventing cognitive decline in SAMP8 mice. Collectively, our findings provide evidence that the CaN pathway is a critical component of the neuroprotective effects of I<sub>2</sub>-IR ligands on SAMP8 model mice, providing insight into several molecular modifications observed after I<sub>2</sub>-IR ligand treatment. In the future, a deeper knowledge of the role of the I<sub>2</sub>-IR signaling cascade in AD will provide new therapeutic targets for cognitive decline and AD.





factor-erythroid2-related factor 1; OFT, open field test; OS, oxidative stress; p-Tau, hyperphosphorylated Tau; PD, Parkinson's disease; PKA, protein kinase A; PP2B, phosphatase 2B; PVDF, polyvinylidene difluoride; ROS, reactive oxygen species; qPCR, real-time quantitative PCR; RT-PCR, reverse transcription-polymerase chain reaction; SAMP8, senescence-accelerated mouse prone 8; sAPP $\alpha$ , soluble APP  $\alpha$ ; sAPP $\beta$ , soluble APP  $\beta$ ; SDS-PAGE, sodium dodecyl sulphate-polyacrylamide gel electrophoresis; SEM, standard error of the mean; TBS-T, tween 20 TBS; TBS, tris-buffered saline; TN, novel object, new location; Tnf- $\alpha$ , tumor necrosis factor alpha; TO, old object, old location; TrkB, tropomyosin-related kinase B; WB, western blotting;  $\Delta\Delta$ Ct, cycle threshold method.

## REFERENCES

- [1] Abás S, Erdozain AM, Keller B, Rodríguez-Arévalo S, Callado LF, García-Sevilla JA, Escolano C. Neuroprotective effects of a structurally new family of high affinity imidazoline I<sub>2</sub> receptors ligands. *ACS Chem. Neurosci.* 2017;8(4):737-742. doi: 10.1021/acschemneuro.6b00426.
- [2] Abás S, Estarellas C, Luque FJ, Escolano C. 2015. Easy access to (2-imidazolin-4-yl)phosphonates by a microwave assisted multicomponent reaction. *Tetrahedron* 2015;71:2872-2881. <https://doi.org/10.1016/j.tet.2015.03.065>.
- [3] Akiguchi I, Pallàs M, Budka H, Akiyama H, Ueno M, Han J, Yagi H, Nishikawa T, Chiba Y, Sugiyama H, Takahashi R, Unno K, Higuchi K, Hosokawa M. SAMP8 mice as a neuropathological model of accelerated brain aging and dementia: Toshio Takeda's legacy and future directions. *Neuropathology.* 2017;37:293-305. doi: 10.1111/neup.12373.
- [4] Antunes M, Biala G. The novel object recognition memory: neuro- biology, test procedure, and its modifications. *Cogn. Process.* 2012;13:93-110. doi: 10.1007/s10339-011-0430-z.
- [5] Baumgärtel, K. & Mansuy, I. M., 2012. Neural functions of CaN in synaptic plasticity and memory. *Learn. Mem. Cold Spring Harb.* 2012;19:375–384. doi: 10.1101/lm.027201.112.
- [6] Bezprozvanny I, Hiesinger PR. The synaptic maintenance problem: membrane recycling, Ca<sup>2+</sup> homeostasis and late onset degeneration. *Mol Neurodegener.* 2013; 8:23 doi: 10.1186/1750-1326-8-23.
- [7] Boersma MCH, Dresselhaus EC, De Biase LM, Mihalas AB, Bergles DE, Meffert MK. A Requirement for Nuclear Factor- $\kappa$ B in Developmental and Plasticity-Associated Synaptogenesis. *J. Neurosci.* 2011;31(14):5414-5425. DOI: 10.1523/JNEUROSCI.2456-10.2011.
- [8] Bon C, Bohme GA, Doble A, Stutzmann JM, Blanchard JC. A role for nitric oxide in long-term potentiation. *Eur J Neurosci.* 1991;4:420–424. doi: 10.1111/j.1460-9568.1992.tb00891.x.
- [9] Bousquet, P, Hudson, A, García-Sevilla, JA, Li, JX. Imidazoline receptors system: the past, the present and the future. *Pharmacol. Rev.* 2020; 72:1-30. Doi: 10.1124/pr.118.016311.
- [10] Bradley CA, Peineau S, Taghibiglou C, Nicolas CS, Whitcomb DG, Bortolotto ZA, Kaang BK, Cho K, Wang YT, Collingridge GL. A pivotal role of GSK3 in synaptic plasticity. *Front Mol*

Neurosci. 2012; 5:13 doi: 10.3389/fnmol.2012.00013.

[11] Bridi MS, Hawk JD, Chatterjee S, Safe S, Abel T. Pharmacological Activators of the NR4A Nuclear Receptors Enhance LTP in a CREB/CBP-Dependent Manner. *Neuropsychopharmacology*. 2017;42(6):1243-1253. doi: 10.1038/npp.2016.253.

[12] Canudas AM, Gutierrez-Cuesta J, Rodríguez MI, Acuña-Castroviejo D, Sureda FX, Camins A, Pallàs M. Hyperphosphorylation of microtubule-associated protein tau in senescence-accelerated mouse (SAM). *Mech Ageing Dev*. 2005;126(12): 1300-4.

[13] Caraveo G, Auluck PK, Whitesell L, Chung CY, Baru V, Mosharov E. V, Yan X, Ben-Johny M, Soste M, Picotti P, Kim H, Caldwell KA, Caldwell GA, Sulzer D, Yue DT, Lindquist S. Calcineurin determines toxic versus beneficial responses to alpha-synuclein. *Proc. Natl. Acad. Sci. USA* 111, 2014;111(34):E3544-E3552.doi:10.1073/pnas.1413201111.

[14] Casanovas A, Olmos G, Ribera J, Boronat MA, Esquerda JE, García-Sevilla JA. Induction of reactive astrogliosis and prevention of motoneuron cell death by the I<sub>2</sub>-imidazoline receptor ligand LSL 60101. *Br J Pharmacol*. 2000;130(8):1767-1776. doi:10.1038/sj.bjp.0703485.

[15] Choi DH, Yun JH, Lee J. Protective effect of the imidazoline I<sub>2</sub> receptor agonist 2-BFI on oxidative cytotoxicity in astrocytes. *Biochem Biophys Res Commun*. 2018;503(4):3011-3016. <https://doi.org/10.1016/j.bbrc.2018.08.086>.

[16] Cummings J, Lee G, Ritter A, Zhong K. Alzheimer's disease drug development pipeline: 2018. *Alzheimers Dement (NY)*. 2018;4:195–214 doi: 10.1016/j.trci.2018.03.009.

[17] Cummings J. Lessons learned from Alzheimer Disease: Clinical Trials with negative outcomes. *Clin Transl Sci*. 2018;11:147-152 doi:10.1111/cts.12491.

[18] Cummings JL, Morstorf T, Zhong K. Alzheimer's disease drug-development pipeline: few candidates, frequent failures. *Alzheimers Res Ther* 2014;6(4):37. doi: 10.1186/alzrt269.

[19] Escolano C, Pallàs M, Griñán-Ferré C, Abás S, Callado LF, García-Sevilla JA. Synthetic I<sub>2</sub> imidazoline receptor ligands for prevention or treatment of human brain disorders. *WO 2019/121853 A1*, June 2019.

[20] Furman JL, Norris CM. Calcineurin and glial signaling: neuroinflammation and beyond. *J Neuroinflammation*. 2014;11:158. doi: 10.1186/s12974-014-0158-7.

[21] Furman JL, Sama DM, Gant JC, Beckett TL, Murphy MP, Bachstetter AD, Van Eldik LJ, Norris CM. Targeting astrocytes ameliorates neurologic changes in a mouse model of Alzheimer's disease. *J Neurosci* 2012; 32:16129 –16140.

[22] García-Sevilla JA, Escribá PV, Walzer C, Bouras C, Guimón J. Imidazoline receptor proteins in brains of patients with Alzheimer's disease. *Neurosci Lett*. 1998;247: 95-98.

[23] Garau C, Miralles A, Garcia-Sevilla JA. Chronic treatment with selective I<sub>2</sub>-imidazoline receptor ligands decreases the content of pro-apoptotic markers in rat brain. *J Psychopharmacol*. 2013;27(2):123–134. doi: 10.1177/0269881112450785.

[24] GBD 2016 Neurology Collaborators. Global, regional, and national burden of neurological disorders, 1990-2016: a systematic analysis for the Global Burden of Disease Study 2019. 2010.

Lancet Neurol. 18(5):459-480. doi: 10.1016/S1474-4422(18)30499-X.

[25] Griñán-Ferré C, Palomera-Avalos V, Puigoriol-Illamola D, Camins A, Porquet D, Plà V, Aguado F, Pallàs M. Behaviour and cognitive changes correlated with hippocampal neuroinflammation and neuronal markers in SAMP8, a model of accelerated senescence. *Exp Gerontol.* 2016;80:57-69. <https://doi.org/10.1016/j.exger.2016.03.014>.

[26] Griñán-Ferré C, Puigoriol-Illamola D, Palomera-Ávalos V. Environmental enrichment modified epigenetic mechanisms in SAMP8 mouse hippocampus by reducing oxidative stress and inflammation and achieving neuroprotection. *Front. Aging Neurosci.* 2016; 8: 1-12.

[27] Griñán-Ferré C, Vasilopoulou F, Abàs S, Rodríguez-Arévalo S, Bagán A, Sureda FX, Pérez B, Callado LF, García-Sevilla JA, García-Fuster MJ, Escolano C, Pallàs M. Behavioral and cognitive improvement induced by novel imidazoline I<sub>2</sub> receptor ligands in female SAMP8 mice. *Neurotherapeutics.* 2019;16:416-431. <https://doi.org/10.1007/s13311-018-00681-5>.

[28] Hopp SC, Bihlmeyer NA, Corradi JP, Vanderburg C, Cacace AM, Das S, Clark TW, Betensky RA, Hyman BT, Hudry E. Neuronal calcineurin transcriptional targets parallel changes observed in Alzheimer disease brain. *J Neurochem.* 2018;147(1): 24-39. doi: 10.1111/jnc.14469.

[29] Horsley V, Pavlath GK. NFAT ubiquitous regulator of cell differentiation and adaptation. *J Cell Biol.* 2002;156(5):771-774 doi: 10.1083/jcb.200111073.

[30] Jin SM1, Cho HJ, Kim YW, Hwang JY, Mook-Jung I. A $\beta$ -induced Ca(2+) influx regulates astrocytic BACE1 expression via calcineurin/NFAT4 signals. *Biochem Biophys Res Commun.* 2012;425(3):649-655 doi: 10.1016/j.bbrc.2012.07.123.

[31] Jiang SX, Zheng RY, Zeng JQ, Li XL, Han Z, Hou ST. Reversible inhibition of intracellular calcium influx through NMDA receptors by imidazoline I(2) receptor antagonists. *Eur J Pharmacol.* 2010;629 (1-3): 12-9. doi:10.1016/j.ejphar.2009.11.063.

[32] Kim S, Violette CJ, Ziff EB. Reduction of increased calcineurin activity rescues impaired homeostatic synaptic plasticity in presenilin 1 M146V mutant. *Neurobiol Aging.* 2015; 36(12): 3239–3246. doi: 10.1016/j.neurobiolaging.2015.09.007.

[33] Kipanyula MJ, Kimaro WH, Seke Etet PF. The Emerging Roles of the Calcineurin-Nuclear Factor of Activated T-Lymphocytes Pathway in Nervous System Functions and Diseases. *J Aging Res.* 2016; 2016:5081021. doi: 10.1155/2016/5081021.

[34] Kuno T, Mukai H, Ito A, Chang CD, Kishima K, Saito N, Tanaka C. Distinct cellular expression of calcineurin A alpha and A beta in rat brain. *J Neurochem.* 1992;58:1643–1651. 10.1111/j.1471-4159.1992.tb10036.x.

[35] Li JX. Imidazoline I<sub>2</sub> receptors: An update. *Pharmacol Ther.* 2017 Oct;178:48-56. doi: 10.1016/j.pharmthera.2017.03.009. Epub 2017 Mar 16.

[36] Lin CH, Lee CC & Gean PW. Involvement of a CaN cascade in amygdala depotentiation and quenching of fear memory. *Mol Pharmacol.* 2003;63:44–52.

[37] Liu J, Si Z, Li S, Huang Z, He Y, Zhang T, Wang A. Prevents Cognitive Impairment by Inhibiting Reactive Astroglialosis in Pilocarpine-Induced Status Epilepticus Rats. *Front Cell Neurosci.*

2018;11:428. doi: 10.3389/fncel.2017.00428.

[38] Martin ZS, Neugebauer V, Dineley KT, Kaye R, Zhang W, Reese LC, Tagliavola G.  $\alpha$ -Synuclein oligomers oppose long-term potentiation and impair memory through a calcineurin-dependent mechanism: relevance to human synucleinopathies. *J Neurochem*. 2012;120(3):440-452. doi: 10.1111/j.1471-4159.2011.07576.x.

[39] Papa L, Latypova X, Wilson CM, Magnaudeix A, Perrin ML, Terro F. Tau protein phosphatases in Alzheimer's disease: The leading role of PP2A. *Ageing Res Rev*. 2003;12: 39-49.

[40] McDonald GR, Olivieri A, Ramsat RR, Holt A. On the formation and nature of the imidazole I<sub>2</sub> binding site on human monoamine oxidase-B. *Pharmacol. Res.* 2010;62(6): 475-488 <https://doi.org/10.1016/j.phrs.2010.09.001>.

[41] Morley JE, Farr SA, Kumar VB, Armbricht HJ. The SAMP8 mouse: a model to develop therapeutic interventions for Alzheimer's disease. *Curr. Pharm. Des.* 2012; 18:1123-1130. doi: 10.2174/138161212799315795.

[42] Mukherjee A, Morales-Scheihing D, Gonzalez-Romero D, Green K, Tagliavola G, Soto C. CaN inhibition at the clinical phase of prion disease reduces neurodegeneration, improves behavioral alterations and increases animal survival. *PLoS Pathog*. 2010;6(10)

[43] Mulkey RM, Endo S, Shenolikar S, Malenka RC. Involvement of a calcineurin/inhibitor-1 phosphatase cascade in hippocampal long-term depression. *Nature*. 1994;369(6480): 486-8.

[44] O'Donnell JC, Jackson JG, Robinson MB. Transient oxygen/glucose deprivation causes a delayed loss of mitochondria and increases spontaneous calcium signaling in astrocytic processes. *J. Neurosci*. 2016;36, 7109-7127. doi: 10.1523/JNEUROSCI.4518-15.2016.

[45] Olmos G, DeGregorio-Rocasolano N, Paz Regalado M, Gasull T, Assumpcio Boronat M, Trullas R, Garcia-Sevilla JA. Protection by imidazole drugs and agmatine of glutamate-induced neurotoxicity in cultured cerebellar granule cells through blockade of NMDA receptor. *Br J Pharmacol*. 1999;127(6):1317-1326. doi: 10.1038/sj.bjp.0702679.

[46] Olmos G, Ribera J, Garcia-Sevilla JA. Imidazole compounds interact with the phencyclidine site of NMDA receptors in the rat brain. *Eur J Pharmacol*. 1996;310(2-3):273-276.

[47] Pallàs M. Senescence-accelerated mice P8: a tool to study brain aging and Alzheimer's disease in a mouse model. *ISRN Cell Biol*. 2012; 2012:1-12. doi: 10.5402/2012/917167. [48] Papa M, Pellicano MP, Sadile AG. Nitric oxide and long-term habituation to novelty in the rat. *Ann NY Acad Sci*. 1994;738:316-324.

[49] Pleiss MM, Sompol P, Kraner SD, Mohammad Abdul H, Furman JL, Guttmann RP, Wilcock DM, Nelson PT, Norris CM. Calcineurin proteolysis in astrocytes: Implications for impaired synaptic function. *Biochim Biophys Acta*. 2016;1862(9):1521-1532.

[50] Reese LC and Tagliavola G. A role of Calcineurin in Alzheimer's disease. *Current Neuropharmacology*. 2011;9(4):685-692 doi: 10.2174/157015911798376316.

[51] Reynolds GP, Boulton RM, Pearson SJ, Hudson AL, Nutt DJ. Imidazole binding sites in Huntington's and Parkinson's disease putamen. *Eur J Pharmacol*. 1996;301(1-3):R19-21

- [52] Ruiz J, Martin I, Callado LF, Meana JJ, Barturen F, Garca-Sevilla JA. Non-adrenoreceptor [3H]idazoxan binding sites (I<sub>2</sub>-imidazoline sites) are increased in postmortem brain from patients with Alzheimer's disease. *Neuroscience letters*. 1993;160:109-112.
- [53] Rusnak F, Mertz P. Calcineurin: form and function. *Physiol Rev*. 2000;80(4):1483-521
- [54] Sée V, Loeffler JP. Oxidative stress induces neuronal death by recruiting a protease and phosphatase-gated mechanism. *J Biol Chem*. 2001;276(37):35049-59.
- [55] Serrano-Pozo A, Frosch MP, Masliah E, Hyman BT. Neuropathological alterations in Alzheimer disease. *Cold Spring Harb Perspect Med*. 2011. Sep;1(1):a006189.
- [56] Sheridan CM, Heist EK, Beals CR, Crabtree GR, Gardner P, 2002 Protein kinase A negatively modulates the nuclear accumulation of NF-ATc1 by priming for subsequent phosphorylation by glycogen synthase kinase-3. *J Biol Chem*. 2002; 277(50): 48664-76. doi: 10.1074/jbc.M20702920.
- [57] Sompol P and Norris C. Ca<sup>2+</sup>, astrocyte activation and calcineurin/NFAT signaling in age-related neurodegenerative diseases. *Front Aging Neurosci*. 2018;10:199.
- [58] Su ZZ, Leszczyniecka M, Kang DC, Sarkar D, Chao W, Volsky DJ, Fisher PB. Insights into glutamate transport regulation in human astrocytes: cloning of the promoter for excitatory amino acid transporter 2 (EAAT2). *Proc Natl Acad Sci U S A*. 2003;100:1955–196
- [59] Sun J, Nan G. The extracellular signal-regulated kinase 1/2 pathway in neurological diseases: A potential therapeutic target (Review) *Int J Mol Med*. 2017;39(6):1338–1346. doi: 10.3892/ijmm.2017.2962.
- [60] Szatmari E, Habas A, Yang P, Zheng JJ, Hagg T, Hetman M. A positive feedback loop between glycogen synthase kinase 3beta and protein phosphatase 1 after stimulation of NR2B NMDA receptors in forebrain neurons. *J Biol Chem*. 2004;280(45):37526-35. doi: 10.1074/jbc.M502699200.
- [61] Takeda T. Senescence-accelerated mouse (SAM) with special references to neurodegeneration models, SAMP8 and SAMP10 mice. *Neurochem Res*. 2009;34:639-659. doi: 10.1007/s11064-009-9922-y.
- [62] Tyacke RJ, Myers JFM, Venkataraman A, Mick I, Turton S, Passchier J, Husbands SM, Rabiner EA, Gunn RN, Murphy PS, Parker CA, Nutt DJ. Evaluation of 11C-BU99008, a PET Ligand for the Imidazoline2 Binding Site in Human Brain. *J Nucl Med*. 2018;59(10):1597-1602. doi: 10.2967/jnumed.118.208009.
- [63] Vehmas AK, Kawas CH, Stewart WF, Troncoso JC. Immune reactive cells in senile plaques and cognitive decline in Alzheimer's disease. *Neurobiol Aging*. 2003;24(2):321-331.
- [64] Wang XS, Chen YY, Shang XF, Zhu ZG, Chen GQ, Han Z, Shao B, Yang HM, Xu HQ, Chen JF, Zheng RY. Idazoxan attenuates spinal cord injury by enhanced astrocytic activation and reduced microglial activation in rat experimental autoimmune encephalomyelitis. *Brain Res*. 2009;1253:198-209. <https://doi.org/10.1016/j.brainres.2008.11.059>.
- [65] Wang Y, Tang JL, Xu X, Zhou XP, Du J, Wang X, Zhou Y, Zhu Q, Yao LL, Wang YG, Hou S, Huang Z. NMDA receptors inhibit axonal outgrowth by inactivating AKT and activating GSK-3β via calcineurin in cultured immature hippocampal neurons. *Exp Cell Res*. 2018; 371(2):389-398.

doi: 10.1016/j.yexcr.2018.08.033.

[66] Watanabe K, Uemura K, Asada M, Masato M, Akiyama H, Shinohama S, Takahashi R, Kinoshita A. The participation of insuline-like growth factor- binding protein 3 released by astrocytes in the pathology of Alzheimer's disease. *Molecular Brain*. 2015;8:82. doi: 10.1186/s13041-015-0174-2.

[67] Wilson H, Dervenoulas G, Pagano G, Tyacke RJ, Polychronis S, Myers J, Gunn RN, Rabiner EA, Nutt D, Politis M. Imidazoline 2 binding sites reflecting astroglia pathology in Parkinson's disease: an in vivo 11C-BU99008 PET study. *Brain*, 2019;142(10):3116–3128.

[68] Wu HY, Hudry E, Hashimoto T, Kuchibhotla K, Rozkalne A, Fan Z, Spires-Jones T, Xie H, Arbel-Ornath M, Grosskreutz CL, Bacskai BJ, Hyman BT. Amyloid beta induces the morphological neurodegenerative triad of spine loss, dendritic simplification, and neuritic dystrophies through calcineurin activation. *J Neurosci*. 2010;30(7):2636-49. doi: 10.1523/JNEUROSCI.4456-0.

[69] Xiong TQ, Chen LM, Tan BH, Guo CY, Li YN, Zhang YF, Li SL, Zhao H, Li YC. The effects of calcineurin inhibitor FK506 on actin cytoskeleton, neuronal survival and glial reactions after pilocarpine-induced status epilepticus in mice. *Epilepsy Res*. 2018;140:138–147. doi: 10.1016/j.eplesyres.2018.01.007.

[70] Yu D, Tong L, Song G, Lin W, Zhang L, Bai W, Gong H, Yin Y, Wei Q. Tau binds both subunits of CaN, and binding is impaired by calmodulin. *Biochim Biophys Acta*. 2008;1783, 2255–2261

[71] Zhang F, Kang Z, Li W, Xiao Z, Zhou X. Roles of brain-derived neurotrophic factor/tropomyosin-related kinase B (BDNF/TrkB) signalling in Alzheimer's disease. *J Clin Neurosci*. 2012;19(7):946-949. doi:10.1016/j.jocn.2011.12.022.

[72] Zhao H, Jin-Long Y, Susan XJ, Sheng-Tao H, Rong-Yuan Z. Fast, Non-Competitive and Reversible inhibition of NMDA-Activated Currents by 2-BFI confers Neuroprotection. *PLoS One*. 2013; 8(5):e64894. doi: 10.1371/journal.pone.0064894.

[73] Zhu D, Liu SH, Sun HS, Lu YM. Expression of Inducible Nitric Oxide Synthase after Focal Cerebral Ischemia Stimulates Neurogenesis in the Adult Rodent Dentate Gyrus. *J Neurosci*. 2003;23(1):223–229. <https://doi.org/10.1523/JNEUROSCI.23-01-00223.2003>.

[74] Zhu X, Castellani RJ, Takeda A, Nunomura A, Atwood CS, Perry G, Smith MA. Differential activation of neuronal ERK, JNK/SAPK and p38 in Alzheimer disease: the 'two hit' hypothesis. *Mech Ageing Dev*. 2001;123:39–46. doi: 10.1016/S0047-6374(01)00342-6.

## SUPPLEMENTARY MATERIAL

**Table 4:** Antibodies used in Western blot studies.

Antibody	Host	Source/Catalog	WB dilution
AKT	Rabbit	Cell Signaling/#9272	1:1000
Bad	Mouse	Santa Cruz/sc-8044	1:1000
Bax	Rabbit	Cell signaling/#2772	1:1000
Bcl-2	Rabbit	Cell Signaling/#2870	1:1000
Calcineurin A	Rabbit	BioRad/VPA00329	1:1000
Calpain	Mouse	BioRad/AHP2443	1:1000
CaMKII	Rabbit	Abcam/ab52476	1:1000
Caspase-3	Rabbit	Cell Signaling/#9662	1:1000
Cdk5	Rabbit	Santa Cruz/sc-173	1:1000
CREB (48H2)	Rabbit	Cell Signaling/#9197	1:1000
EAAT2	Mouse	Santa Cruz/sc-365634	1:1000
GFAP	Rabbit	Gene Tex/GTX100850	1:1000
GSK-3 $\beta$	Rabbit	Cell Signaling/#9315S	1:1000
NFATc1	Rabbit	St John's/STJ24751	1:1000
NMDA2A	Mouse	Santa Cruz/sc-515148	1:1000
NMDA2B	Mouse	Santa Cruz/sc-365597	1:1000
P35/p25	Rabbit	Cell Signaling/#C64B10	1:1000
pAKT (Ser473)	Rabbit	Cell Signaling/#4060	1:1000
pBAD (Ser136)	Rabbit	Cell Signaling/#4366S	1:500
pCaMKII (Thr286)	Rabbit	SAB/#11287	1:1000
pCdk5 (Y15)	Rabbit	Abcam/ab63550	1:1000
pCREB (Ser133)	Rabbit	Cell Signaling/#9198	1:1000
P-p44/42 (T202/Y204)	Rabbit	Cell Signaling/#9101	1:1000
p-GSK-3beta	Rabbit	Cell Signaling/#9336	1:1000
PKA	Mouse	Santa Cruz/sc-28315	1:1000
p-NFAT (Ser172)	Rabbit	Invitrogen/PA5-64696	1:500
p-NMDAR2B (Tyr1472)	Rabbit	Invitrogen/OPA1-04116	1:1000
p-Tau Ser396	Rabbit	Invitrogen/44-752G	1:1000
p-Tau Ser404	Rabbit	Invitrogen/44-758G	1:1000
sAPP $\alpha$	Rabbit	Covance/SIG-39139-005	1:2000
sAPP $\beta$	Rabbit	Covance/SIG-39138-05	1:2000
Tau total	Mouse	Invitrogen/AHB0042	1:1000
TBP	Mouse	Abcam/ab51841	1:1000
Actin	Mouse	Invitrogen/MA5-15739	1:2000
GAPDH	Mouse	Millipore/MAB374	1:5000



**Table 4 continued from previous page**

Goat-anti-mouse HRP conjugated	Biorad/170-5047	1:2000
Goat-anti-rabbit HRP conjugated	Biorad/170-6515	1:2000

**Table 5:** Reagents used in IHC studies.

Antibody	Host	Source/Catalog	IHC dilution
GFAP	Rabbit	DAKO/Z0334	1:400
S100A9	Mouse	R&D Systems/AF2065	1:400
Alexa Fluor 594		Invitrogen/A21044	1:1000
Goat anti-mouse IgM			
Alexa Fluor 488		Invitrogen/A11078	1:400
Rabbit anti-goat IgG			
Hoechst 33258 solution		Sigma-Aldrich/94403	

**Table 6:** Primers and probes used in qPCR studies.

Target	Product size (bp)	Forward primer (5'-3')	Reverse primer (5'-3')
<i>Ide</i>	128	GCAACACCATACCCTGCTCT	TCCACATAAGCAAACGGGCT
<i>Adam10</i>	125	GGGAAGAAATGCAAGCTGAA	CTGTACAGCAGGGTCCCTTGAC
<i>Cxcl10</i>	72	GGCTAGTCCTAATTGCCCTTGG	TTGTCTCAGGACCATGGCTTG
<i>Il-6</i>	189	ATCCAGTTGCCTTCTTGGGACTGA	TAAGCCTCCGACTTGTGAAGTGGT
<i>Il-18</i>	151	GTTTACAAGCATCCAGGCACAG	GAAGGTTTGAGGCGGCTTTC
<i>Il-1<math>\beta</math></i>	179	TGTGAAATGCCACCTTTTGA	GGTCAAAGGTTTGGAAGCAG
<i>Ifn-<math>\gamma</math></i>	87	CCTTCTCAGCAACAGCAAGGCG	CTTGCGCTGGACCTGTGGG
<i>Tnf-<math>\alpha</math></i>	157	TCGGGGTGATCGGTCCCCAA	TGGTTTGCTACGACGTGGGCT
<i>iNOS</i>	125	GGCAGCCTGAGAGACCTTTG	GGAAGCGTTTCGGGATCTGAA
<i>Nrf1</i>	114	AGCACGGAGTGACCCAAAC	TGTACGTGGCTACATGGACCT
<i>Aldh2</i>	189	GCAGGCGTACACAGAAGTGA	TGAGCTTCATCCCCTACCCA
<i>Neo</i>	196	TTGGGAGACCTGGCGGAAAC	CATTCTTGGACCCTCACCCC
<i><math>\beta</math>-actin</i>	190	CAACGAGCGGTTCCGAT	GCCACAGGTTCCATACCCA

### Taqman Probes

Target	Product size (bp)	Reference
<i>Hmox1</i>	69	Mm00516005_m1
<i>Bdnf</i>	71	Mm01334042_m1
<i>Gapdh</i>	109	Mm99999915_g1



### **3.4 Publication 4**

**Disease-modifying treatment with I<sub>2</sub> imidazoline receptor ligand  
LSL60101 in an Alzheimer's disease mouse model:  
A Comparative study with donepezil.**

Adapted from: **Vasilopoulou F**, Rodríguez-Arévalo S, Bagán A, Escolano C,  
Griñán-Ferré C, Pallàs M., *British Journal of Pharmacology*. 2021

Aug;178(15):3017-3033

doi: <https://doi.org/10.1111/bph.15478>

## SUMMARY

The current therapeutic options against AD provide only symptomatic relief at the clinical level, while disease modifying drugs in clinical trials are increasing. Moreover, co-treatment of symptomatic treatment Ache inhibitors with neuroprotective drugs has been shown to deliver better outcomes in the prevention of cognitive decline. However, the development of effective therapeutic strategies still remains a challenge, increasing the necessity for the identification of novel targets. Given the implication of I<sub>2</sub>-IR receptors in AD and the neuroprotective role of I<sub>2</sub>-IR ligands in brain disorders, in this study we assessed the potential therapeutic effects after chronic treatment with a well-established I<sub>2</sub>-IR ligand LSL60101, an AChE inhibitor donepezil, as well as their combination in the 5XFAD mouse model of EOAD.

5XFAD female mice were treated with low doses ( $1 \text{ mg} \cdot \text{kg}^{-1} \cdot \text{day}^{-1}$ ) of LSL60101, donepezil, and donepezil plus LSL60101, during 4 weeks per os. Novel object recognition, Morris water maze, Open field, Elevated plus maze, and Three-chamber tests were employed to evaluate the cognitive and behavioural status after treatment. The effects of the treatments on AD-like pathology were assessed with immunohistochemistry, Western blot, ELISA and qPCR.

Chronic low-dose treatment with LSL60101 and donepezil reversed cognitive deficits and impaired social behaviour. LSL60101 treatment did not improve anxiety-like behaviour in contrast to donepezil. In the 5XFAD brains, LSL60101 and donepezil/LSL60101 treatments attenuated A $\beta$ -pathology by decreasing A $\beta$ <sub>40</sub>, A $\beta$ <sub>42</sub> levels and A $\beta$  plaques number, and tau hyperphosphorylation. These alterations were accompanied by a decrease in the microglia marker Iba-1 levels and an increase in *Trem2* gene expression in the LSL60101 treated mice. LSL60101 and donepezil decreased GFAP astrocytic marker reactivity. However, only LSL60101 and donepezil/LSL60101 treatments significantly increased the synaptic markers' levels PSD95 and synaptophysin in the 5XFAD brains, providing in whole a greater effect in AD neuropathological characteristics. Our results suggest that chronic low dose treatment with selective I<sub>2</sub>-IR ligands can be an effective disease modifying strategy against AD and provide insights into combination treatments of symptomatic and disease-modifying drugs.

## Disease-modifying treatment with I<sub>2</sub> imidazoline receptor ligand LSL60101 in an Alzheimer's disease mouse model: A Comparative study with donepezil.

Foteini Vasilopoulou,<sup>1</sup> Sergio Rodríguez-Arévalo,<sup>2</sup> Andrea Bagán,<sup>2</sup> Carmen Escolano,<sup>2</sup> Christian Griñán-Ferré,<sup>1</sup> Mercè Pallàs<sup>1</sup>

<sup>1</sup>Pharmacology Section. Department of Pharmacology, Toxicology and Medicinal Chemistry, Faculty of Pharmacy and Food Sciences, and Institut de Neurociències, University of Barcelona, Av. Joan XXIII, 27-31, 08028 Barcelona, Spain.

<sup>2</sup>Laboratory of Medicinal Chemistry (Associated Unit to CSIC), Department of Pharmacology, Toxicology and Medicinal Chemistry, Faculty of Pharmacy and Food Sciences, and Institute of Biomedicine (IBUB), University of Barcelona, Av. Joan XXIII, 27-31, 08028 Barcelona, Spain.

**Keywords:** Alzheimer's disease, donepezil, I<sub>2</sub> imidazoline receptors, neuroinflammation, synaptic plasticity,  $\beta$ -amyloid

### ABSTRACT

**Background and Purpose:** The development of effective therapeutic strategies against Alzheimer's disease (AD) remains a challenge. I<sub>2</sub> imidazoline receptor ligands have a neuroprotective role in AD. Moreover, co-treatment of AChE inhibitors with neuroprotective agents have shown better effects on the prevention of dementia. Here, we assessed the potential therapeutic effect of the I<sub>2</sub> ligand LSL60101, donepezil, and their combination in 5XFAD mice.

**Experimental Approach:** 5XFAD female mice were treated with low doses ( $1 \text{ mg} \cdot \text{kg}^{-1} \cdot \text{day}^{-1}$ ), of LSL60101, donepezil, and donepezil plus LSL60101, during 4 weeks per os. Novel object recognition, Morris water maze, open field, elevated plus maze, and three-chamber tests were employed to evaluate the cognitive and behavioural status after treatment. The effects on AD-like pathology were assessed with immunohistochemistry, western blot, ELISA and qPCR.

**Key results:** Chronic low-dose treatment with LSL60101 and donepezil reversed cognitive deficits and impaired social behaviour. LSL60101 treatment did not affect anxiety-like behaviour in contrast to donepezil. In the 5XFAD brains, LSL60101 and donepezil/LSL60101 treatments attenuated amyloid- $\beta$  pathology by decreasing amyloid- $\beta_{40}$  and amyloid- $\beta_{42}$ , amyloid- $\beta$  plaque number, and tau hyperphosphorylation. These alterations were accompanied by reduced microglia marker Iba-1 levels and increased *Trem2* gene expression. LSL60101 and donepezil decreased glial fibrillary acidic protein (GFAP) astrocytic marker reactivity. However, only LSL60101 and donepezil/LSL60101 treatments

significantly increased the synaptic marker levels of post-synaptic density protein 95 and synaptophysin.

**Conclusion and implications:** Chronic low dose treatment with selective I<sub>2</sub> ligands can be an effective treatment for AD and provide insights into combination treatments of symptomatic and disease-modifying drugs.

### 3.4.1 INTRODUCTION

Alzheimer's disease (AD) is the leading cause of dementia among the elderly and the most common irreversible and incurable neurodegenerative disorder, clinically characterised by progressive behavioural disturbances and memory loss (Murray et al., 2011). Amyloid- $\beta$  plaques and neurofibrillary tangles, consisting of hyperphosphorylated tau (p-Tau), are two major neuropathological AD markers, which lead to synaptic failure (DeTure & Dickson, 2019; Selkoe, 2008; Walsh & Selkoe, 2004). Moreover, the inflammatory response triggered by amyloid- $\beta$  deposits and tau hyperphosphorylation, among others and mediated by activated microglia and reactive astrocytes has a key role in the progression of AD (Dickson & Rogers, 1992; Meraz Rios et al., 2013). Thus, targeting amyloid- $\beta$  aggregation, p-Tau and neuroinflammation has been proved so far, the main disease-modifying strategy for treating AD.

However, up to date, only symptomatic treatments, including the AChE inhibitors and the N-methyl-D-aspartate (NMDA) antagonists, are available for AD therapy. Those drugs showed modest symptomatic benefits on behaviour and cognition, but they did not halt the progression of AD (Grossberg, 2003; Mehta et al., 2012). Among AChE inhibitors, donepezil is clinically used for cognitive dysfunction in AD (Giacobini, 2000). Besides its main effects on the enhancement of cholinergic transmission, donepezil has been demonstrated to exert the potential for disease pathway modifications in AD, including attenuation of amyloid- $\beta$  load and anti-inflammatory properties *in vitro* and *in vivo* (Kim et al., 2014). However, it lacks a curative effect. Therefore, identifying new molecular targets for the development of treatments is crucial. In this context, to further enhance the noncholinergic therapeutic effects of donepezil, a combination of donepezil with other neuroprotective agents could provide a novel approach to preserve cognitive function and/or delay AD pathology.

I<sub>2</sub> imidazoline receptors are receiving growing attention due to the neuroprotective effects in the CNS (Bousquet et al., 2020). In the brain, I<sub>2</sub> receptors are found in both neurons and glial cells (Olmos et al., 1994; Regunathan et al., 1993) and their modulation has been associated with neurodegenerative disorders, including AD (Ruiz et al., 1993). Most notably, the density of I<sub>2</sub> receptors was found to increase in AD patients (Garcia-Sevilla et

al., 1998). Several lines of evidence provided by our group demonstrated that selective I<sub>2</sub> ligands protected against cognitive impairment and ameliorated AD pathological features related to amyloid precursor protein processing, tau hyper-phosphorylation, neuroinflammation and oxidative stress processes, using well-established AD animal models (Abás et al., 2017, 2020; Griñan-Ferré et al., 2019; Vasilopoulou, Griñan-Ferré, et al., 2020). Likewise, agmatine, the proposed endogenous ligand for I<sub>2</sub> receptors, prevented cognitive deficits in amyloid- $\beta$  1–42 peptide-injected mice and of note, its effect was augmented and attenuated by I<sub>2</sub> agonists and antagonists, respectively (Kotagale et al., 2020). Collectively, this evidence supports the potential therapeutic effect of I<sub>2</sub> ligands in AD.

Among the I<sub>2</sub> ligands, the selective I<sub>2</sub> ligand LSL60101 [2-(2-benzofuranyl)imidazole] (K<sub>i</sub> ratio for  $\alpha_2$ /I<sub>2</sub> receptors = 286) has been associated with the induction of several central effects, such as acute hyperphagic effects (Menargues et al., 1995) and inhibition of the development of opioid-induced tolerance and potentiation of morphine analgesia (Boronat et al., 1998). Interestingly, LSL60101 was shown to promote neuronal protection mediated by the induction of reactive astrocytes (Casanovas et al., 2000). However, the neuro-protective effect of LSL60101 on AD pathological conditions has not been reported.

In the present *in vivo* study, we explored the I<sub>2</sub> receptor ligand LSL60101 beneficial effects on the behavioural capabilities and cognitive impairments presented in AD, as well as on AD markers, including neuroinflammation, glial reactivity and synaptic plasticity in 5XFAD mice, a widely accepted transgenic mouse model for early-onset AD. Considering that women have a higher risk of dementia and females are under-represented in rodent models of AD, we used 5XFAD females. Additionally, the comparative effect with donepezil, considered a symptomatic AD treatment, was investigated alone and in combination therapy with the I<sub>2</sub> ligand LSL60101 to explore the joint effects of both compounds in ameliorating AD pathology and molecular changes presented by 5XFAD mice.

### 3.4.2 METHODS

#### Animals

The 5XFAD mouse model is a well-characterised double transgenic amyloid precursor protein/PSEN1 model, which co-expressed five familial AD mutations (JAX MMRRC Stock# 034840). This animal model incorporates AD pathological characteristics, including early plaque formation and gliosis starting at 2 months, robust cognitive and behavioural deficits such as memory impairment, reduced anxiety and social disturbances starting at 4–5 months and neuronal loss at 6 months (Griñan-Ferré et al., 2018; Landel et al., 2014; Oakley et al., 2006). Thus, at the selected age of 7 months, 5XFAD mice provide a severe

AD pathological landscape suitable for evaluating the drug effects.

In the present study, 5XFAD (n = 47) and wild-type (WT, n = 46) female mice (7 months old) were used to perform behavioural and molecular analyses. Females were used because AD incidence is higher in women and few studies are available. WT animals were randomly divided into WT control (WT Ct) (n = 11), WT treated with donepezil ( $1 \text{ mg} \cdot \text{kg}^{-1} \cdot \text{day}^{-1}$ ) (WT Dp) (n = 12) and LSL60101 (WT LSL) ( $1 \text{ mg} \cdot \text{kg}^{-1} \cdot \text{day}^{-1}$ ) (n = 12), and the cotreatment of donepezil ( $1 \text{ mg} \cdot \text{kg}^{-1} \cdot \text{day}^{-1}$ ) and LSL60101 ( $1 \text{ mg} \cdot \text{kg}^{-1} \cdot \text{day}^{-1}$ ) (WT Dp + LSL). 5XFAD mice were randomly divided into: 5XFAD control (5XFAD Ct) (n = 11), 5XFAD treated with donepezil ( $1 \text{ mg} \cdot \text{kg}^{-1} \cdot \text{day}^{-1}$ ) (5XFAD Dp) (n = 12) and LSL60101 (5XFAD LSL) ( $1 \text{ mg} \cdot \text{kg}^{-1} \cdot \text{day}^{-1}$ ) (n = 12) and the co-treatment of donepezil ( $1 \text{ mg} \cdot \text{kg}^{-1} \cdot \text{day}^{-1}$ ) and LSL60101 ( $1 \text{ mg} \cdot \text{kg}^{-1} \cdot \text{day}^{-1}$ ) (5XFAD Dp + LSL).

The animals had free access to food and water and were kept under standard temperature conditions ( $22 \pm 2^\circ\text{C}$ ) and 12-h light/dark cycles (300/0 lux). Compounds were dissolved in 1.8% (2-hydroxypropyl)- $\beta$ -cyclodextrin and administered through drinking water. Control groups received water plus 1.8% (2-hydroxypropyl)- $\beta$ -cyclodextrin during the treatment period. For the drugs administration, dosages were calculated on the basis of average daily water consumption recorded in each cage and they were confirmed by recalculations once a week. Each animal's weight was also recorded once a week during the treatment period and the drug dosages were recalculated, when necessary, based on the results obtained. The average daily water consumption was 5 ml day<sup>-1</sup> for each animal without observing significant differences among the groups. Likewise, the body weight of the control and treated groups did not change significantly during the treatment period (Figure S1). The intervention sample size was chosen following previous studies in our laboratory and using one of the available interactive tools (<http://www.biomath.info/power/index.html>). Moreover, the animal number mismatch among experimental groups was due to the exclusion of mice by death or ethical reasons according to the final point indicated in the approved protocol.

After 4 weeks of treatment, behavioural and cognitive tests were performed to study the effects of treatment on learning, memory, anxiety behaviour and social interaction (Figure 1a). Mice were also treated during this period and up to their killing (46 days in total). All studies and procedures for the mouse behaviour tests brain dissection and extractions followed the standard ethical guidelines (European Communities Council Directive 2010/63/EU and Guidelines for the Care and Use of Mammals in Neuroscience and Behavioural Research, National Research Council 2003). Animal studies are reported in compliance with the ARRIVE guidelines (Percie du Sert et al., 2020) and with the recommendations made by the British Journal of Pharmacology (Lilley et al., 2020).



They were approved by Bioethical Committees from the University of Barcelona and the Government of Catalonia.

### **Behavioural tests**

#### *Novel Object Recognition Test*

A modification of the novel object recognition test protocol was performed (Ennaceur & Delacour, 1988). In brief, mice were placed in a 90 two-arm (25 x 20 x 5 cm) black maze, with removable walls for easy cleaning and light intensity in midfield was 30 lux. Before the memory, trial mice were habituated to the apparatus for 10 min for 3 days. On Day 4, the animals were submitted to a 10-min acquisition trial, in which they were allowed to freely explore two identical objects located at the end of each arm (first trial—familiarisation). After 2 h (for short-term memory evaluation) and 24 h (for long-term memory evaluation) from the first trial, the mice were submitted to a 10-min retention trial, in which one of the two identical objects had been replaced by a novel one. The behaviour was recorded and the time that the mice spent exploring the new object (TN) and the old one (TO) was measured manually. Exploration was defined as sniffing or touching the objects with nose and/or forepaws. The discrimination index (DI) was calculated as  $(TN - TO)/(TN + TO)$ . To avoid object preference biases, objects were alternated; 70% EtOH was used to clean the arms and objects after each trial to eliminate olfactory cues.

#### *Morris Water Maze*

The Morris water maze test was performed as described previously (Griñan-Ferré et al., 2016) in an open circular pool, filled with water, which temperature was maintained at  $22 \pm 1^\circ\text{C}$ . The water surface was divided into four quadrants (Q1, Q2, Q3 and Q4) by two principal perpendicular axes and five starting points were set. Four visual clues were placed on the walls of the tank. The animals' swimming paths were recorded, and the data were analysed with SMART Version 3.0 software (Panlab, Cornellà, Spain). On Day 1, mice were placed individually into the pool, facing the wall and allowed to swim for 60 s to be habituated to the experimental conditions. On Day 2, a white platform was submerged 1.5 cm below the water level in the middle of the Q1 platform and the acquisition phase took place for 5 days. Each day, the animals were submitted to five trials starting from the positions set in random order. At each trial, mice were allowed to swim for 60 s and, if not able to find the platform within 60 s, were guided to the visible platform. The mice remained for 30 s onto the platform for spatial orientation. There was no resting phase between each trial and the subsequent one; 24 h after the last training, a memory test was performed. For this, the platform was removed from the pool and the mice were tested for 60 s. The distance to the target and the time spent in the platform quadrant (Q1), among

other parameters, were measured.

#### *Open Field*

Emotional alterations and locomotor activity were evaluated by the open field test using a white plywood apparatus (50 x 50 x 25 cm) as previously described (Archer, 1973; Griñan-Ferré et al., 2016). The apparatus' ground was divided into the centre and peripheral area. Each individual was placed at the centre of the open field and allowed to explore the apparatus for 5 min. The apparatus was cleaned with 70% ethanol after between trials. The behaviour was recorded and later analysed with SMART Version 3.0 software. The locomotor activity of the mice calculated as the sum of total distance travelled in 5 min, the centre stay duration and the number of rearings were evaluated.

#### *Elevated Plus Maze*

Animals were tested for anxiety-like behaviour by performing the elevated plus maze test, based on a previously described protocol (Walf & Frye, 2007). The elevated plus maze apparatus consisted of two open arms (30 x 5 x 15 cm) and two closed arms (30 x 5 x 15 cm). The mice were placed at the arms' junction and allowed to explore the apparatus for 5 min freely. Elevated plus maze apparatus was cleaned with 70% ethanol between tests. The behaviour was recorded and later analysed with SMART Version 3.0 software. Parameters recorded included the total distance travelled during the 5 min test; the time spent in open arms, closed arms and centre; and the number of rearings.

#### *Three-Chamber Test*

Three-chamber test evaluated mice social behaviour following a previously described protocol (Companys-Aleman et al., 2020). A box (15 x 15 x 20 cm) divided into three equally dimensioned rooms with openings among them was used. The mice were submitted to 15-min trials. First, each mouse was placed in the centre of the box and allowed to explore the three chambers for 5 min (habituation). The entries to each room were measured manually. Afterwards, an intruder (same sex and age) was placed in a metal cage in one of the rooms and behaviour was recorded for 10 min. The time spent in each room and interacting with the intruder (e.g. sniffing and grooming) was measured manually. The three-chamber test apparatus was cleaned with 70% ethanol between the trials to eliminate olfactory cues.

### **Brain processing**

Mice were killed by cervical dislocation 3 days after the behavioural and cognitive tests were completed. The brains were immediately removed from the skulls, and the hippocampi

were dissected, frozen and maintained at 80°C. For immunohistochemistry experiments, mice were anaesthetised (ketamine 100 mg · kg<sup>-1</sup> and xylazine 10 mg · kg<sup>-1</sup>, i.p.) and then perfused with 4% paraformaldehyde (PFA) diluted in 0.1M phosphate buffer solution intracardially. Their brains were removed and postfixed in 4% PFA overnight at 4°C. Afterwards, the solutions were changed to PFA + 15% sucrose. Finally, the brains were frozen on powdered dry ice and stored at 80°C until sectioning. All immuno-related procedures involved comply with the editorial on immunoblotting and immunohistochemistry (Alexander et al., 2018).

### **Protein levels determination by Western blotting**

For protein extraction, hippocampus samples were thawed and mixed in 200 µl lysis buffer (50-mM Tris-HCl pH 7.4, 150-mM NaCl, 5-mM EDTA and 1% Triton X-100) containing phosphatase and protease inhibitor cocktail (Cocktail II, Sigma-Aldrich, St. Louis, MO, USA). Once homogenised, samples were maintained on ice for 30 min. Afterwards, the samples were centrifuged at 10,000g for 30 min at 4°C and the supernatants were collected and maintained at 80°C. Total protein amount was quantified with the method of Bradford as described previously (Bradford, 1976).

For western blot aliquots of 15 µg of hippocampal protein were used. Protein samples were separated by SDS-PAGE (8–16%) and transferred onto PVDF membranes (Millipore, Burlington, MA, USA). Afterwards, membranes were blocked in 5% BSA in 0.1% Tris-buffered saline-Tween 20 (TBS-T) for 1 h at room temperature by overnight incubation at 4°C with the primary antibodies listed in Table S1. Membranes were washed and incubated with secondary antibodies for 1 h at room temperature. Immunoreactive proteins were viewed with a chemiluminescence-based detection kit, following the manufacturer's protocol (ECL Kit; Millipore) and digital images were acquired using a ChemiDoc XRS+ System (Bio-Rad Laboratories, Hercules, CA, USA). Semiquantitative analyses were carried out using Image Lab software (Bio-Rad Laboratories) and results were expressed in arbitrary units (AU), considering control protein levels as 100%. Protein loading was monitored by immunodetection of GAPDH or β-actin. For p-Tau quantification, blots were also normalised by total tau (t-Tau) protein levels.

### **RNA extraction and gene expression determination**

Total RNA isolation from hippocampal samples was performed using the TRIzol® reagent according to the manufacturer's instructions (Bioline Reagents, London, UK). The yield, purity and quality of RNA were determined spectrophotometrically with a NanoDrop™ ND-1000 apparatus (Thermo Fisher, Waltham, MA, USA) and an Agilent 2100B Bioanalyzer (Agilent Technologies, Santa Clara, CA, USA). RNA samples with 260/280 ratios

and RINs higher than 7.5, respectively, were selected. RT-PCR was performed. Briefly, 2  $\mu\text{g}$  of mRNA was reverse transcribed using a high-capacity cDNA reverse transcription kit (Applied Biosystems, Foster City, CA, USA).

SYBR® Green real-time PCR was performed using a Step One Plus Detection System (Applied Biosystems) with SYBR Green PCR Master Mix (Applied Biosystems). Each reaction mixture contained 6.75  $\mu\text{l}$  of cDNA (with a concentration of 2  $\mu\text{g}$ ), 0.75  $\mu\text{l}$  of each primer (with a concentration of 100 nM) and 6.75  $\mu\text{l}$  of SYBR Green PCR Master Mix (2) (Applied Biosystems).

The data were analysed utilising the comparative cycle threshold (Ct) ( $\Delta\Delta\text{Ct}$ ) method, in which the levels of a housekeeping gene are used to normalise differences in sample loading and preparation. The normalisation of expression levels was performed with  $\beta$ -actin. The primer sequences and TaqMan probes used in this study are presented in Table S2. Each sample was analysed in duplicate and the results represent the n-fold difference in the transcript levels among different groups.

#### **Amyloid- $\beta$ levels quantification by ELISA**

Amyloid- $\beta_{40}$  and amyloid- $\beta_{42}$  protein levels were measured by ELISA with the human amyloid- $\beta_{40}$  ELISA Kit (Invitrogen, #KHB3481; Thermo Fisher) and human amyloid- $\beta_{42}$  Ultrasensitive ELISA Kit (Invitrogen, #KHB3441), respectively. The samples were diluted by standard dilution buffer at a percentage of 50% and all procedures followed the manufacturer's instructions.

#### **Glial immunohistochemical identification**

For immunohistochemical studies, the frozen brains were embedded in OCT Cryostat Embedding Compound (Tissue-Tek, Torrance, CA, USA) and 30- $\mu\text{m}$ -thick brain coronal sections were obtained at 20°C on a cryostat (Leica Microsystems CM 3050S cryostat, Wetzlar, Germany) and kept in a cryoprotectant solution at 20C until use. Free-floating slices were placed in a 24-well plate and washed with 0.01-M PBS. Next, the free-floating sections were blocked with 0.1-M PBS solution containing 1% BSA and 0.3% Triton X-100 for 20 min at room temperature. Afterwards, slices were washed with PBS 0.01M two times for 5 min each and were incubated with the primary antibodies listed in Table S1 overnight at 4°C. The primary antibodies were diluted in a 0.1M PBS solution containing 1% BSA and 0.3% Triton X-100. On the following day, the coronal slices were washed with 0.1M PBS two times for 5 min each and then incubated with the secondary antibodies listed in Table S1 at room temperature for 1 h. Later, the sections were washed two times for 5 min each with 0.1-M PBS and were incubated with 5 $\mu\text{M}$  Hoechst staining solution

(Sigma-Aldrich) for 5 min in the dark at room temperature. After being washed, the slices were mounted using Fluoromount-G (EMS, Hatfield, PA, USA).

### **Amyloid- $\beta$ plaques histology**

Amyloid- $\beta$  plaques were stained with thioflavin S. Brain coronal sections of 30  $\mu\text{m}$  were obtained (Leica Microsystems CM 3050S cryostat, Wetzlar, Germany) and kept in a cryoprotectant solution at 20°C until use. Free-floating slices were placed in a 24-well plate and washed with 0.01-M PBS for 5 min at room temperature to be rehydrated. Next, the brain sections were washed with 70% ethanol for 1 min, followed by a wash with 80% ethanol for 1 min. The slices were then incubated with 0.3% thioflavin S (Sigma-Aldrich) solution for 15 min at room temperature in the dark. Afterwards, the samples were washed using 80%, 70% and 50% EtOH for 1 min. Three 2-min washes with 0.1-M PBS and the slices were mounted using Fluoromount-G (EMS).

### **Image acquisition and analysis**

Image acquisition was performed with a fluorescence laser microscope (Olympus BX51, Hamburg, Germany) using 4, 10 and 20 objectives, and images were analysed by using ImageJ software (RRID:SCR\_003070) as previously described. For quantification of amyloid plaques, similar and comparable histological areas were selected, focusing on the adjacent positioning of the whole cortical area and the hippocampus of the one brain hemisphere. The images were converted to 8-bit greyscale images, thresholded within the linear range and the number of particles (analyse particle function 10-Infinity), as well as the percentage of area covered by thioflavin S (20X objective), was calculated and averaged from two different sections from each animal. Glial fibrillary acidic protein (GFAP) and Iba-1-stained images (10X objective) were acquired, maintaining constant exposure for all samples across single experiments. The fluorescence intensity of the positive cells was measured in hippocampal CA1, CA3 and dentate gyrus areas and quantification was averaged from two to three different sections from each animal.

### **Statistical Analysis**

The data and statistical analysis comply with the recommendations of the British Journal of Pharmacology on experimental design and analysis in pharmacology (Curtis et al., 2018). Group size may vary according to power analysis and expertise of the authors regarding the behavioural tests (Griñan-Ferré et al., 2016; Griñan-Ferré et al., 2018) and statistical analysis was undertaken only for studies where each group size was at least  $n = 5$ . The blinded analysis was performed for behavioural tests. All data are expressed as the mean  $\pm$  SEM. Statistical analysis was conducted using GraphPad Prism Version

8 statistical software (RRID:SCR\_002798). All data were tested for normal distribution and equal variance. In the cognitive and behavioural studies, means were compared with two-way ANOVA or one-way ANOVA when necessary, followed by Tukey's post hoc tests. In molecular studies, means were compared with two-tailed unpaired Student's t-test (WT control vs. 5XFAD control) or one-way ANOVA followed by Tukey's post hoc tests (5XFAD control vs. 5XFAD-treated groups). The post hoc tests were conducted only if F in ANOVA achieved  $P < .05$  and there was no significant variance in homogeneity. Statistical significance was considered when P values were  $<.05$ . Statistical outliers were determined with Grubbs' test and, when necessary, were removed.

### **Nomenclature of Targets and Ligands**

Key protein targets and ligands in this article are hyperlinked to corresponding entries in the IUPHAR/BPS Guide to PHARMACOLOGY <http://www.guidetopharmacology.org> and are permanently archived in the Concise Guide to PHARMACOLOGY 2019/20 (Alexander et al., 2019).

## **3.4.3 RESULTS**

### **I<sub>2</sub> ligand LSL60101 and donepezil improve memory deficits in 5XFAD mice.**

Short- and long-term working memory were evaluated by novel object recognition test. 7-month-old 5XFAD mice presented robust cognitive deficits compared with WT (Figure 1b, c). LSL60101 treatment resulted in a rapid and sustained recovery of cognitive function by increasing the discrimination index in both 2- and 24-h memory tests (Figure 1b, c). Donepezil enhanced but did not sustain memory function in 5XFAD mice, as a significant increase of the discrimination index was found after 2 h, but not at 24-h memory test (Figure 1b, c). Co-treatment did not improve cognition in comparison with individual treatments (Figure 1b, c). Treatments had no significant effects on WT cognitive performance (Figure 1b, c).

For spatial learning and memory evaluation, the Morris water maze was performed. After 5 days of training, all experimental groups presented curves with progressively shorter path length on consecutive days. Of note, the path length to the platform was significantly decreased in LSL60101-treated 5XFAD mice when compared with 5XFAD controls (Figure 1d). In the probe trial, 5XFAD mice showed a reduced percentage of time spent in the platform quadrant, whereas the mice spent significantly more time in the quadrant opposite to the platform. Moreover, 5XFAD control mice presented increased latency to target compared with WT mice and, overall, a weaker cognitive performance (Figures 1e, g, h and S2). LSL60101 treatment significantly increased the time spent in the platform quadrant

in the 5XFAD- treated mice compared with both vehicle and donepezil-treated 5XFAD, whereas LSL60101 treatment had no effect on WT (Figure 1e, f, h). Neither donepezil nor co-treatment improved 5XFAD mice spatial memory (Figure 1d, e), although WT-treated mice performed better (Figure 1d, f, h). All treatments decreased the path length to the platform, albeit not significantly, due to the different performance of individual mice (Figure S2).

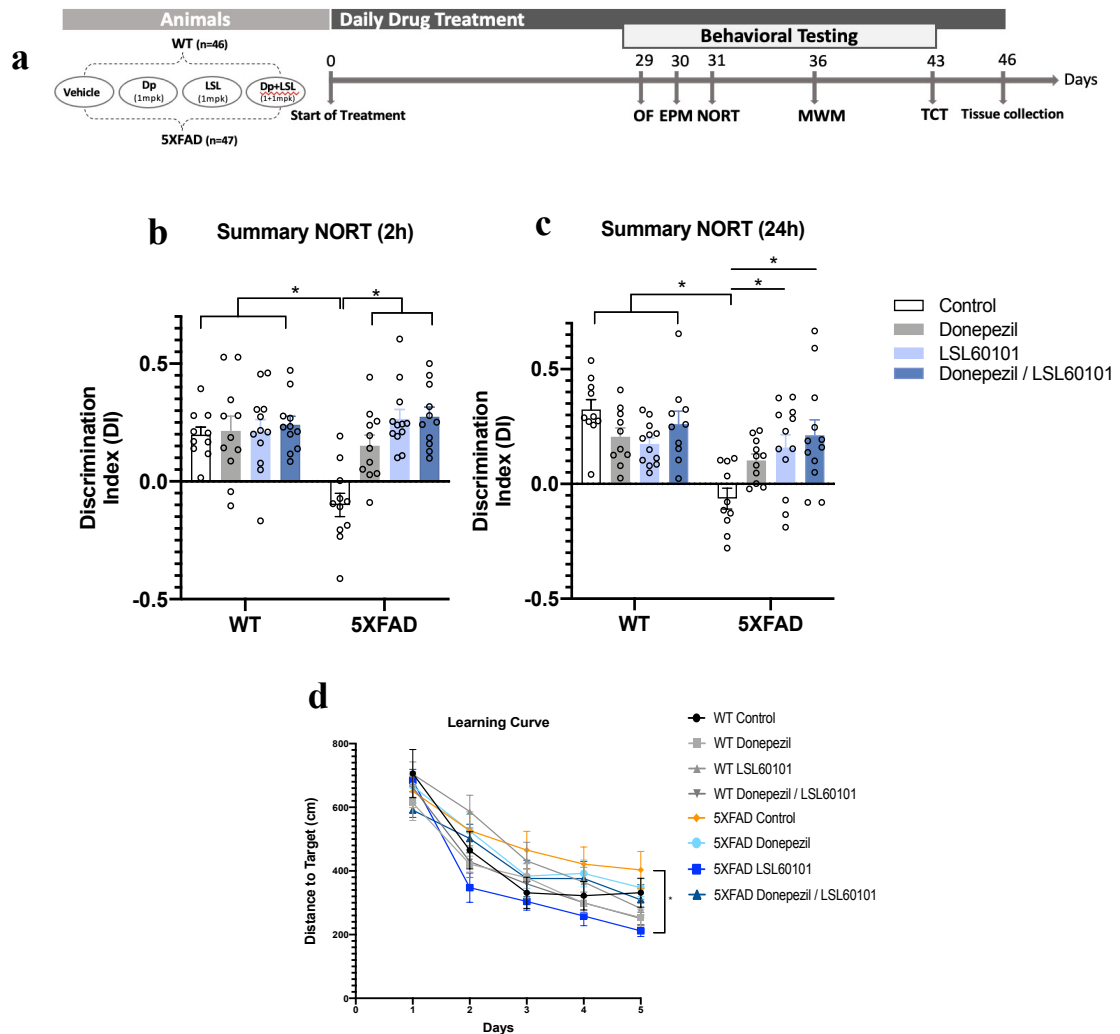
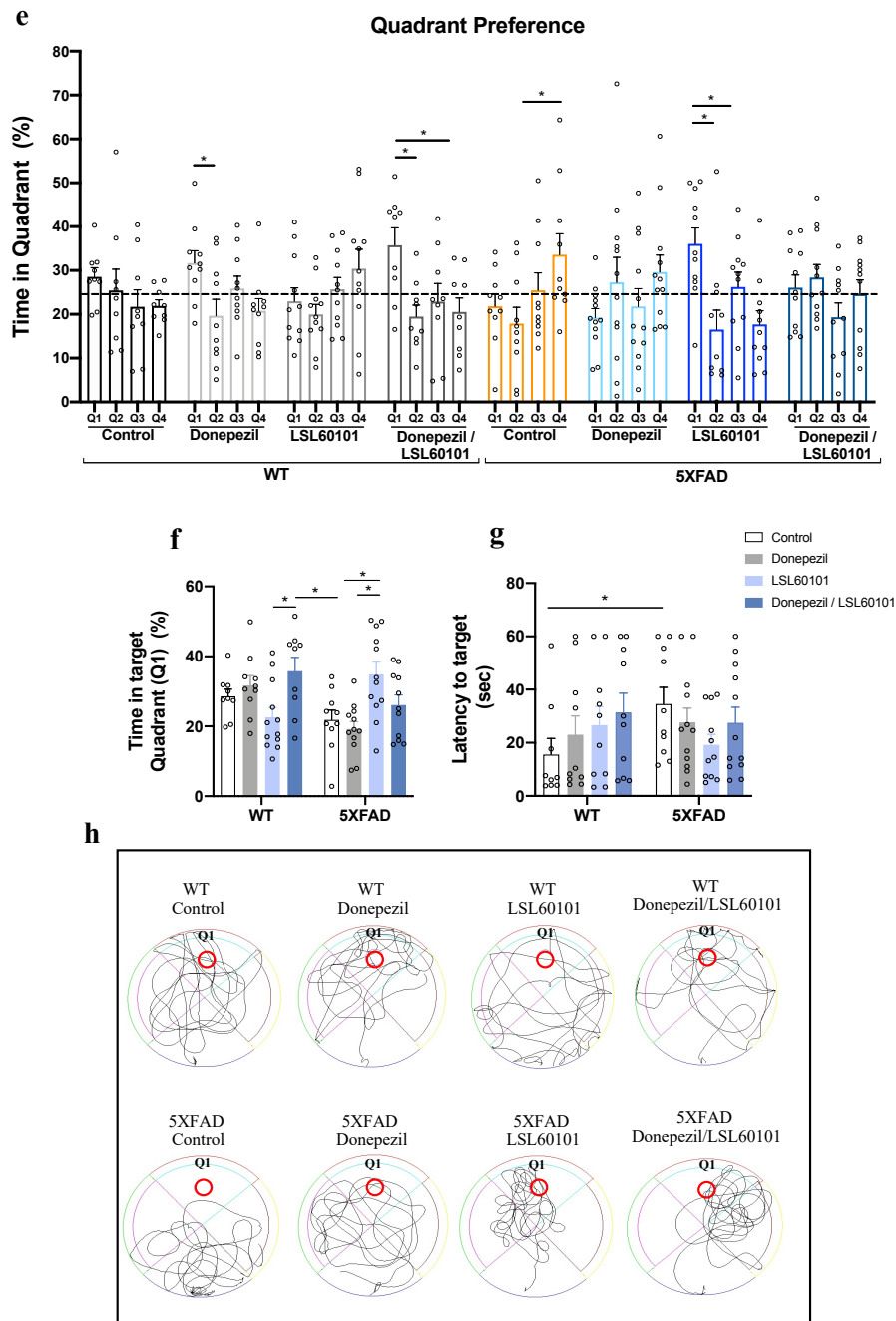


Figure 1: (Continued)



**Figure 1:** (Continued) **Effects of low-dose chronic treatment with  $I_2$  receptor ligand LSL60101, donepezil and co-administration on cognitive status in 5XFAD and WT mice.** (a) Scheme of experimental design:- open field (OF), elevated plus maze (EPM), novel object recognition test (NORT), Morris water maze (MWM) and three-chamber test (TCT). Results of NORT:- discrimination index calculated by using exploration time for novel and familiar object in (b) the short-term memory test session (2 h) (WT, n = 10–12 per group; 5XFAD n = 11–12 per group; two-way ANOVA with Tukey's post hoc analysis showing significant effect of genotype and treatment, with significant interaction) and (c) the long-term memory test session (24 h) (WT, n = 10–12 per group; 5XFAD n = 10–12 per group; two-way ANOVA with Tukey's post hoc analysis showing significant effect of genotype and treatment, with significant interaction). (Continued)



**Figure 1:** (Continued) Results of Morris water maze (MWM): (d) distance to target (platform) (cm) during the training session (WT n = 10–11 per group; 5XFAD n = 10–12 per group; two-way ANOVA with Tukey's post hoc analysis for each day; Day 5; showing non significant effect of genotype and treatment, with significant interaction). (e) Quadrant preference in the test session as time (%) spent in each quadrant (WT n = 9–12 per group; 5XFAD n = 10–12 per group; one-way ANOVA with Tukey's post hoc analysis between quadrants for each experimental group). (f) Time (%) spent in platform quadrant in the test session (WT n = 9–12 per group; 5XFAD n = 10–12 per group; two-way ANOVA with Tukey's post hoc analysis; showing significant effect of genotype and treatment, with significant interaction). (g) Latency to target (platform) (s) in the test session (WT n = 9–12 per group; 5XFAD n = 10–12 per group; two-way ANOVA with Tukey's post hoc analysis). (h) Representative images of trajectory during memory test. Bars show mean  $\pm$  SEM; \*P < .05.

### **I<sub>2</sub> LSL60101 does not affect behavioural and emotional disturbances in 5XFAD mice in contrast to donepezil.**

We also investigated the effect of the treatments on the 5XFAD and WT mice anxiety-like behaviour by performing the open field and elevated plus maze tests. No differences in locomotor activity were observed among the WT and 5XFAD groups (Figure 2a). 5XFAD mice presented a significant increase in the time spent in the centre of the open field compared with WT mice (Figure 2b). No effect was observed on the WT mice behaviour after treatments. 5XFAD treated with donepezil but not with LSL60101 showed a significant decrease in the time spent in the centre compared with 5XFAD controls, reverting to the WT healthy phenotype (Figure 2b). Co-treatment LSL60101/donepezil displayed the same results that showed donepezil alone in all parameters evaluated (Figure 2b and Table S3). Similarly, in the elevated plus maze, 5XFAD mice spent significantly more time in the open arms and less in the closed arms in comparison with age-matched WTs (Figure 2d,e). Donepezil had a positive effect by reverting the evaluated 5XFAD elevated plus maze parameters to those shown by WT group (Figure 2d–f and Table S4). I<sub>2</sub> ligand treatment alone did not affect any of the elevated plus maze parameters studied, whereas cotreatment maintained the donepezil values. Treatments did not induce significant changes in elevated plus maze parameters evaluated in WT mice (Table S4).

### **I<sub>2</sub> ligand LSL60101 and donepezil ameliorate social deficits presented by 5XFAD mice.**

To evaluate the effect of treatments on social behaviour, mice were subjected to the three-chamber test. No differences in the number of entries to each chamber were determined in the habituation phase in any tested group (Figure 2g). On the contrary, mice spent more time in the intruder's chamber during the test phase in all experimental conditions (Figure 2h). When the social interaction was evaluated, 5XFAD mice spent significantly less time interacting with the intruder compared with the WT healthy control (Figure 2i).

All treatments improved social impairments in 5XFAD-treated groups by increasing the time of interaction compared with the 5XFAD controls, but only 5XFAD treated with donepezil reached significance (Figure 2i), whereas for LSL60101,  $P < .06$  was calculated. WT-treated mice presented no differences compared with WT controls.

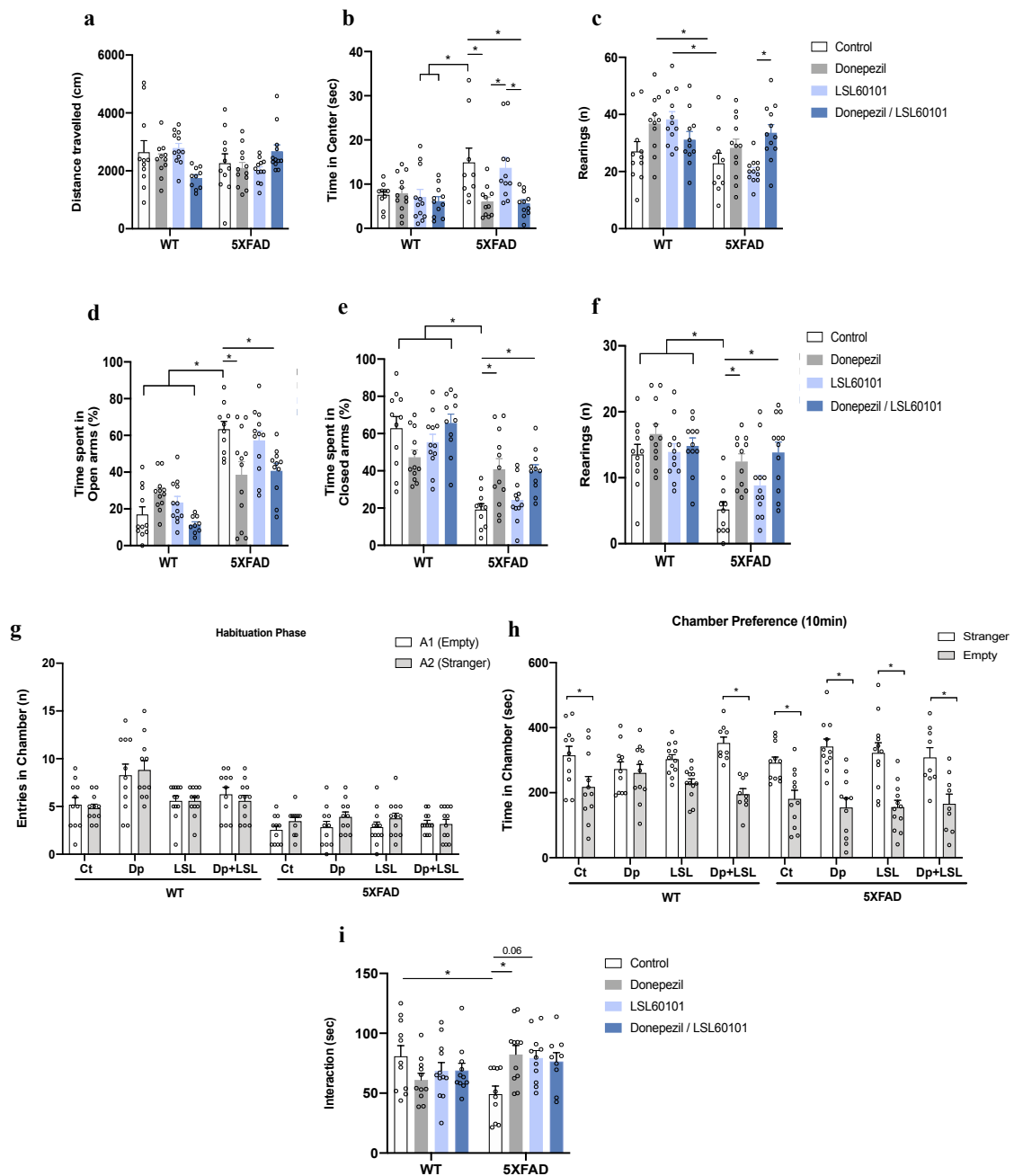


Figure 2: (Caption next page)

**Figure 2:** (Previous page) **Effects of low-dose chronic treatments I<sub>2</sub>-IR LSL60101, donepezil and co-administration on behavioural and social status in 5XFAD mice and WT controls.** Results of open field:- (a) locomotor activity measured as distance travelled (cm) (WT n = 10–12 per group; 5XFAD n = 11–12 per group; two-way ANOVA with Tukey's post hoc analysis). (b) Time spent in the centre (s) (WT n = 10–12 per group; 5XFAD n = 9–11 per group; two-way ANOVA with post hoc analysis showing significant effect of genotype and treatment, with significant interaction). (c) Number of rearings (WT n = 11–12 per group; 5XFAD n = 10–12 per group; two-way ANOVA with Tukey's post hoc analysis showing significant effect of genotype and treatment, with significant interaction). Results of elevated plus maze (EPM):- (d) time (%) spent in open arms (WT n = 11–12 per group; 5XFAD n = 10–12 per group; two-way ANOVA with Tukey's post hoc analysis showing significant effect of genotype and treatment, with significant interaction). (e) Time (%) spent in closed arms (WT n = 11–12 per group; 5XFAD n = 10–12 per group; two-way ANOVA with post hoc analysis showing significant effect of genotype and treatment, with significant interaction). (f) Number of rearings (WT n = 11–12 per group; 5XFAD n = 11–12 per group; two-way ANOVA with post hoc analysis showing significant effect of genotype and treatment, with significant interaction). Results of three-chamber test (TCT): (g) entries in chambers (A1 and A2) in the habituation phase (n) (WT n = 11–12 per group; 5XFAD n = 11–12 per group; unpaired Student's t test). (h) Time in chambers (empty and stranger) during the test session (WT n = 10–11 per group; 5XFAD n = 9–11 per group; unpaired Student's t-test). (i) Time of interaction with intruder (s) in the test session (WT n = 11–12 per group; 5XFAD n = 10–11 per group two-way ANOVA showing non-significant effect of genotype and treatment, with significant interaction). Bars show mean  $\pm$  SEM; \*P < .05

**I<sub>2</sub> ligand LSL60101, but not donepezil, reduces amyloid- $\beta$  plaques; by contrast, donepezil/LSL60101 attenuates amyloid- $\beta$  pathology in 5XFAD mice.**

The number of amyloid plaques in 5XFAD hippocampus and cortex mice was assessed by histochemical staining with thioflavin S. LSL60101 induced a significant decrease in the total number and area (%) covered by the plaques in 5XFAD mice compared with the 5XFAD controls, demonstrating a neuroprotective function of I<sub>2</sub> ligand regarding the senile plaque formation. Treatment with donepezil did not reduce the number of amyloid plaques or area significantly in 5XFAD mice (Figure 3a–c). The protein levels of amyloid- $\beta$  determined by western blots tended to decrease in all treated groups without reaching significance (Figure 3d, h). Protein concentrations of amyloid- $\beta_{40}$  and amyloid- $\beta_{42}$ , determined by ELISA, were significantly higher in 5XFAD in comparison with WT healthy control, whereas treatment with LSL60101 reduced significantly amyloid- $\beta_{40}$  and amyloid- $\beta_{42}$  levels. Donepezil did not modify amyloid- $\beta$  concentration species significantly and combination of donepezil and LSL60101 treatment did not modify the effect of LSL60101 alone (Figure 3e, f). As expected, full-length amyloid precursor protein levels were increased in 5XFAD mice compared with WT mice and treatments did not modify protein expression (Figure 4a, h). Interestingly, alterations in the levels of proteins implicated in the amyloid precursor protein processing showed complementary results in the combination of LSL60101 and donepezil treatment. In this line, the protein levels of C-terminal fragments were found significantly reduced in LSL60101-treated

group compared with the 5XFAD controls. LSL60101/donepezil-treated group showed a significant decrease in C-terminal fragments compared with monotherapy (Figure 4b, h). The protein levels of phosphorylated amyloid precursor protein at Th668 were decreased significantly only for the combination of donepezil/ LSL60101-treated animals (Figure 4c, h). Soluble amyloid precursor protein  $\beta$  levels were found increased in 5XFAD controls compared with WT mice, confirming the amyloid pathology process. Furthermore, a significant decrease in donepezil/LSL60101-treated group was determined (Figure 4d, h). Soluble amyloid precursor protein  $\alpha$  levels were found increased after combination treatment when compared with 5XFAD controls or donepezil-treated mice (Figure 4e, h). Regarding the levels of BACE1 ( $\beta$ -secretase 1) and ADAM10, no significant differences were observed among the 5XFAD groups (Figure 4f–h). However, when the gene expression of enzymes implicated in amyloid degradation was studied, treatments slightly increased gene expression of insulin-degrading enzyme (*IDE*), whereas neutral endopeptidase neprilysin (*Nep*) was only reduced in the donepezil and LSL60101 groups (Figure 4i).

### **I<sub>2</sub> ligand LSL60101 and combination with donepezil reduce Tau hyperphosphorylation in 5XFAD mice.**

Tau hyperphosphorylation, another major marker of AD, was evaluated in the hippocampus of the 5XFAD mice. I<sub>2</sub> ligand LSL60101 and the cotreatment donepezil/LSL60101 decreased the tau phosphorylation at the Ser404 and Ser396, diminutions that reached significance for the donepezil/LSL60101-treated 5XFAD mice. Of note, significant differences in p-Tau levels were also found between the donepezil/LSL60101 5XFAD-treated mice and the donepezil or LSL60101-treated ones (Figure 3g,h).

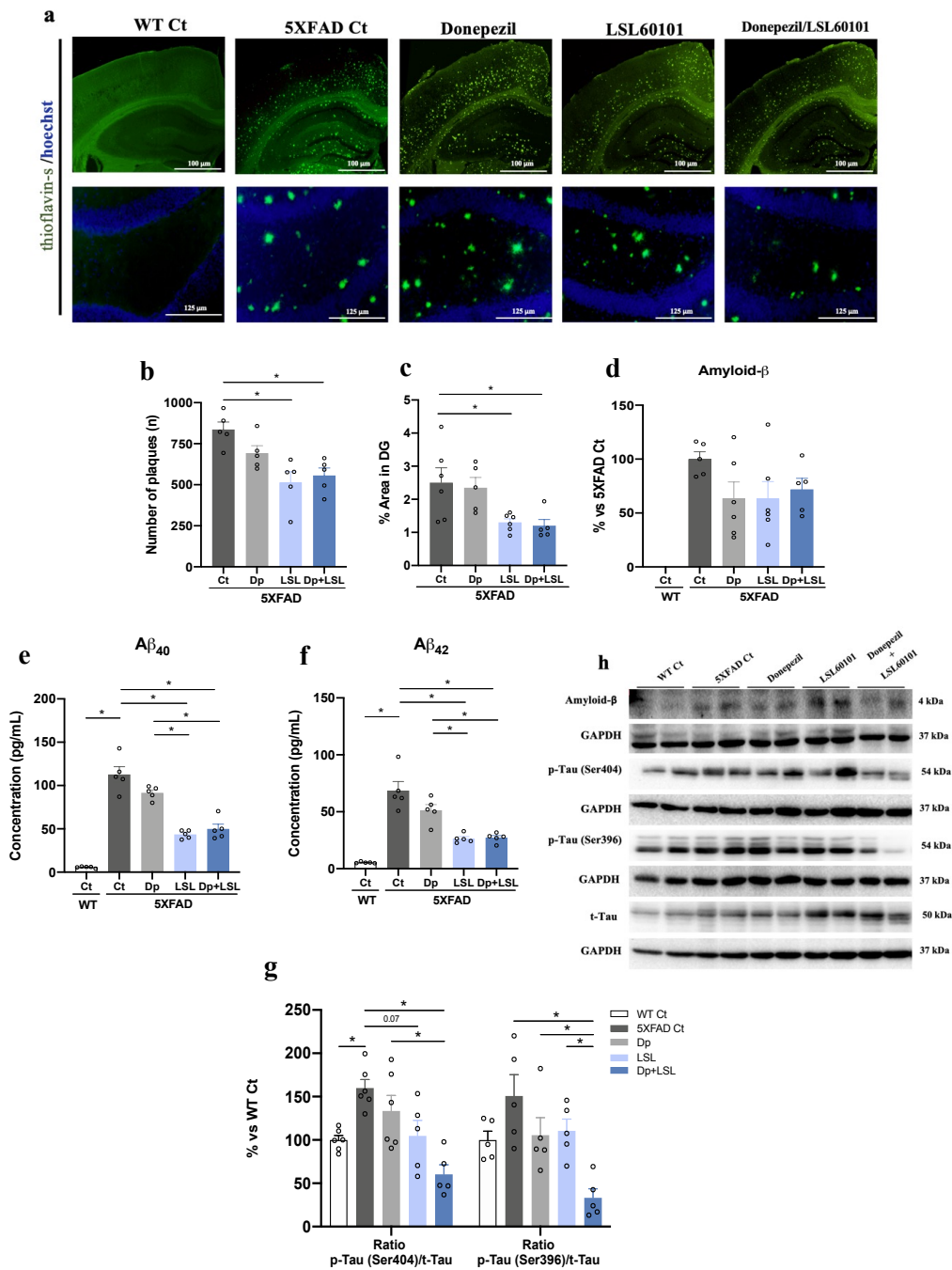


**Figure 3: Effects of low-dose treatments with I<sub>2</sub> receptor ligand LSL60101, donepezil and co-administration on AD markers in 5XFAD mice.** (a) Representative images of thioflavin S staining of amyloid plaques and quantification of (b) amyloid plaque number in cortex and hippocampus and (c) area (%) covered by plaques in the dentate gyrus area of the hippocampus in the 5XFAD mice. Data are presented as the mean  $\pm$  SEM and each dot represents one mouse ( $n = 5$  per group); averaged from 2–3 sections from the same brain area per animal. Levels of amyloid- $\beta_{40}$  and amyloid- $\beta_{42}$  and representative western blot and quantifications for (d–h)  $\beta$ -amyloid, p-Tau (Ser404) and p-Tau (Ser396) in the hippocampus of 5XFAD mice. Values in bar graphs are adjusted to 100% for protein levels of the control WT or the control 5XFAD. Bars represent mean  $\pm$  SEM. Student's t-test or one-way ANOVA with Tukey's post hoc analysis, \* $P < .05$ ;  $n = 5$ –6 per group

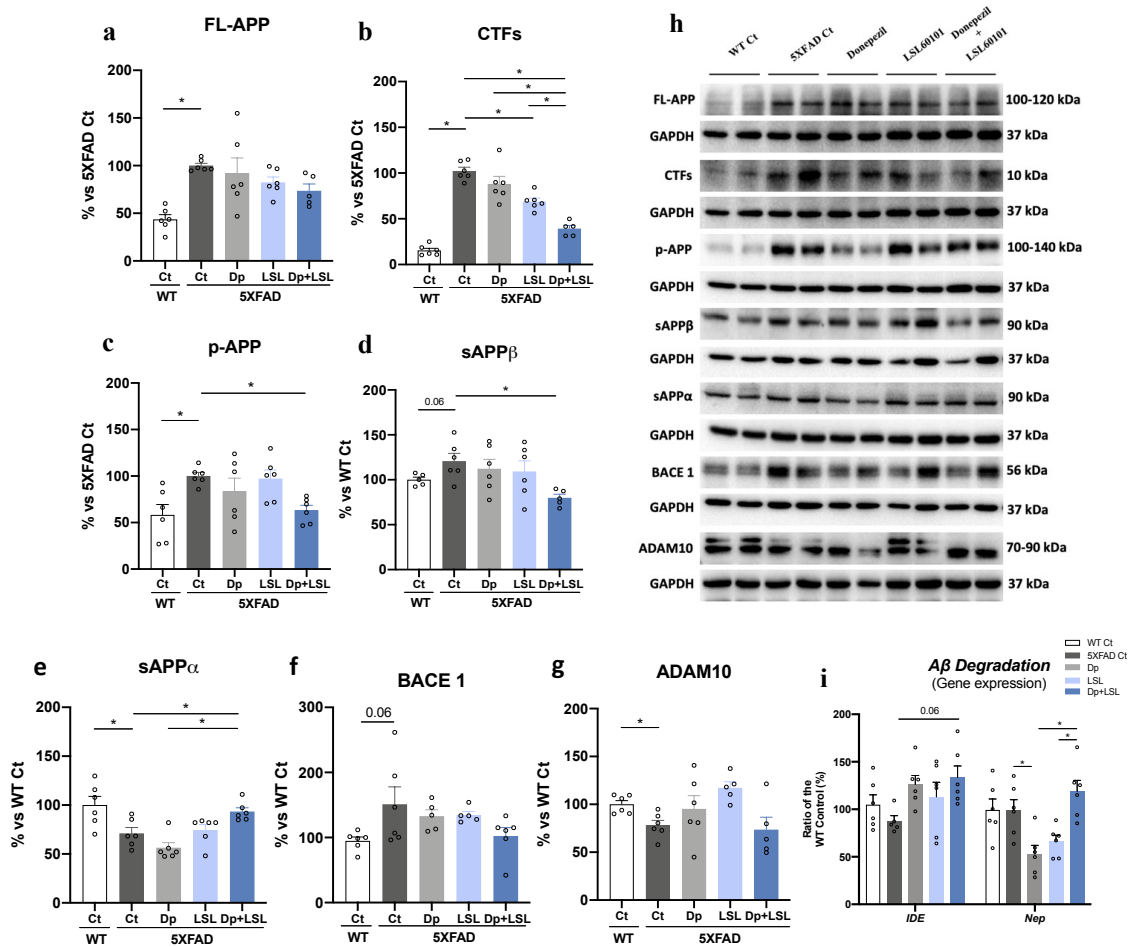


**Figure 4:** Effects of low-dose chronic treatments I<sub>2</sub> receptor ligand LSL60101, donepezil and co-administration on amyloid- $\beta$  (A $\beta$ ) pathology and amyloid precursor protein (APP) processing in 5XFAD mice. Representative western blots and quantifications for (a–h) FL-APP, C-terminal fragments (CTFs), p-APP, sAPP $\beta$ , sAPP $\alpha$ , BACE 1 and ADAM10 in the hippocampus of 5XFAD mice. Values in bar graphs are adjusted to 100% for protein levels of the control WT or the control 5XFAD. Representative gene expression in the hippocampus of the 5XFAD mice for *IDE* and *Nep* (i). Gene expression levels were determined by real-time PCR. Values in bar graphs are adjusted to 100% for relative gene expression of the WT control. Bars represent mean  $\pm$  SEM. Unpaired Student's t-test or one-way ANOVA with Tukey's post hoc analysis, \*P < .05; n = 5–6 per group

### Effects of LSL60101 on microglia activation and inflammatory marker expression.

In the AD brain, the formation of amyloid- $\beta$  plaques leads to the activation of astrocytes and reactive gliosis. To examine changes in microglia reactivity, ionized calcium-binding adaptor molecule 1 (Iba-1) was determined by immunohistochemistry experiments. Importantly, LSL60101 treatment resulted in a significant decrease in Iba-1 levels in the hippocampus (Figure 5a–d) and in the cortex (Figure S3) of 5XFAD mice, whereas donepezil did not affect Iba-1 immunoreactivity (Figure 5a–d). Donepezil/LSL60101 combination reduced significantly Iba-1 levels in the cortex (Figure S3) and the dentate gyrus area in the hip-

pocampus (Figure 5a–d). The gene expression of different inflammatory mediators was evaluated in the hippocampus of 5XFAD mice. In whole, 5XFAD mice presented an evident exacerbation of inflammatory response compared with WT mice, whereas treatments led to the up-regulation of specific markers studied. No significant changes were determined in IL-1 $\beta$  (*Il-1b*) and IL-6 (*Il-6*) markers in treated groups compared with 5XFAD controls (Figure 5e). However, chemokine (C–C motif) ligand 12 (*Ccl12*) and IL-18 (*Il-18*) genes were found increased in LSL60101 group and donepezil/LSL60101-treated groups compared with 5XFAD controls (Figure 5e). Moreover, the gene expression of triggering receptor expressed on myeloid cells 2 (*Trem2*) was increased significantly after treatment with the I<sub>2</sub> ligand LSL60101 and the combination-treated group (Figure 5f), confirming the results of *Il-18* and *Ccl12*.

#### **LSL60101 effects on astroglial activation and synaptic dysfunction.**

All treatments were able to attenuate astrogliosis in the hippocampus of 5XFAD brains by decreasing GFAP immunoreactivity in dentate gyrus, CA1 and CA3 areas in 5XFAD mice groups in comparison with untreated mice (Figure 6a–d). Similar results were observed in the cortex (Figure S3). Likewise, synaptic plasticity markers were evaluated by western blot. Decreases in the protein levels of postsynaptic density protein 95 (PSD95) and synaptophysin were determined in 5XFAD mice when compared with WT mice (Figure 6e–g). I<sub>2</sub> ligand LSL60101 increased PSD95 levels when compared with 5XFAD control (Figure 6e, g). Synaptophysin levels were found to increase in LSL60101 and donepezil/LSL60101-treated 5XFAD mice, reaching significance only for the combination-treated group. Donepezil treatment was not able to modify these markers significantly (Figure 6f, g).

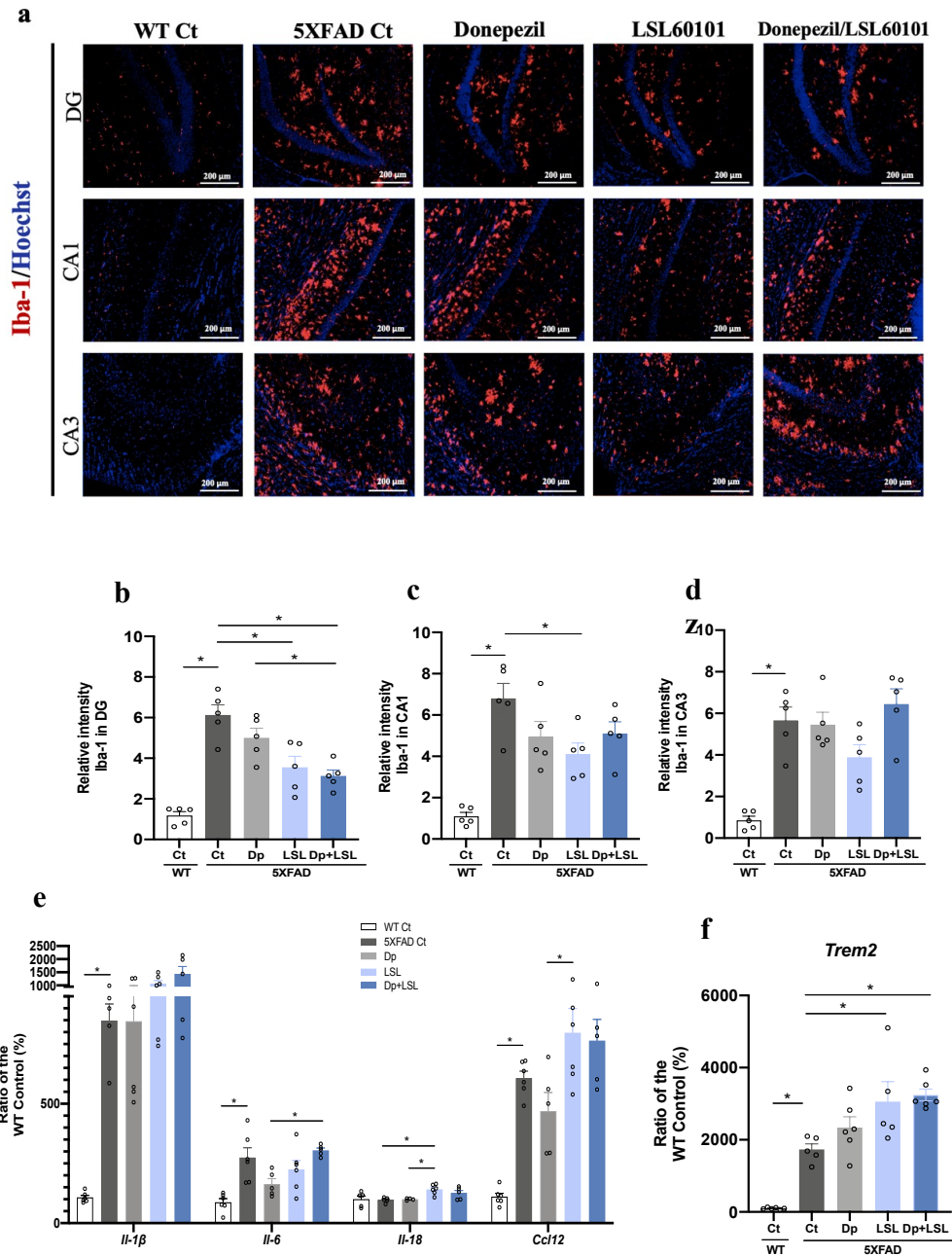


**Figure 5: Effects of low- dose chronic treatments I<sub>2</sub> receptor ligand LSL60101, donepezil and co-administration on microgliosis and inflammatory markers in 5XFAD mice.** (a) Representative images of Iba-1 immunostaining and quantification in (b–d) dentate gyrus (DG), cornu ammonis (CA) 1 and CA3 areas of the hippocampus of the 5XFAD mice. Data are presented as the mean  $\pm$  SEM of relative fluorescent intensity of the positive cells averaged from 2–3 different sections from the same brain area per animal and each dot represents one mouse (n = 5 per group). Representative gene expression in the hippocampus of the 5XFAD mice for (e) *Il-1 $\beta$* , *Il-6*, *Il-18* and *Ccl12* and (f) *Trem2*. Gene expression levels were determined by real-time PCR. Values in bar graphs are adjusted to 100% for relative gene expression of the WT control. Bars show mean  $\pm$  SEM. Unpaired Student’s t-test or one-way ANOVA with Tukey’s post hoc analysis, \*P < .05; n = 5–6 per group



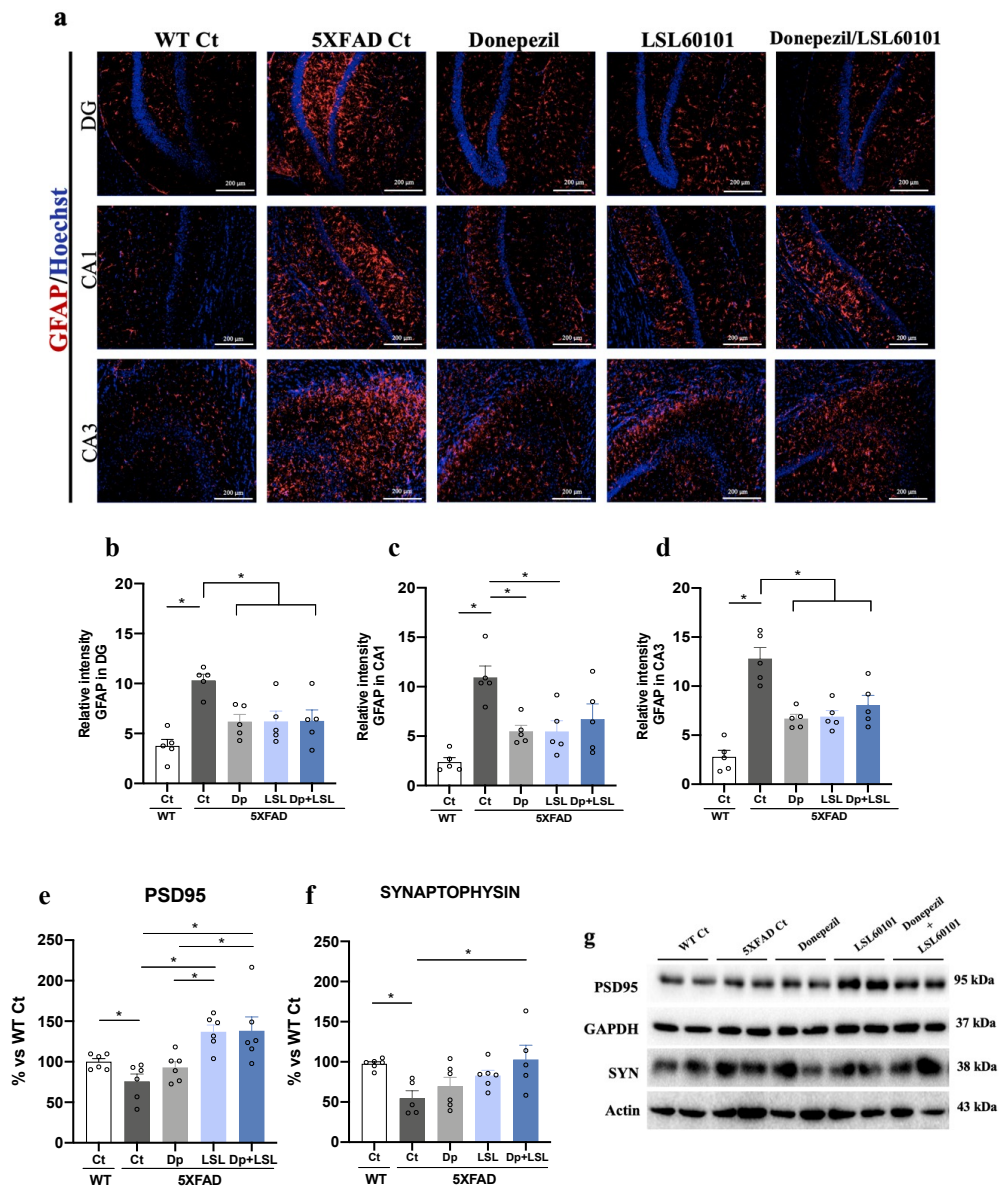


**Figure 6:** Effects of low-dose chronic treatments I<sub>2</sub> receptor ligand LSL60101, donepezil and co-administration on astrogliosis and synaptic plasticity in 5XFAD mice. (a) Representative images of GFAP immunostaining and quantification in (b–d) dentate gyrus (DG), cornu ammonis (CA) 1 and CA3 areas of the hippocampus of the 5XFAD mice. Data are presented as the mean  $\pm$  SEM of relative fluorescent intensity of the positive cells averaged from 2–3 different sections from the same brain area per animal and each dot represents one mouse (n = 5 per group). Representative western blot and quantifications for (e–g) postsynaptic density protein 95 (PSD95) and synaptophysin in the hippocampus of 5XFAD mice. Values in bar graphs are adjusted to 100% for protein levels of the control WT. Bars show mean  $\pm$  SEM. Unpaired Student's t-test or one-way ANOVA with Tukey's post hoc analysis, \*P < .05; n = 5–6 per group

### 3.4.4 DISCUSSION

The identification of new targets for AD treatment is required due to the lack of effective treatment. At present, AChE inhibitors are one of the standard therapeutic options clinically available for AD patients, however those treatments provide only symptomatic benefit in AD (Rosini et al., 2014; Sinforiani et al., 2003). Fortunately, the number of disease-modifying drugs targeting AD markers such as aducanumab (BIIB037), which is currently in Phase 3 trials, is increasing (Cummings et al., 2020). Combination therapies of symptomatic and disease-modifying drugs have centred attention due to the multifactorial origin of the disease and most current clinical trials combine donepezil with novel neuroprotective drugs (Frölich et al., 2019). However, it remains a challenge that must be addressed to unveil new strategies that could be more effective in disease-modifying treatment rather than address symptoms (Schmitt et al., 2004).

Several studies have described the symptomatic effects of donepezil in animal models of dementia and AD, but few *in vivo* studies have evaluated donepezil neuroprotective effects regarding the disease-modifying actions of this compound alone or in combination (Jiangbo & Liyun, 2018; Krishna et al., 2020; Ongnok et al., 2021; Yang et al., 2020). Here, we studied the effect of chronic low doses of an I<sub>2</sub> ligand, donepezil and their combination. In the light of our studies, we demonstrated for the first time the neuroprotective effects of selective I<sub>2</sub> ligands in the senescence-accelerated mouse prone 8 (SAMP8), a mouse model of late-onset AD (Griñan-Ferré et al., 2019). LSL60101, a selective I<sub>2</sub> ligand, has been shown to induce several biological effects associated with I<sub>2</sub> receptor occupancy and, most importantly, neuroprotective effects in the CNS (Boronat et al., 1998; Casanovas et al., 2000; Menargues et al., 1995; Sanchez-Blazquez et al., 2000). Therefore, it represents a suitable drug candidate to validate this receptor as a target for AD. Here, we demonstrated the efficacy of chronic low-dose I<sub>2</sub> ligand LSL60101 treatment compared with donepezil by assessing the beneficial outcomes in a model of familial AD.

Cognitive abilities are the essential indicators to unveil pharmacological effects in AD. First, chronic low-dose treatment with the I<sub>2</sub> ligand LSL60101 or donepezil reversed the cognitive deficits presented by 7-month-old 5XFAD mice without affecting WT mice in the novel object recognition test paradigm. However, in the spatial memory test, only LSL60101 showed improvements in memory. Likewise, 5XFAD exhibited improved social behaviour after LSL60101 or donepezil treatment. In agreement with these results, donepezil has been shown to improve social interactions in scopolamine-induced memory impairments in mice (Riedel et al., 2009) and in drug trials for AD (Boada-Rovira et al., 2004). Nevertheless, the beneficial effect of an I<sub>2</sub> ligand treatment on social interaction deficits has not been described previously.

By contrast, I<sub>2</sub> ligand LSL60101 did not modify anxiety-like behaviour, albeit previous studies have shown the *in vivo* anxiolytic and antidepressant-like effects induced by I<sub>2</sub> ligands (Finn et al., 2003; Tonello et al., 2012). Interestingly, the absence of antidepressant effect after treatment with LSL60101 in healthy rats was recently described (Hernandez-Hernandez et al., 2020), further supporting our results because anxiety-like and depressive-like behaviours are strongly associated, sharing common molecular pathways (Gatt et al., 2009). In contrast, and according to literature (Fitzgerald et al., 2020), chronic treatment with donepezil showed beneficial effects on the anxiety-related disturbances exhibited by 5XFAD mice. Recently, we reported that the amyloidogenic amyloid precursor protein processing pathway was suppressed in senescence-accelerated mouse prone 8 and 5XFAD mice after treatment with novel I<sub>2</sub> ligands, anticipating the role of I<sub>2</sub> modulation in the amyloid- $\beta$  biogenesis (Abas et al., 2020; Griñan-Ferré et al., 2019; Vasilopoulou, Griñan-Ferré, et al., 2020). Accordingly, in this study, we demonstrated for the first time that chronic low-dose treatment with I<sub>2</sub> ligand LSL60101 attenuated the amyloid plaque burden in 5XFAD mice. In addition, amyloid- $\beta$  plaque reduction was accompanied by a decrease in C-terminal fragments, amyloid- $\beta_{40}$  and amyloid- $\beta_{42}$  protein levels. Conversely, recently, it was reported that the I<sub>2</sub> ligand BU224 does not ameliorate amyloid- $\beta$  amyloidosis in 5XFAD mice but improves memory (Mirzaei et al., 2020). In contrast with LSL60101 like molecules, BU224 blocked the memory-enhancing effect of agmatine in memory deficits induced by amyloid- $\beta_{42}$  in mice (Kotagale et al., 2020). These discrepancies between I<sub>2</sub> ligands can be explained by differences in compound administration conditions, such as dose, time (subchronic vs. chronic) and administration route. Thus, we hypothesise that low doses of LSL60101, as well as chronic treatment, have a clear beneficial effect on amyloid burden because of differential characteristics among I<sub>2</sub> ligands (Garau et al., 2013; Sanchez-Blazquez et al., 2000). Several studies have demonstrated the effect of donepezil on amyloid- $\beta$  pathology in AD models, reporting either beneficial changes (Dong et al., 2009; Takada-Takatori et al., 2019) or lack of effect (Ju & Tam, 2020). Here, low-dose donepezil treatment did not induce significant changes either in amyloid- $\beta$  plaques or in amyloid precursor protein processing in 7-month-old 5XFAD. Of note, co-administration of I<sub>2</sub> LSL60101 and donepezil showed a greater effect on amyloid precursor protein processing than monotherapy. Regarding the amyloid- $\beta$  degradation, the co-treatment of donepezil/LSL60101 induced an increase in amyloid- $\beta$  degradation enzyme gene expression in 5XFAD mice, which was not determined in the other treated groups. To sum up, this is the first time an I<sub>2</sub> ligand was shown to effectively reduce the amyloid- $\beta$  plaques in a mouse model of AD.

The presence of p-Tau, another major AD marker, in the 5XFAD model is supported by previous studies suggesting that tau pathology may be downstream from amyloid- $\beta$  pathology (Blanchard et al., 2003; Saul et al., 2013). I<sub>2</sub> ligand LSL60101 ameliorated tau

pathology in the hippocampus of 5XFAD mice. Interestingly, it was shown recently that chronic treatment with idazoxan, a mixed  $\alpha_2/I_2$  ligand, reduced p-Tau reversing cognitive deficits in AD mice because of its  $\alpha_2$  blockade action (Zhang et al., 2020). In this case, the effect of LSL60101 on tau pathology can be attributed to its  $I_2$  selectivity, more than to the  $\alpha_2$  one. Surprisingly, the p-Tau reduction reached significance in the 5XFAD mice treated with the combination of LSL60101 with donepezil demonstrating, in this case, a putative additive effect of the drugs on tau pathology. Indeed, amelioration of tau pathology has been induced in AD animal models both by donepezil (Yoshiyama et al., 2010) and by  $I_2$  ligand treatments (Griñan-Ferré et al., 2019; Vasilopoulou, Griñan-Ferré, et al., 2020). It is possible that the activation of distinct molecular pathways by the two molecules with different modes of actions resulted in a remarkable p-Tau reduction observed in the donepezil/LSL60101-treated mice group.

It is well established that amyloid- $\beta$  accumulation jointly with p-Tau increases microglial activation and inflammatory mediators' production in AD brains (Akiyama et al., 2000; Serrano-Pozo et al., 2011; Zhang & Jiang, 2015). On the one hand, chronic low-dose LSL60101 treatment reduced microgliosis in 5XFAD mice in contrast to the standard of care donepezil, explaining the decrease in the amyloid deposition that in turn would lead to a decrease in gliotic response after LSL60101 treatment. On the other hand, inflammatory gene expression increase (*Il-18* and *Ccl12*) was observed after treatment with  $I_2$  ligand LSL60101 and LSL60101/donepezil, but not with donepezil. Interestingly, this was further supported by a significant up-regulation of *Trem2* gene expression determined in the LSL60101-treated mice, further confirming the neuroinflammatory modulation by  $I_2$  ligand LSL60101 (Griñan-Ferré et al., 2019; Hwang et al., 2010; Vasilopoulou, Bagan, et al., 2020). In fact, increased *Trem2* expression has been shown to reprogram microglia responsivity mediating microglial cytokine release, migration and clearance of amyloid- $\beta$  deposits, ameliorating neuropathological and behavioural deficits of AD mouse models (Lee et al., 2018; Zhao et al., 2018).

It has been described that the  $I_2$  receptors modulate the expression of astrocyte marker GFAP, especially considering their primary location in astrocytes (Olmos et al., 1994; Regunathan et al., 1993, 1999). GFAP diminution was observed *in vivo* and *in vitro* after treatment with selective  $I_2$  ligands (Griñan-Ferré et al., 2019; Siemian et al., 2018; Vasilopoulou, Griñan-Ferré, et al., 2020). In agreement with those results, chronic low-dose treatment with  $I_2$  ligand LSL60101 attenuated astrogliosis in 5XFAD mice. By contrast, it has been shown that chronic treatment with LSL60101 increased GFAP immunoreactivity (Alemany et al., 1995), resulting in reactive astrogliosis and preventing motoneuron cell death in neonatal rats (Casanovas et al., 2000). However, here, in a neurodegenerative landscape provided by the 5XFAD model, the diminution of GFAP reactivity ran in parallel

with the attenuation of the amyloid- $\beta$  pathology and microglial activation observed after LSL60101 and donepezil treatment, given further support to the beneficial effects of I<sub>2</sub> ligand on mice behaviour. Ultimately, we demonstrated that chronic low-dose treatment with I<sub>2</sub> ligand and donepezil enhanced synaptic plasticity, further supporting the cognitive and behavioural improvement induced by the LSL60101 in 5XFAD mice.

Nevertheless, one limitation of our study was that only female 5XFAD mice were used to establish the protective effect of LSL60101 on AD markers and cognition. It would be of great interest to carry out experiments on male mice once we have demonstrated the disease-modifying effects promoted by LSL60101 in a female mice model of AD.

### 3.4.5 CONCLUSIONS

Collectively, we report that chronic low-dose treatment with I<sub>2</sub> ligand LSL60101 reversed cognitive deficits in 5XFAD mice, altering AD neuropathological markers, including glial activation and synaptic dysfunction. Strikingly, treatment with I<sub>2</sub> ligand LSL60101 was found to exert greater beneficial effects under the neurodegenerative process caused by amyloid- $\beta$  pathology than donepezil. However, combination treatment only showed discrete synergistic effects at the molecular level (e.g. tau hyperphosphorylation or synaptic plasticity), suggesting that increased dosage and/or duration of the treatment may be able to produce better effects on both behaviour and AD markers, targeting simultaneously pathological and symptomatic reliefs. In conclusion, our findings demonstrate the therapeutic potential of the I<sub>2</sub> receptor ligands for AD treatment as a disease-modifying single therapy and provide new insights into their efficacy.

**Acknowledgements:** This study was supported by Ministerio de Economía y Competitividad of Spain and FEDER (Ministerio de Ciencia e Innovación; PID2019-107991RB-I00 and PID2019-106285RB-I00) and 2017SGR106 (Agència de Gestió d'Ajuts Universitaris i de Recerca [AGAUR], Catalonia). The project leading to these results has received funding from “la Caixa” Foundation (ID100010434), under Agreement CI18-00002. F.V. thanks the Universitat de Barcelona (UB) for the APIF grant (UB2016); S. R.-A. to Generalitat de Catalunya (2018FI-B- 00227); and A.B. for the APIF Grant Institute of Biomedicine (UB2018).

**Author Contributions:** FV, CG-F and MP conceived the study, designed all the experiments, and interpreted the data; FV, CG-F performed the experiments and data analysis; all authors revised the manuscript draft. S R-A, AB and CE synthesised compounds tested; FV, CG-F and MP wrote, revised, and finalised the manuscript.

**Conflict of interest:** The authors declare no conflicts of interest.

**Abbreviations:** AD, Alzheimer's disease; Ccl12, chemokine (C–C motif) ligand 12; GFAP, glial fibrillary acidic protein; I<sub>2</sub>, imidazoline-2 receptors; Iba-1, ionized calcium-binding adaptor molecule 1; PSD95, postsynaptic density protein 95; p-Tau, hyperphosphorylated tau; Trem2, triggering receptor expressed on myeloid cells 2.

## REFERENCES

Abás, S., Erdozain, A. M., Keller, B., Rodríguez-Arévalo, S., Callado, L. F., García-Sevilla, J. A., & Escolano, C. (2017). Neuroprotective effects of a structurally new family of high affinity imidazoline I<sub>2</sub> receptor ligands. *ACS Chemical Neuroscience*, 8(4), 737–742. <https://doi.org/10.1021/acschemneuro.6b00426>

Abás, S., Rodríguez-Arévalo, S., Bagán, A., Griñan-Ferré, C., Vasilopoulou, F., Brocos-Mosquera, I., Muguruza, C., Pérez, B., Molins, E., Luque, F. J., Pérez-Lozano, P., de Jonghe, S., Daelemans, D., Naesens, L., Brea, J., Loza, M. I., Hernández-Hernández, E., García-Sevilla, J. A., García-Fuster, M. J., ... Escolano, C. (2020). Bicyclic  $\alpha$ -iminophosphonates as high affinity imidazoline I<sub>2</sub> receptor ligands for Alzheimer's disease. *Journal of Medicinal Chemistry*, 63, 3610–3633. <https://doi.org/10.1021/acs.jmedchem.9b02080>

Akiyama, H., Barger, S., Barnum, S., Bradt, B., Bauer, J., Cole, G. M., Wyss-Coray, T., Eikelenboom, P., Emmerling, M., Fiebich, B. L., Finch, C. E., Frautschy, S., Griffin, W. S., Hampel, H., Hull, M., Landreth, G., Lue, L., Mrak, R., Mackenzie, I. R., ... Wyss-Coray, T. (2000). Inflammation and Alzheimer's disease. *Neurobiology of Aging*, 21, 383–421. [https://doi.org/10.1016/s0197-4580\(00\)00124-x](https://doi.org/10.1016/s0197-4580(00)00124-x)

Aleman, R., Olmos, G., Escribá, P. V., Menargues, A., Obach, R., & García-Sevilla, J. A. (1995). LSL 60101, a selective ligand for imidazoline I<sub>2</sub> receptors, on glial fibrillary acidic protein concentration. *European Journal of Pharmacology*, 280, 205–210. [https://doi.org/10.1016/0014-2999\(95\)00214-6](https://doi.org/10.1016/0014-2999(95)00214-6)

Alexander, S. P. H., Kelly, E., Mathie, A., Peters, J. A., Veale, E. L., Armstrong, J. F., Faccenda, E., Harding, S. D., Pawson, A. J., Sharman, J. L., Southan, C., Buneman, O. P., Cidlowski, J. A., Christopoulos, A., Davenport, A. P., Fabbro, D., Spedding, M., Striessnig, J., Davies, J. A., ... Wong, S. S. (2019). The Concise Guide to PHARMACOLOGY 2019/20: Introduction and other protein targets. *British Journal of Pharmacology*, 176(Suppl 1), S1–S20. <https://doi.org/10.1111/bph.14747> PMID: 31710719; PMCID: PMC6844537

Alexander, S. P., Roberts, R.E., Broughton, B. R., Sobey, C. G., George, C. H., Stanford, S. C., Cirino, G., Docherty, J. R., Giembycz, M. A., Hoyer, D., & Insel, P. A. (2018). Goals and practicalities of immunoblotting and immunohistochemistry: A guide for submission to the *British Journal of Pharmacology*. *British Journal of Pharmacology*, 175, 407–411. <https://doi.org/10.1111/bph.14112>

Archer, J. (1973). Tests for emotionality in rats and mice: A review. *Animal Behaviour*, 21,

205–235. [https://doi.org/10.1016/S0003-3472\(73\)80065-X](https://doi.org/10.1016/S0003-3472(73)80065-X)

Blanchard, V., Moussaoui, S., Czech, C., Touchet, N., Bonici, B., Planche, M., Canton, T., Jedidi, I., Gohin, M., Wirths, O., Bayer, T. A., Langui, D., Duyckaerts, C., Tremp, G., & Pradier, L. (2003). Time sequence of maturation of dystrophic neurites associated with A $\beta$  deposits in APP/PS1 transgenic mice. *Experimental Neurology*, 184, 247–263. [https://doi.org/10.1016/S0014-4886\(03\)00252-8](https://doi.org/10.1016/S0014-4886(03)00252-8)

Boada-Rovira, M., Brodaty, H., Cras, P., Baloyannis, S., Emre, M., Zhang, R., Bahra, R., & 322 Study Group. (2004). Efficacy and safety of donepezil in patients with Alzheimer's disease. *Drugs & Aging*, 21, 43–53. <https://doi.org/10.2165/00002512-200421010-00004>

Boronat, M. A., Olmos, G., & García-Sevilla, J. A. (1998). Attenuation of tolerance to opioid-induced antinociception and protection against morphine-induced decrease of neurofilament proteins by idazoxan and other I<sub>2</sub>-imidazoline ligands. *British Journal of Pharmacology*, 125, 175–185. <https://doi.org/10.1038/sj.bjp.0702031>

Bousquet, P., Hudson, A., García-Sevilla, J. A., & Li, J. X. (2020). Imidazoline receptor system: The past, the present, and the future. *Pharmacological Reviews*, 72, 50–79. <https://doi.org/10.1124/pr.118.016311>

Bradford, M. M. (1976). A rapid and sensitive method for the quantitation of microgram quantities of protein utilizing the principle of protein-dye binding. *Analytical Biochemistry*, 72, 248–254. [https://doi.org/10.1016/0003-2697\(76\)90527-3](https://doi.org/10.1016/0003-2697(76)90527-3)

Casanovas, A., Olmos, G., Ribera, J., Boronat, M. A., Esquerda, J. E., & García-Sevilla, J. A. (2000). Induction of reactive astrogliosis and prevention of motoneuron cell death by the I<sub>2</sub>-imidazoline receptor ligand LSL 60101. *British Journal of Pharmacology*, 130, 1767–1776. <https://doi.org/10.1038/sj.bjp.0703485>

Companys-Aleman, J., Turcu, A. L., Bellver-Sanchis, A., Loza, M. I., Brea, J.M., Canudas, A.M., Leiva, R., Vázquez, S., Pallàs, M., & Griñan-Ferré, C. (2020). A novel NMDA receptor antagonist protects against cognitive decline presented by senescent mice. *Pharmaceutics*, 12, 1–17. <https://doi.org/10.3390/pharmaceutics12030284>

Cummings, J., Lee, G., Ritter, A., Sabbagh, M., & Zhong, K. (2020). Alzheimer's disease drug development pipeline: 2020. *Alzheimer's & Dementia: Translational Research & Clinical Interventions*, 6, 1–29.

Curtis, M. J., Alexander, S., Cirino, G., Docherty, J. R., George, C. H., Giembycz, M. A., Hoyer, D., Insel, P. A., Izzo, A. A., Ji, Y., MacEwan, D. J., Sobey, C. G., Stanford, S. C., Teixeira, M. M., Wonnacott, S., & Ahluwalia, A. (2018). Experimental design and analysis and their reporting II: Updated and simplified guidance for authors and peer reviewers. *British Journal of Pharmacology*,

175, 987–993. <https://doi.org/10.1111/bph.14153>

DeTure, M. A., & Dickson, D. W. (2019). The neuropathological diagnosis of Alzheimer's disease. *Molecular Neurodegeneration*, 14, 32. <https://doi.org/10.1186/s13024-019-0333-5>

Dickson, D. W., & Rogers, J. (1992). Neuroimmunology of Alzheimer's disease: A conference report. *Neurobiology of Aging*, 13, 793–798. [https://doi.org/10.1016/0197-4580\(92\)90104-6](https://doi.org/10.1016/0197-4580(92)90104-6)

Dong, H., Yuede, C. M., Coughlan, C. A., Murphy, K. M., & Csernansky, J. G. (2009). Effects of donepezil on amyloid- $\beta$  and synapse density in the Tg2576 mouse model of Alzheimer's disease. *Brain Research*, 1303, 169–178. <https://doi.org/10.1016/j.brainres.2009.09.097>

Ennaceur, A., & Delacour, J. (1988). A new one-trial test for neurobiological studies of memory in rats. 1: Behavioral data. *Behavioural Brain Research*, 31, 47–59.

Finn, D. P., Martí, O., Harbuz, M. S., Vallès, A., Belda, X., Marquez, C., Jessop, D. S., Lalies, M. D., Armario, A., Nutt, D. J., & Hudson, A. L. (2003). Behavioral, neuroendocrine and neurochemical effects of the imidazoline I<sub>2</sub> receptor selective ligand BU224 in naive rats and rats exposed to the stress of the forced swim test. *Psychopharmacology*, 167, 195–202. <https://doi.org/10.1007/s00213-003-1392-3>

Fitzgerald, P. J., Hale, P. J., Ghimire, A., & Watson, B. O. (2020). The cholinesterase inhibitor donepezil has antidepressant-like properties in the mouse forced swim test. *Translational Psychiatry*, 10, 255. <https://doi.org/10.1038/s41398-020-00928-w>

Frölich, L., Atri, A., Ballard, C., Tariot, P. N., Molinuevo, J. L., Boneva, N., Geist, M. A., Raket, L. L., & Cummings, J. L. (2019). Open-label, multicenter, phase III extension study of idalopirdine as adjunctive to donepezil for the treatment of mild-moderate Alzheimer's disease. *Journal of Alzheimer's Disease*, 67, 303–313. <https://doi.org/10.3233/JAD-180595>

Garau, C., Miralles, A., & Garcia-Sevilla, J. A. (2013). Chronic treatment with selective I<sub>2</sub>-imidazoline receptor ligands decreases the content of pro-apoptotic markers in rat brain. *Journal of Psychopharmacology*, 27, 123–134. <https://doi.org/10.1177/0269881112450785>

Garcia-Sevilla, J., Escriba, P., Walzer, C., Bouras, C., & Guimon, J. (1998). Imidazoline receptor proteins in brains of patients with Alzheimer's disease. *Neuroscience Letters*, 247, 95–98. [https://doi.org/10.1016/S0304-3940\(98\)00265-1](https://doi.org/10.1016/S0304-3940(98)00265-1)

Gatt, J. M., Nemeroff, C. B., Dobson-Stone, C., Paul, R. H., Bryant, R. A., Schofield, P. R., Gordon, E., Kemp, A. H., & Williams, L. M. (2009). Interactions between BDNF Val66Met polymorphism and early life stress predict brain and arousal pathways to syndromal depression and anxiety. *Molecular Psychiatry*, 14, 681–695. <https://doi.org/10.1038/mp.2008.143>

Giacobini, E. (2000). Cholinesterase inhibitors stabilize Alzheimer disease. *Neurochemical*



Research, 25, 1185–1190. <https://doi.org/10.1023/A:1007679709322>

Griñan-Ferré, C., Palomera-Ávalos, V., Puigoriol-Illamola, D., Camins, A., Porquet, D., Plá, V., Aguado, F., & Pallàs, M. (2016). Behaviour and cognitive changes correlated with hippocampal neuroinflammation and neuronal markers in female SAMP8, a model of accelerated senescence. *Experimental Gerontology*, 80, 57–69. <https://doi.org/10.1016/j.exger.2016.03.014>

Griñan-Ferré, C., Izquierdo, V., Otero, E., Puigoriol-Illamola, D., Corpas, R., Sanfeliu, C., Ortuño-Sahagún, D., & Pallàs, M. (2018). Environmental enrichment improves cognitive deficits, AD hallmarks and epigenetic alterations presented in 5xFAD mouse model. *Frontiers in Cellular Neuroscience*, 12, 224. <https://doi.org/10.3389/fncel.2018.00224>

Griñan-Ferré, C., Vasilopoulou, F., Abás, S., Rodríguez-Arévalo, S., Bagán, A., Sureda, F. X., Pérez, B., Callado, L. F., García-Sevilla, J. A., García-Fuster, M. J., Escolano, C., & Pallàs, M. (2019). Behavioral and cognitive improvement induced by novel imidazoline I<sub>2</sub> receptor ligands in female SAMP8 mice. *Neurotherapeutics*, 16, 416–431. <https://doi.org/10.1007/s13311-018-00681-5>

Grossberg, G. T. (2003). Cholinesterase inhibitors for the treatment of Alzheimer's disease: Getting on and staying on. *Current Therapeutic Research, Clinical and Experimental*, 64, 216–235. [https://doi.org/10.1016/S0011-393X\(03\)00059-6](https://doi.org/10.1016/S0011-393X(03)00059-6)

Hernández-Hernández, E., García-Sevilla, J. A., & García-Fuster, M. J. (2020). Exploring the antidepressant-like potential of the selective I<sub>2</sub>-imidazoline receptor ligand LSL 60101 in adult male rats. *Pharmacol. Reports*, 73, 288–295. <https://doi.org/10.1007/s43440-020-00148-5>

Hwang, J., Hwang, H., Lee, H.-W., & Suk, K. (2010). Microglia signaling as a target of donepezil. *Neuropharmacology*, 58, 1122–1129. <https://doi.org/10.1016/j.neuropharm.2010.02.003>

Jiangbo, N., & Liyun, Z. (2018). Effect of donepezil hydrochloride & aerobic exercise training on learning and memory and its mechanism of action in an Alzheimer's disease rat model. *Pakistan Journal of Pharmaceutical Sciences*, 31, 2897–2901.

Ju, Y., & Tam, K. Y. (2020). 9R, the cholinesterase and amyloid beta aggregation dual inhibitor, as a multifunctional agent to improve cognitive deficit and neuropathology in the triple-transgenic Alzheimer's disease mouse model. *Neuropharmacology*, 181, 108354.

Kim, H. G., Moon, M., Choi, J. G., Park, G., Kim, A.-J., Hur, J., Lee, K. T., & Oh, M. S. (2014). Donepezil inhibits the amyloid-beta oligomer-induced microglial activation in vitro and in vivo. *Neurotoxicology*, 40, 23–32. <https://doi.org/10.1016/j.neuro.2013.10.004>

Kotagale, N., Dixit, M., Garmelwar, H., Bhondekar, S., Umekar, M., & Taksande, B. (2020). Agmatine reverses memory deficits induced by A $\beta$ 1–42 peptide in mice: A key role of imidazoline receptors. *Pharmacology, Biochemistry, and Behavior*, 196, 172976. <https://doi.org/10.1016/j.pbb.2020.172976>

Krishna, K. V., Saha, R. N., & Dubey, S. K. (2020). Biophysical, biochemical, and behavioral implications of ApoE3 conjugated donepezil nanomedicine in a A $\beta$ 1–42 induced Alzheimer's disease rat model. *ACS Chemical Neuroscience*, 11, 4139–4151. <https://doi.org/10.1021/acscchem-neuro.0c00430>

Landel, V., Baranger, K., Virard, I., Loriod, B., Khrestchatsky, M., Rivera, S., Benech, P., & Féron, F. (2014). Temporal gene profiling of the 5XFAD transgenic mouse model highlights the importance of microglial activation in Alzheimer's disease. *Molecular Neurodegeneration*, 9, 33. <https://doi.org/10.1186/1750-1326-9-33>

Lee, C. Y. D., Daggett, A., Gu, X., Jiang, L. L., Langfelder, P., Li, X., Wang, N., Zhao, Y., Park, C. S., Cooper, Y., Ferando, I., Mody, I., Coppola, G., Xu, H., & Yang, X. W. (2018). Elevated TREM2 gene dose reprograms microglia responsiveness and ameliorates pathological phenotypes in Alzheimer's disease models. *Neuron*, 97, 1032–1048e5.

Lilley, E., Stanford, S. C., Kendall, D. E., Alexander, S. P. H., Cirino, G., Docherty, J. R., George, C. H., Insel, P. A., Izzo, A. A., Ji, Y., Panettieri, R. A., Sobey, C. G., Stefanska, B., Stephens, G., Teixeira, M., & Ahluwalia, A. (2020). ARRIVE 2.0 and the British Journal of Pharmacology: Updated guidance for 2020. *British Journal of Pharmacology*, 177, 3611–3616. <https://doi.org/10.1111/bph.15178>

Mehta, M., Adem, A., & Sabbagh, M. (2012). New acetylcholinesterase inhibitors for Alzheimer's disease. *International Journal of Alzheimer's Disease*, 2012, 728983.

Menargues, A., Cedo, M., Artiga, O., Obach, R., & García-Sevilla, J. A. (1995). Effects of the I<sub>2</sub>-imidazoline receptor ligand LSL 60101 on various models of anorexia in rats. *Annals of the New York Academy of Sciences*, 763, 494–494. <https://doi.org/10.1111/j.1749-6632.1995.tb32439.x>  
Meraz Rios, M. A., Toral-Rios, D., Franco-Bocanegra, D., Villeda-Hernandez, J., & Campos-Peña, V. (2013). Inflammatory process in Alzheimer's disease. *Frontiers in Integrative Neuroscience*, 7, 59.

Mirzaei, N., Mota, B. C., Birch, A. M., Davis, N., Romero-Molina, C., Katsouri, L., Palmer, E. O. C., Golbano, A., Riggall, L. J., Nagy, I., Tyacke, R., Nutt, D. J., & Sastre, M. (2020). Imidazoline ligand BU224 reverses cognitive deficits, reduces microgliosis and enhances synaptic connectivity in a mouse model of Alzheimer's disease. *British Journal of Pharmacology*, 178, 654–671. <https://doi.org/10.1111/bph.15312>

Murray, M. E., Graff-Radford, N. R., Ross, O. A., Petersen, R. C., Duara, R., & Dickson, D. W. (2011). Neuropathologically defined subtypes of Alzheimer's disease with distinct clinical characteristics: A retrospective study. *Lancet Neurology*, 10, 785–796. [https://doi.org/10.1016/S1474-4422\(11\)70156-9](https://doi.org/10.1016/S1474-4422(11)70156-9)

Oakley, H., Cole, S. L., Logan, S., Maus, E., Shao, P., Craft, J., Guillozet-Bongaarts, A., Ohno, M.,

Disterhoft, J., van Eldik, L., Berry, R., & Vassar, R. (2006). Intraneuronal  $\beta$ -amyloid aggregates, neurodegeneration, and neuron loss in transgenic mice with five familial Alzheimer's disease mutations: Potential factors in amyloid plaque formation. *The Journal of Neuroscience*, 26, 10129–10140. <https://doi.org/10.1523/JNEUROSCI.1202-06.2006> Olmos, G., Alemany, R., Escriba, P. V., & García-Sevilla, J. A. (1994). The effects of chronic imidazoline drug treatment on glial fibrillary acidic protein concentrations in rat brain. *British Journal of Pharmacology*, 111, 997–1002. <https://doi.org/10.1111/j.1476-5381.1994.tb14842.x>

Ongnok, B., Khuanjing, T., Chunchai, T., Kerdphoo, S., Jaiwongkam, T., Chattipakorn, N., & Chattipakorn, S. C. (2021). Donepezil provides neuroprotective effects against brain injury and Alzheimer's pathology under conditions of cardiac ischemia/reperfusion injury. *Biochimica et Biophysica Acta - Molecular Basis of Disease*, 1867, 165975.

Percie du Sert, N., Hurst, V., Ahluwalia, A., Alam, S., Avey, M. T., Baker, M., Browne, W. J., Clark, A., Cuthill, I. C., Dirnagl, U., Emerson, M., Garner, P., Holgate, S. T., Howells, D. W., Karp, N. A., Lazic, S. E., Lidster, K., MacCallum, C. J., Macleod, M., ... Würbel, H. (2020). The ARRIVE guidelines 2.0: Updated guidelines for reporting animal research. *PLoS Biology*, 18(7), e3000410. <https://doi.org/10.1371/journal.pbio.3000410>

Regunathan, S., Feinstein, D. L., & Reis, D. J. (1993). Expression of non-adrenergic imidazoline sites in rat cerebral cortical astrocytes. *Journal of Neuroscience Research*, 34, 681–688. <https://doi.org/10.1002/jnr.490340611>

Regunathan, S., Feinstein, D. L., & Reis, D. J. (1999). Anti-proliferative and anti-inflammatory actions of imidazoline agents: Are imidazoline receptors involved? *Annals of the New York Academy of Sciences*, 881, 410–419. <https://doi.org/10.1111/j.1749-6632.1999.tb09389.x>

Riedel, G., Kang, S. H., Choi, D. Y., & Platt, B. (2009). Scopolamine-induced deficits in social memory in mice: Reversal by donepezil. *Behavioural Brain Research*, 204, 217–225.

Rosini, M., Simoni, E., Minarini, A., & Melchiorre, C. (2014). Multi-target design strategies in the context of Alzheimer's disease: Acetylcholinesterase inhibition and NMDA receptor antagonism as the driving forces. *Neurochemical Research*, 39, 1914–1923. <https://doi.org/10.1007/s11064-014-1250-1>

Ruiz, J., Martín, I., Callado, L. F., Meana, J. J., Barturen, F., & García-Sevilla, J. A. (1993). Non-adrenoceptor [ $^3$ H]idazoxan binding sites ( $I_2$ -imidazoline sites) are increased in postmortem brain from patients with Alzheimer's disease. *Neuroscience Letters*, 160, 109–112.

Sánchez-Blázquez, P., Boronat, M. A., Olmos, G., García-Sevilla, J. A., & Garzon, J. (2000). Activation of  $I_2$ -imidazoline receptors enhances supraspinal morphine analgesia in mice: A model to detect agonist and antagonist activities at these receptors. *British Journal of Pharmacology*, 130, 146–152. <https://doi.org/10.1038/sj.bjp.0703294>

- Saul, A., Sprenger, F., Bayer, T. A., & Wirths, O. (2013). Accelerated tau pathology with synaptic and neuronal loss in a novel triple transgenic mouse model of Alzheimer's disease. *Neurobiology of Aging*, 34, 2564–2573. <https://doi.org/10.1016/j.neurobiolaging.2013.05.003>
- Schmitt, B., Bernhardt, T., Moeller, H.-J., Heuser, I., & Frölich, L. (2004). Combination therapy in Alzheimer's disease: A review of current evidence. *CNS Drugs*, 18, 827–844.
- Selkoe, D. J. (2008). Soluble oligomers of the amyloid  $\beta$ -protein impair synaptic plasticity and behavior. *Behavioural Brain Research*, 192, 106–113. <https://doi.org/10.1016/j.bbr.2008.02.016>
- Serrano-Pozo, A., Frosch, M. P., Masliah, E., & Hyman, B. T. (2011). Neuropathological alterations in Alzheimer disease. *Cold Spring Harbor Perspectives in Medicine*, 1, a006189.
- Siemian, J. N., LaMacchia, Z. M., Spreuer, V., Tian, J., Ignatowski, T. A., Paez, P. M., Zhang, Y., & Li, J. X. (2018). The imidazoline I<sub>2</sub> receptor agonist 2-BFI attenuates hypersensitivity and spinal neuroinflammation in a rat model of neuropathic pain. *Biochemical Pharmacology*, 153, 260–268. <https://doi.org/10.1016/j.bcp.2018.01.032>
- Sinforiani, E., Banchieri, L. M., Zucchella, C., Bernasconi, L., & Nappi, G. (2003). Cholinesterase inhibitors in Alzheimer's disease: Efficacy in a non-selected population. *Functional Neurology*, 18, 233–237.
- Takada-Takatori, Y., Nakagawa, S., Kimata, R., Nao, Y., Mizukawa, Y., Urushidani, T., Izumi, Y., Akaike, A., Tsuchida, K., & Kume, T. (2019). Donepezil modulates amyloid precursor protein endocytosis and reduction by up-regulation of SNX33 expression in primary cortical neurons. *Scientific Reports*, 9, 11922. <https://doi.org/10.1038/s41598-019-47462-4>
- Tonello, R., Villarinho, J. G., da Silva Sant'Anna, G., Tamiozzo, L., Machado, P., Trevisan, G., & Rubin, M. A. (2012). The potential antidepressant-like effect of imidazoline I<sub>2</sub> ligand 2-BFI in mice. *Progress in Neuro-Psychopharmacology and Biological Psychiatry*, 37, 15–21. <https://doi.org/10.1016/j.pnpbp.2011.11.005>
- Vasilopoulou, F., Bagan, A., Rodriguez-Arevalo, S., Escolano, C., Griñan-Ferré, C., & Pallàs, M. (2020). Amelioration of BPSD-like phenotype and cognitive decline in SAMP8 mice model accompanied by molecular changes after treatment with I<sub>2</sub>-imidazoline receptor ligand MCR5. *Pharmaceutics*, 12, 475. <https://doi.org/10.3390/pharmaceutics12050475>
- Vasilopoulou, F., Griñan-Ferré, C., Rodríguez-Arévalo, S., Bagán, A., Abás, S., Escolano, C., & Pallàs, M. (2020). I<sub>2</sub> imidazoline receptor modulation protects aged SAMP8 mice against cognitive decline by suppressing the calcineurin pathway. *GeroScience*, 27–31.
- Walf, A. A., & Frye, C. A. (2007). The use of the elevated plus maze as an assay of anxiety-related behavior in rodents. *Nature Protocols*, 2, 322–328. <https://doi.org/10.1038/nprot.2007.44>

- Walsh, D. M., & Selkoe, D. J. (2004). Oligomers on the brain: The emerging role of soluble protein aggregates in neurodegeneration. *Protein and Peptide Letters*, 11, 213–228.
- Yang, H., Mu, W., Wei, D., Zhang, Y., Duan, Y., Gao, J. X., Gong, X.-Q., Wang, H.-J., Wu, X.-l., Tao, H., & Chang, J. (2020). A novel targeted and high-efficiency nanosystem for combinational therapy for Alzheimer's disease. *Advancement of Science*, 7, 1–13.
- Yoshiyama, Y., Kojima, A., Ishikawa, C., & Arai, K. (2010). Anti-inflammatory action of donepezil ameliorates tau pathology, synaptic loss, and neurodegeneration in a tauopathy mouse model. *Journal of Alzheimer's Disease*, 22, 295–306. <https://doi.org/10.3233/JAD-2010-100681>
- Zhang, F., Gannon, M., Chen, Y., Yan, S., Zhang, S., Feng, W., Tao, J., Sha, B., Liu, Z., Saito, T., Saido, T., Keene, C. D., Jiao, K., Roberson, E. D., Xu, H., & Wang, Q. (2020).  $\beta$ -Amyloid redirects norepinephrine signaling to activate the pathogenic GSK3 $\beta$ /tau cascade. *Science Translational Medicine*, 12, eaay6931. <https://doi.org/10.1126/scitranslmed.aay6931>
- Zhang, F., & Jiang, L. (2015). Neuroinflammation in Alzheimer's disease. *Neuropsychiatric Disease and Treatment*, 11, 243–256. <https://doi.org/10.2147/NDT.S75546>
- Zhao, Y., Wu, X., Li, X., Jiang, L.-L., Gui, X., Liu, Y., Sun, Y., Zhu, B., Piña-Crespo, J. C., Zhang, M., Zhang, N., Chen, X., Bu, G., An, Z., Huang, T. Y., & Xu, H. (2018). TREM2 is a receptor for  $\beta$ -amyloid that mediates microglial function. *Neuron*, 97, 1023–1031.e7. <https://doi.org/10.1016/j.neuron.2018.01.031>

## SUPPLEMENTARY MATERIAL

**Figure S1:** Weekly body weight control during treatment period. Bars represent mean  $\pm$  SEM. Statistics: One-Way ANOVA with Tukey's Post hoc analysis between weekly controls for each group.

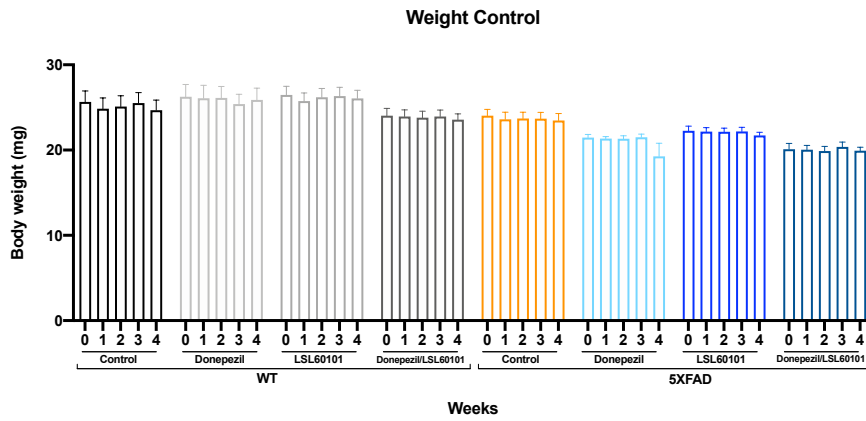


**Figure S2:** Effects of low-dose chronic treatment with I2 ligand LSL60101, donepezil and co-administration on cognitive status in 5XFAD and WT mice. Results of MWM: (a) Latency to 1st platform quadrant entry (sec) (b) Entries in platform Quadrant (c) Distance to target (cm). Bars represent mean  $\pm$  SEM. Two-way ANOVA with Tukey post hoc analysis, \* $P < 0.05$ ;  $n = 9-12$  per group; 5XFAD  $n = 10-12$  per group.

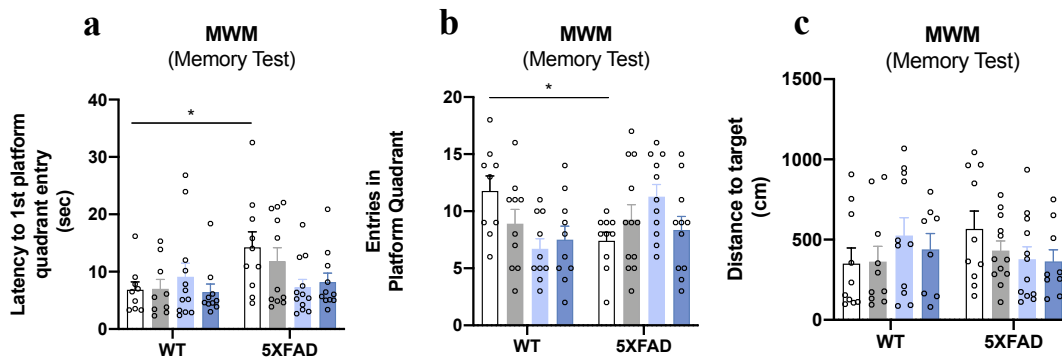


**Figure S3:** Effects of low dose chronic treatments I2 ligand LSL60101, donepezil and co-administration on microgliosis and astrogliosis in 5XFAD mice. Representative images and quantification of Iba-1 (a,c) and GFAP (b,d) immunostaining in the cortex. Data are presented as the mean  $\pm$  SEM of relative fluorescent intensity of the positive cells averaged from 2-3 different sections from the same brain area/animal and each dot represents one mouse (n=5 per group). Bars represent mean  $\pm$  SEM. Unpaired Student's t-test or one-way ANOVA with Tukey post hoc analysis, \*P<0.05.

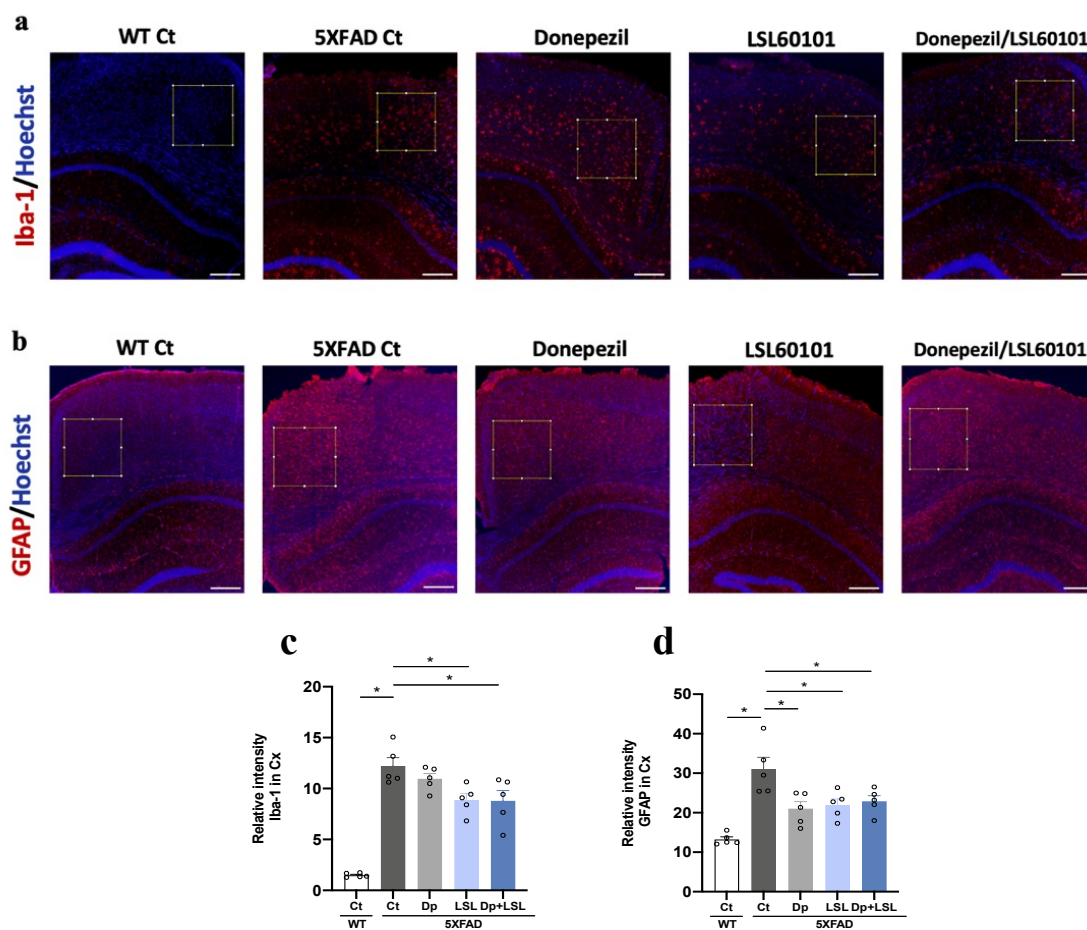


**Table S1:** Antibodies used in Western Blot (WB) and Immunohistochemistry (IHC)

Antibody (WB)	Host	Source/Catalog/RRID	WB dilution
beta Amyloid(H31L21)	Rabbit	Invitrogen Thermo Fisher, Waltham, MA, USA /700254/AB_2532306	1:500
ADAM10	Rabbit	Abcam (Cambridge, UK)/ab39177/ AB_2223064	1:1000
APP C-Terminal	Mouse	Covance (Princeton, NJ, USA)/SIG-39152/ AB_10717336	1:500
BACE (D10E5)	Rabbit	Cell Signaling (Danvers, MA, USA)/5606/AB_190390	1:1000
p-APP (T668)	Rabbit	Cell Signaling /3823S/AB_205641	1:1000
PSD95	Rabbit	Abcam/ab18258/AB_444362	1:1000
p-Tau (Ser396)	Rabbit	Invitrogen/44752G/AB_253374	1:1000
p-Tau (Ser404)	Rabbit	Invitrogen/44758G/AB_2533746	1:1000
sAPP $\alpha$	Rabbit	Covance/SIG39139/ AB_10721469	1:500
sAPP $\beta$	Rabbit	Covance/SIG-39138-050/ AB_66287	1:500
SYN	Mouse	Millipore (Burlington, MA, USA)/MAB5258/ AB_2313839	1:1000
Tau Total	Mouse	Invitrogen/AHB0042/AB_2533746	1:1000
GAPDH	Mouse	Millipore/MAB374/ AB_2107445	1:2500
$\beta$ -Actin	Mouse	Invitrogen/MA5-15739/ AB_10979409	1:2500
Goat-anti-mouse HRP conjugated		Biorad Lab (Hercules, CA, USA)/170-5047/AB_11125753	1:6000
Goat-anti-rabbit HRP conjugated		Biorad Lab/170-6515/AB_11125142	1:6000
Antibody (IHC)	Host	Source/Catalog/RRID	IHC dilution
GFAP	Rabbit	Dako(Santa Clara, CA, USA ) /Z0334/ AB_10013382	1:400
IBA-1	Rabbit	Abcam/ab178847/ AB_2832244	1:400
Donkey-anti-rabbit Alexa Fluor 647		Invitrogen/ A31573/ AB_253618	1:500

**Table S2:** Primers and probes used in qPCR studies.

Target	Product size (bp)	Forward primer (5'-3')	Reverse primer (5'-3')
<i>Ide</i>	287	CCAAAAGGAAGCGTTCGCC	GGGATCGCTGATGAGAAGCA
<i>Nep</i>	196	TTGGGAGACCTGGCGGAAAC	CATTCCTTGGACCCTCACCCC
<i>Trem2</i>	269	CCTGAAGAAGCGGAATGGG	CTTGATTCTGGAGGTGCT
<i>Il-1<math>\beta</math></i>	179	ACAGAATATCAACCAACAAGTGATATTCTC	GATTCTTTCCTTTGAGGCCCA
<i>Il-18</i>	151	GTTTACAAGCATCCAGGCACAG	GAAGGTTTGAGGCGGCTTTC
<i>Il-6</i>	189	ATCCAGTTGCCTTCTTGGGACTGA	TAAGCCTCCGACTTGTGAAGTGGT
<i>Ccl12</i>	110	ACACTGGTTTCTGACTCCTCT	ACCTGAGGACTGATGGTGGT
<i>Actin</i>	190	CAACGAGCGGTTCCGAT	GCCACAGTTCCATACCCA



### **3.5 Publication 5**

**Microarray analysis revealed inflammatory transcriptomic changes after LSL60101 treatment in 5XFAD mice model.**

Adapted from: **Vasilopoulou F**, Escolano C, Pallàs M, Griñán-Ferré C. *Genes*. 2021; 12(9):1315

doi: <https://doi.org/10.3390/genes12091315>

## SUMMARY

I<sub>2</sub> imidazoline receptors (I<sub>2</sub>-IR) are receiving growing attention due to the neuroprotective effects of selective I<sub>2</sub>-IR ligands, attributable to their anti-inflammatory actions, among others. Remarkably, I<sub>2</sub>-IR have been found dysregulated in patients with Alzheimer's Disease (AD), in which the importance of neuroinflammation in the establishment and maintenance of cognitive decline is well-documented. To go deeper into the implication of I<sub>2</sub>-IR in neuroinflammatory pathways altered in AD, we determined the expression profile of genes associated with inflammation in the 5XFAD model treated with LSL60101, a well-established I<sub>2</sub>-IR ligand. We performed a Real-time quantitative PCR array containing 84 inflammation-related genes in 5XFAD and wild-type (WT) animals treated with LSL60101 (1mg/kg/day) for four weeks. We analyzed clustering, gene ontology (GO) and gene set enrichment and we validated the results obtained from gene profiling analysis with qPCR. We identified three gene clusters, two of which had alterations in processes such as inflammatory response, chemotaxis, chemokine-mediated signaling pathway, among others. Changes induced by LSL60101 in 5XFAD were validated for *Cxcr2*, *Tlr5*, *Sele* and a clear tendency to decrease was observed for *CD40lg*, *Ccl7*, *Ccr4*. On the contrary, a tendency to increase in 5XFAD LSL60101 were found for *Ccl12*, *Ccl8*. Likewise, we found a similar pattern induced by LSL60101 in WT, but the results were not statistically significant. Interestingly we identified several genes presented in the clusters associated with the NF- $\kappa$ B pathway to be reduced after treatment. Taken together, these results suggest that treatment with I<sub>2</sub>-IR LSL60101 in the 5XFAD model reverses the inflammatory process during the development of AD by acting on gene transcription.

## **Microarray analysis revealed inflammatory transcriptomic changes after LSL60101 treatment in 5XFAD mouse model.**

Foteini Vasilopoulou,<sup>1</sup> Carmen Escolano,<sup>2</sup> Mercè Pallàs,<sup>1</sup> Christian Griñán-Ferré,<sup>1</sup>

<sup>1</sup>*Pharmacology Section. Department of Pharmacology, Toxicology and Medicinal Chemistry, Faculty of Pharmacy and Food Sciences, and Institut de Neurociències, University of Barcelona, Av. Joan XXIII, 27-31, 08028 Barcelona, Spain.*

<sup>2</sup>*Laboratory of Medicinal Chemistry (Associated Unit to CSIC), Department of Pharmacology, Toxicology and Medicinal Chemistry, Faculty of Pharmacy and Food Sciences, and Institute of Biomedicine (IBUB), University of Barcelona, Av. Joan XXIII, 27-31, 08028 Barcelona, Spain.*

**Keywords:** I<sub>2</sub> imidazoline receptors, neuroinflammation, LSL60101, Alzheimer's disease, transcriptomics, 5XFAD

### **ABSTRACT**

I<sub>2</sub>-IR have been found dysregulated in patients with neurodegenerative diseases, such as Alzheimer's Disease (AD), in which the importance of neuroinflammation in the establishment and maintenance of cognitive decline is well-documented. To go deeper into the implication of I<sub>2</sub>-IR in neuroinflammatory pathways altered in AD, we determined the expression profile of genes associated with inflammation in the 5XFAD model treated with LSL60101, a well-established I<sub>2</sub>-IR ligand. Thus, we performed a qPCR array containing 84 inflammation-related genes. Hierarchical clustering analysis revealed three gene clusters, suggesting that treatment with LSL60101 affects the gene expression associated with inflammation in the 5XFAD model. Furthermore, we evaluated the functions of the three clusters, and thereby we performed a pathway enrichment analysis using the GO database. As we expected, clusters 2 and 3 have alterations in the inflammatory response, chemotaxis, chemokine-mediated signaling pathway, among others. To validate previous results from the gene profiling analysis, the expression levels of a representative subset of mRNAs were selected according to the intensity of the observed changes and their biological relevance. Interestingly, changes induced by LSL60101 in 5XFAD were validated for several genes. These results suggest that treatment with LSL60101 in the 5XFAD model reverses the inflammatory process during the development of AD.

### **3.5.1 INTRODUCTION**

Imidazoline receptors (IR) were described in the late 1880s as binding sites for adrenergic ligands such as clonidine, idazoxan and related compounds, but not for adrenaline; thus, they constitute non-adrenergic receptors [1–3]. IR has been divided into two classes I<sub>1</sub>-IR

and I<sub>2</sub>-IR, primarily based on their sensitivity to clonidine and idazoxan, respectively, whereas a third atypical imidazoline subtype has also been identified [4,5]. I<sub>1</sub>-IR activation has been associated with cardiovascular and metabolic effects [6–8], whereas I<sub>2</sub>-IR are widely distributed in the brain and primarily in glial cells [4], and the binding of specific ligands to I<sub>2</sub>-IR has been shown to induce several pharmacological effects, such as analgesia, anti-inflammatory effects, or neuroprotection [8,9].

Regarding I<sub>2</sub>-IR primary localization in astrocytes and glial cells, it has been demonstrated that I<sub>2</sub>-IR ligands modulate glial activity in mice model brain or spinal cord injury [10,11]. In these studies, using an experimental autoimmune encephalomyelitis model, 2-BFI administration reduced the expression of inflammatory cytokines, including interferon- $\gamma$  (IFN- $\gamma$ ) and tumor necrosis factor- $\alpha$  (TNF- $\alpha$ ), and microglial activation. Similarly, in a traumatic injury model, 2-BFI reduced interleukin 1 $\beta$  (IL-1 $\beta$ ) secretion and microglia activation [12]. In vitro studies corroborate that I<sub>2</sub>-IR ligands exert their action on the glial cells by suppressing astrocytic activation induced by lipopolysaccharide (LPS) and decreasing TNF- $\alpha$  levels [13]. Consistent with these changes, the recently described I<sub>2</sub>-IR ligands MCR5 and B06 decrease the expression of pro-inflammatory markers, such as *Tnf- $\alpha$* , *Il-1 $\beta$* , Interleukin 6 (*Il-6*), and promote synaptic plasticity in a mouse model of ageing and neurodegeneration [14–16]. Interestingly, I<sub>2</sub>-IR have been found dysregulated in patients with neurodegenerative diseases, such as Alzheimer's Disease (AD)[17,18]. AD is a neurodegenerative disease with special histochemical hallmarks, namely amyloid plaques and neurofibrillary tangles [19]. Besides the precise etiology of the pathology, it is well known that neuroinflammation, including the inflammatory levels of cytokines and their corresponding pathways, is the landscape that must be faced in the challenge to find new therapeutic tools to treat AD [20].

The 5XFAD mouse model is a well-characterized double transgenic APP/PSEN1 model, co-expressing five familial AD mutations. This animal model incorporates AD pathological characteristics, including early plaque formation and gliosis, robust cognitive and behavioural deficits such as memory impairment [21]. The well-established I<sub>2</sub>-IR ligand LSL60101, first described in 1995 and recently evaluated in depth by our group, presents high selectivity for the I<sub>2</sub>-IR receptors and optimal pharmacokinetic and safety profile [22,23]; thus it has proven to be a useful tool in the I<sub>2</sub>-IR research throughout the years [24–26]. Remarkably, LSL60101 similarly to BU224, demonstrated a neuroprotective effect in the familial AD mouse model 5XFAD [27,28]. LSL60101 reduced inflammation inherent to AD, and microglial activation in this mouse model, in agreement with the reports mentioned above, further indicating the modulation of inflammatory pathways by I<sub>2</sub>-IR ligands in the brain and its contribution to glial function and activation.

This work aims to unravel the effect of LSL60101, and consequently the implication of I<sub>2</sub>-IR receptors in inflammatory pathways related to AD, and by extension, to other neurodegenerative diseases which pathology includes neuroinflammation. To this end, we analyzed a set of gene expression panel related to inflammation, including several cytokines and their receptors, regulators, and mediators of signaling pathways and factors implicated in the regulation of immune response after LSL60101 treatment in wild type and 5XFAD mice.

### 3.5.2 METHODS

#### Animals and Treatments

The 5XFAD is a double transgenic APP/PSEN1 that co-expresses AD mutations and presents a robust inflammation background [21]. 7-month-old female 5XFAD mice (n = 23) and wild type (WT) (n = 23) mice were used to perform molecular analyses. The animals were randomly allocated to experimental groups and divided into four groups: WT Control and 5XFAD Control, administrated with vehicle (2-hydroxypropyl)- $\beta$ -cyclodextrin 1.8 %) and WT and 5XFAD treated with I<sub>2</sub>-IR ligand, administrated with LSL60101 diluted in vehicle (1mg/kg/day). Treatment was administered through drinking water for 4 weeks. The animals had free access to food and water and were kept under standard temperature conditions (22  $\pm$  2 °C) and 12 h: 12 h light-dark cycles (300 lux/0 lux). The water consumption was controlled each week and the I<sub>2</sub>-IR ligand concentration was adjusted accordingly to reach the precise dose.

All studies and procedures for the mouse behavior tests, brain dissection and extractions followed the ARRIVE and standard ethical guidelines (European Communities Council Directive 2010/63/EU) and Guidelines for the Care and Use of Mammals in Neuroscience and Behavioral Research (National Research Council 2003) and were approved by Bioethical Committees from the University of Barcelona (670/14/8102) and the Government of Catalonia 10291).

#### Brain processing and RNA extraction

Mice were euthanized by cervical dislocation after the treatment period. The brains were immediately removed from the skulls, and the hippocampi were dissected, frozen and maintained at 80°C. Total RNA isolation from hippocampal samples was performed using the TRIzol® reagent according to the manufacturer's instructions (Bioline Reagent, London, UK). The yield, purity and quality of RNA were determined spectrophotometrically with a NanoDrop™ND-1000 apparatus (Thermo Fisher, Waltham, MA, USA) and an Agilent 2100B Bioanalyzer (Agilent Technologies, Santa Clara, CA, USA). RNA samples

with 260/280 ratios and RINs higher than 1.9 and 7.5, respectively, were selected. Reverse Transcription-Polymerase Chain Reaction (RT-PCR) was performed. Briefly, 1  $\mu\text{g}$  and 2  $\mu\text{g}$  of messenger RNA (mRNA) was reverse transcribed using a high-capacity cDNA reverse transcription kit (Applied Biosystems, Foster City, CA, USA) for PCR Array performance and q-PCR validation, respectively.

### **Real-time quantitative PCR Array**

Real-time quantitative PCR array containing 84 inflammation-related genes (qPCR Sign Arrays 96 system, Any genes, Paris, France) was used for screening according to the instructions of the manufacturer. Briefly, 2  $\mu\text{L}$  of diluted cDNA pooled samples ( $n=3-4$ ) (2  $\mu\text{g}$  cDNA diluted at the 1/12 from Reverse Transcription (20  $\mu\text{L}$ ) performed with 1  $\mu\text{g}$  of RNA) was mixed with 10  $\mu\text{L}$  of 2X Perfect Master Mix SYBR Green and 8  $\mu\text{L}$  Ultra-pure H<sub>2</sub>O and added to each well; consequently, the total reaction volume was 20  $\mu\text{L}$  per well. After 20  $\mu\text{L}$  of the reaction mix was in each well of the 96-well plate, the plate was centrifuged and then the qPCR run was performed using a Step One Plus Detection System (Applied-Biosystems), following the manufacturer's recommendations and protocols. PCR reaction conditions were 95°C, 10 min; 95°C, 5 s and 60°C, 30 s,  $\times 40$  cycles. After completion of the reaction, the melting curve was analyzed, 95°C, 10 s, 65°C-95°C, 30 s.

### **Hierarchical clustering**

We performed a hierarchical clustering with the genes analyzed in the qPCR Sign Arrays 96 system to evaluate the expression profile between the expression profile the study groups. These genes were clustered into three groups based on the expression profile using the R package pheatmap. The expression data were clustered by Euclidean distances between genes and applying the complete method for hierarchical clustering. Furthermore, complete microarray gene expression data are presented in Supplementary Table S2.

### **Protein-protein interaction network and functional annotation**

To determine the interactions between the groups, we perform protein-protein interactions networks using the database STRING [29]. A PPI enrichment p-value  $<0.001$  was considered statistically significant, indicating that the proteins are at least partially biologically connected. To determine the functional annotation of the three groups, we determined the Gene Ontology (GO) and performed pathway analysis with the Kyoto Encyclopedia of Genes and Genomes (KEGG), using the Database for Annotation, Visualization and Integrated Discovery (DAVID) [30]. GO terms and KEGG pathways with an adjusted p-value  $<0.05$  were considered statistically significant. We use the KEGG mapping tool to display the down-regulated (green) and up-regulated genes (red) in KEGG pathway

maps [31]. To evaluate the transcriptional regulatory interactions between the three groups of genes and mouse transcriptional factors (TFs), we used the TRRUST database [32]. TRRUST identifies potential TFs involved in the regulation of genes of interest. TFs with an adjusted p-value < 0.05 were considered statistically significant.

### **Gene expression validation with Real-time quantitative PCR**

To confirm the PCR array results, which identified specific genes as responding to I<sub>2</sub>-IR treatment, quantitative SYBR® Green real-time PCR was performed using a Step One Plus Detection System (Applied-Biosystems) with SYBR® Green PCR Master Mix (Applied-Biosystems). Each reaction mixture contained 6.75 µL of complementary DNA (cDNA) (with a concentration of 2 µg), 0.75 µL of each primer (with a concentration of 100 nM), and 6.75 µL of SYBR® Green PCR Master Mix (2x). The data were analyzed utilizing the comparative cycle threshold (Ct) ( $\Delta\Delta\text{Ct}$ ) method, in which the levels of a housekeeping gene are used to normalize differences in sample loading and preparation. Normalization of expression levels was performed with  $\beta$ -actin. The primer sequences used are presented in Supplementary Table S1. Each sample was analyzed in duplicate, and the results represent the ratio percentage of the transcript levels among different groups compared to the Control group.

### **Statistical Analysis**

Data analysis was conducted using GraphPad Prism ver. 8 statistical software. Data are expressed as the mean  $\pm$  Standard error of the mean (SEM) of 5-6 samples per group. All data were tested for normal distribution and equal variance. Means were compared with Two-way Analysis of variance (ANOVA), followed by the Tukey post hoc test. Comparison between groups was also performed by two-tailed Student's t-test for independent samples when it was necessary. Statistical significance was considered when p values were < 0.05. The statistical outliers were determined with Grubbs' test and when necessary were removed from the analysis.

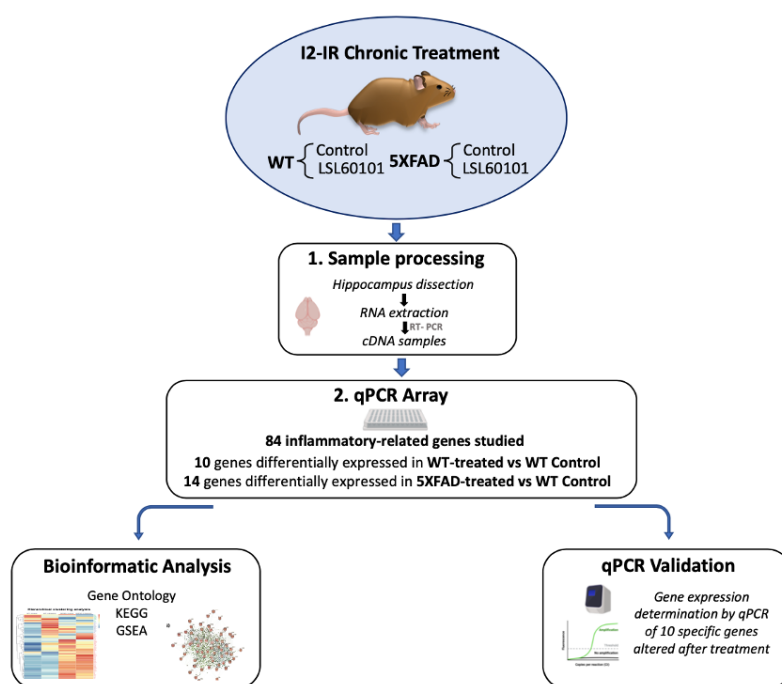


**Figure 1:** Experimental design of sample processing, bioinformatic analysis and qPCR validation.

### 3.5.3 RESULTS

#### LSL60101 treatment regulates genes associated with the inflammatory response

To determine the expression profile of genes associated with inflammation in the 5XFAD model treated with LSL60101, we performed a Real-time quantitative PCR array containing 84 inflammation-related genes. Hierarchical clustering analysis revealed three gene clusters (Figure 2A). Interestingly, cluster 2 was characterized by genes with reduced expression after LSL60101 treatment (Figure 2A). Cluster 3 has increased expression of genes after treatment in the 5XFAD mice (Figure 2A). These results suggest that treatment with LSL60101 reverses some of the inflammatory genes related to cognitive decline in the 5XFAD model.

To evaluate the functions of the three clusters, we performed a pathway enrichment analysis using the GO database. As we expected, clusters 2 and 3 have alterations in processes such as inflammatory response, chemotaxis, chemokine-mediated signaling pathway, among others (Figure 2B), indicating that these mechanisms are involved in the effects observed after treatment with LSL60101 in 5XFAD mice. Additionally, KEGG analysis demonstrated alteration in the Chemokine signaling pathway and Cytokine-cytokine receptor interaction (Figures 3A, B). Remarkably, in the pathway of Figure 3B, among the deregulated genes detected in response to treatment with LSL60101, we can observe a reduction in TNF- $\alpha$  and IL-6, two cytokines with high expression in the development of AD [33]. These results



suggest that treatment with LSL60101 in the 5XFAD model reverses the inflammatory process during the development of AD.

#### **NF-kappa B pathway regulates the inflammatory response in LSL60101 treatment**

NF-kappa B is a transcription factor that regulates multiple aspects associated with inflammatory responses [34]. Using the TRRUST database, a manually curated database of human and mouse transcriptional regulatory networks [35], we found that the genes present in clusters 2 and 3 can be regulated by RELA and NFKB1 (Figure 4A), two subunits of the transcription factor NF- $\kappa$ B [35], suggesting that NF- $\kappa$ B regulates the neuroinflammation process in the 5XFAD model after treatment. Interestingly, several members of the NF- $\kappa$ B signaling pathway, such as IL-1 $\beta$ , cyclooxygenase 2 (COX2), TNF- $\alpha$ , and MIP-2, are reduced in the treatment group (Figure 4B). Altogether, we suggest that treatment with LSL60101 alters the expression of genes associated with neuroinflammation processes in the 5XFAD model, which could be dependent on the NF-kappa B pathway, reinforcing the role of this pathway as a therapeutic target for AD [35].

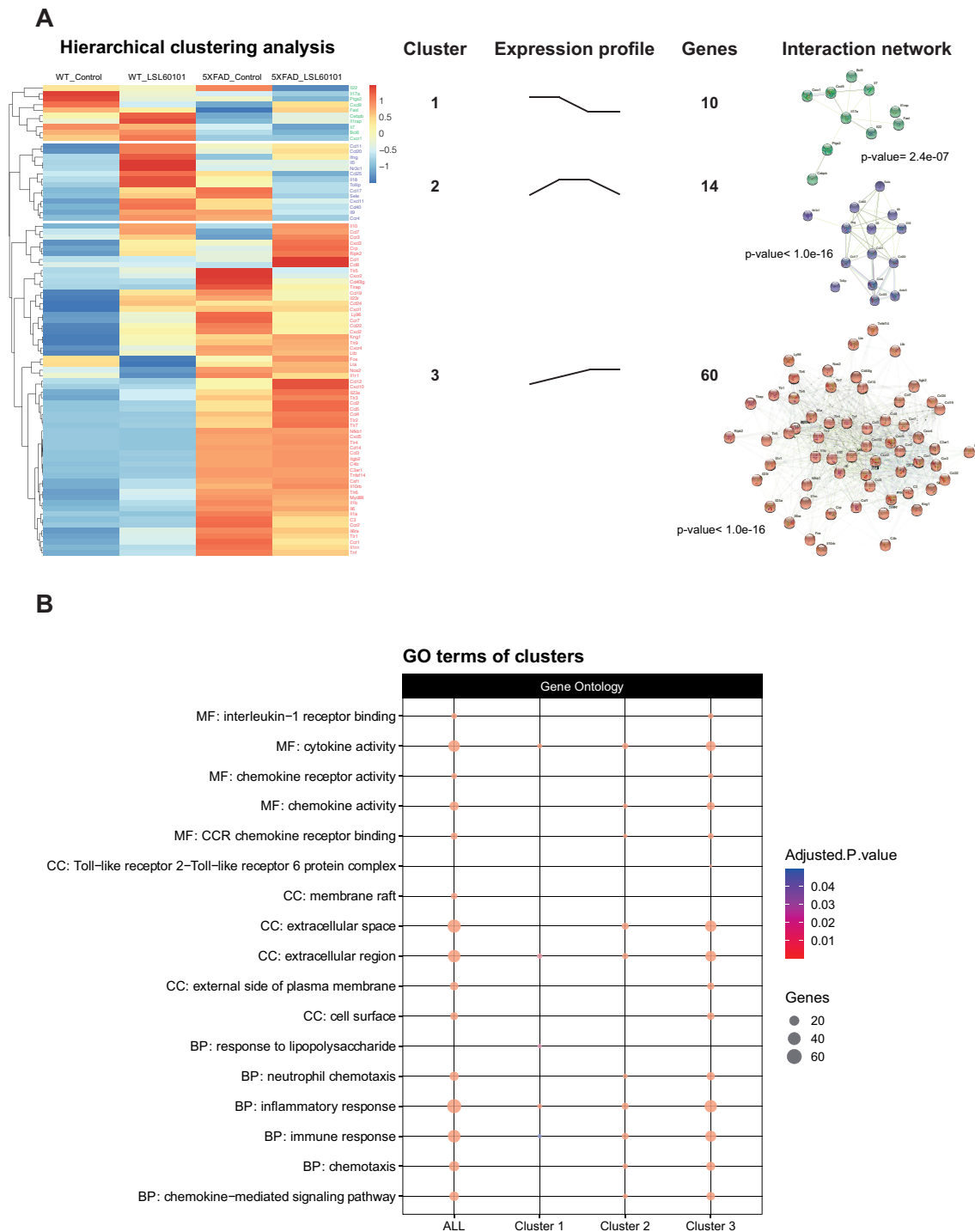
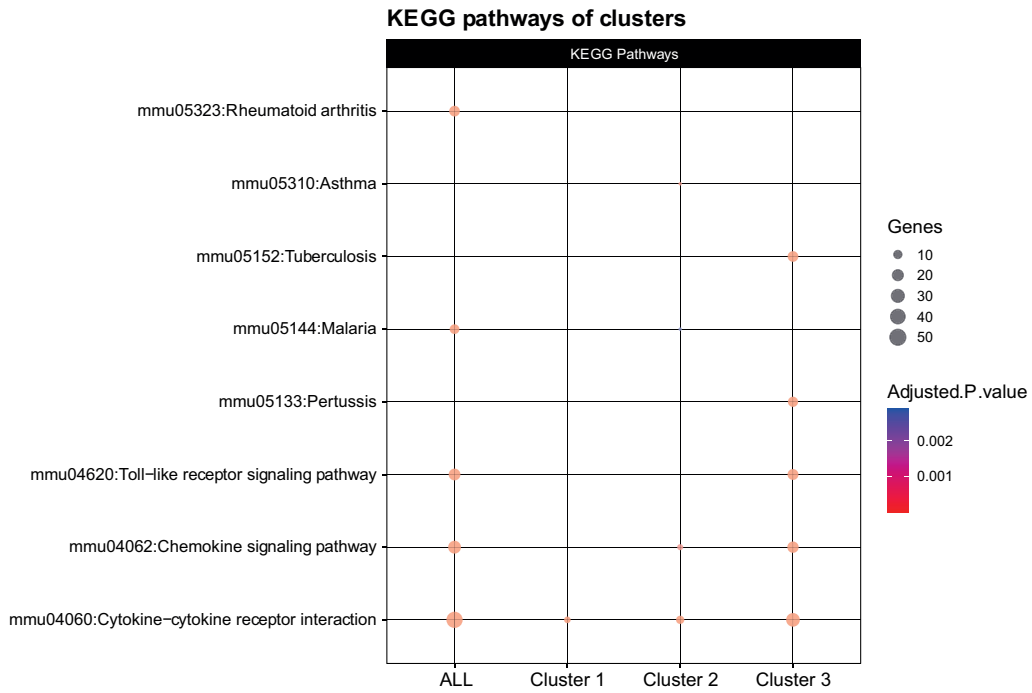


**Figure 2: Hierarchical clustering and Gene Ontology of inflammatory genes in WT and 5XFAD mice treated with LSL60101.** (A) The genes present in the qPCR Array were subjected to hierarchical clustering analysis. The heatmap shows three clusters with a specific expression profile between the experimental conditions represented in "expression profile". The predicted protein-protein interactions analysis is shown, as well as the PPI enrichment p-value of each cluster. (B) The dotplot shows the top GO terms of the clusters. An adjusted  $p$ -value<0.05 was considered statistically significant.

A



B

### Cytokine-Cytokine receptor interaction in the 5XFAD model with LSL60101

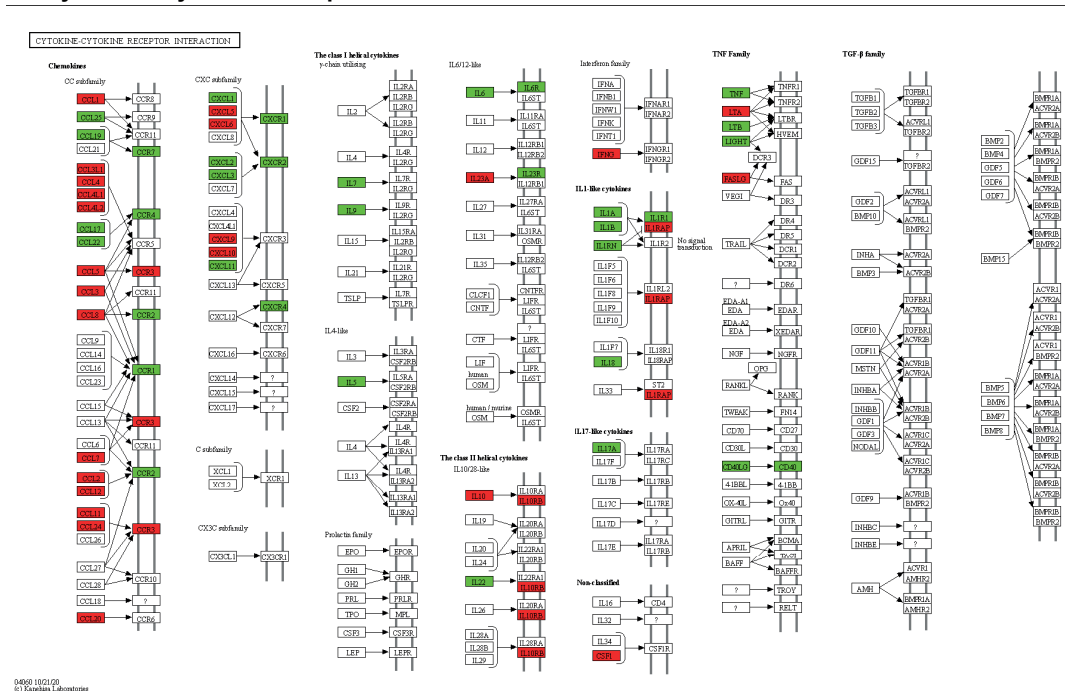


**Figure 3: KEGG pathway analysis and Cytokine-cytokine receptor interaction pathway.** (A) The dotplot shows the top KEGG pathways of the clusters. The Cytokine-cytokine receptor interaction is representative of the three clusters. An adjusted p-value<0.05 was considered statistically significant. (B) The KEGG pathway map Cytokine-cytokine receptor interaction (mmu04060) is shown. The down-regulated (green) and up-regulated genes (red) in the 5XFAD control condition versus the 5XFAD LSL60101 condition are shown.

### Validation of a representative subset of genes involved in neuroinflammation and AD

To validate previous results from the gene profiling analysis, the expression levels of a representative subset of mRNAs were selected according to the intensity of the observed changes and their biological relevance and were measured by single real-time PCR in the hippocampus samples from each group. We evaluated the expression of C-X-C Motif Chemokine Receptor 2 (*Cxcr2*), Toll-like receptor 5 (*Tlr5*), CD40 Ligand (*CD40lg*), Chemokine (C-C motif) ligand 7 (*Ccl7*), C-C chemokine receptor type 4 (*Ccr4*), Interferon-gamma (*Ifn- $\gamma$* ), E-Selectin (*Sele*), Chemokine (C-C motif) ligand 12 (*Ccl12*), Chemokine (C-C motif) ligand 8 (*Ccl8*) and C-X-C motif chemokine ligand 10 (*Cxcl10*) (Figures 5A-J). Interestingly, changes induced by LSL60101 in 5XFAD were validated for *Cxcr2*, *Tlr5*, *Sele* (Figures 5A, 5B, 5G), and a clear tendency to decrease in 5XFAD LSL60101 treated group for *CD40lg*, *Ccl7*, *Ccr4* was observed (Figures 5C-E). On the contrary, a tendency to increase in 5XFAD LSL60101-treated group was found for *Ccl12*, *Ccl8*, *Cxcl10* (Figures 5F, 5H-J). Likewise, changes induced by LSL60101 in WT were not statistically significant; however, a tendency to decrease for *CD40lg*, *Ccl8* and *Cxcl10* (Figures 5C, 5I, 5J) and a tendency to increase for *Ccr4*, *Ccl7* were observed (Figures 5D-E). Significant changes between WT LSL60101 and 5XFAD LSL60101 treated groups were found for *CD40lg*, *Ccl12*, *Ccl8*, *Cxcl10* (Figures 5C, 5H-J).

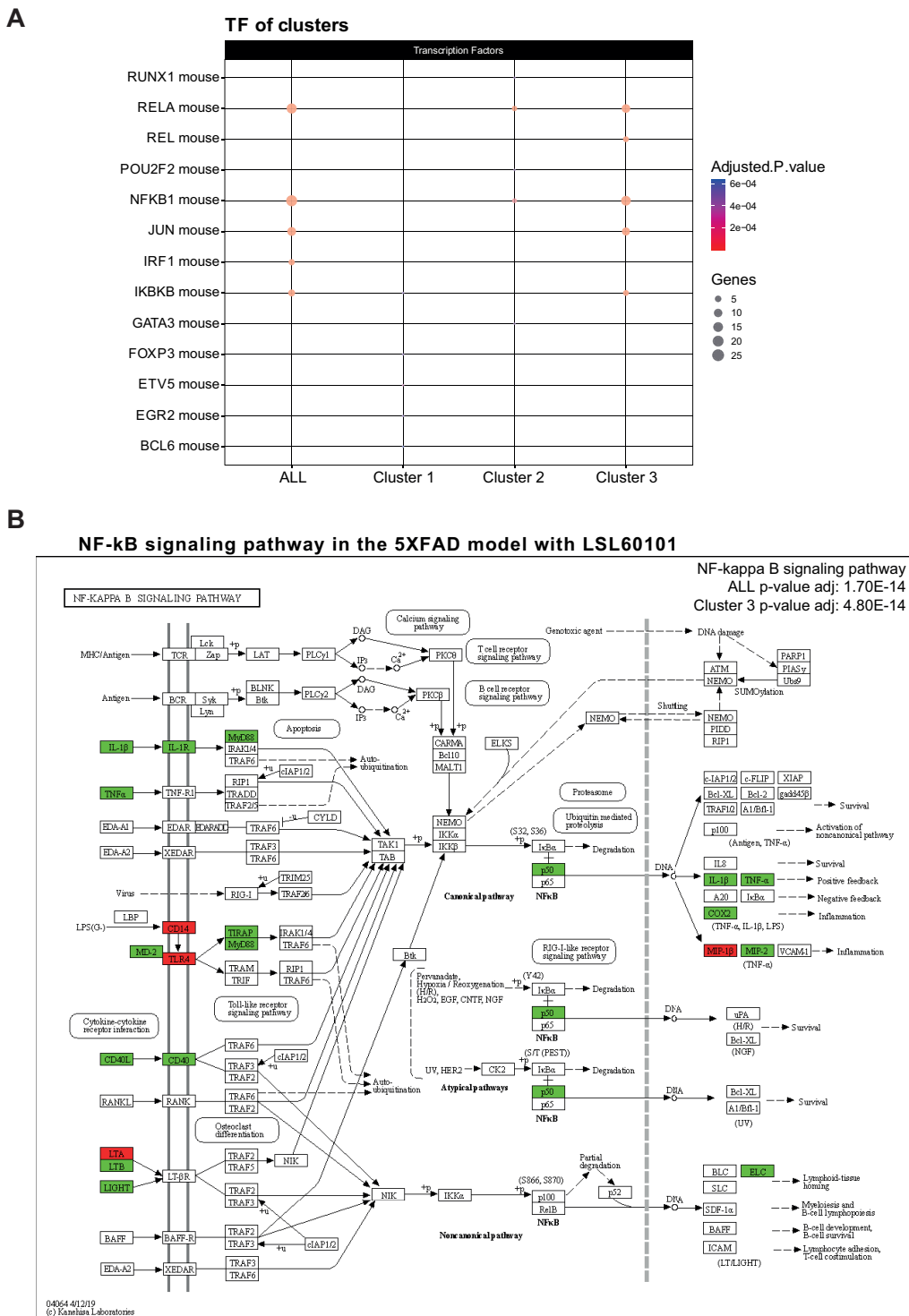


**Figure 4: Transcriptional regulatory interactions analysis and NF-kappa B signaling pathway.** (A) The dotplot shows the top TFs involved in the regulation of the clusters identified with TRRUST. An adjusted p-value < 0.05 was considered statistically significant. (B) The KEGG pathway map NF-κB signaling pathway (mmu04064) and the adjusted p-value of the significant clusters are shown. The down-regulated (green) and up-regulated genes (red) in the 5XFAD control condition versus the 5XFAD LSL60101 condition are shown.

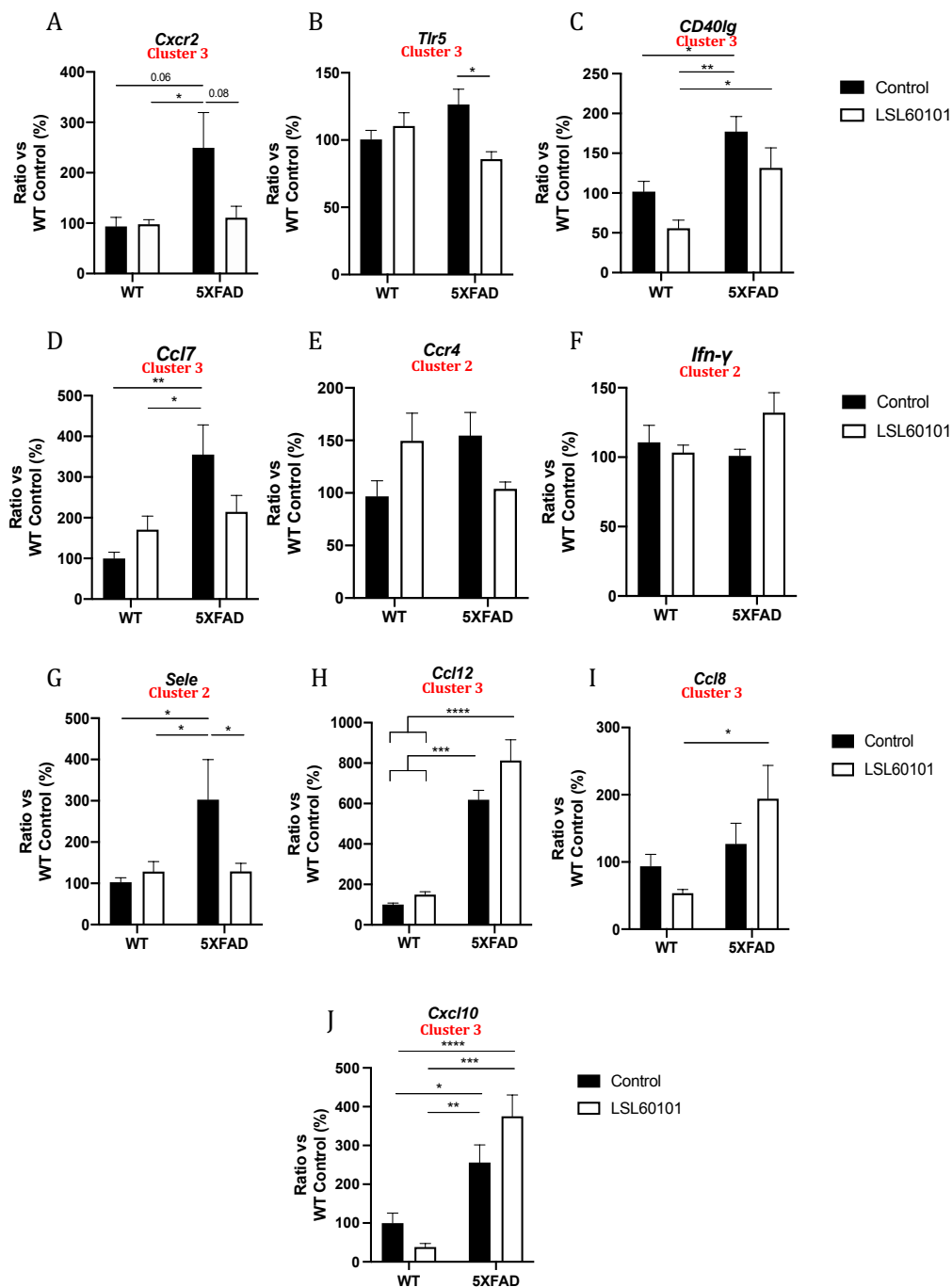


**Figure 5: Validation of representative subset of mRNAs.** Gene expression of *Cxcr2*, *Tlr5*, *Cd40lg*, *Ccl7*, *Ccr4*, *Ifn- $\gamma$* , *Sele*, *Ccl12*, *Ccl8*, *Cxcl10* (A-J) in the hippocampus of WT and 5XFAD control and LSL60101 treated mice. Gene expression levels were determined by real-time PCR. Values in bar graphs are adjusted to 100% for relative gene expression of the WT control. Bars represent mean  $\pm$  SEM. Two-way ANOVA with Tukey post hoc analysis, \*  $p < 0.05$ ; \*\*  $p < 0.01$ ; \*\*\*  $p < 0.001$ ; \*\*\*\*  $p < 0.0001$ ;  $n=5-6$  per group.

### 3.5.4 DISCUSSION

As aforementioned, AD is characterized by multiple molecular signatures at different stages of the disease, being neuroinflammation one of the most relevant early events in the disease [36]. Indeed, chronic inflammation contributes to neuronal dysfunction and cognitive decline [37]. In the current AD drug development pipeline, inflammation is addressed by several drugs with different mechanisms of action, demonstrating its potential as a major target for an effective AD treatment [38]. Evidence provided by our group and others demonstrates that selective I<sub>2</sub>-IR ligands can modulate neuroinflammation, promoting changes in inflammatory cytokines protein levels and/or gene expression in AD mice models [14,16,27,39]. Nevertheless, going deeper into the specific mechanisms whereby I<sub>2</sub>-IR ligands modulate inflammatory pathways is necessary to understand better the potential link between their neuroprotective and anti-inflammatory effects. Thus, the main goal of this work was to study and identify new inflammatory transcriptome biomarkers after LSL60101 treatment and validate some of the inflammatory markers that were found altered in our previous works. Here, we used the hippocampal transcriptome of 5XFAD mice, which harbor five APP/PSEN1 mutations leading to a robust A $\beta$  production and deposition in their brains [21]. Interestingly, we recently demonstrated that chronic treatment with LSL60101 improved cognitive impairment and reduced A $\beta$  plaques and tau pathology in 7-month-old 5XFAD mice [28].

In the present study, a gene expression profile study of the hippocampus samples from 5XFAD mice indicated that LSL60101 treatment significantly modified the expression of several genes, generating three hierarchical clusters based on the enrichment heatmap. Not surprisingly, two clusters were characterized by genes with reduced expression after LSL60101 treatment, suggesting an anti-inflammatory effect of LSL60101. In line with these results, in the AD landscape provided by 5XFAD mice, LSL60101 was shown to decrease microglial and astroglial reactivity by reducing Iba-1 and GFAP levels, respectively [28]. Indeed, microglia and astrocytes are central players in the neuroinflammatory process producing pro-inflammatory or anti-inflammatory cytokines upon pathological insults [40]. Likewise, one hierarchical cluster was characterized by increased anti-inflammatory genes expression in the LSL60101 group, confirming our hypothesis of anti-inflammatory properties of the selective I<sub>2</sub>-IR ligand. Notably, 17 genes in the hippocampus of LSL60101-treated mice displayed a significant change of more than 2-fold in their expression, and we were able to validate the modifications for *Ccr4*, *Ifn- $\gamma$* , *Sele* (Cluster 2) and *Cxcr2*, *Tlr5*, *CD40lg*, *Ccl7*, *Ccl12*, *Ccl8*, *Cxcl10* (Cluster 3). Among them, *Cxcr2*, *Sele*, *CD40lg*, *Ccl7* and *Ccr4* were found to significantly decrease or presented a clear tendency to decrease after treatment while *Ccl8*, *Ccl12* and *Cxcl10* gene expression tended to increase after treatment in 5XFAD mice.

Thus, our results indicated an anti-inflammatory landscape, with several reduced pro-inflammatory and several increased anti-inflammatory cytokines. For instance, the receptor CXCR2 presents a prominent expression at microglia in AD compared to the normal brain tissue and could be used as a strategic therapeutic target to counterbalance inflammatory microenvironments in AD [41,42]. On the other hand, it has been suggested that the CD40-CD40LG interaction may be involved in the inflammatory pathways in AD. It has been demonstrated that CD40LG and A $\beta$  synergistically increase TNF- $\alpha$  and promote neuronal death reinforcing the AD pathology [43]. Finally, overexpression of different chemokine receptors, including CCR4, has been identified in T-cells of AD patients, linking these inflammatory cells to brain damage [44]. Taken together, the results suggest that treatment with I<sub>2</sub>-IR ligand LSL60101 might attenuate the neuroinflammatory process in AD by reversing the expression of inflammatory mediators.

Moreover, as we expected, our results showed alterations in GO enrichment analysis in processes such as inflammatory response, chemotaxis, chemokine-mediate signaling pathway, among others. Likewise, KEGG pathways are related to chemokine signaling pathways, cytokine-cytokine receptor interaction and Toll-like receptor signaling, among others. Altogether, this evidence suggests that the selective I<sub>2</sub>-IR ligand, LSL60101, presents diversity in the modulation of pathways and biological functions in AD. In accordance with our results, the selective I<sub>2</sub>-IR ligand has been shown to mediate pleiotropic central effects *in vivo* and *in vitro*, including alterations in dopamine and serotonin levels, acute hyperphagic effects, inhibition of the development of the opioid-induced tolerance, potentiation of morphine analgesia, glia modulation and neuroprotection among others [22,24,45-48]. Interestingly, gene set enrichment analysis identified several genes such as *Il-1 $\beta$* , *Cox2*, *Tnf- $\alpha$* , and *MIP-2* presented in clusters 2 and 3 associated with the NF- $\kappa$ B pathway that are reduced in the treatment LSL60101 group. Of note, activation of NF- $\kappa$ B pathway is intimately related to neurodegeneration and particularly to AD [35], while its inhibition has been shown to improve cognitive deficits in *in vivo* models of AD [49]. In turn, decreases in NF- $\kappa$ B regulated genes such as *Il-1 $\beta$* , *Cox2*, *Tnf- $\alpha$*  were found after treatments with selective I<sub>2</sub>-IR ligands delivering neuroprotection in mouse models of aging neurodegeneration and AD [14-16,39]. Therefore, downregulation of NF- $\kappa$ B pathway by LSL60101 might partially account for the altered gene expression of inflammatory markers and further explain its neuroprotective effect in this AD mouse model. In this line of evidence, NF- $\kappa$ B has been implicated in APP processing and facilitation of A $\beta$  generation [50]; thus, its downregulation is in accordance with the amelioration of A $\beta$  pathology induced by LSL60101 treatment in 5XFAD mice.

In conclusion, our study identified several genes, modulated pathways, transcriptional factor signatures and their transcriptional regulatory networks that correlated with cognitive



improvement after LSL60101 treatment in 5XFAD presented in our previous study [28], demonstrating the potential of selective I<sub>2</sub>-IR ligands for AD treatment.

**Funding:** This study was supported by Ministeria de Economía y Competitividad of Spain and FEDER (PID2019-107991RB-I00, PID2019-106285RB-I00), María de Maeztu Unit of Excellence (Institute of Neurosciences, University of Barcelona) MDM-2017-0729, and 2017SGR106 (AGAUR, Cata-lonia). The project leading to these results has received funding from “la Caixa” Foundation (ID100010434), under agreement CI18-00002. F.V. partially thanks the UB for the APIF grant (UB2016).

**Author Contributions:** Conceptualization, C.G.F. and M.P.; Experiments, F.V.; Bioinformatic analysis, C.G.F.; writing—original draft preparation, C.G.F. and F.V.; writing—review and editing, C.G., 506 F.V., M.P.; funding acquisition, C.E., M.P. All authors have read and agreed to the published version 507 of the manuscript.

**Conflicts of Interest:** The authors declare no conflict of interest.

**Abbreviations:** I<sub>2</sub>-IR, I<sub>2</sub> imidazoline receptors; AD, Alzheimer’s Disease; TNF- $\alpha$ , tumor necrosis factor- $\alpha$ ; IL-1 $\beta$ , interleukin 1 $\beta$ ; IL-6, Interleukin 6; GO, Gene Ontology; KEGG, Kyoto Encyclopedia of Genes and Genomes; DAVID, Database for Annotation, Visualization, and Integrated Discovery; TFs, transcriptional factors; NF- $\kappa$ B, NF- $\kappa$  $\beta$ ; Cxcr2, C-X-C Motif Chemokine Receptor 2; Tlr5, Toll-like receptor 5; CD40lg, CD40 Ligand; Ccl7, Chemokine (C-C motif) ligand 7; Ccr4, C-C chemokine receptor type 4; Ifn- $\gamma$ , Interferon-gamma; Sele, E-Selectin; Ccl12, Chemokine (C-C motif) ligand 12; Ccl8, Chemokine (C-C motif) ligand 8; Cxcl10, C-X-C motif chemokine ligand 10 (Cxcl10)

## REFERENCES

1. Bousquet, P.; Feldman, J.; Schwartz, J. Central Cardiovascular Effects of Alpha Adrenergic Drugs: Differences between Catecholamines and Imidazolines. *J. Pharmacol. Exp. Ther.* 1984, 230, 232–236.
2. Ernsberger, P.; Meeley, M.P.; Mann, J.J.; Reis, D.J. Clonidine Binds to Imidazole Binding Sites as Well as Alpha 2-Adrenoceptors in the Ventrolateral Medulla. *Eur. J. Pharmacol.* 1987, 134, 1–13, doi:10.1016/0014-2999(87)90125-7.
3. Diamant, S.; Eldar-Geva, T.; Atlas, D. Imidazoline Binding Sites in Human Placenta: Evidence for Heterogeneity and a Search for Physiological Function. *Br. J. Pharmacol.* 1992, 106, 101–108, doi:10.1111/j.1476-5381.1992.tb14300.x.
4. Regunathan, S.; Reis, D.J. Imidazoline Receptors and Their Endogenous Ligands. *Annu. Rev. Pharmacol. Toxicol.* 1996, 36, 511–544, doi:10.1146/annurev.pa.36.040196.002455.

5. Chan, S.L.; Brown, C.A.; Scarpello, K.E.; Morgan, N.G. The Imidazoline Site Involved in Control of Insulin Secretion: Characteristics That Distinguish It from I1- and I2-Sites. *Br. J. Pharmacol.* 1994, 112, 1065–1070, doi:10.1111/j.1476-5381.1994.tb13191.x.
6. Ernsberger, P.; Haxhiu, M.A. The I1-Imidazoline-Binding Site Is a Functional Receptor Mediating Vasodepression via the Ventral Medulla. *Am. J. Physiol.* 1997, 273, R1572-9, doi:10.1152/ajpregu.1997.273.5.R1572.
7. Head, G.; Mayorov, D. Imidazoline Receptors, Novel Agents and Therapeutic Potential. *Cardio-vasc. Hematol. Agents Med. Chem.* 2008, 4, 17–32, doi:10.2174/187152506775268758.
8. Bousquet, P.; Hudson, A.; García-Sevilla, J.A.; Li, J.-X. Imidazoline Receptor System: The Past, the Present, and the Future. *Pharmacol. Rev.* 2020, 72, 50–79, doi:10.1124/pr.118.016311.
9. Li, J.-X. Imidazoline I2 Receptors: An Update. *Pharmacol. Ther.* 2017, 178, 48–56, doi:10.1016/j.pharmthera.2017.03.009.
10. Li, F.; Zhang, Z.-X.; Liu, Y.-F.; Xu, H.-Q.; Hou, S.-T.; Zheng, R.-Y. 2-BFI Ameliorates EAE-Induced Mouse Spinal Cord Damage: Effective Therapeutic Time Window and Possible Mechanisms. *Brain Res.* 2012, 1483, 13–19, doi:10.1016/j.brainres.2012.09.016.
11. Zhu, Y.-B.; Xia, N.-G.; Zhang, Y.-T.; Wang, X.-S.; Liang, S.-S.; Yin, W.-Y.; Xu, H.-Q.; Hou, S.-T.; Zheng, R.-Y. Brain Protection Conferred by Long-Term Administration of 2-(2-Benzofuranyl)-2-Imidazoline against Experimental Autoimmune Encephalomyelitis. *Neurochem. Res.* 2015, 40, 572–578, doi:10.1007/s11064-014-1502-0.
12. Ni, H.; Rui, Q.; Lin, X.; Li, D.; Liu, H.; Chen, G. 2-BFI Provides Neuroprotection Against Inflammation and Necroptosis in a Rat Model of Traumatic Brain Injury. *Front. Neurosci.* 2019, 13, 674, doi:10.3389/fnins.2019.00674.
13. Siemian, J.N.; LaMacchia, Z.M.; Spreuer, V.; Tian, J.; Ignatowski, T.A.; Paez, P.M.; Zhang, Y.; Li, J.-X. The Imidazoline I2 Receptor Agonist 2-BFI Attenuates Hypersensitivity and Spinal Neuroinflammation in a Rat Model of Neuropathic Pain. *Biochem. Pharmacol.* 2018, 153, 260–268, doi:10.1016/j.bcp.2018.01.032.
14. Griñán-Ferré, C.; Vasilopoulou, F.; Abás, S.; Rodríguez-Arévalo, S.; Bagán, A.; Sureda, F.X.; Pérez, B.; Callado, L.F.; García-Sevilla, J.A.; García-Fuster, M.J.; et al. Behavioral and Cognitive Improvement Induced by Novel Imidazoline I2 Receptor Ligands in Female SAMP8 Mice. *Neurotherapeutics* 2019, 16, 416–431, doi:10.1007/s13311-018-00681-5.
15. Vasilopoulou, F.; Bagan, A.; Rodriguez-Arevalo, S.; Escolano, C.; Griñán-Ferré, C.; Pallàs, M. Amelioration of BPSD-Like Phenotype and Cognitive Decline in SAMP8 Mice Model Accompanied by Molecular Changes after Treatment with I2-Imidazoline Receptor Ligand MCR5. *Pharmaceutics* 2020, 12, 475, doi:10.3390/pharmaceutics12050475.

16. Vasilopoulou, F.; Griñán-Ferré, C.; Rodríguez-Arévalo, S.; Bagán, A.; Abás, S.; Escolano, C.; Pallàs, M. I2 Imidazoline Receptor Modulation Protects Aged SAMP8 Mice against Cognitive Decline by Suppressing the Calcineurin Pathway. *GeroScience* 2021, 43, 965–983, doi:10.1007/s11357-020-00281-2.
17. Ruiz, J.; Martín, I.; Callado, L.F.; Meana, J.J.; Barturen, F.; García-Sevilla, J.A. Non-Adrenoceptor [3H]Idazoxan Binding Sites (I2-Imidazoline Sites) Are Increased in Post-mortem Brain from Patients with Alzheimer's Disease. *Neurosci. Lett.* 1993, 160, 109–112, doi:10.1016/0304-3940(93)90925-b.
18. García-Sevilla, J.A.; Escribá, P.V.; Walzer, C.; Bouras, C.; Guimón, J. Imidazoline Receptor Proteins in Brains of Patients with Alzheimer's Disease. *Neurosci Lett.* 1998, 247, 95–98, doi:10.1016/s0304-3940(98)00265-1.
19. Serrano-Pozo, A.; Mielke, M.L.; Gómez-Isla, T.; Betensky, R.A.; Growdon, J.H.; Frosch, M.P.; Hyman, B.T. Reactive Glia Not Only Associates with Plaques but Also Parallels Tangles in Alzheimer's Disease. *Am. J. Pathol.* 2011, 179, 1373–1384, doi:10.1016/j.ajpath.2011.05.047.
20. Ardura-Fabregat, A.; Boddeke, E.W.G.M.; Boza-Serrano, A.; Brioschi, S.; Castro-Gomez, S.; Ceyzeriat, K.; Dansokho, C.; Dierkes, T.; Gelders, G.; Heneka, M.T.; et al. Targeting Neuroinflammation to Treat Alzheimer's Disease. *CNS Drugs* 2017, 31, 1057–1082, doi:10.1007/s40263-017-0483-3.
21. Oakley, H.; Cole, S.L.; Logan, S.; Maus, E.; Shao, P.; Craft, J.; Guillozet-Bongaarts, A.; Ohno, M.; Disterhoft, J.; Van Eldik, L.; et al. Intraneuronal Beta-Amyloid Aggregates, Neurodegeneration, and Neuron Loss in Transgenic Mice with Five Familial Alzheimer's Disease Mutations: Potential Factors in Amyloid Plaque Formation. *J. Neurosci.* 2006, 26, 10129–10140, doi:10.1523/JNEUROSCI.1202-06.2006.
22. García-Sevilla, J.A.; Alemany, R.; Olmos, G.; Menargues, A.; Obach, R. Chronic Imidazoline Drug Treatment Increases the Immunoreactivity of Glial Fibrillary Acidic Protein in Rat Brain. LSL 60101 as a Novel and Selective Ligand for I2-Imidazoline Receptors. *Ann. N. Y. Acad. Sci.* 1995, 763, 486–489, doi:10.1111/j.1749-6632.1995.tb32437.x.
23. Rodríguez-Arévalo, S.; Bagán, A.; Griñán-Ferré, C.; Vasilopoulou, F.; Pallàs, M.; Brocos-Mosquera, I.; Callado, L.F.; Loza, M.I.; Martínez, A.L.; Brea, J.; et al. Benzofuranyl-2-Imidazoles as Imidazoline I2 Receptor Ligands for Alzheimer's Disease. *Eur. J. Med. Chem.* 2021, 222, 113540, doi:10.1016/j.ejmech.2021.113540.
24. Alemany, R.; Olmos, G.; García-Sevilla, J.A. Chronic Treatment with Phenelzine and Other Irreversible Monoamine Oxidase Inhibitors Downregulates I2-Imidazoline Receptors in the Brain and Liver. *Ann. N. Y. Acad. Sci.* 1995, 763, 506–509, doi:10.1111/j.1749-6632.1995.tb32442.x.

25. Escribá, P.V.; Alemany, R.; Sastre, M.; Olmos, G.; Ozaita, A.; García-Sevilla, J.A. Pharmacological Modulation of Immunoreactive Imidazoline Receptor Proteins in Rat Brain: Relationship with Non-Adrenoceptor [3H]-Idazoxan Binding Sites. *Br. J. Pharmacol.* 1996, 118, 2029–2036, doi:10.1111/j.1476-5381.1996.tb15640.x.
26. Sánchez-Blázquez, P.; Boronat, M.A.; Olmos, G.; García-Sevilla, J.A.; Garzón, J. Activation of I2-Imidazoline Receptors Enhances Supraspinal Morphine Analgesia in Mice: A Model to Detect Agonist and Antagonist Activities at These Receptors. *Br. J. Pharmacol.* 2000, 130, 146–152, doi:10.1038/sj.bjp.0703294.
27. Mirzaei, N.; Mota, B.C.; Birch, A.M.; Davis, N.; Romero-Molina, C.; Katsouri, L.; Palmer, E.O.C.; Golbano, A.; Riggall, L.J.; Nagy, I.; et al. Imidazoline Ligand BU224 Reverses Cognitive Deficits, Reduces Microgliosis and Enhances Synaptic Connectivity in a Mouse Model of Alzheimer's Disease. *Br. J. Pharmacol.* 2021, 178, 654–671, doi:10.1111/bph.15312.
28. Vasilopoulou, F.; Rodríguez-Arévalo, S.; Bagán, A.; Escolano, C.; Griñán-Ferré, C.; Pallàs, M. Disease-modifying Treatment with I 2 Imidazoline Receptor Ligand LSL60101 in an Alzheimer's Disease Mouse Model: A Comparative Study with Donepezil. *Br. J. Pharmacol.* 2021, bph.15478, doi:10.1111/bph.15478.
29. Szklarczyk, D.; Gable, A.L.; Nastou, K.C.; Lyon, D.; Kirsch, R.; Pyysalo, S.; Doncheva, N.T.; Legeay, M.; Fang, T.; Bork, P.; et al. The STRING Database in 2021: Customizable Protein–Protein Networks, and Functional Characterization of User-Uploaded Gene/Measurement Sets. *Nucleic Acids Res.* 2021, 49, D605–D612, doi:10.1093/nar/gkaa1074.
30. Dennis, G.; Sherman, B.T.; Hosack, D.A.; Yang, J.; Gao, W.; Lane, H.C.; Lempicki, R.A. DAVID: Database for Annotation, Visualization, and Integrated Discovery. *Genome Biol.* 2003, 4, R60, doi:10.1186/gb-2003-4-9-r60.
31. Dai, Z.; Tang, H.; Pan, Y.; Chen, J.; Li, Y.; Zhu, J. Gene Expression Profiles and Pathway Enrichment Analysis of Human Osteosarcoma Cells Exposed to Sorafenib. *FEBS Open Bio* 2018, 8, 860–867, doi:10.1002/2211-5463.12428.
32. Han, H.; Cho, J.-W.; Lee, S.; Yun, A.; Kim, H.; Bae, D.; Yang, S.; Kim, C.Y.; Lee, M.; Kim, E.; et al. TRRUST v2: An Expanded Reference Database of Human and Mouse Transcriptional Regulatory Interactions. *Nucleic Acids Res.* 2018, 46, D380–D386, doi:10.1093/nar/gkx1013.
33. Nagae, T.; Araki, K. Cytokines and Cytokine Receptors Involved in the Pathogenesis of Alzheimers Disease. *J. Clin. Cell Immunol.* 2016, 7, doi:10.4172/2155-9899.1000441.
34. Liu, T.; Zhang, L.; Joo, D.; Sun, S.-C. NF-B Signaling in Inflammation. *Sig. Transduct. Target. Ther.* 2017, 2, 17023, doi:10.1038/sigtrans.2017.23.
35. Jha, N.K.; Jha, S.K.; Kar, R.; Nand, P.; Swati, K.; Goswami, V.K. Nuclear Factor-

Kappa as a Therapeutic Target for Alzheimer's Disease. *J. Neurochem.* 2019, 150, 113–137, doi:10.1111/jnc.14687.

36. Leng, F.; Edison, P. Neuroinflammation and Microglial Activation in Alzheimer Disease: Where Do We Go from Here? *Nat. Rev. Neurol.* 2021, 17, 157–172, doi:10.1038/s41582-020-00435-y.

37. Passamonti, L.; Tsvetanov, K.A.; Jones, P.S.; Bevan-Jones, W.R.; Arnold, R.; Borchert, R.J.; Mak, E.; Su, L.; O'Brien, J.T.; Rowe, J.B. Neuroinflammation and Functional Connectivity in Alzheimer's Disease: Interactive Influences on Cognitive Performance. *J. Neurosci.* 2019, 39, 7218–7226, doi:10.1523/JNEUROSCI.2574-18.2019.

38. Gyengesi, E.; Münch, G. In Search of an Anti-Inflammatory Drug for Alzheimer Disease. *Nat. Rev. Neurol.* 2020, 16, 131–132, doi:10.1038/s41582-019-0307-9.

39. Abás, S.; Rodríguez-Arévalo, S.; Bagán, A.; Griñán-Ferré, C.; Vasilopoulou, F.; Brocos-Mosquera, I.; Muguruza, C.; Pérez, B.; Molins, E.; Luque, F.J.; et al. Bicyclic  $\alpha$ -Iminophosphonates as High Affinity Imidazoline I2 Receptor Ligands for Alzheimer's Disease. *J. Med. Chem.* 2020, 63, 3610–3633, doi:10.1021/acs.jmedchem.9b02080.

40. Fakhoury, M. Microglia and Astrocytes in Alzheimer's Disease: Implications for Therapy. *CN* 2018, 16, 508–518, doi:10.2174/1570159X15666170720095240.

41. Martin, E.; Delarasse, C. Complex Role of Chemokine Mediators in Animal Models of Alzheimer's Disease. *Biomed. J.* 2018, 41, 34–40, doi:10.1016/j.bj.2018.01.002.

42. Ryu, J.K.; Cho, T.; Choi, H.B.; Jantaratnotai, N.; McLarnon, J.G. Pharmacological Antagonism of Interleukin-8 Receptor CXCR2 Inhibits Inflammatory Reactivity and Is Neuroprotective in an Animal Model of Alzheimer's Disease. *J. Neuroinflammation* 2015, 12, 144, doi:10.1186/s12974-015-0339-z.

43. Tan, J. Microglial Activation Resulting from CD40-CD40L Interaction After  $\beta$ -Amyloid Stimulation. *Science* 1999, 286, 2352–2355, doi:10.1126/science.286.5448.2352.

44. Goldeck, D.; Larbi, A.; Pellicanó, M.; Alam, I.; Zerr, I.; Schmidt, C.; Fulop, T.; Pawelec, G. Enhanced Chemokine Receptor Expression on Leukocytes of Patients with Alzheimer's Disease. *PLoS ONE* 2013, 8, e66664, doi:10.1371/journal.pone.0066664.

45. Boronat, M.A.; Olmos, G.; García-Sevilla, J.A. Attenuation of Tolerance to Opioid-Induced Antinociception and Protection against Morphine-Induced Decrease of Neurofilament Proteins by Idazoxan and Other I2-Imidazoline Ligands. *Br. J. Pharmacol.* 1998, 125, 175–185, doi:10.1038/sj.bjp.0702031.

46. Casanovas, A.; Olmos, G.; Ribera, J.; Boronat, M.A.; Esquerda, J.E.; García-Sevilla, J.A. Induction of Reactive Astrocytosis and Prevention of Motoneuron Cell Death by the I(2)-Imidazoline

- Receptor Ligand LSL 60101. *Br. J. Pharmacol.* 2000, 130, 1767–1776, doi:10.1038/sj.bjp.0703485.
47. Menargues, A.; Cedó, M.; Artiga, O.; Obach, R.; García-Sevilla, J.A. Effects of the I2-Imidazoline Receptor Ligand LSL 60101 on Various Models of Anorexia in Rats. *Ann. N. Y. Acad. Sci.* 1995, 763, 494–496, doi:10.1111/j.1749-6632.1995.tb32439.x.
48. Ozaita, A.; Olmos, G.; Boronat, M.A.; Lizcano, J.M.; Unzeta, M.; García-Sevilla, J.A. Inhibition of Monoamine Oxidase A and B Activities by Imidazol(ine)/Guanidine Drugs, Nature of the Interaction and Distinction from I2-Imidazoline Receptors in Rat Liver. *Br. J. Pharmacol.* 1997, 121, 901–912, doi:10.1038/sj.bjp.0701214.
49. Yan, S.; Xuan, Z.; Yang, M.; Wang, C.; Tao, T.; Wang, Q.; Cui, W. CSB6B Prevents  $\beta$ -Amyloid-Associated Neuroinflammation and Cognitive Impairments via Inhibiting NF- $\kappa$ B and NLRP3 in Microglia Cells. *Int. Immunopharmacol.* 2020, 81, 106263, doi:10.1016/j.intimp.2020.106263.
50. Jones, S.V.; Kounatidis, I. Nuclear Factor-Kappa B and Alzheimer Disease, Unifying Genetic and Environmental Risk Factors from Cell to Humans. *Front. Immunol.* 2017, 8, 1805, doi:10.3389/fimmu.2017.01805.

## SUPPLEMENTARY MATERIAL

**Table S1:** SYBR Green Primers used in qPCR studies.

<b>Target</b>	<b>Forward primer (5'-3')</b>	<b>Reverse primer (5'-3')</b>
<i>Cxcr2</i>	AGCCTTGAGTCACAGAGAGTT	CATCACCAAGGAGTTCCCCAC
<i>Tlr5</i>	GAATCCCGCTTGGGAGAACA	TTCCAAGCGTAGGTGCTCTG
<i>Cd40lg</i>	ACACGTTGTAAGCGAAGCCA	AACCGTCAGCTGTTTCCCAT
<i>Ccl7</i>	CCATCAGAAGTGGGTCGAGG	ACCATTCCCTTAGGCGTGACC
<i>Ifn-<math>\gamma</math></i>	CCTTCTTCAGCAACAGCAAGGCG	CTTGGCGCTGGACCTGTGGG
<i>Ccr4</i>	TGCTGGGTGGAGGAAATCAC	TCTCTACGCTTGTAACCAGGC
<i>Sele</i>	TAGCGCCTGGATGAAAGCAA	GAGCTCACTGGAGGCATTGT
<i>Cxcl10</i>	GGCTAGTCCTAATTGCCCTTGG	TTGTCTCAGGACCATGGCT
<i>Ccl12</i>	AACTGGTTCCTGACTCCTCT	ACCTGAGGACTGATGGTGGT
<i>Ccl8</i>	GCCAGATAAGGCTCCAGTCA	TGCCTGGAGAAGATTAGGGGA
<i><math>\beta</math>-Actin</i>	CAACGAGCGGTTCCGAT	GCCACAGGTTCCATACCCA





# Chapter 4

## Discussion

At present, I<sub>2</sub>-IR are recognized as promising biological targets due to the analgesic, anti-inflammatory and neuroprotective effects elicited by I<sub>2</sub>-IR ligands in the CNS (Bousquet et al., 2020; J.-X. Li, 2017). In the past decades, extensive investigation regarding the analgesic effects of selective I<sub>2</sub>-IR ligands has established their effectiveness in chronic pain (J. X. Li & Zhang, 2011), giving rise to the first-in-class I<sub>2</sub>-IR analgesic, CR4056, which recently completed a phase II clinical trial for osteoarthritis pain (Ferrari et al., 2011; Rovati et al., 2020). Nonetheless, the evidence regarding the neuroprotective effects of I<sub>2</sub>-IR ligands and the I<sub>2</sub>-IR implication in neurodegeneration and particularly in AD (J. García-Sevilla et al., 1995; J. A. García-Sevilla et al., 1998; Ruiz et al., 1993) has not been translated yet into a comprehensive investigation of the I<sub>2</sub>-IR ligands' therapeutic potential against AD. This is of particular importance since AD is an irreversible neurodegenerative disease that still lacks effective pharmacotherapeutic options for prevention and treatment, and consequently, the identification of new targets for halting the disease progression is a pressing need. Recent evidence suggests the I<sub>2</sub>-IR ligand BU99008 as a promising clinical astrocytic PET marker for neurodegenerative diseases (Kumar et al., 2021; Wilson et al., 2019), launching the potential of I<sub>2</sub>-IR ligands for clinical use in the AD field.

In this doctoral dissertation, we expand our knowledge about the previously underexplored I<sub>2</sub>-IR pharmacological possibilities for AD treatment by assessing the effectiveness of both structurally novel and well-established I<sub>2</sub>-IR ligands in widely used mice models of AD. The novel I<sub>2</sub>-IR ligands, namely **MCR5**, **MCR9** and **B06**, showed high affinity and selectivity for the I<sub>2</sub>-IR receptors over the  $\alpha_2$ -AR and I<sub>1</sub>-IR as well as a good BBB permeation and were devoid of cytotoxicity (Abás et al., 2017, 2020). Therefore, we considered them to be appropriate candidates for evaluating the pharmacological actions of I<sub>2</sub>-IR in *in vivo* models. Moreover, to endorse the therapeutic potential of I<sub>2</sub>-IR modu-

lation in AD, we further selected the well-established I<sub>2</sub>-IR ligand **LSL60101** for *in vivo* evaluation. The I<sub>2</sub>-IR ligand **LSL60101**, first described in 1995 (Alemany et al., 1995; J. A. García-Sevilla et al., 1995) displays a very low affinity for  $\alpha_2$ -AR and has proven to be a useful tool in the I<sub>2</sub>-IR research (Escribá et al., 1996; MacInnes & Handley, 2002; Sánchez-Blázquez et al., 2000) and mediates different central and neuroprotective effects in *in vivo* and *in vitro* experimental models (Boronat et al., 1998; Casanovas et al., 2000; Garau et al., 2013; Menargues et al., 1995; Ozaita et al., 1997). Of note, recently in an in-depth evaluation of the compound, we demonstrated that **LSL60101** ligand also showed a good pharmacokinetic profile with high BBB permeability, no signs of toxicity and ultimately that is orally bioavailable and metabolically stable and thus further suggesting it to be a good candidate for *in vivo* studies (Rodríguez-Arévalo et al., 2021)(Annex A.4). Ultimately, combination treatment with the AChE inhibitor and standard of care donepezil was also investigated in terms of a possible add-on therapy built with I<sub>2</sub>-IR ligands.

## 4.1 Effects of treatment with I<sub>2</sub>-IR ligands on memory loss and BPSD present in AD

Memory loss and cognitive dysfunction are the core symptoms of dementia and AD. Moreover, the non-cognitive symptoms of the disease such as fear-anxiety and depressive-like behaviour are of particular importance since they frequently lead to more rapid cognitive impairment and eventually social deficits. Therefore, the control of memory loss and BPSD is essential to patients as well as to caregivers (Cloak & Al Khalili, 2021; M. Fernández et al., 2010). Current treatment approaches with AChE inhibitors and/or memantine are symptomatic and display modest benefit on cognition, while current management of BPSD is associated with potentially major adverse effects, which sometimes includes worsening of cognitive decline (Devanand & Schultz, 2011; Tampi et al., 2016). In the current project, in order to evaluate the effect of I<sub>2</sub>-IR ligands with high affinity and selectivity for I<sub>2</sub>-IR in cognitive and behavioural capabilities which are impaired in AD, a battery of widely used in preclinical studies cognitive tests (Novel object recognition, object location and Morris water maze tests) and behavioural tests (Open Field, elevated plus maze, three chamber, forced swimming and tail suspension tests) were performed in the SAMP8 and 5XFAD mouse models for AD.

### 4.1.1 Cognitive symptoms

Memory impairment is the most common and debilitating cognitive decline associated with AD, including prominent deficits in working memory, spatial learning, and episodic memory (Gold & Budson, 2008). The common neurobiological source of these specific

types of memory-related deficits is the hippocampus, and in fact, accelerated hippocampal atrophy is a consistent finding in AD (Apostolova et al., 2012; Jahn, 2013). At the same time, I<sub>2</sub>-IR are widely distributed in the CNS and more importantly, early autoradiography studies and more recent PET studies reported the highest I<sub>2</sub>-IR density in hippocampal brain regions and moderate density in the cortex, among other brain regions in human and rodent models (De Vos et al., 1991, 1994; Kawamura et al., 2015; Tyacke et al., 2018), thereby suggesting their implication in cognitive function and memory. Additionally, the demonstration of higher I<sub>2</sub>-IR density in the hippocampus and frontal cortex of AD brains than in healthy brains (J. A. García-Sevilla et al., 1998; Kumar et al., 2021; Ruiz et al., 1993), further implies their involvement in memory impairment. Previous *in vivo* studies, explored the effect of the proposed endogenous IR ligand, agmatine, in rat models of diabetes, showing improvement in cognitive function after treatment (Bhutada et al., 2012; Kang et al., 2017). Of note, agmatine has been shown to bind to both I<sub>1</sub>-IR and I<sub>2</sub>-IR, among other receptors; thus, the evaluation of selective and high-affinity ligands on cognitive decline and memory in AD animal models was of relevance.

In aged **female SAMP8** mice, a mouse model of ageing and **LOAD**, all tested structurally novel compounds **MCR5**, **MCR9** and **B06**, when administered chronically at 5mg/kg/day, attenuated cognitive impairment by improving short- and long-term (recognition) memory. A similar beneficial effect was delivered in **male SAMP8** treated with **MCR5** compound, which additionally ameliorated the spatial memory of the mice. In a parallel study, in 7-month-old **female 5XFAD** transgenic mice of **EOAD**, we showed that I<sub>2</sub>-IR ligand **B06** at the same dose and treatment duration prevented memory loss (Abás et al., 2020)(Annex A.3). Ultimately, when the selective well-established I<sub>2</sub>-IR ligand **LSL60101** was chronically administered in 5XFAD mice at a lower dose (1 mg/kg/day), it reversed cognitive deficits in working and spatial memory. Collectively, this evidence suggests that chronic I<sub>2</sub>-IR treatment with selective ligands improved cognition: **i**) in both LOAD and EOAD mouse models **ii**) in female and male mice **iii**) at a previously reported as I<sub>2</sub>-IR functional dose (5 mg/kg/day) and additionally, at lower doses (1 mg/kg/day). Although we demonstrated for the first time the *in vivo* beneficial effects of I<sub>2</sub>-IR treatments in these two widely used AD mouse models, recent studies, which ran in parallel, further showed cognitive improvement in AD models after I<sub>2</sub>-IR treatment. In particular, sub-chronic intraperitoneal (i.p) treatment BU224 at 5 mg/kg reversed cognitive deficits in 5XFAD (Mirzaei et al., 2021), while i.p. agmatine (10 and 20 mg/kg) and 2-BFI (5 and 10 mg/kg) administration prevented cognitive impairment in A $\beta$ 1-42 injected mice (Kotagale et al., 2020). Therefore, these findings can further extend the reported, by our group, beneficial effect of I<sub>2</sub>-IR modulation on cognitive deficits to different I<sub>2</sub>-IR ligands, as well as to different administration routes and duration.

### 4.1.2 Non-cognitive symptoms

Behavioural and psychological alterations associated with fear- and anxiety disturbances, depressive symptoms, and social deficits observed in AD patients are often present in preclinical AD models, making possible the evaluation of novel drugs potential effect on BPSD-like behaviours. I<sub>2</sub>-IR have been involved in both anxiety and depression (Head & Mayorov, 2008); however, their implication in depression has attracted greater attention so far, based on initial studies reporting altered I<sub>2</sub>-IR densities in depressed patients' brains and influenced by the action of antidepressants (Halaris et al., 2001; Sastre & García-Sevilla, 1997; Piletz et al., 2008). Therefore, several lines of evidence showed the antidepressant and/or anxiolytic activity of I<sub>2</sub>-IR ligands such as 2-BFI, BU224, CR4056, as well as of the endogenous ligand agmatine *in vivo* (Aricioglu & Altunbas, 2003; Finn et al., 2003; Kotagale et al., 2013; Nutt et al., 1995; Siemian et al., 2019; Tonello et al., 2012; Zomkowski et al., 2002), whereas other studies reported no such effect for certain I<sub>2</sub>-IR ligands (Hernández-Hernández et al., 2021; O'Neill et al., 2001; Siemian et al., 2019). Possible explanations concerning the implicated mechanisms, included the involvement of the serotonergic system,  $\alpha_2$ -AR system, or interaction with NMDA receptors, among others (Z.-D. Chen et al., 2018; Finn et al., 2003; Kotagale et al., 2013; Tonello et al., 2012). However, the results obtained in some studies that evaluated the effect of I<sub>2</sub>-IR ligands in the presence or absence of other imidazoline and adrenergic drugs (e.g. after pre-treatment with I<sub>1</sub>-IR, I<sub>2</sub>-IR and  $\alpha_2$ -AR agonists and antagonists) postulated the involvement of I<sub>2</sub>-IR receptors in the induced antidepressant effect (Kotagale et al., 2020; Kotagale et al., 2013; Tonello et al., 2012). This evidence suggests that I<sub>2</sub>-IR ligands with high affinity and selectivity for I<sub>2</sub>-IR over  $\alpha_2$ -AR and I<sub>1</sub>-IR can deliver those effects; thereby, we were prompted to evaluate the effect of I<sub>2</sub>-IR ligands on the BPSD-like behaviours frequently exhibited by AD mouse models.

Indeed, the SAMP8 mice have been shown to display BPSD-like behaviours resembling those of AD patients, including anxiety- and depressive-like behaviours, aggression and reduced social investigation (Maes et al., 2020; Meeker et al., 2013; Pérez-Cáceres et al., 2013), which additionally were shown to correlate with cognitive impairment in aged mice (unpublished results). Interestingly, in aged SAMP8 mice, **MCR5**, **MCR9** and **B06** shared a common anxiolytic-induced effect in female (**MCR5**, **MCR9**, **B06**) and male mice (**MCR5**). Further evaluation of the I<sub>2</sub>-IR ligand **MCR5** in SAMP8 mice revealed that chronic treatment delivered an antidepressant-like effect by decreasing the immobility time in the forced swimming and tail suspension tests. Furthermore, we observed that **MCR5** effect was not attributed either to changes in serotonin receptors levels presented by SAMP8 mice or to **MCR5** binding to 5-HT receptors or transporter. Therefore, our results support an I<sub>2</sub>-IR associated antidepressant-like effect of for **MCR5** ligand, and

more importantly, given that the SAMP8 depressive symptoms constitute an AD-associated phenotype, focus the beneficial effect of I<sub>2</sub>-IR modulation on AD-associated depression. In line with these results, recent studies demonstrated that agmatine attenuated depressive behaviour in A $\beta$ 1-40 and A $\beta$ 1-42 injected mice (Guerra de Souza et al., 2018; Kotagale et al., 2020), further pointing out the clinical relevance of imidazoline drugs for the BPSD in the AD field.

APP overexpressing transgenic models, such as 5XFAD, have also been found to present behaviours akin to BPSD in AD patients, including reduced social investigation, aggression, and anxiety disturbances (Jawhar et al., 2012; Kosel et al., 2019). Unlike the novel I<sub>2</sub>-IR compounds tested in SAMP8, the I<sub>2</sub>-IR **LSL60101** treatment at lower doses had no effect on the anxiety parameters studied in 5XFAD. Although a direct comparison of the I<sub>2</sub>-IR mediated anxiolytic effect among our studies is not possible due to significant differences in the mouse models and dosage used, it is important to note that the I<sub>2</sub>-IR ligand **LSL60101** was also shown to lack antidepressant activity in rats, unlike other I<sub>2</sub>-IR compounds (Hernández-Hernández et al., 2021). Previous studies also reported differential behavioural responses of I<sub>2</sub>-IR ligands, partially attributed to the chemical structure of the compounds and heterogeneity of the I<sub>2</sub>-IR, which different I<sub>2</sub>-IR ligands may differentially modulate; thus, this could also be the case regarding the differences observed in our studies among compounds. However, regarding BPSD related to social function, I<sub>2</sub>-IR ligand **LSL60101** ameliorated social deficits in the 5XFAD mouse model, being the first reported I<sub>2</sub>-IR ligand with such action, further pointing out the potential of I<sub>2</sub>-IR modulation to ameliorate BPSD in AD.

## 4.2 Effects of I<sub>2</sub>-IR ligands on histological and molecular AD hallmarks

Emerging drugs in clinical trials for AD aim not only to alleviate the symptoms but also to modify the disease progression in an attempt to provide an effective cure for AD. In fact, most current drugs in clinical trials are molecules that target the two major pathological hallmarks of AD, A $\beta$  accumulation and tau hyperphosphorylation (Cummings et al., 2020, 2021).

### 4.2.1 A $\beta$ pathology

According to the A $\beta$  cascade hypothesis, A $\beta$ -related toxicity is the primary cause of synaptic dysfunction and neurodegeneration that underlies the AD progression, leading ultimately to dementia (Selkoe, 2002; Selkoe & Hardy, 2016); thus, genetic, neuropatho-

logical, and cell biological evidence postulate that targeting  $A\beta$  could be beneficial for AD patients (Ising et al., 2015; Selkoe, 2013). Until recently, there was no evidence concerning the effect of  $I_2$ -IR ligands on  $A\beta$  pathology. At present, the  $I_2$ -IR disease modifying effect related to  $A\beta$  pathology is supported by several findings obtained in our *in vivo* studies performed in two AD mice models, namely the SAMP8 and the 5XFAD models.

APP processing can follow either an amyloidogenic or a non-amyloidogenic pathway resulting or not, respectively, in  $A\beta$  generation and subsequently to  $A\beta$  plaques formation (R. J. O'Brien & Wong, 2011). Although typical  $A\beta$  plaques are not detected in SAMP8 brains, SAMP8 mice present increased  $A\beta$  levels in older age and altered APP processing (Akiguchi et al., 2017). Herein, chronic treatment with the  $I_2$ -IR ligands **MCR5**, **MCR9** and **B06** in aged female SAMP8 mice promoted the non-amyloidogenic pathway and/or suppressed the amyloidogenic one. In parallel,  $I_2$ -IR treatment favoured  $A\beta$  degradation through enzymatic pathways by increasing the expression of *NEP* (**B06**, **MCR5**) and *IDE* (**B06**). To our knowledge, this data constitutes the first evidence reporting the effect of  $I_2$ -IR treatment in the mechanisms involved in the  $A\beta$  pathology in AD.

To further evaluate the  $A\beta$ -associated effect of  $I_2$ -IR treatment, the following studies were performed using the transgenic 5XFAD mouse model. 5XFAD mice rapidly develop  $A\beta$  pathology (accelerated  $A\beta$  accumulation and  $A\beta$  plaques) due to the incorporation of five familial  $A\beta$ -associated mutations into a line, being a valuable tool for testing  $A\beta$ -modifying drugs (Oakley et al., 2006). Chronic treatment with  $I_2$ -IR ligand **B06** in 5XFAD suppressed the amyloidogenic pathway corroborating the results obtained in SAMP8 mice (Abás et al., 2020)(Annex A.3). Conversely, it was recently reported that sub-chronic treatment with  $I_2$ -IR ligand BU224 in 6-month-old 5XFAD female mice failed to reduce  $A\beta$  load and plaques, although it reversed cognitive deficits (Mirzaei et al., 2021). Notwithstanding, in our last study, we provide the ultimate robust evidence of the  $I_2$ -IR effect on  $A\beta$  pathology after an in-depth evaluation of the selective  $I_2$ -IR ligand **LSL60101** in 7-month-old 5XFAD female mice. Chronic and low-dose **LSL60101** treatment decreased  $A\beta_{40}$ ,  $A\beta_{42}$  levels and  $A\beta$  plaques in the 5XFAD brains, and these results were accompanied by beneficial effects in APP processing. Therefore, based on the evidence to date, the  $A\beta$ -associated effect of  $I_2$ -IR treatment in 5XFAD mice appears to depend on the experimental design, including but not limited to  $I_2$ -IR drug particularities, pharmacokinetic factors, and administration conditions. Concretely, a possible explanation arises from differences in the duration of the treatment (chronic versus sub-chronic), especially given that the 5XFAD mice by 6 months of age have developed an advanced  $A\beta$  pathology, which attenuation probably requires longer treatments. Besides, the duration of the  $I_2$ -IR administration (acute vs chronic) has proven to be critical in a previous study evaluating  $I_2$ -IR mediated effects (Garau et al., 2013). However, differences related to  $I_2$ -IR ligand structural variances cannot be

excluded since discrepancies regarding the *in vivo* effects of different I<sub>2</sub>-IR ligands upon the same experimental and pathological conditions have also been reported (Garau et al., 2013; Sánchez-Blázquez et al., 2000), pointing out once again the heterogeneity of I<sub>2</sub>-IR and the necessity for simultaneous evaluation of different I<sub>2</sub>-IR ligands.

To sum up, in our hands, all I<sub>2</sub>-IR ligands tested, **MCR5**, **MCR9**, **B06** and **LSL60101**, delivered an A $\beta$ -related modifying effect in LOAD and/or EOAD mouse models after chronic treatments. Provided that A $\beta$  plaques and especially A $\beta$  oligomers are strongly associated with synapse loss as well as memory and synaptic plasticity (Marsh & Alifragis, 2018; Sasaguri et al., 2017), the beneficial effects of I<sub>2</sub>-IR ligand treatments on cognition can be attributable to amelioration of A $\beta$  pathology.

### 4.2.2 Tau hyperphosphorylation

Tau-hyperphosphorylation and aggregation are highly associated with disruption of neuronal and synaptic function. Moreover, the spreading of tau pathology in the AD affected brains correlates with cognitive decline, and thus jointly with amyloidosis abnormalities, it is considered an indicator of AD progression (Cicognola et al., 2021; Thal et al., 2000). Evidence regarding the effect of I<sub>2</sub>-IR modulation on tau pathology is limited to a recent study reporting that chronic treatment with idazoxan (mixed  $\alpha_2$ -AR/I<sub>2</sub>-IR ligand) reduced tau hyperphosphorylation and increased inactive GSK3 $\beta$  (phosphorylated at Ser9) levels in APP Knock-in, as well as A $\beta$ , injected mice; however, its effects were attributed by the authors to  $\alpha_2$ -AR blockade rather to I<sub>2</sub>-IR modulation (Zhang et al., 2020).

All novel and selective I<sub>2</sub>-IR ligands, devoid of  $\alpha_2$ -AR affinity, **MCR5**, **MCR9** and **B06** led to a remarkable reduction in tau hyperphosphorylation when administered chronically in aged SAMP8 mice, a model characterized by age-dependent abnormal levels of tau phosphorylation (Pallas et al., 2008). In our studies, the decreases in the evaluated p-tau epitopes (Ser396, Ser404) levels were accompanied by reduced activity of the major tau kinases, namely GSK3 $\beta$ , CDK5, ERK1/2, and alterations in upstream molecules implicated in the process. Notably, we determined increased inactive GSK3 $\beta$  phosphorylated at Ser9 and phosphorylated AKT (p-AKT) levels and/or reduced phosphorylated CDK5 (p-CDK5) consistently with a decrease in p25/35 ratio after treatments in SAMP8 mice. Likewise, in 5XFAD mice, chronic treatment with I<sub>2</sub>-IR ligand **LSL60101** followed a similar trend by decreasing tau pathology. Therefore, in our studies, all tested selective I<sub>2</sub>-IR compounds treatments effectively reduced p-tau levels in the AD mouse models used.

In attempts to understand the links between A $\beta$  and tau, it has been accepted that both proteins might interact and cooperate to cause neurodegeneration (Roberson et al., 2007; Shipton et al., 2011). For instance, the involvement of tau in A $\beta$  oligomers-mediated

synapse loss has been demonstrated (Roberson et al., 2011). In this context, the effect of I<sub>2</sub>-IR treatment on tau pathology appears to be in line with the amelioration of A $\beta$  pathology, and together their attenuation may account for the reversion of synaptic damage and cognitive decline.

### 4.3 Effects of I<sub>2</sub>-IR ligands on neuroinflammation

Along with the abnormal protein accumulation which characterizes AD, neuroinflammation is recognized as a central player in AD development and progression (Heneka et al., 2015; Kinney et al., 2018). In fact, chronic neuroinflammation occurs in the early stages of AD and may contribute to neural dysfunction and cell death independently (McGeer & McGeer, 2010; Sudduth et al., 2013). For this reason, therapeutic approaches that target neuroinflammation have been shown to deliver neuroprotection (Krause & Müller, 2010). Although nonsteroidal anti-inflammatory drugs (NSAID) did not show benefit in randomized trials with symptomatic AD patients, decreased AD incidence was observed in NSAID treated asymptomatic individuals after 2-3 years (Breitner et al., 2011). Then, long-term use of NSAID has been shown to delay AD progression. Besides, inflammation is targeted by several drugs in the current AD drug development pipeline, highlighting its potential as a therapeutic target for the development of effective AD drugs (Cummings et al., 2021).

Unlike the classic AD hallmarks, neuroinflammation has previously proven to be intimately related to I<sub>2</sub>-IR modulation. I<sub>2</sub>-IR are expressed primarily in glial cells and can influence glial activity (Keller & García-Sevilla, 2015; Regunathan et al., 1993, 1999). The first evidence for I<sub>2</sub>-IR inflammatory modulation was provided *in vitro* when the I<sub>2</sub>-IR ligand idazoxan was shown to attenuate the induction of NOS-2 inflammatory mediator in LPS-stimulated cells (Feinstein et al., 1999; Regunathan et al., 1999). Since then, the inflammatory-associated effects of established I<sub>2</sub>-IR ligands have been well documented in certain scenarios. For example, I<sub>2</sub>-IR ligand 2-BFI dose-dependently reduced microglial reactivity and/or the expression of inflammatory cytokines in rodent models of experimental autoimmune encephalomyelitis [TNF- $\alpha$ , IL-17A, Interferon gamma (IFN- $\gamma$ )] (Zhu et al., 2015), neuropathic pain (Iba-1 and TNF- $\alpha$ ) (Siemian, LaMacchia, et al., 2018), traumatic brain injury (Iba-1, IL-1 $\beta$ ) (Ni et al., 2019), delivering neuroprotection. In the inflammatory landscape of AD provided by the SAMP8 and 5XFAD model (A. Fernández et al., 2021; Oakley et al., 2006), we provide evidence that chronic I<sub>2</sub>-IR treatment exerts anti-inflammatory properties accordingly.

In aged SAMP8 brains, decreased gene expression of pro-inflammatory cytokines was determined after treatment with the I<sub>2</sub>-IR ligands **MCR5** (IL-1 $\beta$ , Tnf- $\alpha$ ) and, **B06** (IL-6, IL-



I<sub>2</sub>, *Tnf-α*) compounds. Likewise, in the 5XFAD mice, **B06** treatment downregulated certain cytokines (Abás et al., 2020)(Annex A.3). Chronic low-dose **LSL60101** ligand treatment reduced microglia reactivity by decreasing Iba-1 levels in 5XFAD brains, like what was shown after BU224 administration in this model (Mirzaei et al., 2020). Furthermore, we report a not previously described upregulation of *Trem2* gene expression after **LSL60101** treatment in 5XFAD mice accompanied by consistent alterations in inflammatory markers expression (*Ccl12*, *Il-18*). TREM2 is a single-pass transmembrane receptor expressed in myeloid cells and microglia, and its importance in the AD neuroinflammation process has been largely established (Gratuze et al., 2018; J.-T. Li & Zhang, 2018). All this evidence prompted us to go deeper in the implication of I<sub>2</sub>-IR in inflammatory pathways by determining the expression profile of genes associated with inflammation, including different cytokines, chemokines, inflammatory regulators and their receptors after chronic treatment with the ligand **LSL60101** in both 5XFAD and WT mice. Our results further indicate that **LSL60101** treatment reverses the inflammatory process in AD mice and remarkably, point out the nuclear factor- $\kappa$ B (NF- $\kappa$ B) pathway to be involved in the observed effects. NF- $\kappa$ B transcription factor is a key mediator of brain inflammation regulating the gene expression of several inflammatory markers such as *Il-1 $\beta$* , cyclooxygenase -2 (*Cox-2*), *Tnf-α* and its impaired regulation can trigger together with glia activation, OS, and apoptotic cell death in AD (Jha et al., 2019). Therefore, collectively it can be deduced that the anti-inflammatory effect of the I<sub>2</sub>-IR ligands accounts—at least in part—in part for the delivered neuroprotection in SAMP8 and 5XFAD mice and further postulates that I<sub>2</sub>-IR serve a pivotal role in glial functions.

One of the glial functions of I<sub>2</sub>-IR has proven to be specifically the regulation of GFAP, a cytoskeletal protein (astrocytes) with critical functional implications, especially considering the predominant localization of I<sub>2</sub>-IR in astrocytes among glial cells (Regunathan & Reis, 1996). Several studies demonstrated a direct physiological function of I<sub>2</sub>-IR in the regulation of GFAP levels by reporting increased mRNA levels and protein expression induced by I<sub>2</sub>-IR drugs in astrocyte cultures, as well as after chronic I<sub>2</sub>-IR treatment *in vivo* (Olmos et al., 1994; Sastre & García-Sevilla, 1993). The functional relevance of GFAP changes under I<sub>2</sub>-IR treatment was also investigated and eventually associated with neuroprotection in certain neuropathological conditions. For example, increased GFAP expression and astrocytic activation by the I<sub>2</sub>-IR ligand **LSL60101** treatment was suggested to serve as a protective mechanism in neuronal function after brain injury in rats (Casanovas et al., 2000). Conversely, I<sub>2</sub>-IR treatment with 2-BFI attenuated GFAP expression *in vivo*, delivering neuroprotection (Siemian, LaMacchia, et al., 2018). In the latter study, 2-BFI treatment also suppressed astrocytic activation in stimulated astrocyte cultures *in vitro*, corroborating a primary site of I<sub>2</sub>-IR action on astrocytes. In AD, astrocytic pathological responses are represented by reactive astrocytes, which are characterized by increased

expression of GFAP (Heneka et al., 2015). Reactive astrocytes are commonly found in AD post-mortem human tissues (Dossi et al., 2018), and intriguingly, parallel links between GFAP and I<sub>2</sub>-IR have also been demonstrated in AD brains (J. A. García-Sevilla et al., 1998; Olmos et al., 1994). In line with these observations, the AD model SAMP8 presents marked astrogliosis and increased GFAP expression (Sureda et al., 2006). In the SAMP8 brains, I<sub>2</sub>-IR ligands **MCR5**, **MCR9** and **B06** markedly decreased GFAP reactivity and/or protein levels. Likewise, astrogliosis is one of the specific hallmarks of disease progression in the 5XFAD mouse model (Oakley et al., 2006). In 5XFAD brains, chronic treatment with I<sub>2</sub>-IR ligand **LSL60101** led to a robust reduction of astrogliosis by decreasing GFAP reactivity in the hippocampus and the cortex. Of note, reduced astrogliosis in SAMP8 and 5XFAD brains is consistent with inflammatory markers decrease in mice brains, since similarly to microglia, astrocytes release cytokines and ILs among other cytotoxic molecules, upon inflammatory stimuli (e.g. A $\beta$  peptides), thus exacerbating neuroinflammation. Ultimately, our preliminary *in vitro* experiments in human iPSC-derived AD (APP swedish mutated) astrocytes corroborate the results obtained *in vivo*, indicating a decrease in cytokine secretion upon inflammatory stimulation induced by the selective I<sub>2</sub>-IR compounds **MCR5** and **B06**, and thus postulating a direct effect of I<sub>2</sub>-IR ligands on astroglia (Annex A.1).

In whole, we provide strong evidence that the selective I<sub>2</sub>-IR ligands reduce neuroinflammation in AD, which conceivably underlies their effect on the behavioural and cognitive status of the models. Interestingly, the mitigation of astrogliosis, microgliosis and the subsequent decrease in inflammatory markers secretion delivered by I<sub>2</sub>-IR treatments in the AD models are concomitant with the observed attenuation of both classical AD hallmarks in these models. Indeed, in the case of 5XFAD, an A $\beta$ -cascade-hypothesis based model, the reduction of inflammation is more likely to arise from the reduction of A $\beta$  plaques. However, another study showed that I<sub>2</sub>-IR ligand treatment reduced neuroinflammation in the same model without affecting A $\beta$  load and plaques (Mirzaei et al 2020). At the same time I<sub>2</sub>-IR ligand treatments reduced neuroinflammation in the SAMP8 mice, in which the AD-like pathology is attributed to age-related events and unknown risk factors other than the A $\beta$  plaques presence. Therefore, the parallel attenuation of A $\beta$  pathology, tau pathology and neuroinflammation delivered by I<sub>2</sub>-IR treatment in our studies may represent an interactive combination of I<sub>2</sub>-IR mediated effects which synergistically contribute to cognitive improvement in the AD models.

Interestingly, there is evidence to suggest that neuroinflammation is a missing link between the cognitive and non-cognitive symptoms in AD (Selles et al., 2018). Particularly, depressive and anxiety-related disorders have been associated with microglial dysfunction and increased secretion of pro-inflammatory cytokines, while antidepressants have been shown to prevent this process (Felger, 2019; Zheng et al., 2021). In this context, blocking

TNF- $\alpha$ , which is increased in AD brains, has been reported to attenuate BPSD along with the cognitive decline in mice treated with A $\beta$  (Ledo et al., 2016). Moreover, serotonin (5-HT) depletion, which is related to depressive behaviour, appears to be modulated by inflammation, as 5-HT turnover in the brain has been observed to be enhanced by pro-inflammatory cytokines (Felger & Lotrich, 2013; Song et al., 1999; Wichers et al., 2005), further supporting the close relationship between BPSD and neuroinflammation. More importantly, a previous study associated the agmatine's antidepressant effect with decreased pro-inflammatory markers (IL-6, TNF- $\alpha$ ) in a mouse model of AD (Kotagale et al., 2020). These findings correlate with our observations in **MCR5** treated SAMP8 mice, in which amelioration of depressive-like and anxiety-like behaviours was accompanied by decreased gene expression of pro-inflammatory cytokines such as *Tnf- $\alpha$*  and, additionally, positive alterations in key proteins implicated in the AKT/GSK3/mammalian target of rapamycin (mTOR) signalling, which has been involved in mental illnesses. The AKT inactivation of GSK3 $\beta$  by phosphorylation has been shown to influence cytokine expression (Kitagishi et al., 2012). At the same time, activation of the mTOR complex appears to constrain immune cell activation by inhibiting pro-inflammatory cytokines and upregulating anti-inflammatory cytokines (Weichhart et al., 2015; Weichhart & Säemann, 2009). Besides, antidepressants have been shown to upregulate p-AKT protein (David et al., 2010), whereas mood stabilizer lithium has been shown to inhibit GSK3, further indicating the contribution of these kinases to depressive symptoms (W. T. O'Brien & Klein, 2009). Overall, the inflammatory attenuation by **MCR5** in this study not only confirmed the previously obtained results in SAMP8 females but also conferred a protective effect against the BPSD-like phenotype in the SAMP8 model. Thus, modulating glial activation by I<sub>2</sub>-IR ligands may favour protective mechanisms, which—at least in part—explain the protection against behavioural abnormalities and cognitive impairment.

#### 4.4 Changes in oxidative stress process induced by I<sub>2</sub>-IR ligands

OS is a major sign of ageing, which, in turn, has been suggested to represent the main link between OS neurodegenerative diseases (Floyd & Hensley, 2002). Alterations in mitochondrial function that promote an increased ROS production and altered antioxidant defence contribute to the early stages of AD before developing A $\beta$  pathology and cognitive dysfunction (Uttara et al., 2009). Interestingly, OS is also linked to the inflammatory process, being microglia and astroglia dysfunction the connection, through abnormal ROS and RNS production (González-Reyes et al., 2017; Simpson & Oliver, 2020). Currently, some of the under development therapeutic strategies for AD aim to correct the imbalance between ROS production and degradation (Liu et al., 2017).

An association of I<sub>2</sub>-IR with the OS process may arise from the following facts: i) I<sub>2</sub>-IR are mainly located on the outer membrane of mitochondria in glial cells, which are involved in OS regulation (Y. Chen et al., 2020) ii) I<sub>2</sub>-IR have been associated with MAO enzyme which in turn is considered a marker of OS, linked to the production of ROS, and thus contributing to AD neurodegeneration (Cai, 2014). In this context, neuroprotective effects mediated by I<sub>2</sub>-IR ligands have been related to OS attenuation. For example, the I<sub>2</sub>-IR ligand 2-BFI decreased OS and altered the levels of antioxidant enzymes in A $\beta$ <sub>42</sub> injected rats (Tian et al., 2018), and protected against OS-induced astrocytic cell death *in vitro* (Choi et al., 2018). Likewise, agmatine was shown to increase Nrf2 protein levels and enhance its nuclear translocation, with subsequent upregulation of its downstream antioxidant HMOX1, thus attenuating ROS generation in LPS-induced macrophages *in vitro* (Chai et al., 2016), while *in vivo*, agmatine attenuated oxidative damage in rodent models of neurodegeneration (Bilge et al., 2020; Guerra de Souza et al., 2018). In line with these results, chronic treatment with the novel I<sub>2</sub>-IR compounds **MCR5**, **MCR9** and **B06** reduced OS in aged SAMP8 mice. Concretely, decreased H<sub>2</sub>O<sub>2</sub> levels were detected in the brains of SAMP8 mice treated with either **MCR5** or **MCR9**. This effect was accompanied by increased *Hmox1* gene expression, while **MCR5** additionally decreased SOD-1 levels. Similarly, **B06** treatment in aged SAMP8 decreased H<sub>2</sub>O<sub>2</sub> levels, increased *Hmox1*, inducible NOS (*iNOS*) and decreased aldehyde dehydrogenase (*Aldh2*) expression; however, it failed to deliver a similar antioxidant effect when administered in 5XFAD chronically (Abás et al., 2020)(Annex A.3). Conversely, in 5XFAD mice, I<sub>2</sub>-IR ligand **LSL60101** treatment altered OS markers such as *iNOS*, *Aldh2* expression and SOD-1, GPX-1 protein levels, mitigating oxidative damage in 5XFAD brains compared to WT counterparts (Rodriguez-Arévalo et al., 2021)(Annex A.4).

The present evidence is not sufficient to explain why the I<sub>2</sub>-IR ligands alter differentially specific OS parameters (either upregulation or downregulation) in the experimental models used. Moreover, in our hands, **MCR5** and **MCR9** compounds did not shown to inhibit MAO enzymes activity (Annex A.2). However, an overall beneficial effect of the I<sub>2</sub>-IR modulation on this detrimental process present in AD progression was detected and could further support the improved cognitive performance of the mice in our studies. Besides, OS mitigation agrees with the attenuation of AD hallmarks and neuroinflammation observed in the AD models after I<sub>2</sub>-IR treatment. In fact, OS is per se able to produce A $\beta$ , p-tau and trigger glial inflammatory response, and in turn, these features can lead to OS production and eventually apoptosis; thus, this vicious cycle appears to break in SAMP8 and 5XFAD mice after I<sub>2</sub>-IR treatment, further highlighting the potential disease-modifying effect of the selective I<sub>2</sub>-IR ligands.

## 4.5 Alterations in Ca<sup>2+</sup> signaling after treatment with I<sub>2</sub>-IR ligands

Emerging evidence indicates the fundamental role of Ca<sup>2+</sup> signalling in modulating AD pathogenesis (Guo et al., 2020). A balanced concentration of Ca<sup>2+</sup> characterizes healthy neurons; however, Ca<sup>2+</sup> homeostasis is disturbed in AD conditions. This can occur due to several factors, including AD features such as p-tau, neurotoxic APP products and OS, while the mitochondria function is also critical in Ca<sup>2+</sup> regulation. In turn, Ca<sup>2+</sup> dysregulation, once triggered, has been shown to further exacerbate AD pathology, leading eventually to apoptosis and impaired synaptic plasticity (Guo et al., 2020).

At the same time, I<sub>2</sub>-IR activation has been shown to alter Ca<sup>2+</sup> levels and signalling; however, the exact intracellular signalling cascades through which this occurs remains unclear. Several explanations have been given, including increased mobilization of mitochondrial Ca<sup>2+</sup> stores (Boronat et al., 1998; J. García-Sevilla et al., 1995), or binding of I<sub>2</sub>-IR ligands to Ca<sup>2+</sup> influx-associated receptors. For example, one of the proposed mechanisms of I<sub>2</sub>-IR mediated neuroprotection involves the blockade of NMDA gated Ca<sup>2+</sup> channels and subsequent inhibition of Ca<sup>2+</sup> entry *in vitro* and *in vivo* (Han et al., 2013; Olmos et al., 1996, 1999). In the AD context, I<sub>2</sub>-IR ligand BU224 was shown to mediate its beneficial effect on cognition in 5XFAD mice by restoring NMDA function in A $\beta$ -treated cell cultures (Mirzaei et al., 2021). In our hands, the novel I<sub>2</sub>-IR ligands did not alter the Ca<sup>2+</sup> entry by NMDA activation in primary neurons (Annex A.2). However, I<sub>2</sub>-IR treatment with **B06** and **MCR5** ligands was shown to influence NMDA receptor functionality in the neurodegenerative brains of SAMP8 mice by increasing phosphorylated NMDA receptors 2B (NMDAR2B) (Tyr1472) and/or altering subunits composition favourably. Interestingly, changes in NMDA active states and subunits induced by I<sub>2</sub>-IR treatment were consistent with alterations in downstream cascade events involved in synaptic plasticity (see section 4.6).

All the above background argued for going deeper into the Ca<sup>2+</sup> intracellular signalling in the study of I<sub>2</sub>-IR ligand **B06** in the SAMP8 model. Our results reveal that **B06** treatment mediated an effect on Ca<sup>2+</sup> signalling by altering the levels of Ca<sup>2+</sup>-dependent enzymes (e.g. CaN, calpain). Remarkably, **B06** treatment in SAMP8 mice, decreased CaN protein levels, a Ca<sup>2+</sup>/calmodulin-dependent phosphatase sensitive to subtle rises in intracellular Ca<sup>2+</sup> levels, which involvement in AD neurodegeneration is well documented (Reese & Tagliatela, 2011). This important finding was reinforced by the observed downstream changes in the phosphorylation state of CREB, NFAT, for which we also confirmed their translocation to the nucleus, BAD and GSK3 $\beta$ , as well as the downstream targets of them. For instance, after **B06** treatment, CREB-regulated *Bdnf* gene expression

was found increased, NFAT-regulated pro-inflammatory cytokines were decreased, and BAD downstream components such as Bcl-2, Bax and Caspase-3 were found decreased accordingly. All these results can be translated into increased synaptic plasticity, reduced inflammation and apoptosis, respectively, and suggest a neuroprotective effect of I<sub>2</sub>-IR treatment through CaN regulation. Of note, these results were in line with modifications mediated by the I<sub>2</sub>-IR ligands **MCR5** and **MCR9** treatments in SAMP8. In summary, although a direct effect on Ca<sup>2+</sup> levels was not largely explored, indirect alterations on the levels of the enzymes implicated in Ca<sup>2+</sup> intracellular signalling propose a Ca<sup>2+</sup>-associated mechanism whereby I<sub>2</sub>-IR ligands mediate neuroprotection.

## 4.6 Effects on neuronal and synaptic loss delivered by I<sub>2</sub>-IR ligands

Cognitive impairment in AD eventually occurs due to brain atrophy resulting from progressive neuronal and synaptic loss (Niikura et al., 2006). So far, the beneficial effect of I<sub>2</sub>-IR treatment on the central AD detrimental processes has been evidenced; therefore, the ultimate demonstration of the AD modifying effect of I<sub>2</sub>-IR modulation would be the prevention of neuronal death and synaptic dysfunction delivered by I<sub>2</sub>-IR ligands.

### 4.6.1 Apoptotic factors

The exact mechanisms of neuronal death in AD are not yet fully understood; however, apoptosis is considered the primary mechanism among the signal pathways that eventually mediate neuronal death (Mukhin et al., 2017). The apoptotic extrinsic/death receptors and intrinsic/mitochondrial pathways converge to activate caspases that cleave major substrates leading to cell death. Interestingly, mechanisms of neuroprotection induced by imidazoline drugs have been associated with the mitigation of apoptotic cell death. Sustained activation of I<sub>2</sub>-IR receptors by selective ligands has been shown to induce anti-apoptotic effects through inhibition of crucial components of apoptotic signalling, such as Fas associated protein with death domain (FADD)/Fas (extrinsic pathways) and/or Bax, Bcl-2, c-Jun N-terminal kinase ½ (JNK1/2) (intrinsic pathways), caspase-3 decrease, as well as upregulation of anti-apoptotic factors (Ser191/194 phosphorylated FADD) *in vivo* and *in vitro* (Garau et al., 2013; Montolio et al., 2012; Tian et al., 2018). In previous work, I<sub>2</sub>-IR ligand **MCR5** modified FADD in the hippocampus of mice showing non-apoptotic actions (Abás et al., 2017). In the AD background provided by the SAMP8 model, chronic treatments with **MCR5**, **MCR9** and **B06** compounds decreased Bax, Bcl-2 and Caspase-3 protein levels. These results were in line with a decrease in calpain's levels (**B06** treatment) and activity (**MCR5**, **MCR9** treatments), a Ca<sup>2+</sup>-dependent protease

which triggers the classical caspase cascade of the apoptosis reaction. Ultimately, the endogenous imidazoline ligand agmatine was shown to inhibit A $\beta$ -induced apoptosis *in vitro* involving ERK, AKT/GSK3 $\beta$  and TNF- $\alpha$  (Hooshmandi et al., 2019), while the novel I<sub>2</sub>-IR ligands induced similar molecular alterations in the SAMP8 brains. Collectively, this evidence suggests the I<sub>2</sub>-IR mediated anti-apoptotic actions as a possible mechanism for the observed neuroprotective effects of the novel I<sub>2</sub>-IR ligands.

#### 4.6.2 Synaptic plasticity

Synaptic dysfunction is one of the major contributors to AD pathogenesis and is considered a downstream effect of amyloidosis, tau pathology, neuroinflammation and other mechanisms occurring in AD (Selkoe, 2002; Colom-Cadena et al., 2020). More importantly, synaptic function underlies cognitive performance, and for this reason, synapse loss appears to most strongly correlates with cognitive decline in AD (de Wilde et al., 2016; DeKosky & Scheff, 1990). Herein, I<sub>2</sub>-IR ligands increased synaptic plasticity in both SAMP8 and 5XFAD mice, indicated as increased levels of pre-synaptic (e.g. synaptophysin) and post-synaptic (e.g. PSD95) protein levels and importantly, these changes went in parallel with the cognitive improvement of the mice.

Along with the increase in synaptic plasticity markers, novel I<sub>2</sub>-IR treatments enhanced phosphorylated CREB as well as kinases responsible for its phosphorylation (e.g. p-AKT, PKA). CREB is crucial in long-lasting changes in synaptic plasticity and memory formation in the hippocampus, and consequently, memory and synapse loss in AD is mediated by the CREB signalling pathway, among others (Saura & Valero, 2011). Moreover, CREB phosphorylation was in accordance with changes in NMDA activity and synaptic composition promoted by the I<sub>2</sub>-IR ligands **MCR5** and **B06**. Favourable alterations in the involved pathways corroborate our findings. For example, **MCR5** was shown to inhibit NMDA/CDK5/DARPP32 signalling pathway, which regulates CREB phosphorylation (Svenningsson et al., 2004). Particularly, decreased CDK5 activation and p-DARPP32 at Th75 induced by **MCR5** correlated with increased PKA and phosphorylated CREB levels giving further insight into the I<sub>2</sub>-IR mediated CREB signalling enhancement.

Increased synaptic plasticity by I<sub>2</sub>-IR ligands could also be associated with I<sub>2</sub>-IR astrocytic modulation. In fact, astrocytes are involved in synaptic transmission and plasticity mainly, by the reuptake of glutamate, through their membrane glutamate transporters excitatory amino acid transporter 2 (EAAT-2) and EAAT-1 (Oliet et al., 2001). Thus, modulation of astrocytic I<sub>2</sub>-IR receptors by selective ligands may be involved in this process, along with the remarkable modulation of astrocytic GFAP observed. Although this possibility was not investigated in depth in this thesis, our finding regarding the slight increase in EAAT-2 protein levels in the hippocampus of SAMP8 mice after **B06** treatment is relevant.

Interestingly, this is further supported by the observed inhibition of CaN/NFAT after **B06** treatment. Several studies suggest that the CaN/NFAT pathway serves as a putative connection between Ca<sup>2+</sup> dysregulation and glutamate dysregulation in activated astrocytes through EAAT/GLT-1 expression (Sompol & Norris, 2018). Therefore, the direct effect of the I<sub>2</sub>-IR treatment on this pathway and the astrocytic functions related to synaptic transmission and plasticity deserves further investigation.

Along with the cognitive improvement, the reported BPSD alleviation in the AD models might also be attributable to the increased synaptic plasticity delivered by the I<sub>2</sub>-IR ligands treatment. In fact, in the molecular alterations that underlie BPSD, synaptic dysfunction and neurotrophins deficits play a crucial role (Duman, 2002). Interestingly, alterations in synaptic plasticity in stress and depression have been suggested to correlate changes to several signal transduction pathways, including cAMP-PKA, PI3K-AKT, GSK3, mTOR and CREB as well as upstream receptors such as NMDA receptors, TrkB and NGF receptors (Marsden, 2013). Strikingly, I<sub>2</sub>-IR treatment altered these pathways favourably as already discussed for most cases. In this context, we hypothesized that I<sub>2</sub>-IR ligand **MCR5** might deliver antidepressant effects in SAMP8 males through CREB-regulated BDNF restoration, which is found decreased both in AD and depressive hippocampus (Duman, 2002; Ng et al., 2019). In fact, agmatine was found to rescue BPSD in A $\beta$  administered mice by increasing hippocampal BDNF levels (Kotagale et al., 2020). However, unlike the **B06** treatment, which showed to increase *Bdnf* gene expression, in our hands, **MCR5** failed to increase BDNF concentration in the hippocampus of SAMP8 mice. Conversely, treatment with **MCR5** mediated alterations in BDNF receptors (TrkB, NGF receptors) which, together with the observed increases in synaptic plasticity markers, such as PSD95 and upstream factors [mammalian target of rapamycin complex 1 (m-TORC1), p70 S6 kinase (p70S6K)], could result in an enhanced BDNF signalling and, thus, improved BPSD-like phenotype after I<sub>2</sub>-IR treatment.

## 4.7 Combination treatment of I<sub>2</sub>-IR ligand with AChE Inhibitor

Due to the multifactorial pathogenesis of AD, the use of a multimodal therapeutic intervention, such as combination treatments, could be more effective to modify AD progression than monotherapy. Pharmacodynamic combinations for the treatment of AD often consist of symptomatic drugs and disease-modifying therapies. Indeed, disease-modifying agents are currently in clinical trials as add-on therapies to the standard of care, AChE inhibitors or memantine (Cummings et al., 2019; Kabir et al., 2020). As already described, treatment with selective I<sub>2</sub>-IR ligands is able to modify the disease progression in the AD models



used. Therefore, in a comparative study with donepezil, we further investigated possible additive effects after combination treatment with I<sub>2</sub>-IR ligand **LSL60101** and the AChE inhibitor donepezil in the 5XFAD mouse model of AD.

In our study, co-administration of low doses of I<sub>2</sub>-IR ligand **LSL60101** and donepezil did not deliver greater cognitive improvement than the one observed with monotherapies in 5XFAD mice. Moreover, the amelioration of anxiety disturbances observed in the combination treated group compared to I<sub>2</sub>-IR treated mice was attributed to the donepezil treatment. At a molecular level, the beneficial effect of the combination treatment on A $\beta$  pathology, neuroinflammation and synaptic plasticity appeared to be attributable to I<sub>2</sub>-IR treatment, which was greater than donepezil treatment alone in certain parameters (A $\beta$  load, microglial reactivity, synaptic plasticity). Nevertheless, discrete additive effects in the combination treated group were observed in specific processes, such as APP processing and tau pathology, which combination treatment was shown to improve to a greater extent than monotherapies. Although AChE inhibitors are symptomatic drugs, in preclinical studies, donepezil was shown to exert neuroprotective effects against A $\beta$  toxicity (Kimura et al., 2005, p. 200; Meunier et al., 2006), tau pathology and neuroinflammation (Hamano et al., 2013; Yoshiyama et al., 2010), through mechanisms other than inhibition of cholinesterase (S. H. Kim et al., 2017; Takada-Takatori et al., 2009). Thus, the activation of distinct molecular pathways by the I<sub>2</sub>-IR ligand and AChE inhibitor donepezil with different modes of action could explain the effects of combination treatment on these parameters.

The lack of apparent synergistic or additive effects on cognition after I<sub>2</sub>-IR ligand co-treatment with donepezil in the 5XFAD model, could be attributed to parameters related to the selected dosage, paradigms, treatment duration and administration route among others. Indeed, the dosage selection when possible synergy of different drugs is investigated constitutes a pivotal factor (Tallarida, 2011). In our study, we administered the **LSL60101** compound at the lowest reported dose with neuroprotective efficacy for I<sub>2</sub>-IR ligands, while for donepezil, the dose of 1mg/kg was selected based on the literature which reports moderate effects of donepezil treatment in AD mouse models, including the 5XFAD model (Kang et al., 2018; H. Y. Kim et al., 2016; Rochais et al., 2020). Thus, increased dosage and/or duration of the treatment could probably deliver greater beneficial effects on both cognitive status and AD-hallmarks. This is further supported by the moderate additive effects observed on certain molecular markers after combination treatment, which do not rule out the possible synergistic or additive effects of the two drugs. Therefore, albeit further studies are required to assess in depth possible synergy of the drugs, the obtained results provide insights in the combination treatment with I<sub>2</sub>-IR drugs.

## 4.8 Final Considerations

At present, there is increasing recognition of the complexity of AD, the diversity of the pathology and the dynamic interactive network of components that influence the disease progression. AD complexity suggests that for halting its progression, potential therapeutic approaches should interfere with more than one pathogenic step responsible for the clinical symptoms, such as extracellular A $\beta$  plaques, NFTs formation, inflammation, OS. Indeed, treatment with selective I<sub>2</sub>-IR ligands addressed most of these central etiological processes in two preclinical AD models, preventing them from the generalized cognitive downfall (fig. 15).

When interpreting functional results elicited by I<sub>2</sub>-IR ligands, it has proven helpful to consider that I<sub>2</sub>-IR are a heterogeneous group of proteins, which structure remains to be elucidated. Moreover, structural differences among I<sub>2</sub>-IR compounds could lead to binding to I<sub>2</sub>-IR with different affinity and/or selectivity, which, in certain cases, result in inconsistencies in their reported biological effects (Bousquet et al., 2020; J.-X. Li, 2017). Some of these differences were discussed in the present doctoral thesis while reporting the effects of novel I<sub>2</sub>-IR compounds on AD mouse models, jointly with relevant functional results from previous literature. Moreover, it is also important to note that among these studies, there is a variety of pathological conditions, disease models, and I<sub>2</sub>-IR compounds used, which altogether likely account for these functional differences. In this context, I<sub>2</sub>-IR ligands with higher affinity and selectivity for I<sub>2</sub>-IR over other related receptors such as I<sub>1</sub>-IR or  $\alpha_2$ -AR, such as **MCR5**, **MCR9** and **B06** were shown to overcome some of these hurdles, giving better insights into their pharmacological possibilities and the molecular mechanisms whereby the I<sub>2</sub>-IR ligands mediate their action in AD. Indeed, the novel I<sub>2</sub>-IR ligands **MCR5**, **MCR9** and **B06** elicited their pharmacological effects on the major components of AD in a relatively homogeneous way at the dose and experimental conditions tested.

Nevertheless, a lack of structural and molecular information on I<sub>2</sub>-IR denotes a significant challenge in delineating the mechanistic basis of the effects reported. Indeed, although several studies have dealt with the characterization and functional properties of I<sub>2</sub>-IR since their discovery, the complete cascade of events after ligands' binding to I<sub>2</sub>-IR remains to be fully elucidated. Two recently proposed mechanistic pathways underlying the I<sub>2</sub>-IR ligand-induced analgesia involved interactions with the monoaminergic system via MAO inhibition and inhibition of glial activity; however, as explained by the authors, other I<sub>2</sub>-IR mediated behavioural results cannot be fully explained by these mechanisms (Bousquet et al., 2020; Siemian, LaMacchia, et al., 2018; Siemian, Wang, et al., 2018). Our studies, in accordance with the previous literature, suggest a crucial role of I<sub>2</sub>-IR in modulating glial

reactivity; thus, given that glial cells are fundamental players in the evolution of AD able to influence the other AD major components, direct inhibition of glial activity by I<sub>2</sub>-IR ligands may represent an early mechanism underlying the I<sub>2</sub>-IR ligand-induced effects in the AD models used. Further studies are necessary to decipher the importance of glial I<sub>2</sub>-IR modulation by selective compounds and its impact on AD progression.

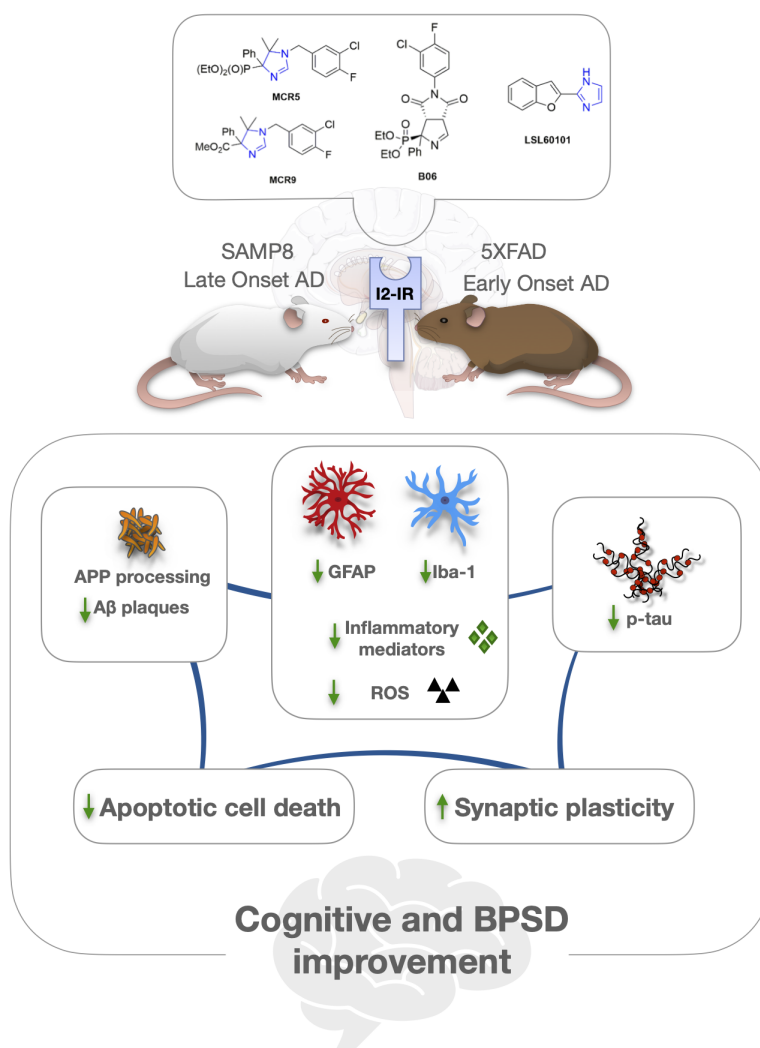


**Figure 15:** Schematic representation of the beneficial effects of novel and well-established I<sub>2</sub>-IR ligands on central AD pathological processes after treatment in SAMP8 and 5XFAD mouse models of AD, delivering neuroprotection and protecting the mice against generalized cognitive downfall and BPSD.



# Chapter 5

## Conclusions

The present doctoral dissertation has shed new insights into the pharmacological possibilities of I<sub>2</sub>-IR. In general, selective I<sub>2</sub>-IR ligands confer neuroprotection in AD mouse models by addressing most of the central etiological processes of the disease. Concretely, the results obtained lead to the following conclusions:

1. Chronic treatment with selective I<sub>2</sub>-IR ligands protects SAMP8 mice, a mouse model of ageing/LOAD, and 5XFAD mice, a mouse model of EOAD, against cognitive impairment.
2. Administration of selective I<sub>2</sub>-IR ligands ameliorates BPSD-like phenotypes addressing anxiety- and depressive-related symptoms and social deficits in aged SAMP8 and 5XFAD mice.
3. Treatment with selective I<sub>2</sub>-IR ligands exerts disease-modifying properties by attenuating AD hallmarks. High affinity and selective I<sub>2</sub>-IR ligands suppress APP amyloidogenic pathway and promote A $\beta$  degradation in aged SAMP8 mice. In 5XFAD mice, low-dose I<sub>2</sub>-IR ligand treatment modifies A $\beta$  pathology by decreasing A $\beta$  peptides levels and plaques in 5XFAD brains. Furthermore, selective I<sub>2</sub>-IR ligands treatments show a robust effect on tau hyperphosphorylation accompanied by alterations in major tau kinases levels (GSK3 $\beta$ , CDK5, ERK1/2).
4. Selective I<sub>2</sub>-IR ligands attenuate the neuroinflammatory process in SAMP8 and 5XFAD mice brains by decreasing astrogliosis, microgliosis and inflammatory cytokines expression; NF- $\kappa$ B signalling appears to be involved in the I<sub>2</sub>-IR anti-inflammatory effects observed after treatment in 5XFAD mice.
5. I<sub>2</sub>-IR ligand treatments deliver an overall beneficial effect against OS damage in AD

mice hippocampus by re-establishing antioxidant defence enzymes and decreasing ROS levels.

6. Treatment with a structurally novel I<sub>2</sub>-IR drug, B06, decreases CaN levels and alters its major downstream components, including NFAT, CREB, BAD and GSK3 $\beta$  levels, allowing to postulate that CaN signalling serves a critical role in I<sub>2</sub>-IR mediated neuroprotection in SAMP8 mice.
7. The neuroprotective effect of I<sub>2</sub>-IR ligand treatments is further reflected by an increase in synaptic plasticity markers (synaptophysin, PSD95) and/or decrease in apoptotic mediators (calpain, caspase-3, Bcl-2, Bax) in SAMP8 and 5XFAD mice, consistently with the cognitive and behavioural improvement of the mice.
8. I<sub>2</sub>-IR ligand, LSL60101, treatment exerts greater effects on AD hallmarks and synaptic plasticity markers than donepezil when administered at a low dose of 1 mg/kg/day. Although combination low-dose treatment of I<sub>2</sub>-IR ligand with donepezil did not show clear synergy in 5XFAD mice, discrete synergistic effects were observed at the molecular level (tau hyperphosphorylation and synaptic plasticity) in 5XFAD mice.
9. I<sub>2</sub>-IR modulation by selective ligands could be a novel therapeutic strategy against AD.

# Bibliography

- 2021 Alzheimer's disease facts and figures - 2021 - Alzheimer's & Dementia - Wiley Online Library. Retrieved June 12, 2021, from <https://alz-journals.onlinelibrary.wiley.com/doi/10.1002/alz.12328>
- Abás, S., Erdozain, A. M., Keller, B., Rodríguez-Arévalo, S., Callado, L. F., García-Sevilla, J. A., & Escolano, C. (2017). Neuroprotective Effects of a Structurally New Family of High Affinity Imidazoline I2 Receptor Ligands. *ACS Chem Neurosci*, 8(4), 737–742. <https://doi.org/10.1021/acchemneuro.6b00426>
- Abás, S., Rodríguez-Arévalo, S., Bagán, A., Griñán-Ferré, C., Vasilopoulou, F., Brocos-Mosquera, I., Muguruza, C., Pérez, B., Molins, E., Luque, F. J., Pérez-Lozano, P., de Jonghe, S., Daelemans, D., Naesens, L., Brea, J., Loza, M. I., Hernández-Hernández, E., García-Sevilla, J. A., García-Fuster, M. J., . . . Escolano, C. (2020). Bicyclic  $\alpha$ -Iminophosphonates as High Affinity Imidazoline I2 Receptor Ligands for Alzheimer's Disease. *J Med Chem*, 63(7), 3610–3633. <https://doi.org/10.1021/acs.jmedchem.9b02080>
- Abdul, H. M., Baig, I., LeVine 3rd, H., Guttmann, R. P., & Norris, C. M. (2011). Proteolysis of calcineurin is increased in human hippocampus during mild cognitive impairment and is stimulated by oligomeric Abeta in primary cell culture [eprint: <https://onlinelibrary.wiley.com/doi/pdf/10.1111/j.1474-9726.2010.00645.x>]. *Aging Cell*, 10(1), 103–113. <https://doi.org/10.1111/j.1474-9726.2010.00645.x>
- Abdul, H. M., Furman, J. L., Sama, M. A., Mathis, D. M., & Norris, C. M. (2010). NFATs and Alzheimer's Disease. *Mol Cell Pharmacol*, 2(1), 7–14. Retrieved June 13, 2021, from <https://www.ncbi.nlm.nih.gov/pmc/articles/PMC2855852/>
- Abdul, H. M., Sama, M. A., Furman, J. L., Mathis, D. M., Beckett, T. L., Weidner, A. M., Patel, E. S., Baig, I., Murphy, M. P., LeVine, H., Kraner, S. D., & Norris, C. M. (2009). Cognitive decline in Alzheimer's disease is associated with selective

- changes in calcineurin/NFAT signaling. *J Neurosci*, 29(41), 12957–12969. <https://doi.org/10.1523/JNEUROSCI.1064-09.2009>
- Abe, K., Abe, Y., & Saito, H. (2000). Agmatine suppresses nitric oxide production in microglia. *Brain research*, 872(1-2), 141–148.
- Ahn, S. K., Hong, S., Park, Y. M., Choi, J. Y., Lee, W. T., Park, K. A., & Lee, J. E. (2012). Protective effects of agmatine on lipopolysaccharide-injured microglia and inducible nitric oxide synthase activity. *Life Sciences*, 91(25), 1345–1350. <https://doi.org/10.1016/j.lfs.2012.10.010>
- Akiguchi, I., Pallàs, M., Budka, H., Akiyama, H., Ueno, M., Han, J., Yagi, H., Nishikawa, T., Chiba, Y., Sugiyama, H., Takahashi, R., Unno, K., Higuchi, K., & Hosokawa, M. (2017). SAMP8 mice as a neuropathological model of accelerated brain aging and dementia: Toshio Takeda's legacy and future directions: SAMP8 as a model of aging and dementia. *Neuropathology*, 37(4), 293–305. <https://doi.org/10.1111/neup.12373>
- Alahari, S. K., Lee, J. W., & Juliano, R. L. (2000). Nischarin, a novel protein that interacts with the integrin alpha5 subunit and inhibits cell migration. *The Journal of cell biology*, 151(6), 1141–1154. <https://doi.org/10.1083/jcb.151.6.1141>
- Alderson, R. F., Alterman, A. L., Barde, Y. A., & Lindsay, R. M. (1990). Brain-derived neurotrophic factor increases survival and differentiated functions of rat septal cholinergic neurons in culture. *Neuron*, 5(3), 297–306. [https://doi.org/10.1016/0896-6273\(90\)90166-d](https://doi.org/10.1016/0896-6273(90)90166-d)
- Aleman, R., Olmos, G., Escribá, P. V., Menargues, A., Obach, R., & García-Sevilla, J. A. (1995a). LSL 60101, a selective ligand for imidazoline I2 receptors, on glial fibrillary acidic protein concentration. *Eur J Pharmacol*, 280(2), 205–210. [https://doi.org/10.1016/0014-2999\(95\)00214-6](https://doi.org/10.1016/0014-2999(95)00214-6)
- Aleman, R., Olmos, G., & García-Sevilla, J. A. (1995b). Chronic treatment with phenelzine and other irreversible monoamine oxidase inhibitors downregulates I2-imidazoline receptors in the brain and liver. *Ann N Y Acad Sci*, 763, 506–509. <https://doi.org/10.1111/j.1749-6632.1995.tb32442.x>
- Alexander, S. P. H., Mathie, A., & Peters, J. A. (2011). Guide to Receptors and Channels (GRAC), 5th edition [Publisher: John Wiley & Sons, Ltd]. *British Journal of Pharmacology*, 164(s1), S1–S2. [https://doi.org/10.1111/j.1476-5381.2011.01649\\_1.x](https://doi.org/10.1111/j.1476-5381.2011.01649_1.x)
- Allen, S. J., Watson, J. J., & Dawbarn, D. (2011). The Neurotrophins and Their Role in Alzheimer's Disease. *Curr Neuropharmacol*, 9(4), 559–573. <https://doi.org/10.2174/157015911798376190>
- Amadoro, G., Corsetti, V., Atlante, A., Florenzano, F., Capsoni, S., Bussani, R., Mercanti, D., & Calissano, P. (2012). Interaction between NH(2)-tau fragment and A $\beta$  in



- Alzheimer's disease mitochondria contributes to the synaptic deterioration. *Neurobiol Aging*, 33(4), 833.e1–25. <https://doi.org/10.1016/j.neurobiolaging.2011.08.001>
- Amor, S., & Woodroffe, M. N. (2014). Innate and adaptive immune responses in neurodegeneration and repair. *Immunology*, 141(3), 287–291. <https://doi.org/10.1111/imm.12134>
- Anderson, N. J., Seif, I., Nutt, D. J., Hudson, A. L., & Robinson, E. S. J. (2006a). Autoradiographical distribution of imidazoline binding sites in monoamine oxidase A deficient mice. *J Neurochem*, 96(6), 1551–1559. <https://doi.org/10.1111/j.1471-4159.2006.03662.x>
- Anderson, N. J., Tyacke, R. J., Husbands, S. M., Nutt, D. J., Hudson, A. L., & Robinson, E. S. (2006b). In vitro and ex vivo distribution of [3h] harmaline, an endogenous  $\beta$ -carboline, in rat brain. *Neuropharmacology*, 50(3), 269–276.
- Apostolova, L. G., Green, A. E., Babakchian, S., Hwang, K. S., Chou, Y.-Y., Toga, A. W., & Thompson, P. M. (2012). Hippocampal atrophy and ventricular enlargement in normal aging, mild cognitive impairment (MCI), and Alzheimer Disease. *Alzheimer Dis Assoc Disord*, 26(1), 17–27. <https://doi.org/10.1097/WAD.0b013e3182163b62>
- Aricioglu, F., & Altunbas, H. (2003). Harmaline induces anxiolysis and antidepressant-like effects in rats. *Ann N Y Acad Sci*, 1009, 196–201. <https://doi.org/10.1196/annals.1304.024>
- Armbrecht, H. J., Boltz, M. A., Kumar, V. B., Flood, J. F., & Morley, J. E. (1999). Effect of age on calcium-dependent proteins in hippocampus of senescence-accelerated mice. *Brain Res*, 842(2), 287–293. [https://doi.org/10.1016/s0006-8993\(99\)01802-8](https://doi.org/10.1016/s0006-8993(99)01802-8)
- Armstrong, J., & Boura, A. (1973). Effects of clonidine and guanethidine on peripheral sympathetic nerve function in the pithed rat. *British journal of pharmacology*, 47(4), 850–852.
- Armstrong, R. A. (2019). Risk factors for Alzheimer's disease. *Folia Neuropathol*, 57(2), 87–105.
- Arriagada, P. V., Growdon, J. H., Hedley-Whyte, E. T., & Hyman, B. T. (1992). Neurofibrillary tangles but not senile plaques parallel duration and severity of Alzheimer's disease. *Neurology*, 42(3 Pt 1), 631–639. <https://doi.org/10.1212/wnl.42.3.631>
- Atlas, D., & Burstein, Y. (1984). Isolation and partial purification of a clonidine-displacing endogenous brain substance. *Eur J Biochem*, 144(2), 287–293. <https://doi.org/10.1111/j.1432-1033.1984.tb08462.x>
- Babbar, M., & Sheikh, M. S. (2013). Metabolic Stress and Disorders Related to Alterations in Mitochondrial Fission or Fusion. *Mol Cell Pharmacol*, 5(3), 109–133.
- Baharudin, A. D., Din, N. C., Subramaniam, P., & Razali, R. (2019). The associations between behavioral-psychological symptoms of dementia (BPSD) and coping strategy, burden of care and personality style among low-income caregivers of

- patients with dementia. *BMC Public Health*, 19(Suppl 4), 447. <https://doi.org/10.1186/s12889-019-6868-0>
- Baki, L., Shioi, J., Wen, P., Shao, Z., Schwarzman, A., Gama-Sosa, M., Neve, R., & Robakis, N. K. (2004). Ps1 activates pi3k thus inhibiting gsk-3 activity and tau overphosphorylation: Effects of fad mutations. *The EMBO journal*, 23(13), 2586–2596.
- Ballard, C., & Corbett, A. (2010). Management of neuropsychiatric symptoms in people with dementia. *CNS drugs*, 24(9), 729–739.
- Ballesteros, J., Maeztu, A. I., Callado, L. F., Gutiérrez, M., García-Sevilla, J. A., & Meana, J. J. (2000). I2-Imidazoline receptors and monoamine oxidase B enzyme sites in human brain: Covariation with age. *Neurosci Lett*, 288(2), 135–138. [https://doi.org/10.1016/s0304-3940\(00\)01218-0](https://doi.org/10.1016/s0304-3940(00)01218-0)
- Bamberger, M. E., & Landreth, G. E. (2002). Inflammation, apoptosis, and alzheimer's disease. *The Neuroscientist*, 8(3), 276–283.
- Banks, W. A., Farr, S. A., Morley, J. E., Wolf, K. M., Geylis, V., & Steinitz, M. (2007). Anti-amyloid beta protein antibody passage across the blood-brain barrier in the SAMP8 mouse model of Alzheimer's disease: An age-related selective uptake with reversal of learning impairment. *Exp Neurol*, 206(2), 248–256. <https://doi.org/10.1016/j.expneurol.2007.05.005>
- Barzilai, A. (2010). DNA damage, neuronal and glial cell death and neurodegeneration. *Apoptosis*, 15(11), 1371–1381. <https://doi.org/10.1007/s10495-010-0501-0>
- Baumann, K., Mandelkow, E.-M., Biernat, J., Piwnica-Worms, H., & Mandelkow, E. (1993). Abnormal alzheimer-like phosphorylation of tau-protein by cyclin-dependent kinases cdk2 and cdk5. *FEBS letters*, 336(3), 417–424.
- Berkels, R., Taubert, D., Gründemann, D., & Schömig, E. (2004). Agmatine signaling: Odds and threads. *Cardiovasc Drug Rev*, 22(1), 7–16. <https://doi.org/10.1111/j.1527-3466.2004.tb00128.x>
- Bhutada, P., Mundhada, Y., Humane, V., Rahigude, A., Deshmukh, P., Latad, S., & Jain, K. (2012). Agmatine, an endogenous ligand of imidazoline receptor protects against memory impairment and biochemical alterations in streptozotocin-induced diabetic rats. *Prog Neuropsychopharmacol Biol Psychiatry*, 37(1), 96–105. <https://doi.org/10.1016/j.pnpbp.2012.01.009>
- Bilge, S. S., Günaydin, C., Önger, M. E., Bozkurt, A., & Avcı, B. (2020). Neuroprotective action of agmatine in rotenone-induced model of Parkinson's disease: Role of BDNF/cREB and ERK pathway. *Behav Brain Res*, 392, 112692. <https://doi.org/10.1016/j.bbr.2020.112692>
- Billingsley, M. L., & Kincaid, R. L. (1997). Regulated phosphorylation and dephosphorylation of tau protein: Effects on microtubule interaction, intracellular trafficking

- and neurodegeneration. *Biochem J*, 323 ( Pt 3), 577–591. <https://doi.org/10.1042/bj3230577>
- Bloom, G. S. (2014). Amyloid- $\beta$  and tau: The trigger and bullet in Alzheimer disease pathogenesis. *JAMA Neurol*, 71(4), 505–508. <https://doi.org/10.1001/jamaneurol.2013.5847>
- Bojarski, L., Herms, J., & Kuznicki, J. (2008). Calcium dysregulation in Alzheimer's disease. *Neurochemistry International*, 52(4-5), 621–633. <https://doi.org/10.1016/j.neuint.2007.10.002>
- Boronat, M. A., Olmos, G., & García-Sevilla, J. A. (1998). Attenuation of tolerance to opioid-induced antinociception and protection against morphine-induced decrease of neurofilament proteins by idazoxan and other  $\alpha$ -imidazoline ligands. *British journal of pharmacology*, 125(1), 175–185.
- Bousquet, P., Feldman, J., Bloch, R., & Schwartz, J. (1981). The nucleus reticularis lateralis: A region highly sensitive to clonidine. *European journal of pharmacology*, 69(3), 389–392. [https://doi.org/10.1016/0014-2999\(81\)90490-8](https://doi.org/10.1016/0014-2999(81)90490-8)
- Bousquet, P., Feldman, J., & Schwartz, J. (1984). Central cardiovascular effects of alpha adrenergic drugs: Differences between catecholamines and imidazolines. *Journal of Pharmacology and Experimental Therapeutics*, 230(1), 232–236.
- Bousquet, P., Hudson, A., García-Sevilla, J. A., & Li, J.-X. (2020). Imidazoline Receptor System: The Past, the Present, and the Future. *Pharmacol Rev*, 72(1), 50–79. <https://doi.org/10.1124/pr.118.016311>
- Boyajian, C. L., Loughlin, S. E., & Leslie, F. M. (1987). Anatomical evidence for alpha-2 adrenoceptor heterogeneity: Differential autoradiographic distributions of [ $^3$ H]rauwolscine and [ $^3$ H]idazoxan in rat brain. *The Journal of pharmacology and experimental therapeutics*, 241(3), 1079–1091.
- Bozdagi, O., Wang, X., Martinelli, G. P., Prell, G, Friedrich Jr, V. L., Huntley, G. W., & Holstein, G. R. (2011). Imidazoleacetic acid-ribotide induces depression of synaptic responses in hippocampus through activation of imidazoline receptors. *Journal of neurophysiology*, 105(3), 1266–1275.
- Bradley-Whitman, M. A., & Lovell, M. A. (2013). Epigenetic changes in the progression of Alzheimer's disease. *Mech Ageing Dev*, 134(10), 486–495. <https://doi.org/10.1016/j.mad.2013.08.005>
- Breitner, J. C., Baker, L. D., Montine, T. J., Meinert, C. L., Lyketsos, C. G., Ashe, K. H., Brandt, J., Craft, S., Evans, D. E., Green, R. C., Ismail, M. S., Martin, B. K., Mullan, M. J., Sabbagh, M., Tariot, P. N., & ADAPT Research Group. (2011). Extended results of the Alzheimer's disease anti-inflammatory prevention trial. *Alzheimers Dement*, 7(4), 402–411. <https://doi.org/10.1016/j.jalz.2010.12.014>
- Bricca, G, Dontenwill, M, Molines, A, Feldman, J, Belcourt, A, & Bousquet, P. (1988). Evidence for the existence of a homogeneous population of imidazoline receptors

- in the human brainstem. *European journal of pharmacology*, 150(3), 401–402. [https://doi.org/10.1016/0014-2999\(88\)90028-3](https://doi.org/10.1016/0014-2999(88)90028-3)
- Bricca, G, Dontenwill, M, Molines, A, Feldman, J, Belcourt, A, & Bousquet, P. (1989). The imidazoline preferring receptor: Binding studies in bovine, rat and human brainstem. *European journal of pharmacology*, 162(1), 1–9. [https://doi.org/10.1016/0014-2999\(89\)90597-9](https://doi.org/10.1016/0014-2999(89)90597-9)
- Bricca, G, Greney, H, Zhang, J, Dontenwill, M, Stutzmann, J, Belcourt, A, & Bousquet, P. (1994). Human brain imidazoline receptors: Further characterization with [3H]clonidine. *European journal of pharmacology*, 266(1), 25–33. [https://doi.org/10.1016/0922-4106\(94\)90205-4](https://doi.org/10.1016/0922-4106(94)90205-4)
- Bricca, G, Zhang, J, Greney, H, Dontenwill, M, Stutzmann, J, Belcourt, A, & Bousquet, P. (1993). Relevance of the use of [3H]-clonidine to identify imidazoline receptors in the rabbit brainstem. *British journal of pharmacology*, 110(4), 1537–1543. <https://doi.org/10.1111/j.1476-5381.1993.tb13998.x>
- Bruban, V, Feldman, J, Greney, H, Dontenwill, M, Schann, S, Jarry, C, Payard, M, Boutin, J, Scalbert, E, Pfeiffer, B, Renard, P, Vanhoutte, P, & Bousquet, P. (2001). Respective contributions of alpha-adrenergic and non-adrenergic mechanisms in the hypotensive effect of imidazoline-like drugs. *British journal of pharmacology*, 133(2), 261–266. <https://doi.org/10.1038/sj.bjp.0704080>
- Bruban, V., Estato, V., Schann, S., Ehrhardt, J.-D., Monassier, L., Renard, P., Scalbert, E., Feldman, J., & Bousquet, P. (2002). Evidence for synergy between alpha(2)-adrenergic and nonadrenergic mechanisms in central blood pressure regulation. *Circulation*, 105(9), 1116–1121. <https://doi.org/10.1161/hc0802.104328>
- Busciglio, J., Lorenzo, A., Yeh, J., & Yankner, B. A. (1995). -amyloid fibrils induce tau phosphorylation and loss of microtubule binding. *Neuron*, 14(4), 879–888. [https://doi.org/https://doi.org/10.1016/0896-6273\(95\)90232-5](https://doi.org/https://doi.org/10.1016/0896-6273(95)90232-5)
- Buskila, Y., Crowe, S. E., & Ellis-Davies, G. C. (2013). Synaptic deficits in layer 5 neurons precede overt structural decay in 5xfad mice. *Neuroscience*, 254, 152–159.
- Butterfield, D. A., Howard, B. J., Yatin, S., Allen, K. L., & Carney, J. M. (1997). Free radical oxidation of brain proteins in accelerated senescence and its modulation by n-tert-butyl- $\alpha$ -phenylnitron. *Proceedings of the National Academy of Sciences*, 94(2), 674–678.
- Butterfield, D. A., & Lauderback, C. M. (2002). Lipid peroxidation and protein oxidation in Alzheimer's disease brain: Potential causes and consequences involving amyloid beta-peptide-associated free radical oxidative stress. *Free Radic Biol Med*, 32(11), 1050–1060. [https://doi.org/10.1016/s0891-5849\(02\)00794-3](https://doi.org/10.1016/s0891-5849(02)00794-3)
- Butterfield, D. A., & Poon, H. F. (2005). The senescence-accelerated prone mouse (SAMP8): A model of age-related cognitive decline with relevance to alterations of

- the gene expression and protein abnormalities in Alzheimer's disease. *Exp Gerontol*, 40(10), 774–783. <https://doi.org/10.1016/j.exger.2005.05.007>
- Byers, A. L., Covinsky, K. E., Barnes, D. E., & Yaffe, K. (2012). Dysthymia and depression increase risk of dementia and mortality among older veterans. *Am J Geriatr Psychiatry*, 20(8), 664–672. <https://doi.org/10.1097/JGP.0b013e31822001c1>
- Cacace, R., Slegers, K., & Van Broeckhoven, C. (2016). Molecular genetics of early-onset Alzheimer's disease revisited. *Alzheimers Dement*, 12(6), 733–748. <https://doi.org/10.1016/j.jalz.2016.01.012>
- Cai, Z. (2014). Monoamine oxidase inhibitors: Promising therapeutic agents for Alzheimer's disease (Review). *Mol Med Rep*, 9(5), 1533–1541. <https://doi.org/10.3892/mmr.2014.2040>
- Cai, Z., Yan, L.-J., Li, K., Quazi, S. H., & Zhao, B. (2012). Roles of amp-activated protein kinase in alzheimer's disease. *Neuromolecular medicine*, 14(1), 1–14.
- Calissano, P., Matrone, C., & Amadoro, G. (2009). Apoptosis and in vitro Alzheimer disease neuronal models. *Commun Integr Biol*, 2(2), 163–169. Retrieved June 13, 2021, from <https://www.ncbi.nlm.nih.gov/pmc/articles/PMC2686374/>
- Campion, D., Dumanchin, C., Hannequin, D., Dubois, B., Belliard, S., Puel, M., Thomas-Anterion, C., Michon, A., Martin, C., Charbonnier, F., Raux, G., Camuzat, A., Penet, C., Mesnage, V., Martinez, M., Clerget-Darpoux, F., Brice, A., & Frebourg, T. (1999). Early-onset autosomal dominant Alzheimer disease: Prevalence, genetic heterogeneity, and mutation spectrum. *Am J Hum Genet*, 65(3), 664–670. <https://doi.org/10.1086/302553>
- Canudas, A. M., Gutierrez-Cuesta, J., Rodríguez, M. I., Acuña-Castroviejo, D., Sureda, F. X., Camins, A., & Pallàs, M. (2005). Hyperphosphorylation of microtubule-associated protein tau in senescence-accelerated mouse (SAM). *Mech Ageing Dev*, 126(12), 1300–1304. <https://doi.org/10.1016/j.mad.2005.07.008>
- Canudas, A. M., Pubill, D., Sureda, F. X., Verdaguer, E., Camps, P., Muñoz-Torrero, D., Jiménez, A., Camins, A., & Pallàs, M. (2003). Neuroprotective effects of (+/-)-huprine Y on in vitro and in vivo models of excitotoxicity damage. *Exp Neurol*, 180(2), 123–130. [https://doi.org/10.1016/s0014-4886\(02\)00029-8](https://doi.org/10.1016/s0014-4886(02)00029-8)
- Carpéné, C., Collon, P., Remaury, A., Cordi, A., Hudson, A., Nutt, D., & Lafontan, M. (1995). Inhibition of amine oxidase activity by derivatives that recognize imidazoline I2 sites. *J Pharmacol Exp Ther*, 272(2), 681–688.
- Casanovas, A., Olmos, G., Ribera, J., Boronat, M. A., Esquerda, J. E., & García-Sevilla, J. A. (2000). Induction of reactive astrocytosis and prevention of motoneuron cell death by the I(2)-imidazoline receptor ligand LSL 60101. *Br J Pharmacol*, 130(8), 1767–1776. <https://doi.org/10.1038/sj.bjp.0703485>
- Chai, J., Luo, L., Hou, F., Fan, X., Yu, J., Ma, W., Tang, W., Yang, X., Zhu, J., Kang, W., Yan, J., & Liang, H. (2016). Agmatine Reduces Lipopolysaccharide-Mediated

- Oxidant Response via Activating PI3K/Akt Pathway and Up-Regulating Nrf2 and HO-1 Expression in Macrophages (F. Gallyas, Ed.). *PLoS ONE*, *11*(9), e0163634. <https://doi.org/10.1371/journal.pone.0163634>
- Chakraborty, S., Lennon, J. C., Malkaram, S. A., Zeng, Y., Fisher, D. W., & Dong, H. (2019). Serotonergic System, Cognition, and BPSD in Alzheimer's disease. *Neurosci Lett*, *704*, 36–44. <https://doi.org/10.1016/j.neulet.2019.03.050>
- Chan, S. L., Brown, C. A., Scarpello, K. E., & Morgan, N. G. (1994). The imidazoline site involved in control of insulin secretion: Characteristics that distinguish it from I1- and I2-sites. *British journal of pharmacology*, *112*(4), 1065–1070. <https://doi.org/10.1111/j.1476-5381.1994.tb13191.x>
- Cheignon, C., Tomas, M., Bonnefont-Rousselot, D., Faller, P., Hureau, C., & Collin, F. (2018). Oxidative stress and the amyloid beta peptide in Alzheimer's disease. *Redox Biol*, *14*, 450–464. <https://doi.org/10.1016/j.redox.2017.10.014>
- Chen, G.-H., Wang, C., Yangcheng, H.-Y., Liu, R.-Y., & Zhou, J.-N. (2007). Age-related changes in anxiety are task-specific in the senescence-accelerated prone mouse 8. *Physiol Behav*, *91*(5), 644–651. <https://doi.org/10.1016/j.physbeh.2007.03.023>
- Chen, L., Na, R., Gu, M., Richardson, A., & Ran, Q. (2008). Lipid peroxidation up-regulates BACE1 expression in vivo: A possible early event of amyloidogenesis in Alzheimer's disease. *J Neurochem*, *107*(1), 197–207. <https://doi.org/10.1111/j.1471-4159.2008.05603.x>
- Chen, Y., Dang, M., & Zhang, Z. (2021). Brain mechanisms underlying neuropsychiatric symptoms in Alzheimer's disease: A systematic review of symptom-general and -specific lesion patterns. *Mol Neurodegener*, *16*, 38. <https://doi.org/10.1186/s13024-021-00456-1>
- Chen, Y., Qin, C., Huang, J., Tang, X., Liu, C., Huang, K., Xu, J., Guo, G., Tong, A., & Zhou, L. (2020). The role of astrocytes in oxidative stress of central nervous system: A mixed blessing. *Cell Prolif*, *53*(3). <https://doi.org/10.1111/cpr.12781>
- Chen, Z.-D., Chen, W.-Q., Wang, Z.-Y., Cao, D.-N., Wu, N., & Li, J. (2018). Antidepressant-like action of agmatine in the acute and sub-acute mouse models of depression: A receptor mechanism study. *Metab Brain Dis*, *33*(5), 1721–1731. <https://doi.org/10.1007/s11011-018-0280-9>
- Cho, H.-J., Sharma, A. K., Zhang, Y., Gross, M. L., & Mirica, L. M. (2020). A Multifunctional Chemical Agent as an Attenuator of Amyloid Burden and Neuroinflammation in Alzheimer's Disease. *ACS Chem. Neurosci.*, *11*(10), 1471–1481. <https://doi.org/10.1021/acscchemneuro.0c00114>
- Choi, D.-H., Yun, J. H., & Lee, J. (2018). Protective effect of the imidazoline I2 receptor agonist 2-BFI on oxidative cytotoxicity in astrocytes. *Biochem Biophys Res Commun*, *503*(4), 3011–3016. <https://doi.org/10.1016/j.bbrc.2018.08.086>

- Choi, S.-H., Choi, D.-H., Lee, J.-J., Park, M.-S., & Chun, B.-G. (2002). Imidazoline drugs stabilize lysosomes and inhibit oxidative cytotoxicity in astrocytes. *Free Radic Biol Med*, 32(5), 394–405. [https://doi.org/10.1016/s0891-5849\(01\)00819-x](https://doi.org/10.1016/s0891-5849(01)00819-x)
- Chow, V. W., Mattson, M. P., Wong, P. C., & Gleichmann, M. (2010). An overview of APP processing enzymes and products. *Neuromolecular Med*, 12(1), 1–12. <https://doi.org/10.1007/s12017-009-8104-z>
- Cicognola, C., Hansson, O., Scheltens, P., Kvartsberg, H., Zetterberg, H., Teunissen, C. E., & Blennow, K. (2021). Cerebrospinal fluid N-224 tau helps discriminate Alzheimer's disease from subjective cognitive decline and other dementias. *Alzheimer's Research & Therapy*, 13(1), 38. <https://doi.org/10.1186/s13195-020-00756-6>
- Cioffi, F., Adam, R. H. I., & Broersen, K. Molecular Mechanisms and Genetics of Oxidative Stress in Alzheimer's Disease. *J Alzheimers Dis*, 72(4), 981–1017. <https://doi.org/10.3233/JAD-190863>
- Cloak, N., & Al Khalili, Y. Behavioral And Psychological Symptoms In Dementia. eng. In: *StatPearls*. Treasure Island (FL): StatPearls Publishing, 2021. Retrieved June 13, 2021, from <http://www.ncbi.nlm.nih.gov/books/NBK551552/>
- Colom-Cadena, M., Spires-Jones, T., Zetterberg, H., Blennow, K., Caggiano, A., DeKosky, S. T., Fillit, H., Harrison, J. E., Schneider, L. S., Scheltens, P., et al. (2020). The clinical promise of biomarkers of synapse damage or loss in alzheimer's disease. *Alzheimer's research & therapy*, 12(1), 1–12.
- Colovic, M. B., Krstic, D. Z., Lazarevic-Pasti, T. D., Bondzic, A. M., & Vasic, V. M. (2013). Acetylcholinesterase inhibitors: Pharmacology and toxicology. *Current neuropharmacology*, 11(3), 315–335.
- Comi, E., Lanza, M., Ferrari, F., Mauri, V., Caselli, G., & Rovati, L. C. (2017). Efficacy of CR4056, a first-in-class imidazoline-2 analgesic drug, in comparison with naproxen in two rat models of osteoarthritis. *J Pain Res*, 10, 1033–1043. <https://doi.org/10.2147/JPR.S132026>
- Counts, S. E., Nadeem, M., Lad, S. P., Wu, J., & Mufson, E. J. (2006). Differential expression of synaptic proteins in the frontal and temporal cortex of elderly subjects with mild cognitive impairment. *J Neuropathol Exp Neurol*, 65(6), 592–601. <https://doi.org/10.1097/00005072-200606000-00007>
- Coupry, I., Atlas, D., Podevin, R. A., Uzielli, I., & Parini, A. (1990). Imidazoline-guanidinium receptive site in renal proximal tubule: Asymmetric distribution, regulation by cations and interaction with an endogenous clonidine displacing substance. *J Pharmacol Exp Ther*, 252(1), 293–299.
- Cummings, J., Lee, G., Ritter, A., Sabbagh, M., & Zhong, K. (2020). Alzheimer's disease drug development pipeline: 2020. *Alzheimer's & Dementia: Translational Research & Clinical Interventions*, 6(1), e12050.

- Cummings, J., Lee, G., Zhong, K., Fonseca, J., & Taghva, K. (2021). Alzheimer's disease drug development pipeline: 2021. *Alzheimer's & Dementia: Translational Research & Clinical Interventions*, 7(1), e12179.
- Cummings, J. L., Tong, G., & Ballard, C. (2019). Treatment Combinations for Alzheimer's Disease: Current and Future Pharmacotherapy Options. *J Alzheimers Dis*, 67(3), 779–794. <https://doi.org/10.3233/JAD-180766>
- Daniilidou, M, Koutroumani, M, & Tsolaki, M. (2011). Epigenetic mechanisms in alzheimer's disease. *Current medicinal chemistry*, 18(12), 1751–1756.
- Danysz, W., & Parsons, C. G. (2012). Alzheimer's disease,  $\beta$ -amyloid, glutamate, nmda receptors and memantine—searching for the connections. *British journal of pharmacology*, 167(2), 324–352.
- David, D. J., Wang, J., Samuels, B. A., Rainer, Q., David, I., Gardier, A. M., & Hen, R. (2010). Implications of the Functional Integration of Adult-Born Hippocampal Neurons in Anxiety-Depression Disorders. *Neuroscientist*, 16(5), 578–591. <https://doi.org/10.1177/1073858409360281>
- de Wilde, M. C., Overk, C. R., Sijben, J. W., & Masliah, E. (2016). Meta-analysis of synaptic pathology in Alzheimer's disease reveals selective molecular vesicular machinery vulnerability. *Alzheimers Dement*, 12(6), 633–644. <https://doi.org/10.1016/j.jalz.2015.12.005>
- De Vos, H., Bricca, G., De Keyser, J., De Backer, J. P., Bousquet, P., & Vauquelin, G. (1994). Imidazoline receptors, non-adrenergic idazoxan binding sites and alpha 2-adrenoceptors in the human central nervous system. *Neuroscience*, 59(3), 589–598. [https://doi.org/10.1016/0306-4522\(94\)90179-1](https://doi.org/10.1016/0306-4522(94)90179-1)
- De Vos, H, Convents, A, De Keyser, J, De Backer, J. P., Van Megen, I. J., Ebinger, G, & Vauquelin, G. (1991). Autoradiographic distribution of alpha 2 adrenoceptors, NAIBS, and 5-HT1A receptors in human brain using [3H]idazoxan and [3H]rauwolscine. *Brain research*, 566(1-2), 13–20. [https://doi.org/10.1016/0006-8993\(91\)91675-q](https://doi.org/10.1016/0006-8993(91)91675-q)
- Deary, I. J., Corley, J., Gow, A. J., Harris, S. E., Houlihan, L. M., Marioni, R. E., Penke, L., Rafnsson, S. B., & Starr, J. M. (2009). Age-associated cognitive decline. *Br Med Bull*, 92, 135–152. <https://doi.org/10.1093/bmb/ldp033>
- Degregorio-Rocasolano, N, Olmos, G, Gasull, T, Boronat, M., Trullas, R, & García-Sevilla, J. (1999). Protection by imidazol (ine) compounds of l-glutamate neurotoxicity through nmda receptor blockade. *Annals of the New York Academy of Sciences*, 881(1), 452–452.
- DeKosky, S. T., & Scheff, S. W. (1990). Synapse loss in frontal cortex biopsies in Alzheimer's disease: Correlation with cognitive severity. *Ann Neurol*, 27(5), 457–464. <https://doi.org/10.1002/ana.410270502>



- DeTure, M. A., & Dickson, D. W. (2019). The neuropathological diagnosis of Alzheimer's disease. *Mol Neurodegener*, *14*(1), 32. <https://doi.org/10.1186/s13024-019-0333-5>
- Devanand, D. P., & Schultz, S. K. (2011). Consequences of antipsychotic medications for the dementia patient. *Am J Psychiatry*, *168*(8), 767–769. <https://doi.org/10.1176/appi.ajp.2011.11040629>
- Deverman, B. E., & Patterson, P. H. (2009). Cytokines and cns development. *Neuron*, *64*(1), 61–78.
- Diamant, S., Eldar-Geva, T., & Atlas, D. (1992). Imidazoline binding sites in human placenta: Evidence for heterogeneity and a search for physiological function. *British journal of pharmacology*, *106*(1), 101–108. <https://doi.org/10.1111/j.1476-5381.1992.tb14300.x>
- Diaz, A., Mayet, S., & Dickenson, A. H. (1997). BU-224 produces spinal antinociception as an agonist at imidazoline I2 receptors. *European journal of pharmacology*, *333*(1), 9–15. [https://doi.org/10.1016/s0014-2999\(97\)01118-7](https://doi.org/10.1016/s0014-2999(97)01118-7)
- Dickerson, B. C., Stoub, T. R., Shah, R. C., Sperling, R. A., Killiany, R. J., Albert, M. S., Hyman, B. T., Blacker, D., & Detoleto-Morrell, L. (2011). Alzheimer-signature MRI biomarker predicts AD dementia in cognitively normal adults. *Neurology*, *76*(16), 1395–1402. <https://doi.org/10.1212/WNL.0b013e3182166e96>
- Dickerson, B. C., Bakkour, A., Salat, D. H., Feczko, E., Pacheco, J., Greve, D. N., Grodstein, F., Wright, C. I., Blacker, D., Rosas, H. D., Sperling, R. A., Atri, A., Growdon, J. H., Hyman, B. T., Morris, J. C., Fischl, B., & Buckner, R. L. (2009a). The cortical signature of Alzheimer's disease: Regionally specific cortical thinning relates to symptom severity in very mild to mild AD dementia and is detectable in asymptomatic amyloid-positive individuals. *Cereb Cortex*, *19*(3), 497–510. <https://doi.org/10.1093/cercor/bhn113>
- Dickerson, B. C., Feczko, E., Augustinack, J. C., Pacheco, J., Morris, J. C., Fischl, B., & Buckner, R. L. (2009b). Differential effects of aging and Alzheimer's disease on medial temporal lobe cortical thickness and surface area. *Neurobiol Aging*, *30*(3), 432–440. <https://doi.org/10.1016/j.neurobiolaging.2007.07.022>
- Dong, X.-X., Wang, Y., & Qin, Z.-H. (2009). Molecular mechanisms of excitotoxicity and their relevance to pathogenesis of neurodegenerative diseases. *Acta Pharmacologica Sinica*, *30*(4), 379–387. <https://doi.org/10.1038/aps.2009.24>
- Dossi, E., Vasile, F., & Rouach, N. (2018). Human astrocytes in the diseased brain. *Brain Research Bulletin*, *136*, 139–156. <https://doi.org/10.1016/j.brainresbull.2017.02.001>
- Drewes, G, Lichtenberg-Kraag, B, Döring, F, Mandelkow, E. M., Biernat, J, Goris, J, Dorée, M, & Mandelkow, E. (1992). Mitogen activated protein (MAP) kinase transforms tau protein into an Alzheimer-like state. *EMBO J*, *11*(6), 2131–2138. Retrieved June 12, 2021, from <https://www.ncbi.nlm.nih.gov/pmc/articles/PMC556680/>

- Du, L., Zhang, Y., Chen, Y., Zhu, J., Yang, Y., & Zhang, H.-L. (2017). Role of Microglia in Neurological Disorders and Their Potentials as a Therapeutic Target. *Mol Neurobiol*, 54(10), 7567–7584. <https://doi.org/10.1007/s12035-016-0245-0>
- Duman, R. S. (2002). Pathophysiology of depression: The concept of synaptic plasticity. *Eur Psychiatry*, 17 Suppl 3, 306–310. [https://doi.org/10.1016/s0924-9338\(02\)00654-5](https://doi.org/10.1016/s0924-9338(02)00654-5)
- Duncan, G. W. (2011). The aging brain and neurodegenerative diseases. *Clin Geriatr Med*, 27(4), 629–644. <https://doi.org/10.1016/j.cger.2011.07.008>
- Edwards III, G. A., Gamez, N., Escobedo Jr., G., Calderon, O., & Moreno-Gonzalez, I. (2019). Modifiable Risk Factors for Alzheimer’s Disease. *Front. Aging Neurosci.*, 11. <https://doi.org/10.3389/fnagi.2019.00146>
- Ernsberger, P., & Haxhiu, M. A. (1997). The I1-imidazoline-binding site is a functional receptor mediating vasodepression via the ventral medulla. *The American journal of physiology*, 273(5), R1572–9. <https://doi.org/10.1152/ajpregu.1997.273.5.R1572>
- Ernsberger, P., Meeley, M. P., Mann, J. J., & Reis, D. J. (1987). Clonidine binds to imidazole binding sites as well as alpha 2-adrenoceptors in the ventrolateral medulla. *European journal of pharmacology*, 134(1), 1–13. [https://doi.org/10.1016/0014-2999\(87\)90125-7](https://doi.org/10.1016/0014-2999(87)90125-7)
- Escribá, P. V., Ozaita, A., & García-Sevilla, J. A. (1999). Pharmacologic characterization of imidazoline receptor proteins identified by immunologic techniques and other methods. *Ann N Y Acad Sci*, 881, 8–25. <https://doi.org/10.1111/j.1749-6632.1999.tb09336.x>
- Escribá, P. V., Sastre, M., Wang, H., Regunathan, S., Reis, D. J., & García-Sevilla, J. A. (1994). Immunodetection of putative imidazoline receptor proteins in the human and rat brain and other tissues. *Neuroscience letters*, 178(1), 81–84. [https://doi.org/10.1016/0304-3940\(94\)90295-x](https://doi.org/10.1016/0304-3940(94)90295-x)
- Escribá, P. V., Alemany, R., Sastre, M., Olmos, G., Ozaita, A., & García-Sevilla, J. A. (1996). Pharmacological modulation of immunoreactive imidazoline receptor proteins in rat brain: Relationship with non-adrenoceptor [3H]-idazoxan binding sites. *British Journal of Pharmacology*, 118(8), 2029–2036. <https://doi.org/10.1111/j.1476-5381.1996.tb15640.x>
- Esteras, N., Kundel, F., Amodeo, G. F., Pavlov, E. V., Klenerman, D., & Abramov, A. Y. (2021). Insoluble tau aggregates induce neuronal death through modification of membrane ion conductance, activation of voltage-gated calcium channels and NADPH oxidase. *FEBS J*, 288(1), 127–141. <https://doi.org/10.1111/febs.15340>
- Farlow, M. R., Salloway, S., Tariot, P. N., Yardley, J., Moline, M. L., Wang, Q., Brand-Schieber, E., Zou, H., Hsu, T., & Satlin, A. (2010). Effectiveness and tolerability of high-dose (23 mg/d) versus standard-dose (10 mg/d) donepezil in moderate

- to severe Alzheimer's disease: A 24-week, randomized, double-blind study. *Clin Ther*, 32(7), 1234–1251. <https://doi.org/10.1016/j.clinthera.2010.06.019>
- Feinstein, D. L., Reis, D. J., & Regunathan, S. (1999). Inhibition of astroglial nitric oxide synthase type 2 expression by idazoxan. *Mol Pharmacol*, 55(2), 304–308. <https://doi.org/10.1124/mol.55.2.304>
- Feldman, H. H., Schmitt, F. A., Olin, J. T., & Memantine MEM-MD-02 Study Group. (2006). Activities of daily living in moderate-to-severe Alzheimer disease: An analysis of the treatment effects of memantine in patients receiving stable donepezil treatment. *Alzheimer Dis Assoc Disord*, 20(4), 263–268. <https://doi.org/10.1097/01.wad.0000213859.35355.59>
- Felger, J. C. Role of Inflammation in Depression and Treatment Implications (M. Macaluso & S. H. Preskorn, Eds.). en. In: In *Antidepressants: From Biogenic Amines to New Mechanisms of Action* (M. Macaluso & S. H. Preskorn, Eds.). Ed. by Macaluso, M., & Preskorn, S. H. *Handbook of Experimental Pharmacology*. Cham: Springer International Publishing, 2019, pp. 255–286. ISBN: 978-3-030-10949-3. [https://doi.org/10.1007/164\\_2018\\_166](https://doi.org/10.1007/164_2018_166).
- Felger, J. C., & Lotrich, F. E. (2013). Inflammatory Cytokines in Depression: Neurobiological Mechanisms and Therapeutic Implications. *Neuroscience*, 246, 199–229. <https://doi.org/10.1016/j.neuroscience.2013.04.060>
- Fenton, C., Keating, G. M., & Lyseng-Williamson, K. A. (2006). Moxonidine: A review of its use in essential hypertension. *Drugs*, 66(4), 477–496. <https://doi.org/10.2165/00003495-200666040-00006>
- Fernández, A., Quintana, E., Velasco, P., Moreno-Jimenez, B., de Andrés, B., Gaspar, M. L., Liste, I., Vilar, M., Mira, H., & Cano, E. (2021). Senescent accelerated prone 8 (SAMP8) mice as a model of age dependent neuroinflammation. *J Neuroinflammation*, 18(1), 75. <https://doi.org/10.1186/s12974-021-02104-3>
- Fernández, M., Gobartt, A. L., Balañá, M., & COOPERA Study Group. (2010). Behavioural symptoms in patients with Alzheimer's disease and their association with cognitive impairment. *BMC Neurol*, 10, 87. <https://doi.org/10.1186/1471-2377-10-87>
- Ferrari, A., Hoerndli, F., Baechi, T., Nitsch, R. M., & Gotz, J. (2003).  $\beta$ -amyloid induces paired helical filament-like tau filaments in tissue culture. *Journal of Biological Chemistry*, 278(41), 40162–40168.
- Ferrari, F., Fiorentino, S., Mennuni, L., Garofalo, P., Letari, O., Mandelli, S., Giordani, A., Lanza, M., & Caselli, G. (2011). Analgesic efficacy of CR4056, a novel imidazoline-2 receptor ligand, in rat models of inflammatory and neuropathic pain. *J Pain Res*, 4, 111–125. <https://doi.org/10.2147/JPR.S18353>
- Ferreira, A. (2012). Calpain Dysregulation in Alzheimer's Disease. *ISRN Biochem*, 2012. <https://doi.org/10.5402/2012/728571>

- Filosto, M., Scarpelli, M., Cotelli, M. S., Vielmi, V., Todeschini, A., Gregorelli, V., Tonin, P., Tomelleri, G., & Padovani, A. (2011). The role of mitochondria in neurodegenerative diseases. *J Neurol*, *258*(10), 1763–1774. <https://doi.org/10.1007/s00415-011-6104-z>
- Finkel, S. I., Costa e Silva, J., Cohen, G., Miller, S., & Sartorius, N. (1996). Behavioral and psychological signs and symptoms of dementia: A consensus statement on current knowledge and implications for research and treatment. *Int Psychogeriatr*, *8 Suppl 3*, 497–500. <https://doi.org/10.1017/s1041610297003943>
- Finn, D. P., Martí, O., Harbuz, M. S., Vallès, A., Belda, X., Márquez, C., Jessop, D. S., Lalies, M. D., Armario, A., Nutt, D. J., & Hudson, A. L. (2003). Behavioral, neuroendocrine and neurochemical effects of the imidazoline I2 receptor selective ligand BU224 in naive rats and rats exposed to the stress of the forced swim test. *Psychopharmacology*, *167*(2), 195–202. <https://doi.org/10.1007/s00213-003-1392-3>
- Flood, J. F., & Morley, J. E. (1998). Learning and memory in the SAMP8 mouse. *Neurosci Biobehav Rev*, *22*(1), 1–20. [https://doi.org/10.1016/s0149-7634\(96\)00063-2](https://doi.org/10.1016/s0149-7634(96)00063-2)
- Floyd, R. A., & Hensley, K. (2002). Oxidative stress in brain aging. Implications for therapeutics of neurodegenerative diseases. *Neurobiol Aging*, *23*(5), 795–807. [https://doi.org/10.1016/s0197-4580\(02\)00019-2](https://doi.org/10.1016/s0197-4580(02)00019-2)
- Fu, W.-Y., Wang, X., & Ip, N. Y. (2018). Targeting neuroinflammation as a therapeutic strategy for alzheimer's disease: Mechanisms, drug candidates, and new opportunities. *ACS chemical neuroscience*, *10*(2), 872–879.
- Fukunari, A., Kato, A., Sakai, Y., Yoshimoto, T., Ishiura, S., Suzuki, K., & Nakajima, T. (1994). Colocalization of prolyl endopeptidase and amyloid beta-peptide in brains of senescence-accelerated mouse. *Neurosci Lett*, *176*(2), 201–204. [https://doi.org/10.1016/0304-3940\(94\)90082-5](https://doi.org/10.1016/0304-3940(94)90082-5)
- Gamblin, T. C., King, M. E., Kuret, J., Berry, R. W., & Binder, L. I. (2000). Oxidative regulation of fatty acid-induced tau polymerization. *Biochemistry*, *39*(46), 14203–14210. <https://doi.org/10.1021/bi001876l>
- Garau, C., Miralles, A., & García-Sevilla, J. A. (2013). Chronic treatment with selective I2-imidazoline receptor ligands decreases the content of pro-apoptotic markers in rat brain. *J Psychopharmacol*, *27*(2), 123–134. <https://doi.org/10.1177/0269881112450785>
- García-Matas, S., Gutierrez-Cuesta, J., Coto-Montes, A., Rubio-Acero, R., Díez-Vives, C., Camins, A., Pallàs, M., Sanfeliu, C., & Cristòfol, R. (2008). Dysfunction of astrocytes in senescence-accelerated mice SAMP8 reduces their neuroprotective capacity. *Aging Cell*, *7*(5), 630–640. <https://doi.org/10.1111/j.1474-9726.2008.00410.x>

- García-Sevilla, J., Miralles, A., Sastre, M., Escribá, P. V., Olmos, G., & Meana, J. J. (1995a). I2-imidazoline receptors in the healthy and pathologic human brain. *Ann N Y Acad Sci*, 763, 178–193. <https://doi.org/10.1111/j.1749-6632.1995.tb32406.x>
- García-Sevilla, J. A., Alemany, R., Olmos, G., Menargues, A., & Obach, R. (1995b). Chronic imidazoline drug treatment increases the immunoreactivity of glial fibrillary acidic protein in rat brain. LSL 60101 as a novel and selective ligand for I2-imidazoline receptors. *Ann N Y Acad Sci*, 763, 486–489. <https://doi.org/10.1111/j.1749-6632.1995.tb32437.x>
- García-Sevilla, J. A., Escribá, P. V., Sastre, M., Walzer, C., Busquets, X., Jaquet, G., Reis, D. J., & Guimón, J. (1996). Immunodetection and quantitation of imidazoline receptor proteins in platelets of patients with major depression and in brains of suicide victims. *Arch Gen Psychiatry*, 53(9), 803–810. <https://doi.org/10.1001/archpsyc.1996.01830090049008>
- García-Sevilla, J. A., Escribá, P. V., Walzer, C., Bouras, C., & Guimón, J. (1998). Imidazoline receptor proteins in brains of patients with Alzheimer's disease. *Neurosci Lett*, 247(2-3), 95–98. [https://doi.org/10.1016/s0304-3940\(98\)00265-1](https://doi.org/10.1016/s0304-3940(98)00265-1)
- García-Sevilla, J. A., Escribá, P. V., & Guimón, J. (1999). Imidazoline receptors and human brain disorders a. *Annals of the new York Academy of Sciences*, 881(1), 392–409.
- García-Sevilla, J. A., & Ferrer-Alcon, M. (2003). In vivo effects of the I(2)-alkylating agent BU99006 on the immunodensity of imidazoline receptor proteins in the mouse brain. *Ann N Y Acad Sci*, 1009, 323–331. <https://doi.org/10.1196/annals.1304.041>
- García-Sevilla, J. A., Sastre, M., & Escribá, P. V. (1995). Age-dependent increases of immunoreactive imidazoline receptors in the human brain: Possible association of a 2930kda protein with the i2-imidazoline receptor identified by [3h] idazoxan. *Neuroscience letters*, 184(2), 133–136.
- Gargalidis-Moudanos, C., Pizzinat, N., Javoy-Agid, F., Remaury, A., & Parini, A. (1997). I2-imidazoline binding sites and monoamine oxidase activity in human postmortem brain from patients with Parkinson's disease. *Neurochem Int*, 30(1), 31–36. [https://doi.org/10.1016/s0197-0186\(96\)00035-6](https://doi.org/10.1016/s0197-0186(96)00035-6)
- Ghosh, A., Carnahan, J., & Greenberg, M. E. (1994). Requirement for BDNF in activity-dependent survival of cortical neurons. *Science*, 263(5153), 1618–1623. <https://doi.org/10.1126/science.7907431>
- Giannakopoulos, P., Herrmann, F. R., Bussièrè, T., Bouras, C., Kövari, E., Perl, D. P., Morrison, J. H., Gold, G., & Hof, P. R. (2003). Tangle and neuron numbers, but not amyloid load, predict cognitive status in Alzheimer's disease. *Neurology*, 60(9), 1495–1500. <https://doi.org/10.1212/01.wnl.0000063311.58879.01>
- Giannoni, P., Arango-Lievano, M., Neves, I. D., Rousset, M.-C., Baranger, K., Rivera, S., Jeanneteau, F., Claeysen, S., & Marchi, N. (2016). Cerebrovascular pathology dur-

- ing the progression of experimental alzheimer's disease. *Neurobiology of disease*, 88, 107–117.
- Gilad, G. M., Salame, K., Rabey, J. M., & Gilad, V. H. (1996). Agmatine treatment is neuroprotective in rodent brain injury models. *Life Sci*, 58(2), PL 41–46. [https://doi.org/10.1016/0024-3205\(95\)02274-0](https://doi.org/10.1016/0024-3205(95)02274-0)
- Godin, S. K., Seo, J., & Tsai, L.-H. Chapter 17 - Neurodegenerative Diseases and the Aging Brain (M. S. Wolfe, Ed.). en. In: In *The Molecular and Cellular Basis of Neurodegenerative Diseases* (M. S. Wolfe, Ed.). Ed. by Wolfe, M. S. Academic Press, 2018, January, pp. 509–526. ISBN: 978-0-12-811304-2. <https://doi.org/10.1016/B978-0-12-811304-2.00017-1>.
- Gold, C. A., & Budson, A. E. (2008). Memory loss in Alzheimer's disease: Implications for development of therapeutics. *Expert Rev Neurother*, 8(12), 1879–1891. <https://doi.org/10.1586/14737175.8.12.1879>
- Gong, X., Tang, X., Wiedmann, M., Wang, X., Peng, J., Zheng, D., Blair, L. A. C., Marshall, J., & Mao, Z. (2003). Cdk5-mediated inhibition of the protective effects of transcription factor MEF2 in neurotoxicity-induced apoptosis. *Neuron*, 38(1), 33–46. [https://doi.org/10.1016/s0896-6273\(03\)00191-0](https://doi.org/10.1016/s0896-6273(03)00191-0)
- González-Reyes, R. E., Nava-Mesa, M. O., Vargas-Sánchez, K., Ariza-Salamanca, D., & Mora-Muñoz, L. (2017). Involvement of Astrocytes in Alzheimer's Disease from a Neuroinflammatory and Oxidative Stress Perspective. *Front Mol Neurosci*, 10. <https://doi.org/10.3389/fnmol.2017.00427>
- Gotz, J., & Chen, F. Van, dj, nitsch, rm, 2001. formation of neurofibrillary tangles in p3011 tau transgenic mice induced by abeta 42 fibrils. *Science*, 293, 14911495.
- Gratuze, M., Leyns, C. E. G., & Holtzman, D. M. (2018). New insights into the role of TREM2 in Alzheimer's disease. *Molecular Neurodegeneration*, 13(1), 66. <https://doi.org/10.1186/s13024-018-0298-9>
- Greenberg, D. A., Prichard, D. C., & Snyder, S. H. (1976). Alpha-noradrenergic receptor binding in mammalian brain: Differential labeling of agonist and antagonist states. *Life sciences*, 19(1), 69–76. [https://doi.org/10.1016/0024-3205\(76\)90375-1](https://doi.org/10.1016/0024-3205(76)90375-1)
- Griñan-Ferré, C., Palomera-Ávalos, V., Puigoriol-Illamola, D., Camins, A., Porquet, D., Plá, V., Aguado, F., & Pallàs, M. (2016). Behaviour and cognitive changes correlated with hippocampal neuroinflammation and neuronal markers in female SAMP8, a model of accelerated senescence. *Exp Gerontol*, 80, 57–69. <https://doi.org/10.1016/j.exger.2016.03.014>
- Groth, R. D., Dunbar, R. L., & Mermelstein, P. G. (2003). Calcineurin regulation of neuronal plasticity. *Biochem Biophys Res Commun*, 311(4), 1159–1171. <https://doi.org/10.1016/j.bbrc.2003.09.002>
- Guerra de Souza, A. C., Gonçalves, C. L., de Souza, V., Hartwig, J. M., Farina, M., & Prediger, R. D. (2018). Agmatine attenuates depressive-like behavior and hippocampal

- oxidative stress following amyloid  $\beta$  (A $\beta$ 1-40) administration in mice. *Behav Brain Res*, 353, 51–56. <https://doi.org/10.1016/j.bbr.2018.06.032>
- Guerreiro, R., Wojtas, A., Bras, J., Carrasquillo, M., Rogaeva, E., Majounie, E., Cruchaga, C., Sassi, C., Kauwe, J. S. K., Younkin, S., Hazrati, L., Collinge, J., Pocock, J., Lashley, T., Williams, J., Lambert, J.-C., Amouyel, P., Goate, A., Rademakers, R., ... Alzheimer Genetic Analysis Group. (2013). TREM2 variants in Alzheimer's disease. *N Engl J Med*, 368(2), 117–127. <https://doi.org/10.1056/NEJMoa1211851>
- Guo, T., Zhang, D., Zeng, Y., Huang, T. Y., Xu, H., & Zhao, Y. (2020). Molecular and cellular mechanisms underlying the pathogenesis of Alzheimer's disease. *Mol Neurodegeneration*, 15(1), 40. <https://doi.org/10.1186/s13024-020-00391-7>
- Gustafson, I., Westerberg, E., & Wieloch, T. (1990). Protection against ischemia-induced neuronal damage by the alpha 2-adrenoceptor antagonist idazoxan: Influence of time of administration and possible mechanisms of action. *J Cereb Blood Flow Metab*, 10(6), 885–894. <https://doi.org/10.1038/jcbfm.1990.145>
- Hagiwara, M., Alberts, A., Brindle, P., Meinkoth, J., Feramisco, J., Deng, T., Karin, M., Shenolikar, S., & Montminy, M. (1992). Transcriptional attenuation following cAMP induction requires PP-1-mediated dephosphorylation of CREB. *Cell*, 70(1), 105–113. [https://doi.org/10.1016/0092-8674\(92\)90537-m](https://doi.org/10.1016/0092-8674(92)90537-m)
- Halaris, A., & Piletz, J. E. (2003). Relevance of imidazoline receptors and agmatine to psychiatry: A decade of progress. *Annals of the New York Academy of Sciences*, 1009, 1–20. <https://doi.org/10.1196/annals.1304.001>
- Halaris, A., & Piletz, J. E. (2001). Imidazoline receptors: Possible involvement in the pathophysiology and treatment of depression. *Hum. Psychopharmacol. Clin. Exp.*, 16(1), 65–69. <https://doi.org/10.1002/hup.185>
- Hamano, T., Shirafuji, N., Sasaki, H., Ishi-da, A., Ueno, A., Yen, S.-H., Yoneda, M., Kuriyama, M., & Nakamoto, Y. (2013). P1-401: Donepezil reduces phosphorylation levels of tau protein in a cellular model of tauopathy. *Alzheimer's & Dementia*, 9, P305–P305. <https://doi.org/10.1016/j.jalz.2013.05.629>
- Han, Z., Xiao, M.-J., Shao, B., Zheng, R.-Y., Yang, G.-Y., & Jin, K. (2009a). Attenuation of ischemia-induced rat brain injury by 2-(-2-benzofuranyl)-2-imidazoline, a high selectivity ligand for imidazoline i2 receptors. *Neurological research*, 31(4), 390–395.
- Han, Z., Xiao, M.-J., Shao, B., Zheng, R.-Y., Yang, G.-Y., & Jin, K. (2009b). Attenuation of ischemia-induced rat brain injury by 2-(-2-benzofuranyl)-2-imidazoline, a high selectivity ligand for imidazoline I(2) receptors. *Neurol Res*, 31(4), 390–395. <https://doi.org/10.1179/174313209X444116>
- Han, Z., Zhang, H.-X., Tian, J.-S., Zheng, R.-Y., & Hou, S. T. (2010). 2-(-2-benzofuranyl)-2-imidazoline induces bcl-2 expression and provides neuroprotection against transient cerebral ischemia in rats. *Brain research*, 1361, 86–92.

- Haque, M. M., Murale, D. P., Kim, Y. K., & Lee, J.-S. (2019). Crosstalk between Oxidative Stress and Tauopathy. *Int J Mol Sci*, 20(8). <https://doi.org/10.3390/ijms20081959>
- Head, G., & Mayorov, D. (2008). Imidazoline Receptors, Novel Agents and Therapeutic Potential. *Cardiovascular & Hematological Agents in Medicinal Chemistry*, 4(1), 17–32. <https://doi.org/10.2174/187152506775268758>
- Hemmings, H. C., Nairn, A. C., Elliott, J. I., & Greengard, P. (1990). Synthetic peptide analogs of DARPP-32 (Mr 32,000 dopamine- and cAMP-regulated phosphoprotein), an inhibitor of protein phosphatase-1. Phosphorylation, dephosphorylation, and inhibitory activity. *J Biol Chem*, 265(33), 20369–20376.
- Heneka, M. T., Carson, M. J., El Khoury, J., Landreth, G. E., Brosseron, F., Feinstein, D. L., Jacobs, A. H., Wyss-Coray, T., Vitorica, J., Ransohoff, R. M., Herrup, K., Frautschy, S. A., Finsen, B., Brown, G. C., Verkhratsky, A., Yamanaka, K., Koistinaho, J., Latz, E., Halle, A., . . . Kummer, M. P. (2015). Neuroinflammation in Alzheimer's disease. *Lancet Neurol*, 14(4), 388–405. [https://doi.org/10.1016/S1474-4422\(15\)70016-5](https://doi.org/10.1016/S1474-4422(15)70016-5)
- Heneka, M. T., Kummer, M. P., & Latz, E. (2014). Innate immune activation in neurodegenerative disease. *Nat Rev Immunol*, 14(7), 463–477. <https://doi.org/10.1038/nri3705>
- Hensley, K. (2010). Neuroinflammation in alzheimer's disease: Mechanisms, pathologic consequences, and potential for therapeutic manipulation. *Journal of Alzheimer's disease*, 21(1), 1–14.
- Hernández-Hernández, E., García-Sevilla, J. A., & García-Fuster, M. J. (2021). Exploring the antidepressant-like potential of the selective I2-imidazoline receptor ligand LSL 60101 in adult male rats. *Pharmacol Rep*, 73(1), 288–295. <https://doi.org/10.1007/s43440-020-00148-5>
- Hippius, H., & Neundörfer, G. (2003). The discovery of Alzheimer's disease. *Dialogues Clin Neurosci*, 5(1), 101–108. Retrieved June 12, 2021, from <https://www.ncbi.nlm.nih.gov/pmc/articles/PMC3181715/>
- Holt, A. (2003). Imidazoline binding sites on receptors and enzymes: Emerging targets for novel antidepressant drugs? *Journal of psychiatry & neuroscience : JPN*, 28(6), 409–414.
- Hooshmandi, E., Ghasemi, R., Iloun, P., & Moosavi, M. (2019). The neuroprotective effect of agmatine against amyloid  $\beta$ -induced apoptosis in primary cultured hippocampal cells involving ERK, Akt/GSK-3 $\beta$ , and TNF- $\alpha$ . *Mol Biol Rep*, 46(1), 489–496. <https://doi.org/10.1007/s11033-018-4501-4>
- Hosokawa, M. (2002). A higher oxidative status accelerates senescence and aggravates age-dependent disorders in SAMP strains of mice. *Mechanisms of Ageing and Development*, 123(12), 1553–1561. [https://doi.org/10.1016/S0047-6374\(02\)00091-X](https://doi.org/10.1016/S0047-6374(02)00091-X)



- Hou, Y., Dan, X., Babbar, M., Wei, Y., Hasselbalch, S. G., Croteau, D. L., & Bohr, V. A. (2019). Ageing as a risk factor for neurodegenerative disease. *Nat Rev Neurol*, *15*(10), 565–581. <https://doi.org/10.1038/s41582-019-0244-7>
- Howard, R., McShane, R., Lindesay, J., Ritchie, C., Baldwin, A., Barber, R., Burns, A., Dening, T., Findlay, D., Holmes, C., et al. (2012). Donepezil and memantine for moderate-to-severe alzheimer's disease. *New England Journal of Medicine*, *366*(10), 893–903.
- Huang, E. J., & Reichardt, L. F. (2001). Neurotrophins: Roles in Neuronal Development and Function. *Annu Rev Neurosci*, *24*, 677–736. <https://doi.org/10.1146/annurev.neuro.24.1.677>
- Hudson, A. L., Luscombe, S., Gouch, R. E., Nutt, D. J., & Tyacke, R. J. (1999). Endogenous indoleamines demonstrate moderate affinity for I2 binding sites. *Ann N Y Acad Sci*, *881*, 212–216. <https://doi.org/10.1111/j.1749-6632.1999.tb09363.x>
- Hudson, A. L. (2015). Borne identity: Leading endogenous suspects at imidazoline binding sites. *ARCHIVOS DE MEDICINA*, *6*(2), 11.
- Hugo, J., & Ganguli, M. (2014). Dementia and Cognitive Impairment: Epidemiology, Diagnosis, and Treatment. *Clin Geriatr Med*, *30*(3), 421–442. <https://doi.org/10.1016/j.cger.2014.04.001>
- Husbands, S. M., Glennon, R. A., Gorgerat, S., Gough, R., Tyacke, R., Crosby, J., Nutt, D. J., Lewis, J. W., & Hudson, A. L. (2001).  $\beta$ -carboline binding to imidazoline receptors. *Drug and alcohol dependence*, *64*(2), 203–208.
- Hyman, C., Hofer, M., Barde, Y.-A., Juhasz, M., Yancopoulos, G. D., Squinto, S. P., & Lindsay, R. M. (1991). Bdnf is a neurotrophic factor for dopaminergic neurons of the substantia nigra. *Nature*, *350*(6315), 230–232.
- Ising, C., Stanley, M., & Holtzman, D. M. (2015). Current thinking on the mechanistic basis of Alzheimer's and implications for drug development. *Clin Pharmacol Ther*, *98*(5), 469–471. <https://doi.org/10.1002/cpt.200>
- Ivanov, T. R., Zhu, H., Regunathan, S., Reis, D. J., Dontenwill, M., Vonthron, C., Bousquet, P., & Piletz, J. E. (1998). Co-detection by two imidazoline receptor protein antisera of a novel 85 kilodalton protein. *Biochemical Pharmacology*, *55*(5), 649–655. [https://doi.org/10.1016/S0006-2952\(97\)00537-6](https://doi.org/10.1016/S0006-2952(97)00537-6)
- J Allen, S., J Watson, J., & Dawbarn, D. (2011). The neurotrophins and their role in alzheimer's disease. *Current neuropharmacology*, *9*(4), 559–573.
- Jackson, H. C., Griffin, I. J., & Nutt, D. J. (1991). The effects of idazoxan and other alpha 2-adrenoceptor antagonists on food and water intake in the rat. *British journal of pharmacology*, *104*(1), 258–262. <https://doi.org/10.1111/j.1476-5381.1991.tb12416.x>

- Jahn, H. (2013). Memory loss in Alzheimer's disease. *Dialogues Clin Neurosci*, *15*(4), 445–454. Retrieved June 13, 2021, from <https://www.ncbi.nlm.nih.gov/pmc/articles/PMC3898682/>
- Jawhar, S., Trawicka, A., Jenneckens, C., Bayer, T. A., & Wirths, O. (2012). Motor deficits, neuron loss, and reduced anxiety coinciding with axonal degeneration and intraneuronal A $\beta$  aggregation in the 5XFAD mouse model of Alzheimer's disease. *Neurobiol Aging*, *33*(1), 196.e29–40. <https://doi.org/10.1016/j.neurobiolaging.2010.05.027>
- Jeppesen, D. K., Bohr, V. A., & Stevnsner, T. (2011). DNA repair deficiency in neurodegeneration. *Prog Neurobiol*, *94*(2), 166–200. <https://doi.org/10.1016/j.pneurobio.2011.04.013>
- Jha, N. K., Jha, S. K., Kar, R., Nand, P., Swati, K., & Goswami, V. K. (2019). Nuclear factor-kappa  $\beta$  as a therapeutic target for Alzheimer's disease [Publisher: John Wiley & Sons, Ltd]. *Journal of Neurochemistry*, *150*(2), 113–137. <https://doi.org/10.1111/jnc.14687>  
<https://doi.org/10.1111/jnc.14687>
- Jiang, S. X., Zheng, R.-Y., Zeng, J.-Q., Li, X.-L., Han, Z., & Hou, S. T. (2010). Reversible inhibition of intracellular calcium influx through NMDA receptors by imidazoline I(2) receptor antagonists. *Eur J Pharmacol*, *629*(1-3), 12–19. <https://doi.org/10.1016/j.ejphar.2009.11.063>
- Johri, A., & Beal, M. F. (2012). Mitochondrial dysfunction in neurodegenerative diseases. *J Pharmacol Exp Ther*, *342*(3), 619–630. <https://doi.org/10.1124/jpet.112.192138>
- Jonsson, T., Stefansson, H., Steinberg, S., Jonsdottir, I., Jonsson, P. V., Snaedal, J., Bjornsson, S., Huttenlocher, J., Levey, A. I., Lah, J. J., et al. (2013). Variant of trem2 associated with the risk of alzheimer's disease. *New England Journal of Medicine*, *368*(2), 107–116.
- Jordan, S., Jackson, H., Nutt, D., & Handley, S. (1996). Discriminative stimulus produced by the imidazoline i2 site ligand, 2-bfi. *Journal of Psychopharmacology*, *10*(4), 273–278.
- Kabir, M. T., Uddin, M. S., Mamun, A. A., Jeandet, P., Aleya, L., Mansouri, R. A., Ashraf, G. M., Mathew, B., Bin-Jumah, M. N., & Abdel-Daim, M. M. (2020). Combination Drug Therapy for the Management of Alzheimer's Disease. *IJMS*, *21*(9), 3272. <https://doi.org/10.3390/ijms21093272>
- Kang, S., Ha, S., Park, H., Nam, E., Suh, W. H., Suh, Y.-H., & Chang, K.-A. (2018). Effects of a Dehydroevodiamine-Derivative on Synaptic Destabilization and Memory Impairment in the 5xFAD, Alzheimer's Disease Mouse Model. *Front. Behav. Neurosci.*, *12*, 273. <https://doi.org/10.3389/fnbeh.2018.00273>
- Kang, S., Kim, C.-H., Jung, H., Kim, E., Song, H.-T., & Lee, J. E. (2017). Agmatine ameliorates type 2 diabetes induced-Alzheimer's disease-like alterations in high-fat

- diet-fed mice via reactivation of blunted insulin signalling. *Neuropharmacology*, 113(Pt A), 467–479. <https://doi.org/10.1016/j.neuropharm.2016.10.029>
- Kanno, T., Tsuchiya, A., & Nishizaki, T. (2014). Hyperphosphorylation of Tau at Ser396 occurs in the much earlier stage than appearance of learning and memory disorders in 5XFAD mice. *Behav Brain Res*, 274, 302–306. <https://doi.org/10.1016/j.bbr.2014.08.034>
- Karasawa, N., Nagatsu, I., Sakai, K., Nagatsu, T., Watanabe, K., & Onozuka, M. (1997). Immunocytochemical study of catecholaminergic neurons in the senescence-accelerated mouse (SAM-P8) brain. *J Neural Transm (Vienna)*, 104(11-12), 1267–1275. <https://doi.org/10.1007/BF01294727>
- Karege, F., Perret, G., Bondolfi, G., Schwald, M., Bertschy, G., & Aubry, J.-M. (2002). Decreased serum brain-derived neurotrophic factor levels in major depressed patients. *Psychiatry research*, 109(2), 143–148.
- Karppanen, H., Paakkari, I., Paakkari, P., Huotari, R., & Orma, A. L. (1976). Possible involvement of central histamine H<sub>2</sub>-receptors in the hypotensive effect of clonidine. *Nature*, 259(5544), 587–588. <https://doi.org/10.1038/259587a0>
- Kashyap, G., Bapat, D., Das, D., Gowaikar, R., Amritkar, R. E., Rangarajan, G., Ravindranath, V., & Ambika, G. (2019). Synapse loss and progress of Alzheimer's disease -A network model [Number: 1 Publisher: Nature Publishing Group]. *Sci Rep*, 9(1), 6555. <https://doi.org/10.1038/s41598-019-43076-y>
- Kawamata, T., Akiguchi, I., Maeda, K., Tanaka, C., Higuchi, K., Hosokawa, M., & Takeda, T. (1998). Age-related changes in the brains of senescence-accelerated mice (SAM): Association with glial and endothelial reactions. *Microsc Res Tech*, 43(1), 59–67. [https://doi.org/10.1002/\(SICI\)1097-0029\(19981001\)43:1<59::AID-JEMT9>3.0.CO;2-X](https://doi.org/10.1002/(SICI)1097-0029(19981001)43:1<59::AID-JEMT9>3.0.CO;2-X)
- Kawamoto, E. M., Vivar, C., & Camandola, S. (2012). Physiology and Pathology of Calcium Signaling in the Brain. *Front Pharmacol*, 3. <https://doi.org/10.3389/fphar.2012.00061>
- Kawamura, K., Kimura, Y., Yui, J., Wakizaka, H., Yamasaki, T., Hatori, A., Kumata, K., Fujinaga, M., Yoshida, Y., Ogawa, M., Nengaki, N., Fukumura, T., & Zhang, M.-R. (2012). PET study using [11C]FTIMD with ultra-high specific activity to evaluate I<sub>2</sub>-imidazoline receptors binding in rat brains. *Nucl Med Biol*, 39(2), 199–206. <https://doi.org/10.1016/j.nucmedbio.2011.07.008>
- Kawamura, K., Naganawa, M., Konno, F., Yui, J., Wakizaka, H., Yamasaki, T., Yanamoto, K., Hatori, A., Takei, M., Yoshida, Y., Sakaguchi, K., Fukumura, T., Kimura, Y., & Zhang, M.-R. (2010). Imaging of I<sub>2</sub>-imidazoline receptors by small-animal PET using 2-(3-fluoro-[4-<sup>11</sup>C]tolyl)-4,5-dihydro-1H-imidazole ([<sup>11</sup>C]FTIMD). *Nucl Med Biol*, 37(5), 625–635. <https://doi.org/10.1016/j.nucmedbio.2010.02.013>

- Kawamura, K., Shimoda, Y., Kumata, K., Fujinaga, M., Yui, J., Yamasaki, T., Xie, L., Hatori, A., Wakizaka, H., Kurihara, Y., Ogawa, M., Nengaki, N., & Zhang, M.-R. (2015). In vivo evaluation of a new 18F-labeled PET ligand, [18F]FEBU, for the imaging of I2-imidazoline receptors. *Nuclear Medicine and Biology*, 42(4), 406–412. <https://doi.org/10.1016/j.nucmedbio.2014.12.014>
- Kawecka-Jaszcz, K., Czarnecka, D., Klocek, M., Zabojszcz, M., Kucharska, M., Jaworski, R., & Pachocki, R. (2006). Rilmenidine—its antihypertensive efficacy, safety and impact on quality of life in perimenopausal women with mild to moderate essential hypertension. *Blood pressure*, 15(1), 51–58. <https://doi.org/10.1080/08037050600565969>
- Keller, B., & García-Sevilla, J. A. (2015). Immunodetection and subcellular distribution of imidazoline receptor proteins with three antibodies in mouse and human brains: Effects of treatments with I and Iimidazoline drugs. *Journal of Psychopharmacology*, 29(9), 996–1012. <https://doi.org/10.1177/0269881115586936>
- Kessing, L. V. (2012). Depression and the risk for dementia. *Curr Opin Psychiatry*, 25(6), 457–461. <https://doi.org/10.1097/YCO.0b013e328356c368>
- Kim, H. Y., Kim, H. V., Lee, D. K., Yang, S.-H., & Kim, Y. (2016). Rapid and sustained cognitive recovery in APP/PS1 transgenic mice by co-administration of EPPS and donepezil. *Sci Rep*, 6(1), 34165. <https://doi.org/10.1038/srep34165>
- Kim, S. H., Kandiah, N., Hsu, J., Suthisisang, C., Udommongkol, C., & Dash, A. (2017). Beyond symptomatic effects: Potential of donepezil as a neuroprotective agent and disease modifier in Alzheimer's disease. *Br J Pharmacol*, 174(23), 4224–4232. <https://doi.org/10.1111/bph.14030>
- Kim, S. U., & de Vellis, J. (2005). Microglia in health and disease. *Journal of neuroscience research*, 81(3), 302–313.
- Kim, W.-Y., Wang, X., Wu, Y., Doble, B. W., Patel, S., Woodgett, J. R., & Snider, W. D. (2009). Gsk-3 is a master regulator of neural progenitor homeostasis. *Nature neuroscience*, 12(11), 1390–1397.
- Kimura, A., Tyacke, R. J., Robinson, J. J., Husbands, S. M., Minchin, M. C., Nutt, D. J., & Hudson, A. L. (2009). Identification of an imidazoline binding protein: Creatine kinase and an imidazoline-2 binding site. *Brain research*, 1279, 21–28.
- Kimura, M., Akasofu, S., Ogura, H., & Sawada, K. (2005). Protective effect of donepezil against Abeta(1-40) neurotoxicity in rat septal neurons. *Brain Res*, 1047(1), 72–84. <https://doi.org/10.1016/j.brainres.2005.04.014>
- Kinney, J. W., Bemiller, S. M., Murtishaw, A. S., Leisgang, A. M., Salazar, A. M., & Lamb, B. T. (2018). Inflammation as a central mechanism in Alzheimer's disease. *Alzheimers Dement (N Y)*, 4, 575–590. <https://doi.org/10.1016/j.trci.2018.06.014>

- Kitagishi, Y., Kobayashi, M., Kikuta, K., & Matsuda, S. (2012). Roles of pi3k/akt/gsk3/mtor pathway in cell signaling of mental illnesses. *Depression research and treatment*, 2012.
- Klupp, H, Knappen, F, Otsuka, Y, Streller, I, & Teichmann, H. (1970). Effects of clonidine on central sympathetic tone. *European Journal of Pharmacology*, 10(2), 225–229. [https://doi.org/10.1016/0014-2999\(70\)90276-1](https://doi.org/10.1016/0014-2999(70)90276-1)
- Kobinger, W. (1967). On the mechanism of action of a new antihypertensive substance with imidazoline structure. *Naunyn-Schmiedebergs Archiv fur experimentelle Pathologie und Pharmakologie*, 258(1), 48–58.
- Kobinger, W, & Walland, A. (1972a). Evidence for a central activation of a vagal cardiodepressor reflex by clonidine. *European journal of pharmacology*, 19(2), 203–209. [https://doi.org/10.1016/0014-2999\(72\)90010-6](https://doi.org/10.1016/0014-2999(72)90010-6)
- Kobinger, W, & Walland, A. (1972b). Facilitation of vagal reflex bradycardia by an action of clonidine on central -receptors. *European journal of pharmacology*, 19(2), 210–217. [https://doi.org/10.1016/0014-2999\(72\)90011-8](https://doi.org/10.1016/0014-2999(72)90011-8)
- Kobinger, W, & Walland, A. (1967). Investigations into the mechanism of the hypotensive effect of 2-(2,6-dichlorophenylamino)-2-imidazoline-HCl. *European journal of pharmacology*, 2(3), 155–162. [https://doi.org/10.1016/0014-2999\(67\)90080-5](https://doi.org/10.1016/0014-2999(67)90080-5)
- Kolch, W. (2000). Meaningful relationships: The regulation of the ras/raf/mek/erk pathway by protein interactions. *Biochemical Journal*, 351(2), 289–305.
- Koopman, W. J., Nijtmans, L. G., Dieteren, C. E., Roestenberg, P., Valsecchi, F., Smeitink, J. A., & Willems, P. H. (2010). Mammalian Mitochondrial Complex I: Biogenesis, Regulation, and Reactive Oxygen Species Generation. *Antioxidants & Redox Signaling*, 12(12), 1431–1470. <https://doi.org/10.1089/ars.2009.2743>
- Kosel, F., Torres Munoz, P., Yang, J. R., Wong, A. A., & Franklin, T. B. (2019). Age-related changes in social behaviours in the 5xFAD mouse model of Alzheimer's disease. *Behav Brain Res*, 362, 160–172. <https://doi.org/10.1016/j.bbr.2019.01.029>
- Kotagale, N., Dixit, M., Garmelwar, H., Bhondekar, S., Umekar, M., & Taksande, B. (2020). Agmatine reverses memory deficits induced by A $\beta$ 1-42 peptide in mice: A key role of imidazoline receptors. *Pharmacol Biochem Behav*, 196, 172976. <https://doi.org/10.1016/j.pbb.2020.172976>
- Kotagale, N. R., Tripathi, S. J., Aglawe, M. M., Chopde, C. T., Umekar, M. J., & Taksande, B. G. (2013). Evidences for the agmatine involvement in antidepressant like effect of bupropion in mouse forced swim test. *Pharmacol Biochem Behav*, 107, 42–47. <https://doi.org/10.1016/j.pbb.2013.03.019>
- Krause, D. L., & Müller, N. (2010). Neuroinflammation, microglia and implications for anti-inflammatory treatment in Alzheimer's disease. *Int J Alzheimers Dis*, 2010. <https://doi.org/10.4061/2010/732806>

- Kültz, D. (2005). Molecular and evolutionary basis of the cellular stress response. *Annu Rev Physiol*, 67, 225–257. <https://doi.org/10.1146/annurev.physiol.67.040403.103635>
- Kumar, A., Koistinen, N. A., Malarte, M.-L., Nennesmo, I., Ingelsson, M., Ghetti, B., Lemoine, L., & Nordberg, A. (2021). Astroglial tracer BU99008 detects multiple binding sites in Alzheimer's disease brain. *Mol Psychiatry*. <https://doi.org/10.1038/s41380-021-01101-5>
- Kumar, V. B., Farr, S. A., Flood, J. F., Kamlesh, V., Franko, M., Banks, W. A., & Morley, J. E. (2000). Site-directed antisense oligonucleotide decreases the expression of amyloid precursor protein and reverses deficits in learning and memory in aged SAMP8 mice. *Peptides*, 21(12), 1769–1775. [https://doi.org/10.1016/s0196-9781\(00\)00339-9](https://doi.org/10.1016/s0196-9781(00)00339-9)
- Kumar, V. B., Vyas, K., Franko, M., Choudhary, V., Buddhiraju, C., Alvarez, J., & Morley, J. E. (2001). Molecular cloning, expression, and regulation of hippocampal amyloid precursor protein of senescence accelerated mouse (SAMP8). *Biochem Cell Biol*, 79(1), 57–67.
- Kumar, V. B., Franko, M., Banks, W. A., Kasinadhuni, P., Farr, S. A., Vyas, K., Choudhuri, V., & Morley, J. E. (2009). Increase in Presenilin 1 (PS1) levels in senescence-accelerated mice(SAMP8) may indirectly impair memory by affecting amyloid precursor protein(APP) processing. *Journal of Experimental Biology*, 212(4), 494–498. <https://doi.org/10.1242/jeb.022780>
- Kurokawa, T., Asada, S., Nishitani, S., & Hazeki, O. (2001). Age-related changes in manganese superoxide dismutase activity in the cerebral cortex of senescence-accelerated prone and resistant mouse. *Neurosci Lett*, 298(2), 135–138. [https://doi.org/10.1016/s0304-3940\(00\)01755-9](https://doi.org/10.1016/s0304-3940(00)01755-9)
- LANGER, S. Z., ADLER-GRASCHINSKY, E., & GIORGI, O. (1977). Physiological significance of  $\alpha$ -adrenoceptor-mediated negative feedback mechanism regulating noradrenaline release during nerve stimulation. *Nature*, 265(5595), 648–650. <https://doi.org/10.1038/265648a0>
- Ledo, J. H., Azevedo, E. P., Beckman, D., Ribeiro, F. C., Santos, L. E., Razolli, D. S., Kincheski, G. C., Melo, H. M., Bellio, M., Teixeira, A. L., Velloso, L. A., Foguel, D., De Felice, F. G., & Ferreira, S. T. (2016). Cross Talk Between Brain Innate Immunity and Serotonin Signaling Underlies Depressive-Like Behavior Induced by Alzheimer's Amyloid- Oligomers in Mice. *Journal of Neuroscience*, 36(48), 12106–12116. <https://doi.org/10.1523/JNEUROSCI.1269-16.2016>
- Lee, M.-s., Kwon, Y. T., Li, M., Peng, J., Friedlander, R. M., & Tsai, L.-H. (2000). Neurotoxicity induces cleavage of p35 to p25 by calpain. *Nature*, 405(6784), 360–364.
- Leng, F., & Edison, P. (2021). Neuroinflammation and microglial activation in Alzheimer disease: Where do we go from here? [Number: 3 Publisher: Nature Publishing

- Group]. *Nat Rev Neurol*, 17(3), 157–172. <https://doi.org/10.1038/s41582-020-00435-y>
- Lewis, J., Dickson, D. W., Lin, W. L., Chisholm, L., Corral, A., Jones, G., Yen, S. H., Sahara, N., Skipper, L., Yager, D., Eckman, C., Hardy, J., Hutton, M., & McGowan, E. (2001). Enhanced neurofibrillary degeneration in transgenic mice expressing mutant tau and APP. *Science*, 293(5534), 1487–1491. <https://doi.org/10.1126/science.1058189>
- Li, F., Zhang, Z.-X., Liu, Y.-F., Xu, H.-Q., Hou, S.-T., & Zheng, R.-Y. (2012). 2-BFI ameliorates EAE-induced mouse spinal cord damage: Effective therapeutic time window and possible mechanisms. *Brain Res*, 1483, 13–19. <https://doi.org/10.1016/j.brainres.2012.09.016>
- Li, G., Regunathan, S., Barrow, C. J., Eshraghi, J., Cooper, R., & Reis, D. J. (1994). Agmatine: An endogenous clonidine-displacing substance in the brain. *Science*, 263(5149), 966–969. <https://doi.org/10.1126/science.7906055>
- Li, H.-L., Wang, H.-H., Liu, S.-J., Deng, Y.-Q., Zhang, Y.-J., Tian, Q., Wang, X.-C., Chen, X.-Q., Yang, Y., Zhang, J.-Y., Wang, Q., Xu, H., Liao, F.-F., & Wang, J.-Z. (2007). Phosphorylation of tau antagonizes apoptosis by stabilizing beta-catenin, a mechanism involved in Alzheimer's neurodegeneration. *Proc Natl Acad Sci U S A*, 104(9), 3591–3596. <https://doi.org/10.1073/pnas.0609303104>
- Li, J.-T., & Zhang, Y. (2018). TREM2 regulates innate immunity in Alzheimer's disease. *J Neuroinflammation*, 15(1), 107. <https://doi.org/10.1186/s12974-018-1148-y>
- Li, J.-X. (2017). Imidazoline I2 receptors: An update. *Pharmacol Ther*, 178, 48–56. <https://doi.org/10.1016/j.pharmthera.2017.03.009>
- Li, J. X., & Zhang, Y. (2011). Imidazoline I2 receptors: Target for new analgesics? [Publisher: Elsevier B.V.]. *European Journal of Pharmacology*, 658(2-3), 49–56. <https://doi.org/10.1016/j.ejphar.2011.02.038>
- Li, K., Li, J., Zheng, J., & Qin, S. (2019). Reactive Astrocytes in Neurodegenerative Diseases. *Aging Dis*, 10(3), 664–675. <https://doi.org/10.14336/AD.2018.0720>
- Li, T., Shi, H., & Zhao, Y. (2018). Phosphorylation of microtubule-associated protein tau by mitogen-activated protein kinase in Alzheimer's disease. *IOP Conf. Ser.: Mater. Sci. Eng.*, 394, 022023. <https://doi.org/10.1088/1757-899X/394/2/022023>
- Li, Y., Cheng, K.-C., Asakawa, A., Amitani, H., Takimoto, Y., Runtuwene, J., & Inui, A. (2015). Activation of imidazoline-I3 receptors ameliorates pancreatic damage. *Clinical and experimental pharmacology & physiology*, 42(9), 964–971. <https://doi.org/10.1111/1440-1681.12441>
- Li, Y. F., Gong, Z. H., Cao, J. B., Wang, H. L., Luo, Z. P., & Li, J. (2003). Antidepressant-like effect of agmatine and its possible mechanism. *Eur J Pharmacol*, 469(1-3), 81–88. [https://doi.org/10.1016/s0014-2999\(03\)01735-7](https://doi.org/10.1016/s0014-2999(03)01735-7)

- Limon, I., Coupry, I., Lanier, S. M., & Parini, A. (1992). Purification and characterization of mitochondrial imidazoline-guanidinium receptive site from rabbit kidney. *J Biol Chem*, 267(30), 21645–21649.
- Lindholm, D., Carroll, P., Tzimagiorgis, G., & Thoenen, H. (1996). Autocrine—paracrine regulation of hippocampal neuron survival by igf-1 and the neurotrophins bdnf, nt-3 and nt-4. *European journal of neuroscience*, 8(7), 1452–1460.
- Lione, L. A., Nutt, D. J., & Hudson, A. L. (1998). Characterisation and localisation of [3H]2-(2-benzofuranyl)-2-imidazoline binding in rat brain: A selective ligand for imidazoline I2 receptors. *European Journal of Pharmacology*, 353(1), 123–135. [https://doi.org/10.1016/S0014-2999\(98\)00389-6](https://doi.org/10.1016/S0014-2999(98)00389-6)
- Liu, B., Liu, J., & Shi, J.-S. (2020). SAMP8 Mice as a Model of Age-Related Cognition Decline with Underlying Mechanisms in Alzheimer’s Disease. *J Alzheimers Dis*, 75(2), 385–395. <https://doi.org/10.3233/JAD-200063>
- Liu, Z., Zhou, T., Ziegler, A. C., Dimitrion, P., & Zuo, L. (2017). Oxidative Stress in Neurodegenerative Diseases: From Molecular Mechanisms to Clinical Applications. *Oxidative Medicine and Cellular Longevity*, 2017, 1–11. <https://doi.org/10.1155/2017/2525967>
- Livingston, G., Sommerlad, A., Orgeta, V., Costafreda, S. G., Huntley, J., Ames, D., Ballard, C., Banerjee, S., Burns, A., Cohen-Mansfield, J., Cooper, C., Fox, N., Gitlin, L. N., Howard, R., Kales, H. C., Larson, E. B., Ritchie, K., Rockwood, K., Sampson, E. L., . . . Mukadam, N. (2017). Dementia prevention, intervention, and care. *Lancet*, 390(10113), 2673–2734. [https://doi.org/10.1016/S0140-6736\(17\)31363-6](https://doi.org/10.1016/S0140-6736(17)31363-6)
- Lladó, J., Esteban, S., & García-Sevilla, J. A. (1996). The alpha 2-adrenoceptor antagonist idazoxan is an agonist at 5-HT1A autoreceptors modulating serotonin synthesis in the rat brain in vivo. *Neurosci Lett*, 218(2), 111–114. [https://doi.org/10.1016/s0304-3940\(96\)13132-3](https://doi.org/10.1016/s0304-3940(96)13132-3)
- Lleó, A. (2007). Current therapeutic options for alzheimer’s disease. *Current genomics*, 8(8), 550–558.
- López-Otín, C., Blasco, M. A., Partridge, L., Serrano, M., & Kroemer, G. (2013). The hallmarks of aging. *Cell*, 153(6), 1194–1217. <https://doi.org/10.1016/j.cell.2013.05.039>
- Lucas, S.-M., Rothwell, N. J., & Gibson, R. M. (2006). The role of inflammation in CNS injury and disease. *Br J Pharmacol*, 147 Suppl 1, S232–240. <https://doi.org/10.1038/sj.bjp.0706400>
- MacInnes, N., & Handley, S. L. (2002). Characterization of the discriminable stimulus produced by 2-BFI: Effects of imidazoline I(2)-site ligands, MAOIs, beta-carbolines, agmatine and ibogaine. *Br J Pharmacol*, 135(5), 1227–1234. <https://doi.org/10.1038/sj.bjp.0704579>



- Maes, T., Mascaró, C., Rotllant, D., Lufino, M. M. P., Estiarte, A., Guibourt, N., Cavalcanti, F., Griñan-Ferré, C., Pallàs, M., Nadal, R., Armario, A., Ferrer, I., Ortega, A., Valls, N., Fyfe, M., Martinell, M., Castro Palomino, J. C., & Buesa Arjol, C. (2020). Modulation of KDM1A with vafidemstat rescues memory deficit and behavioral alterations. *PLoS One*, *15*(5). <https://doi.org/10.1371/journal.pone.0233468>
- Maidment, I. D., Fox, C. G., Boustani, M., Rodriguez, J., Brown, R. C., & Katona, C. L. (2008). Efficacy of memantine on behavioral and psychological symptoms related to dementia: A systematic meta-analysis. *Annals of Pharmacotherapy*, *42*(1), 32–38.
- Maiese, K., Pek, L., Berger, S. B., & Reis, D. J. (1992). Reduction in focal cerebral ischemia by agents acting at imidazole receptors. *J Cereb Blood Flow Metab*, *12*(1), 53–63. <https://doi.org/10.1038/jcbfm.1992.7>
- Mallard, N. J., Hudson, A. L., & Nutt, D. J. (1992). Characterization and autoradiographical localization of non-adrenoceptor idazoxan binding sites in the rat brain. *British journal of pharmacology*, *106*(4), 1019–1027. <https://doi.org/10.1111/j.1476-5381.1992.tb14450.x>
- Mamounas, L. A., Blue, M. E., Siuciak, J. A., & Altar, C. A. (1995). Brain-derived neurotrophic factor promotes the survival and sprouting of serotonergic axons in rat brain. *J Neurosci*, *15*(12), 7929–7939.
- Mandelkow, E.-M., Drewes, G., Biernat, J., Gustke, N., Van Lint, J., Vandenheede, J. v., & Mandelkow, E. (1992). Glycogen synthase kinase-3 and the alzheimer-like state of microtubule-associated protein tau. *FEBS letters*, *314*(3), 315–321.
- Marambaud, P., Dreses-Werringloer, U., & Vingtdeux, V. (2009). Calcium signaling in neurodegeneration. *Mol Neurodegeneration*, *4*(1), 20. <https://doi.org/10.1186/1750-1326-4-20>
- Marksteiner, J., Kaufmann, W. A., Gurka, P., & Humpel, C. (2002). Synaptic proteins in Alzheimer's disease. *J Mol Neurosci*, *18*(1), 53–63. <https://doi.org/10.1385/JMN:18:1-2:53>
- Marsden, W. N. (2013). Synaptic plasticity in depression: Molecular, cellular and functional correlates. *Prog Neuropsychopharmacol Biol Psychiatry*, *43*, 168–184. <https://doi.org/10.1016/j.pnpbp.2012.12.012>
- Marsh, J., & Alifragis, P. (2018). Synaptic dysfunction in Alzheimer's disease: The effects of amyloid beta on synaptic vesicle dynamics as a novel target for therapeutic intervention. *Neural Regen Res*, *13*(4), 616–623. <https://doi.org/10.4103/1673-5374.230276>
- Martin, L., Latypova, X., & Terro, F. (2011). Post-translational modifications of tau protein: Implications for Alzheimer's disease. *Neurochem Int*, *58*(4), 458–471. <https://doi.org/10.1016/j.neuint.2010.12.023>

- Masters, C. L., Bateman, R., Blennow, K., Rowe, C. C., Sperling, R. A., & Cummings, J. L. (2015). Alzheimer's disease. *Nat Rev Dis Primers*, *1*, 15056. <https://doi.org/10.1038/nrdp.2015.56>
- McAuley, J. D., Miller, J. P., & Pang, K. C. H. (2004). Age-Related Changes in the Spontaneous Motor Rhythms of the Senescence-Accelerated Mouse (SAMP8). *Experimental Aging Research*, *30*(1), 113–127. <https://doi.org/10.1080/03610730490251513>
- McDonald, G. R., Olivieri, A., Ramsay, R. R., & Holt, A. (2010). On the formation and nature of the imidazoline I2 binding site on human monoamine oxidase-B. *Pharmacol Res*, *62*(6), 475–488. <https://doi.org/10.1016/j.phrs.2010.09.001>
- McGeer, E. G., & McGeer, P. L. (2010). Neuroinflammation in Alzheimer's disease and mild cognitive impairment: A field in its infancy. *J Alzheimers Dis*, *19*(1), 355–361. <https://doi.org/10.3233/JAD-2010-1219>
- Meana, J. J., Barturen, F., Martin, I., & García-Sevilla, J. A. (1993). Evidence of increased non-adrenoceptor [3H]idazoxan binding sites in the frontal cortex of depressed suicide victims. *Biol Psychiatry*, *34*(7), 498–501. [https://doi.org/10.1016/0006-3223\(93\)90243-7](https://doi.org/10.1016/0006-3223(93)90243-7)
- Meeker, H. C., Chadman, K. K., Heaney, A. T., & Carp, R. I. (2013). Assessment of social interaction and anxiety-like behavior in senescence-accelerated-prone and -resistant mice. *Physiol Behav*, *118*, 97–102. <https://doi.org/10.1016/j.physbeh.2013.05.003>
- Melov, S., Adlard, P. A., Morten, K., Johnson, F., Golden, T. R., Hinerfeld, D., Schilling, B., Mavros, C., Masters, C. L., Volitakis, I., Li, Q.-X., Laughton, K., Hubbard, A., Cherny, R. A., Gibson, B., & Bush, A. I. (2007). Mitochondrial oxidative stress causes hyperphosphorylation of tau. *PLoS One*, *2*(6), e536. <https://doi.org/10.1371/journal.pone.0000536>
- Menargues, A., Cedó, M., Artiga, O., Obach, R., & García-Sevilla, J. A. (1995). Effects of the I2-Imidazoline Receptor Ligand LSL 60101 on Various Models of Anorexia in Ratsfn1 [eprint: <https://nyaspubs.onlinelibrary.wiley.com/doi/pdf/10.1111/j.1749-6632.1995.tb32439.x>]. *Annals of the New York Academy of Sciences*, *763*(1), 494–496. <https://doi.org/10.1111/j.1749-6632.1995.tb32439.x>
- Meunier, J, Ieni, J, & Maurice, T. (2006). The anti-amnesic and neuroprotective effects of donepezil against amyloid  $\beta$ 25-35 peptide-induced toxicity in mice involve an interaction with the 1 receptor. *Br J Pharmacol*, *149*(8), 998–1012. <https://doi.org/10.1038/sj.bjp.0706927>
- Michel, M. C., & Insel, P. A. (1989). Are there multiple imidazoline binding sites? *Trends Pharmacol Sci*, *10*(9), 342–344. [https://doi.org/10.1016/0165-6147\(89\)90002-3](https://doi.org/10.1016/0165-6147(89)90002-3)
- Miralles, A., Olmos, G., Sastre, M., Barturen, F., Martin, I., & Garcia-Sevilla, J. A. (1993). Discrimination and pharmacological characterization of I2-imidazoline sites with [3H] idazoxan and alpha-2 adrenoceptors with [3H] RX821002 (2-methoxy ida-

- zoxan) in the human and rat brains. [Publisher: Citeseer]. *Journal of Pharmacology and Experimental Therapeutics*, 264(3), 1187–1197.
- Mirzaei, N., Mota, B. C., Birch, A. M., Davis, N., Romero-Molina, C., Katsouri, L., Palmer, E. O. C., Golbano, A., Riggall, L. J., Nagy, I., Tyacke, R., Nutt, D. J., & Sastre, M. (2021). Imidazoline ligand BU224 reverses cognitive deficits, reduces microgliosis and enhances synaptic connectivity in a mouse model of Alzheimer's disease [eprint: <https://bpspubs.onlinelibrary.wiley.com/doi/pdf/10.1111/bph.15312>]. *British Journal of Pharmacology*, 178(3), 654–671. <https://doi.org/10.1111/bph.15312>
- Miyamoto, M. (1997). Characteristics of age-related behavioral changes in senescence-accelerated mouse SAMP8 and SAMP10. *Exp Gerontol*, 32(1-2), 139–148. [https://doi.org/10.1016/s0531-5565\(96\)00061-7](https://doi.org/10.1016/s0531-5565(96)00061-7)
- Miyamoto, M., Kiyota, Y., Yamazaki, N., Nagaoka, A., Matsuo, T., Nagawa, Y., & Takeda, T. (1986). Age-related changes in learning and memory in the senescence-accelerated mouse (SAM). *Physiol Behav*, 38(3), 399–406. [https://doi.org/10.1016/0031-9384\(86\)90112-5](https://doi.org/10.1016/0031-9384(86)90112-5)
- Miyamoto, M. (2004). Emotional disorders and memory deficits in senescence-accelerated mice, SAMP8 and SAMP10. *International Congress Series*, 1260, 99–106. [https://doi.org/10.1016/S0531-5131\(03\)01597-8](https://doi.org/10.1016/S0531-5131(03)01597-8)
- Miyamoto, M., Kiyota, Y., Nishiyama, M., & Nagaoka, A. (1992). Senescence-accelerated mouse (SAM): Age-related reduced anxiety-like behavior in the SAM-P/8 strain. *Physiology & Behavior*, 51(5), 979–985. [https://doi.org/10.1016/0031-9384\(92\)90081-C](https://doi.org/10.1016/0031-9384(92)90081-C)
- Molderings, G. J., Moura, D, Fink, K, Bönisch, H, & Göthert, M. (1993). Binding of [3H]clonidine to I1-imidazoline sites in bovine adrenal medullary membranes. *Naunyn-Schmiedeberg's archives of pharmacology*, 348(1), 70–76. <https://doi.org/10.1007/BF00168539>
- Möller, H. J., & Graeber, M. B. (1998). The case described by Alois Alzheimer in 1911. Historical and conceptual perspectives based on the clinical record and neurohistological sections. *Eur Arch Psychiatry Clin Neurosci*, 248(3), 111–122. <https://doi.org/10.1007/s004060050027>
- Montolio, M., Gregori-Puigjané, E., Pineda, D., Mestres, J., & Navarro, P. (2012). Identification of small molecule inhibitors of amyloid  $\beta$ -induced neuronal apoptosis acting through the imidazoline I(2) receptor. *J Med Chem*, 55(22), 9838–9846. <https://doi.org/10.1021/jm301055g>
- Moosavi, M., Zarifkar, A. H., Farbood, Y., Dianat, M., Sarkaki, A., & Ghasemi, R. (2014). Agmatine protects against intracerebroventricular streptozotocin-induced water maze memory deficit, hippocampal apoptosis and akt/gsk3 $\beta$  signaling disruption. *European journal of pharmacology*, 736, 107–114.

- Moreira, P., Duarte, A., Santos, M., Rego, A. C., & Oliveira, C. (2009). An Integrative View of the Role of Oxidative Stress, Mitochondria and Insulin in Alzheimer's Disease. *Journal of Alzheimer's disease : JAD*, *16*, 741–61. <https://doi.org/10.3233/JAD-2009-0972>
- Morgan, N. G., Cooper, E. J., Squires, P. E., Hills, C. E., Parker, C. A., & Hudson, A. L. (2003). Comparative effects of efaroxan and b-carbolines on the secretory activity of rodent and human b cells. *Annals of the New York Academy of Sciences*, *1009*(1), 167–174.
- Mori, A., Utsumi, K., Liu, J., & Hosokawa, M. (1998). Oxidative Damage in the Senescence-accelerated Mouse. *Annals of the New York Academy of Sciences*, *854*(1), 239–250. <https://doi.org/10.1111/j.1749-6632.1998.tb09906.x>
- Morley, J. E., Kumar, V. B., Bernardo, A. E., Farr, S. A., Uezu, K., Tumosa, N., & Flood, J. F. (2000). Beta-amyloid precursor polypeptide in SAMP8 mice affects learning and memory. *Peptides*, *21*(12), 1761–1767. [https://doi.org/10.1016/s0196-9781\(00\)00342-9](https://doi.org/10.1016/s0196-9781(00)00342-9)
- Morley, J. E., Armbricht, H. J., Farr, S. A., & Kumar, V. B. (2012). The senescence accelerated mouse (SAMP8) as a model for oxidative stress and Alzheimer's disease. *Biochimica et Biophysica Acta (BBA) - Molecular Basis of Disease*, *1822*(5), 650–656. <https://doi.org/10.1016/j.bbadis.2011.11.015>
- Mukhin, V. N., Pavlov, K. I., & Klimenko, V. M. (2017). Mechanisms of Neuron Loss in Alzheimer's Disease. *Neurosci Behav Physi*, *47*(5), 508–516. <https://doi.org/10.1007/s11055-017-0427-x>
- Mullard, A. (2021). Landmark alzheimer's drug approval confounds research community. *Nature*.
- Musgrave, I. F., & Badoer, E. (2000). Harmane produces hypotension following microinjection into the RVLM: Possible role of I(1)-imidazoline receptors. *Br J Pharmacol*, *129*(6), 1057–1059. <https://doi.org/10.1038/sj.bjp.0703142>
- Ndountse, L. T., & Chan, H. M. (2009). Role of N-methyl-D-aspartate receptors in polychlorinated biphenyl mediated neurotoxicity. *Toxicol Lett*, *184*(1), 50–55. <https://doi.org/10.1016/j.toxlet.2008.10.013>
- Neumeister, K. L., & Riepe, M. W. (2012). Synergistic Effects of Antidementia Drugs on Spatial Learning and Recall in the APP23 Transgenic Mouse Model of Alzheimer's Disease. *JAD*, *30*(2), 245–251. <https://doi.org/10.3233/JAD-2012-111643>
- Ng, T. K. S., Ho, C. S. H., Tam, W. W. S., Kua, E. H., & Ho, R. C.-M. (2019). Decreased Serum Brain-Derived Neurotrophic Factor (BDNF) Levels in Patients with Alzheimer's Disease (AD): A Systematic Review and Meta-Analysis. *Int J Mol Sci*, *20*(2). <https://doi.org/10.3390/ijms20020257>

- Ni, H., Rui, Q., Lin, X., Li, D., Liu, H., & Chen, G. (2019). 2-BFI Provides Neuroprotection Against Inflammation and Necroptosis in a Rat Model of Traumatic Brain Injury. *Front Neurosci*, *13*, 674. <https://doi.org/10.3389/fnins.2019.00674>
- Niccoli, T., & Partridge, L. (2012). Ageing as a risk factor for disease. *Curr Biol*, *22*(17), R741–752. <https://doi.org/10.1016/j.cub.2012.07.024>
- Niikura, T., Tajima, H., & Kita, Y. (2006). Neuronal Cell Death in Alzheimer's Disease and a Neuroprotective Factor, Humanin. *Curr Neuropharmacol*, *4*(2), 139–147. Retrieved June 13, 2021, from <https://www.ncbi.nlm.nih.gov/pmc/articles/PMC2430668/>
- Nishi, A., Bibb, J. A., Matsuyama, S., Hamada, M., Higashi, H., Nairn, A. C., & Greengard, P. (2002). Regulation of DARPP-32 dephosphorylation at PKA- and Cdk5-sites by NMDA and AMPA receptors: Distinct roles of calcineurin and protein phosphatase-2A. *J Neurochem*, *81*(4), 832–841. <https://doi.org/10.1046/j.1471-4159.2002.00876.x>
- Nishikawa, T., Takahashi, J. A., Fujibayashi, Y., Fujisawa, H., Zhu, B., Nishimura, Y., Ohnishi, K., Higuchi, K., Hashimoto, N., & Hosokawa, M. (1998). An early stage mechanism of the age-associated mitochondrial dysfunction in the brain of SAMP8 mice; an age-associated neurodegeneration animal model. *Neuroscience Letters*, *254*(2), 69–72. [https://doi.org/10.1016/S0304-3940\(98\)00646-6](https://doi.org/10.1016/S0304-3940(98)00646-6)
- Nizami, S., Hall-Roberts, H., Warriar, S., Cowley, S. A., & Daniel, E. D. (2019). Microglial inflammation and phagocytosis in Alzheimer's disease: Potential therapeutic targets [eprint: <https://bpspubs.onlinelibrary.wiley.com/doi/pdf/10.1111/bph.14618>]. *British Journal of Pharmacology*, *176*(18), 3515–3532. <https://doi.org/10.1111/bph.14618>
- Noble, W., Olm, V., Takata, K., Casey, E., Mary, O, Meyerson, J., Gaynor, K., LaFrancois, J., Wang, L., Kondo, T., et al. (2003). Cdk5 is a key factor in tau aggregation and tangle formation in vivo. *Neuron*, *38*(4), 555–565.
- Nutt, D. J., French, N., Handley, S., Hudson, A., Husbands, S., Jackson, H., Jordan, S., Lalies, M. D., Lewis, J., & Lione, L. (1995). Functional studies of specific imidazoline-2 receptor ligands. *Ann N Y Acad Sci*, *763*, 125–139. <https://doi.org/10.1111/j.1749-6632.1995.tb32397.x>
- Oakley, H., Cole, S. L., Logan, S., Maus, E., Shao, P., Craft, J., Guillozet-Bongaarts, A., Ohno, M., Disterhoft, J., Van Eldik, L., Berry, R., & Vassar, R. (2006). Intraneuronal beta-amyloid aggregates, neurodegeneration, and neuron loss in transgenic mice with five familial Alzheimer's disease mutations: Potential factors in amyloid plaque formation. *J Neurosci*, *26*(40), 10129–10140. <https://doi.org/10.1523/JNEUROSCI.1202-06.2006>

- O'Brien, R. J., & Wong, P. C. (2011). Amyloid precursor protein processing and Alzheimer's disease. *Annu Rev Neurosci*, *34*, 185–204. <https://doi.org/10.1146/annurev-neuro-061010-113613>
- O'Brien, W. T., & Klein, P. S. (2009). Validating GSK3 as an in vivo target of lithium action. *Biochem Soc Trans*, *37*(Pt 5), 1133–1138. <https://doi.org/10.1042/BST0371133>
- Oda, A., Tamaoka, A., & Araki, W. (2010). Oxidative stress up-regulates presenilin 1 in lipid rafts in neuronal cells. *J Neurosci Res*, *88*(5), 1137–1145. <https://doi.org/10.1002/jnr.22271>
- Oh, J., Lee, Y. D., & Wagers, A. J. (2014). Stem cell aging: Mechanisms, regulators and therapeutic opportunities. *Nat Med*, *20*(8), 870–880. <https://doi.org/10.1038/nm.3651>
- Oliet, S. H., Piet, R., & Poulain, D. A. (2001). Control of glutamate clearance and synaptic efficacy by glial coverage of neurons. *Science*, *292*(5518), 923–926. <https://doi.org/10.1126/science.1059162>
- Olmos, G., Alemany, R., Boronat, M. A., & García-Sevilla, J. A. (1999a). Pharmacologic and molecular discrimination of I2-imidazoline receptor subtypes. *Ann N Y Acad Sci*, *881*, 144–160. <https://doi.org/10.1111/j.1749-6632.1999.tb09354.x>
- Olmos, G., Alemany, R., Escriba, P. V., & García-Sevilla, J. A. (1994). The effects of chronic imidazoline drug treatment on glial fibrillary acidic protein concentrations in rat brain. *Br J Pharmacol*, *111*(4), 997–1002. <https://doi.org/10.1111/j.1476-5381.1994.tb14842.x>
- Olmos, G., DeGregorio-Rocasolano, N., Paz Regalado, M., Gasull, T., Assumpció Boronat, M., Trullas, R., Villarroya, A., Lerma, J., & García-Sevilla, J. A. (1999b). Protection by imidazol(ine) drugs and agmatine of glutamate-induced neurotoxicity in cultured cerebellar granule cells through blockade of NMDA receptor. *Br J Pharmacol*, *127*(6), 1317–1326. <https://doi.org/10.1038/sj.bjp.0702679>
- Olmos, G., Gabilondo, A. M., Miralles, A., Escriba, P. V., & García-Sevilla, J. A. (1993). Chronic treatment with the monoamine oxidase inhibitors clorgyline and pargyline down-regulates non-adrenoceptor [3H]-idazoxan binding sites in the rat brain. *Br J Pharmacol*, *108*(3), 597–603. <https://doi.org/10.1111/j.1476-5381.1993.tb12848.x>
- Olmos, G., Ribera, J., & García-Sevilla, J. A. (1996a). Imidazoli(di)ne compounds interact with the phencyclidine site of NMDA receptors in the rat brain. *Eur J Pharmacol*, *310*(2-3), 273–276. [https://doi.org/10.1016/0014-2999\(96\)00519-5](https://doi.org/10.1016/0014-2999(96)00519-5)
- Olmos, G., Alemany, R., & García-Sevilla, J. A. (1996b). Pharmacological and molecular discrimination of brain I2-imidazoline receptor subtypes. *Naunyn-Schmiedeberg's Archives of Pharmacology*, *354*(6), 709–716. <https://doi.org/10.1007/BF00166896>
- O'Neill, M. F., Osborne, D. J., Woodhouse, S. M., & Conway, M. W. (2001). Selective imidazoline I2 ligands do not show antidepressant-like activity in the forced

- swim test in mice. *J Psychopharmacol*, 15(1), 18–22. <https://doi.org/10.1177/026988110101500104>
- Ownby, R. L., Crocco, E., Acevedo, A., John, V., & Loewenstein, D. (2006). Depression and risk for Alzheimer disease: Systematic review, meta-analysis, and metaregression analysis. *Arch Gen Psychiatry*, 63(5), 530–538. <https://doi.org/10.1001/archpsyc.63.5.530>
- Oxidative stress and the amyloid beta peptide in Alzheimer's disease - PubMed. Retrieved June 12, 2021, from <https://pubmed.ncbi.nlm.nih.gov/29080524/>
- Ozaita, A., Olmos, G., Boronat, M. A., Lizcano, J. M., Unzeta, M., & García-Sevilla, J. A. (1997). Inhibition of monoamine oxidase A and B activities by imidazol(ine)/guanidine drugs, nature of the interaction and distinction from I2-imidazoline receptors in rat liver. *Br J Pharmacol*, 121(5), 901–912. <https://doi.org/10.1038/sj.bjp.0701214>
- Pallas, M., Camins, A., Smith, M. A., Perry, G., Lee, H.-g., & Casadesus, G. (2008). From aging to Alzheimer's disease: Unveiling "the switch" with the senescence-accelerated mouse model (SAMP8). *J Alzheimers Dis*, 15(4), 615–624. <https://doi.org/10.3233/jad-2008-15408>
- Pallàs, M. (2012). Senescence-Accelerated Mice P8: A Tool to Study Brain Aging and Alzheimer's Disease in a Mouse Model. *ISRN Cell Biology*, 2012, 1–12. <https://doi.org/10.5402/2012/917167>
- Parini, A., Moudanos, C. G., Pizzinat, N., & Lanier, S. M. (1996). The elusive family of imidazoline binding sites. *Trends Pharmacol Sci*, 17(1), 13–16. [https://doi.org/10.1016/0165-6147\(96\)81564-1](https://doi.org/10.1016/0165-6147(96)81564-1)
- Parker, C. A., Anderson, N. J., Robinson, E. S. J., Price, R., Tyacke, R. J., Husbands, S. M., Dillon, M. P., Eglen, R. M., Hudson, A. L., Nutt, D. J., Crump, M. P., & Crosby, J. (2004). Harmane and harmalan are bioactive components of classical clonidine-displacing substance. *Biochemistry*, 43(51), 16385–16392. <https://doi.org/10.1021/bi048584v>
- Parker, C. A., Nabulsi, N., Holden, D., Lin, S.-f., Cass, T., Labaree, D., Kealey, S., Gee, A. D., Husbands, S. M., Quelch, D., et al. (2014). Evaluation of 11c-bu99008, a pet ligand for the imidazoline2 binding sites in rhesus brain. *Journal of Nuclear Medicine*, 55(5), 838–844.
- Parsons, C. G., Stöffler, A., & Danysz, W. (2007). Memantine: A nmda receptor antagonist that improves memory by restoration of homeostasis in the glutamatergic system- too little activation is bad, too much is even worse. *Neuropharmacology*, 53(6), 699–723.
- Paterson, L. M., Tyacke, R. J., Robinson, E. S. J., Nutt, D. J., & Hudson, A. L. (2007). In vitro and in vivo effect of BU99006 (5-isothiocyano-2-benzofuranyl-2-imidazoline) on I2 binding in relation to MAO: Evidence for two distinct I2 binding

- sites. *Neuropharmacology*, 52(2), 395–404. <https://doi.org/10.1016/j.neuropharm.2006.08.010>
- Pawate, S., Shen, Q., Fan, F., & Bhat, N. R. (2004). Redox regulation of glial inflammatory response to lipopolysaccharide and interferon $\gamma$ . *Journal of neuroscience research*, 77(4), 540–551.
- Penney, J., Ralvenius, W. T., & Tsai, L.-H. (2020). Modeling alzheimer's disease with ipsc-derived brain cells. *Molecular psychiatry*, 25(1), 148–167.
- Perl, D. P. (2010). Neuropathology of Alzheimer's disease. *Mt Sinai J Med*, 77(1), 32–42. <https://doi.org/10.1002/msj.20157>
- Perry, G., Roder, H., Nunomura, A., Takeda, A., Friedlich, A. L., Zhu, X., Raina, A. K., Holbrook, N., Siedlak, S. L., Harris, P. L., & Smith, M. A. (1999). Activation of neuronal extracellular receptor kinase (ERK) in Alzheimer disease links oxidative stress to abnormal phosphorylation. *Neuroreport*, 10(11), 2411–2415. <https://doi.org/10.1097/00001756-199908020-00035>
- Perry, V. H., & Teeling, J. (2013). Microglia and macrophages of the central nervous system: The contribution of microglia priming and systemic inflammation to chronic neurodegeneration. *Semin Immunopathol*, 35(5), 601–612. <https://doi.org/10.1007/s00281-013-0382-8>
- Piletz, J. E., Deleersnijder, W, Roth, B. L., Ernsberger, P, Zhu, H, & Ziegler, D. (2003). IRAS splice variants. *Annals of the New York Academy of Sciences*, 1009, 419–426. <https://doi.org/10.1196/annals.1304.056>
- Piletz, J. E., Halaris, A., & Ernsberger, P. R. (1994). Psychopharmacology of imidazoline and alpha 2-adrenergic receptors: Implications for depression. *Crit Rev Neurobiol*, 9(1), 29–66.
- Piletz, J. E., Ivanov, T. R., Sharp, J. D., Ernsberger, P, Chang, C. H., Pickard, R. T., Gold, G, Roth, B, Zhu, H, Jones, J. C., Baldwin, J, & Reis, D. J. (2000a). Imidazoline receptor antisera-selected (IRAS) cDNA: Cloning and characterization. *DNA and cell biology*, 19(6), 319–329. <https://doi.org/10.1089/10445490050043290>
- Piletz, J. E., Jones, J. C., Zhu, H, Bishara, O, & Ernsberger, P. (1999). Imidazoline receptor antisera-selected cDNA clone and mRNA distribution. *Annals of the New York Academy of Sciences*, 881, 1–7. <https://doi.org/10.1111/j.1749-6632.1999.tb09335.x>
- Piletz, J. E., Zhu, H., Ordway, G., Stockmeier, C., Dilly, G., Reis, D., & Halaris, A. (2000b). Imidazoline receptor proteins are decreased in the hippocampus of individuals with major depression. *Biol Psychiatry*, 48(9), 910–919. [https://doi.org/10.1016/s0006-3223\(00\)00892-1](https://doi.org/10.1016/s0006-3223(00)00892-1)
- Piletz, J., Baker, R., & Halaris, A. (2008). Platelet imidazoline receptors as state marker of depressive symptomatology. *Journal of psychiatric research*, 42(1), 41–49.



- Piletz, J. E., Aricioglu, F., Cheng, J.-T., Fairbanks, C. A., Gilad, V. H., Haenisch, B., Halaris, A., Hong, S., Lee, J. E., Li, J., Liu, P., Molderings, G. J., Rodrigues, A. L. S., Satriano, J., Seong, G. J., Wilcox, G., Wu, N., & Gilad, G. M. (2013). Agmatine: Clinical applications after 100 years in translation. *Drug Discov Today*, 18(17-18), 880–893. <https://doi.org/10.1016/j.drudis.2013.05.017>
- Pinton, P., Giorgi, C., Siviero, R., Zecchini, E., & Rizzuto, R. (2008). Calcium and apoptosis: ER-mitochondria Ca<sup>2+</sup> transfer in the control of apoptosis. *Oncogene*, 27(50), 6407–6418. <https://doi.org/10.1038/onc.2008.308>
- Podtelezhnikov, A. A., Tanis, K. Q., Nebozhyn, M., Ray, W. J., Stone, D. J., & Loboda, A. P. (2011). Molecular insights into the pathogenesis of Alzheimer's disease and its relationship to normal aging. *PLoS One*, 6(12), e29610. <https://doi.org/10.1371/journal.pone.0029610>
- Polidori, C., Gentili, F., Pignini, M., Quaglia, W., Panocka, I., & Massi, M. (2000). Hyperphagic effect of novel compounds with high affinity for imidazoline I(2) binding sites. *European journal of pharmacology*, 392(1-2), 41–49. [https://doi.org/10.1016/s0014-2999\(00\)00014-5](https://doi.org/10.1016/s0014-2999(00)00014-5)
- Prell, G. D., Martinelli, G. P., Holstein, G. R., Matulić-Adamić, J., Watanabe, K. A., Chan, S. L., Morgan, N. G., Haxhiu, M. A., & Ernsberger, P. (2004). Imidazoleacetic acid-ribotide: An endogenous ligand that stimulates imidazol (in) e receptors. *Proceedings of the National Academy of Sciences*, 101(37), 13677–13682.
- P´rez-Cáceres, D., Ciudad-Roberts, A., Rodrigo, M. T., Pubill, D., Camins, A., Camarasa, J., Escubedo, E., & Pallàs, M. (2013). Depression-like behavior is dependent on age in male SAMP8 mice. *Biogerontology*, 14(2), 165–176. <https://doi.org/10.1007/s10522-013-9420-0>
- Qiu, Y., He, X.-H., Zhang, Y., & Li, J.-X. (2014). Discriminative stimulus effects of the novel imidazoline I receptor ligand CR4056 in rats. *Sci Rep*, 4, 6605. <https://doi.org/10.1038/srep06605>
- Qiu, Y., Zhang, Y., & Li, J.-X. (2015). Discriminative stimulus effects of the imidazoline I2 receptor ligands BU224 and phenyzoline in rats. *Eur J Pharmacol*, 749, 133–141. <https://doi.org/10.1016/j.ejphar.2015.01.013>
- Quintana, A., Giralt, M., Rojas, S., Penkowa, M., Campbell, I. L., Hidalgo, J., & Molinero, A. (2005). Differential role of tumor necrosis factor receptors in mouse brain inflammatory responses in cryolesion brain injury. *Journal of neuroscience research*, 82(5), 701–716.
- Raasch, W., Muhle, H., & Dominiak, P. (1999). Modulation of MAO activity by imidazoline and guanidine derivatives. *Ann N Y Acad Sci*, 881, 313–331. <https://doi.org/10.1111/j.1749-6632.1999.tb09376.x>

- Raasch, W., Regunathan, S., Li, G., & Reis, D. J. (1995). Agmatine is widely and unequally distributed in rat organs. *Annals of the New York Academy of Sciences*, 763(1), 330–334.
- Raddatz, R., Parini, A., & Lanier, S. M. (1997). Localization of the imidazoline binding domain on monoamine oxidase B. *Mol Pharmacol*, 52(4), 549–553. <https://doi.org/10.1124/mol.52.4.549>
- Raynaud, F., & Marcilhac, A. (2006). Implication of calpain in neuronal apoptosis. A possible regulation of Alzheimer's disease. *FEBS J*, 273(15), 3437–3443. <https://doi.org/10.1111/j.1742-4658.2006.05352.x>
- Reese, L. C., & Tagliatela, G. (2011). A role for calcineurin in Alzheimer's disease. *Curr Neuropharmacol*, 9(4), 685–692. <https://doi.org/10.2174/157015911798376316>
- Regunathan, S., Feinstein, D. L., & Reis, D. J. (1993). Expression of non-adrenergic imidazoline sites in rat cerebral cortical astrocytes. *J Neurosci Res*, 34(6), 681–688. <https://doi.org/10.1002/jnr.490340611>
- Regunathan, S., Feinstein, D., & Reis, D. (1999). Anti-proliferative and anti-inflammatory actions of imidazoline agents: Are imidazoline receptors involved? *Annals of the New York Academy of Sciences*, 881(1), 410–419.
- Regunathan, S., & Reis, D. J. (1996). Imidazoline receptors and their endogenous ligands. *Annual Review of Pharmacology and Toxicology*, 36(50), 511–544. <https://doi.org/10.1146/annurev.pa.36.040196.002455>
- Reis, D. J., & Regunathan, S. (2000). Is agmatine a novel neurotransmitter in brain? *Trends Pharmacol Sci*, 21(5), 187–193. [https://doi.org/10.1016/s0165-6147\(00\)01460-7](https://doi.org/10.1016/s0165-6147(00)01460-7)
- Reis, D. J., & Regunathan, S. (1999). Agmatine: An endogenous ligand at imidazoline receptors is a novel neurotransmitter a. *Annals of the New York Academy of Sciences*, 881(1), 65–80.
- Reitz, C., & Mayeux, R. (2014). Alzheimer disease: Epidemiology, diagnostic criteria, risk factors and biomarkers. *Biochem Pharmacol*, 88(4), 640–651. <https://doi.org/10.1016/j.bcp.2013.12.024>
- Remaury, A., Missy, K., & Parini, A. (1998). Characterization of [3H]idazoxan binding proteins in solubilized membranes from rabbit and human liver. *J Auton Nerv Syst*, 72(2-3), 111–117. [https://doi.org/10.1016/s0165-1838\(98\)00095-2](https://doi.org/10.1016/s0165-1838(98)00095-2)
- Remaury, A., Ordener, C., Shih, J., & Parini, A. (1999). Relationship between I2 imidazoline binding sites and monoamine oxidase B in liver. *Ann N Y Acad Sci*, 881, 32–34. <https://doi.org/10.1111/j.1749-6632.1999.tb09338.x>
- Remaury, A., Raddatz, R., Ordener, C., Savic, S., Shih, J. C., Chen, K., Seif, I., De Maeyer, E., Lanier, S. M., & Parini, A. (2000). Analysis of the pharmacological and molecular heterogeneity of I(2)-imidazoline-binding proteins using monoamine oxidase-deficient mouse models. *Mol Pharmacol*, 58(5), 1085–1090. <https://doi.org/10.1124/mol.58.5.1085>

- Reynolds, G. P., Boulton, R. M., Pearson, S. J., Hudson, A. L., & Nutt, D. J. (1996). Imidazoline binding sites in Huntington's and Parkinson's disease putamen. *Eur J Pharmacol*, *301*(1-3), R19–21. [https://doi.org/10.1016/0014-2999\(96\)00196-3](https://doi.org/10.1016/0014-2999(96)00196-3)
- Richard, B. C., Kurdakova, A., Baches, S., Bayer, T. A., Weggen, S., & Wirths, O. (2015). Gene dosage dependent aggravation of the neurological phenotype in the 5xfad mouse model of alzheimer's disease. *Journal of Alzheimer's Disease*, *45*(4), 1223–1236.
- Roberson, E. D., Halabisky, B., Yoo, J. W., Yao, J., Chin, J., Yan, F., Wu, T., Hamto, P., Devidze, N., Yu, G.-Q., Palop, J. J., Noebels, J. L., & Mucke, L. (2011). Amyloid- $\beta$ /Fyn-induced synaptic, network, and cognitive impairments depend on tau levels in multiple mouse models of Alzheimer's disease. *J Neurosci*, *31*(2), 700–711. <https://doi.org/10.1523/JNEUROSCI.4152-10.2011>
- Roberson, E. D., Scarce-Levie, K., Palop, J. J., Yan, F., Cheng, I. H., Wu, T., Gerstein, H., Yu, G.-Q., & Mucke, L. (2007). Reducing endogenous tau ameliorates amyloid beta-induced deficits in an Alzheimer's disease mouse model. *Science*, *316*(5825), 750–754. <https://doi.org/10.1126/science.1141736>
- Rochais, C., Lecoutey, C., Hamidouche, K., Giannoni, P., Gaven, F., Cem, E., Mignani, S., Baranger, K., Freret, T., Bockaert, J., Rivera, S., Boulouard, M., Dallemagne, P., & Claeysen, S. (2020). Donecopride, a Swiss army knife with potential against Alzheimer's disease. *Br J Pharmacol*, *177*(9), 1988–2005. <https://doi.org/10.1111/bph.14964>
- Rodriguez-Arévalo, S., Bagán, A., Griñán-Ferré, C., Vasilopoulou, F., Pallàs, M., Brocos-Mosquera, I., Callado, L. F., Loza, M. I., Martínez, A. L., Brea, J., Pérez, B., Molins, E., De Jonghe, S., Daelemans, D., Radan, M., Djikic, T., Nikolic, K., Hernández-Hernández, E., García-Fuster, M. J., ... Escolano, C. (2021). Benzofuranyl-2-imidazoles as imidazoline I2 receptor ligands for Alzheimer's disease. *European Journal of Medicinal Chemistry*, *222*, 113540. <https://doi.org/10.1016/j.ejmech.2021.113540>
- Rossi, D., & Volterra, A. (2009). Astrocytic dysfunction: Insights on the role in neurodegeneration. *Brain research bulletin*, *80*(4-5), 224–232.
- Rouot, B. R., & Snyder, S. H. (1979). [3H]Para-amino-clonidine: A novel ligand which binds with high affinity to alpha-adrenergic receptors. *Life sciences*, *25*(9), 769–774. [https://doi.org/10.1016/0024-3205\(79\)90521-6](https://doi.org/10.1016/0024-3205(79)90521-6)
- Rovati, L. C., Brambilla, N., Blicharski, T., Connell, J., Vitalini, C., Bonazzi, A., Giacobelli, G., Girolami, F., & D'Amato, M. (2020). Efficacy and safety of the first-in-class imidazoline-2 receptor ligand CR4056 in pain from knee osteoarthritis and disease phenotypes: A randomized, double-blind, placebo-controlled phase 2 trial. *Osteoarthritis and Cartilage*, *28*(1), 22–30. <https://doi.org/10.1016/j.joca.2019.09.002>

- Rubinsztein, D. C., Mariño, G., & Kroemer, G. (2011). Autophagy and aging. *Cell*, *146*(5), 682–695. <https://doi.org/10.1016/j.cell.2011.07.030>
- Ruffolo, R. R., Turowski, B. S., & Patil, P. N. (1977). Lack of cross-desensitization between structurally dissimilar alpha-adrenoceptor agonists. *The Journal of pharmacy and pharmacology*, *29*(6), 378–380. <https://doi.org/10.1111/j.2042-7158.1977.tb11344.x>
- Ruffolo, R. R. J., Rice, P. J., Patil, P. N., Hamada, A., & Miller, D. D. (1983). Differences in the applicability of the easson-stedman hypothesis to the alpha 1- and alpha 2-adrenergic effects of phenethylamines and imidazolines. *European journal of pharmacology*, *86*(3-4), 471–475. [https://doi.org/10.1016/0014-2999\(83\)90199-1](https://doi.org/10.1016/0014-2999(83)90199-1)
- Ruggiero, D. A., Regunathan, S., Wang, H., Milner, T. A., & Reis, D. J. (1995). Distribution of imidazoline receptor binding protein in the central nervous system. *Ann N Y Acad Sci*, *763*, 208–221. <https://doi.org/10.1111/j.1749-6632.1995.tb32408.x>
- Ruggiero, D. A., Regunathan, S., Wang, H., Milner, T. A., & Reis, D. J. (1998). Immunocytochemical localization of an imidazoline receptor protein in the central nervous system. *Brain Res*, *780*(2), 270–293. [https://doi.org/10.1016/s0006-8993\(97\)01203-1](https://doi.org/10.1016/s0006-8993(97)01203-1)
- Ruiz, J, Martin, I, Callado, L., Meana, J., Barturen, F, & Garcia-Sevilla, J. (1993). Non-adrenoceptor [3h] idazoxan binding sites (i2-imidazoline sites) are increased in postmortem brain from patients with alzheimer's disease. *Neuroscience letters*, *160*(1), 109–112.
- Sama, D. M., & Norris, C. M. (2013). Calcium dysregulation and neuroinflammation: Discrete and integrated mechanisms for age-related synaptic dysfunction. *Ageing Res Rev*, *12*(4). <https://doi.org/10.1016/j.arr.2013.05.008>
- S'anchez-Blázquez, P., Boronat, M. A., Olmos, G., García-Sevilla, J. A., & Garzón, J. (2000). Activation of I2-imidazoline receptors enhances supraspinal morphine analgesia in mice: A model to detect agonist and antagonist activities at these receptors. *Br J Pharmacol*, *130*(1), 146–152. <https://doi.org/10.1038/sj.bjp.0703294>
- Sasaguri, H., Nilsson, P., Hashimoto, S., Nagata, K., Saito, T., De Strooper, B., Hardy, J., Vassar, R., Winblad, B., & Saido, T. C. (2017). APP mouse models for Alzheimer's disease preclinical studies. *EMBO J*, *36*(17), 2473–2487. <https://doi.org/10.15252/embj.201797397>
- Sastre, M., & García-Sevilla, J. A. (1997). Densities of I2-imidazoline receptors, alpha 2-adrenoceptors and monoamine oxidase B in brains of suicide victims. *Neurochem Int*, *30*(1), 63–72. [https://doi.org/10.1016/s0197-0186\(96\)00032-0](https://doi.org/10.1016/s0197-0186(96)00032-0)
- Sastre, M., & García-Sevilla, J. A. (1993). Opposite age-dependent changes of alpha 2A-adrenoceptors and nonadrenoceptor [3H]idazoxan binding sites (I2-imidazoline

- sites) in the human brain: Strong correlation of I2 with monoamine oxidase-B sites. *J Neurochem*, 61(3), 881–889. <https://doi.org/10.1111/j.1471-4159.1993.tb03599.x>
- Sastre, M., Ventayol, P., & García-Sevilla, J. A. (1996). Decreased density of I2-imidazoline receptors in the postmortem brain of heroin addicts. *Neuroreport*, 7(2), 509–512. <https://doi.org/10.1097/00001756-199601310-00032>
- Sastre-Coll, A., Esteban, S., & García-Sevilla, J. A. (1999). Effects of imidazoline receptor ligands on monoamine synthesis in the rat brain in vivo. *Naunyn Schmiedeberg's Arch Pharmacol*, 360(1), 50–62. <https://doi.org/10.1007/s002109900032>
- Sato, E., Kurokawa, T., Oda, N., & Ishibashi, S. (1996a). Early appearance of abnormality of microperoxisomal enzymes in the cerebral cortex of senescence-accelerated mouse. *Mech Ageing Dev*, 92(2-3), 175–184. [https://doi.org/10.1016/s0047-6374\(96\)01832-5](https://doi.org/10.1016/s0047-6374(96)01832-5)
- Sato, E., Oda, N., Ozaki, N., Hashimoto, S., Kurokawa, T., & Ishibashi, S. (1996b). Early and transient increase in oxidative stress in the cerebral cortex of senescence-accelerated mouse. *Mech Ageing Dev*, 86(2), 105–114. [https://doi.org/10.1016/0047-6374\(95\)01681-3](https://doi.org/10.1016/0047-6374(95)01681-3)
- Saura, C. A., & Valero, J. (2011). The role of CREB signaling in Alzheimer's disease and other cognitive disorders. *Rev Neurosci*, 22(2), 153–169. <https://doi.org/10.1515/RNS.2011.018>
- Scheff, S. W., Neltner, J. H., & Nelson, P. T. (2014). Is synaptic loss a unique hallmark of Alzheimer's disease? *Biochem Pharmacol*, 88(4), 517–528. <https://doi.org/10.1016/j.bcp.2013.12.028>
- Schmitt, H., & Fénard, S. (1973). Action of -adrenergic blocking drugs on the sympathetic centres and their interactions with the central sympatho-inhibitory effect of clonidine. *Arzneimittel-Forschung*, 23(1), 40–45.
- Selkoe, D. J. (2002). Alzheimer's disease is a synaptic failure. *Science*, 298(5594), 789–791. <https://doi.org/10.1126/science.1074069>
- Selkoe, D. J. (2013). The therapeutics of Alzheimer's disease: Where we stand and where we are heading. *Ann Neurol*, 74(3), 328–336. <https://doi.org/10.1002/ana.24001>
- Selkoe, D. J., & Hardy, J. (2016). The amyloid hypothesis of Alzheimer's disease at 25 years. *EMBO Mol Med*, 8(6), 595–608. <https://doi.org/10.15252/emmm.201606210>
- Selkoe, D. J., & Podlisny, M. B. (2002). Deciphering the genetic basis of Alzheimer's disease. *Annu Rev Genomics Hum Genet*, 3, 67–99. <https://doi.org/10.1146/annurev.genom.3.022502.103022>
- Selles, M. C., Oliveira, M. M., & Ferreira, S. T. (2018). Brain Inflammation Connects Cognitive and Non-Cognitive Symptoms in Alzheimer's Disease. *J Alzheimers Dis*, 64(s1), S313–S327. <https://doi.org/10.3233/JAD-179925>

- Shin, J., Park, S., Lee, H., & Kim, Y. (2021). Thioflavin-positive tau aggregates complicating quantification of amyloid plaques in the brain of 5XFAD transgenic mouse model [Number: 1 Publisher: Nature Publishing Group]. *Sci Rep*, *11*(1), 1617. <https://doi.org/10.1038/s41598-021-81304-6>
- Shinosaki, K., Nishikawa, T., & Takeda, M. (2000). Neurobiological basis of behavioral and psychological symptoms in dementia of the Alzheimer type. *Psychiatry Clin Neurosci*, *54*(6), 611–620. <https://doi.org/10.1046/j.1440-1819.2000.00773.x>
- Shipton, O. A., Leitz, J. R., Dworzak, J., Acton, C. E. J., Tunbridge, E. M., Denk, F., Dawson, H. N., Vitek, M. P., Wade-Martins, R., Paulsen, O., & Vargas-Caballero, M. (2011). Tau protein is required for amyloid {beta}-induced impairment of hippocampal long-term potentiation. *J Neurosci*, *31*(5), 1688–1692. <https://doi.org/10.1523/JNEUROSCI.2610-10.2011>
- Shukla, V., Zheng, Y.-L., Mishra, S. K., Amin, N. D., Steiner, J., Grant, P., Kesavapany, S., & Pant, H. C. (2013). A truncated peptide from p35, a Cdk5 activator, prevents Alzheimer's disease phenotypes in model mice. *FASEB J*, *27*(1), 174–186. <https://doi.org/10.1096/fj.12-217497>
- Sica, D. A. (2007). Centrally acting antihypertensive agents: An update. *Journal of clinical hypertension (Greenwich, Conn.)*, *9*(5), 399–405. <https://doi.org/10.1111/j.1524-6175.2007.07161.x>
- Siemian, J. N., LaMacchia, Z. M., Spreuer, V., Tian, J., Ignatowski, T. A., Paez, P. M., Zhang, Y., & Li, J.-X. (2018a). The imidazoline I2 receptor agonist 2-BFI attenuates hypersensitivity and spinal neuroinflammation in a rat model of neuropathic pain. *Biochem Pharmacol*, *153*, 260–268. <https://doi.org/10.1016/j.bcp.2018.01.032>
- Siemian, J. N., Obeng, S., Zhang, Y., Zhang, Y., & Li, J.-X. (2016). Antinociceptive interactions between the imidazoline i2 receptor agonist 2-bfi and opioids in rats: Role of efficacy at the  $\mu$ -opioid receptor. *Journal of Pharmacology and Experimental Therapeutics*, *357*(3), 509–519.
- Siemian, J. N., Shang, L., Seaman, R. W., Zhu, Q., Zhang, Y., & Li, J.-X. (2019). Effects of imidazoline I2 receptor agonists on reserpine-induced hyperalgesia and depressive-like behavior in rats. *Behavioural Pharmacology*, *30*(5), 429–434. <https://doi.org/10.1097/FBP.0000000000000454>
- Siemian, J. N., Wang, K., Zhang, Y., & Li, J. (2018b). Mechanisms of imidazoline I2 receptor agonist-induced antinociception in rats: Involvement of monoaminergic neurotransmission. *Br J Pharmacol*, *175*(9), 1519–1534. <https://doi.org/10.1111/bph.14161>
- Sierksma, A., Escott-Price, V., & Strooper, B. D. (2020). Translating genetic risk of Alzheimer's disease into mechanistic insight and drug targets [Publisher: American Association for the Advancement of Science Section: Review]. *Science*, *370*(6512), 61–66. <https://doi.org/10.1126/science.abb8575>

- Simpson, D. S. A., & Oliver, P. L. (2020). ROS Generation in Microglia: Understanding Oxidative Stress and Inflammation in Neurodegenerative Disease. *Antioxidants (Basel)*, 9(8). <https://doi.org/10.3390/antiox9080743>
- Sompol, P., & Norris, C. M. (2018). Ca<sup>2+</sup>, astrocyte activation and calcineurin/nfat signaling in age-related neurodegenerative diseases. *Frontiers in aging neuroscience*, 10, 199.
- Song, C., Merali, Z., & Anisman, H. (1999). Variations of nucleus accumbens dopamine and serotonin following systemic interleukin-1, interleukin-2 or interleukin-6 treatment. *Neuroscience*, 88(3), 823–836. [https://doi.org/10.1016/s0306-4522\(98\)00271-1](https://doi.org/10.1016/s0306-4522(98)00271-1)
- Spires-Jones, T. L., & Hyman, B. T. (2014). The intersection of amyloid beta and tau at synapses in Alzheimer's disease. *Neuron*, 82(4), 756–771. <https://doi.org/10.1016/j.neuron.2014.05.004>
- Stähle, H. (2000). A historical perspective: Development of clonidine. *Best Practice & Research Clinical Anaesthesiology*, 14(2), 237–246. <https://doi.org/10.1053/bean.2000.0079>
- Sudduth, T. L., Schmitt, F. A., Nelson, P. T., & Wilcock, D. M. (2013). Neuroinflammatory phenotype in early Alzheimer's disease. *Neurobiol Aging*, 34(4), 1051–1059. <https://doi.org/10.1016/j.neurobiolaging.2012.09.012>
- Sun, Z., Chang, C.-H., & Ernsberger, P. (2007). Identification of IRAS/Nischarin as an I1-imidazoline receptor in PC12 rat pheochromocytoma cells. *Journal of neurochemistry*, 101(1), 99–108. <https://doi.org/10.1111/j.1471-4159.2006.04413.x>
- Sureda, F. X., Gutierrez-Cuesta, J., Romeu, M., Mulero, M., Canudas, A. M., Camins, A., Mallol, J., & Pallàs, M. (2006). Changes in oxidative stress parameters and neurodegeneration markers in the brain of the senescence-accelerated mice SAMP-8. *Exp Gerontol*, 41(4), 360–367. <https://doi.org/10.1016/j.exger.2006.01.015>
- Svenningsson, P., Nishi, A., Fisone, G., Girault, J.-A., Nairn, A. C., & Greengard, P. (2004). DARPP-32: An integrator of neurotransmission. *Annu Rev Pharmacol Toxicol*, 44, 269–296. <https://doi.org/10.1146/annurev.pharmtox.44.101802.121415>
- Swerdlow, R. H., Burns, J. M., & Khan, S. M. (2010). The Alzheimer's Disease Mitochondrial Cascade Hypothesis (X. Zhu, M. F. Beal, X. Wang, G. Perry, & M. A. Smith, Eds.). *JAD*, 20(s2), S265–S279. <https://doi.org/10.3233/JAD-2010-100339>
- Takada-Takatori, Y., Kume, T., Izumi, Y., Ohgi, Y., Niidome, T., Fujii, T., Sugimoto, H., & Akaike, A. (2009). Roles of nicotinic receptors in acetylcholinesterase inhibitor-induced neuroprotection and nicotinic receptor up-regulation. *Biol Pharm Bull*, 32(3), 318–324. <https://doi.org/10.1248/bpb.32.318>
- Takashima, A., Noguchi, K., Michel, G., Mercken, M., Hoshi, M., Ishiguro, K., & Imahori, K. (1996). Exposure of rat hippocampal neurons to amyloid  $\beta$  peptide (25–35) induces the inactivation of phosphatidylinositol-3 kinase and the activation of tau

- protein kinase I/glycogen synthase kinase-3 $\beta$ . *Neuroscience Letters*, 203(1), 33–36. [https://doi.org/10.1016/0304-3940\(95\)12257-5](https://doi.org/10.1016/0304-3940(95)12257-5)
- Takeda, T. (1999). Senescence-accelerated mouse (SAM): A biogerontological resource in aging research. *Neurobiol Aging*, 20(2), 105–110. [https://doi.org/10.1016/s0197-4580\(99\)00008-1](https://doi.org/10.1016/s0197-4580(99)00008-1)
- Takeda, T., Hosokawa, M., & Higuchi, K. (1991). Senescence-accelerated mouse (SAM): A novel murine model of accelerated senescence. *J Am Geriatr Soc*, 39(9), 911–919. <https://doi.org/10.1111/j.1532-5415.1991.tb04460.x>
- Takeda, T., Hosokawa, M., & Higuchi, K. (1997a). Senescence-accelerated mouse (SAM): A novel murine model of senescence. *Exp Gerontol*, 32(1-2), 105–109. [https://doi.org/10.1016/s0531-5565\(96\)00036-8](https://doi.org/10.1016/s0531-5565(96)00036-8)
- Takeda, T., Matsushita, T., Kurozumi, M., Takemura, K., Higuchi, K., & Hosokawa, M. (1997b). Pathobiology of the senescence-accelerated mouse (SAM). *Exp Gerontol*, 32(1-2), 117–127. [https://doi.org/10.1016/s0531-5565\(96\)00068-x](https://doi.org/10.1016/s0531-5565(96)00068-x)
- Takemura, M., Nakamura, S., Akiguchi, I., Ueno, M., Oka, N., Ishikawa, S., Shimada, A., Kimura, J., & Takeda, T. (1993a). Beta/A4 proteinlike immunoreactive granular structures in the brain of senescence-accelerated mouse. *Am J Pathol*, 142(6), 1887–1897. Retrieved June 13, 2021, from <https://www.ncbi.nlm.nih.gov/pmc/articles/PMC1886996/>
- Takemura, M., Nakamura, S., Akiguchi, I., Ueno, M., Oka, N., Ishikawa, S., Shimada, A., Kimura, J., & Takeda, T. (1993b). Beta/a4 proteinlike immunoreactive granular structures in the brain of senescence-accelerated mouse. *The American journal of pathology*, 142(6), 1887.
- Tallarida, R. J. (2011). Quantitative Methods for Assessing Drug Synergism. *Genes & Cancer*, 2(11), 1003–1008. <https://doi.org/10.1177/1947601912440575>
- Tamagno, E., Bardini, P., Obbili, A., Vitali, A., Borghi, R., Zaccheo, D., Pronzato, M. A., Danni, O., Smith, M. A., Perry, G., & Tabaton, M. (2002). Oxidative stress increases expression and activity of BACE in NT2 neurons. *Neurobiol Dis*, 10(3), 279–288. <https://doi.org/10.1006/nbdi.2002.0515>
- Tampi, R. R., Tampi, D. J., Balachandran, S., & Srinivasan, S. (2016). Antipsychotic use in dementia: A systematic review of benefits and risks from meta-analyses. *Therapeutic advances in chronic disease*, 7(5), 229–245.
- Tanaka, K., & Matsuda, N. (2014). Proteostasis and neurodegeneration: The roles of proteasomal degradation and autophagy. *Biochim Biophys Acta*, 1843(1), 197–204. <https://doi.org/10.1016/j.bbamcr.2013.03.012>
- Tang, Y.-P., & Gershon, E. S. (2003). Genetic studies in alzheimer's disease. *Dialogues in clinical neuroscience*, 5(1), 17.
- Tannenberg, R. K., Scott, H. L., Tannenberg, A. E. G., & Dodd, P. R. (2006). Selective loss of synaptic proteins in Alzheimer's disease: Evidence for an increased severity



- with APOE 4. *Neurochemistry International*, 49(7), 631–639. <https://doi.org/10.1016/j.neuint.2006.05.004>
- Tariot, P. N., Farlow, M. R., Grossberg, G. T., Graham, S. M., McDonald, S., Gergel, I., Group, M. S., Group, M. S., et al. (2004). Memantine treatment in patients with moderate to severe alzheimer disease already receiving donepezil: A randomized controlled trial. *Jama*, 291(3), 317–324.
- Terry, R. D., Peck, A., DeTeresa, R., Schechter, R., & Horoupian, D. S. (1981). Some morphometric aspects of the brain in senile dementia of the Alzheimer type. *Ann Neurol*, 10(2), 184–192. <https://doi.org/10.1002/ana.410100209>
- Terwel, D., Muyliaert, D., Dewachter, I., Borghgraef, P., Croes, S., Devijver, H., & Van Leuven, F. (2008). Amyloid activates GSK-3beta to aggravate neuronal tauopathy in bigenic mice. *Am J Pathol*, 172(3), 786–798. <https://doi.org/10.2353/ajpath.2008.070904>
- Tesson, F., Limon-Boulez, I., Urban, P., Puype, M., Vandekerckhove, J., Couprie, I., Pompon, D., & Parini, A. (1995). Localization of I2-imidazoline binding sites on monoamine oxidases. *J Biol Chem*, 270(17), 9856–9861. <https://doi.org/10.1074/jbc.270.17.9856>
- Tesson, F., & Parini, A. (1991). Identification of an imidazoline-guanidinium receptive site in mitochondria from rabbit cerebral cortex. *Eur J Pharmacol*, 208(1), 81–83. [https://doi.org/10.1016/0922-4106\(91\)90055-m](https://doi.org/10.1016/0922-4106(91)90055-m)
- Tesson, F., Prip-Buus, C., Lemoine, A., Pegorier, J. P., & Parini, A. (1991). Subcellular distribution of imidazoline-guanidinium-receptive sites in human and rabbit liver. Major localization to the mitochondrial outer membrane. *J Biol Chem*, 266(1), 155–160.
- Tesson, F., Limon, I., & Parini, A. (1992). Tissue-specific localization of mitochondrial imidazoline-guanidinium receptive sites. *European Journal of Pharmacology*, 219(2), 335–338. [https://doi.org/10.1016/0014-2999\(92\)90316-V](https://doi.org/10.1016/0014-2999(92)90316-V)
- Thal, D. R., Holzer, M., Rüb, U., Waldmann, G., Günzel, S., Zedlick, D., & Schober, R. (2000). Alzheimer-related tau-pathology in the perforant path target zone and in the hippocampal stratum oriens and radiatum correlates with onset and degree of dementia. *Exp Neurol*, 163(1), 98–110. <https://doi.org/10.1006/exnr.2000.7380>
- Thorn, D. A., An, X.-F., Zhang, Y., Pignini, M., & Li, J.-X. (2012). Characterization of the hypothermic effects of imidazoline I receptor agonists in rats. *British journal of pharmacology*, 166(6), 1936–1945. <https://doi.org/10.1111/j.1476-5381.2012.01894.x>
- Thorn, D. A., Siemian, J. N., Zhang, Y., & Li, J.-X. (2015). Anti-hyperalgesic effects of imidazoline I2 receptor ligands in a rat model of inflammatory pain: Interactions with oxycodone. *Psychopharmacology (Berl)*, 232(18), 3309–3318. <https://doi.org/10.1007/s00213-015-3983-1>

- Thorn, D. A., Zhang, Y., & Li, J.-X. (2016). Effects of the imidazoline I2 receptor agonist 2-BFI on the development of tolerance to and behavioural/physical dependence on morphine in rats. *Br J Pharmacol*, *173*(8), 1363–1372. <https://doi.org/10.1111/bph.13435>
- Thorn, D. A., Zhang, Y., & Li, J.-X. (2017). Tolerance and cross-tolerance to the antinociceptive effects of oxycodone and the imidazoline I2 receptor agonist phenyzo-line in adult male rats. *Psychopharmacology (Berl)*, *234*(12), 1871–1880. <https://doi.org/10.1007/s00213-017-4599-4>
- Thorn, D. A., Zhang, Y., Peng, B.-W., Winter, J. C., & Li, J.-X. (2011). Effects of imidazoline i2 receptor ligands on morphine-and tramadol-induced antinociception in rats. *European journal of pharmacology*, *670*(2-3), 435–440.
- Tian, J.-S., Zhai, Q.-J., Zhao, Y., Chen, R., & Zhao, L.-D. (2018a). 2-(2-benzofuranyl)-2-imidazoline (2-BFI) improved the impairments in AD rat models by inhibiting oxidative stress, inflammation and apoptosis. *JIN*, *16*(4), 385–400. <https://doi.org/10.3233/JIN-170032>
- Tian, J., Chen, R., Hu, L., Zhang, L., Chen, J., Cao, Y., Guo, X., Wang, L., & Han, Z. (2018b). The protective effect of 2-(2-benzofuranyl)-2-imidazoline against oxygen-glucose deprivation in cultured rat cortical astrocytes. *Neuroscience research*, *133*, 1–6.
- Tonello, R., Villarinho, J. G., da Silva Sant'Anna, G., Tamiozzo, L., Machado, P., Trevisan, G., Pinto Martins, M. A., Ferreira, J., & Rubin, M. A. (2012). The potential antidepressant-like effect of imidazoline I2 ligand 2-BFI in mice. *Prog Neuropsychopharmacol Biol Psychiatry*, *37*(1), 15–21. <https://doi.org/10.1016/j.pnpbp.2011.11.005>
- Tong, B. C.-K., Wu, A. J., Li, M., & Cheung, K.-H. (2018). Calcium signaling in Alzheimer's disease & therapies. *Biochim Biophys Acta Mol Cell Res*, *1865*(11 Pt B), 1745–1760. <https://doi.org/10.1016/j.bbamcr.2018.07.018>
- Town, T., Zolton, J., Shaffner, R., Schnell, B., Crescentini, R., Wu, Y., Zeng, J., DelleDonne, A., Obregon, D., Tan, J., & Mullan, M. (2002). P35/Cdk5 pathway mediates soluble amyloid-beta peptide-induced tau phosphorylation in vitro. *J Neurosci Res*, *69*(3), 362–372. <https://doi.org/10.1002/jnr.10299>
- Tseng, H. C., Zhou, Y., Shen, Y., & Tsai, L. H. (2002). A survey of Cdk5 activator p35 and p25 levels in Alzheimer's disease brains. *FEBS Lett*, *523*(1-3), 58–62. [https://doi.org/10.1016/s0014-5793\(02\)02934-4](https://doi.org/10.1016/s0014-5793(02)02934-4)
- Tyacke, R. J., Myers, J. F. M., Venkataraman, A., Mick, I., Turton, S., Passchier, J., Husbands, S. M., Rabiner, E. A., Gunn, R. N., Murphy, P. S., Parker, C. A., & Nutt, D. J. (2018). Evaluation of 11C-BU99008, a PET Ligand for the Imidazoline2 Binding Site in Human Brain. *J Nucl Med*, *59*(10), 1597–1602. <https://doi.org/10.2967/jnumed.118.208009>

- Tinnies, E., & Trushina, E. (2017). Oxidative Stress, Synaptic Dysfunction, and Alzheimer's Disease. *J Alzheimers Dis*, 57(4), 1105–1121. <https://doi.org/10.3233/JAD-161088>
- Uddin, M. S., & Kabir, M. T. Oxidative Stress in Alzheimer's Disease: Molecular Hallmarks of Underlying Vulnerability (G. M. Ashraf & A. Alexiou, Eds.). en. In: *Biological, Diagnostic and Therapeutic Advances in Alzheimer's Disease* (G. M. Ashraf & A. Alexiou, Eds.). Ed. by Ashraf, G. M., & Alexiou, A. Singapore: Springer Singapore, 2019, pp. 91–115. ISBN: 9789811396359 9789811396366. [https://doi.org/10.1007/978-981-13-9636-6\\_5](https://doi.org/10.1007/978-981-13-9636-6_5).
- Ugedo, L., Pineda, J., Martín-Ruiz, R., Ruiz-Ortega, J. A., & Artigas, F. (1999). Imidazoline-induced inhibition of firing rate of 5-HT neurons in rat dorsal raphe by modulation of extracellular 5-HT levels. *Ann N Y Acad Sci*, 881, 365–368. <https://doi.org/10.1111/j.1749-6632.1999.tb09382.x>
- Uttara, B., Singh, A. V., Zamboni, P., & Mahajan, R. T. (2009). Oxidative stress and neurodegenerative diseases: A review of upstream and downstream antioxidant therapeutic options. *Curr Neuropharmacol*, 7(1), 65–74. <https://doi.org/10.2174/157015909787602823>
- van Weeren, P. C., de Bruyn, K. M., de Vries-Smits, A. M., van Lint, J., & Burgering, B. M. (1998). Essential role for protein kinase B (PKB) in insulin-induced glycogen synthase kinase 3 inactivation. Characterization of dominant-negative mutant of PKB. *J Biol Chem*, 273(21), 13150–13156. <https://doi.org/10.1074/jbc.273.21.13150>
- Van Cauwenberghe, C., Van Broeckhoven, C., & Sleegers, K. (2016). The genetic landscape of Alzheimer disease: Clinical implications and perspectives. *Genet Med*, 18(5), 421–430. <https://doi.org/10.1038/gim.2015.117>
- Van Dam, D., & De Deyn, P. P. (2011). Animal models in the drug discovery pipeline for Alzheimer's disease. *Br J Pharmacol*, 164(4), 1285–1300. <https://doi.org/10.1111/j.1476-5381.2011.01299.x>
- Vorbrodt, A. W., Dobrogowska, D. H., Ueno, M., & Tarnawski, M. (1995). A quantitative immunocytochemical study of blood-brain barrier to endogenous albumin in cerebral cortex and hippocampus of senescence-accelerated mice (SAM). *Folia Histochem Cytobiol*, 33(4), 229–237.
- Wang, F., Feng, T.-Y., Yang, S., Preter, M., Zhou, J.-N., & Wang, X.-P. (2016). Drug therapy for behavioral and psychological symptoms of dementia. *Current neuropharmacology*, 14(4), 307–313.
- Wang, H., Regunathan, S., Meeley, M. P., & Reis, D. J. (1992). Isolation and characterization of imidazoline receptor protein from bovine adrenal chromaffin cells. [Place: United States]. *Mol Pharmacol*, 42(5), 792–801.

- Wang, H, Regunathan, S, Ruggiero, D. A., & Reis, D. J. (1993). Production and characterization of antibodies specific for the imidazoline receptor protein. *Molecular pharmacology*, 43(4), 509–515.
- Wang, P., Wang, Z.-W., Lin, F.-H., Han, Z., Hou, S.-T., & Zheng, R.-Y. (2011). 2-bfi attenuates experimental autoimmune encephalomyelitis-induced spinal cord injury with enhanced b-ck, caatpase, but reduced calpain activity. *Biochemical and biophysical research communications*, 406(1), 152–157.
- Wang, Q. M., Fiol, C. J., DePaoli-Roach, A., & Roach, P. J. (1994). Glycogen synthase kinase-3 beta is a dual specificity kinase differentially regulated by tyrosine and serine/threonine phosphorylation. *Journal of Biological Chemistry*, 269(20), 14566–14574.
- Wei, X., Zhang, Y., & Zhou, J. (1999). Alzheimer's disease-related gene expression in the brain of senescence accelerated mouse. *Neuroscience Letters*, 268(3), 139–142. [https://doi.org/10.1016/S0304-3940\(99\)00396-1](https://doi.org/10.1016/S0304-3940(99)00396-1)
- Weichhart, T., Hengstschläger, M., & Linke, M. (2015). Regulation of innate immune cell function by mTOR [Number: 10 Publisher: Nature Publishing Group]. *Nat Rev Immunol*, 15(10), 599–614. <https://doi.org/10.1038/nri3901>
- Weichhart, T., & Säemann, M. D. (2009). The multiple facets of mTOR in immunity. *Trends Immunol*, 30(5), 218–226. <https://doi.org/10.1016/j.it.2009.02.002>
- Weingarten, M. D., Lockwood, A. H., Hwo, S.-Y., & Kirschner, M. W. (1975). A protein factor essential for microtubule assembly. *Proceedings of the National Academy of Sciences*, 72(5), 1858–1862.
- Wichers, M. C., Koek, G. H., Robaey, G., Verkerk, R., Scharpé, S., & Maes, M. (2005). IDO and interferon- $\alpha$ -induced depressive symptoms: A shift in hypothesis from tryptophan depletion to neurotoxicity [Number: 6 Publisher: Nature Publishing Group]. *Mol Psychiatry*, 10(6), 538–544. <https://doi.org/10.1038/sj.mp.4001600>
- Wiendl, H., Elger, C., Förstl, H., Hartung, H.-P., Oertel, W., Reichmann, H., & Schwab, S. (2015). Gaps Between Aims and Achievements in Therapeutic Modification of Neuronal Damage ("Neuroprotection"). *Neurotherapeutics : the journal of the American Society for Experimental NeuroTherapeutics*, 12(2), 449–454. <https://doi.org/10.1007/s13311-015-0348-8>
- Wikberg, J. E. (1989). High affinity binding of idazoxan to a non-catecholaminergic binding site in the central nervous system: Description of a putative idazoxan-receptor. *Pharmacology & toxicology*, 64(1), 152–155. <https://doi.org/10.1111/j.1600-0773.1989.tb00620.x>
- Wikberg, J. E., & Uhlén, S. (1990). Further characterization of the guinea pig cerebral cortex idazoxan receptor: Solubilization, distinction from the imidazole site, and demonstration of cirazoline as an idazoxan receptor-selective drug. *Journal of*

- neurochemistry*, 55(1), 192–203. <https://doi.org/10.1111/j.1471-4159.1990.tb08838.x>
- Wiley, C. D., Velarde, M. C., Lecot, P., Liu, S., Sarnoski, E. A., Freund, A., Shirakawa, K., Lim, H. W., Davis, S. S., Ramanathan, A., Gerencser, A. A., Verdin, E., & Campisi, J. (2016). Mitochondrial Dysfunction Induces Senescence with a Distinct Secretory Phenotype. *Cell Metab*, 23(2), 303–314. <https://doi.org/10.1016/j.cmet.2015.11.011>
- Wilson, H., Dervenoulas, G., Pagano, G., Tyacke, R. J., Polychronis, S., Myers, J., Gunn, R. N., Rabiner, E. A., Nutt, D., & Politis, M. (2019). Imidazoline 2 binding sites reflecting astroglia pathology in Parkinson's disease: An in vivo <sup>11</sup>C-BU99008 PET study. *Brain*, 142(10), 3116–3128. <https://doi.org/10.1093/brain/awz260>
- Wu, Y., Zhang, A.-Q., & Yew, D. T. (2005). Age related changes of various markers of astrocytes in senescence-accelerated mice hippocampus. *Neurochem Int*, 46(7), 565–574. <https://doi.org/10.1016/j.neuint.2005.01.002>
- Wu, Y., Dissing-Olesen, L., MacVicar, B. A., & Stevens, B. (2015). Microglia: Dynamic Mediators of Synapse Development and Plasticity. *Trends Immunol*, 36(10), 605–613. <https://doi.org/10.1016/j.it.2015.08.008>
- Wyss-Coray, T. (2016). Ageing, neurodegeneration and brain rejuvenation. *Nature*, 539(7628), 180–186. <https://doi.org/10.1038/nature20411>
- Xu, H., Garcia-Ptacek, S., Jönsson, L., Wimo, A., Nordström, P., & Eriksson, M. (2021). Long-term effects of cholinesterase inhibitors on cognitive decline and mortality. *Neurology*, 96(17), e2220–e2230.
- Yakovlev, A. G., & Faden, A. I. (2004). Mechanisms of neural cell death: Implications for development of neuroprotective treatment strategies. *NeuroRx : the journal of the American Society for Experimental NeuroTherapeutics*, 1(1), 5–16. <https://doi.org/10.1602/neurorx.1.1.5>
- Yanai, S., & Endo, S. (2016). Data on the optimization of behavioral tasks for senescence-accelerated mouse prone 8 (SAMP8). *Data in Brief*, 8, 262–266. <https://doi.org/10.1016/j.dib.2016.05.044>
- Yang, X.-C., & Reis, D. J. (1999). Agmatine selectively blocks then-methyl-d-aspartate subclass of glutamate receptor channels in rat hippocampal neurons. *Journal of Pharmacology and Experimental Therapeutics*, 288(2), 544–549.
- Yankner, B. A., Lu, T., & Loerch, P. (2008). The aging brain. *Annu Rev Pathol*, 3, 41–66. <https://doi.org/10.1146/annurev.pathmechdis.2.010506.092044>
- Yoon, S.-S., & Jo, S. A. (2012). Mechanisms of Amyloid- $\beta$  Peptide Clearance: Potential Therapeutic Targets for Alzheimer's Disease. *Biomol Ther (Seoul)*, 20(3), 245–255. <https://doi.org/10.4062/biomolther.2012.20.3.245>
- Yoshiyama, Y., Kojima, A., Ishikawa, C., & Arai, K. (2010). Anti-Inflammatory Action of Donepezil Ameliorates Tau Pathology, Synaptic Loss, and Neurodegeneration in a

- Tauopathy Mouse Model. *JAD*, 22(1), 295–306. <https://doi.org/10.3233/JAD-2010-100681>
- Yu, B. P. (1994). Cellular defenses against damage from reactive oxygen species. *Physiological reviews*, 74(1), 139–162.
- Zaplatic, E., Bule, M., Shah, S. Z. A., Uddin, M. S., & Niaz, K. (2019). Molecular mechanisms underlying protective role of quercetin in attenuating alzheimer's disease. *Life sciences*, 224, 109–119.
- Zec, R. F., & Burkett, N. R. (2008). Non-pharmacological and pharmacological treatment of the cognitive and behavioral symptoms of Alzheimer disease. *NeuroRehabilitation*, 23(5), 425–438.
- Zhang, F., Gannon, M., Chen, Y., Yan, S., Zhang, S., Feng, W., Tao, J., Sha, B., Liu, Z., Saito, T., Saido, T., Keene, C. D., Jiao, K., Roberson, E. D., Xu, H., & Wang, Q. (2020).  $\beta$ -amyloid redirects norepinephrine signaling to activate the pathogenic GSK3 $\beta$ /tau cascade. *Sci. Transl. Med.*, 12(526), eaay6931. <https://doi.org/10.1126/scitranslmed.aay6931>
- Zhang, Z., Yang, J.-L., Zhang, L.-L., Chen, Z.-Z., Chen, J.-O., Cao, Y.-G., Qu, M., Lin, X.-D., Ji, X.-M., & Han, Z. (2018). 2-(2-Benzofuranyl)-2-imidazoline treatment within 5 hours after cerebral ischemia/reperfusion protects the brain. *Neural Regen Res*, 13(12), 2111–2118. <https://doi.org/10.4103/1673-5374.241461>
- Zhao, Y., & Zhao, B. (2013). Oxidative stress and the pathogenesis of Alzheimer's disease. *Oxid Med Cell Longev*, 2013, 316523. <https://doi.org/10.1155/2013/316523>
- Zheng, W.-H., Bastianetto, S., Mennicken, F., Ma, W., & Kar, S. (2002). Amyloid beta peptide induces tau phosphorylation and loss of cholinergic neurons in rat primary septal cultures. *Neuroscience*, 115(1), 201–211. [https://doi.org/10.1016/s0306-4522\(02\)00404-9](https://doi.org/10.1016/s0306-4522(02)00404-9)
- Zheng, Z.-H., Tu, J.-L., Li, X.-H., Hua, Q., Liu, W.-Z., Liu, Y., Pan, B.-X., Hu, P., & Zhang, W.-H. (2021). Neuroinflammation induces anxiety- and depressive-like behavior by modulating neuronal plasticity in the basolateral amygdala. *Brain, Behavior, and Immunity*, 91, 505–518. <https://doi.org/10.1016/j.bbi.2020.11.007>
- Zhu, H., & Piletz, J. E. (2003). Association between I(2) binding sites and monoamine oxidase-B activity in platelets. *Ann N Y Acad Sci*, 1009, 347–352. <https://doi.org/10.1196/annals.1304.044>
- Zhu, H., Halaris, A., & Piletz, J. E. (1997). Chronic imipramine treatment downregulates IR1-imidazoline receptors in rat brainstem. *Life Sciences*, 61(19), 1973–1983. [https://doi.org/10.1016/S0024-3205\(97\)00837-0](https://doi.org/10.1016/S0024-3205(97)00837-0)
- Zomkowski, A. D. E., Hammes, L., Lin, J., Calixto, J. B., Santos, A. R. S., & Rodrigues, A. L. S. (2002). Agmatine produces antidepressant-like effects in two models of depression in mice. *Neuroreport*, 13(4), 387–391. <https://doi.org/10.1097/00001756-200203250-00005>

# **Annex A**





## A.1

### **Preliminary evaluation of the effect of I<sub>2</sub> Imidazoline receptor ligands in human APP Swedish mutated iPSC-derived astrocytes from Alzheimer's disease patients.**

#### **A.1.1 Background**

The complexity of the I<sub>2</sub>-IR receptors make crucial the conduction of *in vitro* studies for a deeper understanding of the intrinsic mechanisms that lead to the neuroprotection described *in vivo*. At the same time both the fact that the I<sub>2</sub>-IR have been associated with the astrocytes and that our published results in SAMP8 (Publications 1,2,3) and 5XFAD mice (Publications 4,5) show a strong effect of the I<sub>2</sub>-treatment on GFAP and inflammatory response strengthened our interest in the evaluation of I<sub>2</sub>-IR treatment effect on AD astrocytes *in vitro*. To address this, we performed experiments in human induced pluripotent stem cell (iPSC) derived astrocytes from patients with familial AD (Oksanen et al., 2018). Models that are based on iPSC technology share important anatomical, physiological, and genetic features with humans, thus contributing to advancing new treatments for CNS diseases, such as AD (Oksanen et al., 2017; Penney et al., 2020). Furthermore, the I<sub>2</sub>-IR, as already mentioned in terms of the present thesis are heterogeneous and differentially expressed among different species. In this context, evaluating the effect of selective I<sub>2</sub>-IR ligands (**MCR5**, **B06**) in iPSC-derived astrocytes from AD patients could not only contribute to knowledge regarding their direct effect on astroglia, but also to extending our previously reported results in AD mouse models, to human-based models.

#### **A.1.2 Methods and Results**

##### **Astrocytic lines and astrocytic maturation**

The experiments were performed based on previously described protocols (Oksanen et al., 2017, 2018, 2020). Briefly, 5.5-month-old differentiated astrocytic spheres from different human iPSC-lines (from individuals carrying APP Swedish mutation-AD astrocytes and from healthy individuals- CTRL astrocytes) were thawed and maintained in Astrocyte differentiation Medium (ADM) [(DMEM/F12, 1% N2, 1% Glutamax, 1% nonessential amino acids, 0.5% P/S (50 IU/50 µg/ml) and 0.5 IU/ml heparin] supplemented with 10 ng/ml bFGF, and 10 ng/ml epidermal growth factor (EGF) for approximately 4 weeks. When spheres completed between 200-220 days *in vitro* were dissociated with accutase to single cells and plated on Matrigel coated 48-well plates (60.000 cells/well) or 96-well plate (20.000/well) in ADM supplemented with 10ng/ml ciliary neurotrophic factor (CNTF) and 10ng/ml bone morphogenetic protein 4 (BMP4). Cells were maintained for 7

days in ADM supplemented with CNT and BMP4 (changed every 2 days) until mature astrocytes were obtained and before any analysis.

### **I<sub>2</sub>-IR ligand treatment, chemical stimulation of the cells and cytokine bead array**

The iPSC-astrocytes (AD and CTRL astrocytes) were matured on Matrigel-coated 48-well plates and treated with 1uM and 10uM imidazoline ligands Idazoxan, MCR5, B06 at 1uM and 10uM or vehicle (DMSO) for 24 hr. After the 24 hr pre-treatment period, the cells were stimulated for 24h with 50 ng/ml TNF- $\alpha$  and 10 ng/ml IL-1 $\beta$  for 24 hr in the absence (inflammatory stimulated DMSO controls) or presence of the imidazoline drugs (inflammatory stimulated treated astrocytes). Additional non-stimulated DMSO cells were maintained in the regular culture medium. Medium was collected and centrifuged at 1000g for 5 min to remove cell debris and 10 $\mu$ l of supernatant was used for analysis. Cytokine concentrations (pg/uL) were analyzed by CBA Flex Sets. Human Soluble Protein flex sets were used for detecting C-C Motif Chemokine Ligand 5 (CCL5)/RANTES, granulocyte-macrophage colony-stimulating factor (GM-CSF), Interleukin-6 (IL-6), Interleukin-8 (IL-8) and monocyte chemoattractant protein-1 (MCP-1) according to manufacturer's instructions with minor modifications. Mean concentrations of each group were compared with two way ANOVA followed by Tukey's post hoc tests and presented as fold change to inflammatory stimulated control astrocytes. Statistical analysis was conducted using GraphPad Prism version 9.

### **Effect of I<sub>2</sub>-IR ligands on cytokine secretion upon inflammatory stimulation in AD and healthy iPSC- derived astrocytes.**

All I<sub>2</sub>-IR ligands showed to exert anti-inflammatory properties on human iPSC-derived astrocytes upon inflammatory stimulation with Tnf- $\alpha$  and IL-1 $\beta$ . Idazoxan (10uM) treatment was shown to reduce cytokine secretion in a genotype-independent manner which is consistent with previously published *in vivo* and *in vitro* results (Feinstein et al., 1999; Regunathan et al., 1999). In contrast, the selective compounds B06 and especially the compound MCR5 showed a greater effect on AD stimulated astrocytes cytokines secretion than in control, which together with their beneficial effect on APP processing *in vivo* (Chapter 1, 3) suggest that their AD-specific anti-inflammatory effects may be associated with A $\beta$  pathology.

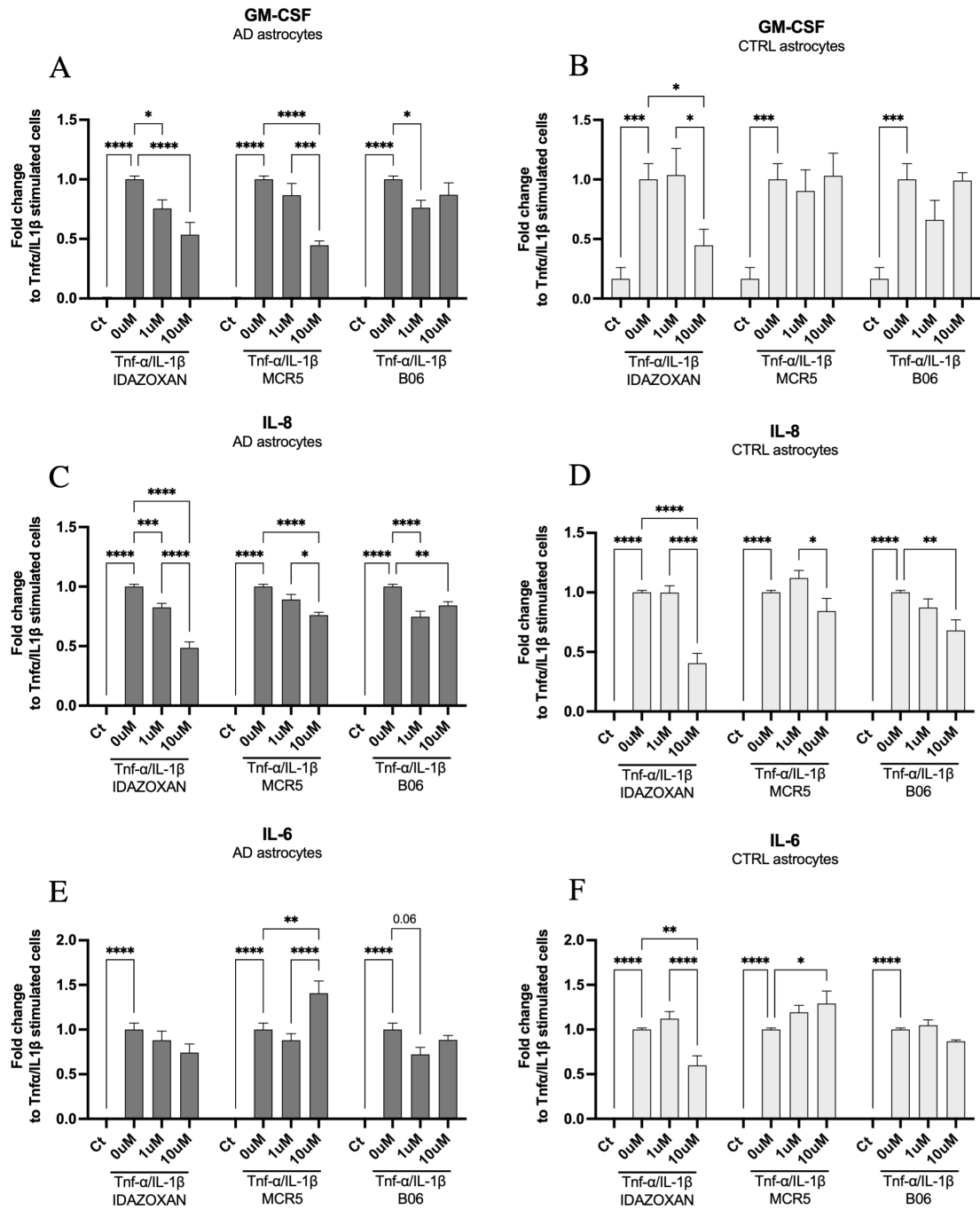
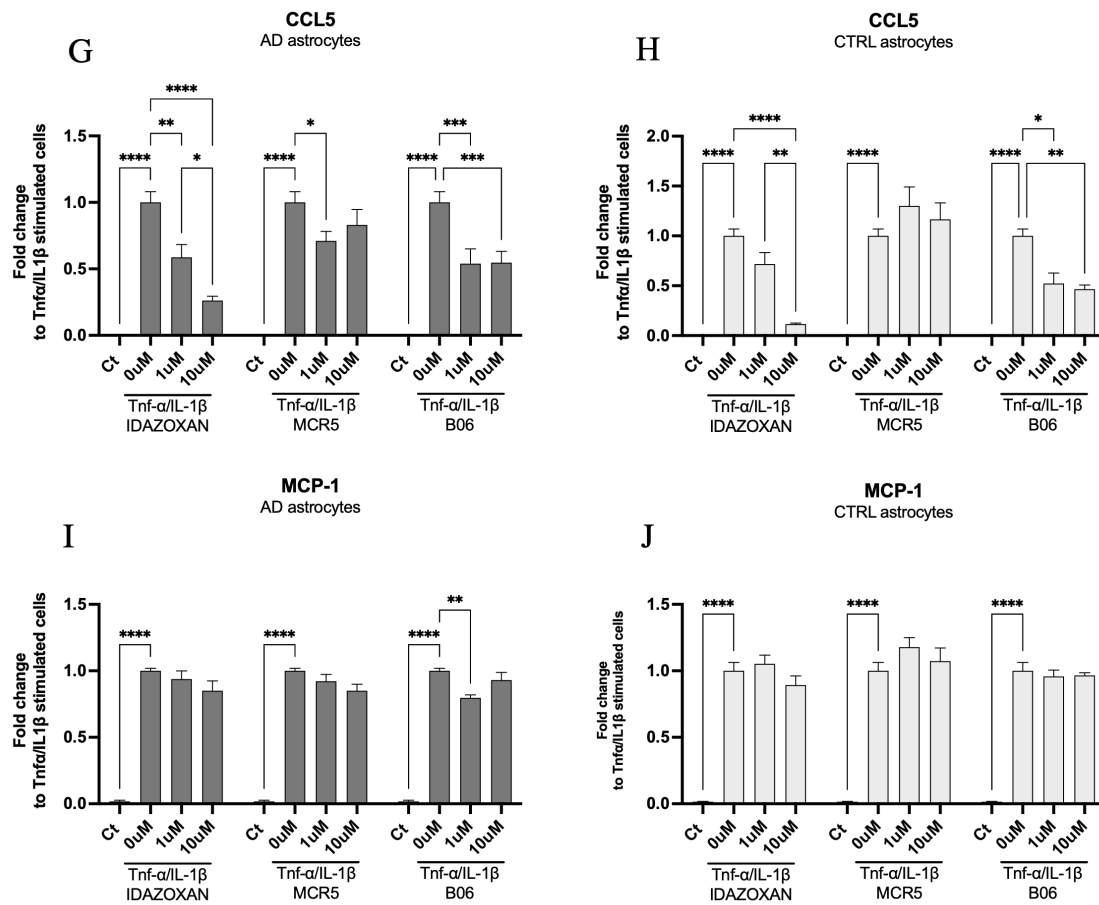


Figure 1: Continued



**Figure 1:** I<sub>2</sub>-IR ligand treatment (1uM, 10uM) shows anti-inflammatory effects. Cytokine secretion from astrocytes upon inflammatory stimulation. (A) GM-CSF, (C) IL-8, (E) IL-6 (G) CCL5, (I) MCP-1 in AD astrocytes, (B) GM-CSF, (D) IL-8, (F) IL-6 (H) CCL5, (J) MCP-1 in CTRL astrocytes. I<sub>2</sub>-IR ligands treatment reduces cytokine secretion from cells of Control (CTRL) and/or AD astrocytes. Relative levels are shown as fold change to inflammatory stimulated control astrocytes and presented as mean ± SEM (n=2 (CTRL) and n=3 (AD) independent experiment performed in duplicates per each line). \*\*\*\*p<0.0001, \*\*\*p<0.001, \*p<0.01, \*p<0.05.

## ACKNOWLEDGEMENTS

This study was performed in the context of the author's short-term visit in the Neuroscience Center of the University of Helsinki. We thank the supervisor of the study Dr. Jari Koistinaho for hosting the author and providing the necessary equipment and material for the conduction of the experiments. The author also deeply thanks Dr Taisia Rolova, Marja Koskivi and Pinja Kettunen for the invaluable guidance, help and advice in terms of this project and training. Ultimately, the author acknowledges support from the Montcelimar Foundation fellowship (2020) awarded by the University of Barcelona.

**REFERENCES**

- Feinstein, D. L., Reis, D. J., & Regunathan, S. (1999). Inhibition of astroglial nitric oxide synthase type 2 expression by idazoxan. *Molecular Pharmacology*, 55(2), 304–308.
- Oksanen, M., Hyötyläinen, I., Trontti, K., Roloova, T., Wojciechowski, S., Koskuvi, M., Viitanen, M., Levonen, A.-L., Hovatta, I., Roybon, L., Lehtonen, Š., Kanninen, K. M., Hämäläinen, R. H., & Koistinaho, J. (2020). NF-E2-related factor 2 activation boosts antioxidant defenses and ameliorates inflammatory and amyloid properties in human Presenilin-1 mutated Alzheimer's disease astrocytes. *Glia*, 68(3), 589–599.
- Oksanen, M., Hyötyläinen, I., Voutilainen, J., Puttonen, K. A., Hämäläinen, R. H., Graff, C., Lehtonen, Š., & Koistinaho, J. (2018). Generation of a human induced pluripotent stem cell line (LL008 1.4) from a familial Alzheimer's disease patient carrying a double KM670/671NL (Swedish) mutation in APP gene. *Stem Cell Research*, 31, 181–185.
- Oksanen, M., Petersen, A. J., Naumenko, N., Puttonen, K., Lehtonen, Š., Gubert Olivé, M., Shakirzyanova, A., Leskelä, S., Sarajärvi, T., Viitanen, M., Rinne, J. O., Hiltunen, M., Haapasalo, A., Giniatullin, R., Tavi, P., Zhang, S.-C., Kanninen, K. M., Hämäläinen, R. H., & Koistinaho, J. (2017). PSEN1 Mutant iPSC-Derived Model Reveals Severe Astrocyte Pathology in Alzheimer's Disease. *Stem Cell Reports*, 9(6), 1885–1897.
- Penney, J., Ralvenius, W. T., & Tsai, L.-H. (2020). Modeling Alzheimer's disease with iPSC-derived brain cells. *Molecular Psychiatry*, 25(1), 148–167. <https://doi.org/10.1038/s41380-019-0468-3>
- Regunathan, S., Feinstein, D. L., & Reis, D. J. (1999). Anti-proliferative and anti-inflammatory actions of imidazoline agents. Are imidazoline receptors involved? *Annals of the New York Academy of Sciences*, 881, 410–419.



## A.2

### Evaluation of MAO inhibitory activity and NMDA antagonistic activity of selective I<sub>2</sub>-IR compounds MCR5 and MCR9

#### A.2.1 Background

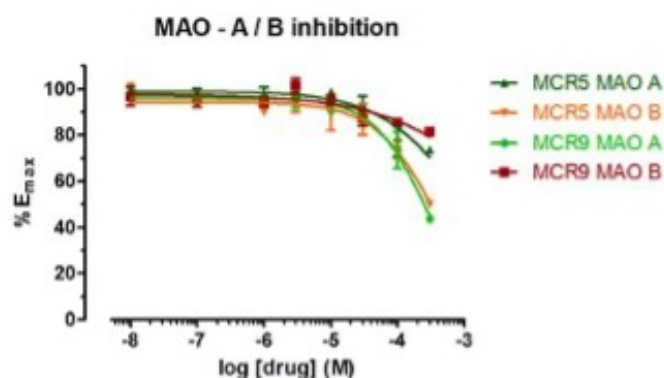
As already stated in the present thesis, it has been proposed that I<sub>2</sub>-IR can be located in the outer mitochondrial membrane and on allosteric sites on MAO A/B (Jones et al., 2007; McDonald et al., 2010). Moreover, several I<sub>2</sub>-IR ligands have shown to inhibit MAO suggesting this to be a possible mechanism of the observed functional effects induced by I<sub>2</sub>-IR ligands (). Furthermore, several experimental data described that I<sub>2</sub>-IR ligands exerted protective effects against glutamate-induced neurotoxicity interacting at the NMDA receptor (Olmos et al., 1999) and that I<sub>2</sub>-IR compounds inhibit NMDA or glutamate-induced calcium increases *in vitro* (Han et al., 2013). Based on this background we tested the effect of the structurally new compounds MCR5 and MCR9 on MAO and NMDA activity *in vitro*.

#### A.2.2 Background

##### MAO Inhibitory activity

Investigative compounds were evaluated for their *in vitro* human MAO A or MAO B activity on separate experiments, using a commercial bioluminescence kit (MAO-Glo™ Assay, Promega). Inhibitory assays were performed according to the protocol provided by the manufacturer, in a range from 0.01 to 300  $\mu$ M for each compound using 96-well black plates (Greiner). MAO-A and B were from a recombinant origin, expressed in baculovirus-infected BTI insect cells (Sigma-Aldrich). As positive controls, we used clorgyline for MAO-A (1  $\mu$ M) or selegiline for MAO B (10  $\mu$ M). The quantity of MAO A or B was 1  $\mu$ g per well, and the time of incubation was set to one hour at room temperature. Readings were performed 1 hour later in a Synergy HT multimode reader (Biotek). All the experiments were the mean of three different experiments performed in duplicate.

The *in vitro* assays did not show any inhibitory activity at recombinant human MAO-B in a range from 10 nM to 300  $\mu$ M. MCR5 and MCR9 only inhibited recombinant human MAO-A at concentrations in the high micromolar range ( $IC_{50} > 200\mu$ M). Clorgyline (0.1  $\mu$ M) and selegiline (10  $\mu$ M) were used as selective positive controls. Both compounds inhibited completely the activity of MAO-A and MAO-B respectively. These results should be in accordance with other reports that postulated that I<sub>2</sub>-IR should not be associated with MAO enzymes (Halaris & Piletz, 2001; Zhu & Piletz, 2003).

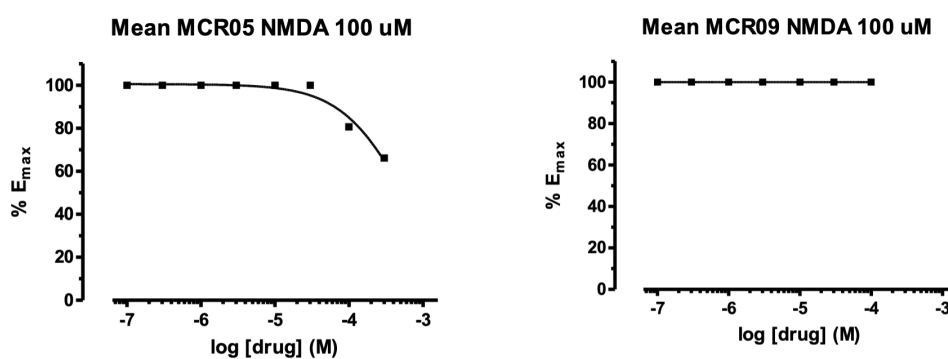


### Antagonist activity against NMDA receptors

The functional assay for antagonist activity against NMDA receptors was performed using primary cultures of rat cerebellar granule neurons that were prepared according to established protocols (Canudas et al., 2003). Briefly, cells were dissociated from the cerebella of 7-8 day-old pups and grown on 24-well culture plates containing 10 mm poly-L-lysine coated glass coverslips. Density was adjusted to  $1 \times 10^6$  cells/ml. Cultures were grown in basal medium with Eagle's salts (BME, Gibco-ThermoFisher) containing 10% FCS, 2 mM L-glutamine, 0.1 mg/ml gentamicin and 25 mM KCl. Cytosine arabinoside (10  $\mu$ M) was added 16-18h after plating to prevent excessive proliferation of astrocytes. Cells were allowed to differentiate in a Sanyo CO<sub>2</sub> cell incubator (37 °C, 5% CO<sub>2</sub>) and were ready to be used for the experiments after 6–10 days in vitro. The day of the experiment cells were loaded with 6  $\mu$ M Fura-2 AM (Molecular Probes-ThermoFisher) for 30 min and the coverslip was mounted on a fluorimeter quartz cuvette containing a Mg-free Locke–Hepes buffer (in mM: NaCl 154, KCl 5.6, NaHCO<sub>3</sub> 3.6, CaCl<sub>2</sub> 1.3, D-glucose 5.6, HEPES 10 and 0.1% BSA, pH=7.35) using a special holder (coverslip accessory L2250008, PerkinElmer). Measurements were made at 37°C under continuous mild stirring in an LS55 PerkinElmer fluorescence spectrometer, equipped with a fast-filter accessory for Fura-2 fluorescence ratio measurements. Emission data (510 nm) were collected with alternate excitation at 340 and 380 nm, and the ratio F<sub>340</sub>/F<sub>380</sub> was calculated in real time, using proprietary software (FL WinLab 2.0). After stimulation with NMDA (100  $\mu$ M, in the presence of 10  $\mu$ M glycine), increasing cumulative concentrations of the compound to be tested were added (range 0.1-300  $\mu$ M). The percentages of inhibition at every tested concentration were calculated and fitted using a non-linear regression curve (variable slope) by using the software GraphPad Prism 5.0. All experiments were performed at least three times using different batches of cultures.

MCR5 and MCR9 had little effect on NMDA-mediated calcium increases in cerebellar granule cells (approximately 35% inhibition at 300  $\mu$ M for MCR5, no effect for MCR9).





## Acknowledgements

We deeply thank Dr. Francesc Xavier Sureda for performing MAO enzymatic activity and calcium entry experiments in the Department of Basic Medical Sciences, Faculty of Medicine and Health Sciences, Universitat Rovira I Virgili, Reus (Spain).

## REFERENCES

- Canudas, A. M., Pubill, D., Sureda, F. X., Verdaguer, E., Camps, P., Muñoz-Torrero, D., Jiménez, A., Camins, A., & Pallàs, M. (2003). Neuroprotective effects of (+/-)-huprine Y on in vitro and in vivo models of excitotoxicity damage. *Experimental Neurology*, 180(2), 123–130. [https://doi.org/10.1016/s0014-4886\(02\)00029-8](https://doi.org/10.1016/s0014-4886(02)00029-8)
- Halaris, A., & Piletz, J. E. (2001). Imidazoline receptors: Possible involvement in the pathophysiology and treatment of depression. *Human Psychopharmacology: Clinical and Experimental*, 16(1), 65–69. <https://doi.org/10.1002/hup.185>
- Han, Z., Yang, J.-L., Jiang, S. X., Hou, S.-T., & Zheng, R.-Y. (2013). Fast, non-competitive and reversible inhibition of NMDA-activated currents by 2-BFI confers neuroprotection. *PloS One*, 8(5), e64894. <https://doi.org/10.1371/journal.pone.0064894>
- Jones, T. Z. E., Giurato, L., Guccione, S., & Ramsay, R. R. (2007). Interactions of imidazoline ligands with the active site of purified monoamine oxidase A. *The FEBS Journal*, 274(6), 1567–1575. <https://doi.org/10.1111/j.1742-4658.2007.05704.x>
- McDonald, G. R., Olivieri, A., Ramsay, R. R., & Holt, A. (2010). On the formation and nature of the imidazoline I<sub>2</sub> binding site on human monoamine oxidase-B. *Pharmacological Research*, 62(6), 475–488. <https://doi.org/10.1016/j.phrs.2010.09.001>
- Olmos, G., DeGregorio-Rocasolano, N., Paz Regalado, M., Gasull, T., Assumpció Boronat, M., Trullas, R., Villarroel, A., Lerma, J., & García-Sevilla, J. A. (1999). Protection by imidazol(ine) drugs and agmatine of glutamate-induced neurotoxicity in cultured cerebellar

granule cells through blockade of NMDA receptor. *British Journal of Pharmacology*, 127(6), 1317–1326. <https://doi.org/10.1038/sj.bjp.0702679>

Zhu, H., & Piletz, J. E. (2003). Association between I(2) binding sites and monoamine oxidase-B activity in platelets. *Annals of the New York Academy of Sciences*, 1009, 347–352. <https://doi.org/10.1196/annals.1304.044>

### A.3

#### **Bicyclic $\alpha$ -Iminophosphonates as High Affinity Imidazoline I<sub>2</sub> Receptor ligands for Alzheimer's Disease**

Abás S, Rodríguez-Arévalo S, Bagán A, Griñán-Ferré C, **Vasilopoulou F**, Brocos-Mosquera I, Muguruza C, Pérez B, Molins E, Luque FJ, Pérez-Lozano P, de Jonghe S, Daelemans D, Naesens L, Brea J, Loza MI, Hernández-Hernández E, García-Sevilla JA, García-Fuster MJ, Radan M, Djikic T, Nikolic K, Pallàs M, Callado LF, Escolano C.

*Journal of Medicinal Chemistry*. 2020 63(7):3610-3633.

doi: <https://doi.org/10.1021/acs.jmedchem.9b02080>



Bicyclic  $\alpha$ -Iminophosphonates as High Affinity Imidazoline I<sub>2</sub> Receptor Ligands for Alzheimer's Disease

Sònia Abás,<sup>▲</sup> Sergio Rodríguez-Arévalo,<sup>▲</sup> Andrea Bagán, Christian Griñán-Ferré, Foteini Vasilopoulou, Iria Brocos-Mosquera, Carolina Muguruza, Belén Pérez, Elies Molins, F. Javier Luque, Pilar Pérez-Lozano, Steven de Jonghe, Dirk Daelemans, Lieve Naesens, José Brea, M. Isabel Loza, Elena Hernández-Hernández, Jesús A. García-Sevilla, M. Julia García-Fuster, Milica Radan, Teodora Djikic, Katarina Nikolic, Mercè Pallàs, Luis F. Callado, and Carmen Escolano\*

Cite This: *J. Med. Chem.* 2020, 63, 3610–3633

Read Online

ACCESS |



Metrics &amp; More

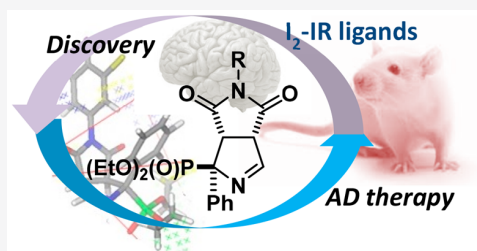


Article Recommendations



Supporting Information

**ABSTRACT:** Imidazoline I<sub>2</sub> receptors (I<sub>2</sub>-IR), widely distributed in the CNS and altered in patients that suffer from neurodegenerative disorders, are orphans from a structural point of view, and new I<sub>2</sub>-IR ligands are urgently required for improving their pharmacological characterization. We report the synthesis and three-dimensional quantitative structure–activity relationship (3D-QSAR) studies of a new family of bicyclic  $\alpha$ -iminophosphonates endowed with relevant affinities for human brain I<sub>2</sub>-IR. Acute treatment in mice with a selected compound significantly decreased Fas-associated protein with death domain (FADD) in the hippocampus, a key signaling mediator of neuroprotective actions. Additionally, *in vivo* studies in the familial Alzheimer's disease 5xFAD murine model revealed beneficial effects in behavior and cognition. These results are supported by changes in molecular pathways related to cognitive decline and Alzheimer's disease. Therefore, bicyclic  $\alpha$ -iminophosphonates are tools that may open new therapeutic avenues for I<sub>2</sub>-IR, particularly for unmet neurodegenerative conditions.



## INTRODUCTION

The imidazoline receptors (IRs) (nonadrenergic receptors for imidazolines)<sup>1</sup> have attracted the attention of the scientific community during decades building a body of knowledge that place them as relevant biological targets.<sup>2,3</sup> IRs are classified in I<sub>1</sub>-, I<sub>2</sub>-, and I<sub>3</sub>-types depending on the specific radiolabeled ligands that recognize their binding sites. These receptors are situated in different locations and are involved in different physiological functions.<sup>4</sup> I<sub>1</sub>-, I<sub>2</sub>-, and I<sub>3</sub>-IRs have been unequally studied. Pharmacologically, I<sub>1</sub>-IRs are well characterized and understood, leading to the clinically approved antihypertensive drugs moxonidine<sup>5</sup> and rilmenidine.<sup>6</sup> The most unknown are I<sub>3</sub>-IRs, identified in pancreatic  $\beta$ -cells and involved in insulin secretion.<sup>7</sup> Regarding I<sub>2</sub>-IRs, although structurally undescribed, a considerable understanding has been achieved on these heterogeneous receptors by using well-characterized I<sub>2</sub>-IR ligands.<sup>8</sup> I<sub>2</sub>-IRs are widely distributed in the brain and, at the molecular level, are located in the outer membrane of mitochondria. Selective I<sub>2</sub>-IR ligands have proven that I<sub>2</sub>-IRs are involved in analgesia,<sup>9</sup> inflammation,<sup>10</sup> and a plethora of human brain disorders.<sup>11</sup> Dysregulation of the levels of I<sub>2</sub>-IRs is a hallmark in illnesses such as glial tumors,<sup>12,13</sup> Huntington's disease,<sup>14</sup> Parkinson's disease,<sup>15</sup> and depression,<sup>16,17</sup> among others. In particular, I<sub>2</sub>-IRs are reported to be increased in the brains of patients that suffered from

Alzheimer's disease (AD).<sup>18,19</sup> Recently, two I<sub>2</sub>-IR ligands, CR4056 (**1**) and [<sup>13</sup>C]BU99008 (**2**), have been progressed to clinical trials. CR4056 (**1**),<sup>20,21</sup> described as the first-in-class I<sub>2</sub>-IR ligand embodying analgesic properties, is in clinical phase II studies for osteoarthritis and postoperative dental pain, and [<sup>13</sup>C]BU99008 (**2**)<sup>22,23</sup> is in early clinical phase I for PET diagnosis for patients that suffer from AD.

The implication of I<sub>2</sub>-IRs in many physiological and pathological processes emphasizes their pharmacological relevance, and they deserve in-depth studies. Since the structural data for I<sub>2</sub>-IRs remains unknown, the discovery of better and more selective I<sub>2</sub>-IR ligands is crucial to build a comprehensive understanding of the pharmacological implications of I<sub>2</sub>-IR.

Although there are a few exceptions, LSL60101 (**3**) and most notably the clinical candidate CR4056 (**1**), the vast majority of known I<sub>2</sub>-IR ligands (idazoxan, **4**; trazicoline, **5**, and 2-BFI, **6**) are 2-substituted 2-imidazolines without further decoration in the 1-, 4-, and 5-positions (Figure 1).<sup>24</sup>

Received: December 14, 2019

Published: March 9, 2020



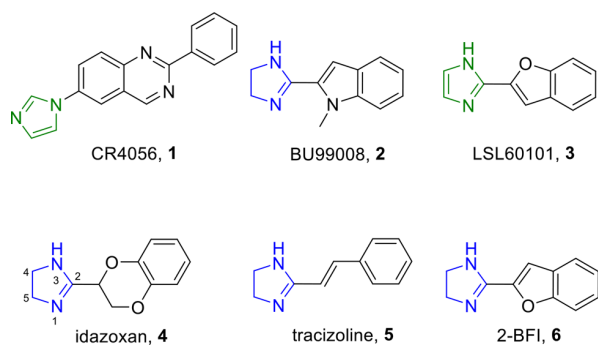


Figure 1. Representative I<sub>2</sub>-IR ligands.

In order to explore new imidazoline-based I<sub>2</sub>-IR ligands moving out of the comfort zone offered by the rather structurally homogeneous I<sub>2</sub>-IR ligands reported so far (Figure 1), we have recently disclosed a family of (2-imidazolin-4-yl)phosphonates.<sup>25,26</sup> The putative therapeutic relevance of a member of this new family of I<sub>2</sub>-IR ligands, MCR5 (7), was validated in a murine model of neurodegeneration, the senescence accelerated mouse-prone 8 (SAMP8).<sup>27</sup> An improvement in the cognitive decline and related biomarkers was found when MCR5 (7) was orally administered to the animals. This study was the first *in vivo* evidence that reinforced I<sub>2</sub>-IRs as a promising target for the treatment of cognitive impairment associated with multiple neurodegenerative diseases.<sup>27</sup>

Separately, we had reported that the diastereoselective [3 + 2] cycloaddition of diethyl isocyanomethylphosphonate with 10 diversely substituted maleimides in acetonitrile under AgOAc catalysis furnished a series of bicycles of general structure Ia (Scheme 1a).<sup>28</sup> The presence within this series of compounds of an  $\alpha$ -iminophosphonate unit, also featured in the above-mentioned (2-imidazolin-4-yl)phosphonates, prompted us to evaluate whether these bicyclo derivatives would also behave as I<sub>2</sub>-IR ligands. We indeed found that two of these 10 already reported compounds, 8a and 8c (Scheme 1b), displayed an affinity for the I<sub>2</sub>-IRs similar to that of idazoxan, 4 (see below). These promising results encouraged us to resume our research with this family of bicyclic  $\alpha$ -

iminophosphonates with the twofold aim of further exploring the scope of the aforementioned [3 + 2] cycloaddition reaction and of establishing their structure–activity relationships (SARs) as I<sub>2</sub>-IR ligands.

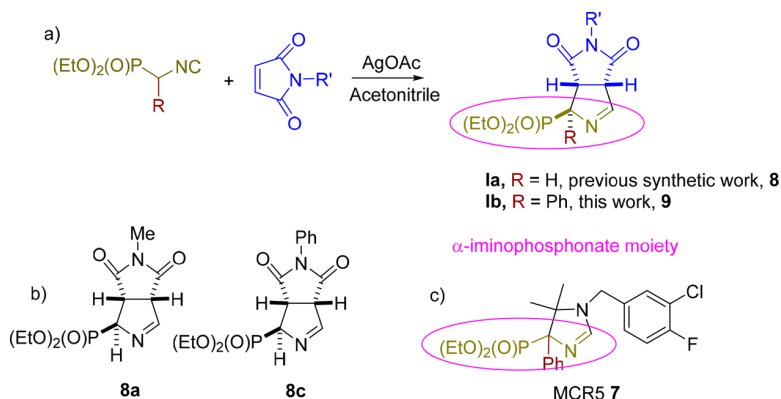
Herein, we explore the synthetic scope of the [3 + 2] cycloaddition reaction of  $\alpha$ -substituted PhosMic derivatives and diversely substituted maleimides. Particular attention was given to derivatives including a phenyl substituent in the  $\alpha$ -position of the phosphonate leading to general structures 9 depicted as Ib in the Scheme 1a, in order to resemble the structure of MCR5, 7 (Scheme 1c). We also assessed the pharmacological profile and selectivity of a wide range of bicyclic  $\alpha$ -iminophosphonates through competition binding studies against the selective I<sub>2</sub>-IR radioligand [<sup>3</sup>H]2-[(2-benzofuranyl)-2-imidazoline] ([<sup>3</sup>H]2-BFI).<sup>29</sup> Selectivity versus two related targets, the I<sub>1</sub>-IR and the  $\alpha_2$ -adrenergic receptor ( $\alpha_2$ -AR), was evaluated through competition studies using the selective radioligands [<sup>3</sup>H]clonidine and [<sup>3</sup>H]RX821002 (2-methoxyidazoxan), respectively. Complementarily, we performed 3D-QSAR studies. Compound 9d (named also B06), endowed with outstanding I<sub>2</sub>-IR affinity and excellent selectivity index regarding I<sub>1</sub>-IR and  $\alpha_2$ -AR, was selected for further studies. We first compared the affinity for the human I<sub>2</sub>-IR of 9d with those of the standards shown in Figure 1. Additionally, the affinity for I<sub>2</sub>-IR from different species was considered for idazoxan (4) and 9d. Next, we performed preliminary drug metabolism and pharmacokinetics (DMPK) studies for 9d, including chemical stability, parallel artificial membrane permeability assay (PAMPA)–blood–brain barrier (BBB) permeability assay, solubility, cytotoxicity, microsomal stability, cytochromes inhibition, and safety. Finally, we characterized its *in vivo* neuroprotective effects in the SxPAD murine model of AD.

## RESULTS AND DISCUSSION

### Chemistry. Synthesis and Structural Characterization.

Considering the previously described compounds 8a and 8c as promising starting points for designing potent I<sub>2</sub>-IR ligands, we resolved to prepare bicyclic compounds functionally close to MCR5 (7) by including an  $\alpha$ -phenyliminophosphonate moiety in their structure. To this end, we decided to increase the

Scheme 1. (a) General Structure of Bicyclic  $\alpha$ -Iminophosphonates Ia (Previously Reported) and Ib (Reported Herein),<sup>a</sup> (b) Chemical Structures of 8a and 8c, and (c) Chemical Structure of MCR5 (7)



<sup>a</sup>Reagents and conditions: *N*-substituted maleimide derivative (1.5 mmol), PhosMic (1 mmol), AgOAc (0.06 mmol), acetonitrile, room temperature, overnight.

scope of the original [3 + 2] cycloaddition by using diversely  $\alpha$ -substituted PhosMic derivatives (Figure 2).

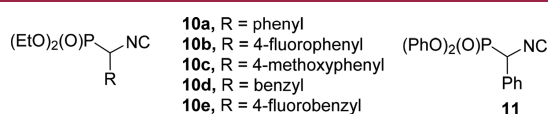


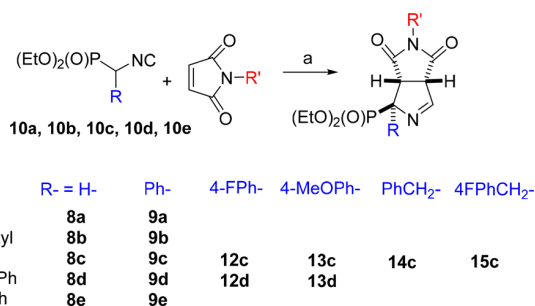
Figure 2.  $\alpha$ -Substituted PhosMic derivatives used in this work.

The preparation of the  $\alpha$ -substituted PhosMic derivatives was performed adapting previously described procedures (for references and experimental procedures, see Supporting Information). Briefly, the four phenylisocyanomethylphosphonates **10a**, **10b**, **10c**, and **11** were prepared by conversion of the required ( $\alpha$ -aminophenyl)phosphonate derivative to the corresponding formamide followed by dehydration with phosphorus oxychloride. While diethyl ( $\alpha$ -aminophenyl)phosphonate is a commercially available compound, the other three precursors were synthesized according to published procedures. A different approach was followed for the  $\alpha$ -benzylisocyanomethyl derivatives **10d** and **10e**. Alkylation of commercially available PhosMic with either benzylbromide or 4-fluorobenzylbromide, using potassium *tert*-butoxide furnished diethyl benzylisocyanomethylphosphonate **10d** and diethyl 4-fluorobenzylisocyanomethylphosphonate **10e**, respectively.

The maleimides used in the cycloaddition reaction were commercially available or were prepared following previously described procedures.

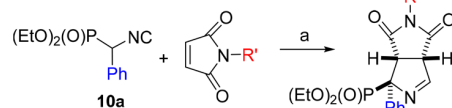
Gratifyingly, although the targeted compounds feature increased steric hindrance in the  $\alpha$ -phosphonate position, our previously optimized set of conditions for the [3 + 2] cycloaddition reaction of maleimides with PhosMic also worked for the current set of  $\alpha$ -substituted PhosMic derivatives.<sup>28</sup> In this way, 36 new bicycloderivatives (Schemes 2 and 3) having a quaternary stereocenter, were synthesized in medium to high yields (Experimental Section). The products were purified by column chromatography, and when they were solids, analytical samples were obtained by recrystallization. For the sake of clarity in the section I<sub>2</sub>-IR Binding Activity and Structure–Activity Relationships, the new  $\alpha$ -substituted bi-

### Scheme 2. General Procedure for the Synthesis of Bicyclic $\alpha$ -Iminophosphonates<sup>a</sup>



<sup>a</sup>Compounds prepared in previous work (R = H)<sup>28</sup> and compounds prepared in this work (R = Ph, 4FPh, 4-MeOPh, PhCH<sub>2</sub>, 4FPhCH<sub>2</sub>). Reagents and conditions: (a) *N*-substituted maleimide derivative (1.5 mmol),  $\alpha$ -substituted PhosMic (**10a**, **10b**, **10c**, **10d**, **10e**, 1 mmol), AgOAc (0.06 mmol), acetonitrile, room temperature, overnight.

### Scheme 3. Second Round of Compounds Synthesized, Featuring Modified *N*-Maleimide Substituents Inspired by Compounds **9a** and **9b**, R' = Alkyl, and **9c** and **9d**, R' = Aryl<sup>a</sup>



R' = alkyl, **9a**–**9b**

**9f**, ethyl  
**9g**, propyl  
**9h**, *t*-butyl  
**9i**, (1-adamantyl)methyl-

**9j**, PhCH<sub>2</sub>-  
**9k**, PhCH<sub>2</sub>CH<sub>2</sub>-  
**9l**, 4-FPhCH<sub>2</sub>CH<sub>2</sub>-  
**9m**, Ph(CH<sub>2</sub>)<sub>2</sub>CH-

R' = aryl, **9c**–**9d**

**9n**, 4-CF<sub>3</sub>Ph-  
**9o**, 3-CF<sub>3</sub>Ph-  
**9p**, 4-FPh-  
**9q**, 4-ClPh-  
**9r**, 2-ClPh-  
**9s**, 3-ClPh-  
**9t**, 4-BrPh-  
**9u**, 3,5-diClPh-  
**9v**, 3,4-diClPh-  
**9w**, 2,4,6-triClPh-  
**9x**, 3-NO<sub>2</sub>Ph-  
**9y**, 3-NO<sub>2</sub>,6-CH<sub>3</sub>Ph-

**9z**, 4-PhPh-  
**9aa**, 4-CH<sub>3</sub>Ph-  
**9ab**, 4-PhOPh-

**9ac**, 1-naphthyl  
**9ad**, 2-Cl,3-pyridyl

<sup>a</sup>Reagents and conditions: (a) *N*-alkyl- or *N*-aryl-substituted maleimide derivative (1.5 mmol),  $\alpha$ -PhenylPhosMic (**10a**, 1 mmol), AgOAc (0.06 mmol), acetonitrile, room temperature, overnight.

cycles, depicted in Schemes 2 and 3, were ordered and numbered attending to the SAR discussion.

Analogously to our previous work,<sup>28</sup> all the [3 + 2] cycloaddition reactions occurred in a diastereoselective manner, and only one of the two possible diastereoisomers was formed. The relative configuration of the three stereocenters in the new compounds was unambiguously confirmed by X-ray crystallographic analysis for five examples, and the stereochemistry of the other compounds was assigned by comparison of their <sup>1</sup>H and <sup>13</sup>C NMR spectra (Tables S12 and S13).

As previously noted, the [3 + 2] cycloaddition reaction between  $\alpha$ -substituted PhosMic derivatives and diversely substituted maleimides was completely diastereoselective, only one of the two possible diastereoisomers was observed. Iminophosphonates **9b**, **9c**, **9d**, **9v**, and **9ab** were recrystallized as monocrystals from ethyl acetate. Their relative configuration was unambiguously confirmed by X-ray crystallographic analysis, indicating a *trans* relationship between the hydrogen atoms on the bridged positions and the substituent at the  $\alpha$  phosphonate carbon atom (Figure 3).

Finally, the origin of the diastereoselective [3 + 2] cycloaddition was investigated by quantum mechanical (QM) calculations that were performed for the addition of *N*-methylmaleimide to  $\alpha$ -phenylPhosMic (in this latter case, the ethyl groups were replaced by methyl in order to reduce the cost of QM computations). In addition, a silver cation bound to acetonitrile was introduced to account for the catalytic effect on the chemical reaction. Reactants, transition states, and products for the *cis* and *trans* [3 + 2] cycloadditions were determined from geometry optimizations at the B3LYP/6-31+G(d) (LANL2DZ for silver) level, and the nature of the

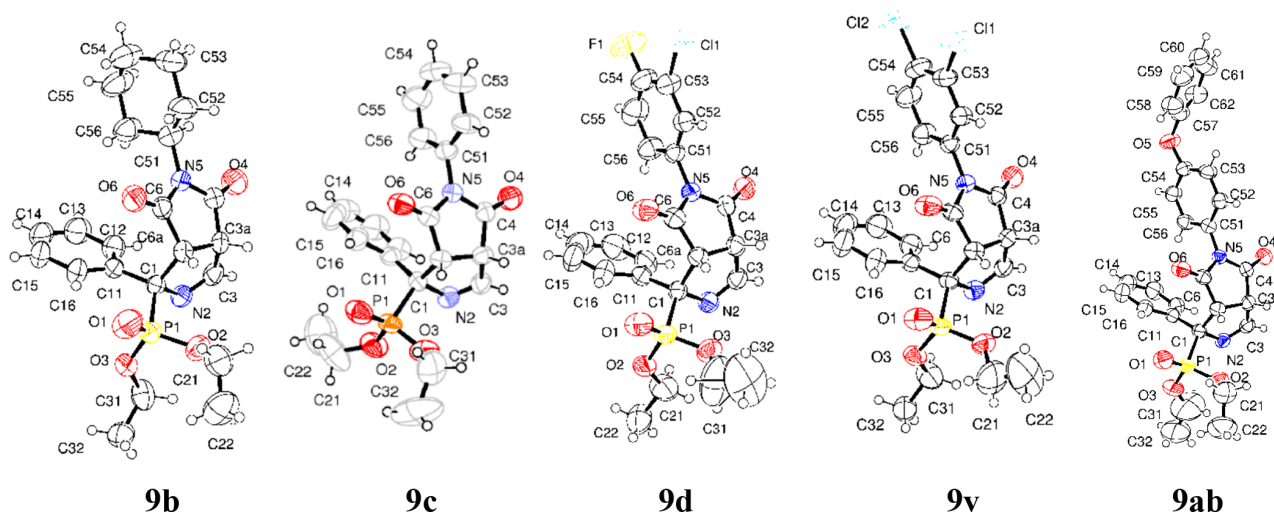


Figure 3. X-ray structures of **9b**, **9c**, **9d**, **9v**, and **9ab**.

stationary points was verified from the analysis of the vibrational frequencies. The geometries of the transition states point out that the cycloaddition occurs via an asynchronous concerted process as the length of the bond that is formed by carbon atom **3a** is shorter than the bond formed by carbon atom **6a** by 0.51 and 0.23 Å in the *cis* and *trans* addition, respectively (Figure 4). Moreover, a significant deviation from

of the *trans* transition state was further checked by geometry optimizations performed for the *cis* and *trans* cycloadditions with the MN15L density functional, leading to a free energy difference of 1.2 kcal mol<sup>-1</sup> favoring the *trans* cycloaddition. The contribution due to the solvation effects in acetonitrile was determined by means of continuum solvation calculations (see Experimental Section). The results (Table S1) reveal that solvation leads to a slight destabilization of the transition state relative to the reactants. Nevertheless, this effect cancels out for the *cis* and *trans* addition, which can be understood from the similar structural features of the two transition states. Overall, these results justify the preferential formation of the diastereoselective compound originating from the *trans* cycloaddition (Figure 4).

**I<sub>2</sub>-IR Binding Activity and Structure–Activity Relationships.** The pharmacological activity of the compounds depicted in Schemes 2 and 3 was evaluated through competition binding studies against the selective I<sub>2</sub>-IR radioligand [<sup>3</sup>H]2-BFI and the selective α<sub>2</sub>-AR radioligand [<sup>3</sup>H]RX821002. The studies were performed in membranes from post-mortem human frontal cortex, a brain area that shows an important density of I<sub>2</sub>-IR and α<sub>2</sub>-AR.<sup>30</sup> Idazoxan (**4**), a compound with well-established affinity for I<sub>2</sub>-IR (pK<sub>i</sub> = 7.27 ± 0.07) and α<sub>2</sub>-AR (pK<sub>i</sub> = 7.51 ± 0.07), was used as reference. The inhibition constant (K<sub>i</sub>) for each compound was obtained and is expressed as the corresponding pK<sub>i</sub> (Table 1). The selectivity for these two receptors was expressed by the I<sub>2</sub>-IR/α<sub>2</sub>-AR index, calculated as the antilogarithm of the ratio between pK<sub>i</sub> value for I<sub>2</sub>-IR and pK<sub>i</sub> value for α<sub>2</sub>-AR (Table 1). Competition experiments against [<sup>3</sup>H]2-BFI were monophasic for most of the compounds (for a few exceptions, see below).

Among the set of 10 bicycles of general structure **1a** (Scheme 1a) already reported,<sup>28</sup> five representative compounds, **8a**, **8b**, **8c**, **8d**, and **8e**, were selected for evaluation as potential I<sub>2</sub>-IR ligands considering the substitution in the *N*-maleimide by an alkyl (**8a**), cycloalkyl (**8b**), unsubstituted phenyl (**8c**), electron withdrawing-disubstituted phenyl (**8d**), and electron donating-substituted phenyl (**8e**) groups.

Pleasantly, **8a** and **8c** displayed pK<sub>i</sub> I<sub>2</sub> affinity of 6.79 and 7.73, respectively, in the range of that of idazoxan (**4**) (7.41). However, no promising results were found for **8b**, **8d**, and **8e** (Table 1). As a first structural approximation, we turned our

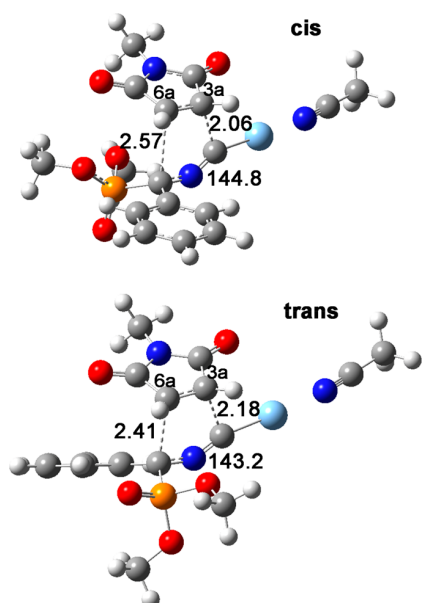


Figure 4. Representation of the transition states for the *cis* and *trans* [3 + 2] cycloaddition between *N*-methylmaleimide and α-phenyl-PhosMic (ethyl groups substituted by methyl) located from B3LYP calculations (C...C distances in Å; C–N–C angle in deg).

linearity is observed in the isocyano group, as the C–N–C angle is close to 144° in the two transition states. The results also point out that the transition state leading to the *trans* addition was more stable by 2.3 kcal mol<sup>-1</sup> relative to the *cis* cycloaddition (Table S1), presumably due to the destabilizing electrostatic interactions between the oxygen atoms of the phosphonate and maleimide moieties. The preferred stability



Table 1. I<sub>2</sub>-IR and α<sub>2</sub>-AR Binding Affinities (pK<sub>i</sub>) of Five Previously Reported Compounds **8**<sup>28</sup> and New Compounds

Compound General structure	R-	R'-	pK <sub>i</sub>			
			<sup>a</sup> [ <sup>3</sup> H]-2-BFI, I <sub>2</sub> one site	<sup>b</sup> [ <sup>3</sup> H]-2-BFI, I <sub>2</sub> two sites	<sup>a</sup> Selectivity I <sub>2</sub> /α <sub>2</sub>	
	<b>Idazoxan</b>					
	<b>8a</b>	H	Me	7.41 ± 0.63	8.35 ± 0.16	-
	<b>8b</b>	H	cyclohexyl	6.79 ± 0.51	9.49 ± 0.18	5
	<b>8c</b>	H	Ph	5.74 ± 0.51	5.02 ± 0.58	-
	<b>8d</b>	H	3-Cl,4-FPh	7.73 ± 0.19	8.49 ± 0.36	-
	<b>8e</b>	H	4-MeOPh	<3	10.27 ± 0.32	-
	<b>9a</b>	Ph	Me	5.11 ± 0.13	6.14 ± 0.85	-
	<b>9b</b>	Ph	cyclohexyl	7.97 ± 0.55	5.93 ± 0.41	110
	<b>9c</b>	Ph	Ph	9.74 ± 0.29	9.01 ± 0.51	5
	<b>9d</b>	Ph	3-Cl,4-FPh	10.28 ± 0.37	10.38 ± 0.22	1
<b>9e</b>	Ph	4-MeOPh	8.56 ± 0.32	6.27 ± 0.56	195	
<b>12c</b>	4-FPh	Ph	8.61 ± 0.28/ 4.29 ± 0.20; 3.7 ± 4	6.77 ± 0.64	219	
<b>12d</b>	4-FPh	3-Cl,4-FPh	7.55 ± 0.32	3.38 ± 0.33	14791	
<b>13c</b>	4-MeOPh	Ph	3.39 ± 0.62	3.85 ± 0.31	-	
<b>13d</b>	4-MeOPh	3-Cl,4-FPh	7.87 ± 0.40	<3	74131	
<b>14c</b>	CH <sub>2</sub> Ph	Ph	6.59 ± 0.77	3.94 ± 0.16	447	
<b>15c</b>	4-FCH <sub>2</sub> Ph	Ph	5.35 ± 0.35	7.20 ± 1.02	-	
<b>9f</b>	Ph	Et	8.37 ± 0.27	5.85 ± 0.53	331	
<b>9g</b>	Ph	propyl	8.95 ± 0.36/ 5.86 ± 0.66; 6.2 ± 1.1	±	1259	
<b>9h</b>	Ph	<i>t</i> -butyl	4.02 ± 0.41	6.77 ± 0.66	3	

Compound General structure	R-	R'-	pK <sub>i</sub>			
			<sup>a</sup> [ <sup>3</sup> H]-2-BFI, I <sub>2</sub> one site	<sup>b</sup> [ <sup>3</sup> H]-2-BFI, I <sub>2</sub> two sites	<sup>a</sup> Selectivity I <sub>2</sub> /α <sub>2</sub>	
	<b>9i</b>	Ph	(1-adamantyl)methyl	7.01 ± 0.76	4.31 ± 0.29	501
	<b>9j</b>	Ph	PhCH <sub>2</sub>	5.26 ± 0.22	8.11 ± 0.28	-
	<b>9k</b>	Ph	PhCH <sub>2</sub> CH <sub>2</sub>	6.35 ± 0.38	3.77 ± 0.09	380
	<b>9l</b>	Ph	4-FPhCH <sub>2</sub> CH <sub>2</sub>	<3	5.65 ± 0.39	-
	<b>9m</b>	Ph	Ph(CH <sub>2</sub> ) <sub>2</sub> CH <sub>2</sub>	3.84 ± 0.31	3.44 ± 0.28	2
	<b>9n</b>	Ph	4-CF <sub>3</sub> Ph	6.87 ± 0.81/ 3.20 ± 0.99; 22 ± 2	4.73 ± 0.60	-
	<b>9o</b>	Ph	3-CF <sub>3</sub> Ph	<3	±	-
	<b>9p</b>	Ph	4-FPh	<3	5.34 ± 0.35	-
	<b>9q</b>	Ph	4-ClPh	<3	±	-
	<b>9r</b>	Ph	2-ClPh	5.09 ± 0.16	6.15 ± 0.44	-
	<b>9s</b>	Ph	3-ClPh	7.53 ± 0.66/ 4.74 ± 0.23; 25 ± 7	±	24
	<b>9t</b>	Ph	4-BrPh	<3	±	-
	<b>9u</b>	Ph	3,5-diClPh	5.81 ± 0.37	6.22 ± 0.26	-
	<b>9v</b>	Ph	3,4-diClPh	<3	±	-
	<b>9w</b>	Ph	2,4,6-triClPh	<3	5.16 ± 0.19	-
	<b>9x</b>	Ph	3-NO <sub>2</sub> Ph	6.81 ± 0.27	10.18 ± 0.41	-
	<b>9y</b>	Ph	3-NO <sub>2</sub> -6-CH <sub>3</sub> Ph	<3	±	-
	<b>9z</b>	Ph	4-PhPh	7.90 ± 0.46	5.12 ± 0.14	602
	<b>9aa</b>	Ph	4-CH <sub>3</sub> Ph	5.44 ± 0.16	±	-
	<b>9ab</b>	Ph	4-PhOPh	6.96 ± 0.30	5.43 ± 0.21	34
<b>9ac</b>	Ph	1-naphthyl	3.11 ± 0.7	<3	-	
<b>9ad</b>	Ph	2-Cl,3-pyridyl	7.96 ± 0.41	<3	91201	

<sup>a</sup>Selectivity I<sub>2</sub>-IR/α<sub>2</sub>-AR expressed as the antilog (pK<sub>i</sub> I<sub>2</sub>-IR – pK<sub>i</sub> α<sub>2</sub>-AR). <sup>b</sup>The best fit of the data for **9d**, **9f**, **9m**, and **9r** was to a two-site binding model of binding with high pK<sub>i</sub> (pK<sub>iH</sub>) and low pK<sub>i</sub> (pK<sub>iL</sub>) affinities for both binding sites, respectively.

attention to compounds bearing a quaternary center in the α-position by including a phenyl group. In this manner, the new compounds would resemble the α-phenyliminophosphonate moiety of MCR5, **7** (in pink color in Scheme 1a,c). In order to maintain the homology with the first series of evaluated compounds (Scheme 2, R = H), analogous maleimide derivatives were considered to give access to compounds **9a**, **9b**, **9c**, **9d**, and **9e** (Scheme 2, R = phenyl). Indeed, this change was highly positive for the whole series, increasing the pK<sub>i</sub> I<sub>2</sub> affinity for all the phenyl-substituted derivatives compared to their unsubstituted congeners, with the added benefit, in three cases (**9a**, **9d**, and **9e**), of an enhanced I<sub>2</sub>-IR/α<sub>2</sub>-AR selectivity ratio up to 195. A remarkable benefit in the I<sub>2</sub>-IR affinity, pK<sub>i</sub> I<sub>2</sub> 9.74 (K<sub>i</sub> = 0.18 nM), was observed in *N*-cyclohexyl derived **9b**, 4-fold improvement compared with analogous **8b**, with an I<sub>2</sub>-IR/α<sub>2</sub>-AR selectivity of 5. The rise in the affinity was also conserved in compounds bearing an *N*-arylimide substitution. In particular, the presence of an *N*-phenyl group **9c** led to an outstanding activity binding pK<sub>i</sub> I<sub>2</sub> 10.28 (K<sub>i</sub> = 52.48 pM) but not I<sub>2</sub>-IR/α<sub>2</sub>-AR selectivity. Gratifyingly, introduction of halogen atoms (3-chloro-4-fluoro) in the *N*-phenyl ring of **9c** giving congener **9d** kept a nice affinity, with a pK<sub>i</sub> I<sub>2</sub> 8.56. Of note, **9d** fitted significantly better to a two-site binding model, with a high pK<sub>i</sub> I<sub>2</sub> 8.61 (K<sub>iH</sub> = 2.45 nM) and a low pK<sub>i</sub> I<sub>2</sub> 4.29 (K<sub>iL</sub> = 51.2 μM), with the high-affinity site representing a calculated 37% of the specific binding of [<sup>3</sup>H]2-BFI at 2 nM concentration.

The enhancement, in terms of both affinity and selectivity, observed when moving from the α-unsubstituted to the α-substituted phosphonates prompted us to briefly consider

additional variations. The introduction in the α-phosphonate position of *p*-fluorophenyl (**12c**) or *p*-methoxyphenyl (**13c**), benzyl (**14c**), and *p*-fluorobenzyl (**15c**) groups was highly deleterious for the affinity (pK<sub>i</sub> I<sub>2</sub> = 6.59 for **14c** and pK<sub>i</sub> I<sub>2</sub> < 3 up to 5.35 for **12c**, **13c**, and **15c**, respectively). However, for the *p*-substituted phenyl derivatives, the further introduction of halogen atoms (3-chloro-4-fluoro) in the *N*-phenyl ring (compounds **12d** and **13d**) nicely restored the affinity (pK<sub>i</sub> I<sub>2</sub> 7.55 for **12d** and pK<sub>i</sub> I<sub>2</sub> 7.87 for **13d**). Additionally, due to the lack of binding of **12d** and **13d** to α<sub>2</sub>-AR, their I<sub>2</sub>-IR/α<sub>2</sub>-AR selectivity was outstanding, 14791 and 74131, respectively.

Taking into account the aforementioned results for a second round of compounds, the general structure depicted in Scheme 3 was conserved, featuring the unsubstituted phenyl group in the α-position of the phosphonate and modifying the substituents in the maleimide. New compounds were classified in two groups taking into consideration whether an alkyl or an aryl substituent was introduced in the *N*-maleimide.

Inspired by **9a** and **9b**, compounds bearing alkyl substituents with different lengths, **9f** and **9g**, ramified alkyl, **9h**, and polycycloalkane, **9i**, were prepared. From **9a**, the elongation of the *N*-alkyl chain, from methyl to ethyl, led to **9f**, with an increase in the affinity to pK<sub>i</sub> I<sub>2</sub> = 8.37 (K<sub>i</sub> = 4.3 nM) and in the I<sub>2</sub>-IR/α<sub>2</sub>-AR selectivity to 331, while the *n*-propyl derivative, **9g**, demonstrated much lower affinity, pK<sub>i</sub> I<sub>2</sub> = 4.02. For **9f**, the best fit was a two-site model of binding with a high pK<sub>i</sub> I<sub>2</sub> = 8.95 and a low pK<sub>i</sub> I<sub>2</sub> = 5.86; high affinity site occupancy is 62%. Further increase of the size of the *N*-alkyl substituent to a *tert*-butyl, **9h**, or an adamantylmethyl, **9i**, did not improve the affinity. Taking together the affinity values for **9a**, **9b**, **9f**, **9g**, **9h**

and **9i**, it seems that small and large substituents are compatible with good affinity values but that conformational freedom, as in **9g**, is deleterious.

Compounds **9j**, **9k**, **9l**, and **9m**, with *N*-benzyl, *N*-phenethyl, *N*-4-fluorophenethyl, and *N*-phenylpropyl substituents, respectively, were accessed to increase the examples in the SAR study. However, their affinities revealed a remarkable decrease in the biological properties, leading to  $pK_i I_2 = 5.26, 6.35, <3,$  and  $3.84$  values, respectively.

Taking into account that **9c** displayed an outstanding affinity for  $I_2$ -IR but lacked selectivity over  $\alpha_2$ -AR, further  $R' =$  aryl derivatives were explored. As we knew that **9d** ( $pK_i I_2 = 8.56, I_2$ -IR/ $\alpha_2$ -AR = 195) was endowed with excellent affinity and remarkable selectivity, we mainly focused on electron withdrawing groups (**9n**, **9o**, **9p**, **9q**, **9r**, **9s**, **9t**, **9u**, **9v**, **9w**, **9x**, and **9y**), although a few electron donating substituents were briefly examined (**9z**, **9aa**, and **9ab**). Overall, neither these new phenyl derivatives nor the *N*-naphthyl derivative **9ac** outperformed the excellent affinity of **9c** (Table 1), although **9z** ( $pK_i I_2 = 7.90$ ) had an improved  $I_2$ -IR/ $\alpha_2$ -AR ratio of 602. Finally, **9ad** with an *N*-(2-chloro-3-pyridyl) substituent gave a  $pK_i I_2 = 7.96$ , in the range of standard idazoxan (**4**), but it offered as an outstanding advantage a null affinity for  $\alpha_2$ -AR, leading to an  $I_2$ -IR/ $\alpha_2$ -AR selectivity of 91201.

**Selectivity for  $I_2$ -IR versus  $I_1$ -IR.** After evaluating the affinity of the indicated compounds for  $\alpha_2$ -AR, we assessed the affinity of some representative compounds for  $I_1$ -IR. To this end,  $I_1$ -IR binding site assays were conducted in membranes obtained from the rat kidney using moxonidine, a known  $I_1$ -IR selective compound, as reference. The results are summarized in Table 2, and only **8e** deserves a mention with a  $pK_i I_1 8.09$ .

**Table 2.**  $I_1$ -IR Potencies ( $pIC_{50}$ ) of Representative Compounds

compound	$pIC_{50}$ , [ $^3H$ ]-clonidine
moxonidine	$8.45 \pm 0.85$
<b>8a</b>	$5.13 \pm 0.44$
<b>8b</b>	$5.14 \pm 0.54$
<b>8c</b>	$5.47 \pm 0.31$
<b>8d</b>	<3
<b>8e</b>	$8.09 \pm 0.34$
<b>9a</b>	$6.19 \pm 0.27$
<b>9b</b>	$7.54 \pm 0.79$
<b>9c</b>	$6.74 \pm 0.74$
<b>9d</b>	$3.04 \pm 0.45$
<b>9e</b>	$3.22 \pm 0.67$
<b>14c</b>	$5.12 \pm 0.85$
<b>9j</b>	$5.87 \pm 0.19$
<b>9k</b>	$7.98 \pm 0.31$
<b>9x</b>	$5.26 \pm 0.43$
<b>9z</b>	$7.19 \pm 0.33$

Gratifyingly, the values for the rest of the assessed compounds led to the conclusion that there was not a significant interaction with  $I_1$ -IR, highlighting the  $I_2$ -IR selective behavior of this family of ligands.

Overall, considering its excellent  $I_2$ -IR affinity ( $K_i = 2.8$  nM) and the remarkable selectivity versus  $\alpha_2$ -AR ( $K_i = 53$   $\mu$ M) and  $I_1$ -IR ( $K_i = 912$   $\mu$ M), we identified **9d** as the most promising compound for performing further studies.

#### Comparison of $I_2$ -IR Human Receptor Binding Affinities ( $pK_i$ ) of **9d** and Other Ligands and across

**Species.** A problem typically encountered when working with  $I_2$ -IR ligands is that the binding experiments reported in the bibliography have been performed in a variety of non-human species and using tissues from different anatomical parts (e.g., kidney, whole brain, cortex). Another factor of potential discrepancies is that different radioligands have been used. Overall, this makes difficult the comparison among studies. For this reason and in order to better place **9d** as a new  $I_2$ -IR ligand, unprecedented experiments of displacement of [ $^3H$ ]2-BFI<sup>31</sup> in samples from post-mortem human brains were performed with clinical candidates [ $^{13}C$ ]BU99008 (**2**)<sup>32</sup> and CR4056 (**1**)<sup>33</sup> and the widely used  $I_2$ -IR ligands trazicoline (**5**), LSL60101 (**3**), and 2-BFI (**6**) (Table 3).

As previously observed with **9d**, the affinity data found for BU99008 (**2**) and CR4056 (**1**) fit best to a two-site model of binding. In particular, BU99008 (**2**) showed a  $pK_{iH} I_2 = 6.89$  ( $K_{iH} = 128$  nM) and  $pK_{iL} I_2 = 3.82$  ( $K_{iL} = 151$   $\mu$ M), and a good  $I_2$ -IR/ $\alpha_2$ -AR selectivity ratio of 331. CR4056 (**1**) showed a  $pK_{iH} I_2 = 7.72$  ( $K_{iH} = 19.0$  nM) and  $pK_{iL} I_2 = 5.45$  ( $K_{iL} = 3.5$   $\mu$ M) with an excellent  $I_2$ -IR/ $\alpha_2$ -AR selectivity of 117490. The percentage of occupancy for the high affinity site was different for BU99008 (**2**) (51%) compared with CR4056 (**1**) (29%). Other well-established  $I_2$ -IR ligands, trazicoline (**5**), LSL60101 (**3**), and 2-BFI (**6**) also resulted in clearly biphasic curves. Trazicoline (**5**) displayed a  $pK_{iH} I_2 = 8.48$  ( $K_{iH} = 3.3$  nM) and  $pK_{iL} I_2 = 6.48$  with an excellent  $I_2$ -IR/ $\alpha_2$ -AR selectivity of 14125. 2-BFI (**6**) had a  $pK_{iH} I_2 = 9.87$  ( $K_{iH} = 0.13$  nM) and  $pK_{iL} I_2 = 7.94$ , with a good  $I_2$ -IR/ $\alpha_2$ -AR selectivity of 1698, and LSL60101 (**3**) a  $pK_{iH} I_2 = 9.03$  ( $K_{iH} = 0.9$  nM) and  $pK_{iL} I_2 = 5.25$  ( $K_{iL} = 5.6$   $\mu$ M), with a good  $I_2$ -IR/ $\alpha_2$ -AR selectivity of 7244. The high-affinity site represented 38%, 21%, and 49% occupancy for trazicoline (**5**), 2-BFI (**6**), and LSL60101 (**3**), respectively (Table 3). Previous studies have reported [ $^3H$ ]2-BFI identifying two binding sites in rabbit,<sup>34</sup> rat,<sup>35,36</sup> and human brain.<sup>31</sup> It remains unclear whether these two sites observed represent distinct receptors or interconvertible conformational states of the  $I_2$ -IR. For trazicoline (**5**), a single binding site of  $pK_i I_2 = 8.72$ , similar to the affinity described for human tissues, was described in the rabbit kidney membranes.<sup>37</sup> In the rat cerebral cortex, LSL60101 (**3**) shows lower affinity than in human tissues, with a  $K_{iH} = 350$  nM and  $K_{iL} = 116$   $\mu$ M.<sup>38</sup>

Therefore, compounds BU99008 (**2**), trazicoline (**5**), and 2-BFI (**6**), which have a nonsubstituted 2-(imidazolin-2-yl) group, CR4056 (**1**) and LSL60101 (**3**), which feature an imidazole ring, and the structurally dissimilar **9d** have similar affinity profiles to  $I_2$ -IR in human brain.

Of note, the ability of BU99008 (**2**) to displace [ $^3H$ ]2-BFI from  $I_2$ -IR in rat brain was fit to a two-site model of binding, with a  $K_{iH} = 1.4 \pm 0.6$  nM and  $K_{iL} = 238.6 \pm 63.3$  nM and with a percentage fraction of high occupancy of  $58\% \pm 7\%$ . That is, an enhanced affinity by 100 times in rat brain compared with human brain, the % of occupancy being similar in the high site. Regarding selectivity, a good  $I_2$ -IR/ $\alpha_2$ -AR ratio of 909 was reported in rat, 4.5 times higher than that found in human. Of note, the opposite trend was found for CR4056 (**1**): the inhibition recorded in rat whole-brain for [ $^3H$ ]2-BFI binding was  $IC_{50}$  of  $596 \pm 76$  nM, with an improved affinity of 19 nM shown in human brain.<sup>39</sup> Therefore, significant differences between species occur within the two  $I_2$ -IR ligands in clinical trials, BU99008 (**2**) and CR4056 (**1**).

In an attempt to incorporate additional data regarding the differences in  $I_2$ -IR binding affinities between species, idazoxan

**Table 3.** I<sub>2</sub>-IR and  $\alpha_2$ -AR Binding Affinities (pK<sub>i</sub>) of BU99008 2, CR4056 1, Tracizoline 5, LSL60101 3, and 9d in Post-mortem Human Brain Cortical Membranes

compound	<sup>3</sup> H]-2-BFI I <sub>2</sub> pK <sub>i</sub> , two sites		high-affinity site (%)	<sup>3</sup> H]-RX821002 $\alpha_2$ pK <sub>i</sub>	selectivity I <sub>2</sub> -IR/ $\alpha_2$ -AR for [ <sup>3</sup> H]-2-BFI (high-affinity site)
	high-affinity	low-affinity			
BU99008, 2	6.89 ± 0.21	3.82 ± 0.30	51 ± 6	4.37 ± 0.17	331
CR4056, 1	7.72 ± 0.31	5.45 ± 0.15	29 ± 6	2.65 ± 1.24	117490
tracizoline, 5	8.48 ± 0.51	6.48 ± 0.32	38 ± 13	4.33 ± 0.22	14125
2-BFI, 6	9.87 ± 0.33	7.94 ± 0.11	21 ± 5	6.64 ± 0.38	1698
LSL60101, 3	9.03 ± 0.21	5.25 ± 0.24	49 ± 4	5.17 ± 1.32	7244
9d	8.61 ± 0.28	4.29 ± 0.20	37 ± 4	6.27 ± 0.56	219

**Table 4.** I<sub>2</sub>-IR Binding Affinities (pK<sub>i</sub>) of Idazoxan 4 and 9d in the Brain Cortex of Different Species

	human	rat	mice
idazoxan, 4	7.74 ± 0.10	7.17 ± 0.11	5.68 ± 0.31
9d	8.61 ± 0.28	4.29 ± 0.20	6.41 ± 0.39

(4) and 9d were investigated (Table 4). In our hands, idazoxan (4) gave similar results in human frontal cortex, pK<sub>i</sub> 7.74, as compared to rat brain cortex, pK<sub>i</sub> 7.17, and had considerably less affinity in mouse brain cortical membranes, pK<sub>i</sub> 5.68. Importantly, differences for 9d were found not only among species but also in its binding characteristics. As previously mentioned, the binding to I<sub>2</sub>-IR in human frontal cortex displayed a biphasic curve, whereas a monophasic one was observed in rat and mouse brain cortex with affinity values of pK<sub>i</sub> 6.92 and 6.41, respectively.

Finally, in order to verify if the high affinity site observed for 9d in competition experiments against [<sup>3</sup>H]2-BFI corresponded to the I<sub>2</sub>-IR, we performed additional experiments in the presence of MCR5 (7), a high-affinity I<sub>2</sub>-IR selective compound previously reported by our group.<sup>25</sup> Interestingly, in the presence of MCR5 (7) (10<sup>-5</sup> M), the 9d competition curve against [<sup>3</sup>H]2-BFI became monophasic (pK<sub>i</sub> = 6.96 ± 0.46), and the high-affinity site recognized by 9d was completely blocked. These results confirm that the high affinity site bound by 9d is the I<sub>2</sub>-IR.

**3D-QSAR Study.** 3D-QSAR studies were performed to rationalize the differences in activity and gain insights for improved bicyclic  $\alpha$ -iminophosphonate-based I<sub>2</sub>-IR ligands. 3D-QSAR models were created using Pentacle program,<sup>40</sup> which calculates GRIND descriptors (GRIND and GRIND2) from molecular interaction fields, and were evaluated by internal and external validation parameters (Tables S2 and S3). The data set included structurally diverse bicyclic  $\alpha$ -iminophosphonates (Schemes 2 and 3) with a wide range of binding activity on I<sub>2</sub>-IR (pK<sub>i</sub> I<sub>2</sub> = 3.11–10.28) and  $\alpha_2$ -AR (pK<sub>i</sub>  $\alpha_2$  = 3.38–10.27) ensuring the good quality and applicability of the 3D-QSAR models. Additionally, we added four I<sub>2</sub>-IR standard ligands (tracizoline, 5; idazoxan, 4; BU99008, 2; LSL60101, 3) in both data sets to compare and validate our results. Created 3D-QSAR models were used to analyze statistically significant variables that describe distance between chemical groups in the examined compounds. These variables are presented as interactions between two same (e.g., DRY–DRY) or different (e.g., DRY–TIP) MIF probes in PLS coefficient plots (Figures S1 and S2).

Describing the most significant GRIND variables with positive and negative influence on I<sub>2</sub>-IR and  $\alpha_2$ -AR binding activity gave us the deeper insight into crucial interactions for enhancing activity and selectivity on I<sub>2</sub>-IR against  $\alpha_2$ -AR. Based on comprehensive 3D-QSAR analysis presented in Supporting

Information, we can conclude that the presence of two steric hot spots (var183, TIP–TIP), such as halogen atoms (3-chloro-4-fluoro) in the *N*-phenyl ring at the distance range 6.00–6.40 Å, may be crucial for enhancing I<sub>2</sub>-IR binding activity and selectivity. The highest values are calculated for compounds 13d and 12d, which possess high selectivity toward I<sub>2</sub>-IR (Figure 5B). Likewise, var19 (DRY–DRY, 7.60–8.00 Å) implies that introduction of hydrophobic regions such as phenyl ring in the *N*-maleimide group may be crucial for establishing favorable van der Waals interactions with aromatic amino acids of the active pocket of I<sub>2</sub>-IR (Figure 5A,B). Comparing to compounds that possess *N*-alkyl substituents instead of *N*-phenyl, such as 8a or 9a, we can conclude that introduction of this aromatic ring positively correlates with I<sub>2</sub>-IR binding activity. Contrarily, the  $\alpha_2$ -AR model pointed out a negative DRY–DRY variable (var25, 10.00–10.40 Å), which suggests that introduction of a phenyl substituent in the  $\alpha$ -phosphonate position negatively correlates with  $\alpha_2$ -AR activity. This is in agreement with experimental findings, which show that  $\alpha$ -substituted ligands possess higher affinity and selectivity toward I<sub>2</sub>-IR (8a, 8c, 8d, and 8e). Additionally, analysis of negative variables var200 (TIP–TIP, 12.80–13.20 Å), var314 (DRY–N1, 13.60–14.00 Å), and var377 (DRY–TIP, 16.40–16.80 Å) emphasizes that introduction of bulkier substituents in the *N*-maleimide group unfavorably affects the fit in the binding site of I<sub>2</sub>-IR and may decrease the potency of I<sub>2</sub> ligands (Figure 6A,B). The highest values of these variables are pronounced in compounds 9z, 9m, 9k, 9j, 9ab, and 9ac.

**In Silico Analysis of Physicochemical and Pharmacokinetic Parameters.** *In silico* analysis of key parameters is one of the most important steps in drug discovery processes.<sup>41</sup> Thus, ADMET Predictor software 9.5,<sup>42</sup> and SwissADME web tool<sup>43</sup> were used to foresee ADMET and physicochemical properties on the most potent bicyclic  $\alpha$ -iminophosphonate I<sub>2</sub>-IR ligands (pK<sub>i</sub> > 7) and four standards. The obtained results are presented in the Supporting Information (Tables S4 and S5) including solubility and lipophilicity, BBB-penetration, elimination rate, and interactions with targets. Note that introduction of aromatic rings increases log *P* values and affinity for albumin, while it decreases the water solubility (9d, 9z, 12d, and 13d). Based on results obtained from different computational methods, we can conclude that all examined compounds possess good water solubility and lipophilicity. Furthermore, calculated values of topological polar surface area (TPSA) descriptor revealed acceptable polarity of all

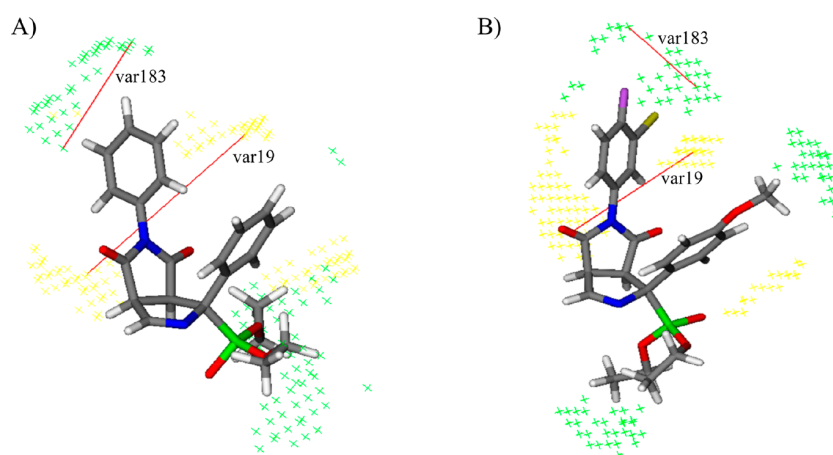


**Figure 5.** Representation of positive (in red) interactions of **9c** (A) and **13d** (B) in  $I_2$ -IR 3D-QSAR model. The steric hot spots (TIP) are presented in green and hydrophobic regions (DRY) in yellow.

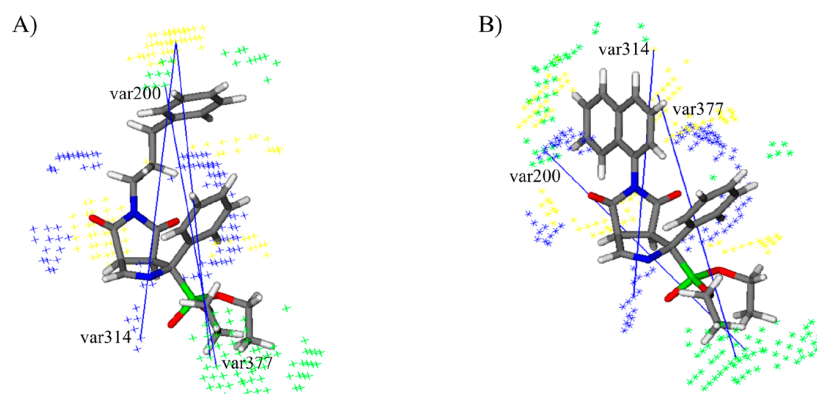


**Figure 6.** Representation of negative (in blue) interactions of **9m** (A) and **9ac** (B) in  $I_2$ -IR 3D-QSAR model. The steric hot spots (TIP) are presented in green, hydrophobic regions (DRY) in yellow, and H-bond acceptor regions (N1) in blue.

molecules. The Lipinski's Rule of 5 was used to describe drug-likeness properties of compounds based on physicochemical analysis ( $M \log P \leq 4.15$ ;  $MW \leq 500$ ;  $N$  or  $O \leq 10$ ;  $OH$  or  $NH \leq 5$ ). Because of the slightly higher molecular weight, **9z** and **13d** violated only one rule. Analysis of pharmacokinetic parameters shows that all compounds possess high BBB permeation. Compared to standards, bicyclic  $\alpha$ -iminophosphonates have lower percentage of unbound drug in plasma. Also, they are estimated to have lower metabolic CYP risk compared to idazoxan. Only three compounds, **9z**, **12d**, and **13d** were identified as P-gp inhibitors. Performed calculations also show that bicyclic  $\alpha$ -iminophosphonates possess lower toxicity risk, while compound **13d** had no predicted toxicity.

The theoretical effort paved the way to continue with crucial *in vitro* experiments (drug-like) due to the lack of warnings that had stopped the progress of this family of  $\alpha$ -iminophosphonates as  $I_2$ -IR ligands.

**BBB Permeation Assay.** Considering the localization of  $I_2$ -IR in the CNS, a good ability to cross the BBB is an essential requirement for developing effective  $I_2$ -IR ligands with potential therapeutic applications in the neuroprotective field. For this reason, the *in vitro* permeability ( $P_e$ ) of all the novel compounds was determined by using the PAMPA-BBB permeability assay (Table S6). In particular, our representative compound **9d** had a  $P_e$  value of  $(9.7 \pm 0.7) \times 10^{-6} \text{ cm s}^{-1}$ , well above the threshold established for high BBB permeation ( $P_e >$

$5.198 \times 10^{-6} \text{ cm s}^{-1}$ ). Thus, compounds were considered suitable to envisage further *in vitro* and *in vivo* studies oriented to in-depth pharmacological profiling of the new family of  $I_2$ -IR ligands.

**Cytotoxicity.** All the synthesized compounds were devoid of cytotoxicity in human embryonic lung fibroblast cell cultures (highest concentration tested,  $100 \mu\text{M}$ ). Further evaluation of eight selected compounds, including the outstanding  $I_2$ -IR ligands **9d**, **9b**, and **9c** and representative compounds **8d**, **9e**, **8b**, **9x**, and **9j** was performed in different mammalian cell lines, such as HeLa (human cervix carcinoma), Vero (African green monkey kidney), MDCK (Mandin-Darby canine kidney), and MT4 (human T-lymphocyte). Serial compound dilutions were added to semiconfluent cell cultures, and after 3–5 days incubation at  $37^\circ\text{C}$ , cytotoxicity was estimated by microscopic inspection of cell morphology and by colorimetric cell viability assays. None of the compounds produced any cytotoxicity at  $100 \mu\text{M}$ , the highest concentration tested. Additionally, the cytotoxicity of **9d** was tested in MRC-5 (human embryonic lung fibroblast) cells ( $CC_{50} > 100 \mu\text{M}$ ).

**ADME–DMPK Profiling of 9d.** In order to further progress **9d** to *in vivo* assays with the confidence that the *in silico* studies offered (see above), we evaluated its physicochemical properties, such as solubility and chemical stability, microsomal stability, cytochromes inhibition, hERG inhibition, and plasma protein binding.

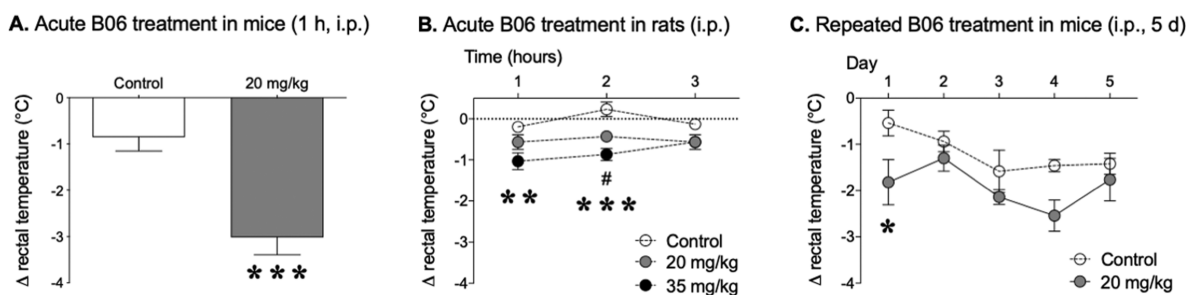


**Figure 7.** Hypothermic effects of **9d** (B06) in rodents. (A) Acute effect of **9d** (20 mg/kg, ip) in mice. Columns are means  $\pm$  SEM of the difference ( $\Delta$ , 1 h minus basal value) in body temperature ( $^{\circ}$ C) for each treatment group. \*\*\* $p$  < 0.001 vs control group (Student's  $t$ -test). (B) Acute effect of **9d** (20 or 35 mg/kg, ip) in rats. Columns are means  $\pm$  SEM of the difference ( $\Delta$ , 1, 2, or 3 h minus basal value) in body temperature ( $^{\circ}$ C) for each treatment group. # $p$  < 0.05 for dose of 20 mg/kg and \*\* $p$  < 0.01 and \*\*\* $p$  < 0.001 for dose of 35 mg/kg vs control group (repeated measures ANOVA followed by Sidak's comparison test). (C) Repeated (5 days) effect of **9d** (20 mg/kg, ip) in mice. Circles are means  $\pm$  SEM of the daily difference ( $\Delta$ , 1 h minus basal value) in body temperature ( $^{\circ}$ C) for each treatment group. \* $p$  < 0.05 vs control group (repeated measures ANOVA followed by Sidak's comparison test).

The solubility of **9d** was determined in several media. An excellent solubility of 92  $\mu$ M was found in 1% DMSO and 99% PBS buffer. Additional solvents, methanol, acetonitrile, and water, were also evaluated with good solubility.<sup>44</sup> To evaluate the stability of **9d**, forced degradation studies were performed under various stress conditions for a period of 9 weeks, with HPLC and  $^1$ H NMR monitoring every week.<sup>45</sup> Particularly, **9d** was subjected to the effect of daylight with temperatures between 0 and 23  $^{\circ}$ C and a relative humidity of 25–85%, to the effect of high temperature (thermal stability at 75  $^{\circ}$ C), and to the continuous light of a 100 W (230 V) bulb. Analysis by HPLC showed that the compound was completely stable under all the aforementioned conditions. Overall, these studies confirmed that **9d** is sufficiently stable to undertake further experiments.

Selected compound **9d** was further studied *in vitro* for ascertaining their microsomal stability, CYP inhibition, and protein plasma binding. The microsomal stability was assessed in three species (human, mouse, and rat), considering that the affinity and selectivity studies were performed in human samples, the cognition studies were envisaged in mice, and the hypothermia evaluation was planned in mice and rats (see below). Compound **9d** showed good microsomal stability (Table S7) and inhibited neither cytochromes [CYP1A2, CYP2C9, CYP2C19, CYP3A4 (BFC and DBF), and CYP2D6] nor hERG. Plasma protein binding was measured in mice and human species (Table S8) with a slight difference that should be taken into consideration if **9d** progress through additional preclinical studies.

**Receptor Characterization Panel.** In a Lead Profiling Screen (Eurofins)<sup>46</sup> of 44 potential off targets, **9d** showed a clean ancillary pharmacology (Table S9). Only one target, the cholecystinin type A receptor (CCK<sub>A</sub>), was inhibited more than 50% at the tested concentration of 10  $\mu$ M. CCK receptors belong to the G-protein-coupled receptor superfamily and are involved in a range of biological actions mediated by two distinct receptor types, CCK<sub>A</sub> (present in gastrointestinal tract and discrete regions of the brain) and CCK<sub>B</sub> (present in the CNS).<sup>47</sup> Compound **9d** exhibited an IC<sub>50</sub> of 5.94  $\mu$ M upon CCK<sub>A</sub> and an IC<sub>50</sub> > 10  $\mu$ M for CCK<sub>B</sub>. Taking into account the relative high IC<sub>50</sub> of **9d** for CCK<sub>A</sub> and the lack of significant interaction with the other off targets evaluated, we conclude that **9d** shows a very selective profile.

**Hypothermic Effects of 9d.** It is known that I<sub>2</sub>-IR ligands such as idazoxan (**4**) or 2-(4,5-dihydroimidazol-2-yl)quinoline (BU224) induce hypothermia in rats.<sup>48,49</sup> We have also found hypothermic effects with compound MCR5 (**7**) in mice.<sup>25,27</sup>

In the same line, acute **9d** (20 mg/kg) exposure induced hypothermia in adult CD1 mice as observed by reductions of core body temperature (ranging from  $-1.8$  to  $-3.0$   $^{\circ}$ C) measured 1 h postinjection (Figure 7A,C, day 1). To test for differences between species, a pilot study was performed in adult rats, which showed that acute **9d** (20 and 35 mg/kg) treatment induced moderate drops in temperature ( $-0.4$  to  $-1.0$   $^{\circ}$ C) as measured 1 and 2 h postinjection (Figure 7B). Repeated administration of **9d** (20 mg/kg, 5 days) in mice revealed the induction of tolerance to the acute hypothermic effect of this drug from day 2 of treatment (Figure 7C), effects previously observed for other I<sub>2</sub>-IR compounds.<sup>25,27</sup>

Of note, hypothermia is well established as having a neuroprotective effect in cerebral ischemia and even mild temperature drops cause significant neuroprotection.<sup>50</sup> Also, hypothermia has been clinically used to improve the neurological outcome under various pathological conditions, including stroke and traumatic brain injury.<sup>51,52</sup> Thus, the hypothermic effects showed by **9d** might be a relevant feature that could mediate neuroprotection.

**Effects of Acute and Repeated Treatments with 9d on Hippocampal FADD Protein Content in Mice.** FADD multifunctional protein is an adaptor of cell death receptors that can also mediate antiapoptotic or neuroprotective actions in rodents.<sup>25,53,54</sup> Acute treatment with **9d** significantly decreased ( $-30\%$ ) the content of FADD protein in the hippocampus when compared to vehicle-treated mice (Figure 8, left panel). Following repeated (5 days) administration, no effects were observed on FADD modulation (Figure 8, right panel). The significant decrease in hippocampal proapoptotic FADD following acute **9d** treatment suggests that this compound might be mediating some of its neuroplastic or neuroprotective actions through the regulation of this key brain marker, similarly with other I<sub>2</sub>-IR compounds.<sup>25</sup>

**5xFAD *In Vivo* Behavioral Studies on Selected Compound 9d.** Recently, we reported the first *in vivo* study that validates I<sub>2</sub>-IR as a target for cognitive impairment using a mouse model of age-related cognitive decline and late-onset AD, the SAMP8, a murine model that displays a phenotype of accelerated aging.<sup>27</sup> To further support the effect of I<sub>2</sub>-IR

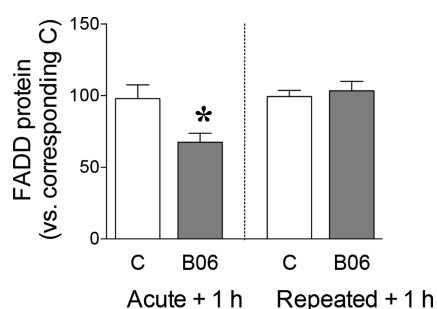


**Figure 8.** Effects of acute (20 mg/kg, ip) and repeated (20 mg/kg, ip, 5 days) treatments with **9d** (B06) on the contents of FADD protein in the hippocampus of mice. Columns are means  $\pm$  SEM of FADD in **9d**- and vehicle-treated groups. \* $p < 0.05$  vs control group (Student's  $t$ -test).

ligands as a putative treatment for neurodegenerative diseases, herein we evaluate **9d** in the 5xFAD, a well-established murine model of early on-set AD.<sup>55</sup>

Because one of the signs of AD is memory loss (cognitive decline), the effect of orally administered **9d** (5 (mg/kg)/day for 28 days) on cognitive performance was evaluated in the novel object recognition test (NORT). The NORT is a widely used behavioral task to assess visual recognition memory.<sup>56</sup> This brain activity relies on the hippocampus and involves the cortex to remember and recognize new and old objects. The NORT is based on an animal's innate preference for novelty. The task consists of three parts: a habituation phase; a training phase, where mice are presented with two identical objects; and a trial phase, in which following an interval time (2 or 24 h) memory was assessed by presenting the mice with a trained object and a novel one. Mice with cognitive ability preserved preferentially explore the novel object in the different time exposition studied. After a 2 h acquisition trial, one of the familiar objects was replaced with a novel object, and the time spent investigating each of the objects was recorded, and the discrimination index (DI) was calculated as the percentage of novel object interaction time relative to total interaction time during the retention trial. As expected, untreated 5xFAD did not exhibit differences between exploration times for the familiar and novel objects (DI close to 0), indicating deterioration or loss of memory for the familiar object. As shown in Figure 9A, the oral administration of **9d** to 5xFAD enhanced recognition memory at short-term, reaching DI

values of WT mice (Figure 9A). Of note, 24 h after the retention trial, **9d** treated 5xFAD mice, explored the novel object for a longer time, obtaining a higher DI, indicative of preserved memory for the familiar object presented during the acquisition trial (Figure 9B). These results suggest that compound **9d** enhanced recognition memory during the NORT in 5xFAD mice.

#### Effects of Selected Compound **9d** in 5xFAD Hippocampus: Neuroinflammation and Oxidative Stress Parameters.

Inflammation is an omnipresent sign in neurodegeneration and can act as a propagation method for the deleterious effects for the characteristic event in AD.<sup>57</sup> Oxidative stress (OS) is another key risk factor that can promote ignition of degenerative processes.<sup>58</sup> The reduction in the memory impairment of the **9d** treated animals prompted us to determine indicators of brain neuroinflammation and OS by comparison of WT and 5xFAD mice (vehicle and **9d** treated). 5xFAD mice had higher gene expression of *Cxcl10* (C-X-C motif chemokine 10) and *Tnf- $\alpha$*  (tumor necrosis factor  $\alpha$ ) compared to WT mice (Figure 10A) that decreased after treatment of 5xFAD mice with **9d** (5 (mg/kg)/day). Of note, it has been reported that TNF- $\alpha$  contributes to amyloidogenesis via  $\beta$ -secretase regulation, apart from being involved in AD-related brain neuroinflammation.<sup>59</sup> In fact, when amyloid precursor protein (APP) processing was studied in treated 5xFAD mice, an increase in sAPP $\alpha$ , correlating with a significant decrease in sAPP $\beta$  protein levels, was determined compared with untreated mice (Figure 10B).

In reference to OS, 5xFAD mice showed no changes in gene expression for *iNOS* (inducible nitric oxide synthase, a pro-oxidant key driver)<sup>60</sup> and *Hmox1* (an enzyme implicated in antioxidant defense) (Figure 10A).<sup>61</sup> Those results correlated with published results in 5xFAD mice, and in agreement, **9d** treatment did not modify either *iNOS* or *Hmox1* (Figure 10A). Nonetheless, total levels of hydrogen peroxide (H<sub>2</sub>O<sub>2</sub>), although not significant, were higher in 5xFAD than in the WT and were reduced after **9d** treatment (Figure 10C). The increase of OS, without increases in *iNOS* expression, was also described in 5xFAD mice; concretely the increase in 4-HNE (4-hydroxy-2-nonenal), a protein derivative obtained when reactive species of oxygen, ROS (such as H<sub>2</sub>O<sub>2</sub>), increase, is significant in 6-month-old 5xFAD mice compared to WT mice.<sup>62</sup> All the evaluated parameters are consistent with a mild reduction in the oxidative environment in treated 5xFAD mice.

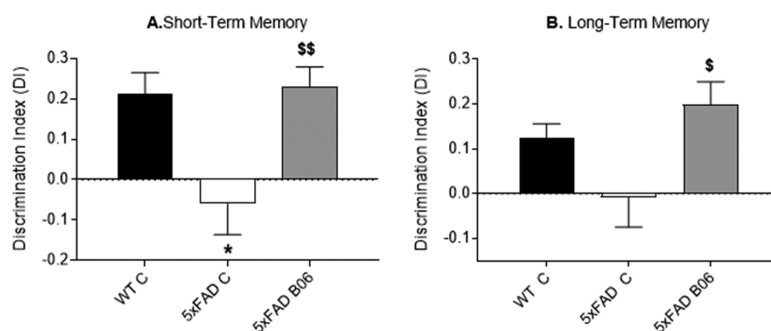


**Figure 9.** DI of NORT in 6-month-old (WT C,  $n = 12$ ), 5xFAD (C,  $n = 14$ ) control mice and 5xFAD mice after treatment with **9d** (B06) at 5 mg/kg for 4 weeks ( $n = 25$ ). Summary from (A) Short-Term Memory and (B) Long-Term Memory. Values represented are mean  $\pm$  standard error of the mean (SEM). One-way ANOVA followed by (Tukey post hoc test);  $P$ -value: \* $p < 0.05$  vs WT-Control,  $^{\$}p < 0.05$ ;  $^{\$\$}p < 0.01$  vs 5xFAD-Control.

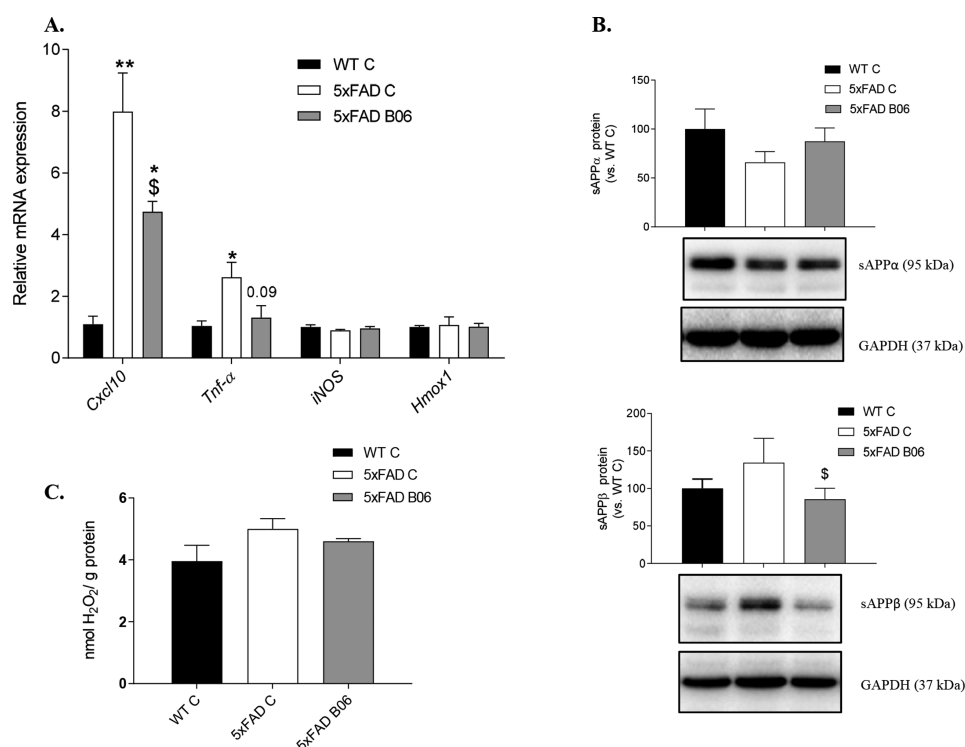


**Figure 10.** (A) Gene expression of inflammatory markers, *Cxcl10* and *Tnf- $\alpha$* , and OS markers, *iNOS* and *Hmox1* ( $n = 4$  for each group). (B) H<sub>2</sub>O<sub>2</sub> concentration ( $n = 10$  for each group) and (C) representative Western blot and bar chart sAPP $\alpha$  and sAPP $\beta$  ( $n = 4$ –6 for each group) in the hippocampus of 6-month-old female WT, 5xFAD Control mice, and 5xFAD mice after treatment with 9d (B06) at 5 mg/kg for 4 weeks. Bars represent mean  $\pm$  standard error of the mean (SEM).

## CONCLUSIONS

To sum up, we have explored the scope of diastereoselective [3 + 2] cycloaddition reaction of  $\alpha$ -substituted-PhosMic derivatives with diversely substituted maleimides leading to a family of bicyclic  $\alpha$ -iminophosphonates. A combination of X-ray crystallographic analyses and NMR studies allowed a full stereochemical characterization, and theoretical calculations provided a basis to justify the excellent diastereoselectivity observed. The pharmacological profiling of the new compounds led to the identification of high affinity and selective I<sub>2</sub>-IR ligands devoid of  $\alpha_2$ -AR and I<sub>1</sub>-IR affinities. 3D-QSAR study revealed key structural parameters for the design of future promising structures, and theoretical DMPK and physicochemical parameters were calculated in order to rule out warnings to continue the medicinal chemistry program. DMPK and cytotoxicity assays and a safety panel were carried out for the selected compound 9d. Taking in account the improvement in the cognitive impairment in a 5xFAD model treated with 9d, modulation of I<sub>2</sub>-IR can be proposed as a new therapeutic strategy for AD treatment.

## EXPERIMENTAL SECTION

**Chemistry. General Information.** Reagents, solvents, and starting products were acquired from commercial sources. The term “concentration” refers to vacuum evaporation using a Büchi rotavapor. When indicated, the reaction products were purified by flash chromatography on silica gel (35–70  $\mu$ m) with the indicated solvent system. The melting points were measured in a MFB 59510M Gallenkamp instruments. IR spectra were performed in a spectrophotometer, Nicolet Avantar 320 FTR-IR or Spectrum Two FT-IR, and only noteworthy IR absorptions (cm<sup>-1</sup>) are listed. NMR spectra were recorded in CDCl<sub>3</sub> at 400 MHz (<sup>1</sup>H) and 100.6 MHz (<sup>13</sup>C), and 162

MHz (<sup>31</sup>P). Chemical shifts are reported in  $\delta$  values downfield from TMS or relative to residual chloroform (7.26 ppm, 77.0 ppm) as an internal standard. Data are reported in the following manner: chemical shift, multiplicity, coupling constant ( $J$ ) in hertz (Hz), integrated intensity, and assignment (when possible). Multiplicities are reported using the following abbreviations: s, singlet; d, doublet; dd, doublet of doublets; ddd, double doublet of doublets; dq, double quadruplet; t, triplet; qu, quintet; m, multiplet; br s, broad signal; app, apparent. Assignments and stereochemical determinations are given only when they are derived from definitive two-dimensional NMR experiments (g-HSQC-COSY). The accurate mass analyses were carried out using a LC/MSD-TOF spectrophotometer. The elemental analyses were carried out in a Flash 1112 series Thermofinnigan elemental microanalyzer (A5) to determine C, H, and N. HPLC-MS (Agilent 1260 Infinity II) analysis was conducted on a Poroshell 120 EC-C15 (4.6 mm  $\times$  50 mm, 2.7  $\mu$ m) at 40 °C with mobile phase A (H<sub>2</sub>O + 0.05% formic acid) and B (ACN + 0.05% formic acid) using a gradient elution and flow rate 0.6 mL/min. The DAD detector was set at 254 nm, the injection volume was 5  $\mu$ L, and oven temperature was 40 °C. All tested compounds possess a purity of at least 95%.

**General Procedure for the [3 + 2] Cycloaddition Reaction.** To a solution of silver acetate (0.06–0.1 mmol) and maleimide (1.0–1.5 mmol) in acetonitrile was added diethyl  $\alpha$ -methylisocyanomethylphosphonate, diethyl  $\alpha$ -phenylisocyanomethylphosphonate, diphenyl  $\alpha$ -phenylisocyanomethylphosphonate, diethyl  $\alpha$ -(4-fluorophenyl)-isocyanomethylphosphonate, diethyl  $\alpha$ -(4-methoxyphenyl)-isocyanomethylphosphonate, or diethyl  $\alpha$ -benzylisocyanomethylphosphonate (1.0 mmol). The reaction mixture was stirred at room temperature overnight and concentrated, and the resulting residue was purified by column chromatography to afford pure products.

**Diethyl (1*R*,3*aSR*,6*aSR*)-5-Methyl-4,6-dioxo-1-phenyl-1,3*a*,4,5,6,6*a*-hexahydropyrrolo[3,4-*c*]pyrrole-1-phosphonate (9a).** Following the general procedure, AgOAc (13 mg, 0.08 mmol), *N*-methylmaleimide (133 mg, 1.2 mmol), acetonitrile (6 mL), and diethyl  $\alpha$ -phenylisocyanomethylphosphonate (202 mg, 0.8 mmol)

gave **9a** (184 mg, 64%) as a yellowish oil, after column chromatography (EtOAc/hexane 95:5). IR (NaCl) 3472, 2981, 1709, 1432, 1281, 1248, 1051, 967  $\text{cm}^{-1}$ .  $^1\text{H}$  NMR (400 MHz,  $\text{CDCl}_3$ , HETCOR)  $\delta$  1.15 (t,  $J = 7.0$  Hz, 3H,  $\text{CH}_2\text{CH}_3$ ), 1.27 (t,  $J = 7.0$  Hz, 3H,  $\text{CH}_2\text{CH}_3$ ), 2.70 (s, 3H,  $\text{NCH}_3$ ), 3.83 (m, 1H,  $\text{CH}_2\text{CH}_3$ ), 4.01–4.18 (m, 4H, H-6a and  $\text{CH}_2\text{CH}_3$ ), 4.34 (ddd,  $J = 8.5, 4.0, 1.0$  Hz, 1H, H-3a), 7.29–7.37 (m, 3H, ArH), 7.68–7.70 (m, 2H, ArH), 7.95 (dd,  $J = 5.5, 1.0$  Hz, 1H, H-3).  $^{13}\text{C}$  NMR (100.6 MHz)  $\delta$  16.1 (d,  $J = 5.0$  Hz,  $\text{CH}_2\text{CH}_3$ ), 16.2 (d,  $J = 5.0$  Hz,  $\text{CH}_2\text{CH}_3$ ), 25.0 ( $\text{NCH}_3$ ), 47.7 (d,  $J = 2.0$  Hz, C-6a), 60.5 (C-3a), 63.4 (d,  $J = 7.0$  Hz,  $\text{CH}_2\text{CH}_3$ ), 64.6 (d,  $J = 7.0$  Hz,  $\text{CH}_2\text{CH}_3$ ), 85.6 (d,  $J = 154.0$  Hz, C-1), 127.6 (d,  $J = 2.0$  Hz, 2CHAR), 128.4 (d,  $J = 2.5$  Hz, CHAR), 128.5 (d,  $J = 6.0$  Hz, 2CHAR), 133.2 (d,  $J = 4.5$  Hz, C-*ipso*), 162.5 (d,  $J = 11.5$  Hz, C-3), 172.1 (d,  $J = 5.5$  Hz, CO), 172.5 (d,  $J = 14.0$  Hz, CO). MS-EI  $m/z$  364  $\text{M}^+$  (36), 255 (31), 227 (73), 199 (23), 170 (41), 143 (21), 142 (100), 115 (58). HRMS  $\text{C}_{17}\text{H}_{22}\text{N}_2\text{O}_3\text{P}$  [ $\text{M} + \text{H}$ ] $^+$  365.1262; found, 365.1261. Purity 97.0% ( $t_{\text{R}} = 3.89$  min).

**Diethyl (1*R*,3*aSR*,6*aSR*)-5-Cyclohexyl-4,6-dioxo-1-phenyl-1,3*a*,4,5,6,6*a*-hexahydropyrrolo[3,4-*c*]pyrrole-1-phosphonate (**9b**).** Following the general procedure, AgOAc (15 mg, 0.09 mmol), *N*-cyclohexylmaleimide (403 mg, 2.3 mmol), acetonitrile (12 mL), and diethyl  $\alpha$ -phenylisocyanomethylphosphonate (380 mg, 1.5 mmol) gave **9b** (494 mg, 76%) as a white solid, after column chromatography (EtOAc). Mp 128–132 °C (EtOAc). IR (NaCl) 3467, 2934, 2858, 1705, 1370, 1249, 1191, 1025, 971, 755  $\text{cm}^{-1}$ .  $^1\text{H}$  NMR (400 MHz,  $\text{CDCl}_3$ , HETCOR)  $\delta$  1.06–1.13 (m, 3H,  $\text{CH}_2\text{cycl}$ ), 1.16 (t,  $J = 7.0$  Hz, 3H,  $\text{CH}_2\text{CH}_3$ ), 1.21 (m, 1H,  $\text{CH}_2\text{cycl}$ ), 1.25 (t,  $J = 7.0$  Hz, 3H,  $\text{CH}_2\text{CH}_3$ ), 1.51–1.54 (m, 2H,  $\text{CH}_2\text{cycl}$ ), 1.57–1.69 (m, 3H,  $\text{CH}_2\text{cycl}$ ), 1.85 (m, 1H,  $\text{CH}_2\text{cycl}$ ), 3.60 (m, 1H,  $\text{CH}_2\text{cycl}$ ), 3.90 (m, 1H,  $\text{CH}_2\text{CH}_3$ ), 4.03 (dd,  $J = 18.5, 8.5$  Hz, 1H, H-6a), 4.06–4.18 (m, 3H,  $\text{CH}_2\text{CH}_3$ ), 4.25 (ddd,  $J = 8.5, 3.0, 1.5$  Hz, 1H, H-3a), 7.29–7.35 (m, 3H, ArH), 7.61–7.63 (m, 2H, ArH), 8.00 (dd,  $J = 5.0, 1.5$  Hz, 1H, H-3).  $^{13}\text{C}$  NMR (100.6 MHz)  $\delta$  16.1 (d,  $J = 5.5$  Hz,  $\text{CH}_2\text{CH}_3$ ), 16.2 (d,  $J = 5.5$  Hz,  $\text{CH}_2\text{CH}_3$ ), 24.7 ( $\text{CH}_2\text{cycl}$ ), 25.6 (2 $\text{CH}_2\text{cycl}$ ), 27.8 ( $\text{CH}_2\text{cycl}$ ), 28.6 ( $\text{CH}_2\text{cycl}$ ), 47.5 (d,  $J = 2.5$  Hz, C-6a), 51.9 ( $\text{CH}_2\text{cycl}$ ), 59.9 (C-3a), 63.3 (d,  $J = 7.5$  Hz,  $\text{CH}_2\text{CH}_3$ ), 64.6 (d,  $J = 7.5$  Hz,  $\text{CH}_2\text{CH}_3$ ), 85.7 (d,  $J = 156.0$  Hz, C-1), 127.7 (d,  $J = 1.6$  Hz, 2CHAR), 128.2 (CHAR), 128.3 (CHAR), 128.4 (CHAR), 133.6 (d,  $J = 4.0$  Hz, C-*ipso*), 162.8 (d,  $J = 12.0$  Hz, C-3), 172.1 (d,  $J = 5.5$  Hz, CO), 172.5 (d,  $J = 12.0$  Hz, CO). MS-EI  $m/z$  432  $\text{M}^+$  (60), 323 (30), 295 (95), 223 (12), 170 (78), 142 (100), 115 (35), 81 (15). HRMS  $\text{C}_{22}\text{H}_{30}\text{N}_2\text{O}_3\text{P}$  [ $\text{M} + \text{H}$ ] $^+$  433.1892; found, 433.1887. Anal. Calcd for  $\text{C}_{22}\text{H}_{30}\text{N}_2\text{O}_3\text{P}$ : C, 61.10%; H, 6.76%; N, 6.48%. Found: C, 61.42%; H, 6.81%; N, 6.47%.

**Diethyl (1*R*,3*aSR*,6*aSR*)-4,6-Dioxo-1,5-diphenyl-1,3*a*,4,5,6,6*a*-hexahydropyrrolo[3,4-*c*]pyrrole-1-phosphonate (**9c**).** Following the general procedure, AgOAc (4 mg, 0.02 mmol), *N*-phenylmaleimide (104 mg, 0.6 mmol), acetonitrile (3 mL), and diethyl  $\alpha$ -phenylisocyanomethylphosphonate (101 mg, 0.4 mmol) gave **9c** (108 mg, 64%) as a white solid, after column chromatography (EtOAc). Mp 158–160 °C (EtOAc). IR (NaCl) 3479, 2969, 1713, 1496, 1390, 1239, 1021, 969  $\text{cm}^{-1}$ .  $^1\text{H}$  NMR (400 MHz,  $\text{CDCl}_3$ , HETCOR)  $\delta$  1.10 (t,  $J = 7.0$  Hz, 3H,  $\text{CH}_2\text{CH}_3$ ), 1.19 (t,  $J = 7.0$  Hz, 3H,  $\text{CH}_2\text{CH}_3$ ), 3.85 (m, 1H,  $\text{CH}_2\text{CH}_3$ ), 3.99–4.14 (m, 3H,  $\text{CH}_2\text{CH}_3$ ), 4.17 (dd,  $J = 18.5, 9.0$  Hz, 1H, H-6a), 4.40 (ddd,  $J = 8.5, 3.0, 1.6$  Hz, 1H, H-3a), 6.62–6.65 (m, 2H, ArH), 7.15–7.30 (m, 6H, ArH), 7.61–7.63 (m, 2H, ArH), 7.97 (dd,  $J = 4.5, 1.6$  Hz, 1H, H-3).  $^{13}\text{C}$  NMR (100.6 MHz)  $\delta$  16.2 (d,  $J = 4.0$  Hz,  $\text{CH}_2\text{CH}_3$ ), 16.3 (d,  $J = 4.0$  Hz,  $\text{CH}_2\text{CH}_3$ ), 48.2 (d,  $J = 2.0$  Hz, C-6a), 60.2 (C-3a), 63.4 (d,  $J = 7.0$  Hz,  $\text{CH}_2\text{CH}_3$ ), 64.6 (d,  $J = 7.0$  Hz,  $\text{CH}_2\text{CH}_3$ ), 86.2 (d,  $J = 157.0$  Hz, C-1), 126.0 (2CHAR), 127.9 (CHAR), 128.0 (CHAR), 128.4 (d,  $J = 6.0$  Hz, CHAR), 128.5 (CHAR), 128.6 (CHAR), 128.7 (CHAR), 129.0 (2CHAR), 131.1 (C-*ipso*), 133.5 (d,  $J = 4.0$  Hz, C-*ipso*), 162.5 (d,  $J = 12.0$  Hz, C-3), 170.9 (d,  $J = 5.5$  Hz, CO), 171.6 (d,  $J = 11.5$  Hz, CO). MS-EI  $m/z$  426  $\text{M}^+$  (43), 317 (20), 289 (47), 244 (11), 170 (43), 142 (100), 115 (43), 81 (11). HRMS  $\text{C}_{22}\text{H}_{24}\text{N}_2\text{O}_3\text{P}$  [ $\text{M} + \text{H}$ ] $^+$  427.1418; found, 427.1417. Anal. Calcd for  $\text{C}_{22}\text{H}_{24}\text{N}_2\text{O}_3\text{P}$ : C, 61.97%; H, 5.44%; N, 6.57%. Found: C, 62.18%; H, 5.36%; N, 6.43%.

**Diethyl (1*R*,3*aSR*,6*aSR*)-5-(3-Chloro-4-fluorophenyl)-4,6-dioxo-1-phenyl-1,3*a*,4,5,6,6*a*-hexahydropyrrolo[3,4-*c*]pyrrole-1-phospho-**

**rate (9d).** Following the general procedure, AgOAc (8 mg, 0.05 mmol), *N*-(3-chloro-4-fluorophenyl)maleimide (250 mg, 1.1 mmol), acetonitrile (6 mL), and diethyl  $\alpha$ -phenylisocyanomethylphosphonate (187 mg, 0.7 mmol) gave **9d** (189 mg, 54%) as a white needles, after column chromatography (EtOAc). Mp 185–186 °C (EtOAc). IR (NaCl) 3437, 2956, 1718, 1499, 1256, 1050, 980  $\text{cm}^{-1}$ .  $^1\text{H}$  NMR (400 MHz,  $\text{CDCl}_3$ , HETCOR)  $\delta$  1.20 (t,  $J = 7.0$  Hz, 3H,  $\text{CH}_2\text{CH}_3$ ), 1.28 (t,  $J = 7.0$  Hz, 3H,  $\text{CH}_2\text{CH}_3$ ), 3.95 (m, 1H,  $\text{CH}_2\text{CH}_3$ ), 4.09–4.20 (m, 3H,  $\text{CH}_2\text{CH}_3$ ), 4.25 (dd,  $J = 18.0, 8.0$  Hz, 1H, H-6a), 4.47 (m, 1H, H-3a), 6.63 (ddd,  $J = 9.0, 4.0, 3.0$  Hz, 1H, ArH), 6.72 (dd,  $J = 6.5, 2.5$  Hz, 1H, ArH), 7.05 (t,  $J = 8.5$  Hz, 1H, ArH), 7.35–7.39 (m, 3H, ArH), 7.67 (m,  $J = 5.0$  Hz, 2H, ArH), 8.05 (d,  $J = 4.5$  Hz, 1H, H-3).  $^{13}\text{C}$  NMR (100.6 MHz)  $\delta$  16.3 (t,  $J = 5.5$  Hz, 2 $\text{CH}_2\text{CH}_3$ ), 48.5 (C-6a), 60.1 (C-3a), 63.7 (d,  $J = 7.0$  Hz,  $\text{CH}_2\text{CH}_3$ ), 64.8 (d,  $J = 7.0$  Hz,  $\text{CH}_2\text{CH}_3$ ), 86.2 (d,  $J = 156.0$  Hz, C-1), 116.8 (d,  $J = 22.5$  Hz, CHAR), 121.5 (d,  $J = 19.5$  Hz, C-*ipso*), 126.1 (d,  $J = 8.0$  Hz, CHAR), 127.4 (d,  $J = 4.0$  Hz, C-*ipso*), 128.1 (2CHAR), 128.3 (d,  $J = 5.5$  Hz, 2CHAR), 128.6 (CHAR), 128.8 (CHAR), 133.5 (d,  $J = 3.0$  Hz, C-*ipso*), 157.7 (d,  $J = 251.0$  Hz, C-*ipso*), 162.0 (d,  $J = 12.5$  Hz, C-3), 170.6 (d,  $J = 5.5$  Hz, CO), 171.3 (d,  $J = 11.0$  Hz, CO).  $^{31}\text{P}$  NMR (162 MHz)  $\delta$  19.71. MS-EI  $m/z$  478  $\text{M}^+$  (2), 341 (12), 281 (41), 207 (100), 191 (11), 147 (14), 73 (31). HRMS  $\text{C}_{22}\text{H}_{22}\text{ClF}_2\text{N}_2\text{O}_3\text{P}$  [ $\text{M} + \text{H}$ ] $^+$  479.0935; found, 479.0933. Anal. Calcd for  $\text{C}_{22}\text{H}_{22}\text{ClF}_2\text{N}_2\text{O}_3\text{P}$ : C, 55.18%; H, 4.42%; N, 5.85%. Found: C, 55.28%; H, 4.49%; N, 5.56%.

**Diethyl (1*R*,3*aSR*,6*aSR*)-5-(4-Methoxyphenyl)-4,6-dioxo-1-phenyl-1,3*a*,4,5,6,6*a*-hexahydropyrrolo[3,4-*c*]pyrrole-1-phosphonate (**9e**).** Following the general procedure, AgOAc (4 mg, 0.02 mmol), *N*-(4-methoxyphenyl)maleimide (122 mg, 0.6 mmol), acetonitrile (3 mL), and diethyl  $\alpha$ -phenylisocyanomethylphosphonate (102 mg, 0.4 mmol) gave **9e** (119 mg, 65%) as a white solid, after column chromatography (EtOAc). Mp 167 °C (EtOAc). IR (NaCl) 3477, 2981, 2930, 1715, 1513, 1384, 1251, 1024, 970, 755  $\text{cm}^{-1}$ .  $^1\text{H}$  NMR (400 MHz,  $\text{CDCl}_3$ , HETCOR)  $\delta$  1.18 (t,  $J = 7.0$  Hz, 3H,  $\text{CH}_2\text{CH}_3$ ), 1.28 (t,  $J = 7.0$  Hz, 3H,  $\text{CH}_2\text{CH}_3$ ), 3.73 (s, 3H,  $\text{OCH}_3$ ), 3.92 (m, 1H,  $\text{CH}_2\text{CH}_3$ ), 4.09–4.19 (m, 3H,  $\text{CH}_2\text{CH}_3$ ), 4.25 (dd,  $J = 18.0, 8.5$  Hz, 1H, H-6a), 4.45 (ddd,  $J = 8.5, 3.0, 1.5$  Hz, 1H, H-3a), 6.60–6.64 (m, 2H, ArH), 6.77–6.81 (m, 2H, ArH), 7.30–7.39 (m, 3H, ArH), 7.68–7.70 (m, 2H, ArH), 8.04 (dd,  $J = 5.0, 1.5$  Hz, 1H, H-3).  $^{13}\text{C}$  NMR (100.6 MHz)  $\delta$  16.2 (d,  $J = 3.5$  Hz,  $\text{CH}_2\text{CH}_3$ ), 16.3 (d,  $J = 3.5$  Hz,  $\text{CH}_2\text{CH}_3$ ), 48.1 (d,  $J = 2.0$  Hz, C-6a), 55.4 ( $\text{OCH}_3$ ), 60.1 (C-3a), 63.5 (d,  $J = 7.5$  Hz,  $\text{CH}_2\text{CH}_3$ ), 64.6 (d,  $J = 7.5$  Hz,  $\text{CH}_2\text{CH}_3$ ), 86.2 (d,  $J = 157.5$  Hz, C-1), 114.3 (2CHAR), 123.6 (C-*ipso*), 127.2 (2CHAR), 127.9 (2CHAR), 128.3 (CHAR), 128.4 (CHAR), 128.5 (CHAR), 133.5 (d,  $J = 4.0$  Hz, C-*ipso*), 159.5 (C-*ipso*), 162.4 (d,  $J = 12.0$  Hz, C-3), 171.1 (d,  $J = 5.0$  Hz, CO), 171.8 (d,  $J = 11.5$  Hz, CO). HRMS  $\text{C}_{23}\text{H}_{26}\text{N}_2\text{O}_6\text{P}$  [ $\text{M} + \text{H}$ ] $^+$  457.1519; found, 457.1523. Anal. Calcd for  $\text{C}_{23}\text{H}_{26}\text{N}_2\text{O}_6\text{P}$ : C, 60.52%; H, 5.52%; N, 6.14%. Found: C, 60.71%; H, 5.75%; N, 5.98%.

**Diethyl (1*R*,3*aSR*,6*aSR*)-1-(4-Fluorophenyl)-4,6-dioxo-5-phenyl-1,3*a*,4,5,6,6*a*-hexahydropyrrolo[3,4-*c*]pyrrole-1-phosphonate (**12c**).** Following the general procedure, AgOAc (10 mg, 0.06 mmol), *N*-phenylmaleimide (156 mg, 0.9 mmol), acetonitrile (4 mL), and diethyl  $\alpha$ -(4-fluorophenyl)isocyanomethylphosphonate (164 mg, 0.6 mmol) gave **12c** (159 mg, 60%) as a white solid, after column chromatography (EtOAc/hexane 4:1). Mp 191–193 °C (EtOAc). IR (ATR) 3491, 2991, 2909, 1775, 1718, 1598, 1506, 1377, 1242, 1189, 1016, 982, 742, 598  $\text{cm}^{-1}$ .  $^1\text{H}$  NMR (400 MHz,  $\text{CDCl}_3$ , HETCOR)  $\delta$  1.20 (t,  $J = 7.0$  Hz, 3H,  $\text{CH}_2\text{CH}_3$ ), 1.29 (t,  $J = 7.0$  Hz, 3H,  $\text{CH}_2\text{CH}_3$ ), 3.93 (m, 1H,  $\text{CH}_2\text{CH}_3$ ), 4.08–4.19 (m, 3H,  $\text{CH}_2\text{CH}_3$ ), 4.25 (dd,  $J = 18.0, 8.5$  Hz, 1H, H-6a), 4.49 (dq,  $J = 8.5, 1.5$  Hz, 1H, H-3a), 6.79–6.81 (m, 2H, ArH), 7.03–7.08 (m, 2H, ArH), 7.29–7.35 (m, 3H, ArH), 7.70–7.73 (m, 2H, ArH), 8.04 (dd,  $J = 5.0, 1.5$  Hz, 1H, H-3).  $^{13}\text{C}$  NMR (100.6 MHz)  $\delta$  16.4 (d,  $J = 5.5$  Hz,  $\text{CH}_2\text{CH}_3$ ), 16.5 (d,  $J = 5.0$  Hz,  $\text{CH}_2\text{CH}_3$ ), 48.1 (d,  $J = 3.0$  Hz, C-6a), 60.5 (C-3a), 63.8 (d,  $J = 8.0$  Hz,  $\text{CH}_2\text{CH}_3$ ), 64.9 (d,  $J = 8.0$  Hz,  $\text{CH}_2\text{CH}_3$ ), 85.9 (d,  $J = 156.0$  Hz, C-1), 114.9 (d,  $J = 2.0$  Hz, CHAR), 115.1 (d,  $J = 2.0$  Hz, CHAR), 126.2 (2CHAR), 129.0 (CHAR), 129.3 (2CHAR), 129.4 (dd,  $J = 4.0, 3.5$  Hz, C-*ipso*), 130.6 (d,  $J = 6.0$  Hz, CHAR), 130.7 (d,  $J = 6.0$  Hz, CHAR), 131.1 (C-*ipso*), 162.8 (d,  $J = 12.0$  Hz, C-3), 162.9 (dd,  $J = 246.0, 2.5$  Hz, C-*ipso*), 171.0 (d,  $J = 6.0$  Hz, CO), 171.8 (d,  $J = 12.0$



Hz, CO). HRMS  $C_{22}H_{23}FN_2O_3P$   $[M + H]^+$  445.1323; found, 445.1324. Anal. Calcd for  $C_{22}H_{23}FN_2O_3P$ : C, 59.46%; H, 4.99%; N, 6.30%. Found: C, 59.90%; H, 5.13%; N, 6.20%.

**Diethyl (1*RS*,3*aSR*,6*aSR*)-5-(3-Chloro-4-fluorophenyl)-1-(4-fluorophenyl)-4,6-dioxo-1,3*a*,4,5,6,6*a*-hexahydropyrrolo[3,4-*c*]pyrrole-1-phosphonate (12*d*).** Following the general procedure, AgOAc (7 mg, 0.04 mmol), *N*-(3-chloro-4-fluorophenyl)maleimide (135 mg, 0.6 mmol), acetonitrile (3 mL), and diethyl  $\alpha$ -(4-fluorophenyl)isocyanomethylphosphonate (108 mg, 0.4 mmol) gave **12d** (124 mg, 62%) as a white solid, after column chromatography (EtOAc). Mp 179–181 °C (EtOAc). IR (ATR) 3483, 2962, 2903, 1719, 1504, 1236, 1051, 1012, 978, 739, 593  $cm^{-1}$ .  $^1H$  NMR (400 MHz,  $CDCl_3$ , HETCOR)  $\delta$  1.20 (t,  $J = 7.0$  Hz, 3H,  $CH_2CH_3$ ), 1.28 (t,  $J = 7.0$  Hz, 3H,  $CH_2CH_3$ ), 3.94 (m, 1H,  $CH_2CH_3$ ), 4.08–4.19 (m, 3H,  $CH_2CH_3$ ), 4.25 (dd,  $J = 18.0, 8.5$  Hz, 1H, H-6*a*), 4.49 (ddd,  $J = 8.5, 3.0, 1.5$  Hz, 1H, H-3*a*), 6.71 (m, 1H, ArH), 6.87 (dd,  $J = 6.5, 2.5$  Hz, 1H, ArH), 7.04–7.09 (m, 3H, ArH), 7.68–7.71 (m, 2H, ArH), 8.02 (dd,  $J = 5.0, 1.5$  Hz, 1H, H-3).  $^{13}C$  NMR (100.6 MHz)  $\delta$  16.4 (d,  $J = 5.5$  Hz,  $CH_2CH_3$ ), 16.5 (d,  $J = 5.5$  Hz,  $CH_2CH_3$ ), 48.2 (d,  $J = 3.0$  Hz, C-6*a*), 60.3 (C-3*a*), 63.9 (d,  $J = 7.0$  Hz,  $CH_2CH_3$ ), 64.9 (d,  $J = 8.0$  Hz,  $CH_2CH_3$ ), 86.0 (d,  $J = 156.0$  Hz, C-1), 115.1 (dd,  $J = 21.0, 2.0$  Hz, 2CHAr), 117.1 (d,  $J = 22.0$  Hz, CHAr), 121.8 (d,  $J = 19.0$  Hz, C-*ipso*), 126.1 (CHAr), 127.4 (d,  $J = 3.0$  Hz, C-*ipso*), 128.7 (CHAr), 129.2 (dd,  $J = 4.0, 3.0$  Hz, C-*ipso*), 130.6 (dd,  $J = 7.0, 2.0$  Hz, 2CHAr), 157.9 (d,  $J = 251.0$  Hz, C-*ipso*), 162.4 (d,  $J = 12.0$  Hz, C-3), 163.0 (d,  $J = 249.5$  Hz, C-*ipso*), 170.5 (d,  $J = 5.0$  Hz, CO), 171.5 (d,  $J = 13.0$  Hz, CO). HRMS  $C_{22}H_{21}ClF_2N_2O_3P$   $[M + H]^+$  497.0839; found, 497.0840. Anal. Calcd for  $C_{22}H_{20}ClF_2N_2O_3P$ : C, 53.19%; H, 4.06%; N, 5.64%. Found: C, 53.45%; H, 4.24%; N, 5.46%.

**Diethyl (1*RS*,3*aSR*,6*aSR*)-1-(4-Methoxyphenyl)-4,6-dioxo-5-phenyl-1,3*a*,4,5,6,6*a*-hexahydropyrrolo[3,4-*c*]pyrrole-1-phosphonate (13*c*).** Following the general procedure, AgOAc (8 mg, 0.05 mmol), *N*-phenylmaleimide (138 mg, 0.8 mmol), acetonitrile (4 mL), and diethyl  $\alpha$ -(4-methoxyphenyl)isocyanomethylphosphonate (142 mg, 0.5 mmol) gave **13c** (155 mg, 69%) as a white solid, after column chromatography (EtOAc/hexane 4:1). Mp 184–186 °C (EtOAc). IR (ATR) 3481, 2986, 2914, 1785, 1713, 1607, 1511, 1386, 1247, 1189, 1021, 737, 694, 598  $cm^{-1}$ .  $^1H$  NMR (400 MHz,  $CDCl_3$ , HETCOR)  $\delta$  1.20 (t,  $J = 7.0$  Hz, 3H,  $CH_2CH_3$ ), 1.28 (t,  $J = 7.0$  Hz, 3H,  $CH_2CH_3$ ), 3.79 (s, 3H, OCH<sub>3</sub>), 3.92 (m, 1H,  $CH_2CH_3$ ), 4.08–4.18 (m, 3H,  $CH_2CH_3$ ), 4.23 (dd,  $J = 18.0, 8.5$  Hz, 1H, H-6*a*), 4.46 (ddd,  $J = 8.5, 3.0, 1.5$  Hz, 1H, H-3*a*), 6.76–6.78 (m, 2H, ArH), 6.88 (d,  $J = 9.0$  Hz, 2H, ArH), 7.27–7.32 (m, 3H, ArH), 7.60–7.63 (m, 2H, ArH), 8.02 (dd,  $J = 5.5, 1.5$  Hz, 1H, H-3).  $^{13}C$  NMR (100.6 MHz)  $\delta$  16.4 (d,  $J = 5.0$  Hz,  $CH_2CH_3$ ), 48.3 (d,  $J = 3.0$  Hz, C-6*a*), 55.3 (OCH<sub>3</sub>), 60.3 (C-3*a*), 63.5 (d,  $J = 8.0$  Hz,  $CH_2CH_3$ ), 64.8 (d,  $J = 8.0$  Hz,  $CH_2CH_3$ ), 86.0 (d,  $J = 157.0$  Hz, C-1), 113.4 (d,  $J = 2.0$  Hz, 2CHAr), 125.5 (d,  $J = 4.0$  Hz, C-*ipso*), 126.3 (2CHAr), 128.8 (CHAr), 129.2 (2CHAr), 129.9 (d,  $J = 6.0$  Hz, 2CHAr), 131.2 (C-*ipso*), 159.7 (d,  $J = 2.0$  Hz, C-*ipso*), 162.3 (d,  $J = 12.0$  Hz, C-3), 171.2 (d,  $J = 6.0$  Hz, CO), 171.9 (d,  $J = 12.0$  Hz, CO). HRMS  $C_{23}H_{25}N_2O_6P$   $[M + H]^+$  457.1523; found, 457.1520. Anal. Calcd For  $C_{23}H_{25}N_2O_6P$ : C, 60.52%; H, 5.52%; N, 6.14%. Found: C, 60.85%; H, 5.51%; N, 5.94%.

**Diethyl (1*RS*,3*aSR*,6*aSR*)-5-(3-Chloro-4-fluorophenyl)-1-(4-methoxyphenyl)-4,6-dioxo-1,3*a*,4,5,6,6*a*-hexahydropyrrolo[3,4-*c*]pyrrole-1-phosphonate (13*d*).** Following the general procedure, AgOAc (8 mg, 0.05 mmol), *N*-(3-chloro-4-fluorophenyl)maleimide (181 mg, 0.8 mmol), acetonitrile (4 mL) and diethyl  $\alpha$ -(4-methoxyphenyl)isocyanomethylphosphonate (142 mg, 0.5 mmol) gave **13d** (170 mg, 67%) as a white solid, after column chromatography (EtOAc). Mp 227–228 °C (EtOAc). IR (ATR) 3481, 2986, 2905, 1771, 1718, 1612, 1497, 1386, 1237, 1184, 1026, 968, 752, 656  $cm^{-1}$ .  $^1H$  NMR (400 MHz,  $CDCl_3$ , HETCOR)  $\delta$  1.21 (t,  $J = 7.0$  Hz, 3H,  $CH_2CH_3$ ), 1.28 (t,  $J = 7.0$  Hz, 3H,  $CH_2CH_3$ ), 3.81 (s, 3H, OCH<sub>3</sub>), 3.94 (m, 1H,  $CH_2CH_3$ ), 4.09–4.18 (m, 3H,  $CH_2CH_3$ ), 4.22 (dd,  $J = 18.0, 8.5$  Hz, 1H, H-6*a*), 4.46 (ddd,  $J = 8.5, 3.0, 1.5$  Hz, 1H, H-3*a*), 6.69–6.73 (m, 2H, ArH), 6.89 (d,  $J = 9.0$  Hz, 2H, ArH), 7.07 (m, 1H, ArH), 7.59 (d,  $J = 7.5$  Hz, 2H, ArH), 8.02 (dd,  $J = 5.0, 1.5$  Hz, 1H, H-3).  $^{13}C$  NMR (100.6 MHz)  $\delta$  16.4 (d,  $J = 5.0$  Hz,  $CH_2CH_3$ ), 16.5 (d,  $J = 5.0$  Hz,  $CH_2CH_3$ ), 48.6 (d,  $J = 3.0$  Hz,

C-6*a*), 55.3 (OCH<sub>3</sub>), 60.1 (C-3*a*), 63.7 (d,  $J = 8.0$  Hz,  $CH_2CH_3$ ), 64.8 (d,  $J = 7.0$  Hz,  $CH_2CH_3$ ), 86.0 (d,  $J = 158.0$  Hz, C-1), 113.5 (d,  $J = 1.0$  Hz, 2CHAr), 117.0 (d,  $J = 22.0$  Hz, CHAr), 121.7 (d,  $J = 19.0$  Hz, C-*ipso*), 125.3 (d,  $J = 4.0$  Hz, C-*ipso*), 126.2 (d,  $J = 8.0$  Hz, CHAr), 127.5 (d,  $J = 4.0$  Hz, C-*ipso*), 128.7 (CHAr), 129.8 (d,  $J = 6.0$  Hz, 2CHAr), 157.9 (d,  $J = 250.0$  Hz, C-*ipso*), 159.9 (d,  $J = 2.0$  Hz, C-*ipso*), 161.8 (d,  $J = 13.0$  Hz, C-3), 170.7 (d,  $J = 5.0$  Hz, CO), 171.6 (d,  $J = 11.0$  Hz, CO). HRMS  $C_{23}H_{24}ClFN_2O_6P$   $[M + H]^+$  509.1039; found, 509.1037. Anal. Calcd for  $C_{23}H_{23}ClFN_2O_6P$ : C, 54.29%; H, 4.56%; N, 5.51%. Found: C, 54.66%; H, 4.63%; N, 5.36%.

**Diethyl (1*RS*,3*aSR*,6*aSR*)-1-Benzyl-4,6-dioxo-5-phenyl-1,3*a*,4,5,6,6*a*-hexahydropyrrolo[3,4-*c*]pyrrole-1-phosphonate (14*c*).** Following the general procedure, AgOAc (8 mg, 0.05 mmol), *N*-phenylmaleimide (139 mg, 0.8 mmol), acetonitrile (6 mL), and diethyl  $\alpha$ -benzylisocyanomethylphosphonate (213 mg, 0.8 mmol) gave **14c** (32 mg, 9%) as a yellowish oil, after column chromatography (EtOAc/hexane 1:1). IR (ATR) 3738, 2926, 2843, 1730, 1492, 1385, 1220, 1181, 1059, 1020, 782, 700  $cm^{-1}$ .  $^1H$  NMR (400 MHz,  $CDCl_3$ , HETCOR)  $\delta$  1.29 (t,  $J = 7.0$  Hz, 3H,  $CH_2CH_3$ ), 1.40 (t,  $J = 7.0$  Hz, 3H,  $CH_2CH_3$ ), 3.29 (dd,  $J = 15.0, 12.5$  Hz, 1H,  $CH_2$ -Ar), 3.86 (dd,  $J = 15.0, 9.5$  Hz, 1H,  $CH_2$ -Ar), 3.97 (dd,  $J = 19.0, 9.0$  Hz, 1H, H-6*a*), 4.11–4.26 (m, 4H,  $CH_2CH_3$ ), 4.39 (dq,  $J = 9.0, 1.5$  Hz, 1H, H-3*a*), 6.73–6.75 (m, 2H, ArH), 7.10–7.12 (m, 3H, ArH), 7.21–7.23 (m, 2H, ArH), 7.33–7.36 (m, 3H, ArH), 7.82 (dd,  $J = 5.0, 1.5$  Hz, 1H, H-3).  $^{13}C$  NMR (100.6 MHz)  $\delta$  16.3 (d,  $J = 6.0$  Hz,  $CH_2CH_3$ ), 16.5 (d,  $J = 6.0$  Hz,  $CH_2CH_3$ ), 36.8 (d,  $J = 2.0$  Hz,  $CH_2$ -Ar), 45.9 (d,  $J = 3.0$  Hz, C-6*a*), 59.9 (C-3*a*), 63.4 (d,  $J = 7.0$  Hz,  $CH_2CH_3$ ), 64.0 (d,  $J = 6.0$  Hz,  $CH_2CH_3$ ), 83.7 (d,  $J = 158.0$  Hz, C-1), 126.5 (2CHAr), 126.7 (CHAr), 127.8 (2CHAr), 128.7 (CHAr), 128.8 (2CHAr), 131.0 (C-*ipso*), 131.8 (2CHAr), 134.9 (d,  $J = 12.0$  Hz, C-*ipso*), 161.3 (d,  $J = 13.0$  Hz, C-3), 171.1 (d,  $J = 6.0$  Hz, CO), 173.1 (d,  $J = 8.0$  Hz, CO). HRMS  $C_{23}H_{26}N_2O_5P$   $[M + H]^+$  441.1574; found, 441.1580. Additional column chromatography led to sample for testing. Purity 95.7% ( $t_R = 4.50$  min).

**Diethyl (1*RS*,3*aSR*,6*aSR*)-1-(4-Fluorobenzyl)-4,6-dioxo-5-phenyl-1,3*a*,4,5,6,6*a*-hexahydropyrrolo[3,4-*c*]pyrrole-1-phosphonate (15*c*).** Following the general procedure, AgOAc (12 mg, 0.07 mmol), *N*-phenylmaleimide (121 mg, 0.7 mmol), acetonitrile (5 mL) and diethyl  $\alpha$ -(4-fluorobenzyl)isocyanomethylphosphonate (200 mg, 0.7 mmol) gave **15c** (67 mg, 21%) as an oil, after column chromatography (EtOAc). IR (ATR) 3471, 2924, 2853, 1780, 1711, 1509, 1378, 1221, 1049, 1017, 968, 691  $cm^{-1}$ .  $^1H$  NMR (400 MHz,  $CDCl_3$ , HETCOR)  $\delta$  1.30 (td,  $J = 7.0, 0.5$  Hz, 3H,  $CH_2CH_3$ ), 1.40 (td,  $J = 7.0, 0.5$  Hz, 3H,  $CH_2CH_3$ ), 3.25 (dd,  $J = 14.5, 12.5$  Hz, 1H,  $CH_2$ -Ar), 3.81 (dd,  $J = 14.5, 9.0$  Hz, 1H,  $CH_2$ -Ar), 3.96 (dd,  $J = 19.0, 9.5$  Hz, 1H, H-6*a*), 4.11–4.27 (m, 4H,  $CH_2CH_3$ ), 4.39 (ddd,  $J = 9.5, 3.5, 1.5$  Hz, 1H, H-3*a*), 6.76–6.82 (m, 3H, ArH), 7.14–7.19 (m, 2H, ArH), 7.33–7.47 (m, 4H, ArH), 7.82 (dd,  $J = 5.0, 1.5$  Hz, 1H, H-3).  $^{13}C$  NMR (100.6 MHz)  $\delta$  16.3 (d,  $J = 6.0$  Hz,  $CH_2CH_3$ ), 16.5 (d,  $J = 5.5$  Hz,  $CH_2CH_3$ ), 36.0 (CHAr), 45.9 (d,  $J = 2.5$  Hz, C-6*a*), 59.9 (C-3*a*), 63.4 (d,  $J = 7.5$  Hz,  $CH_2CH_3$ ), 64.4 (d,  $J = 7.0$  Hz,  $CH_2CH_3$ ), 83.7 (d,  $J = 159.5$  Hz, C-1), 114.5 (d,  $J = 2.0$  Hz, 2CHAr), 126.3 (2CHAr), 128.9 (CHAr), 129.0 (2CHAr), 130.5 (d,  $J = 12.5$  Hz, C-*ipso*), 130.9 (C-*ipso*), 133.4 (d,  $J = 8.0$  Hz, 2CHAr), 161.5 (d,  $J = 12.5$  Hz, C-3), 161.8 (d,  $J = 245.5$  Hz, C-*ipso*), 171.0 (d,  $J = 6.0$  Hz, CO), 173.2 (d,  $J = 12.5$  Hz, CO). HRMS  $C_{23}H_{25}FN_2O_5P$   $[M + H]^+$  459.1480; found, 459.1483. Purity 96.4% ( $t_R = 4.56$  min).

**Diethyl (1*RS*,3*aSR*,6*aSR*)-5-Ethyl-4,6-dioxo-1-phenyl-1,3*a*,4,5,6,6*a*-hexahydropyrrolo[3,4-*c*]pyrrole-1-phosphonate (9*f*).** Following the general procedure, AgOAc (11 mg, 0.07 mmol), *N*-ethylmaleimide (213 mg, 1.7 mmol), acetonitrile (8 mL), and diethyl  $\alpha$ -phenylisocyanomethylphosphonate (279 mg, 1.1 mmol) gave **9f** (130 mg, 31%) as a yellowish oil, after column chromatography (EtOAc). IR (ATR) 3476, 2981, 2929, 1780, 1698, 1626, 1396, 1251, 1055, 1026, 968, 766  $cm^{-1}$ .  $^1H$  NMR (400 MHz,  $CDCl_3$ , HETCOR)  $\delta$  0.75 (t,  $J = 7.0$  Hz, 3H,  $NCH_2CH_3$ ), 1.15 (t,  $J = 7.0$  Hz, 3H,  $CH_2CH_3$ ), 1.25 (t,  $J = 7.0$  Hz, 3H,  $CH_2CH_3$ ), 3.21–3.27 (m, 2H,  $NCH_2CH_3$ ), 3.88 (m, 1H,  $CH_2CH_3$ ), 4.06–4.15 (m, 4H,  $CH_2CH_3$  and H-6*a*), 4.29 (ddd,  $J = 8.5, 3.5, 1.5$  Hz, 1H, H-3*a*), 7.31–7.34 (m, 3H, ArH), 7.65 (dbr,  $J = 11.6$  Hz, 2H, ArH), 7.96 (dd,  $J = 5.0, 1.5$  Hz,

1H, H-3).  $^{13}\text{C}$  NMR (100.6 MHz)  $\delta$  12.6 (NCH<sub>2</sub>CH<sub>3</sub>), 16.4 (d,  $J$  = 5.5 Hz, CH<sub>2</sub>CH<sub>3</sub>), 16.4 (d,  $J$  = 5.5 Hz, CH<sub>2</sub>CH<sub>3</sub>), 34.0 (NCH<sub>2</sub>CH<sub>3</sub>), 47.9 (d,  $J$  = 2.0 Hz, C-6a), 60.5 (C-3a), 63.6 (d,  $J$  = 8.0 Hz, CH<sub>2</sub>CH<sub>3</sub>), 64.8 (d,  $J$  = 8.0 Hz, CH<sub>2</sub>CH<sub>3</sub>), 85.8 (d,  $J$  = 155.0 Hz, C-1), 127.9 (d,  $J$  = 1.0 Hz, 2CHAR), 128.6 (d,  $J$  = 2.0 Hz, 2CHAR), 128.6 (CHAR), 133.6 (d,  $J$  = 4.0 Hz, C-*ipso*), 162.7 (d,  $J$  = 12.0 Hz, C-3), 171.0 (d,  $J$  = 6.0 Hz, CO), 172.5 (d,  $J$  = 12.0 Hz, CO). HRMS C<sub>18</sub>H<sub>24</sub>N<sub>2</sub>O<sub>5</sub>P [M + H]<sup>+</sup> 379.1417; found, 379.1418. Additional column chromatography led to sample for testing. Purity 95.5% ( $t_{\text{R}}$  = 4.06 min).

**Diethyl (1*RS*,3*aSR*,6*aSR*)-4,6-Dioxo-1-phenyl-5-propyl-1,3*a*,4,5,6,6*a*-hexahydropyrrolo[3,4-*c*]pyrrole-1-phosphonate (9g).** Following the general procedure, AgOAc (8 mg, 0.05 mmol), *N*-propylmaleimide (200 mg, 1.4 mmol), acetonitrile (7 mL), and diethyl  $\alpha$ -phenylisocyanomethylphosphonate (228 mg, 0.9 mmol) gave **9g** (314 mg, 89%) as a yellowish oil, after column chromatography (EtOAc/hexane 1:1 to 3:2). IR (ATR) 3464, 2976, 2928, 1719, 1631, 1451, 1402, 1202, 1056, 1027, 963, 705, 583 cm<sup>-1</sup>.  $^1\text{H}$  NMR (400 MHz, CDCl<sub>3</sub>, HETCOR)  $\delta$  0.59 (t,  $J$  = 7.0 Hz, 3H, CH<sub>2</sub>CH<sub>2</sub>CH<sub>3</sub>), 1.13–1.19 (m, 2H, CH<sub>2</sub>CH<sub>2</sub>CH<sub>3</sub>), 1.14 (t,  $J$  = 7.0 Hz, 3H, CH<sub>2</sub>CH<sub>3</sub>), 1.25 (t,  $J$  = 7.0 Hz, 3H, CH<sub>2</sub>CH<sub>3</sub>), 3.16 (m, 2H, CH<sub>2</sub>CH<sub>2</sub>CH<sub>3</sub>), 3.85 (m, 1H, CH<sub>2</sub>CH<sub>3</sub>), 4.02–4.14 (m, 4H, CH<sub>2</sub>CH<sub>3</sub> and H-6a), 4.30 (ddd,  $J$  = 8.5, 3.5, 1.5 Hz, 1H, H-3a), 7.29–7.34 (m, 3H, ArH), 7.65 (br d,  $J$  = 8.0 Hz, 2H, ArH), 7.95 (dd,  $J$  = 5.0, 1.5 Hz, 1H, H-3).  $^{13}\text{C}$  NMR (100.6 MHz)  $\delta$  11.0 (CH<sub>2</sub>CH<sub>2</sub>CH<sub>3</sub>), 16.3 (d,  $J$  = 4.0 Hz, CH<sub>2</sub>CH<sub>3</sub>), 16.4 (d,  $J$  = 6.0 Hz, CH<sub>2</sub>CH<sub>3</sub>), 20.7 (CH<sub>2</sub>CH<sub>2</sub>CH<sub>3</sub>), 40.6 (CH<sub>2</sub>CH<sub>2</sub>CH<sub>3</sub>), 47.8 (d,  $J$  = 3.0 Hz, C-6a), 60.5 (C-3a), 63.5 (d,  $J$  = 7.0 Hz, CH<sub>2</sub>CH<sub>3</sub>), 64.7 (d,  $J$  = 7.0 Hz, CH<sub>2</sub>CH<sub>3</sub>), 85.9 (d,  $J$  = 154.0 Hz, C-1), 127.8 (d,  $J$  = 2.0 Hz, 2CHAR), 128.5 (d,  $J$  = 3.0 Hz, CHAR), 128.6 (d,  $J$  = 6.0 Hz, 2CHAR), 133.5 (d,  $J$  = 4.0 Hz, C-*ipso*), 162.8 (d,  $J$  = 12.0 Hz, C-3), 172.2 (d,  $J$  = 6.0 Hz, CO), 172.7 (d,  $J$  = 12.0 Hz, CO). HRMS C<sub>19</sub>H<sub>26</sub>N<sub>2</sub>O<sub>5</sub>P [M + H]<sup>+</sup> 393.1574; found, 393.1572. Additional column chromatography led to sample for testing. Purity 95.6% ( $t_{\text{R}}$  = 4.24 min).

**Diethyl (1*RS*,3*aSR*,6*aSR*)-5-(*tert*-Butyl)-4,6-dioxo-1-phenyl-1,3*a*,4,5,6,6*a*-hexahydropyrrolo[3,4-*c*]pyrrole-1-phosphonate (9h).** Following the general procedure, AgOAc (9 mg, 0.05 mmol), *N*-*tert*-butylmaleimide (215 mg, 1.4 mmol), acetonitrile (7 mL), and diethyl  $\alpha$ -phenylisocyanomethylphosphonate (229 mg, 0.9 mmol) gave **9h** (202 mg, 55%) as a yellowish oil, after column chromatography (EtOAc). IR (ATR) 3454, 2981, 2923, 1777, 1709, 1348, 1265, 1241, 1173, 1061, 973, 744, 710, 588 cm<sup>-1</sup>.  $^1\text{H}$  NMR (400 MHz, CDCl<sub>3</sub>, HETCOR)  $\delta$  1.13 [s, 9H, C(CH<sub>3</sub>)<sub>3</sub>], 1.17 (t,  $J$  = 7.0 Hz, 3H, CH<sub>2</sub>CH<sub>3</sub>), 1.24 (t,  $J$  = 7.0 Hz, 3H, CH<sub>2</sub>CH<sub>3</sub>), 3.88–3.95 (m, 2H, CH<sub>2</sub>CH<sub>3</sub> and H-6a), 4.07–4.15 (m, 4H, CH<sub>2</sub>CH<sub>3</sub> and H-3a), 7.28–7.33 (m, 3H, ArH), 7.59 (dbr,  $J$  = 8.0 Hz, 2H, ArH), 7.93 (dd,  $J$  = 5.0, 1.5 Hz, 1H, H-3).  $^{13}\text{C}$  NMR (100.6 MHz)  $\delta$  16.4 (d,  $J$  = 6.0 Hz, CH<sub>2</sub>CH<sub>3</sub>), 16.4 (d,  $J$  = 6.0 Hz, CH<sub>2</sub>CH<sub>3</sub>), 27.7 (C(CH<sub>3</sub>)<sub>3</sub>), 48.1 (d,  $J$  = 2.0 Hz, C-6a), 58.6 [C(CH<sub>3</sub>)<sub>3</sub>], 60.2 (C-3a), 63.5 (d,  $J$  = 8.0 Hz, CH<sub>2</sub>CH<sub>3</sub>), 64.6 (d,  $J$  = 8.0 Hz, CH<sub>2</sub>CH<sub>3</sub>), 86.6 (d,  $J$  = 158.0 Hz, C-1), 127.9 (d,  $J$  = 2.0 Hz, 2CHAR), 128.4 (d,  $J$  = 2.0 Hz, CHAR), 128.5 (d,  $J$  = 6.0 Hz, 2CHAR), 134.1 (d,  $J$  = 4.0 Hz, C-*ipso*), 163.3 (d,  $J$  = 12.0 Hz, C-3), 172.6 (d,  $J$  = 5.0 Hz, CO), 173.6 (d,  $J$  = 10.0 Hz, CO). HRMS C<sub>20</sub>H<sub>28</sub>N<sub>2</sub>O<sub>5</sub>P [M + H]<sup>+</sup> 407.1730; found, 407.1733. Additional column chromatography led to sample for testing. Purity 98.3% ( $t_{\text{R}}$  = 4.46 min).

**Diethyl (1*RS*,3*aSR*,6*aSR*)-5-(Adamantan-1-yl)methyl)-4,6-dioxo-1-phenyl-1,3*a*,4,5,6,6*a*-hexahydropyrrolo[3,4-*c*]pyrrole-1-phosphonate (9i).** Following the general procedure, AgOAc (12 mg, 0.07 mmol), *N*-(adamantan-1-methylphenyl)maleimide (270 mg, 1.1 mmol), acetonitrile (5 mL), and diethyl  $\alpha$ -phenylisocyanomethylphosphonate (177 mg, 0.7 mmol) gave **9i** (220 mg, 63%) as a white solid, after column chromatography (EtOAc/hexane 7:3). Mp 107–108 °C (EtOAc). IR (ATR) 3469, 2908, 2850, 1714, 1446, 1392, 1226, 1158, 1012, 978, 758, 700, 573 cm<sup>-1</sup>.  $^1\text{H}$  NMR (400 MHz, CDCl<sub>3</sub>, HETCOR)  $\delta$  0.95 (dd,  $J$  = 52.0, 12.0 Hz, 6H, 3CH<sub>2</sub>), 1.12 (t,  $J$  = 7.0 Hz, 3H, CH<sub>2</sub>CH<sub>3</sub>), 1.25 (t,  $J$  = 7.0 Hz, 3H, CH<sub>2</sub>CH<sub>3</sub>), 1.47 (dd,  $J$  = 53.0, 12.0 Hz, 6H, 3CH<sub>2</sub>), 1.72 (s, 3H, 3CH), 2.95 (s, 2H, NCH<sub>2</sub>), 3.81 (m, 1H, CH<sub>2</sub>CH<sub>3</sub>), 3.99–3.15 (m, 3H, CH<sub>2</sub>CH<sub>3</sub>), 4.11 (dd,  $J$  = 19.0, 8.5 Hz, 1H, H-6a), 4.29 (ddd,  $J$  = 8.5, 3.0, 1.0 Hz, 1H, H-3a), 7.25–7.33 (m, 3H, ArH), 7.72 (d,  $J$  = 7.0 Hz, 2H, ArH), 7.95

(dd,  $J$  = 5.0, 1.0 Hz, 1H, H-3).  $^{13}\text{C}$  NMR (100.6 MHz)  $\delta$  16.3 (d,  $J$  = 5.5 Hz, CH<sub>2</sub>CH<sub>3</sub>), 16.4 (d,  $J$  = 6.0 Hz, CH<sub>2</sub>CH<sub>3</sub>), 28.1 (3CH), 34.9 (C), 36.5 (3CH<sub>2</sub>), 40.0 (3CH<sub>2</sub>), 47.7 (d,  $J$  = 2.0 Hz, C-6a), 50.2 (NCH<sub>2</sub>), 60.6 (C-3a), 63.6 (d,  $J$  = 7.5 Hz, CH<sub>2</sub>CH<sub>3</sub>), 64.7 (d,  $J$  = 7.5 Hz, CH<sub>2</sub>CH<sub>3</sub>), 86.0 (d,  $J$  = 155.0 Hz, C-1), 127.8 (d,  $J$  = 2.0 Hz, 2CHAR), 128.5 (d,  $J$  = 3.0 Hz, CHAR), 129.0 (d,  $J$  = 4.5 Hz, 2CHAR), 133.5 (d,  $J$  = 5.0 Hz, C-*ipso*), 162.6 (d,  $J$  = 12.0 Hz, C-3), 172.7 (d,  $J$  = 5.0 Hz, CO), 173.2 (d,  $J$  = 13.0 Hz, CO); HRMS C<sub>27</sub>H<sub>36</sub>N<sub>2</sub>O<sub>5</sub>P [M + H]<sup>+</sup> 499.2356; found, 499.2359. Purity 97.8% ( $t_{\text{R}}$  = 5.27 min).

**Diethyl (1*RS*,3*aSR*,6*aSR*)-5-Benzyl-4,6-dioxo-1-phenyl-1,3*a*,4,5,6,6*a*-hexahydropyrrolo[3,4-*c*]pyrrole-1-phosphonate (9j).** Following the general procedure, AgOAc (4 mg, 0.02 mmol), *N*-benzylmaleimide (112 mg, 0.6 mmol), acetonitrile (3 mL), and diethyl  $\alpha$ -phenylisocyanomethylphosphonate (101 mg, 0.4 mmol) gave **9j** (139 mg, 79%) as a yellowish oil, after column chromatography (EtOAc/hexane 9:1). IR (NaCl) 3472, 3068, 2984, 1778, 1698, 1632, 1495, 1249, 1172, 1021, 750, 615 cm<sup>-1</sup>.  $^1\text{H}$  NMR (400 MHz, CDCl<sub>3</sub>, HETCOR)  $\delta$  1.14 (t,  $J$  = 7.0 Hz, 3H, CH<sub>2</sub>CH<sub>3</sub>), 1.25 (t,  $J$  = 7.0 Hz, 3H, CH<sub>2</sub>CH<sub>3</sub>), 3.86 (m, 1H, CH<sub>2</sub>CH<sub>3</sub>), 4.00–4.18 (m, 4H, CH<sub>2</sub>CH<sub>3</sub> and H-6a), 4.33 (ddd,  $J$  = 8.5, 3.5, 1.5 Hz, 1H, H-3a), 4.36 (dd,  $J$  = 53.5, 14.5 Hz, 2H, CH<sub>2</sub>Ar), 6.94–6.96 (m, 2H, ArH), 7.14–7.22 (m, 3H, ArH), 7.23–7.30 (m, 3H, ArH), 7.61–7.63 (m, 2H, ArH), 7.92 (dd,  $J$  = 5.0, 1.5 Hz, 1H, H-3).  $^{13}\text{C}$  NMR (100.6 MHz)  $\delta$  16.1 (d,  $J$  = 5.0 Hz, CH<sub>2</sub>CH<sub>3</sub>), 16.2 (d,  $J$  = 5.0 Hz, CH<sub>2</sub>CH<sub>3</sub>), 42.4 (CH<sub>2</sub>Ar), 47.8 (d,  $J$  = 2.0 Hz, C-6a), 60.4 (C-3a), 63.4 (d,  $J$  = 7.5 Hz, CH<sub>2</sub>CH<sub>3</sub>), 64.6 (d,  $J$  = 7.5 Hz, CH<sub>2</sub>CH<sub>3</sub>), 85.7 (d,  $J$  = 155.0 Hz, C-1), 127.7 (d,  $J$  = 1.0 Hz, 2CHAR), 127.8 (CHAR), 128.3 (br s, 4CHAR), 128.4 (CHAR), 128.5 (2CHAR), 133.2 (d,  $J$  = 4.0 Hz, C-*ipso*), 135.0 (C-*ipso*), 162.3 (d,  $J$  = 11.5 Hz, C-3), 171.6 (d,  $J$  = 5.5 Hz, CO), 172.2 (d,  $J$  = 13.5 Hz, CO). HRMS C<sub>23</sub>H<sub>25</sub>N<sub>2</sub>O<sub>5</sub>P [M + H]<sup>+</sup> 441.1574; found, 441.1579. Additional column chromatography led to sample for testing. Purity 95.4% ( $t_{\text{R}}$  = 4.43 min).

**Diethyl (1*RS*,3*aSR*,6*aSR*)-4,6-Dioxo-5-phenethyl-1-phenyl-1,3*a*,4,5,6,6*a*-hexahydropyrrolo[3,4-*c*]pyrrole-1-phosphonate (9k).** Following the general procedure, AgOAc (7 mg, 0.04 mmol), *N*-phenethylmaleimide (200 mg, 1.0 mmol), acetonitrile (5 mL), and diethyl  $\alpha$ -phenylisocyanomethylphosphonate (170 mg, 0.7 mmol) gave **9k** (110 mg, 36%) as an oil, after column chromatography (EtOAc/hexane 1:1). IR (NaCl) 3468, 3027, 2981, 1709, 1627, 1394, 1250, 1162, 1052, 1025, 968, 792, 750 cm<sup>-1</sup>.  $^1\text{H}$  NMR (400 MHz, CDCl<sub>3</sub>, HETCOR)  $\delta$  1.14 (t,  $J$  = 7.0 Hz, 3H, CH<sub>2</sub>CH<sub>3</sub>), 1.25 (t,  $J$  = 7.0 Hz, 3H, CH<sub>2</sub>CH<sub>3</sub>), 2.40–2.53 (m, 2H, CH<sub>2</sub>), 3.46 (t,  $J$  = 7.5 Hz, 2H, CH<sub>2</sub>), 3.83 (m, 1H, CH<sub>2</sub>CH<sub>3</sub>), 3.99–4.16 (m, 4H, CH<sub>2</sub>CH<sub>3</sub> and H-6a), 4.24 (ddd,  $J$  = 8.5, 4.0, 1.0 Hz, 1H, H-3a), 6.97–6.99 (m, 2H, ArH), 7.16–7.25 (m, 3H, ArH), 7.30–7.38 (m, 3H, ArH), 7.68–7.70 (m, 2H, ArH), 7.85 (dd,  $J$  = 5.0, 1.0 Hz, 1H, H-3).  $^{13}\text{C}$  NMR (100.6 MHz)  $\delta$  16.1 (d,  $J$  = 4.0 Hz, CH<sub>2</sub>CH<sub>3</sub>), 16.2 (d,  $J$  = 4.5 Hz, CH<sub>2</sub>CH<sub>3</sub>), 33.0 (CH<sub>2</sub>), 39.9 (CH<sub>2</sub>), 47.5 (d,  $J$  = 2.5 Hz, C-6a), 60.2 (C-3a), 63.4 (d,  $J$  = 7.5 Hz, CH<sub>2</sub>CH<sub>3</sub>), 64.6 (d,  $J$  = 7.5 Hz, CH<sub>2</sub>CH<sub>3</sub>), 126.6 (CHAR), 127.6 (CHAR), 127.7 (CHAR), 128.4 (d,  $J$  = 2.5 Hz, CHAR), 128.5 (2CHAR), 128.6 (CHAR), 128.7 (CHAR), 128.8 (2CHAR), 133.2 (d,  $J$  = 4.5 Hz, C-*ipso*), 137.1 (C-*ipso*), 162.6 (d,  $J$  = 11.5 Hz, C-3), 171.6 (d,  $J$  = 5.5 Hz, CO), 172.3 (d,  $J$  = 13.5 Hz, CO). HRMS C<sub>24</sub>H<sub>28</sub>N<sub>2</sub>O<sub>5</sub>P [M + H]<sup>+</sup> 455.1730; found, 455.1731. Additional column chromatography led to sample for testing. Purity 98.0% ( $t_{\text{R}}$  = 4.54 min).

**Diethyl (1*RS*,3*aSR*,6*aSR*)-5-(4-Fluorophenethyl)-4,6-dioxo-1-phenyl-1,3*a*,4,5,6,6*a*-hexahydropyrrolo[3,4-*c*]pyrrole-1-phosphonate (9l).** Following the general procedure, AgOAc (8 mg, 0.05 mmol), *N*-(4-fluorophenethyl)maleimide (263 mg, 1.2 mmol), acetonitrile (6 mL), and diethyl  $\alpha$ -phenylisocyanomethylphosphonate (202 mg, 0.8 mmol) gave **9l** (201 mg, 53%) as a white solid, after column chromatography (EtOAc). Mp 94–95 °C (EtOAc). IR (NaCl) 3466, 3050, 2976, 1779, 1702, 1632, 1507, 1257, 1153, 1013, 763, 583 cm<sup>-1</sup>.  $^1\text{H}$  NMR (400 MHz, CDCl<sub>3</sub>, HETCOR)  $\delta$  1.23 (t,  $J$  = 7.0 Hz, 3H, CH<sub>2</sub>CH<sub>3</sub>), 1.25 (t,  $J$  = 7.0 Hz, 3H, CH<sub>2</sub>CH<sub>3</sub>), 2.40–2.52 (m, 2H, CH<sub>2</sub>), 3.41–3.46 (m, 2H, CH<sub>2</sub>), 3.80 (m, 1H, CH<sub>2</sub>CH<sub>3</sub>), 3.97–4.15 (m, 4H, CH<sub>2</sub>CH<sub>3</sub> and H-6a), 4.24 (ddd,  $J$  = 8.0, 4.0, 1.5 Hz, 1H, H-3a), 6.86–6.92 (m, 4H, ArH), 7.31–7.37 (m, 3H, ArH), 7.67 (m, 2H, ArH), 7.83 (dd,  $J$  = 5.5, 1.5 Hz, 1H, H-3).  $^{13}\text{C}$  NMR (100.6 MHz)  $\delta$

16.1 (d,  $J = 5.0$  Hz,  $\text{CH}_2\text{CH}_3$ ), 16.2 (d,  $J = 5.0$  Hz,  $\text{CH}_2\text{CH}_3$ ), 32.1 ( $\text{CH}_2$ ), 39.9 ( $\text{CH}_2$ ), 47.5 (d,  $J = 2.0$  Hz, C-6a), 60.3 (C-3a), 63.4 (d,  $J = 7.0$  Hz,  $\text{CH}_2\text{CH}_3$ ), 64.6 (d,  $J = 7.0$  Hz,  $\text{CH}_2\text{CH}_3$ ), 85.7 (d,  $J = 15.0$  Hz, C-1), 115.3 (d,  $J = 2.0$  Hz, 2CHAr), 127.6 (d,  $J = 2.0$  Hz, 2CHAr), 128.4 (d,  $J = 3.0$  Hz, CHAr), 128.6 (d,  $J = 6.0$  Hz, 2CHAr), 130.1 (d,  $J = 8.0$  Hz, 2CHAr), 132.7 (d,  $J = 3.0$  Hz, C-*ipso*), 133.1 (d,  $J = 5.0$  Hz, C-*ipso*), 160.4 (d,  $J = 244.5$  Hz, C-*ipso*), 162.5 (d,  $J = 12.0$  Hz, C-3), 171.6 (d,  $J = 6.0$  Hz, CO), 172.3 (d,  $J = 14.0$  Hz, CO). HRMS  $\text{C}_{24}\text{H}_{27}\text{FN}_2\text{O}_5\text{P}$  [ $\text{M} + \text{H}$ ] $^+$  473.1636; found, 473.1640. Anal. Calcd for  $\text{C}_{24}\text{H}_{26}\text{FN}_2\text{O}_5\text{P}$ : C, 61.01%; H, 5.55%; N, 5.93%. Found: C, 61.14%; H, 5.74%; N, 5.83%.

**Diethyl (1*RS*,3*aSR*,6*aSR*)-5-(2,3-Dihydro-1*H*-inden-2-yl)-4,6-dioxo-1-phenyl-1,3*a*,4,5,6,6*a*-hexahydropyrrolo[3,4-*c*]pyrrole-1-phosphonate (9*m*).** Following the general procedure, AgOAc (7 mg, 0.04 mmol), *N*-(2,3-dihydro-1*H*-inden-2-yl)maleimide (126 mg, 0.6 mmol), acetonitrile (3 mL), and diethyl  $\alpha$ -phenylisocyanomethylphosphonate (100 mg, 0.4 mmol) gave **9m** (158 mg, 85%) as a beige solid, after column chromatography (EtOAc). Mp 124–126 °C (EtOAc). IR (ATR) 3457, 2986, 2943, 2866, 1766, 1698, 1623, 1377, 1252, 1170, 1055, 1021, 790, 704, 574  $\text{cm}^{-1}$ .  $^1\text{H}$  NMR (400 MHz,  $\text{CDCl}_3$ , HETCOR)  $\delta$  1.18 (t,  $J = 7.0$  Hz, 3H,  $\text{CH}_2\text{CH}_3$ ), 1.26 (t,  $J = 7.0$  Hz, 3H,  $\text{CH}_2\text{CH}_3$ ), 2.69 (dd,  $J = 15.0, 9.0$  Hz, 1H, CH<sub>2</sub>), 2.75 (dd,  $J = 15.0, 9.0$  Hz, 1H, CH<sub>2</sub>), 2.77 (dd,  $J = 15.0, 9.0$  Hz, 1H, CH<sub>2</sub>), 3.23 (dd,  $J = 15.0, 9.0$  Hz, 1H, CH<sub>2</sub>), 3.92 (m, 1H,  $\text{CH}_2\text{CH}_3$ ), 4.08–4.17 (m, 4H,  $\text{CH}_2\text{CH}_3$  and H-6a), 4.31 (ddd,  $J = 9.0, 3.0, 1.5$  Hz, 1H, H-3a), 4.62 (qu,  $J = 9.2$  Hz, 1H, CH), 7.09 (m, 1H, ArH), 7.07–7.11 (m, 3H, ArH), 7.32–7.37 (m, 3H, ArH), 7.64 (br d,  $J = 7.5$  Hz, 2H, ArH), 8.00 (dd,  $J = 5.0, 1.5$  Hz, 1H, H-3).  $^{13}\text{C}$  NMR (100.6 MHz)  $\delta$  16.4 (d,  $J = 2.0$  Hz,  $\text{CH}_2\text{CH}_3$ ), 16.5 (d,  $J = 3.0$  Hz,  $\text{CH}_2\text{CH}_3$ ), 34.6 ( $\text{CH}_2$ ), 35.1 ( $\text{CH}_2$ ), 48.0 (d,  $J = 2.0$  Hz, C-6a), 50.8 (CH), 60.2 (C-3a), 63.6 (d,  $J = 7.0$  Hz,  $\text{CH}_2\text{CH}_3$ ), 64.7 (d,  $J = 8.0$  Hz,  $\text{CH}_2\text{CH}_3$ ), 86.1 (d,  $J = 157.0$  Hz, C-1), 124.4 (d,  $J = 2.0$  Hz, 2CHAr), 126.8 (d,  $J = 2.0$  Hz, 2CHAr), 128.0 (d,  $J = 1.0$  Hz, 2CHAr), 128.5 (d,  $J = 8.0$  Hz, 2CHAr), 128.6 (CHAr), 133.7 (C-*ipso*), 133.8 (C-*ipso*), 140.5 (d,  $J = 9.0$  Hz, C-*ipso*), 162.7 (d,  $J = 12.0$  Hz, C-3), 172.1 (d,  $J = 5.0$  Hz, CO), 172.7 (d,  $J = 12.0$  Hz, CO). HRMS  $\text{C}_{25}\text{H}_{28}\text{N}_2\text{O}_5\text{P}$  [ $\text{M} + \text{H}$ ] $^+$  467.1730; found, 467.1728. Anal. Calcd for  $\text{C}_{25}\text{H}_{27}\text{N}_2\text{O}_5\text{P}$ : C, 64.37%; H, 5.83%; N, 6.01%. Found: C, 64.55%; H, 6.11%; N, 5.76%.

**Diethyl (1*RS*,3*aSR*,6*aSR*)-4,6-Dioxo-1-phenyl-5-[4-(trifluoromethyl)phenyl]-1,3*a*,4,5,6,6*a*-hexahydropyrrolo[3,4-*c*]pyrrole-1-phosphonate (9*n*).** Following the general procedure, AgOAc (4 mg, 0.03 mmol), *N*-(4-trifluoromethylphenyl)maleimide (144 mg, 0.6 mmol), acetonitrile (3 mL), and diethyl  $\alpha$ -phenylisocyanomethylphosphonate (101 mg, 0.4 mmol) gave **9n** (133 mg, 67%) as a white solid, after column chromatography (EtOAc). Mp 184–185 °C (EtOAc). IR (NaCl) 3492, 3050, 2984, 1723, 1616, 1378, 1326, 1249, 1170, 1067, 758, 580  $\text{cm}^{-1}$ .  $^1\text{H}$  NMR (400 MHz,  $\text{CDCl}_3$ , HETCOR)  $\delta$  1.19 (t,  $J = 7.0$  Hz, 3H,  $\text{CH}_2\text{CH}_3$ ), 1.28 (t,  $J = 7.0$  Hz, 3H,  $\text{CH}_2\text{CH}_3$ ), 3.95 (m, 1H,  $\text{CH}_2\text{CH}_3$ ), 4.10–4.20 (m, 3H,  $\text{CH}_2\text{CH}_3$ ), 4.28 (dd,  $J = 18.0, 9.0$  Hz, H-6a), 4.51 (ddd,  $J = 8.5, 3.0, 1.5$  Hz, 1H, H-3a), 6.85–6.87 (m, 2H, ArH), 7.34–7.38 (m, 3H, ArH), 7.54–7.56 (m, 2H, ArH), 7.67–7.69 (m, 2H, ArH), 8.05 (dd,  $J = 5.0, 1.5$  Hz, 1H, H-3).  $^{13}\text{C}$  NMR (100.6 MHz)  $\delta$  16.2 (d,  $J = 5.0$  Hz,  $\text{CH}_2\text{CH}_3$ ), 16.3 (d,  $J = 5.0$  Hz,  $\text{CH}_2\text{CH}_3$ ), 48.3 (d,  $J = 3.0$  Hz, C-6a), 60.1 (C-3a), 63.6 (d,  $J = 7.0$  Hz,  $\text{CH}_2\text{CH}_3$ ), 64.7 (d,  $J = 7.0$  Hz,  $\text{CH}_2\text{CH}_3$ ), 86.3 (d,  $J = 157.0$  Hz, C-1), 123.5 (q,  $J = 272.5$  Hz,  $\text{CF}_3$ ), 126.0 (q,  $J = 4.0$  Hz, 2CHAr), 126.3 (2CHAr), 128.0 (d,  $J = 1.0$  Hz, 2CHAr), 128.4 (d,  $J = 6.0$  Hz, 2CHAr), 128.7 (d,  $J = 2.0$  Hz, CHAr), 137.5 (q,  $J = 33.0$  Hz,  $\text{CCF}_3$ ), 133.4 (d,  $J = 4.0$  Hz, C-*ipso*), 134.1 (d,  $J = 1.5$  Hz, C-*ipso*), 162.0 (d,  $J = 13.0$  Hz, C-3), 170.4 (d,  $J = 5.0$  Hz, CO), 171.2 (d,  $J = 12.0$  Hz, CO). HRMS  $\text{C}_{23}\text{H}_{23}\text{F}_3\text{N}_2\text{O}_5\text{P}$  [ $\text{M} + \text{H}$ ] $^+$  495.1291; found, 495.1288. Anal. Calcd for  $\text{C}_{23}\text{H}_{22}\text{F}_3\text{N}_2\text{O}_5\text{P}$ : C, 55.88%; H, 4.49%; N, 5.67%. Found: C, 56.04%; H, 4.71%; N, 5.56%.

**Diethyl (1*RS*,3*aSR*,6*aSR*)-4,6-Dioxo-1-phenyl-5-[3-(trifluoromethyl)phenyl]-1,3*a*,4,5,6,6*a*-hexahydropyrrolo[3,4-*c*]pyrrole-1-phosphonate (9*o*).** Following the general procedure, AgOAc (10 mg, 0.06 mmol), *N*-(3-trifluoromethylphenyl)maleimide (362 mg, 1.5 mmol), acetonitrile (8 mL), and diethyl  $\alpha$ -phenylisocyanomethylphosphonate (253 mg, 1.0 mmol) gave **9o** (218 mg, 44%) as a white solid, after column chromatography (EtOAc). Mp

179–180 °C (EtOAc). IR (ATR) 3483, 3084, 2957, 2036, 1719, 1446, 1382, 1329, 1168, 1027, 978, 739, 573  $\text{cm}^{-1}$ .  $^1\text{H}$  NMR (400 MHz,  $\text{CDCl}_3$ , HETCOR)  $\delta$  1.21 (t,  $J = 7.0$  Hz, 3H,  $\text{CH}_2\text{CH}_3$ ), 1.28 (t,  $J = 7.0$  Hz, 3H,  $\text{CH}_2\text{CH}_3$ ), 3.98 (m, 1H,  $\text{CH}_2\text{CH}_3$ ), 4.11–4.20 (m, 3H,  $\text{CH}_2\text{CH}_3$ ), 4.27 (dd,  $J = 18.0, 9.0$  Hz, 1H, H-6a), 4.50 (ddd,  $J = 9.0, 2.5, 1.5$  Hz, 1H, H-3a), 6.86 (s, 1H, ArH), 6.96 (d,  $J = 9.5$  Hz, 1H, ArH), 7.36–7.39 (m, 3H, ArH), 7.42 (t, 7.5 Hz, 1H, ArH), 7.53 (d,  $J = 8.0$  Hz, 1H, ArH), 7.67 (br d,  $J = 7.0$  Hz, 2H, ArH), 8.06 (dd,  $J = 5.0, 1.5$  Hz, 1H, H-3).  $^{13}\text{C}$  NMR (100.6 MHz)  $\delta$  16.4 (d,  $J = 5.5$  Hz,  $\text{CH}_2\text{CH}_3$ ), 16.4 (d,  $J = 5.5$  Hz,  $\text{CH}_2\text{CH}_3$ ), 48.6 (d,  $J = 2.0$  Hz, C-6a), 60.2 (C-3a), 63.8 (d,  $J = 7.5$  Hz,  $\text{CH}_2\text{CH}_3$ ), 64.9 (d,  $J = 7.5$  Hz,  $\text{CH}_2\text{CH}_3$ ), 86.4 (d,  $J = 158.0$  Hz, C-1), 123.3 (q,  $J = 4.0$  Hz, CHAr), 123.4 (q,  $J = 272.5$  Hz,  $\text{CF}_3$ ), 125.6 (q,  $J = 4.0$  Hz, CHAr), 128.2 (d,  $J = 2.0$  Hz, 2CHAr), 128.5 (d,  $J = 6.0$  Hz, 2CHAr), 128.9 (d,  $J = 2.0$  Hz, CHAr), 129.5 (d,  $J = 1.0$  Hz, CHAr), 129.7 (CHAr), 131.6 (q,  $J = 33.5$  Hz,  $\text{CCF}_3$ ), 131.7 (C-*ipso*), 133.5 (d,  $J = 4.0$  Hz, C-*ipso*), 162.1 (d,  $J = 12.0$  Hz, C-3), 170.6 (d,  $J = 5.0$  Hz, CO), 171.5 (d,  $J = 11.0$  Hz, CO). HRMS  $\text{C}_{23}\text{H}_{23}\text{F}_3\text{N}_2\text{O}_5\text{P}$  [ $\text{M} + \text{H}$ ] $^+$  495.1291; found, 495.1287. Anal. Calcd for  $\text{C}_{23}\text{H}_{22}\text{F}_3\text{N}_2\text{O}_5\text{P}$ : C, 55.88%; H, 4.49%; N, 5.67%. Found: C, 56.00%; H, 4.63%; N, 5.46%.

**Diethyl (1*RS*,3*aSR*,6*aSR*)-5-(4-Fluorophenyl)-4,6-dioxo-1-phenyl-1,3*a*,4,5,6,6*a*-hexahydropyrrolo[3,4-*c*]pyrrole-1-phosphonate (9*p*).** Following the general procedure, AgOAc (7 mg, 0.04 mmol), *N*-(4-fluorophenyl)maleimide (211 mg, 1.1 mmol), acetonitrile (5 mL), and diethyl  $\alpha$ -phenylisocyanomethylphosphonate (177 mg, 0.7 mmol) gave **9p** (198 mg, 64%) as a white solid, after column chromatography (EtOAc). Mp 200–201 °C (EtOAc). IR (NaCl) 3481, 3061, 2980, 1787, 1717, 1511, 1385, 1245, 1017, 969, 700, 583  $\text{cm}^{-1}$ .  $^1\text{H}$  NMR (400 MHz,  $\text{CDCl}_3$ , HETCOR)  $\delta$  1.19 (t,  $J = 7.5$  Hz, 3H,  $\text{CH}_2\text{CH}_3$ ), 1.28 (t,  $J = 7.5$  Hz, 3H,  $\text{CH}_2\text{CH}_3$ ), 3.93 (m, 1H,  $\text{CH}_2\text{CH}_3$ ), 4.10–4.20 (m, 3H,  $\text{CH}_2\text{CH}_3$ ), 4.26 (dd,  $J = 18.0, 9.0$  Hz, H-6a), 4.48 (ddd,  $J = 8.5, 3.0, 1.5$  Hz, 1H, H-3a), 6.67–6.72 (m, 2H, ArH), 6.96–7.00 (m, 2H, ArH), 7.33–7.39 (m, 3H, ArH), 7.68–7.70 (m, 2H, ArH), 8.05 (dd,  $J = 5.0, 1.5$  Hz, 1H, H-3).  $^{13}\text{C}$  NMR (100.6 MHz)  $\delta$  16.2 (d,  $J = 4.0$  Hz,  $\text{CH}_2\text{CH}_3$ ), 16.3 (d,  $J = 4.0$  Hz,  $\text{CH}_2\text{CH}_3$ ), 48.2 (d,  $J = 3.0$  Hz, C-6a), 60.1 (C-3a), 63.6 (d,  $J = 8.0$  Hz,  $\text{CH}_2\text{CH}_3$ ), 63.7 (d,  $J = 7.0$  Hz,  $\text{CH}_2\text{CH}_3$ ), 86.2 (d,  $J = 157.0$  Hz, C-1), 116.1 (d,  $J = 23.0$  Hz, 2CHAr), 126.9 (d,  $J = 3.0$  Hz, C-*ipso*), 127.9 (2CHAr), 128.0 (2CHAr), 128.4 (d,  $J = 6.0$  Hz, 2CHAr), 128.6 (d,  $J = 2.0$  Hz, CHAr), 133.4 (d,  $J = 4.0$  Hz, C-*ipso*), 160.9 (d,  $J = 248.5$  Hz, C-*ipso*), 162.2 (d,  $J = 12.0$  Hz, C-3), 170.9 (d,  $J = 5.0$  Hz, CO), 171.6 (d,  $J = 11.0$  Hz, CO). HRMS  $\text{C}_{22}\text{H}_{22}\text{FN}_2\text{O}_5\text{P}$  [ $\text{M} + \text{H}$ ] $^+$  445.1323; found, 445.1322. Anal. Calcd for  $\text{C}_{22}\text{H}_{22}\text{FN}_2\text{O}_5\text{P}$ : C, 59.46%; H, 4.99%; N, 6.30%. Found: C, 59.73%; H, 5.13%; N, 6.19%.

**Diethyl (1*RS*,3*aSR*,6*aSR*)-5-(4-Chlorophenyl)-4,6-dioxo-1-phenyl-1,3*a*,4,5,6,6*a*-hexahydropyrrolo[3,4-*c*]pyrrole-1-phosphonate (9*q*).** Following the general procedure, AgOAc (5 mg, 0.03 mmol), *N*-(4-chlorophenyl)maleimide (150 mg, 0.7 mmol), acetonitrile (4 mL), and diethyl  $\alpha$ -phenylisocyanomethylphosphonate (118 mg, 0.5 mmol) gave **9q** (136 mg, 59%) as a white solid, after column chromatography (EtOAc). Mp 211–212 °C (EtOAc). IR (ATR) 3078, 2981, 2923, 2855, 1713, 1499, 1377, 1187, 1022, 773, 583  $\text{cm}^{-1}$ .  $^1\text{H}$  NMR (400 MHz,  $\text{CDCl}_3$ , HETCOR)  $\delta$  1.19 (t,  $J = 7.0$  Hz, 3H,  $\text{CH}_2\text{CH}_3$ ), 1.28 (t,  $J = 7.0$  Hz, 3H,  $\text{CH}_2\text{CH}_3$ ), 3.94 (m, 1H,  $\text{CH}_2\text{CH}_3$ ), 4.11–4.19 (m, 3H,  $\text{CH}_2\text{CH}_3$ ), 4.25 (dd,  $J = 18.0, 9.0$  Hz, 1H, H-6a), 4.47 (ddd,  $J = 8.5, 3.0, 1.0$  Hz, 1H, H-3a), 6.65–6.67 (m, 2H, ArH), 7.24–7.27 (m, 2H, ArH), 7.33–7.37 (m, 3H, ArH), 7.67 (br d,  $J = 7.5$  Hz, 2H, ArH), 8.04 (dd,  $J = 5.5, 1.0$  Hz, 1H, H-3).  $^{13}\text{C}$  NMR (100.6 MHz)  $\delta$  16.4 (d,  $J = 3.0$  Hz,  $\text{CH}_2\text{CH}_3$ ), 16.4 (d,  $J = 4.0$  Hz,  $\text{CH}_2\text{CH}_3$ ), 48.4 (d,  $J = 2.0$  Hz, C-6a), 60.2 (C-3a), 63.7 (d,  $J = 7.0$  Hz,  $\text{CH}_2\text{CH}_3$ ), 64.8 (d,  $J = 7.0$  Hz,  $\text{CH}_2\text{CH}_3$ ), 86.4 (d,  $J = 157.0$  Hz, C-1), 127.4 (2CHAr), 128.1 (d,  $J = 1.0$  Hz, 2CHAr), 128.5 (d,  $J = 6.0$  Hz, 2CHAr), 128.7 (d,  $J = 2.0$  Hz, CHAr), 129.4 (2CHAr), 129.6 (C-*ipso*), 133.6 (d,  $J = 4.0$  Hz, C-*ipso*), 134.7 (C-*ipso*), 162.2 (d,  $J = 12.0$  Hz, C-3), 170.8 (d,  $J = 5.0$  Hz, CO), 171.5 (d,  $J = 12.0$  Hz, CO). HRMS  $\text{C}_{22}\text{H}_{22}\text{ClN}_2\text{O}_5\text{P}$  [ $\text{M} + \text{H}$ ] $^+$  461.1028; found, 461.1026. Anal. Calcd for  $\text{C}_{22}\text{H}_{22}\text{ClN}_2\text{O}_5\text{P}$ : C, 57.34%; H, 4.81%; N, 6.08%. Found: C, 57.71%; H, 4.92%; N, 5.96%.

**Diethyl (1*RS*,3*aSR*,6*aSR*)-5-(2-Chlorophenyl)-4,6-dioxo-1-phenyl-1,3*a*,4,5,6,6*a*-hexahydropyrrolo[3,4-*c*]pyrrole-1-phosphonate (9*r*).**

Following the general procedure, AgOAc (6 mg, 0.04 mmol), *N*-(2-chlorophenyl)maleimide (180 mg, 0.9 mmol), acetonitrile (5 mL), and diethyl  $\alpha$ -phenylisocyanomethylphosphonate (152 mg, 0.6 mmol) gave **9r** (200 mg, 72%) as a white solid, after column chromatography (EtOAc/hexane 7:3). Mp 172–174 °C (EtOAc). IR (ATR) 3496, 2981, 2866, 1790, 1718, 1482, 1386, 1237, 1194, 1045, 1021, 973, 757, 579 cm<sup>-1</sup>. <sup>1</sup>H NMR (400 MHz, CDCl<sub>3</sub>, HETCOR)  $\delta$  1.14 (t, *J* = 7.0 Hz, 3H, CH<sub>2</sub>CH<sub>3</sub>-rotamer A), 1.19 (t, *J* = 7.0 Hz, 3H, CH<sub>2</sub>CH<sub>3</sub>-rotamer B), 1.29 (t, *J* = 7.0 Hz, 3H, CH<sub>2</sub>CH<sub>3</sub>-rotamer A), 1.30 (t, *J* = 7.0 Hz, 3H, CH<sub>2</sub>CH<sub>3</sub>-rotamer B), 3.82 (m, 1H, CH<sub>2</sub>CH<sub>3</sub>-rotamer A), 3.93 (m, 1H, CH<sub>2</sub>CH<sub>3</sub>-rotamer B), 4.05–4.20 (m, 6H, CH<sub>2</sub>CH<sub>3</sub>-rotamer A and B), 4.35 (dd, *J* = 18.0, 8.5 Hz, 1H, H-6a rotamer A), 4.36 (dd, *J* = 18.0, 8.5 Hz, 1H, H-6a rotamer B), 4.52 (ddd, *J* = 8.5, 4.5, 1.5 Hz, 1H, H-3a rotamer A), 4.56 (ddd, *J* = 8.5, 3.0, 1.5 Hz, 1H, H-3a rotamer B), 6.30 (dd, *J* = 8.0, 1.5 Hz, 1H, ArH rotamer B), 7.10 (m, 1H, ArH rotamer B), 7.13 (ddd, *J* = 16.0, 8.0, 2.0 Hz, 1H, ArH rotamer A), 7.25–7.43 (m, 10H, 6ArH rotamer A and 4ArH rotamer B), 7.42 (dd, *J* = 8.0, 1.5 Hz, 1H, ArH rotamer B), 7.71 (d, *J* = 8.0 Hz, 2H, ArH rotamer B), 7.78 (d, *J* = 8.0 Hz, 2H, ArH rotamer A), 8.03 (dd, *J* = 5.5 Hz, 1.5 Hz, 1H, H-3 rotamer A), 8.08 (dd, *J* = 5.0, 1.5 Hz, 1H, H-3 rotamer B). <sup>13</sup>C NMR (100.6 MHz)  $\delta$  16.2 (d, *J* = 6.0 Hz, CH<sub>2</sub>CH<sub>3</sub> rotamer A or B), 16.2 (d, *J* = 6.0 Hz, CH<sub>2</sub>CH<sub>3</sub> rotamer A or B), 16.3 (d, *J* = 5.5 Hz, CH<sub>2</sub>CH<sub>3</sub> rotamer A or B), 16.3 (d, *J* = 5.5 Hz, CH<sub>2</sub>CH<sub>3</sub> rotamer A or B), 48.0 (d, *J* = 2.5 Hz, C-6a rotamer A), 48.6 (d, *J* = 2.5 Hz, C-6a rotamer B), 60.3 (C-3a rotamer B), 60.1 (C-3a rotamer A), 63.5 (d, *J* = 7.5 Hz, CH<sub>2</sub>CH<sub>3</sub> rotamer A), 63.6 (d, *J* = 7.5 Hz, CH<sub>2</sub>CH<sub>3</sub> rotamer B), 64.7 (d, *J* = 7.5 Hz, CH<sub>2</sub>CH<sub>3</sub> rotamer B), 64.8 (d, *J* = 7.5 Hz, CH<sub>2</sub>CH<sub>3</sub> rotamer A), 86.0 (d, *J* = 157.5, C-1 rotamer A), 86.6 (d, *J* = 153.5, C-1 rotamer B), 127.6 (CHAr rotamer A or B), 127.7 (d, *J* = 2.0 Hz, CHAr rotamer A or B), 127.8 (CHAr rotamer A), 127.9 (CHAr rotamer A or B), 128.0 (CHAr rotamer A or B), 128.4 (d, *J* = 5.0 Hz, 2CHAr rotamer B), 128.5 (2CHAr rotamer A or B), 128.6 (d, *J* = 2.0 Hz, CHAr rotamer A or B), 128.9 (d, *J* = 6.0 Hz, CHAr rotamer A), 129.1 (C-*ipso* rotamer A), 129.2 (C-*ipso* rotamer B), 129.3 (CHAr rotamer B), 129.6 (CHAr rotamer A), 130.2 (CHAr rotamer B), 130.3 (CHAr rotamer A or B), 130.7 (CHAr rotamer A or B), 130.9 (CHAr rotamer A or B), 132.0 (C-*ipso* rotamer A), 132.2 (C-*ipso* rotamer B), 132.9 (d, *J* = 4.0 Hz, C-*ipso* rotamer A), 133.5 (d, *J* = 4.0 Hz, C-*ipso* rotamer B), 162.0 (d, *J* = 11.5 Hz, C-3 rotamer A), 162.2 (d, *J* = 12.5 Hz, C-3 rotamer B), 170.2 (d, *J* = 5.0 Hz, CO rotamer B), 170.3 (d, *J* = 5.5 Hz, CO rotamer A), 170.7 (d, *J* = 11.5 Hz, CO rotamer A or B), 170.8 (d, *J* = 15.0 Hz, CO rotamer B). HRMS C<sub>22</sub>H<sub>23</sub>ClN<sub>2</sub>O<sub>5</sub>P [M + H]<sup>+</sup> 461.1028; found, 461.1025. Anal. Calcd for C<sub>22</sub>H<sub>22</sub>ClN<sub>2</sub>O<sub>5</sub>P: C, 57.34%; H, 4.81%; N, 6.08%. Found: C, 57.18%; H, 4.86%; N, 5.88%.

**Diethyl (1*R*S,3*a*S*R*,6*a*S*R*)-5-(3-Chlorophenyl)-4,6-dioxo-1-phenyl-1,3*a*,4,5,6,6*a*-hexahydropyrrolo[3,4-*c*]pyrrole-1-phosphonate (9s).** Following the general procedure, AgOAc (8 mg, 0.05 mmol), *N*-(3-chlorophenyl)maleimide (250 mg, 1.2 mmol), acetonitrile (6 mL), and diethyl  $\alpha$ -phenylisocyanomethylphosphonate (203 mg, 0.8 mmol) gave **9s** (167 mg, 45%) as a white solid, after column chromatography (EtOAc). Mp 186–187 °C (EtOAc). IR (ATR) 3488, 3084, 2962, 2928, 1709, 1587, 1475, 1382, 1241, 1183, 1051, 1022, 948, 705 cm<sup>-1</sup>. <sup>1</sup>H NMR (400 MHz, CDCl<sub>3</sub>, HETCOR)  $\delta$  1.19 (t, *J* = 7.0 Hz, 3H, CH<sub>2</sub>CH<sub>3</sub>), 1.28 (t, *J* = 7.0 Hz, 3H, CH<sub>2</sub>CH<sub>3</sub>), 3.94 (m, 1H, CH<sub>2</sub>CH<sub>3</sub>), 4.10–4.19 (m, 3H, CH<sub>2</sub>CH<sub>3</sub>), 4.26 (dd, *J* = 18.0, 9.0 Hz, 1H, H-6a), 4.48 (ddd, *J* = 8.5, 3.0, 1.5 Hz, 1H, H-3a), 6.63–6.68 (m, 2H, ArH), 7.22 (m, 1H, ArH), 7.26 (m, 1H, ArH), 7.35–7.39 (m, 3H, ArH), 7.68 (br d, *J* = 7.5 Hz, 2H, ArH), 8.05 (dd, *J* = 5.0, 1.5 Hz, 1H, H-3). <sup>13</sup>C NMR (100.6 MHz)  $\delta$  16.4 (d, *J* = 5.5 Hz, CH<sub>2</sub>CH<sub>3</sub>), 16.4 (d, *J* = 5.5 Hz, CH<sub>2</sub>CH<sub>3</sub>), 48.5 (d, *J* = 3.0 Hz, C-6a), 60.2 (C-3a), 63.7 (d, *J* = 7.0 Hz, CH<sub>2</sub>CH<sub>3</sub>), 64.8 (d, *J* = 7.0 Hz, CH<sub>2</sub>CH<sub>3</sub>), 86.4 (d, *J* = 157.0 Hz, C-1), 124.4 (CHAr), 126.5 (CHAr), 128.2 (d, *J* = 2.0 Hz, 2CHAr), 128.5 (d, *J* = 6.0 Hz, 2CHAr), 128.9 (d, *J* = 2.0 Hz, CHAr), 129.0 (CHAr), 130.1 (CHAr), 132.2 (C-*ipso*), 133.5 (d, *J* = 4.0 Hz, C-*ipso*), 134.7 (C-*ipso*), 162.3 (d, *J* = 12.0 Hz, C-3), 170.6 (d, *J* = 5.0 Hz, CO), 171.4 (d, *J* = 12.0 Hz, CO). HRMS C<sub>22</sub>H<sub>23</sub>ClN<sub>2</sub>O<sub>5</sub>P [M + H]<sup>+</sup> 461.1028; found, 461.1029. Anal. Calcd for C<sub>22</sub>H<sub>22</sub>ClN<sub>2</sub>O<sub>5</sub>P: C, 57.34%; H, 4.81%; N, 6.08%. Found: C, 57.70%; H, 4.96%; N, 5.59%.

**Diethyl (1*R*S,3*a*S*R*,6*a*S*R*)-5-(4-Bromophenyl)-4,6-dioxo-1-phenyl-1,3*a*,4,5,6,6*a*-hexahydropyrrolo[3,4-*c*]pyrrole-1-phosphonate (9t).** Following the general procedure, AgOAc (7 mg, 0.04 mmol), *N*-(4-bromophenyl)maleimide (275 mg, 1.1 mmol), acetonitrile (5 mL), and diethyl  $\alpha$ -phenylisocyanomethylphosphonate (177 mg, 0.7 mmol) gave **9t** (181 mg, 51%) as a white solid, after column chromatography (EtOAc/hexane 1:1). Mp 180–182 °C (EtOAc). IR (ATR) 3478, 2918, 2845, 1797, 1714, 1480, 1387, 1236, 1187, 1158, 1022, 973, 744, 578 cm<sup>-1</sup>. <sup>1</sup>H NMR (400 MHz, CDCl<sub>3</sub>, HETCOR)  $\delta$  1.19 (t, *J* = 7.0 Hz, 3H, CH<sub>2</sub>CH<sub>3</sub>), 1.28 (t, *J* = 7.0 Hz, 3H, CH<sub>2</sub>CH<sub>3</sub>), 3.93 (m, 1H, CH<sub>2</sub>CH<sub>3</sub>), 4.10–4.19 (m, 3H, CH<sub>2</sub>CH<sub>3</sub>), 4.25 (dd, *J* = 18.0, 9.0 Hz, 1H, H-6a), 4.47 (ddd, *J* = 9.0, 3.0, 1.5 Hz, 1H, H-3a), 6.59–6.61 (m, 2H, ArH), 7.34–7.36 (m, 3H, ArH), 7.40–7.42 (m, 2H, ArH), 7.67 (br s, *J* = 7.5 Hz, 2H, ArH), 8.04 (dd, *J* = 5.0, 1.5 Hz, 1H, H-3). <sup>13</sup>C NMR (100.6 MHz)  $\delta$  16.4 (d, *J* = 3.0 Hz, CH<sub>2</sub>CH<sub>3</sub>), 16.4 (d, *J* = 4.0 Hz, CH<sub>2</sub>CH<sub>3</sub>), 48.4 (d, *J* = 3.0 Hz, C-6a), 60.3 (C-3a), 63.7 (d, *J* = 8.0 Hz, CH<sub>2</sub>CH<sub>3</sub>), 64.8 (d, *J* = 7.0 Hz, CH<sub>2</sub>CH<sub>3</sub>), 86.4 (d, *J* = 157.0 Hz, C-1), 122.7 (C-*ipso*), 127.7 (2CHAr), 128.1 (d, *J* = 2.0 Hz, 2CHAr), 128.5 (d, *J* = 6.0 Hz, 2CHAr), 128.8 (d, *J* = 2.0 Hz, CHAr), 130.2 (C-*ipso*), 132.4 (2CHAr), 133.6 (d, *J* = 4.0 Hz, C-*ipso*), 162.2 (d, *J* = 12.0 Hz, C-3), 170.7 (d, *J* = 5.0 Hz, CO), 171.4 (d, *J* = 11.0 Hz, CO). HRMS C<sub>22</sub>H<sub>23</sub>BrN<sub>2</sub>O<sub>5</sub>P [M + H]<sup>+</sup> 505.0522; found, 505.0522. Anal. Calcd for C<sub>22</sub>H<sub>23</sub>BrN<sub>2</sub>O<sub>5</sub>P: C, 52.99%; H, 4.90%; N, 5.24%. Found: C, 53.30%; H, 4.61%; N, 5.10%.

**Diethyl (1*R*S,3*a*S*R*,6*a*S*R*)-5-(3,5-Dichlorophenyl)-4,6-dioxo-1-phenyl-1,3*a*,4,5,6,6*a*-hexahydropyrrolo[3,4-*c*]pyrrole-1-phosphonate (9u).** Following the general procedure, AgOAc (12 mg, 0.07 mmol), *N*-(3,5-dichlorophenyl)maleimide (267 mg, 1.1 mmol), acetonitrile (5 mL), and diethyl  $\alpha$ -phenylisocyanomethylphosphonate (177 mg, 0.7 mmol) gave **9u** (190 mg, 55%) as a white solid, after column chromatography (EtOAc/hexane 8:2). Mp 207–209 °C (EtOAc). IR (ATR) 3483, 3079, 2952, 2928, 1719, 1573, 1441, 1373, 1226, 1183, 1027, 973, 763, 734, 727, 588 cm<sup>-1</sup>. <sup>1</sup>H NMR (400 MHz, CDCl<sub>3</sub>, HETCOR)  $\delta$  1.20 (t, *J* = 7.0 Hz, 3H, CH<sub>2</sub>CH<sub>3</sub>), 1.28 (t, *J* = 7.0 Hz, 3H, CH<sub>2</sub>CH<sub>3</sub>), 3.94 (m, 1H, CH<sub>2</sub>CH<sub>3</sub>), 4.10–4.19 (m, 3H, CH<sub>2</sub>CH<sub>3</sub>), 4.25 (dd, *J* = 18.0, 8.5 Hz, 1H, H-6a), 4.47 (ddd, *J* = 9.0, 2.5, 1.5 Hz, 1H, H-3a), 6.60 (d, *J* = 2.0 Hz, 2H, ArH), 7.27 (m, 1H, ArH), 7.37–7.40 (m, 3H, ArH), 7.65 (br d, *J* = 5.0 Hz, 2H, ArH), 8.04 (dd, *J* = 5.0, 1.5 Hz, 1H, H-3). <sup>13</sup>C NMR (100.6 MHz)  $\delta$  16.3 (d, *J* = 5.5 Hz, CH<sub>2</sub>CH<sub>3</sub>), 16.4 (d, *J* = 5.5 Hz, CH<sub>2</sub>CH<sub>3</sub>), 48.6 (d, *J* = 3.0 Hz, C-6a), 60.9 (C-3a), 63.8 (d, *J* = 7.0 Hz, CH<sub>2</sub>CH<sub>3</sub>), 64.9 (d, *J* = 7.0 Hz, CH<sub>2</sub>CH<sub>3</sub>), 86.5 (d, *J* = 158.0 Hz, C-1), 124.8 (2CHAr), 128.3 (d, *J* = 2.0 Hz, 2CHAr), 128.5 (d, *J* = 5.0 Hz, 2CHAr), 129.0 (d, *J* = 2.0 Hz, CHAr), 129.1 (CHAr), 132.8 (C-*ipso*), 133.5 (d, *J* = 3.0 Hz, C-*ipso*), 135.3 (2C-*ipso*), 162.0 (d, *J* = 13.0 Hz, C-3), 170.2 (d, *J* = 5.0 Hz, CO), 171.1 (d, *J* = 11.0 Hz, CO). HRMS C<sub>22</sub>H<sub>21</sub>Cl<sub>2</sub>N<sub>2</sub>O<sub>5</sub>P [M + H]<sup>+</sup> 495.0638; found, 495.0638. Anal. Calcd for C<sub>22</sub>H<sub>21</sub>Cl<sub>2</sub>N<sub>2</sub>O<sub>5</sub>P: C, 53.35%; H, 4.27%; N, 5.66%. Found: C, 53.69%; H, 4.35%; N, 5.42%.

**Diethyl (1*R*S,3*a*S*R*,6*a*S*R*)-5-(3,4-Dichlorophenyl)-4,6-dioxo-1-phenyl-1,3*a*,4,5,6,6*a*-hexahydropyrrolo[3,4-*c*]pyrrole-1-phosphonate (9v).** Following the general procedure, AgOAc (8 mg, 0.05 mmol), *N*-(3-chloro-4-chlorophenyl)maleimide (288 mg, 1.2 mmol), acetonitrile (6 mL), and diethyl  $\alpha$ -phenylisocyanomethylphosphonate (202 mg, 0.8 mmol) gave **9v** (210 mg, 53%) as a white solid, after column chromatography (EtOAc/hexane 1:1). Mp 172–174 °C (EtOAc). IR (ATR) 3480, 3075, 2957, 1790, 1716, 1464, 1251, 1187, 1058, 1024, 737, 579 cm<sup>-1</sup>. <sup>1</sup>H NMR (400 MHz, CDCl<sub>3</sub>, HETCOR)  $\delta$  1.20 (t, *J* = 7.0 Hz, 3H, CH<sub>2</sub>CH<sub>3</sub>), 1.28 (t, *J* = 7.0 Hz, 3H, CH<sub>2</sub>CH<sub>3</sub>), 3.95 (m, 1H, CH<sub>2</sub>CH<sub>3</sub>), 4.10–4.20 (m, 3H, CH<sub>2</sub>CH<sub>3</sub>), 4.26 (dd, *J* = 18.0, 8.5 Hz, 1H, H-6a), 4.47 (ddd, *J* = 8.5, 3.0, 1.5 Hz, 1H, H-3a), 6.61 (dd, *J* = 9.0, 2.5 Hz, 1H, ArH), 6.78 (d, *J* = 2.5 Hz, 1H, ArH), 7.35–7.38 (m, 4H, ArH), 7.65–7.68 (m, 2H, ArH), 8.04 (dd, *J* = 4.5, 1.5 Hz, 1H, H-3). <sup>13</sup>C NMR (100.6 MHz)  $\delta$  16.2 (d, *J* = 6.0 Hz, CH<sub>2</sub>CH<sub>3</sub>), 16.3 (d, *J* = 6.0 Hz, CH<sub>2</sub>CH<sub>3</sub>), 48.4 (d, *J* = 3.0 Hz, C-6a), 60.0 (C-3a), 63.6 (d, *J* = 7.0 Hz, CH<sub>2</sub>CH<sub>3</sub>), 64.7 (d, *J* = 8.0 Hz, CH<sub>2</sub>CH<sub>3</sub>), 86.2 (d, *J* = 157.0 Hz, C-1), 125.2 (CHAr), 127.9 (CHAr), 128.0 (d, *J* = 2.0 Hz, 2CHAr), 128.3 (d, *J* = 6.0 Hz, 2CHAr), 128.7 (d, *J* = 2.0 Hz, CHAr), 130.2 (C-*ipso*), 130.6 (CHAr), 132.9 (C-*ipso*), 133.0 (C-*ipso*), 133.3 (d, *J* = 4.0 Hz, C-*ipso*), 161.9 (d, *J* = 13.0 Hz, C-3), 170.2 (d, *J* = 5.0 Hz, CO), 171.1 (d, *J* = 12.0 Hz, CO). HRMS

$C_{22}H_{22}Cl_3N_2O_3P$  [M + H]<sup>+</sup> 495.0638; found, 495.0637. Anal. Calcd for  $C_{22}H_{21}Cl_3N_2O_3P$ : C, 53.35%; H, 4.27%; N, 5.66%. Found: C, 53.42%; H, 4.30%; N, 5.48%.

**Diethyl (1*R*,3*a**S**R*,6*a**S**R*)-4,6-Dioxo-1-phenyl-5-(2,4,6-trichlorophenyl)-1,3*a*,4,5,6,6*a*-hexahydropyrrolo[3,4-*c*]pyrrole-1-phosphonate (9w).** Following the general procedure, AgOAc (8.3 mg, 0.05 mmol), *N*-(2,4,6-trichlorophenyl)maleimide (194 mg, 0.7 mmol), acetonitrile (4 mL), and diethyl  $\alpha$ -phenylisocyanomethylphosphonate (127 mg, 0.5 mmol) gave **9w** (215 mg, 81%) as a yellowish solid, after column chromatography (EtOAc). Mp 146–148 °C (EtOAc). IR (ATR) 3501, 2976, 2854, 1786, 1727, 1471, 1361, 1253, 1043, 1322, 961, 704 cm<sup>-1</sup>. <sup>1</sup>H NMR (400 MHz, CDCl<sub>3</sub>, HETCOR)  $\delta$  1.14 (t, *J* = 7.0 Hz, 3H, CH<sub>2</sub>CH<sub>3</sub>), 1.28 (t, *J* = 7.0 Hz, 3H, CH<sub>2</sub>CH<sub>3</sub>), 3.84 (m, 1H, CH<sub>2</sub>CH<sub>3</sub>), 4.03–4.17 (m, 3H, CH<sub>2</sub>CH<sub>3</sub>), 4.41 (dd, *J* = 18.0, 9.0 Hz, 1H, H-6*a*), 4.57 (ddd, *J* = 8.5, 4.0, 1.0 Hz, 1H, H-3*a*), 7.26 (d, *J* = 3.0 Hz, 1H, ArH), 7.28–7.34 (m, 3H, ArH), 7.36 (d, *J* = 2.0 Hz, 1H, ArH), 7.75 (br d, *J* = 8.0 Hz, 2H, ArH), 8.02 (dd, *J* = 5.0, 1.0 Hz, 1H, H-3). <sup>13</sup>C NMR (100.6 MHz)  $\delta$  16.3 (d, *J* = 6.0 Hz, CH<sub>2</sub>CH<sub>3</sub>), 16.4 (d, *J* = 6.0 Hz, CH<sub>2</sub>CH<sub>3</sub>), 48.3 (d, *J* = 3.0 Hz, C-6*a*), 61.0 (C-3*a*), 63.7 (d, *J* = 7.0 Hz, CH<sub>2</sub>CH<sub>3</sub>), 64.9 (d, *J* = 8.0 Hz, CH<sub>2</sub>CH<sub>3</sub>), 86.7 (d, *J* = 152.0 Hz, C-1), 126.6 (C-*ipso*), 127.8 (d, *J* = 2.0 Hz, 2CHAr), 128.6 (CHAr), 128.7 (CHAr), 128.8 (CHAr), 129.0 (d, *J* = 5.0 Hz, 2CHAr), 133.0 (d, *J* = 5.0 Hz, C-*ipso*), 135.1 (d, *J* = 10.0 Hz, C-*ipso*), 136.8 (2C-*ipso*), 161.8 (d, *J* = 11.0 Hz, C-3), 169.3 (d, *J* = 5.0 Hz, CO), 169.8 (d, *J* = 14.0 Hz, CO). HRMS  $C_{22}H_{21}Cl_3N_2O_3P$  [M + H]<sup>+</sup> 529.0248; found, 529.0242. Purity 98% (*t*<sub>R</sub> = 5.06 min).

**Diethyl (1*R*,3*a**S**R*,6*a**S**R*)-5-(3-Nitrophenyl)-4,6-dioxo-1-phenyl-1,3*a*,4,5,6,6*a*-hexahydropyrrolo[3,4-*c*]pyrrole-1-phosphonate (9x).** Following the general procedure, AgOAc (4 mg, 0.02 mmol), *N*-(3-nitrophenyl)maleimide (131 mg, 0.6 mmol), acetonitrile (3 mL), and diethyl  $\alpha$ -phenylisocyanomethylphosphonate (101 mg, 0.4 mmol) gave **9x** (101 mg, 54%) as a white solid, after column chromatography (EtOAc). Mp 192–195 °C (EtOAc). IR (NaCl) 2984, 1724, 1537, 1351, 1248, 1176, 1050, 971, 758, 674 cm<sup>-1</sup>. <sup>1</sup>H NMR (400 MHz, CDCl<sub>3</sub>, HETCOR)  $\delta$  1.21 (t, *J* = 7.0 Hz, 3H, CH<sub>2</sub>CH<sub>3</sub>), 1.29 (t, *J* = 7.0 Hz, 3H, CH<sub>2</sub>CH<sub>3</sub>), 3.98 (m, 1H, CH<sub>2</sub>CH<sub>3</sub>), 4.10–4.24 (m, 3H, CH<sub>2</sub>CH<sub>3</sub>), 4.30 (dd, *J* = 18.0, 9.0 Hz, 1H, H-6*a*), 4.53 (ddd, *J* = 9.0, 3.0, 1.0 Hz, H-3*a*), 7.11 (dq, *J* = 8.0, 1.0 Hz, 1H, ArH), 7.38–7.41 (m, 3H, ArH), 7.49 (t, *J* = 8.0 Hz, 1H, ArH), 7.58 (t, *J* = 2.0 Hz, 1H, ArH), 7.67–7.69 (m, 2H, ArH), 8.07 (dd, *J* = 5.0, 1.0 Hz, 1H, H-3), 8.14 (ddd, *J* = 8.5, 2.5, 1.0 Hz, 1H, ArH). <sup>13</sup>C NMR (100.6 MHz)  $\delta$  16.2 (d, *J* = 3.0 Hz, CH<sub>2</sub>CH<sub>3</sub>), 16.3 (d, *J* = 3.5 Hz, CH<sub>2</sub>CH<sub>3</sub>), 48.5 (d, *J* = 2.0 Hz, C-6*a*), 60.0 (C-3*a*), 63.6 (d, *J* = 7.5 Hz, CH<sub>2</sub>CH<sub>3</sub>), 64.7 (d, *J* = 7.5 Hz, CH<sub>2</sub>CH<sub>3</sub>), 86.2 (d, *J* = 158.0 Hz, C-1), 121.4 (CHAr), 123.3 (CHAr), 128.1 (2CHAr), 128.2 (CHAr), 128.3 (CHAr), 128.9 (d, *J* = 1.5 Hz, CHAr), 129.8 (CHAr), 131.9 (CHAr), 132.0 (C-*ipso*), 133.2 (d, *J* = 4.0 Hz, C-*ipso*), 148.3 (C-*ipso*), 161.7 (d, *J* = 12.0 Hz, C-3), 170.2 (d, *J* = 5.5 Hz, CO), 171.1 (d, *J* = 11.0 Hz, CO). HRMS  $C_{22}H_{21}N_3O_7P$  [M + H]<sup>+</sup> 472.1268; found, 472.1276. Anal. Calcd for  $C_{22}H_{21}N_3O_7P$ : C, 56.05%; H, 4.70%; N, 8.91%. Found: C, 55.73%; H, 4.74%; N, 8.85%.

**Diethyl (1*R*,3*a**S**R*,6*a**S**R*)-5-(2-Methyl-5-nitrophenyl)-4,6-dioxo-1-phenyl-1,3*a*,4,5,6,6*a*-hexahydropyrrolo[3,4-*c*]pyrrole-1-phosphonate (9y).** Following the general procedure, AgOAc (5 mg, 0.03 mmol), *N*-(2-methyl-5-nitrophenyl)maleimide (138 mg, 0.6 mmol), acetonitrile (3 mL), and diethyl  $\alpha$ -phenylisocyanomethylphosphonate (101 mg, 0.4 mmol) gave **9y** (111 mg, 57%) as a white solid, after column chromatography (EtOAc). Mp 196–198 °C (EtOAc). IR (ATR) 3493, 3079, 2947, 2845, 1724, 1519, 1343, 1192, 1017, 739, 578 cm<sup>-1</sup>. <sup>1</sup>H NMR (400 MHz, CDCl<sub>3</sub>, HETCOR)  $\delta$  1.16 (td, *J* = 7.0, 0.5 Hz, 3H, CH<sub>2</sub>CH<sub>3</sub> rotamer A), 1.22 (td, *J* = 7.0, 0.5 Hz, 3H, CH<sub>2</sub>CH<sub>3</sub> rotamer B), 1.29 (td, *J* = 7.0, 0.5 Hz, 3H, CH<sub>2</sub>CH<sub>3</sub> rotamer B), 1.30 (td, *J* = 7.0, 0.5 Hz, 3H, CH<sub>2</sub>CH<sub>3</sub> rotamer A), 1.51 (s, 3H, CH<sub>3</sub> rotamer A), 2.15 (s, 3H, CH<sub>3</sub> rotamer B), 3.85 (m, 1H, CH<sub>2</sub>CH<sub>3</sub> rotamer A), 3.99 (m, 1H, CH<sub>2</sub>CH<sub>3</sub> rotamer B), 4.03–4.24 (m, 6H, CH<sub>2</sub>CH<sub>3</sub> rotamer A and B), 4.35 (dd, *J* = 18.0, 9.0 Hz, 1H, H-6*a* rotamer B), 4.39 (dd, *J* = 18.5, 9.0 Hz, 1H, H-6*a* rotamer A), 4.55 (ddd, *J* = 10.0, 2.5, 1.5 Hz, 1H, H-3*a* rotamer B), 4.59 (ddd, *J* = 9.0, 3.5, 1.5 Hz, 1H, H-3*a* rotamer A), 6.88 (d, *J* = 2.5 Hz, 1H, ArH rotamer B), 7.47–7.19 (m, 8H, 4ArH rotamer A and 4ArH rotamer

B), 7.69 (br s, 2H, ArH rotamer B), 7.77 (d, *J* = 7.5 Hz, 2H, ArH rotamer A), 7.91 (d, *J* = 2.5 Hz, 1H, ArH rotamer A), 8.05 (dd, *J* = 5.0, 1.5 Hz, 1H, C-3 rotamer A), 8.08 (dd, *J* = 5.5, 2.5 Hz, 1H, C-3 rotamer B), 8.08–8.11 (m, 2H, ArH rotamer A and rotamer B). <sup>13</sup>C NMR (100.6 MHz)  $\delta$  16.3 (d, *J* = 5.5 Hz, CH<sub>2</sub>CH<sub>3</sub> rotamer A), 16.3 (d, *J* = 5.5 Hz, CH<sub>2</sub>CH<sub>3</sub> rotamer B), 16.4 (d, *J* = 5.5 Hz, CH<sub>2</sub>CH<sub>3</sub> rotamer A), 16.4 (d, *J* = 5.5 Hz, CH<sub>2</sub>CH<sub>3</sub> rotamer B), 17.5 (CH<sub>3</sub> rotamer A), 18.2 (CH<sub>3</sub> rotamer B), 48.3 (d, *J* = 2.5 Hz, C-6*a* rotamer A), 49.2 (d, *J* = 2.5 Hz, C-6*a* rotamer B), 60.1 (C-3*a* rotamer B), 61.0 (C-3*a* rotamer A), 63.7 (d, *J* = 7.5 Hz, CH<sub>2</sub>CH<sub>3</sub> rotamer A), 63.8 (d, *J* = 7.5 Hz, CH<sub>2</sub>CH<sub>3</sub> rotamer B), 64.9 (d, *J* = 7.5 Hz, CH<sub>2</sub>CH<sub>3</sub> rotamer B), 65.0 (d, *J* = 7.5 Hz, CH<sub>2</sub>CH<sub>3</sub> rotamer A), 86.3 (d, *J* = 159.0 Hz, C-1 rotamer B), 86.6 (d, *J* = 154.5 Hz, C-1 rotamer A), 123.5 (CHAr rotamer B), 123.7 (CHAr rotamer A), 124.3 (CHAr rotamer A), 124.5 (CHAr rotamer B), 127.9 (CHAr rotamer A), 128.0 (CHAr rotamer B), 128.3 (d, *J* = 5.5 Hz, 2CHAr rotamer B), 128.3 (CHAr rotamer A), 128.4 (CHAr rotamer B), 128.8 (d, *J* = 2.5 Hz, CHAr rotamer A), 128.9 (d, *J* = 6.5 Hz, 2CHAr rotamer A), 129.4 (d, *J* = 2.0 Hz, CHAr rotamer B), 131.1 (C-*ipso* rotamer A), 131.2 (C-*ipso* rotamer B), 131.8 (CHAr rotamer B), 131.9 (CHAr rotamer A), 133.3 (d, *J* = 4.5 Hz, C-*ipso* rotamer A), 133.4 (d, *J* = 4.0 Hz, C-*ipso* rotamer B), 143.8 (C-*ipso* rotamer A), 143.9 (C-*ipso* rotamer B), 146.6 (C-*ipso* rotamer A), 146.7 (C-*ipso* rotamer B), 161.8 (d, *J* = 12.5 Hz, C-3 rotamer B), 161.9 (d, *J* = 11.5 Hz, C-3 rotamer A), 170.4 (d, *J* = 5.0 Hz, CO rotamer B), 170.6 (d, *J* = 5.5 Hz, CO rotamer A), 171.0 (d, *J* = 13.5 Hz, CO rotamer A), 171.3 (d, *J* = 10.0 Hz, CO rotamer B). HRMS  $C_{23}H_{25}N_3O_7P$  [M + H]<sup>+</sup> 486.1425; found, 486.1424. Anal. Calcd for  $C_{23}H_{24}N_3O_7P$ : C, 56.91%; H, 4.98%; N, 8.66%. Found: C, 57.33%; H, 5.11%; N, 8.59%.

**Diethyl (1*R*,3*a**S**R*,6*a**S**R*)-5-(1,1'-Biphenyl)-4-yl-4,6-dioxo-1-phenyl-1,3*a*,4,5,6,6*a*-hexahydropyrrolo[3,4-*c*]pyrrole-1-phosphonate (9z).** Following the general procedure, AgOAc (5 mg, 0.03 mmol), *N*-(*p*-phenylphenyl)maleimide (200 mg, 0.8 mmol), acetonitrile (4 mL), and diethyl  $\alpha$ -phenylisocyanomethylphosphonate (134 mg, 0.5 mmol) gave **9z** (129 mg, 49%) as a yellowish oil, after column chromatography (EtOAc). IR (NaCl) 3483, 2982, 2928, 1716, 1628, 1487, 1378, 1248, 1182, 1052, 1024, 969, 839, 792 cm<sup>-1</sup>. <sup>1</sup>H NMR (400 MHz, CDCl<sub>3</sub>, HETCOR)  $\delta$  1.20 (t, *J* = 7.0 Hz, 3H, CH<sub>2</sub>CH<sub>3</sub>), 1.29 (t, *J* = 7.0 Hz, 3H, CH<sub>2</sub>CH<sub>3</sub>), 3.97 (m, 1H, CH<sub>2</sub>CH<sub>3</sub>), 4.09–4.23 (m, 3H, CH<sub>2</sub>CH<sub>3</sub>), 4.30 (dd, *J* = 18.5, 9.0 Hz, 1H, H-6*a*), 4.51 (ddd, *J* = 9.0, 3.0, 1.5 Hz, 1H, H-3*a*), 6.80 (m, 2H, ArH), 7.31–7.42 (m, 6H, ArH), 7.47–7.51 (m, 4H, ArH), 7.71 (br d, *J* = 7.5 Hz, 2H, ArH), 8.08 (dd, *J* = 5.0, 1.5 Hz, 1H, H-3). <sup>13</sup>C NMR (100.6 MHz)  $\delta$  16.2 (d, *J* = 5.5 Hz, CH<sub>2</sub>CH<sub>3</sub>), 16.3 (d, *J* = 5.5 Hz, CH<sub>2</sub>CH<sub>3</sub>), 48.2 (d, *J* = 2.5 Hz, C-6*a*), 60.2 (C-3*a*), 63.5 (d, *J* = 7.0 Hz, CH<sub>2</sub>CH<sub>3</sub>), 64.6 (d, *J* = 7.5 Hz, CH<sub>2</sub>CH<sub>3</sub>), 86.5 (d, *J* = 157.0 Hz, C-1), 126.3 (2CHAr), 127.1 (2CHAr), 127.7 (CHAr), 127.8 (2CHAr), 127.9 (d, *J* = 1.5 Hz, 2CHAr), 128.4 (d, *J* = 6.0 Hz, 2CHAr), 128.6 (d, *J* = 2.0 Hz, CHAr), 128.8 (2CHAr), 130.0 (C-*ipso*), 133.4 (d, *J* = 4.0 Hz, C-*ipso*), 140.0 (C-*ipso*), 141.7 (C-*ipso*), 162.3 (d, *J* = 12.0 Hz, C-3), 170.9 (d, *J* = 5.5 Hz, CO), 171.7 (d, *J* = 11.5 Hz, CO). HRMS  $C_{28}H_{28}N_2O_3P$  [M + H]<sup>+</sup> 503.1730; found, 503.1727. Purity 98.5% (*t*<sub>R</sub> = 4.71 min).

**Diethyl (1*R*,3*a**S**R*,6*a**S**R*)-4,6-Dioxo-1-phenyl-5-(*p*-tolyl)-1,3*a*,4,5,6,6*a*-hexahydropyrrolo[3,4-*c*]pyrrole-1-phosphonate (9aa).** Following the general procedure, AgOAc (6 mg, 0.04 mmol), *N*-(4-methylphenyl)maleimide (153 mg, 0.9 mmol), acetonitrile (4.5 mL), and diethyl  $\alpha$ -phenylisocyanomethylphosphonate (168 mg, 0.6 mmol) gave **9aa** (199 mg, 75%) as a white solid, after column chromatography (EtOAc/hexane 3:2 to 9:1). Mp 156–158 °C (EtOAc). IR (ATR) 3476, 2936, 2863, 1711, 1632, 1520, 1368, 1240, 1181, 1025, 971, 740, 583 cm<sup>-1</sup>. <sup>1</sup>H NMR (400 MHz, CDCl<sub>3</sub>, HETCOR)  $\delta$  1.19 (t, *J* = 7.0 Hz, 3H, CH<sub>2</sub>CH<sub>3</sub>), 1.29 (t, *J* = 7.0 Hz, 3H, CH<sub>2</sub>CH<sub>3</sub>), 2.28 (s, 3H, CH<sub>3</sub>-Ar), 3.93 (m, 1H, CH<sub>2</sub>CH<sub>3</sub>), 4.11–4.19 (m, 3H, CH<sub>2</sub>CH<sub>3</sub>), 4.24 (dd, *J* = 16.5, 9.0 Hz, 1H, H-6*a*), 4.46 (dd, *J* = 8.5, 3.0, 1.5 Hz, 1H, H-3*a*), 6.60 (m, 2H, ArH), 7.09 (m, 2H, ArH), 7.31–7.38 (m, 3H, ArH), 7.68–7.70 (m, 2H, ArH), 8.05 (dd, *J* = 5.0, 1.5 Hz, 1H, H-3). <sup>13</sup>C NMR (100.6 MHz)  $\delta$  16.2 (d, *J* = 5.5 Hz, CH<sub>2</sub>CH<sub>3</sub>), 16.3 (d, *J* = 5.5 Hz, CH<sub>2</sub>CH<sub>3</sub>), 21.1 (CH<sub>3</sub>-Ar), 48.1 (d, *J* = 3.0 Hz, C-6*a*), 60.2 (C-3*a*), 63.5 (d, *J* = 7.0 Hz, CH<sub>2</sub>CH<sub>3</sub>), 64.6 (d, *J* = 8.0 Hz, CH<sub>2</sub>CH<sub>3</sub>), 86.2 (d, *J* = 156.0 Hz, C-1), 125.8

(2CHAr), 127.9 (d,  $J = 2.0$  Hz, 2CHAr), 128.3 (CHAr), 128.4 (CHAr), 128.5 (d,  $J = 2.0$  Hz, CHAr), 128.5 (C-*ipso*), 129.6 (2CHAr), 133.5 (d,  $J = 4.0$  Hz, C-*ipso*), 138.8 (C-*ipso*), 162.4 (d,  $J = 12.0$  Hz, C-3), 171.1 (d,  $J = 5.0$  Hz, CO), 171.7 (d,  $J = 11.0$  Hz, CO). HRMS  $C_{23}H_{26}N_2O_5P$  [ $M + H$ ]<sup>+</sup> 441.1574; found, 441.1572. Anal. Calcd for  $C_{23}H_{26}N_2O_5P$ : C, 62.72%; H, 5.72%; N, 6.36%. Found: C, 62.87%; H, 5.82%; N, 6.18%.

**Diethyl (1*RS*,3*aSR*,6*aSR*)-4,6-Dioxo-5-(4-phenoxyphenyl)-1-phenyl-1,3*a*,4,5,6*a*-hexahydropyrrolo[3,4-*c*]pyrrole-1-phosphonate (9*ab*).** Following the general procedure, AgOAc (9 mg, 0.05 mmol), *N*-(4-phenoxyphenyl)maleimide (371 mg, 1.4 mmol), acetonitrile (7 mL), and diethyl  $\alpha$ -phenylisocyanomethylphosphonate (228 mg, 0.9 mmol) gave **9ab** (302 mg, 65%) as a white solid, after column chromatography (EtOAc). Mp 165–167 °C (EtOAc). IR (NaCl) 3488, 3057, 2984, 1783, 1715, 1628, 1488, 1242, 1187, 1024, 700, 578  $cm^{-1}$ . <sup>1</sup>H NMR (400 MHz, CDCl<sub>3</sub>, HETCOR)  $\delta$  1.19 (t,  $J = 7.0$  Hz, 3H, CH<sub>2</sub>CH<sub>3</sub>), 1.28 (t,  $J = 7.0$  Hz, 3H, CH<sub>2</sub>CH<sub>3</sub>), 3.95 (m, 1H, CH<sub>2</sub>CH<sub>3</sub>), 4.10–4.19 (m, 3H, CH<sub>2</sub>CH<sub>3</sub>), 4.25 (dd,  $J = 18.0, 8.5$  Hz, 1H, H-6*a*), 4.46–4.49 (ddd,  $J = 8.5, 3.0, 1.5$  Hz, 1H, H-3*a*), 6.64–6.67 (m, 2H, ArH), 6.87–6.89 (m, 2H, ArH), 6.96–6.98 (m, 2H, ArH), 7.12 (m, 1H, ArH), 7.30–7.38 (m, 5H, ArH), 7.69 (d,  $J = 8.0$  Hz, 2H, ArH), 8.01 (dd,  $J = 5.0, 1.5$  Hz, 1H, H-3). <sup>13</sup>C NMR (100.6 MHz)  $\delta$  16.2 (d,  $J = 4.0$  Hz, CH<sub>2</sub>CH<sub>3</sub>), 16.3 (d,  $J = 4.0$  Hz, CH<sub>2</sub>CH<sub>3</sub>), 48.2 (d,  $J = 3.0$  Hz, C-6*a*), 60.1 (C-3*a*), 63.5 (d,  $J = 7.0$  Hz, CH<sub>2</sub>CH<sub>3</sub>), 64.6 (d,  $J = 7.0$  Hz, CH<sub>2</sub>CH<sub>3</sub>), 86.2 (d,  $J = 157.0$  Hz, C-1), 118.5 (2CHAr), 119.6 (2CHAr), 124.0 (2CHAr), 125.6 (C-*ipso*), 127.5 (2CHAr), 127.9 (d,  $J = 2.0$  Hz, 2CHAr), 128.4 (d,  $J = 6.0$  Hz, CHAr), 128.6 (d,  $J = 2.0$  Hz, CHAr), 129.8 (2CHAr), 133.5 (d,  $J = 4.0$  Hz, C-*ipso*), 156.2 (C-*ipso*), 157.6 (C-*ipso*), 162.2 (d,  $J = 12.0$  Hz, C-3), 171.0 (d,  $J = 6.0$  Hz, CO), 171.7 (d,  $J = 11.0$  Hz, CO). HRMS  $C_{28}H_{28}N_2O_6P$  [ $M + H$ ]<sup>+</sup> 519.1679; found, 519.1675. Anal. Calcd for  $C_{28}H_{28}N_2O_6P$ : C, 64.86%; H, 5.25%; N, 5.40%. Found: C, 65.12%; H, 5.26%; N, 5.41%.

**Diethyl (1*RS*,3*aSR*,6*aSR*)-5-(Naphth-1-yl)-4,6-dioxo-1-phenyl-1,3*a*,4,5,6*a*-hexahydropyrrolo[3,4-*c*]pyrrole-1-phosphonate (9*ac*).** Following the general procedure, AgOAc (3 mg, 0.02 mmol), *N*-(naphth-1-yl)maleimide (100 mg, 0.5 mmol), acetonitrile (2 mL), and diethyl  $\alpha$ -phenylisocyanomethylphosphonate (76 mg, 0.3 mmol) gave **9ac** (70 mg, 49%) as a white solid, after column chromatography (EtOAc/hexane 1:1 to 9:1). Mp 197–198 °C (EtOAc). IR (ATR) 3480, 2927, 2853, 1716, 1598, 1446, 1397, 1358, 1240, 1177, 1039, 1025, 961, 775, 706, 583  $cm^{-1}$ . <sup>1</sup>H NMR (400 MHz, CDCl<sub>3</sub>, HETCOR)  $\delta$  1.17 (td,  $J = 7.0, 0.5$  Hz, 3H, CH<sub>2</sub>CH<sub>3</sub> rotamer A), 1.20 (td,  $J = 7.0, 0.5$  Hz, 3H, CH<sub>2</sub>CH<sub>3</sub> rotamer B), 1.31 (t,  $J = 7.0$  Hz, 3H, CH<sub>2</sub>CH<sub>3</sub> rotamer A), 1.31 (t,  $J = 7.0$  Hz, 3H, CH<sub>2</sub>CH<sub>3</sub> rotamer B), 3.90 (m, 1H, CH<sub>2</sub>CH<sub>3</sub> rotamer A), 3.98 (m, 1H, CH<sub>2</sub>CH<sub>3</sub> rotamer B), 4.04–4.26 (m, 6H, CH<sub>2</sub>CH<sub>3</sub> rotamer A and B), 4.43 (dd,  $J = 18.5, 9.0$  Hz, 1H, H-6*a* rotamer A), 4.46 (dd,  $J = 18.0, 8.5$  Hz, 1H, H-6*a* rotamer B), 4.63 (ddd,  $J = 9.0, 3.5, 1.5$  Hz, 1H, H-3*a* rotamer A), 4.67 (ddd,  $J = 8.5, 3.0, 1.5$  Hz, 1H, H-3*a* rotamer B), 6.33 (dd,  $J = 8.5, 1.0$  Hz, 1H, ArH rotamer A), 6.39 (dd,  $J = 7.5, 1.0$  Hz, 1H, ArH rotamer B), 7.12 (ddd,  $J = 8.5, 7.0, 1.5$  Hz, 1H, ArH rotamer A), 7.21 (dd,  $J = 7.5, 1.0$  Hz, 1H, ArH rotamer A), 7.28–7.49 (m, 12H, ArH rotamer A and B), 7.73–7.90 (m, 8H, ArH rotamer A and B), 8.12 (dd,  $J = 5.0$  Hz, 1.5 Hz, 1H, H-3 rotamer B), 8.13 (dd,  $J = 5.0, 1.5$  Hz, 1H, H-3 rotamer A). <sup>13</sup>C NMR (100.6 MHz)  $\delta$  16.2 (d,  $J = 5.0$  Hz, CH<sub>2</sub>CH<sub>3</sub> rotamer A or B), 16.3 (d,  $J = 5.0$  Hz, CH<sub>2</sub>CH<sub>3</sub> rotamer A or B), 16.3 (d,  $J = 6.0$  Hz, 2CH<sub>2</sub>CH<sub>3</sub> rotamer A or B), 48.3 (d,  $J = 2.5$  Hz, C-6*a* rotamer A), 48.6 (d,  $J = 2.5$  Hz, C-6*a* rotamer B), 60.3 (C-3*a* rotamer B), 61.0 (C-3*a* rotamer A), 63.6 (d,  $J = 7.5$  Hz, 2CH<sub>2</sub>CH<sub>3</sub> rotamer A and B), 64.7 (d,  $J = 7.0$  Hz, CH<sub>2</sub>CH<sub>3</sub> rotamer B), 64.7 (d,  $J = 7.5$  Hz, CH<sub>2</sub>CH<sub>3</sub> rotamer A), 86.2 (d,  $J = 157.5$  Hz, C-1 rotamer B), 86.5 (d,  $J = 155.0$  Hz, C-1 rotamer A), 121.2 (CHAr rotamer A), 121.6 (CHAr rotamer B), 125.0 (CHAr rotamer A), 125.1 (CHAr rotamer B), 125.7 (CHAr rotamer B), 126.0 (CHAr rotamer A), 126.3 (CHAr rotamer A), 126.5 (CHAr rotamer B), 127.0 (CHAr rotamer A), 127.2 (CHAr rotamer B), 127.6 (C-*ipso* rotamer A), 127.8 (C-*ipso* rotamer B), 127.9 (d,  $J = 2.0$  Hz, 2CHAr rotamer A), 128.0 (d,  $J = 2.0$  Hz, 2CHAr rotamer B), 128.3 (CHAr rotamer A), 128.4 (d,  $J = 6.0$  Hz, CHAr rotamer B), 128.6 (d,  $J = 2.0$  Hz, 2CHAr rotamer A),

128.7 (d,  $J = 2.5$  Hz, 2CHAr rotamer B), 128.9 (CHAr rotamer B), 129.0 (CHAr rotamer A), 130.0 (CHAr rotamer A), 130.1 (CHAr rotamer B), 133.4 (d,  $J = 4.5$  Hz, C-*ipso* rotamer A), 133.5 (d,  $J = 4.0$  Hz, C-*ipso* rotamer B), 134.1 (C-*ipso* rotamer A), 134.2 (C-*ipso* rotamer B), 162.3 (d,  $J = 11.5$  Hz, C-3 rotamer A), 162.4 (d,  $J = 12.0$  Hz, C-3 rotamer B), 171.3 (d,  $J = 5.5$  Hz, CO rotamer B), 171.4 (d,  $J = 5.5$  Hz, CO rotamer A), 171.7 (d,  $J = 12.5$  Hz, CO rotamer A), 171.9 (d,  $J = 11.5$  Hz, CO rotamer B). HRMS  $C_{26}H_{26}N_2O_5P$  [ $M + H$ ]<sup>+</sup> 477.1574; found, 477.1571. Anal. Calcd For  $C_{26}H_{26}N_2O_5P$ : C, 65.54%; H, 5.29%; N, 5.88%. Found: C, 65.34%; H, 5.12%; N, 5.65%.

**Diethyl (1*RS*,3*aSR*,6*aSR*)-5-(2-Chloropyridin-3-yl)-4,6-dioxo-1-phenyl-1,3*a*,4,5,6*a*-hexahydropyrrolo[3,4-*c*]pyrrole-1-phosphonate (9*ad*).** Following the general procedure, AgOAc (12 mg, 0.07 mmol), *N*-(2-chloropyridin-3-yl)maleimide (250 mg, 1.2 mmol), acetonitrile (6 mL), and diethyl  $\alpha$ -phenylisocyanomethylphosphonate (203 mg, 0.8 mmol) gave **9ad** (224 mg, 61%) as a white solid, after column chromatography (EtOAc). Mp 176–178 °C (EtOAc). IR (ATR) 3483, 2991, 2948, 1790, 1722, 1564, 1420, 1242, 1050, 752, 699, 574  $cm^{-1}$ . <sup>1</sup>H NMR (400 MHz, CDCl<sub>3</sub>, HETCOR)  $\delta$  1.14 (td,  $J = 7.0, 0.5$  Hz, 3H, CH<sub>2</sub>CH<sub>3</sub> rotamer A), 1.19 (td,  $J = 7.0, 0.5$  Hz, 3H, CH<sub>2</sub>CH<sub>3</sub> rotamer B), 1.28 (td,  $J = 7.0, 0.5$  Hz, 3H, CH<sub>2</sub>CH<sub>3</sub> rotamer A), 1.29 (td,  $J = 7.0, 0.5$  Hz, 3H, CH<sub>2</sub>CH<sub>3</sub> rotamer B), 3.82 (m, 1H, CH<sub>2</sub>CH<sub>3</sub> rotamer A), 3.95 (m, 1H, CH<sub>2</sub>CH<sub>3</sub> rotamer B), 4.05–4.20 (m, 6H, CH<sub>2</sub>CH<sub>3</sub> rotamer A and B), 4.36 (dd,  $J = 18.0, 8.5$  Hz, 1H, H-6*a* rotamer A), 4.38 (dd,  $J = 18.0, 8.5$  Hz, 1H, H-6*a* rotamer B), 4.53 (ddd,  $J = 8.5, 4.0, 1.5$  Hz, 1H, H-3*a* rotamer A), 4.58 (ddd,  $J = 8.5, 3.0, 1.5$  Hz, 1H, H-3*a* rotamer B), 6.59 (dd,  $J = 8.0, 2.0$  Hz, 1H, ArH rotamer B), 7.14 (dd,  $J = 8.0, 5.0$  Hz, 1H, ArH rotamer B), 7.27 (dd,  $J = 8.0, 5.0$  Hz, 1H, ArH rotamer A), 7.31–7.37 (m, 6H, 3ArH rotamer A and 3ArH rotamer B), 7.46 (dd,  $J = 8.0, 2.0$  Hz, 1H, ArH rotamer A), 7.69 (m, 2H, ArH rotamer A), 7.76 (m, 2H, ArH rotamer B), 8.02 (dd,  $J = 5.5$  Hz, 1.5 Hz, 1H, H-3 rotamer A), 8.07 (dd,  $J = 5.0, 1.5$  Hz, 1H, H-3 rotamer B), 8.36 (dd,  $J = 5.0, 2.0$  Hz, 2H, ArH rotamer A and rotamer B). <sup>13</sup>C NMR (100.6 MHz)  $\delta$  16.3 (d,  $J = 5.5$  Hz, CH<sub>2</sub>CH<sub>3</sub> rotamer A), 16.4 (d,  $J = 5.5$  Hz, CH<sub>2</sub>CH<sub>3</sub> rotamer B), 16.4 (d,  $J = 6.0$  Hz, CH<sub>2</sub>CH<sub>3</sub> rotamer A), 16.5 (d,  $J = 5.5$  Hz, CH<sub>2</sub>CH<sub>3</sub> rotamer B), 48.4 (d,  $J = 2.5$  Hz, C-6*a* rotamer A), 49.0 (d,  $J = 2.5$  Hz, C-6*a* rotamer B), 60.4 (C-3*a* rotamer A), 61.0 (C-3*a* rotamer B), 63.7 (d,  $J = 7.5$  Hz, CH<sub>2</sub>CH<sub>3</sub> rotamer A), 63.8 (d,  $J = 7.5$  Hz, CH<sub>2</sub>CH<sub>3</sub> rotamer B), 64.9 (d,  $J = 7.5$  Hz, CH<sub>2</sub>CH<sub>3</sub> rotamer B), 65.0 (d,  $J = 7.5$  Hz, CH<sub>2</sub>CH<sub>3</sub> rotamer A), 86.1 (d,  $J = 158.0$  Hz, C-1 rotamer A or B), 86.9 (d,  $J = 153.0$  Hz, C-1 rotamer A or B), 123.0 (CHAr rotamer A), 123.2 (CHAr rotamer B), 126.4 (C-*ipso* rotamer A), 126.5 (C-*ipso* rotamer B), 127.9 (d,  $J = 2.0$  Hz, 2CHAr rotamer A), 128.1 (d,  $J = 1.5$  Hz, 2CHAr rotamer B), 128.6 (d,  $J = 5.5$  Hz, 2CHAr rotamer B), 128.8 (d,  $J = 4.5$  Hz, CHAr rotamer A or B), 128.8 (CHAr rotamer A or B), 128.9 (d,  $J = 5.5$  Hz, 2CHAr rotamer A), 132.9 (d,  $J = 4.5$  Hz, C-*ipso* rotamer A), 133.6 (d,  $J = 4.0$  Hz, C-*ipso* rotamer B), 138.4 (CHAr rotamer B), 138.6 (CHAr rotamer A), 149.2 (C-*ipso* rotamer A), 149.5 (C-*ipso* rotamer B), 150.3 (CHAr rotamer A), 150.5 (CHAr rotamer B), 161.6 (d,  $J = 11.5$  Hz, C-3 rotamer A), 162.0 (d,  $J = 12.5$  Hz, C-3 rotamer B), 169.7 (d,  $J = 5.0$  Hz, CO rotamer A), 169.8 (d,  $J = 5.5$  Hz, CO rotamer B), 170.5 (d,  $J = 11.5$  Hz, CO rotamer A), 170.6 (d,  $J = 14.5$  Hz, CO rotamer B). HRMS  $C_{21}H_{22}ClN_3O_5P$  [ $M + H$ ]<sup>+</sup> 462.0980; found, 462.0980. Anal. Calcd For  $C_{21}H_{22}ClN_3O_5P$ : C, 54.61%; H, 4.58%; N, 9.10%. Found: C, 55.01%; H, 4.67%; N, 8.86%.

**Theoretical Calculations.** The study of the [3 + 2] cycloaddition reaction (Scheme 1) was performed for model systems that include the reactants (dimethyl  $\alpha$ -phenylisocyanomethylphosphonate and *N*-methylmaleimide) and a silver cation bound to acetonitrile as the catalytic moiety. Geometry optimizations were carried out using the B3LYP functional<sup>63,64</sup> and the 6-31+G(d) basis set<sup>65</sup> for all atoms but silver, which was treated with the LANL2DZ basis<sup>66</sup> in conjunction with the effective core potential for inner electrons. The nature of the stationary points (reactant, transition state, and products) was confirmed by inspection of the vibrational frequencies. Intrinsic reaction coordinate calculations<sup>67</sup> were carried out to check the connection between the transition states and the minimum energy structures. To further check the relative stabilities of transition states,

geometry optimizations were also performed using the MN15L functional.<sup>68</sup> Finally, solvation calculations were performed with the SMD version<sup>69</sup> of the IEFPCM model to take into account the contribution due to solvation in acetonitrile. All calculations were performed with Gaussian 16.<sup>70</sup>

**Binding Studies. Preparation of Cellular Membranes.** Male Swiss mice (final age 8–10 weeks) and Sprague–Dawley rats weighting 250–300 g (Harlan Interfauna Iberica, Spain) were killed, and the brain cortex was dissected and stored at  $-70\text{ }^{\circ}\text{C}$  until assays were performed. Kidneys were also obtained from male Sprague–Dawley rats. All animal experimental protocols were performed in agreement with European Union regulations (O.J. of E.C. L 358/1 18/12/1986).

Human brain samples were obtained at autopsy in the Basque Institute of Legal Medicine, Bilbao, Spain. Samples from the prefrontal cortex (Brodmann's area 9) were dissected at the time of autopsy and immediately stored at  $-70\text{ }^{\circ}\text{C}$  until assay. The study was developed in compliance with policies of research and ethical review boards for post-mortem brain studies.

To obtain cellular membranes (P2 fraction), the different samples were homogenized using an ultraturax in 30 volumes of homogenization buffer (0.25 M sucrose, 1 mM  $\text{MgCl}_2$ , 5 mM Tris-HCl, pH 7.4). The crude homogenate was centrifuged for 5 min at 1000g ( $4\text{ }^{\circ}\text{C}$ ), and the supernatant was centrifuged again for 10 min at 4000g ( $4\text{ }^{\circ}\text{C}$ ). The resultant pellet was washed twice in 20 volumes of homogenization buffer and recentrifuged in similar conditions. Protein content was measured according to the method of Bradford using BSA as standard.

**Competition Binding Assays.** The pharmacological activity of the compounds was evaluated through competition binding studies against the  $\text{I}_2$ -IR selective radioligand [ $^3\text{H}$ ]2-[(2-benzofuranyl)-2-imidazoline (2-BFI), the  $\alpha_2$ -adrenergic receptor selective radioligand [ $^3\text{H}$ ]RX821002 (2-methoxyidazoxan) or the  $\text{I}_1$ -IR selective radioligand [ $^3\text{H}$ ]clonidine. Specific binding was measured in 0.25 mL aliquots (50 mM Tris-HCl, pH 7.5) containing 100  $\mu\text{g}$  of membranes, which were incubated in 96-well plates either with [ $^3\text{H}$ ]2-BFI (2 nM) for 45 min at  $25\text{ }^{\circ}\text{C}$ , [ $^3\text{H}$ ]RX821002 (1 nM) for 30 min at  $25\text{ }^{\circ}\text{C}$ , or [ $^3\text{H}$ ]clonidine (5 nM) for 45 min at  $22\text{ }^{\circ}\text{C}$ , in the absence or presence of the competing compounds ( $10^{-12}$  to  $10^{-3}$  M, 10 concentrations). [ $^3\text{H}$ ]Clonidine binding was performed in the presence of 10  $\mu\text{M}$  adrenaline to preclude binding to  $\alpha_2$ -AR.

Incubations were terminated by separating free ligand from bound ligand by rapid filtration under vacuum (1450 Filter Mate Harvester, PerkinElmer) through GF/C glass fiber filters. The filters were then rinsed three times with 300  $\mu\text{L}$  of binding buffer, air-dried (120 min), and counted for radioactivity by liquid scintillation spectrometry using a MicroBeta TriLux counter (PerkinElmer). Specific binding was determined and plotted as a function of the compound concentration. Nonspecific binding was determined in the presence of idazoxan ( $10^{-5}$  M), a compound with well established affinity for  $\text{I}_2$ -IR and  $\alpha_2$ -adrenergic receptors, in [ $^3\text{H}$ ]2-BFI and [ $^3\text{H}$ ]RX821002 assays or rilmenidine ( $10^{-5}$  M) in [ $^3\text{H}$ ]clonidine experiments. Analyses of competition experiments to obtain the inhibition constant ( $K_i$ ) were performed by nonlinear regression using the GraphPad Prism program.  $K_i$  values were normalized to  $\text{p}K_i$  values.  $\text{I}_2$ -IR/ $\alpha_2$  selectivity index was calculated as the antilogarithm of the difference between  $\text{p}K_i$  values for  $\text{I}_2$ -IR and  $\text{p}K_i$  values for  $\alpha_2$ -AR. For [ $^3\text{H}$ ]clonidine experiments,  $\text{IC}_{50}$  values were calculated (the concentration of tested ligand that displaces 50% of specifically bound [ $^3\text{H}$ ]clonidine).

**$\text{I}_1$ -Binding Site Assay.** Kidneys were obtained from male Sprague–Dawley rats (250–280 g) and cellular membranes (P2 fractions) prepared according to established methods. [ $^3\text{H}$ ]RX821002 (2-methoxyidazoxan) binds to  $\alpha_2$ -adrenoceptor subtypes and a nonadrenoceptor imidazoline binding site in rat kidney.<sup>71</sup>

Competition binding assays were performed as previously reported with minor modifications.<sup>25</sup> [ $^3\text{H}$ ]Clonidine (5 nM, Perkin–Elmer) was bound in the presence of 10  $\mu\text{M}$  adrenaline to preclude binding to  $\alpha_2$ -adrenoceptors. The specific component was defined by 1 mM rilmenidine. Membrane aliquots (220  $\mu\text{L}$ , 0.1–0.12 mg of protein)

were incubated with 10 concentrations of the test compounds over the range  $10^{-12}$  to  $10^{-3}$  M.

Incubations were carried out in 96 well plates (final volume 250  $\mu\text{L}$ /well) in 50 mM Tris–HCl buffer (pH 7.4) supplemented with 1 mM  $\text{MgCl}_2$  at  $22\text{ }^{\circ}\text{C}$  for 45 min with agitation (400 rpm). Bound radioligand and free radioactivity were separated by rapid filtration through presoaked (0.5% polyethylenimine) glass-fiber filters (Whatman GFB). Trapped radioligand was determined by liquid scintillation counting, and the data were analyzed with GraphPad Prism version 5.0 for Windows (GraphPad Software, San Diego, CA, USA) to yield  $\text{IC}_{50}$  values (the concentration of tested ligand that displaces 50% of specifically bound [ $^3\text{H}$ ]clonidine).

**3D-QSAR Study. Data Set Preparation.** The data set composed of previously synthesized and in vitro tested bicyclic  $\alpha$ -iminophosphonates with different affinities on  $\text{I}_2$ -IR and  $\alpha_2$ -AR receptors was used for the creation of the 3D-QSAR models (Table 1). Additionally, to compare and validate our results, we have added four standards in both data sets, trazolone, idazoxan, BU99008, and LSL60101. Examined compounds cover wide range of experimental activity ( $\text{p}K_i$   $\text{I}_2$ , 3.11–10.28;  $\text{p}K_i$   $\alpha_2$ , 3.59–10.27) and structural diversity, which ensure good quality and applicability of the created 3D-QSAR models. Selection of dominant forms of studied ligands at physiological pH 7.4 was obtained by the Marvin Sketch 5.5.1.0 program.<sup>72</sup> Subsequently, they were initially preoptimized with semiempirical/PM3 (Parameterized Model revision 3) method<sup>73,74</sup> and then by ab initio Hartree–Fock/3-21G method<sup>75</sup> using Gaussian 09 software<sup>76</sup> included in Chem3D Ultra program.<sup>77</sup> Obtained ligands' conformations were used for calculation of specific molecular descriptors (grid independent descriptors, GRIND)<sup>78</sup> and 3D-QSAR model building.

**3D-QSAR Study.** 3D-QSAR models were created using Pentacle program,<sup>79</sup> which calculates GRID independent descriptors (GRIND and GRIND2) from molecular interaction fields (MIFs). Four different probes were used to calculate MIFs: O probe (hydrogen bond acceptor groups), N1 probe (hydrogen bond donor groups), DRY probe (hydrophobic interactions), and TIP probe (the shape of molecule). The grid spacing was set to 0.5. ALMOND algorithm was used for the extraction of the most relevant regions, which represent favorable interaction positions between ligand and probe. Consistently Large Auto and Cross Correlation (CLACC) algorithm was used to calculate GRIND descriptors using the correlation between same and different nodes. The smoothing window was set to 0.8 Å. Partial Least Square (PLS) regression was applied for 3D-QSAR model building. Initial number of descriptors was reduced using Fractional Factorial Design (FFD) to obtain most significant GRIND variables. The results of node–node energies between the same or a different probe were then presented as correlograms.<sup>79,80</sup>

**In vivo studies in mice.** Studies and procedures involving mouse brain dissection and extractions followed the ARRIVE<sup>81</sup> and standard ethical guidelines (European Communities Council Directive 2010/63/EU and Guidelines for the Care and Use of Mammals in Neuroscience and Behavioral Research, National Research Council 2003) and were approved by the respective Local Bioethical Committees (Universitat de les Illes Balears-CAIB and University of Barcelona-GenCat). All efforts were made to minimize the number of animals used and their suffering.

**Hypothermia.** For this study a total of 35 adult CD-1 mice and 9 adult Sprague–Dawley rats bred and housed in standard cages under defined environmental conditions ( $22\text{ }^{\circ}\text{C}$ , 70% humidity, and 12 h light/dark cycle, lights on at 8:00 AM, with free access to a standard diet and tap water) in the animal facility at the University of the Balearic Islands were used. Animals were habituated to the experimenter by being handled and weighed for 2 days prior to any experimental procedures. For the acute treatment, mice or rats received a single dose of **9d** (20 mg/kg, ip,  $n = 12$  for mice, and 20 or 35 mg/kg, ip,  $n = 3$  per dose for rats) or vehicle (1 mL/kg of DMSO, ip,  $n = 13$  for mice and  $n = 3$  for rats), while for the repeated treatment, mice were daily treated with **9d** (20 mg/kg, ip,  $n = 5$ ) or vehicle (ip,  $n = 5$ ) for 5 consecutive days. The possible hypothermic effect exerted by **9d** was evaluated by measuring changes in rectal

temperature before any drug treatment (basal value) and 1 h (for mice) or 1, 2, and 3 h (for rats) after drug injection by a rectal probe connected to a digital thermometer (Compact LCD display thermometer, SA880-1M, RS, Corby, UK). Animals were sacrificed right after the last rectal temperature measurement, and the hippocampus was freshly dissected and kept at  $-80\text{ }^{\circ}\text{C}$  for future biochemical analysis.

**Western Blot Analysis for FADD Protein.** Hippocampal sample proteins ( $40\text{ }\mu\text{g}$ ) were separated by sodium dodecyl sulfate polyacrylamide electrophoresis (SDS-PAGE) on 10% polyacrylamide minigels (Bio-Rad) and transferred onto nitrocellulose membranes by standard Western blot procedures as described previously.<sup>25</sup> The membranes were incubated overnight with anti-FADD (H-181) Ab, no. sc-5559 (Santa Cruz Biotechnology, Santa Cruz, CA) and then stripped and reprobed for  $\beta$ -actin (clone AC-15) Ab, no. A1978 (Sigma). Following secondary antibody (anti-rabbit or anti-mouse) incubation and ECL detection system (Amersham, Buckinghamshire, UK), proteins were visualized on autoradiographic films (Amersham ECL Hyperfilm). Upon densitometric scanning (GS-800 Imaging Densitometer, Bio-Rad) of immunoreactive bands (integrated optical density, IOD) the amount of FADD protein in brain samples of mice from different treatment groups was compared with that of vehicle-treated controls (100%) in the same gel. Quantification of  $\beta$ -actin contents served as a loading control (no differences between treatment groups, data not shown). Each brain sample (and target protein) was quantified in 2–4 gels, and the mean value was used as a final estimate.

**5xFAD In Vivo Experimental Design.** Female 5xFAD and WT mice, 5-months-old ( $n = 51$ ), were used to carry out cognitive and molecular analyses. The 5xFAD mouse is a double transgenic APP/PS1 that coexpresses five mutations associated with AD and that rapidly develops severe amyloid pathology with high levels of intraneuronal  $A\beta_{42}$  around 2 months of age. The model was generated by the introduction of human APP with the Swedish (K670N/M671L), Florida (I716V), and London (Val717Ile) mutations and the introduction of PS1 M146L and L286V. Moreover, 5xFAD mouse presents neuronal loss and cognitive deficits in spatial learning (at approximately four to five months).<sup>82</sup>

The animals were randomly allocated to three experimental groups: WT control ( $n = 12$ ) and 5xFAD control ( $n = 14$ ), animals administered vehicle (2-hydroxypropyl)- $\beta$ -cyclodextrin 1.8%, and 5xFAD treated with **9d 5** (mg/kg)/day ( $n = 25$ ), diluted in 1.8% (2-hydroxypropyl)- $\beta$ -cyclodextrin and administered through drinking water, up to euthanasia. Weight and water consumption were controlled each week, and the **9d** concentration was adjusted accordingly to reach the precise dose. Animals had free access to food and water and were kept under standard temperature conditions ( $22 \pm 2\text{ }^{\circ}\text{C}$ ) and 12 h/12 h light–dark cycles (300 lx/0 lx).

After 4 weeks of treatment period, animals were subjected to cognitive tests to study the effect of treatment on learning and memory, including short- and long-term memory (NORT). Mice were euthanized 3 days after the behavioral test completion by cervical dislocation. Brains were immediately removed from the skull, and the hippocampus was then isolated and frozen on powdered dry ice. They were maintained at  $-80\text{ }^{\circ}\text{C}$  for biochemical experiments.

**Behavioral Testing: NORT.** In brief, mice were placed in a black L-shape maze consisting of two arms at  $90^{\circ}$ , 25 cm long, 20 cm high, and 5 cm wide. The mice were habituated to the apparatus for 10 min on 3 consecutive days in the habituation phase. Afterward, on day 4, the training session took place, in which two identical objects (A) were placed in the maze and the mice were allowed to explore freely for 10 min. Two hours after training sessions, one of the objects was replaced with a novel object (B) to assess short-term-memory. Again, the amount of time spent exploring each object was scored. During this second trial, objects A and B were placed in the maze, and the times that the animal took to explore the new object (TN) and the old object (TO) were recorded. A discrimination index (DI) was calculated, defined as  $(\text{TN} - \text{TO})/(\text{TN} + \text{TO})$ . Twenty-four hours after the acquisition trial, the mice were tested again to assess long-term memory, with a new object substituting object B and a new DI

calculated. Exploration of an object by a mouse was defined as pointing the nose toward the object at a distance  $\leq 2\text{ cm}$  or touching it with the nose. Turning or sitting around the object was not considered exploration. To avoid object preference biases, objects A and B were counterbalanced so that one-half of the animals in each experimental group were first exposed to object A and then to object B, whereas the other half first saw object B and then object A. All sessions were videotaped, and the time spent with each object was manually recorded. The maze, the surface, and the objects were cleaned with 70% ethanol between the animal trials to eliminate olfactory cues.

**Determination of Oxidative Stress.** Hydrogen peroxide from brain samples of 10 mice of each group was measured as an indicator of OS, and it was quantified using the Hydrogen Peroxide Assay Kit (Sigma-Aldrich, St. Louis, MI) according to the manufacturer's instructions.

**RNA Extraction and Gene Expression Determination.** Total RNA isolation was carried out using TRIzol reagent according to manufacturer's instructions. The yield, purity, and quality of RNA were determined spectrophotometrically with a NanoDrop ND-1000 (Thermo Scientific) apparatus and an Agilent 2100B Bioanalyzer (Agilent Technologies). RNAs with 260/280 ratios and RNA integrity number (RIN) higher than 1.9 and 7.5, respectively, were selected. Reverse transcription-polymerase chain reaction (RT-PCR) was performed as follows:  $2\text{ }\mu\text{g}$  of mRNA (mRNA) was reverse-transcribed using the High Capacity cDNA Reverse Transcription Kit (Applied Biosystems). Real-time quantitative PCR (qPCR) from 48 mice of both strains ( $n = 4\text{--}6$  per group) was used to quantify mRNA expression of OS and inflammatory genes.

SYBR Green real-time PCR was performed on a Step One Plus Detection System (Applied-Biosystems) employing SYBR Green PCR Master Mix (Applied-Biosystems). Each reaction mixture contained  $6.75\text{ }\mu\text{L}$  ( $2\text{ }\mu\text{g}$ ) of complementary DNA (cDNA),  $0.75\text{ }\mu\text{L}$  of each primer (of which concentration was 100 nM), and  $6.75\text{ }\mu\text{L}$  of SYBR Green PCR Master Mix (2 $\times$ ).

TaqMan-based real-time PCR (Applied Biosystems) was also performed in a Step One Plus Detection System (Applied-Biosystems). Each  $20\text{ }\mu\text{L}$  of TaqMan reaction contained  $9\text{ }\mu\text{L}$  (25 ng) of cDNA,  $1\text{ }\mu\text{L}$  of 20 $\times$  probe of TaqMan Gene Expression Assays, and  $10\text{ }\mu\text{L}$  of 2 $\times$  TaqMan Universal PCR Master Mix.

Data were analyzed utilizing the comparative cycle threshold (Ct) method ( $\Delta\Delta\text{Ct}$ ), where the housekeeping gene level was used to normalize differences in sample loading and preparation.<sup>49</sup> Normalization of expression levels was performed with  $\beta$ -actin gene for SYBR Green-based real-time PCR and TATA-binding protein (*Tbp*) gene for TaqMan-based real-time PCR. Primers sequences and TaqMan probes used in this study are presented in Table S10. Each sample was analyzed in duplicate, and the results represent the  $n$ -fold difference of the transcript levels among different groups.

## ■ ASSOCIATED CONTENT

### SI Supporting Information

The Supporting Information is available free of charge at <https://pubs.acs.org/doi/10.1021/acs.jmedchem.9b02080>.

Experimental procedures for synthesis of **10a–10c** and **11**, theoretical calculations, 3D-QSAR study, in vitro BBB assay, DMPK assays, receptor characterization panel, in vivo data, tables of  $^1\text{H}$  and  $^{13}\text{C}$  spectra, and X-ray crystallography data (PDF)

Molecular formula strings (CSV)

## ■ AUTHOR INFORMATION

### Corresponding Author

Carmen Escolano – Laboratory of Medicinal Chemistry (Associated Unit to CSIC), Department of Pharmacology, Toxicology and Medicinal Chemistry, Faculty of Pharmacy and Food Sciences, and Institute of Biomedicine (IBUB), University



of Barcelona, E-08028 Barcelona, Spain; [orcid.org/0000-0002-9117-8239](https://orcid.org/0000-0002-9117-8239); Phone: +34 934024542; Email: cescolano@ub.edu

## Authors

**Sònia Abás** – Laboratory of Medicinal Chemistry (Associated Unit to CSIC), Department of Pharmacology, Toxicology and Medicinal Chemistry, Faculty of Pharmacy and Food Sciences, and Institute of Biomedicine (IBUB), University of Barcelona, E-08028 Barcelona, Spain

**Sergio Rodríguez-Arévalo** – Laboratory of Medicinal Chemistry (Associated Unit to CSIC), Department of Pharmacology, Toxicology and Medicinal Chemistry, Faculty of Pharmacy and Food Sciences, and Institute of Biomedicine (IBUB), University of Barcelona, E-08028 Barcelona, Spain

**Andrea Bagán** – Laboratory of Medicinal Chemistry (Associated Unit to CSIC), Department of Pharmacology, Toxicology and Medicinal Chemistry, Faculty of Pharmacy and Food Sciences, and Institute of Biomedicine (IBUB), University of Barcelona, E-08028 Barcelona, Spain

**Christian Griñán-Ferré** – Pharmacology Section, Toxicology and Medicinal Chemistry, Faculty of Pharmacy and Food Sciences, and Institut de Neurociències, University of Barcelona, E-08028 Barcelona, Spain

**Foteini Vasilopoulou** – Pharmacology Section, Toxicology and Medicinal Chemistry, Faculty of Pharmacy and Food Sciences, and Institut de Neurociències, University of Barcelona, E-08028 Barcelona, Spain

**Iria Brocos-Mosquera** – Department of Pharmacology, University of the Basque Country, UPV/EHU, E-48940 Leioa, Bizkaia, Spain

**Carolina Muguruza** – Department of Pharmacology, University of the Basque Country, UPV/EHU, E-48940 Leioa, Bizkaia, Spain; [orcid.org/0000-0002-0477-5757](https://orcid.org/0000-0002-0477-5757)

**Belén Pérez** – Department of Pharmacology, Therapeutic and Toxicology, Autonomous University of Barcelona, E-08193 Barcelona, Spain

**Elies Molins** – Institut de Ciència de Materials de Barcelona (CSIC), E-08193 Cerdanyola, Spain; [orcid.org/0000-0003-1012-0551](https://orcid.org/0000-0003-1012-0551)

**F. Javier Luque** – Department of Nutrition, Food Sciences and Gastronomy, School of Pharmacy and Food Sciences, Institute of Biomedicine (IBUB), and Institute of Theoretical and Computational Chemistry (IQTCUB), University of Barcelona, E-08921 Santa Coloma de Gramanet, Spain; [orcid.org/0000-0002-8049-3567](https://orcid.org/0000-0002-8049-3567)

**Pilar Pérez-Lozano** – Unit of Pharmaceutical Technology, Pharmacy and Pharmaceutical Technology, and Physical Chemistry Department, Faculty of Pharmacy and Food Sciences, University of Barcelona, E-08028 Barcelona, Spain; [orcid.org/0000-0001-6899-066X](https://orcid.org/0000-0001-6899-066X)

**Steven de Jonghe** – Rega Institute for Medical Research, Katholieke Universiteit Leuven, 3000 Leuven, Belgium; [orcid.org/0000-0002-3872-6558](https://orcid.org/0000-0002-3872-6558)

**Dirk Daelemans** – Rega Institute for Medical Research, Katholieke Universiteit Leuven, 3000 Leuven, Belgium

**Lieve Naesens** – Rega Institute for Medical Research, Katholieke Universiteit Leuven, 3000 Leuven, Belgium

**José Brea** – Innopharma screening platform, BioFarma research group, Centro de Investigación en Medicina Molecular y Enfermedades Crónicas (CIMUS), Universidad de Santiago de Compostela, 15782 Santiago de Compostela, Spain

**M. Isabel Loza** – Innopharma screening platform, BioFarma research group, Centro de Investigación en Medicina Molecular y Enfermedades Crónicas (CIMUS), Universidad de Santiago de Compostela, 15782 Santiago de Compostela, Spain

**Elena Hernández-Hernández** – IUNICS University of the Balearic Islands (UIB), and Health Research Institute of the Balearic Islands (IdISBa), E-07122 Palma de Mallorca, Spain

**Jesús A. García-Sevilla** – IUNICS University of the Balearic Islands (UIB), and Health Research Institute of the Balearic Islands (IdISBa), E-07122 Palma de Mallorca, Spain

**M. Julia García-Fuster** – IUNICS University of the Balearic Islands (UIB), and Health Research Institute of the Balearic Islands (IdISBa), E-07122 Palma de Mallorca, Spain

**Milica Radan** – Department of Pharmaceutical Chemistry, Faculty of Pharmacy, University of Belgrade, 11000 Belgrade, Serbia

**Teodora Djikic** – Department of Pharmaceutical Chemistry, Faculty of Pharmacy, University of Belgrade, 11000 Belgrade, Serbia

**Katarina Nikolic** – Department of Pharmaceutical Chemistry, Faculty of Pharmacy, University of Belgrade, 11000 Belgrade, Serbia

**Mercè Pallàs** – Pharmacology Section, Toxicology and Medicinal Chemistry, Faculty of Pharmacy and Food Sciences, and Institut de Neurociències, University of Barcelona, E-08028 Barcelona, Spain; [orcid.org/0000-0003-3095-4254](https://orcid.org/0000-0003-3095-4254)

**Luis F. Callado** – Department of Pharmacology, University of the Basque Country, UPV/EHU, E-48940 Leioa, Bizkaia, Spain

Complete contact information is available at:

<https://pubs.acs.org/10.1021/acs.jmedchem.9b02080>

## Author Contributions

▲S.A. and S.R.-A. contributed equally to this work. C.G.-F., J.A.G.-S., M.J.G.-F., M.P., and C.E. designed the study. S.A., S.R.-A., and A.B. synthesized, purified, and characterized the I<sub>2</sub>-IR ligands. C.G.-F., F.V., and M.P. carried out the behavior and cognition studies and cellular parameter determination. I.B.-M., C.M., and L.F.C. performed the binding experiments. B.P. performed the PAMPA–BBB permeation experiments. E.M. conducted the X-ray crystallographic analysis. F.J.L. was in charge of the theoretical studies. P.P.-L. performed the physicochemical studies. S.L., D.D., and L.N. carried out the cytotoxicity studies. J.B. and M.I.L. determined the ADMET parameters. E.H.-H., J.A.G.-S., and M.J.G.-S. performed the hypothermic studies and analysis of FADD protein content. M.R., T.D., and K.N. carried out the 3D-QSAR study. C.G.-F., F.J.L., P.P.-L., J.A.G.-S., M.J.G.-S., L.F.C., K.N., M.P., and C.E. contributed to writing the manuscript. All the authors have read and approved the final version of the manuscript.

## Notes

The authors declare the following competing financial interest(s): C.E., M.P., C.G.-F., S.A., L.-F.C., and J.A.G.-S. are inventors of the patent application on I<sub>2</sub> imidazoline receptor ligands, WO2019/121853 (reference 29).

## ACKNOWLEDGMENTS

We strongly acknowledge the advice of Dr. Andrés G. Fernández (our mentor in the CaixaImpulse 2018 program) for invaluable advice. This study was supported by the Ministerio de Economía y Competitividad of Spain (SAF2016-77703) and the Basque Government (IT1211-19).

The project leading to these results has received funding from “la Caixa” Foundation (ID 100010434) under agreement CI18-00002. This activity has received funding from the European Institute of Innovation and Technology (EIT). This body of the European Union receives support from the European Union’s Horizon 2020 research and innovation programme. C.G.-F, F.V., C.E., S.R.-A., A.B., and M.P. belong to 2017SGR106 (Generalitat de Catalunya). J.A.G.-S. is a member emeritus of the Institut d’Estudis Catalans. Financial support was provided for F.V. (University of Barcelona, APIF\_2017), S.R.-A. (Generalitat de Catalunya, 2018FI\_B\_00227), A.B. (Institute of Biomedicine UB\_2018), C.M. (Marie Skłodowska-Curie Actions Individual Fellowships H2020-MSCA-IF-2016, ID747487), and E.H.-H. (Consejería de Innovación, Investigación y Turismo del Gobierno de las Islas Baleares y del Fondo Social Europeo, FPI/2102/2018). F.J.L. acknowledges the financial support from the Spanish Ministerio de Economía, Industria y Competitividad (grant MDM-2017-0767; AEI/FEDER UE), and Generalitat de Catalunya (grant 2017SGR1746). M.R., T.D., and K.N. kindly acknowledge Ministry of Science and Technological Development of the Republic of Serbia, Project Contract No. 172033, and HORIZON2020-COST-Action CA18133 ERNEST: European Research Network on Signal Transduction.

## ABBREVIATIONS

$\alpha_2$ -AR,  $\alpha_2$  adrenergic receptor; 2-BFI, 2-[(2-benzofuranyl)-2-imidazole]; B3LYP, 3-parameter hybrid Becke exchange/Lee–Yang–Parr correlation; BU224, 2-(4,5-dihydroimidazol-2-yl)quinoline; CCK<sub>A</sub>, cholecystokinin type A receptor; CCK<sub>B</sub>, cholecystokinin type B receptor; *Cxcl10*, C-X-C motif chemokine 10 gene; DI, discrimination index; 5xFAD, mouse model of amyloid deposition expressing five familial AD (FAD) mutations; FADD, Fas-associated protein with death domain; GRIND, Grid-independent descriptors; HeLa, human cervical carcinoma cell line; 4-HNE, 4-hydroxy-2-nonenal; Hmox1, heme oxygenase (decycling) 1; H<sub>2</sub>O<sub>2</sub>, hydrogen peroxide; IR, imidazole receptors; I<sub>1</sub>-IRs, imidazole I<sub>1</sub> receptors; I<sub>2</sub>-IRs, imidazole I<sub>2</sub> receptors; I<sub>3</sub>-IRs, imidazole I<sub>3</sub> receptors; LANLD2DZ, Los Alamos National Laboratory 2-double-z (density functional theory); MDCK, Madin-Darby canine kidney; MT4, human T-lymphocyte; MRC-S, human embryonic lung fibroblast; NORT, novel object recognition test; iNOS, inducible nitric oxide synthase; OS, oxidative stress; PhosMic, diethyl isocyanomethylphosphonate;  $P_e$ , permeability;  $pK_i$ , antilog of  $K_i$ ;  $pK_{iL}$ , low  $pK_i$  binding site;  $pK_{iH}$ , high  $pK_i$  binding site; 3D-QSAR, three-dimensional quantitative structure–activity relationship; QM, quantum mechanical; [<sup>3</sup>H]-RX821002, <sup>3</sup>H-labeled 2-methoxyidazoxan; SAMP8, senescence accelerated mouse-prone 8; SEM, standard error of the mean; *Tnf- $\alpha$* , tumor necrosis factor  $\alpha$  gene; TPSA, topological polar surface area; Vero, African green monkey kidney cell line; WT, WT mice

## REFERENCES

- (1) Bousquet, P.; Feldman, J.; Schwartz, J. Central cardiovascular effects of alpha adrenergic drugs: differences between catecholamines and imidazolines. *J. Pharmacol. Exp. Ther.* **1984**, *230*, 232–236.
- (2) Bousquet, P.; Hudson, A.; García-Sevilla, J. A.; Li, J.-X. Imidazole receptor system: the past, the present, and the future. *Pharmacol. Rev.* **2020**, *72*, 50–79.
- (3) Lowry, J. A.; Brown, J. T. Significance of the imidazole receptors in toxicology. *Clin. Toxicol.* **2014**, *52*, 454–469.
- (4) Regunathan, S.; Reis, D. J. Imidazole receptors and their endogenous ligands. *Annu. Rev. Pharmacol. Toxicol.* **1996**, *36*, 511–544.
- (5) Fenton, C.; Keating, G. M.; Lyseng-Williamson, K. A. Moxonidine: a review of its use in essential hypertension. *Drugs* **2006**, *66*, 477–496.
- (6) Reid, J. L. Rilmenidine: a clinical overview. *Am. J. Hypertens.* **2000**, *13*, 106S–111S.
- (7) Chan, S. L.; Brown, C. A.; Scarpello, K. E.; Morgan, N. G. The imidazole site involved in control of insulin secretion: characteristics that distinguish it from I<sub>1</sub>- and I<sub>2</sub>-sites. *Br. J. Pharmacol.* **1994**, *112*, 1065–1070.
- (8) Li, J. X. Imidazole I<sub>2</sub> receptors: an update. *Pharmacol. Ther.* **2017**, *178*, 48–56.
- (9) Li, J. X.; Zhang, Y. Imidazole I<sub>2</sub> receptors: target for new analgesics? *Eur. J. Pharmacol.* **2011**, *658*, 49–56.
- (10) Regunathan, S.; Feinstein, D. L.; Reis, D. J. Anti-proliferative and anti-inflammatory actions of imidazole agents. Are imidazole receptors involved? *Ann. N. Y. Acad. Sci.* **1999**, *881*, 410–419.
- (11) Smith, K. L.; Jessop, D. S.; Finn, D. P. Modulation of stress by imidazole binding sites: implications for psychiatric disorders. *Stress* **2009**, *12*, 97–114.
- (12) Martín-Gómez, J. I.; Ruiz, J.; Callado, L. F.; Garibi, J. M.; Aguinaco, L.; Barturen, F.; Meana, J. J. Increased density of I<sub>2</sub>-imidazole receptors in human glioblastomas. *NeuroReport* **1996**, *7*, 1393–1396.
- (13) Callado, L. F.; Martín-Gómez, J. I.; Ruiz, J.; Garibi, J. M.; Meana, J. J. Imidazole I<sub>2</sub> receptors density increases with the malignancy of human gliomas. *J. Neurol., Neurosurg. Psychiatry* **2004**, *75*, 785–787.
- (14) Reynolds, G. P.; Boulton, R. M.; Pearson, S. J.; Hudson, A. L.; Nutt, D. J. Imidazole binding sites in Huntington’s and Parkinson’s disease putamen. *Eur. J. Pharmacol.* **1996**, *301*, R19–R21.
- (15) Gargalidis-Moudanos, C.; Pizzinat, N.; Javoy-Agid, F.; Remaury, A.; Parini, A. I<sub>2</sub>-imidazole binding sites and monoamine oxidase activity in human postmortem brain from patients with Parkinson’s disease. *Neurochem. Int.* **1997**, *30*, 31–36.
- (16) Meana, J. J.; Barturen, F.; Martín, I.; García-Sevilla, J. A. Evidence of increased non-adrenoreceptor [<sup>3</sup>H]idazoxan binding sites in the frontal cortex of depressed suicide victims. *Biol. Psychiatry* **1993**, *34*, 498–501.
- (17) García-Sevilla, J.; Escribá, P. V.; Sastre, M.; Walzer, C.; Busquets, X.; Jaquet, G.; Reis, D. J.; Guimón, J. Immunodetection and quantitation of imidazole receptor proteins in platelets of patients with major depression and in brains of suicide victims. *Arch. Gen. Psychiatry* **1996**, *53*, 803–810.
- (18) Ruiz, J.; Martín, I.; Callado, L. F.; Meana, J. J.; Barturen, F.; García-Sevilla, J. A. Non-adrenoreceptor [<sup>3</sup>H]idazoxan binding sites (I<sub>2</sub>-imidazole sites) are increased in postmortem brain from patients with Alzheimer’s disease. *Neurosci. Lett.* **1993**, *160*, 109–112.
- (19) García-Sevilla, J. A.; Escribá, P. V.; Walzer, C.; Bouras, C.; Guimón, J. Imidazole receptor proteins in brains of patients with Alzheimer’s disease. *Neurosci. Lett.* **1998**, *247*, 95–98.
- (20) Comi, E.; Lanza, M.; Ferrari, F.; Mauri, V.; Caselli, G.; Rovati, L. C. Efficacy of CR4056, a first-in-class imidazole-2 analgesic drug, in comparison with naproxen in two rat models of osteoarthritis. *J. Pain Res.* **2017**, *10*, 1033–1043.
- (21) Rovati, L. C.; Brambilla, N.; Blicharski, T.; Connell, J.; Vitalini, C.; Bonazzi, A.; Giacobelli, G.; Girolami, F.; D’Amato, M. Efficacy and safety of the first-in-class imidazole-2 receptor ligand CR4056 in pain from knee osteoarthritis and disease phenotypes: a randomized, double-blind, placebo-controlled phase 2 trial. *Osteoarthritis and Cartilage* **2020**, *28*, 22.
- (22) Tyacke, R. J.; Myers, J. F. M.; Venkataraman, A. V.; Mick, I.; Turton, S.; Passchier, J.; Husbands, S. M.; Rabiner, E. A.; Gunn, R. N.; Murphy, P. S.; Parker, C. A.; Nutt, D. J. Evaluation of <sup>11</sup>C-

- BU99008, a PET ligand for the imidazoline<sub>2</sub> binding site in human brain. *J. Nucl. Med.* **2018**, *59*, 1597–1602.
- (23) Wilson, H.; Dervenoulas, G.; Pagano, G.; Tyacke, R. J.; Polychronis, S.; Myers, J.; Gunn, R. N.; Rabiner, E. A.; Nutt, D.; Politis, M. Imidazoline 2 binding sites reflecting astroglia pathology in Parkinson's disease: an *in vivo* <sup>11</sup>C-BU99008 PET study. *Brain* **2019**, *142*, 3116.
- (24) Dardonville, C.; Rozas, I. Imidazoline binding sites and their ligands: an overview of the different chemical structures. *Med. Res. Rev.* **2004**, *24*, 639–661.
- (25) Abás, S.; Erdozain, A. M.; Keller, B.; Rodríguez-Arévalo, S.; Callado, L. F.; García-Sevilla, J. A.; Escolano, C. Neuroprotective effects of a structurally new family of high affinity imidazoline I<sub>2</sub> receptors ligands. *ACS Chem. Neurosci.* **2017**, *8*, 737–742.
- (26) Abás, S.; Estarellas, C.; Luque, F. J.; Escolano, C. Easy access to (2-imidazolyl-4-yl)phosphonates by a microwave assisted multi-component reaction. *Tetrahedron* **2015**, *71*, 2872–2881.
- (27) Griñán-Ferré, C.; Vasilopoulou, F.; Abás, S.; Rodríguez-Arévalo, S.; Bagán, A.; Sureda, F. X.; Pérez, B.; Callado, L. F.; García-Sevilla, J. A.; García-Fuster, M. J.; Escolano, C.; Pallás, M. Behavioral and cognitive improvement induced by novel imidazoline I<sub>2</sub> receptor ligands in female SAMP8 mice. *Neurotherapeutics* **2019**, *16*, 416–431.
- (28) Arróniz, C.; Molina, J.; Abás, S.; Molins, E.; Campanera, J. M.; Luque, F. J.; Escolano, C. First diastereoselective [3 + 2] cycloaddition reaction of diethyl isocyanomethylphosphonate and maleimides. *Org. Biomol. Chem.* **2013**, *11*, 1640–1649.
- (29) Escolano, C.; Pallás, M.; Griñán-Ferré, C.; Abás, S.; Callado, L. F.; García-Sevilla, J. A. Synthetic I<sub>2</sub> Imidazoline Receptor Ligands for Prevention or Treatment of Human Brain Disorders. WO 2019/121853 A1, June 27, 2019.
- (30) Grijalba, B.; Callado, L. F.; Meana, J. J.; García-Sevilla, J. A.; Pazos, A.  $\alpha_2$ -Adrenoceptor subtypes in the human brain: a pharmacological delineation of [<sup>3</sup>H]RX-821002 binding to membranes and tissue sections. *Eur. J. Pharmacol.* **1996**, *310*, 83–93.
- (31) Callado, L. F.; Maeztu, A. I.; Ballesteros, J.; Gutiérrez, M.; Meana, J. J. Differential [<sup>3</sup>H]idazoxan and [<sup>3</sup>H]2-(2-benzofuranyl)-2-imidazoline (2-BFI) binding to imidazoline I<sub>2</sub> receptors in human postmortem frontal cortex. *Eur. J. Pharmacol.* **2001**, *423*, 109–114.
- (32) BU99008 was prepared according to the literature procedure: Tyacke, R. J.; Fisher, A.; Robinson, E. S. J.; Grundt, P.; Turner, E. M.; Husbands, S. M.; Hudson, A. L.; Parker, C. A.; Nutt, D. J. Evaluation and initial *in vitro* and *in vivo* characterization of the potential positron emission tomography ligand, BU99008 (2-(4,5-dihydro-1H-imidazol-2-yl)-1-methyl-1H-indole), for the imidazoline<sub>2</sub> binding site. *Synapse* **2012**, *66*, 542–551.
- (33) CR4056 was prepared according to the literature procedure: Giordani, A.; Mandelli, S.; Verpilio, I.; Zanzola, S.; Tarchino, F.; Caselli, G.; Piepoli, T.; Mazzari, S.; Makovec, F.; Rovati, L. C. 6-1H-Imidazo-quinazoline and Quinolines Derivatives, New Potent Analgesics and Anti-inflammatory Agents. US 8,193,353 B2, June 5, 2012.
- (34) Lione, L. A.; Nutt, D. J.; Hudson, A. L. [<sup>3</sup>H]-2-(2-benzofuranyl)-2-imidazoline: a new selective high affinity radioligand for the study of rabbit brain imidazoline I<sub>2</sub> receptors. *Eur. J. Pharmacol.* **1996**, *304*, 221–229.
- (35) Alemany, R.; Olmos, G.; García-Sevilla, J. A. Labelling I<sub>2B</sub>-imidazoline receptors by [<sup>3</sup>H]-2-(2-benzofuranyl)-2-imidazoline (2-BFI) in rat brain and liver: characterization, regulation and relation to monoamine oxidase enzymes. *Naunyn-Schmiedeberg's Arch. Pharmacol.* **1997**, *356*, 39–47.
- (36) Lione, L. A.; Nutt, D. J.; Hudson, A. L. Characterisation and localisation of [<sup>3</sup>H]-2-(2-benzofuranyl)-2-imidazoline binding in rat brain: a selective ligand for imidazoline I<sub>2</sub> receptors. *Eur. J. Pharmacol.* **1998**, *353*, 123–135.
- (37) Quaglia, W.; Bousquet, P.; Pignini, M.; Carotti, A.; Carrieri, A.; Döntenwill, M.; Gentili, F.; Giannella, M.; Maranca, F.; Piergentili, A.; Brasili, L. 2-(2-Phenylcyclopropyl)imidazolines: reversed enantioselective interaction at I<sub>1</sub> and I<sub>2</sub> imidazoline receptors. *J. Med. Chem.* **1999**, *42*, 2737–2740.
- (38) Alemany, R.; Olmos, G.; Escrivá, P. V.; Menargues, A.; Obach, R.; García-Sevilla, J. A. LSL60101, a selective ligand for imidazoline I<sub>2</sub> receptors, on glial fibrillary acidic protein concentration. *Eur. J. Pharmacol.* **1995**, *280*, 205–210.
- (39) Ferrari, F.; Fiorentino, S.; Mennuni, L.; Garofalo, P.; Letari, O.; Mandelli, S.; Giordani, A.; Lanza, M.; Caselli, G. Analgesic efficacy of CR4056, a novel imidazoline-2 receptor ligand, in rat models of inflammatory and neuropathic pain. *J. Pain Res.* **2011**, *4*, 111–115.
- (40) *Pentacle*, version 1.0.6, Molecular Discovery Ltd., Perugia, Italy, 2009.
- (41) Ghosh, J.; Lawless, M. S.; Waldman, M.; Gombar, V.; Fraczkiwicz, R. Modeling ADMET. *Methods Mol. Biol.* **2016**, *1425*, 63–83.
- (42) ADMET Predictor, v. 9.5, Simulations Plus Inc., Lancaster, CA, USA, 2019, <https://www.simulations-plus.com>.
- (43) Daina, A.; Michielin, O.; Zoete, V. Swiss ADME: a free web tool to evaluate pharmacokinetics, drug-likeness and medicinal chemistry friendliness of small mol. *Sci. Rep.* **2017**, *7*, 42717.
- (44) Biopharmaceutics classification system-based biowaivers, International council for harmonisation of technical requirements for pharmaceutical for human use. [https://www.ich.org/fileadmin/Public\\_Web\\_Site/ICH\\_Products/Guidelines/Multidisciplinary/M9/M9EWG\\_DraftGuideline\\_Step2\\_2018\\_0606.pdf](https://www.ich.org/fileadmin/Public_Web_Site/ICH_Products/Guidelines/Multidisciplinary/M9/M9EWG_DraftGuideline_Step2_2018_0606.pdf).
- (45) International council on harmonisation of technical requirements for registration of pharmaceuticals for human use. ICH harmonized tripartite guideline. "Stability testing of new drug substance and products". Q1A (R2), 2003.
- (46) For information on the Eurofins Lead Profiling Screen, see <http://www.eurofins.com>.
- (47) Cawston, E. E.; Miller, L. J. Therapeutic potential for novel drugs targeting the type 1 cholecystokinin receptor. *Br. J. Pharmacol.* **2010**, *159*, 1009–1021.
- (48) Keller, B.; García-Sevilla, J. A. Inhibitory effects of imidazoline receptor ligands on basal and kainic acid-induced neurotoxic signalling in mice. *J. Psychopharmacol.* **2016**, *30*, 875–886.
- (49) Thorn, D. A.; An, X. F.; Zhang, Y.; Pignini, M.; Li, J. X. Characterization of the hypothermic effects of imidazoline I<sub>2</sub> receptor agonists in rats. *Br. J. Pharmacol.* **2012**, *166*, 1936–1945.
- (50) Craven, J. A.; Conway, E. L. Effects of alpha 2-adrenoceptor antagonists and imidazoline 2-receptor ligands on neuronal damage in global ischaemia in the rat. *Clin. Exp. Pharmacol. Physiol.* **1997**, *24*, 204–207.
- (51) Marion, D. W.; Penrod, L. E.; Kelsey, S. F.; Obrist, W. D.; Kochanek, P. M.; Palmer, A. M.; Wisniewski, S. R.; DeKosky, S. T. Treatment of traumatic brain injury with moderate hypothermia. *N. Engl. J. Med.* **1997**, *336*, 540–546.
- (52) Maier, C. M.; Ahern, K. V.; Cheng, M. L.; Lee, J. E.; Yenari, M. A.; Steinberg, G. K. Optimal depth and duration of mild hypothermia in focal model of transient cerebral ischemia: effects on neurologic outcome, infarct size, apoptosis, and inflammation. *Stroke* **1998**, *29*, 2171–2180.
- (53) Hernández-Hernández, E.; Miralles, A.; Esteban, S.; García-Fuster, M. J. Improved age-related deficits in cognitive performance and affective-like behavior following acute, but not repeated, 8-OH-DPAT treatments in rats: regulation of hippocampal FADD. *Neurobiol. Aging* **2018**, *71*, 115–126.
- (54) Hernández-Hernández, E.; Miralles, A.; Esteban, S.; García-Fuster, M. J. Repeated treatment with the  $\alpha_2$ -adrenoceptor agonist UK-14304 improves cognitive performance in middle-age rats: role of hippocampal Fas-associated death domain. *J. Psychopharmacol.* **2018**, *32*, 248–255.
- (55) Bilkei-Gorzo, A. Genetic mouse models of brain ageing and Alzheimer's disease. *Pharmacol. Ther.* **2014**, *142*, 244–257.
- (56) Antunes, M.; Biala, G. The novel object recognition memory: neurobiology, test procedure, and its modifications. *Cogn. Process.* **2012**, *13*, 93–110.

- (57) Heneka, M. T.; McManus, R. M.; Latz, E. Inflammation signalling in brain function and neurodegenerative disease. *Nat. Rev. Neurosci.* **2018**, *19*, 610–621.
- (58) Gao, H.-M.; Zhou, H.; Hong, J. S. Oxidative stress, neuroinflammation, and neurodegeneration. In *Neuroinflammation and neurodegeneration*; Peterson, P. K., Toborek, M., Eds.; Springer: New York, 2014; pp 81–104.
- (59) Ekert, J. O.; Gould, R. L.; Reynolds, G.; Howard, R. J. TNF alpha inhibitors in Alzheimer's disease: a systematic review. *Int. J. Geriatr. Psychiatry* **2018**, *33*, 688–694.
- (60) Iadecola, C.; Zhang, F.; Casey, R.; Nagayama, M.; Ross, M. E. Delayed reduction of ischemic brain injury and neurological deficits in mice lacking the inducible nitric oxide synthase gene. *J. Neurosci.* **1997**, *17*, 9157–9164.
- (61) Schipper, H. M.; Song, W.; Tavitian, A.; Cressatti, M. The sinister face of heme oxygenase-1 in brain aging and disease. *Prog. Neurobiol.* **2019**, *172*, 40–70.
- (62) Griñán-Ferré, C.; Sarroca, S.; Ivanova, A.; Puigoriol-Illamola, D.; Aguado, F.; Camins, A.; Sanfeliu, C.; Pallàs, M. Epigenetic mechanisms underlying cognitive impairment and Alzheimer disease hallmarks in 5xFAD mice. *Aging* **2016**, *8*, 664–684.
- (63) Becke, A. D. Density-functional thermochemistry. III. The role of exact exchange. *J. Chem. Phys.* **1993**, *98*, 5648.
- (64) Lee, C.; Yang, W.; Parr, R. G. Development of the Colle-Salvetti correlation-energy formula into a functional of the electron density. *Phys. Rev. B: Condens. Matter Mater. Phys.* **1988**, *37*, 785.
- (65) Clark, T.; Chandrasekhar, J.; Spitznagel, G. W.; Schleyer, P. v. R. Efficient diffuse function-augmented basis sets for anion calculations. III. The 3-21+G basis set for first-row elements, Li–F. *J. Comput. Chem.* **1983**, *4*, 294–301.
- (66) Wadt, W. R.; Hay, P. J. Ab initio effective core potentials for molecular calculations. Potentials for K to Au including the outermost core orbitals. *J. Chem. Phys.* **1985**, *82*, 284.
- (67) Gonzalez, C.; Schlegel, H. B. An improved algorithm for reaction path following. *J. Chem. Phys.* **1989**, *90*, 2154.
- (68) Yu, H. S.; He, X.; Truhlar, D. G. MN-15: A new local exchanged-correlation functional for Kohn-Sham density functional theory broad accuracy for atoms, molecules, and solids. *J. Chem. Theory Comput.* **2016**, *12*, 1280–1293.
- (69) Marenich, A. V.; Cramer, C. J.; Truhlar, D. G. Universal solvation model based on solute electron density and on a continuum model of the solvent defined by the bulk dielectric constant and atomic surface tensions. *J. Phys. Chem. B* **2009**, *113*, 6378–6396.
- (70) Frisch, M. J.; et al. *Gaussian 16*, revision B.01, Gaussian, Inc.: Wallingford, CT, 2016.
- (71) Callado, L. F.; Gabilondo, A. M.; Meana, J. J. [<sup>3</sup>H] RX821002 (2-methoxyidazoxan) binds to  $\alpha_2$ -adrenoceptor subtypes and a non-adrenoceptor imidazoline binding site in rat kidney. *Eur. J. Pharmacol.* **1996**, *316*, 359–368.
- (72) MarvinSketch 5.5.1.0. ChemAxon, Budapest, Hungary, 2011; software available at <https://www.chemaxon.com>.
- (73) Stewart, J. J. P. Optimization of parameters for semiempirical methods I. Method. *J. Comput. Chem.* **1989**, *10*, 209–220.
- (74) Stewart, J. J. P. Optimization of parameters for semiempirical methods II. Method. *J. Comput. Chem.* **1989**, *10*, 221–264.
- (75) Hehre, W. J.; Radom, L.; Schleyer, P. v. R.; Pople, J. A. *Ab initio molecular orbital theory*; Wiley: New York, 1986; Vol 1.
- (76) Frisch, M. J.; Trucks, G. W.; Schlegel, H. B.; Scuseria, G. E.; Robb, M. A.; Cheeseman, J. R.; Scalmani, G.; Barone, V.; Mennucci, B.; Petersson, G. A.; Nakatsuji, H.; Caricato, M.; Li, X.; Hratchian, H. P.; Izmaylov, A. F.; Bloino, J.; Zheng, G.; Sonnenberg, J. L.; Hada, M.; Ehara, M.; Toyota, K.; Fukuda, R.; Hasegawa, J.; Ishida, M.; Nakajima, T.; Honda, Y.; Kitao, O.; Nakai, H.; Vreven, T.; Montgomery, J. A., Jr.; Peralta, J. E.; Ogliaro, F.; Bearpark, M.; Heyd, J. J.; Brothers, E.; Kudin, K. N.; Staroverov, V. N.; Kobayashi, R.; Normand, J.; Raghavachari, K.; Rendell, A.; Burant, J. C.; Iyengar, S. S.; Tomasi, J.; Cossi, M.; Rega, N.; Millam, J. M.; Klene, M.; Knox, J. E.; Cross, J. B.; Bakken, V.; Adamo, C.; Jaramillo, J.; Gomperts, R.; Stratmann, R. E.; Yazyev, O.; Austin, A. J.; Cammi, R.; Pomelli, C.; Ochterski, J. W.; Martin, R. L.; Morokuma, K.; Zakrzewski, V. G.; Voth, G. A.; Salvador, P.; Dannenberg, J. J.; Dapprich, S.; Daniels, A. D.; Farkas, O.; Foresman, J. B.; Ortiz, J. V.; Cioslowski, J.; Fox, D. J. *Gaussian 09*, revision D.01, Gaussian Inc.: Wallingford, CT, 2009.
- (77) CambridgeSoft Corporation. *ChemBio3D Ultra*, version 13.0; CambridgeSoft, Cambridge, MA, USA, 2013.
- (78) Durán, A.; Zamora, I.; Pastor, M. Suitability of GRIND-Based principal properties for the description of molecular similarity and ligand-based virtual screening. *J. Chem. Inf. Model.* **2009**, *49*, 2129–2138.
- (79) Durán, A.; Pastor, M. *Pentacle, An advanced tool for computing and handling grid-independent descriptors*. User Manual Version 1.06; 2011.
- (80) Ojha, P. K.; Roy, K. Comparative QSARs for antimalarial endochins: Importance of descriptor-thinning and noise reduction prior to feature selection. *Chemom. Intell. Lab. Syst.* **2011**, *109*, 146–161.
- (81) Kilkenny, C.; Browne, W. J.; Cuthill, I. C.; Emerson, M.; Altman, D. G. Improving biocscience research reporting: the ARRIVE guidelines for reporting animal research. *PLoS Biol.* **2010**, *8*, e1000412.
- (82) Oakley, H.; Cole, S. L.; Logan, S.; Maus, E.; Shao, P.; Craft, J.; Guillozet-Bongaarts, A.; Ohno, M.; Disterhoft, J.; Van Eldik, L.; Berry, R.; Vassar, R. Intraneuronal beta-amyloid aggregates, neurodegeneration, and neuron loss in transgenic mice with five familial Alzheimer's disease mutations: potential factors in amyloid plaque formation. *J. Neurosci.* **2006**, *26*, 10129–10140.

## A.4

### **Benzofuranyl-2-imidazoles as Imidazoline I<sub>2</sub> Receptor ligands for Alzheimer's disease.**

Rodríguez-Arévalo S, Bagán A, Griñán-Ferré C, **Vasilopoulou F**, Pallàs M, Brocos-Mosquera I, Callado LF, Loza MI, Martínez AL, Brea A, Pérez B, Molins E, Jonghe S, Daelemans D, Radan, Djikic T, Nikolic K, Hernández-Hernández E, Julia García-Fuster M, García-Sevilla JA, Escolano C.

*European Journal of Medicinal Chemistry*.doi:  
<https://doi.org/10.1016/j.ejmech.2021.113540>





## Benzofuranyl-2-imidazoles as imidazoline I<sub>2</sub> receptor ligands for Alzheimer's disease



Sergio Rodríguez-Arévalo <sup>a,1</sup>, Andrea Bagán <sup>a</sup>, Christian Griñán-Ferré <sup>b,1</sup>, Foteini Vasilopoulou <sup>b</sup>, Mercè Pallàs <sup>b</sup>, Iria Brocos-Mosquera <sup>c,d</sup>, Luis F. Callado <sup>c,d</sup>, M. Isabel Loza <sup>e</sup>, Antón L. Martínez <sup>e</sup>, José Brea <sup>e</sup>, Belén Pérez <sup>f</sup>, Elies Molins <sup>g</sup>, Steven De Jonghe <sup>h</sup>, Dirk Daelemans <sup>h</sup>, Milica Radan <sup>i</sup>, Teodora Djikic <sup>i</sup>, Katarina Nikolic <sup>i</sup>, Elena Hernández-Hernández <sup>j</sup>, M. Julia García-Fuster <sup>j</sup>, Jesús A. García-Sevilla <sup>j</sup>, Carmen Escolano <sup>a,\*</sup>

<sup>a</sup> Laboratory of Medicinal Chemistry (Associated Unit to CSIC), Department of Pharmacology, Toxicology and Medicinal Chemistry, Faculty of Pharmacy and Food Sciences, Institute of Biomedicine (IBUB), University of Barcelona, Av. Joan XXIII, 27-31, E-08028, Barcelona, Spain

<sup>b</sup> Pharmacology Section, Toxicology and Medicinal Chemistry, Faculty of Pharmacy and Food Sciences, Institut de Neurociències, University of Barcelona, Av. Joan XXIII, 27-31, E-08028, Barcelona, Spain

<sup>c</sup> Department of Pharmacology, University of the Basque Country, UPV/EHU, E-48940, Leioa, Bizkaia, Spain

<sup>d</sup> Centro de Investigación Biomédica en Red de Salud Mental, CIBERSAM, Spain

<sup>e</sup> Innopharma Screening Platform, BioFarma Research Group, Centro de Investigación en Medicina Molecular y Enfermedades Crónicas (CIMUS), Universidad de Santiago de Compostela, E-15782, Santiago de Compostela, Spain

<sup>f</sup> Department of Pharmacology, Therapeutic and Toxicology, Autonomous University of Barcelona, E-08193, Cerdanyola, Spain

<sup>g</sup> Institut de Ciència de Materials de Barcelona (CSIC), Campus UAB, E-08193, Cerdanyola, Spain

<sup>h</sup> KU Leuven, Department of Microbiology, Immunology and Transplantation, Rega Institute, Laboratory of Virology and Chemotherapy, Herestraat 49, 3000, Leuven, Belgium

<sup>i</sup> Department of Pharmaceutical Chemistry, Faculty of Pharmacy, University of Belgrade, 11000, Belgrade, Serbia

<sup>j</sup> IUNICS University of the Balearic Islands (UIB), Health Research Institute of the Balearic Islands (IdISBa), E-07122, Palma de Mallorca, Spain

### ARTICLE INFO

#### Article history:

Received 23 February 2021

Received in revised form

26 April 2021

Accepted 10 May 2021

Available online 20 May 2021

#### Keywords:

Imidazoline I<sub>2</sub> receptors

Imidazoline I<sub>2</sub> receptor ligands

Neuroprotection

5x-FAD

Benzofuranyl-2-imidazoles

Oxidative stress

### ABSTRACT

Recent findings unveil the pharmacological modulation of imidazoline I<sub>2</sub> receptors (I<sub>2</sub>-IR) as a novel strategy to face unmet medical neurodegenerative diseases. In this work, we report the chemical characterization, three-dimensional quantitative structure-activity relationship (3D-QSAR) and ADMET *in silico* of a family of benzofuranyl-2-imidazoles that exhibit affinity against human brain I<sub>2</sub>-IR and most of them have been predicted to be brain permeable. Acute treatment in mice with 2-(2-benzofuranyl)-2-imidazole, known as **LSL60101** (garsevil), showed non-warning properties in the ADMET studies and an optimal pharmacokinetic profile. Moreover, LSL60101 induced hypothermia in mice while decreased pro-apoptotic FADD protein in the hippocampus. *In vivo* studies in the familial Alzheimer's disease 5x-FAD murine model with the representative compound, revealed significant decreases in the protein expression levels of antioxidant enzymes superoxide dismutase and glutathione peroxidase in hippocampus. Overall, **LSL60101** plays a neuroprotective role by reducing apoptosis and modulating oxidative stress.

© 2021 Elsevier Masson SAS. All rights reserved.

### 1. Introduction

Imidazoline I<sub>2</sub> receptors (I<sub>2</sub>-IR) are heterogeneous entities, often described as nonadrenergic binding sites for imidazolines [1], that

bind with high affinity to [<sup>3</sup>H]idazoxan and with lower affinity to [<sup>3</sup>H]*p*-aminoclonidine and [<sup>3</sup>H]clonidine [2,3]. I<sub>2</sub>-IR are present in many organs, tissues and cell types, including brain, kidney, liver, astrocytes, platelets [4], pancreatic cells and, vascular smooth muscle cells [5]. Modifications in the levels of I<sub>2</sub>-IR have been associated with analgesia [6], inflammation [7] and with human brain disorders [8] such as depression [9], Alzheimer's type

\* Corresponding author.

E-mail address: [cescolano@ub.edu](mailto:cescolano@ub.edu) (C. Escolano).

<sup>1</sup> Both authors contribute equally to this work.

dementia [10], Parkinson's disease [11], and glial tumors [12]. The fact that I<sub>2</sub>-IR are altered in many pathophysiological processes and the availability of known I<sub>2</sub>-IR ligands have permitted to place I<sub>2</sub>-IR in a privileged position as new promising therapeutic targets. Representative I<sub>2</sub>-IR ligands [13] emerged from the literature as useful tools to reveal the biological implications of these non-structurally described receptors (Fig. 1). The compelling evidence has demonstrated the neuroprotective role of I<sub>2</sub>-IR through the pharmacological activities observed for their ligands. Agmatine, identified as the endogenous I<sub>2</sub>-IR ligand, has modulated actions in several neurotransmitters leading to neuroprotection in both *in vitro* and in rodent models [14]. Idazoxan reduced neuron damage in the rat brain hippocampus after global ischemia [15]. 2-(2-Benzofuranyl)-2-imidazoline (2-BFI), a selective I<sub>2</sub>-IR ligand, provided neuroprotective benefits against cerebral ischemia in models of chronic opioid therapy [16]. Idazoxan and 2-BFI have been proposed to exert neuroprotection by direct blocking of *N*-methyl-*D*-aspartate receptor (NMDA) mediated intracellular [Ca<sup>2+</sup>] influx [17].

Two out of these seven ligands depicted in Fig. 1, CR4056 and [<sup>11</sup>C]BU99008, are in the process of validating their therapeutic potential by progressing in clinical trials for osteoarthritis [18], and for PET diagnosis for patients that suffer from Alzheimer's disease (AD) [19,20], respectively. Due to the clinical implications of I<sub>2</sub>-IR, the discovery of new I<sub>2</sub>-IR ligands that could modulate the pharmacology involved is a challenging goal for a medicinal chemistry program. In this framework, we recently provided two structurally new families of I<sub>2</sub>-IR ligands and validated their properties ameliorating the devastating cognitive decline in two murine models of neurodegeneration [21–23].

At the subcellular level in the central nervous system (CNS), I<sub>2</sub>-IR are mainly located on the outer membrane of mitochondria in astrocytes [24,25]. Mitochondria are one of the main sources of reactive oxygen species (ROS) and reactive nitrogen species (RNS).

The amyloid cascade hypothesis, that dominates the field of AD, has been replaced by alternative explanations arising from the connection of mitochondrial dysfunction and increased ROS. There is evidence that indicates a pro-oxidant ability of Aβ, mediating an accelerated production of ROS by directly binding to the mitochondrial membranes. Consequently, mitochondrial dynamics and function are altered, disrupting the energy metabolism, and leading to the loss of synaptic function. An excess in ROS/RNS production and a mitochondrial dysfunction could lead to oxidative stress (OS), which is implicated in several neurodegenerative diseases, such as AD [26–28]. In fact, there is growing evidence for the contribution of OS and neuroinflammation to the pathogenesis of AD [29,30]. Recent studies have investigated the role of I<sub>2</sub>-IR in OS processes. Selective 2-BFI [31] decreased OS and altered the levels of antioxidant enzymes in an AD rat model and protected against OS-induced astrocytic cell death. Moreover, our group reported decreased levels of hydrogen peroxide levels and OS markers induced by two new I<sub>2</sub>-IR ligands in aged SAMP8 mice [32].

In this manuscript, we focused our attention on 2-(2-benzofuranyl)-2-imidazole, named as **LSL60101** (garsevil), first described in 1995 by García-Sevilla's group as a I<sub>2</sub>-IR selective ligand involved in astrocyte activation and neuronal regeneration [33,34]. In the following years, some outstanding papers described the biological relevance of **LSL60101** in the attenuation of morphine tolerance and hence proposing a neuroprotective role [35], such as provoking morphological/biochemical changes in astroglia that were neuroprotective after neonatal axotomy [36], and producing discriminable stimulus [37], amongst others. Of note, astrocytes as the main supportive cells in the CNS are significantly involved in the redox homeostasis, and consequently, this could be an indicative of a possible effect of **LSL60101** on OS balance.

From the structural chemical point of view, the nature of known I<sub>2</sub>-IR ligands (Fig. 1) is relatively restricted and the pharmacophore moiety is generally related to 2-imidazoline-like structures.

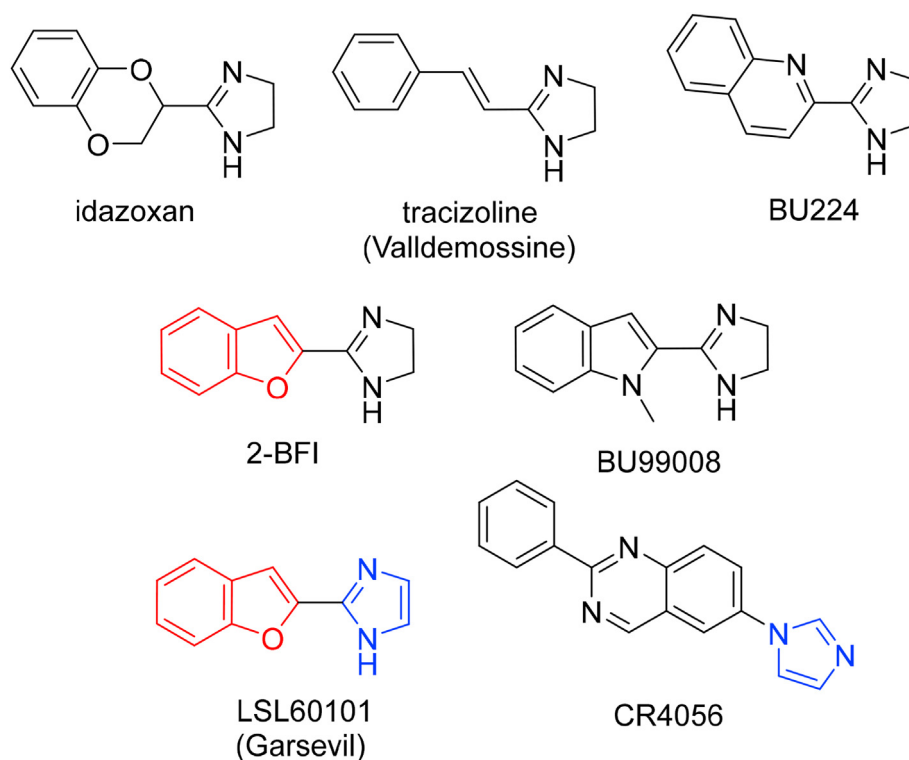


Fig. 1. Representative I<sub>2</sub>-IR ligands.



Structural comparison of **LSL60101** with other known I<sub>2</sub>-IR ligands, and in particular with 2-BFI that shares a benzofuran moiety, suggest a pharmacomodulation involving an unsaturation of the imidazole ring, a drug optimization strategy appealed in the design of new drugs. The presence of an imidazole ring in the successful CR4056 ligand encourages the proposal.

Herein we describe the synthesis and full characterization of ten benzofuranyl-2-imidazole derivatives to shed light on the structural-activity relationship of this family. Note, that the structural exploration involves substituents, either electron donating (methoxy) or electron attractor by inductive effect (bromide), located in different positions of the phenyl ring, and alkylation of the imidazole ring of the benzofuranyl-2-imidazole scaffold. We assessed the pharmacological profile of the ten analogues and selectivity through competition binding studies against the selective I<sub>2</sub>-IR radioligand [<sup>3</sup>H]2-BFI. Selectivity versus two related targets, the imidoline I<sub>1</sub> receptor (I<sub>1</sub>-IR) and the α<sub>2</sub>-adrenergic receptor (α<sub>2</sub>-AR) was evaluated through competition studies using the selective radioligands [<sup>3</sup>H]clonidine and [<sup>3</sup>H]RX821002 (2-methoxyidazoxan), respectively. Complementarily, we performed three-dimensional quantitative structure–activity relationship (3D-QSAR) studies of this compound family and predicted *in silico* the ADMET properties. **LSL60101** endowed with the best I<sub>2</sub>-IR affinity and an excellent selectivity index regarding I<sub>1</sub>-IR and α<sub>2</sub>-AR was selected for further studies. We carried out preliminary drug metabolism and pharmacokinetics (DMPK) studies for **LSL60101**, including chemical stability, PAMPA-BBB permeability assay, solubility, cytotoxicity, microsomal stability, cytochromes inhibition, and safety. The hypothermic properties and FADD multifunctional protein (as a marker of neuroplasticity) regulation were also studied following several **LSL60101** treatments in mice. Pharmacokinetics was carried out prior to an *in vivo* treatment in a proper murine model of AD. Thus, we further assessed the neuroprotective effects of **LSL60101** by evaluating specific OS markers under oxidative damage and several transcription factors related to OS machinery in 5xFAD mice (an early-onset mouse transgenic model of AD).

## 2. Results and discussion

### 2.1. Chemistry

The preparation of the required final benzofuranyl-2-imidazoles was accomplished, based on previous described procedure [33], starting from the corresponding commercially available benzofuran-2-carboxylic acid derivatives (Scheme 1). Except for the commercially available benzofuran-2-carbonitrile, **2a**, the other derivatives **2b**, **2c**, and **2d**, were prepared in two steps. Treatment of the corresponding benzofuran-2-carboxylic acid derivatives with thionyl chloride and ammonium hydroxide furnished the carboxamides **1b**, **1c**, and **1d** in excellent yields. Dehydration reaction with phosphorus oxychloride gave benzofuran-2-carbonitriles, **2b**, **2c**, and **2d**, that were efficiently transformed in the corresponding benzofuran-2-carbimidates hydrochlorides **3a**, **3b**, **3c** and **3d** after treatment with ethereal HCl 2 M. To construct the imidazole moiety, the reaction with 2,2-dimethoxyethylamine was undertaken to give **4a**, **4b**, **4c** and **4d** in quantitative yields, that were treated with aqueous hydrochloric acid accomplish the attack of the nitrogen atom to the ketal electrophilic carbon, affording benzofuranyl-2-imidazoles **5a** (named **LSL60101**), **5b**, **5c** and **5d**. Recrystallization of **5a** as monocrystal confirmed its structure by X-ray crystallographic analysis (see supporting information S51).

To access hydroxybenzofuran-2-imidazole derivatives **6b** and **6c**, hydrolysis of the methylether group of **5b** and **5c** was achieved by treatment with hydrobromic acid. The alkylation of the N-imidazole of compound **5a** with methyl iodide gave compound **7a** and with ethyl iodide yielded **7aa**. Analogously, the reaction of **5b** and **5c** with ethyl bromide furnished the expected products **7b** and **7c** in excellent yields.

All final products **5a–5d**, **6b–6c** and **7a**, **7aa**, **7b** and **7c**, were completely characterized (see experimental section and supporting information S19–S29) and all the tested compounds possess a purity of at least 95% (see supporting information S30–S49).

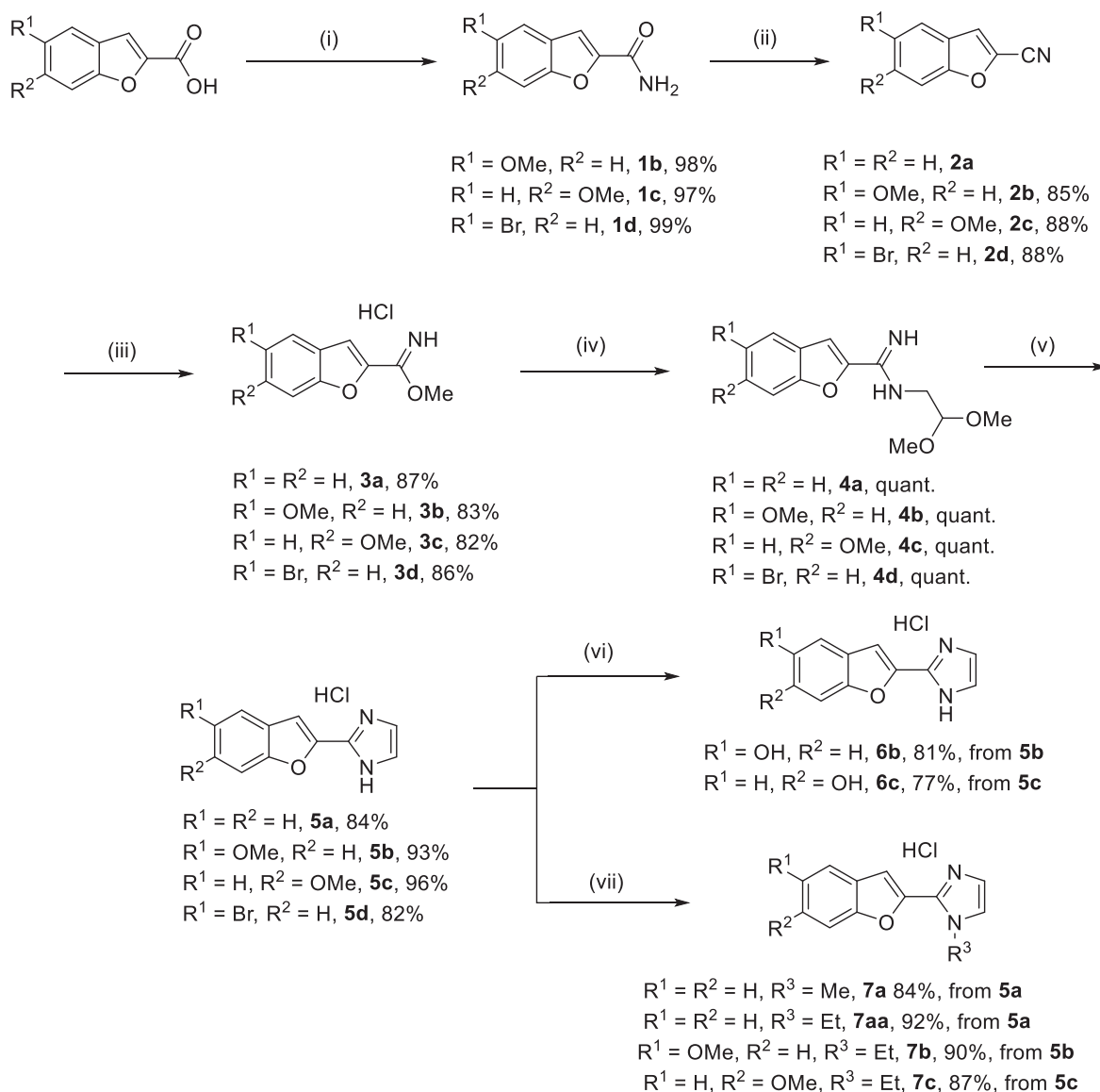
### 2.2. Pharmacological evaluation

#### 2.2.1. Radioligand I<sub>2</sub>-IR binding assays

The pharmacological profile of the ten compounds with the structures **5**, **6** and **7** (Scheme 1) was evaluated through competition binding studies against the selective I<sub>2</sub>-IR radioligand [<sup>3</sup>H]2-BFI and the selective α<sub>2</sub>-AR radioligand [<sup>3</sup>H]RX821002. The studies were performed in membranes from post-mortem human frontal cortex, a brain area that shows an important density of I<sub>2</sub>-IR and α<sub>2</sub>-AR. Idazoxan, a compound with well-established affinity for I<sub>2</sub>-IR (pK<sub>i</sub> = 7.41 ± 0.63) and α<sub>2</sub>-AR (pK<sub>i</sub> = 8.35 ± 0.16) was used as reference. The inhibition constant (K<sub>i</sub>) for each compound was obtained and is expressed as the corresponding pK<sub>i</sub>. The selectivity for these two receptors was expressed by the I<sub>2</sub>/α<sub>2</sub> index, calculated as the antilogarithm of the ratio between pK<sub>i</sub> values for I<sub>2</sub>-IR and pK<sub>i</sub> values for α<sub>2</sub>-AR. Competition experiments against [<sup>3</sup>H]2-BFI were biphasic for most of the compounds (Table 1).

We have previously reported the affinity of 2-BFI in I<sub>2</sub>-IR human brain (pK<sub>iH</sub> = 9.08 and pK<sub>iL</sub> = 7.15). The structural differences between 2-BFI and **LSL60101** rely on the presence of an additional double bond in the five membered ring, from a 2-imidazoline to an imidazole conferring a planar structure to **LSL60101** (see X-ray crystallography discussion in the experimental section). The mentioned structural difference rendered a decrease in the affinity to pK<sub>iH</sub> = 8.17 ± 0.19 and pK<sub>iL</sub> = 6.02 ± 0.10, with 34% occupancy of the high affinity site. The decreased affinity upon α<sub>2</sub>-AR plays in our favor and selectivity had an excellent ratio of 3090.

Next, electron-donating groups in the phenyl ring, such as a methoxy group was considered. Thus, compounds **5b** and **5c** bearing a methoxy group in the position –5 and –6, gave affinity values of pK<sub>i</sub> = 6.41 ± 0.16 and pK<sub>iH</sub> = 6.77 ± 0.29 and pK<sub>iL</sub> = 4.58 ± 0.39, respectively. The introduction of a 5-bromine furnished compound **5d** with similar affinity values as **LSL60101** (pK<sub>iH</sub> = 8.63 ± 0.51 and pK<sub>iL</sub> = 5.85 ± 0.18) but showing less selectivity against α<sub>2</sub>-AR. The hydroxybenzofuran-2-imidazole derivatives **6b** and **6c** showed affinities of pK<sub>iH</sub> = 9.57 ± 0.63 and pK<sub>iL</sub> = 4.6 ± 0.26 and pK<sub>i</sub> = 5.48 ± 0.11, respectively, with a drop in the I<sub>2</sub>/α<sub>2</sub> selectivity in relation to their methoxy derivative partners **5b** and **5c**. Compounds **7a**, **7aa** and **7b** bearing a N-alkylated imidazole nucleus showed affinity that better fit to a two-site binding model with pK<sub>iH</sub> = 6.99 ± 0.28 and pK<sub>iL</sub> = 5.35 ± 0.21, pK<sub>iH</sub> = 7.09 ± 0.42 and pK<sub>iL</sub> = 4.72 ± 0.15, and pK<sub>iH</sub> = 6.95 ± 0.16 and pK<sub>iL</sub> = 4.16 ± 0.12, with high affinity site occupancy of 38, 22 and 35%, respectively. Compared to the non-alkylated partners **LSL60101** and **5b**, the additional N-alkyl group did not result in a significant increase in the pK<sub>i</sub> value but in a drop in the I<sub>2</sub>/α<sub>2</sub> selectivity. N-Ethyl substituted **7c** gave an outstanding pK<sub>iH</sub> = 9.13 ± 0.47 value of I<sub>2</sub> affinity with a 12% high occupancy affinity site, whereas the non-alkylated homologous **5c** displayed a and pK<sub>iL</sub> = 5.11 ± 0.06.



**Scheme 1.** Reagents and conditions: (i)  $\text{SOCl}_2$ , toluene, 3 h, reflux; 25% aq.  $\text{NH}_4\text{OH}$ , rt; (ii)  $\text{POCl}_3$ , dichloroethane,  $75^\circ\text{C}$ , 2 h; (iii)  $\text{Et}_2\text{OHCl}$  2 M,  $4^\circ\text{C}$ , 48 h; (iv) 2,2-dimethoxyethylamine, methanol,  $60^\circ\text{C}$ , 16 h; (v) HCl 2 M,  $60^\circ\text{C}$ , 16 h; (vi) HBr 47%,  $100^\circ\text{C}$ , 7 h; (vii) NaH, methyl iodide or ethyl bromide, DMF,  $0^\circ\text{C}$  to rt, 75 min.

The study highlighted **LSL60101** as the most promising candidate of the benzofuran-2-imidazole family to tackle further *in vitro* and *in vivo* studies.

### 2.2.2. Comparison of $I_2$ -IR binding affinities of **LSL60101** across species

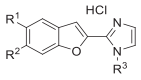
The literature is non-uniform in the  $I_2$ -IR affinity values across species (human, rat, rabbit, mouse, and monkey), given the radioligand considered as a reference (idazoxan, 2-BFI) and the tissues used for analysis (from different anatomical parts: kidney, whole brain, cortex, etc). Thus, we made an effort in the comparison of affinities of standard  $I_2$ -IR ligands, 2-BFI, trazolone, and clinically prominent [ $^{11}\text{C}$ ]BU99008 and CR4056 [23]. When evaluating **LSL60101** a two-site model of binding was observed in human post-mortem brain cortical membranes with a  $\text{pK}_{\text{IH}} = 8.17 \pm 0.19$  and  $\text{pK}_{\text{IL}} = 6.02 \pm 0.10$ , and an occupancy of the high site of 34%. In rat cerebral cortex using idazoxan as radioligand, **LSL60101** was reported a lower affinity than in human tissues, with a  $\text{pK}_{\text{IH}} = 6.45$

and  $\text{pK}_{\text{IL}} = 1.16$ , but a higher percentage fraction of occupancy (79%) [34]. In mice brain cortical membranes, the competition curve against [ $^3\text{H}$ ]2-BFI binding was significantly better with a two-site fit than a one-site binding model, providing a  $\text{pK}_{\text{IH}} = 9.92 \pm 0.17$  and  $\text{pK}_{\text{IL}} = 6.00 \pm 0.14$ . These values were close to those found in human tissues including a similar occupancy of the high site (41%) supporting the *in vivo* experiments in mice.

### 2.3. 3D-QSAR study

The 3D-QSAR method was used to analyse the most significant descriptors that were interpreted in terms of identifying and quantifying structural elements important for  $I_2$ -IR and  $\alpha_2$ -AR activity. The study was conducted on structurally diverse  $I_2$ -IR ligands that were divided into two clusters, based on their chemical structures. Cluster 1 represents compounds synthesized in this manuscript, while cluster 2 contains bicyclic  $\alpha$ -iminophosphonate  $I_2$ -IR ligands previously described by our group (Fig. S1) [23]. To

**Table 1**  
I<sub>2</sub>-IR and  $\alpha_2$ -AR Binding Affinities (pK<sub>i</sub>) of compound idazoxan and 2-BFI and new compounds **5a-5d**, **6b**, **6c**, **7a**, **7aa**, **7b** and **7c**.

Compound R <sup>1</sup> /R <sup>2</sup> /R <sup>3</sup> General structure	<sup>a</sup> [ <sup>3</sup> H]2-BFI I <sub>2</sub> pK <sub>i</sub> one site	<sup>b</sup> [ <sup>3</sup> H]2-BFI I <sub>2</sub> pK <sub>i</sub> two sites	High-affinity site %	[ <sup>3</sup> H]-RX821002 $\alpha_2$ pK <sub>i</sub>	Selectivity I <sub>2</sub> / $\alpha_2$	
	7.41 ± 0.63	7.87 ± 0.74	5.76 ± 0.57	40 ± 7	8.35 ± 0.16	–
<b>2-BFI</b>	8.31 ± 0.13	9.08 ± 0.22	7.15 ± 0.31	58 ± 9	4.58 ± 0.22	5370
<b>5a, LSL60101</b> R <sup>1</sup> = R <sup>2</sup> = R <sup>3</sup> = H	6.67 ± 0.09	8.17 ± 0.19	6.02 ± 0.10	34 ± 4	3.18 ± 0.17	3090
<b>5b</b> R <sup>1</sup> = OMe, R <sup>2</sup> = R <sup>3</sup> = H	6.41 ± 0.16	–	–	–	3.94 ± 0.07	295
<b>5c</b> R <sup>1</sup> = H, R <sup>2</sup> = OMe, R <sup>3</sup> = H	5.88 ± 0.16	6.77 ± 0.29	4.58 ± 0.39	46 ± 9	3.01 ± 0.45	741
<b>5d</b> R <sup>1</sup> = Br, R <sup>2</sup> = H, R <sup>3</sup> = H	6.28 ± 0.18	8.63 ± 0.51	5.85 ± 0.18	20 ± 5	4.92 ± 0.25	23
<b>6b</b> R <sup>1</sup> = OH, R <sup>2</sup> = H, R <sup>3</sup> = H	4.87 ± 0.23	9.57 ± 0.63	4.6 ± 0.25	29 ± 5	3.84 ± 0.16	11
<b>6c</b> R <sup>1</sup> = H, R <sup>2</sup> = OH, R <sup>3</sup> = H	5.48 ± 0.11	–	–	–	3.76 ± 0.12	52
<b>7a</b> R <sup>1</sup> = R <sup>2</sup> = H, R <sup>3</sup> = Me	5.98 ± 0.08	6.99 ± 0.28	5.35 ± 0.21	38 ± 10	3.75 ± 0.12	170
<b>7aa</b> R <sup>1</sup> = R <sup>2</sup> = H, R <sup>3</sup> = Et	5.05 ± 0.10	7.09 ± 0.42	4.72 ± 0.15	22 ± 6	3.77 ± 0.08	19
<b>7b</b> R <sup>1</sup> = OMe, R <sup>2</sup> = H, R <sup>3</sup> = Et	4.96 ± 0.15	6.95 ± 0.16	4.16 ± 0.12	35 ± 3	4.21 ± 0.19	6
<b>7c</b> R <sup>1</sup> = H, R <sup>2</sup> = OMe, R <sup>3</sup> = Et	5.26 ± 0.08	9.13 ± 0.47	5.11 ± 0.06	12 ± 2	3.17 ± 0.25	123

<sup>a</sup> Selectivity I<sub>2</sub>-IR/ $\alpha_2$ -AR expressed as the antilog (pK<sub>i</sub> I<sub>2</sub>-IR – pK<sub>i</sub>  $\alpha_2$ -AR).

<sup>b</sup> The best fit of the data for most of the compounds was to a two-site binding model with high pK<sub>i</sub> (pK<sub>iH</sub>) and low pK<sub>i</sub> (pK<sub>iL</sub>) affinities for both binding sites, respectively.

compare and validate our results, we have added three I<sub>2</sub>-IR standard ligands (tracizoline, idazoxan, and BU99008, Fig. 1), in both data sets. Structural diversity of prepared data set enabled us not only to deeper analyse the most important structural characteristics, but also to suggest modifications to come up with novel compounds with improved I<sub>2</sub>-IR activity and selectivity.

The Pentacle program [38] was used for calculation of GRID independent descriptors (GRIND and GRIND2) and 3D-QSAR model building. The reliability and predictive power of the created 3D-QSAR models were assessed using different internal and external validation parameters (Tables S1 and S2). Obtained results indicated that both models possessed good predictive capability and could be used for activity prediction of newly designed compounds. PLS coefficient plots presented the most important variables with positive and negative influence on I<sub>2</sub>-IR and  $\alpha_2$ -AR activity (Figs. S2 and S3).

Compounds from cluster 1 are compounds reported here (Scheme 1) with pK<sub>i</sub> ranges between 4.87 and 6.67 for I<sub>2</sub>-IR, and 3.01–4.92 for  $\alpha_2$ -AR, while cluster 2 compounds present our bicyclic  $\alpha$ -iminophosphonate derivatives (Fig. S1) with pK<sub>i</sub> ranging from 4.02 to 8.56 for I<sub>2</sub>-IR, and 3.38–6.77 for  $\alpha_2$ -AR. Comparing to molecules from cluster 2, cluster 1 compounds possess lower pK<sub>i</sub> values for I<sub>2</sub>-IR as well as  $\alpha_2$ -AR.

The most potent compound from cluster 1, **LSL60101** (pK<sub>i</sub> = 6.67), displayed all significant variables with the most positive impact on the activity. Positive influence on both I<sub>2</sub>-IR and  $\alpha_2$ -AR activity showed variables var24 (DRY-DRY: 9.60–10.00 Å) and var25 (DRY-DRY: 10.00–10.40 Å), respectively. They described the optimal distance range between two hydrophobic regions, around benzofuranyl and imidazole rings, which may be crucial for establishing favourable van der Waals interactions with amino acids in the active pocket of both receptors (Fig. 2a). Moreover, I<sub>2</sub>-IR 3D-QSAR model pointed out var232 (DRY-O: 6.40–6.80 Å) as the variable with the strongest positive influence on I<sub>2</sub>-IR binding

activity. This variable implies the importance of hydrogen bond donor group, –NH from imidazole ring, located at a certain distance from hydrophobic region, benzofuranyl ring (Fig. 2a). Contrary, it did not possess such a significant influence in the compounds from cluster 2, since they lack hydrogen bond donor groups (Fig. S4). GRIND variable O–N1 (var394: 6.40–6.80 Å) signified a positive influence of the imidazole ring on I<sub>2</sub>-IR activity, describing the distance between hydrogen bond acceptor and donor probes located around nitrogen atoms (Fig. 2a). On the other hand, it did not show a significant effect on  $\alpha_2$ -AR activity. Furthermore, the importance of hydrogen bonding interactions in the binding site of I<sub>2</sub> receptor was confirmed with variables var452 (O–TIP: 8.00–8.40 Å) and var503 (N1–TIP: 6.80–7.20 Å), which underlined optimal distances between the steric region around the benzofuranyl ring and –NH from the imidazole ring as a hydrogen bond donor or acceptor (Fig. 2a). Therefore, we can conclude that the substitution of the –NH imidazole group (R3) and losing of the hydrogen bond donating characteristics negatively correlated with I<sub>2</sub>-IR binding activity and selectivity (**7a**, **7aa**, **7c**, **7b**). Analysis of  $\alpha_2$ -AR 3D-QSAR model showed that the sole introduction of a hydrogen bond acceptor-group, at a certain distance from hydrophobic or steric region around heterocyclic ring, induced a positive impact on  $\alpha_2$ -AR activity.

The compound with the lowest activity within the cluster 1 is **6b** (pK<sub>i</sub> = 4.87). The introduction of a hydroxy or methoxy group on the carbon atom of the benzofuranyl nucleus resulted in reduced affinity, which could be described with var197 (TIP–TIP: 14.00–14.40 Å) and var350 (DRY–TIP: 10.40–10.80 Å) (Fig. 2b). Additionally, the unfavourable impact of these groups is also defined with the negative variable var408 (O–N1), which explains the distance of 12.00–12.40 Å between –NH of imidazole, as a hydrogen bond donor and the oxygen atom in hydroxy or methoxy substituent as a hydrogen bond acceptor (Fig. 2b). Based on these findings we can conclude that the introduction of a hydrogen bond

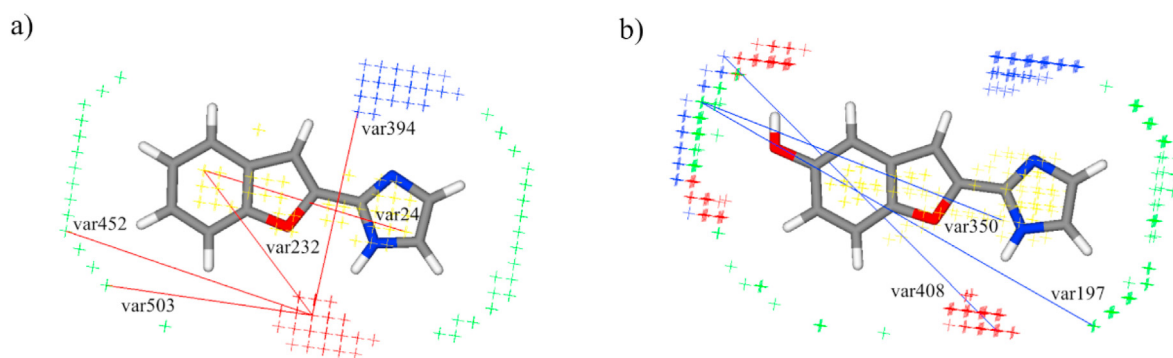


**Fig. 2.** Representation of positive interactions (in red) of **LSL60101** (a) and negative interactions (in blue) of **6b**; (b) in I<sub>2</sub>-IR 3D-QSAR model. The steric hot spots (TIP) are presented in green, hydrophobic regions (DRY) in yellow, H-bond acceptor regions (N1) in blue, and H-bond donor regions (N1) in red.

acceptor substituent on the benzofuranyl ring may not be considered as the most complementary with the binding site of I<sub>2</sub>-IR.

#### 2.4. *In silico* ADMET analysis of physicochemical and pharmacokinetic parameters

The drug discovery pipeline has more and more relied on *in silico* predictions to optimize lead compounds and reduce investments [39]. *In silico* ADMET prediction aims to evaluate individual ADMET behaviours of examined compounds. Pharmacokinetic properties such as absorption, distribution, metabolism, excretion, and toxicity (ADMET) profiling of compounds were determined using ADMET Predictor software [40], while physico-chemical parameters were assessed with SwissADME online programme [41]. The obtained results are presented in Tables S3 and S4. Based on the results obtained from the performed calculations, we can conclude that all studied compounds present good water solubility and lipophilicity. Compounds reported here satisfy the Lipinski's Rule of 5, which supports their drug-likeness properties and potential chance to be orally bioavailable. Moreover, the polarity of compounds was evaluated by the TPSA (topological polar surface area) descriptor and results revealed that benzofuranyl-2-imidazoles possessed lower polarity, similar to idazoxan, when compared to previously described bicyclic  $\alpha$ -iminophosphonate derivatives (see supporting information, Fig. S1) [23]. Regarding pharmacokinetic properties, we noted that all molecules possessed high BBB permeation. Compared to standard molecules, such as idazoxan, all examined compounds possessed lower percentage of unbound drug in plasma. Furthermore, this family showed lower metabolic CYP risk and TOX risk comparing to idazoxan and bicyclic  $\alpha$ -iminophosphonate derivatives. P-gp is believed to play an important role in drug distribution and resistance to CNS drug treatment. The examined compounds were not identified as potential substrates for P-gp transporters. Since blocking hERG channels represents a major therapeutic challenge in drug discovery, we note that the compounds synthesized in this manuscript did not show affinity to inhibit hERG channels.

The absence of warnings of this theoretical study gave us confidence for undertaking further *in vitro* and eventually, *in vivo* experiments to assess the benzofuranyl-2-imidazole family and **LSL60101** as a neuroprotective agent.

#### 2.5. Blood brain barrier permeation assay

Considering the localization of I<sub>2</sub>-IR in the CNS, a good ability to cross the BBB is an essential requirement for developing effective

I<sub>2</sub>-IR ligands with potential therapeutic applications in the neuroprotective field. Guaranteed by the *in silico* parameters the *in vitro* permeability ( $P_e$ ) of all the novel compounds was determined by using the PAMPA-BBB permeability assay (Table 2). The new compounds prepared were well above the threshold established for high BBB permeation ( $P_e > 5.198 \times 10^{-6} \text{ cm s}^{-1}$ ), except for compounds **6b** and **6c**. The aforementioned two compounds bear a hydroxyl group increasing their polarity and decreasing their capability to permeate the artificial PAMPA-BBB membrane with  $P_e$  values of  $0.1 \pm 0.03 \times 10^{-6} \text{ cm s}^{-1}$  and  $0.32 \pm 0.1 \times 10^{-6} \text{ cm s}^{-1}$ , respectively. In particular, the most I<sub>2</sub>-IR affine compound **LSL60101** had a  $P_e$  value of  $13.6 \pm 0.4 \times 10^{-6} \text{ cm s}^{-1}$  and was considered suitable to envisage further *in vitro* and *in vivo* studies oriented to in-depth the pharmacological profile of the new family of I<sub>2</sub>-IR ligands.

According to these data, compounds including a hydroxyl group in its structure, such as **6b** and **6c**, were not suitable for considering their potential in neurodegenerative diseases. In particular, **LSL60101** showed the best affinity and selectivity values and since it had a good ability to cross the BBB it will be used to undertake further studies.

#### 2.6. Selectivity I<sub>2</sub>-IR versus I<sub>1</sub>-IR in **LSL60101**

**LSL60101** showed a remarkable affinity for I<sub>2</sub>-IR and selectivity I<sub>2</sub>/ $\alpha_2$ -AR with a ratio 3090. Then, we assessed the affinity/selectivity

**Table 2**

Permeability results ( $P_e \text{ } 10^{-6} \text{ cm s}^{-1}$ ) from the PAMPA-BBB assay for new report compounds and their prediction of BBB permeation.

Compound	<sup>a</sup> $P_e \text{ } 10^{-6} \text{ cm s}^{-1}$	<sup>b</sup> Prediction
<b>Idazoxan</b>	$3.3 \pm 0.1$	CNS $\pm$
<b>2-BFI</b>	$6.1 \pm 0.2$	CNS+
<b>5a, LSL60101</b>	$13.6 \pm 0.4$	CNS+
<b>5b</b>	$8.3 \pm 1.2$	CNS+
<b>5c</b>	$7.6 \pm 0.1$	CNS+
<b>5d</b>	$20.3 \pm 0.2$	CNS+
<b>6b</b>	$0.32 \pm 0.1$	CNS-
<b>6c</b>	$0.1 \pm 0.03$	CNS-
<b>7a</b>	$17.4 \pm 0.85$	CNS+
<b>7aa</b>	$19.2 \pm 1.1$	CNS+
<b>7b</b>	$12.4 \pm 0.8$	CNS+
<b>7c</b>	$14.85 \pm 0.1$	CNS+

<sup>a</sup> PBS/EtOH (70:30) was used as solvent. Values are expressed as mean  $\pm$  SD of at least three independent experiments.

<sup>b</sup> The *in vitro* permeability ( $P_e$ ) of fourteen commercial drugs through lipid extract of porcine brain membrane together with the test compounds were determined (for the commercial drug values see Table S5).

for the very close receptors I<sub>1</sub>-IR. Specific binding of [<sup>3</sup>H]clonidine (20 nM) to I<sub>1</sub>-IR of rat or human hypothalamic membranes was accomplished after pre-incubation with benextramine (10 μM) to alkylate population of α<sub>2</sub>-AR. Under these experimental conditions [<sup>3</sup>H]clonidine only labelled I<sub>1</sub>-IR and in drug competition experiments moxonidine, a known I<sub>1</sub>-IR selective compound, showed subnanomolar affinity for these I<sub>1</sub>-sites; K<sub>iH</sub> = 0.2 nM; K<sub>iL</sub> = 12 μM. **LSL60101** displayed a very low affinity for I<sub>1</sub>-IR, in rat samples K<sub>i</sub> = 115 μM and in human samples K<sub>i</sub> = 250 μM.

### 2.7. Acute toxicity

Based on the excellent affinity/selectivity upon I<sub>2</sub>-IR of **LSL60101**, the safety evaluation was undertaken to determine the acute toxicity of the compound. **LSL60101** was safe up to a dose level of 100 mg/kg body weight after an intraperitoneal administration, since the LD<sub>50</sub> was considered to be greater than 100 mg/kg (Probit analysis) in male albino mice (lack of toxicity in the range of doses tested: 10–100 mg/kg; n = 10 mice per dose tested).

### 2.8. ADME-DMPK profiling of **LSL60101**

With a compound showing promising binding properties/selectivity, devoid to α<sub>2</sub>-AR and I<sub>1</sub>-IR, and optimal safety, we undertook *in vitro* assays to define its physicochemical properties and chemical stability.

The solubility of **LSL60101** in 1% DMSO and 99% PBS buffer was excellent (52.5 μM). For a better definition, the solubility of **LSL60101** at different pH 1.13, 4.61 and 6.97, simulating the pH range of the gastric and intestinal fluids, was studied (see supporting information S10). Following the solubility terms established in *European Pharmacopoeia* vs.10.0, **LSL60101** is a soluble substance at pH 1.13 and 4.61 and a very slightly soluble substance at pH 6.97 (Table S6).

The chemical evaluation of **LSL60101** implied forced degradation studies under different stress conditions for a period of nine weeks, monitoring weekly the assays by HPLC and <sup>1</sup>H NMR. In particular, **LSL60101** was subjected to the effect of daylight with temperatures between 0 and 23 °C and a relative humidity of 25–85%, to the effect of high temperature (thermal stability at 75 °C), and to the continuous light of a 100W (230V) bulb. Analysis by HPLC showed that the compound was completely stable under all the aforementioned conditions. Calculated lipophilicity of **LSL60101** referring to the consensus log P<sub>o/w</sub> value calculated using the SwissADME program for five predictive log P<sub>o/w</sub> models, iLOGP, XLOGP3, WLOGP, MLOGP and SILICOS-IT, which gave values of 1.51, 2.16, 2.82, 1.15 and 3.02, respectively. Therefore, the calculated log P<sub>o/w</sub> and the other parameters of Lipinski were within the limits and the compounds are suitable for undertaking the characterization of *in vitro* ADME properties.

Microsomal stability, which is widely used to determine the likely degree of primary metabolic clearance in the liver, was assessed in human and mouse recombinant microsomes. The data shown in Table S7 reveals a 36% percentage of remaining compound, after 60 min of incubation in mouse microsomes, and 58% in human, indicating moderate differences in the metabolism depending on the species. The t<sub>1/2</sub> is 1.4-fold bigger in human than in mice, therefore the difference should be taken into consideration through additional preclinical studies.

The inhibition potential of **LSL60101** was evaluated using recombinant human cytochrome P450 enzymes [CYP1A2, CYP2C9, CYP2C19, CYP2D6, CYP3A4 (7-BFC) and CYP3A4 (DBF)] and probe substances with fluorescent detection. The results depicted in Table S8 showed no inhibition of the cytochromes considered at 10 μM concentration. Taking into account the range of nM in the

affinity values of **LSL60101** it is not expected that at therapeutic doses the compound may interfere with the cytochrome P450-mediated metabolism of other drugs.

The plasma stability of **LSL60101** assessed in humans pooled from healthy donors was measured up to 6 h (0 h, 1 h, 2 h and 6 h) revealing 100, 83, 77 and 57% of the remaining percentage (Table S9). In mouse plasma **LSL60101** was inert under the conditions studied, remaining as 100% of the initial compound after 6 h (Table S10).

The extent of plasma protein binding was slightly superior in human than in mouse plasma. The fraction unbound value is also reported in Table S11. Whereas a 7.1% of **LSL60101** can be found in humans as free drug, a 16.0% was observed in mouse.

The effect of **LSL60101** over the activity of hERG, an important safety issue in drug discovery, was assessed and showed an inhibitory activity (%) of 4 ± 1 at 10 μM concentration, discarding any worries on this issue.

### 2.9. Cytotoxicity

In order to exclude compounds with adverse cellular effects, the newly synthesized compounds were evaluated for cytotoxicity. Human primary cells are physiologically more relevant. However, because of the difficulties of working with primary cultures, immortalized cell lines were used as an *in vitro* screening tool for cytotoxicity. In a panel of cancer cell lines, including LN-229 (glioblastoma), Capan-1 (pancreatic adenocarcinoma), HCT-116 (colorectal carcinoma), NCI-H460 (lung carcinoma), DND-41 (acute lymphoblastic leukemia), HL-60 (acute myeloid leukemia), K-562 (chronic myeloid leukemia) and Z-138 (non-Hodgkin lymphoma) cell lines, none of the compounds displayed any cytotoxicity at 100 μM (the highest concentration tested), as determined by a real-time IncuCyte proliferation assay.

### 2.10. Pharmacokinetics

The pharmacokinetic profile of **LSL60101** was investigated prior to the treatment of a murine model of AD (5xFAD). Following a single oral administration of 10 mg/kg of **LSL60101** in CD1 mice, plasma concentrations of drug were found after 15 min of treatment and were detected for 24 h. Absorption of drug from the gastrointestinal tract was slowly reaching C<sub>max</sub> (3.24 μM) at 2 h after dosing and t<sub>1/2β</sub> was around 7 h. The narrow differences in AUC<sub>0</sub><sup>∞</sup> and AUC<sub>0</sub><sup>8</sup> showed complete exposure, good bioavailability and appropriate elimination of **LSL60101** to reach the therapeutic potential of I<sub>2</sub>-IR ligands in the experimental conditions described (Fig. 3).

Furthermore, the remarkable affinity of **LSL60101** for I<sub>2</sub>-IR (pK<sub>i</sub> in mouse brain cortical membranes ranged from 9.92 to 6) and the excellent selectivity ratio I<sub>2</sub>/α<sub>2</sub>-AR (3090) could guarantee, from the kinetic profile observed in plasma, that the concentrations reached at the site of action are enough to demonstrate the efficacy of this drug.

Overall, these studies confirmed that **LSL60101** is orally bioavailable and metabolically stable and can be used for further *in vivo* experiments.

### 2.11. Hypothermic effects of **LSL60101** in naïve mice

Several previous studies have proven the induction of acute hypothermia by I<sub>2</sub>-IR ligands in rats [42,43] and mice [21–23]. In this regard, the present study evaluated the hypothermic effects of **LSL60101** in a wide range of doses (1, 5, 10, 20, 30, 50 mg/kg i.p.) in adult male and female CD1 mice at different times post-injection. The results showed a sharp drop in core body temperature

Pharmacokinetic parameters	
AUC <sub>0-∞</sub> (ug*h/ml)	2.6
AUC <sub>0-t</sub> (ug*h/ml)	2.7
T <sub>max</sub>	2 h
C <sub>max</sub>	0.6 µg/ml
t <sub>1/2 β</sub>	6.7 h

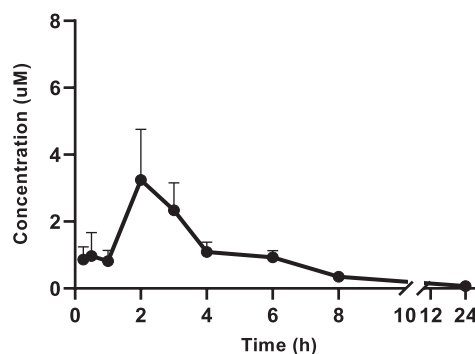


**Fig. 3.** Plasma concentration of **LSL60101** at different times (15 min–24 h) after an oral administration of 10 mg/kg, determined by HPLC/UV-VS at 290 nm. Basic pharmacokinetic parameters were calculated.

(ranging from  $-1.1$  to  $-3.9$  °C) for the larger dose tested (50 mg/kg) and observed 1 and up to 2 h post-injection (Fig. 4). Core body temperature returned to basal levels 3 h after drug administration.

The present results, in line with prior data [42], suggest the need for high doses of **LSL60101** to induce the expected hypothermia characteristic of I<sub>2</sub>-IR ligands [21–23,43]. As for the role of this acute pharmacological effect, hypothermia is known to provide neuroprotection in models of cerebral ischemia; even mild temperature drops can cause significant neuroprotection [44]. In fact, hypothermia has been used to improve the neurological outcome under various pathological conditions, including stroke and traumatic brain injury [45,46]. In this line of thought, **LSL60101** has proven to partially prevent neuronal death in rats following neonatal axotomy [36], and thus, its hypothermic effects might be a relevant feature that could be mediating certain degree of neuroprotection.

Although the agonist or antagonist nature of I<sub>2</sub>-IR ligands has been a topic of debate [2], it has been suggested that I<sub>2</sub>-IR agonists reliably decrease body temperature in a highly quantitative manner in rodents [42], suggesting this assay could be used as a sensitive *in vivo* assay for studying I<sub>2</sub> receptor ligands, and in line with the hypothermic effects observed in the present study in mice treated with **LSL60101**.

#### 2.12. Effects of acute **LSL60101** on hippocampal FADD protein content in naïve mice

In the context of neuroprotection, FADD adaptor emerges as a key multifunctional protein involved in the mechanisms

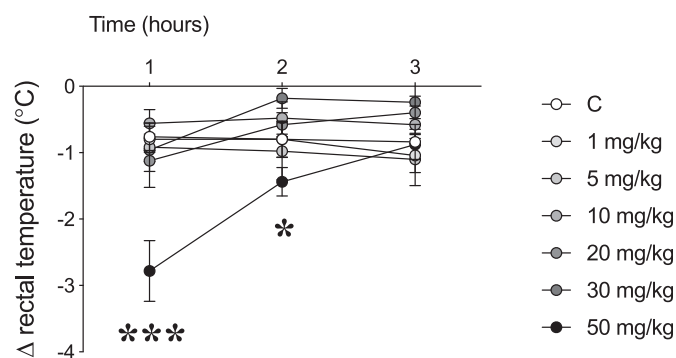


**Fig. 4.** Acute effects of **LSL60101** treatment on core body temperature in mice. Symbols represent means  $\pm$  SEM of the difference ( $\Delta$ , 1, 2 or 3 h minus basal value) in body temperature (°C) for each treatment group. \*\*\* $p$  < 0.001 and \* $p$  < 0.05 when comparing the dose of 50 mg/kg with the control group (repeated measures ANOVA followed by Sidak's comparison test).

controlling cell fate regulation, balancing pro-apoptotic and/or neuroprotective actions in rodents [21,47,48]. The acute treatment with a high dose of **LSL60101** (50 mg/kg, i.p.) significantly decreased (by  $\sim$ 34%) hippocampal FADD protein content as compared to vehicle-treated mice (Fig. 5). The present results replicated earlier studies in which other I<sub>2</sub>-IR ligands decreased FADD hippocampal content [21,23], and suggested the induction of non-apoptotic (e.g., neuroplastic and or neuroprotective) actions initiated by acute **LSL60101** treatment in mice brain and in parallel to the hypothermic effects.

#### 2.13. Effects of chronic **LSL60101** at a low dose in a mice model of Alzheimer's disease

Accumulating evidence support that I<sub>2</sub>-IR exert neuroprotective roles in a plethora of neurodegenerative disorders, such as AD [8,9,11,49,50]. Previous studies suggested that I<sub>2</sub>-IR in the CNS are mainly located on the outer membrane of mitochondria in astrocytes [51]. Given that alterations in mitochondrial function promote an increased ROS production, which combined with an altered antioxidant defence contribute to the early stages of AD before the development of A $\beta$  pathology and cognitive dysfunction [29,30,52], here we tested the effects of a low dose of **LSL60101** administered following a chronic paradigm (1 mg/kg/day, for 4 weeks) on specific OS markers under oxidative damage in 5XFAD mice, an early-onset mouse transgenic model of AD, and as compared to a wild type strain. The results showed increased gene expression of the so-called antioxidant response element (AREs), such as heme oxygenase 1 (Hmox1), aldehyde dehydrogenase 2 (Aldh2) and iNOS [53] in 5XFAD vs. wild type mice (Fig. 6). By contrast, in 5XFAD mice treated with **LSL60101**, the expression of those decreased in a significant way.

On the other hand, an excess in ROS is removed by antioxidant enzymes (e.g., superoxide dismutase, SOD1, and glutathione peroxidase, GPX-1). 5XFAD mice showed a significant decrease in both proteins levels in reference to wild type mice. Interestingly, **LSL60101** was able to significantly increase the levels of these key protein, indicating that **LSL60101** induced the activation of a cellular signalling cascade that led to a reduced OS, and that in turn could have a neuroprotective role in an oxidative environment related with neurodegenerative processes such as AD (Fig. 7).

These results are in agreement with recent studies that demonstrated a key role for I<sub>2</sub>-IR ligands in the OS process. In particular, 2-BFI (a selective ligand to I<sub>2</sub>-IR), decreased OS and altered the level of anti-oxidant enzymes in an AD rat model [54], protecting against OS-induced astrocytic cell death [55]. Ultimately, previous work from our group reported a decrease in hydrogen peroxide levels and OS markers induced by the I<sub>2</sub>-IR ligands **MCR5**

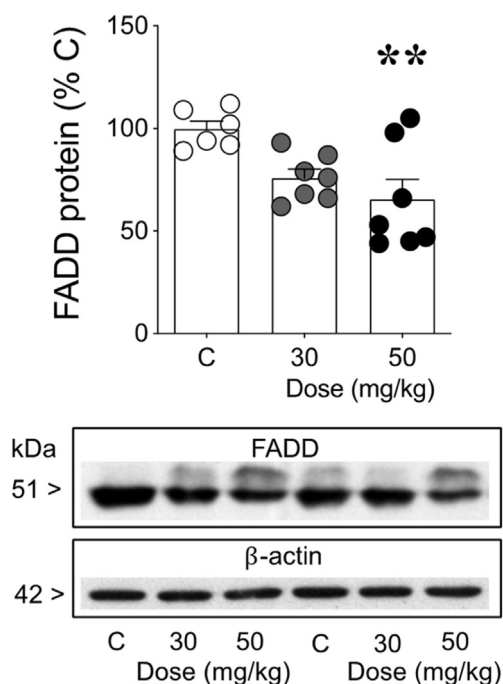


**Fig. 5.** Acute effects of **LSL60101** (30 or 50 mg/kg, i.p.) on hippocampal FADD protein. Columns are means  $\pm$  SEM of FADD content (% C) for each treatment group. Individual symbols are shown for each animal. One-way ANOVA followed by Sidak's multiple comparisons tests: \*\* $p < 0.01$  vs. C (control-treated mice). Representative immunoblots depicting the labelling of FADD and  $\beta$ -actin (as a loading control) for each treatment group are shown below.

and **MCR9** in aged SAMP8 mice [22]. Recently, we demonstrated that **LSL60101** can ameliorate the AD hallmarks and neuroinflammation [56]. Moreover, the chronic treatment with **LSL60101** led to the induction of reactive astrocytes and the up-regulation of the expression of the astrocyte marker glial fibrillary acidic protein (GFAP) [34]. As mentioned, astrocytes are the main supportive cells in the CNS and are significantly involved in the redox homeostasis [57], and thus, and as a consequence, this could be proposed as a possible effect of **LSL60101** on OS balance.

### 3. Conclusions

We have evaluated the binding and selective properties upon  $I_2$ -IR in human brain tissues of a series of benzofuranyl-2-imidazoles diversely substituted in both benzofuranyl and imidazole rings. Due to the lack of structural description of these receptors, 3D-QSAR and *in silico* physicochemical properties were performed in order to determine the relevant elements that may allow the further structural optimization of new molecules. The secure theoretical DMPK of the family led us to undertake *in vitro* studies including PAMPA to confirm their penetration into the CNS to address neurodegenerative issues. The safe *in vitro* DMPK and cytotoxicity assays of the selected **LSL60101** opened the door to *in vivo* studies. After the determination of its pharmacokinetic profile, the treatment of animals with **LSL60101** confirmed a decrease in the content of hippocampal FADD protein, a key signalling mediator of neuroprotective actions. The  $I_2$ -IR ligand **LSL60101** also fostered a diminution in oxidative stress biomarkers in an AD murine model (5xFAD). Thus, the modulation of  $I_2$ -IR by **LSL60101** is proposed as a promising opportunity for addressing AD therapeutics and invites for the further design of new promising benzofuranyl-2-imidazole-base structures to be added to the scarce arsenal of  $I_2$ -IR ligands.

## 4. Experimental section

### 4.1. Chemistry

Reagents, solvents and starting products were acquired from commercial sources. The term "concentration" refers to the vacuum evaporation using a Büchi rotavapor. When indicated, the reaction products were purified by "flash" chromatography on silica gel (35–70  $\mu$ m) with the indicated solvent system. IR spectra were performed in a Spectrum Two FT-IR Spectrometer, and only noteworthy IR absorptions ( $\text{cm}^{-1}$ ) are listed. NMR spectra were recorded in  $\text{DMSO-}d_6$  at 400 MHz ( $^1\text{H}$ ) and 100.6 MHz ( $^{13}\text{C}$ ), and chemical shifts are reported in  $\delta$  values downfield from TMS or relative to residual  $\text{DMSO-}d_6$  (2.50 ppm, 39.5 ppm) as an internal standard. Data are reported in the following manner: chemical shift, multiplicity, coupling constant (J) in hertz (Hz) and integrated intensity. Multiplicities are reported using the following abbreviations: s, singlet; d, doublet; dd, double doublet; q, quadruplet; t, triplet; m, multiplet; br s, broad signal. The accurate mass analyses were carried out using a LC/MSD-TOF spectrophotometer. HPLC-MS (Agilent 1260 Infinity II) analysis was conducted on a Poroshell 120 EC-C15 (4.6 mm  $\times$  50 mm, 2.7  $\mu$ m) at 40  $^\circ\text{C}$  with mobile phase A ( $\text{H}_2\text{O} + 0.05\%$  formic acid) and B (ACN + 0.05% formic acid) using a gradient elution and flow rate 0.6 mL/min. The DAD detector was set at 254 nm, the injection volume was 5  $\mu$ L, and oven temperature was 40  $^\circ\text{C}$ . All tested compounds possess a purity of at least 95%.

#### 4.1.1. General procedures for the synthesis of benzofuran-2-carboxamides **1b**, **1c** and **1d**

Thionyl chloride (1.65 equiv) was added to a suspension of benzofuran-2-carboxylic acid derivatives (1 equiv) in anhydrous toluene (0.4 mmol/mL). After stirring the mixture for 3 h, at reflux, the reaction was cooled and concentrated. Then, the resulting benzofuran-2-carbonyl chloride derivative (1 equiv) was added in small portions to an ice-cold solution of 25% aq.  $\text{NH}_4\text{OH}$  (0.5 mmol/mL). Upon completion of the addition the reaction mixture was allowed to reach rt and a precipitate was formed. The solid was collected by filtration, washed with cold water and dried under vacuum.

**4.1.1.1. 5-Methoxybenzofuran-2-carboxamide (1b).** Following the general procedure, thionyl chloride (17.2 mmol, 1.25 mL), 5-bromobenzofuran-2-carboxylic acid (10.4 mmol, 2.0 g), anhydrous toluene (25 mL) and 25% aq.  $\text{NH}_4\text{OH}$  (20 mL) gave **1b** (1.87 g, 98%) as a beige solid.

**4.1.1.2. 6-Methoxybenzofuran-2-carboxamide (1c).** Following the general procedure, thionyl chloride (8.60 mmol, 0.63 mL), 6-methoxybenzofuran-2-carboxylic acid (5.20 mmol, 1.0 g), anhydrous toluene (13 mL) and 25% aq.  $\text{NH}_4\text{OH}$  (10 mL) gave **1c** (930 mg, 97%) as a beige solid.

**4.1.1.3. 5-Bromobenzofuran-2-carboxamide (1d).** Following the general procedure, thionyl chloride (13.7 mmol, 1.0 mL), 5-bromobenzofuran-2-carboxylic acid (8.30 mmol, 2.0 g), anhydrous toluene (21 mL) and 25% aq.  $\text{NH}_4\text{OH}$  (17 mL) gave **1d** (1.98 g, 99%) as a white solid.

#### 4.1.2. General procedure for the synthesis of benzofuran-2-carbonitrile **2b**, **2c** and **2d**

Phosphoryl chloride (3 equiv) was added to a solution of benzofuran-2-carboxamide derivative (1 equiv) in dichloroethane (0.48 mmol/mL). The reaction was stirred at 75  $^\circ\text{C}$  for 2 h. Then, the reaction mixture was evaporated and neutralized with saturated  $\text{NaHCO}_3$  solution. The aqueous phase was extracted with  $\text{AcOEt}$ , the

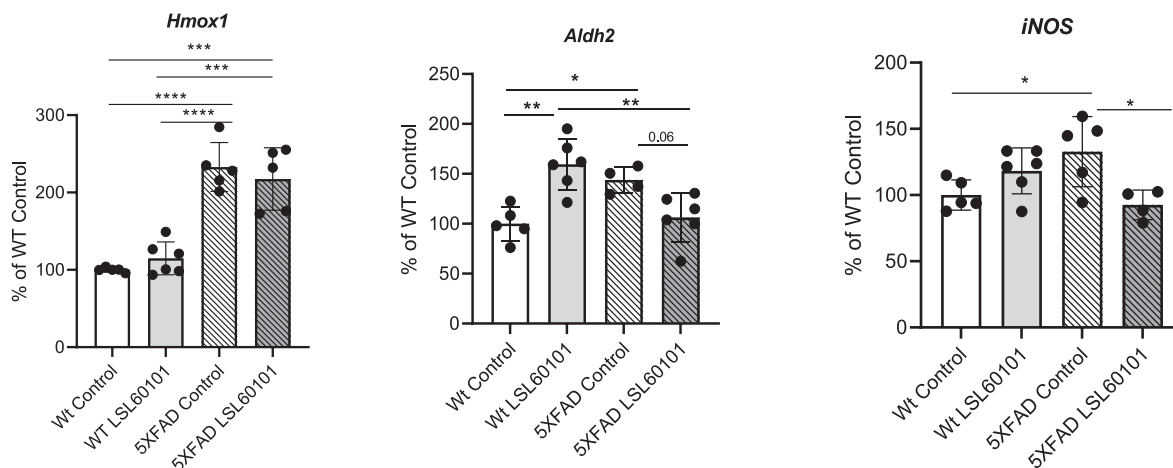


**Fig. 6.** Chronic effects of **LSL60101** (1 mg/kg/day, per os.) on *Hmox1*, *Aldh2* and *iNOS* gene expression in hippocampus. Columns are the mean  $\pm$  SEM for each treatment group. Individual symbols are shown for each animal. Means were compared with two-way ANOVAs, followed by Tukey-Kramer multiple comparison post-hoc analysis: \*\*\*\* $p$  < 0.0001; \*\*\* $p$  < 0.001; \*\* $p$  < 0.01; \* $p$  < 0.05 vs. Wt Controls.

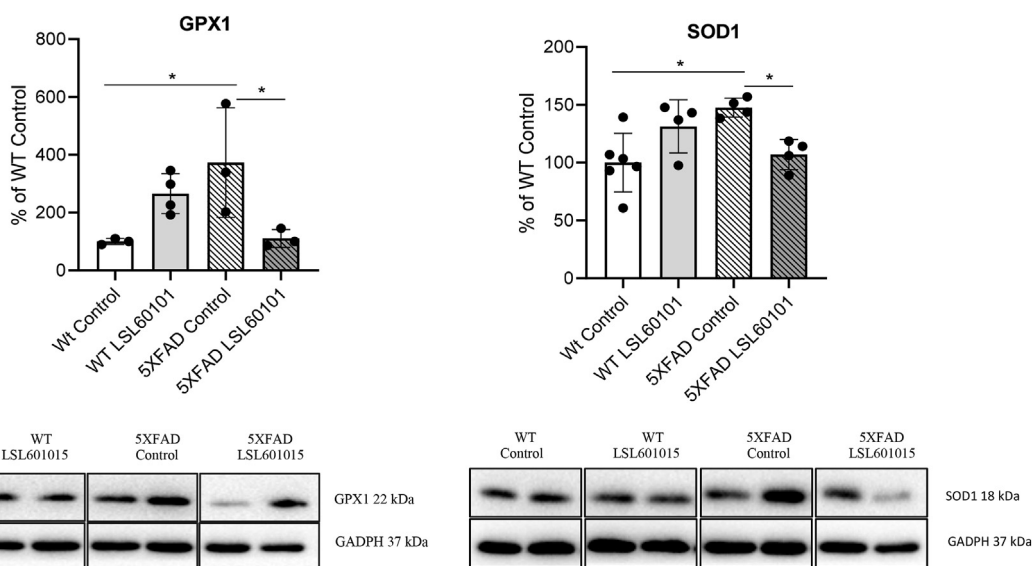


**Fig. 7.** Chronic effects of **LSL60101** (1 mg/kg/day, per os.) on the expression of SOD1 and GPX-1 protein levels in hippocampus. Columns are the mean  $\pm$  SEM for each treatment group. Individual symbols are shown for each animal. Means were compared with two-way ANOVAs, followed by Tukey-Kramer multiple comparisons post-hoc analysis. \* $p$  < 0.01 vs. Wt control mice).

combined organic phases were washed with brine, dried over  $\text{Na}_2\text{SO}_4$ , and evaporated to give a residue, which was purified by flash column chromatography.

**4.1.2.1. 5-Methoxybenzofuran-2-carbonitrile (2b).** Following the general procedure, **1b** (9.62 mmol, 1.84 g), dichloroethane (20 mL) and phosphoryl chloride (28.9 mmol, 2.70 mL) gave **2b** (1.42 g, 85%) as a beige solid, after column chromatography (dichloromethane 100%).

**4.1.2.2. 6-Methoxybenzofuran-2-carbonitrile (2c).** Following the general procedure, **1c** (4.87 mmol, 930 mg), dichloroethane (10 mL) and phosphoryl chloride (14.6 mmol, 1.36 mL) gave **2c** (740 mg, 88%) as a beige solid, after column chromatography (dichloromethane 100%).

**4.1.2.3. 5-Bromobenzofuran-2-carbonitrile (2d).** Following the general procedure, **1d** (7.92 mmol, 1.90 g), dichloroethane (17 mL) and

phosphoryl chloride (23.8 mmol, 2.21 mL) gave **2d** (1.55 g, 88%) as a white solid, after column chromatography (dichloromethane 100%).

#### 4.1.3. General procedure for the synthesis of methyl benzofuran-2-carbimidate hydrochlorides **3a**, **3b**, **3c** and **3d**

The 2-cyanobenzofuran derivative (1 equiv) was dissolved in ethereal HCl 2 M (0.25 mmol/mL) and methanol (5 mmol/mL). The resulting mixture was kept at 4 °C for 48 h. The resulting solid was filtered, washed with cold ether and dried in order to obtain the desired carbimidate hydrochloride.

**4.1.3.1. Methyl benzofuran-2-carbimidate hydrochloride (3a).** Following the general procedure, benzofuran-2-carbonitrile (6.99 mmol, 1.0 g), ethereal HCl 2 M (28 mL) and methanol (1.4 mL) gave **3a** (1.29 g, 87%) as a white solid.



4.1.3.2. *Methyl 5-methoxybenzofuran-2-carbimidate hydrochloride (3b)*. Following the general procedure, **2b** (8.08 mmol, 1.40 g), ethereal HCl 2 M (32 mL), methanol (2 mL) gave **3b** (1.62 g, 83%) as a white solid.

4.1.3.3. *Methyl 6-methoxybenzofuran-2-carbimidate hydrochloride (3c)*. Following the general procedure, **2c** (4.04 mmol, 700 mg), ethereal HCl 2 M (16 mL) and methanol (1 mL) gave **3c** (797 mg, 82%) as a white solid.

4.1.3.4. *Methyl 5-bromobenzofuran-2-carbimidate hydrochloride (3d)*. Following the general procedure, **2d** (4.82 mmol, 1.10 g), ethereal HCl 2 M (19 mL) and methanol (1 mL) gave **3d** (1.20 g, 86%) as a white solid.

#### 4.1.4. General procedure for the synthesis of *N*-(2,2-dimethoxyethyl)benzofuran-2-carboximidamide **4a**, **4b**, **4c** and **4d**

A solution of 2,2-dimethoxyethylamine (1.1 equiv) and methyl benzofuran-2-carbimidate hydrochloride derivative (1 equiv) in methanol (0.47 mmol/mL) was stirred at 60 °C for 16 h. The mixture was evaporated to dryness, which was used directly in the next step without further purification.

4.1.4.1. *N*-(2,2-dimethoxyethyl)benzofuran-2-carboximidamide (**4a**). Following the general procedure, **3a** (5.20 mmol, 1.10 g), 2,2-dimethoxyethylamine (5.72 mmol, 0.62 mL) and methanol (11 mL) gave **4a** (1.29 g, quantitative) as a beige solid.

4.1.4.2. *N*-(2,2-Dimethoxyethyl)-5-methoxybenzofuran-2-carboximidamide (**4b**). Following the general procedure, **3b** (4.34 mmol, 1.05 g), 2,2-dimethoxyethylamine (4.78 mmol, 0.52 mL) and methanol (9 mL) gave **4b** (1.29 g, quantitative) as a beige solid.

4.1.4.3. *N*-(2,2-Dimethoxyethyl)-6-methoxybenzofuran-2-carboximidamide (**4c**). Following the general procedure, **3c** (2.93 mmol, 708 mg), 2,2-dimethoxyethylamine (3.22 mmol, 0.35 mL) and methanol (6 mL) gave **4c** (815 mg, quantitative) as a beige solid.

4.1.4.4. *N*-(2,2-Dimethoxyethyl)-5-bromobenzofuran-2-carboximidamide (**4d**). Following the general procedure, **3d** (2.01 mmol, 584 mg), 2,2-dimethoxyethylamine (2.21 mmol, 0.24 mL) and methanol (4 mL) gave **4d** (657 mg, quantitative) as a beige solid.

#### 4.1.5. General procedure for the synthesis of 2-(benzofuran-2-yl)-1H-imidazole hydrochlorides **LSL60101**, **5b**, **5c** and **5d**

The corresponding *N*-(2,2-dimethoxyethyl)benzofuran-2-carboximidamide was treated with HCl 2 M (0.1 mmol/mL) and the resulting mixture was stirred at 60 °C for 16 h. After cooling, the solution was washed with dichloromethane. The aqueous layer was basified with NaOH 5 M and the free base extracted with AcOEt. The combined organic phases were washed with brine, dried over Na<sub>2</sub>SO<sub>4</sub>, and evaporated to give a residue which was dissolved in diethyl ether/ethanol (5:1). Ethereal HCl 2 M (1.5 mmol/mL) was added and the precipitated salt was collected by filtration and was crystallized with acetonitrile.

4.1.5.1. 2-(Benzofuran-2-yl)-1H-imidazole hydrochloride (**5a**). Following the general procedure, **4a** (5.20 mmol, 1.29 g), HCl 2 M (52 mL) and ethereal HCl 2 M (3.5 mL) gave **LSL60101** (960 mg, 84%) as a white solid. IR (ATR) 3477, 3168, 2535, 1651, 1457, 1310, 1140, 1009, 879, 737, 706 cm<sup>-1</sup>. <sup>1</sup>H NMR (400 MHz, DMSO-*d*<sub>6</sub>) δ 7.40 (t, *J* = 7.5 Hz, 1H), 7.52 (t, *J* = 8.5 Hz, 1H), 7.74 (d, *J* = 8.5 Hz, 1H), 7.83 (s,

2H), 7.88 (d, *J* = 7.5 Hz, 1H), 8.12 (s, 1H). <sup>13</sup>C NMR (100.6 MHz) δ 109.8, 111.6, 120.8 (2C), 122.9, 124.4, 127.1, 127.3, 135.1, 140.6, 154.6. HRMS C<sub>11</sub>H<sub>9</sub>N<sub>2</sub>O [M+H]<sup>+</sup> 185.0709; found, 185.0706. Purity 99.6% (t<sub>R</sub> = 3.08 min).

4.1.5.2. 2-(5-Methoxybenzofuran-2-yl)-1H-imidazole hydrochloride (**5b**). Following the general procedure, **4b** (4.10 mmol, 1.14 g), HCl 2 M (41 mL) and ethereal HCl 2 M (2.7 mL) gave **5b** (950 mg, 93%) as a white solid. IR (ATR) 3449, 3076, 2587, 1647, 1457, 1434, 1206, 1157, 1018, 812, 776, 712 cm<sup>-1</sup>. <sup>1</sup>H NMR (400 MHz, DMSO-*d*<sub>6</sub>) δ 3.81 (s, 3H), 7.08 (dd, *J* = 9.0, 2.5 Hz, 1H), 7.38 (d, *J* = 2.5 Hz, 1H), 7.61 (d, *J* = 9.0 Hz, 1H), 7.82 (s, 2H), 8.10 (s, 1H). <sup>13</sup>C NMR (100.6 MHz) δ 55.7, 104.4, 110.2, 112.2, 116.5, 120.7 (2C), 127.8, 135.0, 141.1, 149.5, 156.5. HRMS C<sub>12</sub>H<sub>11</sub>N<sub>2</sub>O<sub>2</sub> [M+H]<sup>+</sup> 215.0815; found, 215.0816. Purity 98.5% (t<sub>R</sub> = 3.19 min).

4.1.5.3. 2-(6-Methoxybenzofuran-2-yl)-1H-imidazole hydrochloride (**5c**). Following the general procedure, **4c** (2.93 mmol, 815 mg), HCl 2 M (29 mL) and ethereal HCl 2 M (2.0 mL) gave **5c** (702 mg, 96%) as a white solid. IR (ATR) 3349, 3089, 2731, 1614, 1492, 1269, 1151, 1110, 1023, 842, 773, 709 cm<sup>-1</sup>. <sup>1</sup>H NMR (400 MHz, DMSO-*d*<sub>6</sub>) δ 3.86 (s, 3H), 7.02 (dd, *J* = 8.5, 2.0 Hz, 1H), 7.23 (s, 1H), 7.74 (d, *J* = 8.5 Hz, 1H), 7.77 (s, 2H), 8.06 (s, 1H). <sup>13</sup>C NMR (100.6 MHz) δ 55.9, 95.8, 110.2, 113.8, 120.2, 120.4 (2C), 123.2, 135.2, 139.6, 156.0, 159.8. HRMS C<sub>12</sub>H<sub>11</sub>N<sub>2</sub>O<sub>2</sub> [M+H]<sup>+</sup> 215.0815; found, 215.0814. Purity 99.6% (t<sub>R</sub> = 3.20 min).

4.1.5.4. 2-(5-Bromobenzofuran-2-yl)-1H-imidazole hydrochloride (**5d**). Following the general procedure, **4d** (1.99 mmol, 650 mg), HCl 2 M (20 mL) and ethereal HCl 2 M (1.3 mL) gave **5d** (536 mg, 82%) as a white solid. IR (ATR) 3379, 3171, 2703, 1650, 1566, 1447, 1143, 1047, 879, 749, 718 cm<sup>-1</sup>. <sup>1</sup>H NMR (400 MHz, DMSO-*d*<sub>6</sub>) δ 7.62 (dd, *J* = 9.0, 2.0 Hz, 1H), 7.70 (d, *J* = 9.0 Hz, 1H), 7.83 (s, 2H), 8.07 (s, 1H), 8.12 (d, *J* = 2.0 Hz, 1H). <sup>13</sup>C NMR (100.6 MHz) δ 108.9, 113.7, 116.6, 121.1 (2C), 125.3, 129.4, 129.8, 134.6, 142.0, 153.3. HRMS C<sub>11</sub>H<sub>8</sub>BrN<sub>2</sub>O [M+H]<sup>+</sup> 262.9815; found, 262.9813. Purity 98.6% (t<sub>R</sub> = 3.47 min).

#### 4.1.6. General procedure for the synthesis of 1-alkyl-2-(benzofuran-2-yl)-1H-imidazole hydrochlorides **6b** and **6c**

2-(Benzofuran-2-yl)-1H-imidazole hydrochlorides derivatives were neutralized with NaOH 2 N and the free base was extracted with AcOEt. The combined organic phases were washed with brine, dried over Na<sub>2</sub>SO<sub>4</sub>, and evaporated to give the desired amine. To a solution of the free base (1 equiv) generated from the corresponding 2-(benzofuran-2-yl)-1H-imidazole hydrochloride was treated with HBr 47% acid solution (0.5 mL) and the mixture was stirred at 100 °C for 7 h. After cooling the resulting solid was filtered, dissolved in water and basified with saturated NaHCO<sub>3</sub> solution. The free base was extracted with AcOEt. The combined organic phases were washed with brine, dried over Na<sub>2</sub>SO<sub>4</sub>, and evaporated to give a residue which was dissolved in diethyl ether/ethanol. Ethereal HCl 2 M (1.5 mmol/mL) was added and the precipitated salt was collected by filtration and was crystallized with acetonitrile.

4.1.6.1. 2-(5-Hydroxybenzofuran-2-yl)-1H-imidazole hydrochloride (**6b**). Following the general procedure, **5b** (0.93 mmol, 200 mg), HBr 47% acid solution (2 mL) and ethereal HCl 2 M (0.6 mL) gave **6b** (191 mg, 81%) as a yellowish solid. IR (ATR) 3266, 3009, 2819, 2731, 1593, 1443, 1370, 1246, 1195, 1157, 1090, 850, 802, 700 cm<sup>-1</sup>. <sup>1</sup>H NMR (400 MHz, DMSO-*d*<sub>6</sub>) δ 6.99 (dd, *J* = 9.0, 2.0 Hz, 1H), 7.14 (d, *J* = 2.0 Hz, 1H), 7.51 (d, *J* = 9.0 Hz, 1H), 7.80 (s, 2H), 7.97 (d, *J* = 1.0 Hz, 1H). <sup>13</sup>C NMR (100.6 MHz) δ 106.4, 109.9, 111.9, 116.7, 120.6 (2C), 127.9, 135.2, 140.7, 148.9, 154.5. HRMS C<sub>11</sub>H<sub>9</sub>N<sub>2</sub>O<sub>2</sub> [M+H]<sup>+</sup>

201.0659; found, 201.0656. Purity 98.1% ( $t_R = 2.92$  min).

**4.1.6.2. 2-(6-Hydroxybenzofuran-2-yl)-1H-imidazole hydrochloride (6c).** Following the general procedure, **5c** (0.93 mmol, 200 mg), HBr 47% acid solution (1.9 mL) and ethereal HCl 2 M (0.6 mL) gave **6c** (183 mg, 77%) as a yellowish solid. IR (ATR) 3388, 3092, 2813, 2755, 1624, 1430, 1377, 1283, 1150, 1122, 1096, 839, 766, 708  $\text{cm}^{-1}$ .  $^1\text{H}$  NMR (400 MHz, DMSO- $d_6$ )  $\delta$  6.92 (dd,  $J = 8.5, 2.0$  Hz, 1H), 7.10 (s, 1H), 7.63 (d,  $J = 8.5$  Hz, 1H), 7.77 (s, 2H), 8.01 (s, 1H), 10.30 (br s, 1H).  $^{13}\text{C}$  NMR (100.6 MHz)  $\delta$  97.5, 110.6, 114.4, 118.9, 120.2 (2C), 123.2, 135.4, 138.7, 156.2, 158.4. HRMS  $\text{C}_{11}\text{H}_9\text{N}_2\text{O}_2$   $[\text{M}+\text{H}]^+$  201.0659; found, 201.0657. Purity 97.6% ( $t_R = 2.91$  min).

#### 4.1.7. General procedure for the synthesis of 1-alkyl-2-(benzofuran-2-yl)-1H-imidazole hydrochlorides **7a**, **7aa**, **7b** and **7c**

2-(Benzofuran-2-yl)-1H-imidazole hydrochlorides derivatives were neutralized with NaOH 2 N and the free base was extracted with AcOEt. The combined organic phases were washed with brine, dried over  $\text{Na}_2\text{SO}_4$ , and evaporated to give the desired amine. To a solution of the free base (1 equiv) generated from the corresponding 2-(benzofuran-2-yl)-1H-imidazole hydrochloride in DMF (0.34 mmol/mL) at 0 °C was added sodium hydride (1.5 equiv, 60% in mineral oil). After 30 min at rt, methyl iodide/ethyl bromide (1.1 equiv) was added dropwise over 15 min at 0 °C. Then, the mixture was stirred for 30 min at rt, poured into water and extracted with AcOEt. The organic layer was washed with and the product was extracted with HCl 1 M. The aqueous layer was basified with NaOH 2 M and the free base was extracted with AcOEt. The combined organic phases were washed with brine, dried over  $\text{Na}_2\text{SO}_4$ , and evaporated to give a residue which was dissolved in diethyl ether/ethanol. Ethereal HCl 2 M (1.5 mmol/mL) was added and the precipitated salt was collected by filtration and was crystallized with acetonitrile.

**4.1.7.1. 1-Methyl-2-(benzofuran-2-yl)-1H-imidazole hydrochloride (7a).** Following the general procedure, **LSL60101** (0.76 mmol, 140 mg), methyl iodide (0.84 mmol, 0.05 mL), sodium hydride 60% in mineral oil (1.14 mmol, 45.8 mg), DMF (2.3 mL) and ethereal HCl 2 M (0.5 mL) gave **7a** (150 mg, 84%) as a white solid. IR (ATR) 3306, 3095, 2569, 1634, 1445, 1270, 1188, 1131, 1033, 883, 756, 708  $\text{cm}^{-1}$ .  $^1\text{H}$  NMR (400 MHz, DMSO- $d_6$ )  $\delta$  4.13 (s, 3H), 7.43 (t,  $J = 7.5$  Hz, 1H), 7.55 (t,  $J = 8.5$  Hz, 1H), 7.77 (d,  $J = 8.5$  Hz, 1H), 7.80 (d,  $J = 2.0$  Hz, 1H), 7.86–7.91 (m, 2H), 8.01 (s, 1H).  $^{13}\text{C}$  NMR (100.6 MHz)  $\delta$  36.8, 111.5, 112.2, 121.0, 123.2, 124.9, 126.0, 127.4, 127.9, 135.6, 140.5, 154.9. HRMS  $\text{C}_{12}\text{H}_{11}\text{N}_2\text{O}$   $[\text{M}+\text{H}]^+$  199.0866; found, 199.0866. Purity 99.7% ( $t_R = 3.15$  min).

**4.1.7.2. 1-Ethyl-2-(benzofuran-2-yl)-1H-imidazole hydrochloride (7aa).** Following the general procedure, **LSL60101** (1.36 mmol, 250 mg), ethyl bromide (1.42 mmol, 0.10 mL), sodium hydride 60% in mineral oil (2.04 mmol, 82 mg), DMF (4.0 mL) and ethereal HCl 2 M (0.9 mL) gave **7aa** (310 mg, 92%) as a white solid. IR (ATR) 3394, 3104, 2618, 1628, 1428, 1266, 1177, 1111, 929, 836, 761, 708  $\text{cm}^{-1}$ .  $^1\text{H}$  NMR (400 MHz, DMSO- $d_6$ )  $\delta$  1.50 (t,  $J = 7.0$  Hz, 3H), 4.55 (q,  $J = 7.0$  Hz, 2H), 7.41 (d,  $J = 7.5$  Hz, 1H), 7.53 (t,  $J = 8.0$  Hz, 1H), 7.76 (d,  $J = 8.5$  Hz, 1H), 7.86–7.88 (m, 2H), 8.00 (d,  $J = 1.5$  Hz, 1H), 8.12 (s, 1H).  $^{13}\text{C}$  NMR (100.6 MHz)  $\delta$  15.2, 44.3, 111.6, 111.8, 120.8, 122.8, 123.9, 124.5, 126.8, 127.5, 134.1, 139.7, 154.6. HRMS  $\text{C}_{13}\text{H}_{13}\text{N}_2\text{O}$   $[\text{M}+\text{H}]^+$  213.1022; found, 213.1021. Purity 100% ( $t_R = 3.35$  min).

**4.1.7.3. 1-Ethyl-2-(5-methoxybenzofuran-2-yl)-1H-imidazole hydrochloride (7b).** Following the general procedure, **5b** (0.93 mmol, 200 mg), ethyl bromide (0.98 mmol, 0.07 mL), sodium hydride 60% in mineral oil (1.40 mmol, 56 mg), DMF (3 mL) and ethereal HCl 2 M (0.6 mL) gave **7b** (220 mg, 90%) as a white solid. IR (ATR) 3410, 3143,

2532, 1610, 1490, 1420, 1255, 1209, 1021, 928, 810, 758, 709  $\text{cm}^{-1}$ .  $^1\text{H}$  NMR (400 MHz, DMSO- $d_6$ )  $\delta$  1.49 (t,  $J = 7.0$  Hz, 3H), 3.82 (s, 3H), 4.54 (q,  $J = 7.0$  Hz, 2H), 7.10 (dd,  $J = 9.0, 2.5$  Hz, 1H), 7.35 (d,  $J = 2.5$  Hz, 1H), 7.66 (d,  $J = 9.0$  Hz, 1H), 7.85 (d,  $J = 2.0$  Hz, 1H), 7.98 (d,  $J = 2.0$  Hz, 1H), 8.06 (s, 1H).  $^{13}\text{C}$  NMR (100.6 MHz)  $\delta$  15.2, 44.3, 55.7, 104.1, 111.7, 112.5, 116.8, 120.7, 123.8, 127.5, 134.1, 140.3, 149.6, 156.5. HRMS  $\text{C}_{14}\text{H}_{15}\text{N}_2\text{O}_2$   $[\text{M}+\text{H}]^+$  243.1128; found, 243.1128. Purity 98.4% ( $t_R = 3.44$  min).

**4.1.7.4. 1-Ethyl-2-(6-methoxybenzofuran-2-yl)-1H-imidazole hydrochloride (7c).** Following the general procedure, **5c** (0.93 mmol, 200 mg), ethyl bromide (0.98 mmol, 0.07 mL), sodium hydride 60% in mineral oil (1.40 mmol, 56 mg), DMF (2.7 mL) and ethereal HCl 2 M (0.6 mL) gave **7c** (212 mg, 87%) as a white solid. IR (ATR) 3474, 3151, 2728, 1614, 1495, 1417, 1276, 1150, 1108, 1021, 928, 853, 813, 778, 701  $\text{cm}^{-1}$ .  $^1\text{H}$  NMR (400 MHz, DMSO- $d_6$ )  $\delta$  1.49 (t,  $J = 7.0$  Hz, 3H), 3.86 (s, 3H), 4.52 (q,  $J = 7.0$  Hz, 2H), 7.03 (dd,  $J = 8.5, 2.0$  Hz, 1H), 7.33 (s, 1H), 7.73 (d,  $J = 8.5$  Hz, 1H), 7.82 (d,  $J = 2.0$  Hz, 1H), 7.95 (d,  $J = 2.0$  Hz, 1H), 8.05 (s, 1H).  $^{13}\text{C}$  NMR (100.6 MHz)  $\delta$  15.2, 44.2, 55.9, 95.8, 112.0, 114.2, 119.9, 120.3, 123.1, 123.6, 134.3, 138.6, 156.1, 159.9. HRMS  $\text{C}_{14}\text{H}_{15}\text{N}_2\text{O}_2$   $[\text{M}+\text{H}]^+$  243.1128; found, 243.1128. Purity 99.2% ( $t_R = 3.37$  min).

## 4.2. X-ray crystallographic analysis

Crystals of **LSL60101** were obtained from slow evaporation of methanol solutions. The single crystal X-Ray diffraction data set was collected at 294 K up to a max  $2\theta$  of ca. 57° on a Bruker Smart APEX II diffractometer, using monochromatic MoK $\alpha$  radiation  $\lambda = 0.71073$  Å and 0.3° separation between frames. Data integration was performed using SAINT V6.45A and SORTAV (Blessing, 1995) in the diffractometer package. The crystal and collection data and structural refinement parameters are given in Table S14. The structure was solved by direct methods using SHELXT-2014 (Sheldrick, 2014) and Fourier's difference methods, and refined by least squares on  $F^2$  using SHELXL-2014/7 (Sheldrick, 2014) inside the WinGX program environment (Farrugia, 2012). Atom coordinates are given in Table S15 and bond distances and angles in Table S16. The crystal structure shows the chlorohydrate form of **LSL60101**, which is as almost planar, as well as a methanol solvent molecule. Anisotropic displacement parameters were used for non-H atoms (Table S17) and the H-atoms were positioned in calculated positions (except H2) and refined riding on their parent atoms. Fig. 8 exhibits an ORTEP view of the molecule with the atom labelling, as well as its closest intermolecular bonds (Table S18) with the chloride anion (N12–H12...Cl1) and the methanol molecule (N9–H9...O2). These two intermolecular bonds are slightly out of the plane of the **LSL60101** molecule, producing a small torsion of the imidazolium group respect to the molecular mean plane ( $\tau(\text{O1}–\text{C2}–\text{C8}–\text{N9}) = -4.3(11)$ ,  $\tau(\text{C3}–\text{C2}–\text{C8}–\text{N12}) = -1.8(14)^\circ$ ). Methanol is also bonded to the chloride anion through the contact  $\text{O2}–\text{H2} \cdots \text{Cl1}^i$  ( $i = x-1, y, z$ ), giving rise to corrugated chains along **a**, assembled by parallel stacking along **c**. Crystallographic data (excluding structure factors) for the reported structure has been deposited in the Cambridge Crystallographic Data Centre as supplementary publication, CCDC No. 2063533. Copies of this information may be obtained free of charge from The Director, CCDC, 12 Union Road, Cambridge CB2 1EZ, UK. Fax: +44 1223 336 033. E-mail: data\_request@ccdc.cam.ac.uk. Web page: <http://www.ccdc.cam.ac.uk>.

## 4.3. Binding studies

### 4.3.1. Preparation of cellular membranes

Male Swiss mice (final age 8–10 weeks) were killed, and the

brain cortex dissected and stored at  $-70^{\circ}\text{C}$  until assays were performed. All animal experimental protocols were performed in agreement with European Union regulations (O.J. of E.C. L 358/1 18/12/1986).

Human brain samples were obtained at autopsy in the Basque Institute of Legal Medicine, Bilbao, Spain. Samples from the prefrontal cortex (Brodmann's area 9) were dissected at the time of autopsy and immediately stored at  $-70^{\circ}\text{C}$  until assay. The study was developed in compliance with policies of research and ethical review boards for postmortem brain studies.

To obtain cellular membranes (P2 fraction) the different samples were homogenized using an ultraturrax in 10 vol of homogenization buffer (0.25 M sucrose, 5 mM Tris-HCl, pH 7.4). The crude homogenate was centrifuged for 5 min at 1000 g ( $4^{\circ}\text{C}$ ) and the supernatant was centrifuged again for 10 min at 40,000 g ( $4^{\circ}\text{C}$ ). The resultant pellet was washed twice in 5 vol of homogenization buffer and re-centrifuged in similar conditions. Protein content was measured according to the method of Bradford using BSA as standard.

#### 4.3.2. Competition binding assays

The pharmacological activity of the compounds was evaluated through competition binding studies against the  $\text{I}_2$ -IR selective radioligand [ $^3\text{H}$ ]2-BFI or the  $\alpha_2$ -adrenergic receptor selective radioligand [ $^3\text{H}$ ]RX821002. Specific binding was measured in 0.25 mL aliquots (50 mM Tris-HCl, pH 7.5) containing 100  $\mu\text{g}$  of membranes, which were incubated in 96-well plates either with [ $^3\text{H}$ ]2-BFI (2 nM) for 45 min at  $25^{\circ}\text{C}$  or [ $^3\text{H}$ ]RX821002 (1 nM) for 30 min at  $25^{\circ}\text{C}$ , in the absence or presence of the competing compounds ( $10^{-12}$  to  $10^{-3}$  M, 10 concentrations).

Specific binding of [ $^3\text{H}$ ]clonidine (20 nM) to rat or human hypothalamic membranes pre-incubated with benextramine (100  $\mu\text{M}$ ) to alkylate the population of  $\alpha_2$ -adrenoceptors. Under these experimental conditions [ $^3\text{H}$ ]clonidine only labelled  $\text{I}_1$ -sites. In drug competition experiments, moxonidine (the reference compound for  $\text{I}_1$ -IR) showed sub-nanomolar affinity for these  $\text{I}_1$ -sites ( $K_{\text{IH}} = 0.2$  nM;  $K_{\text{IL}} = 32$  mM).

Incubations were terminated by separating free ligand from

bound ligand by rapid filtration under vacuum (1450 Filter Mate Harvester, PerkinElmer) through GF/C glass fiber filters. The filters were then rinsed three times with 300  $\mu\text{L}$  of binding buffer, air-dried (120 min), and counted for radioactivity by liquid scintillation spectrometry using a MicroBeta TriLux counter (PerkinElmer). Specific binding was determined and plotted as a function of the compound concentration. Nonspecific binding was determined in the presence of idazoxan ( $10^{-5}$  M), a compound with well established affinity for  $\text{I}_2$ -IR and  $\alpha_2$ -adrenergic receptors, in [ $^3\text{H}$ ]2-BFI and [ $^3\text{H}$ ]RX821002 assays. To obtain the inhibition constant ( $K_i$ ) analyses of competition experiments were performed by nonlinear regression using the GraphPad Prism program.  $K_i$  values were normalized to  $\text{p}K_i$  values.  $\text{I}_2$ -IR/ $\alpha_2$  selectivity index was calculated as the antilogarithm of the difference between  $\text{p}K_i$  values for  $\text{I}_2$ -IR and  $\text{p}K_i$  values for  $\alpha_2$ -AR.

#### 4.4. Acute toxicity

Lethal dose ( $\text{LD}_{50}$ ) is a statistical derived amount of a compound that can be expected to cause death in 50% of the animals, rodents in general and is used as a measure of its acute toxicity. In this particular study,  $\text{LD}_{50}$  was calculated using the Logarithmic-Probit method, as initially described in Miller and Tainter (1944) [58], and the calculations further elaborated by Randhawa (2009) [59]. Male albino mice were administered i.p. with LSL60101 at a range of doses (10–100 mg/kg;  $n = 10$  mice per dose tested), percentage mortalities were transformed to probits for each dose, and log-doses vs. probits were plotted to calculate  $\text{LD}_{50}$  (see further details in Ref. [59]).

#### 4.5. 3D-QSAR study. Data set preparation

The original data set was divided on training set, that was used for model building and test set, used for model evaluation. The  $\text{I}_2$ -IR 3D-QSAR model contains 24 compounds (Fig. S1), with 16 compounds in the training set and 8 compounds in the test set, while data set for the  $\alpha_2$ -AR 3D-QSAR model contains 22 compounds, with 14 compounds in the training set and 8 compounds in the test set (Tables S1 and S2). In order to compare and validate our results, we added three  $\text{I}_2$ -IR standard ligands (tracizoline, idazoxan, and BU99008, Fig. 1), in both data sets. Test set compounds were chosen based on PCA (Principal Component Analysis) plot, considering that  $\text{p}K_i$  values were homogeneously distributed in the whole range.

After dividing all data sets into training and test sets, variable selection was performed using fractional factorial design (FFD), and Partial Least Square (PLS) regression was applied for building 3D-QSAR models (Figs. S2 and S3).

Dominant forms of ligands at physiological pH 7.4 were obtained with the Marvin Sketch 5.5.1.0 program [60], while geometry was optimized with semiempirical/PM3 (Parameterized Model revision 3) method [61,62] followed by ab initio Hartree-Fock/3-21G method [63] using Gaussian 09 software [64] included in ChemBio3D Ultra 13 program [65].

The Pentacle program [38] was used for calculation of GRID independent descriptors (GRIND and GRIND2) and 3D-QSAR model building. Computation of descriptors is based on Molecular Interaction Fields (MIF), by using four different probes: O probe (hydrogen bond acceptor groups), N1 probe (hydrogen bond donor groups), TIP probe (the shape of molecule), and DRY probe (hydrophobic interactions). After MIFs calculation, ALMOND algorithm was used for the extraction of the most relevant regions, which represented the positions of favourable interactions between the ligand and probe. In the final step, Consistently Large Auto and Cross Correlation (CLACC) algorithm was used to plot node-node energies, between the same or a different probe, into auto- and

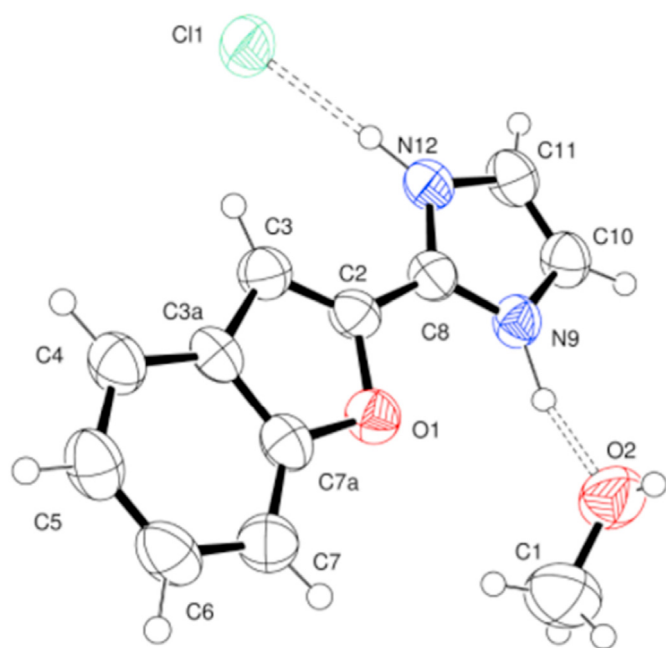


Fig. 8. X-ray crystal structure of LSL60101.

cross-correlograms, with the smoothing window set to 0.8 Å [66].

#### 4.6. Cytotoxicity assays

Cancer cell lines LN-229, Capan-1, HCT-116, NCI-H460, HL-60, K-562 and Z-138 were acquired from the American Type Culture Collection (ATCC, Manassas, VA, USA) and the DND-41 cell line was purchased from the Deutsche Sammlung von Mikroorganismen und Zellkulturen (DSMZ Leibniz-Institut, Germany). All cell lines were cultured as recommended by the suppliers. Adherent cell lines LN-229, Capan-1, HCT-116 and NCI-H460 were seeded at a density between 500 and 1500 cells per well, in 384-well tissue culture plates (Greiner). After overnight incubation, cells were treated with different concentrations of the test compounds. Suspension cell lines HL-60, K-562, Z-138 and DND-41 were seeded at densities ranging from 2500 to 5500 cells per well in 384-well culture plates containing the test compounds at the same concentration points. The plates were incubated and monitored at 37 °C for 72 h in an IncuCyte® (Essen BioScience Inc., Sartorius) for real-time imaging of cell proliferation. Brightfield images were taken every 3 h, with one field imaged per well under 10x magnification. Cell growth was then quantified based on the percent cellular confluence as analysed by the IncuCyte® image analysis software, and used to calculate CC<sub>50</sub> values by linear interpolation.

#### 4.7. Pharmacokinetic analysis and analysis conditions

The pharmacokinetic study was carried on in male CD1 mice (Envigo Laboratories) with a body weight between 40 and 50 g (n = 3–4 per group). Animals were randomized to be included in the treated or control groups. A single intraperitoneal dose of **LSL60101** (10 mg/kg, 10 ml/kg) was administered early in the morning (between 8 and 11 a.m.) without anaesthesia. Compound was dissolved in 10% of 2-hydroxypropyl- $\beta$ -cyclodextrin in physiological saline. Mice were monitored for signs of pain or distress during the time between injection and euthanasia. Mice were sacrificed by cervical dislocation and blood (0.6 mL) was collected at different time points (15 min, 30 min, 45 min, 60 min, 2 h, 3 h, 4 h, 5 h, 8 h and 24 h after injection) in tubes with serum gel and clotting activator (Sarstedt Micro tube 1.1 mL Z-Gel). Samples were centrifuged at 10,000 rpm for 10 min to obtain plasma and stored at –80 °C up to analysis of compound concentration by HPLC-UV. Experimental procedures were in line with the Directive 2010/63/EU and approved by the Institutional Animal Care and Generalitat de Catalunya (#10291, 1/28/2018).

**LSL60101** plasma concentrations versus time curves for the mean of animals were analysed by a non-compartmental model based on statistical moment theory using the “PK Solutions” computer program. The pharmacokinetic parameters calculated were the area under the concentration vs time curve (AUC), calculated using the trapezoidal rule in the interval 0–24 h; the half-life ( $t_{1/2\beta}$ ), determined as  $\ln 2/\beta$ , being  $\beta$ , calculated from the slope of the linear, least-squares regression line; the C<sub>max</sub> and T<sub>max</sub> were read directly from the mean concentration curves.

The HPLC system was a PerkinElmer LC (Perkin Elmer INC, Massachusetts, U.S.) consisting of a Flexar LC pump, a chromatography interface (NCI 900 network), a Flexar LC autosampler PE, and a Waters 2487 dual  $\lambda$  absorbance detector. The chromatographic column was a kromasil 100-5-C18 (4.0 × 200 mm-Teknokroma Analítica S.A. Sant Cugat, Spain). Flux was 0.8 ml/min and the mobile phase consisted in 0.05 M KH<sub>2</sub>PO<sub>4</sub> (30%):acetonitrile (70%) in isocratic conditions. The elution time of **LSL60101** was 4.4 min, and it was detected at 290 nm. The assay had a range of 0.025–5  $\mu$ g/mL. The calibration curves were constructed by plotting the peak area ratio of the analysed peak against the known concentrations.

#### 4.8. In vivo studies in mice

Studies and procedures involving mouse brain dissection and extractions were approved by the respective Local Bioethical Committees (Universitat de les Illes Balears-CAIB and University of Barcelona-GenCat) and followed the ARRIVE [67] and standard ethical guidelines (European Communities Council Directive 2010/63/EU and Guidelines for the Care and Use of Mammals in Neuroscience and Behavioural Research, National Research Council 2003). All efforts were made to minimize the number of animals used and their suffering.

#### 4.9. Hypothermia in naïve mice

This study was performed in male and female adult CD-1 mice bred and housed in the animal facility at the University of the Balearic Islands in standard cages in set environmental conditions (22 °C, 70% humidity, and 12 h light/dark cycle, lights on at 8:00 a.m.) with free access to a standard diet and tap water. Prior to any experimental procedures, mice were habituated to the experimenter by being handled and weighed for 2 days. Mice were treated with a single dose of **LSL60101** (1, 5, 10, 20, 30 or 50 mg/kg, i.p., n = 5 for treatment group) or vehicle (2 ml/kg of saline, i.p., n = 5), and changes in rectal temperature were measured by comparing basal values (before drug treatment) with that obtained 1, 2 and 3 h post-treatment by a rectal probe connected to a digital thermometer (Compact LCD display thermometer, SA880-1 M, RS, Corby, UK).

#### 4.10. Western blot analysis for FADD protein in naïve mice

For evaluating FADD protein regulation, a subgroup of mice received a single dose of **LSL60101** (30 or 50 mg/kg, i.p., n = 7 for treatment group) or vehicle (2 ml/kg of saline, i.p., n = 6) and were sacrificed 1 h after treatment. The hippocampus was freshly dissected and kept at –80 °C until hippocampal sample proteins (40  $\mu$ g) were separated by SDS-PAGE on 10% polyacrylamide minigels (Bio-Rad) and transferred onto nitrocellulose membranes by standard Western blot (Wb) procedures as described previously [21]. Membranes were incubated overnight with anti-FADD (H-181; sc-5559; Santa Cruz Biotechnology, Santa Cruz, CA), and following secondary antibody (anti-rabbit) incubation and ECL detection system (Amersham, Buckinghamshire, UK), proteins were visualized on autoradiographic films (Amersham ECL Hyperfilm). The amount of FADD protein in mice brain samples from different treatment groups was compared with that of vehicle-treated controls (100%) in the same gel by densitometric scanning (GS-800 Imaging Densitometer, Bio-Rad) of immunoreactive bands (integrated optical density, IOD). Each brain sample was quantified in 2–4 gels, and the mean value was used as a final estimate. Quantification of  $\beta$ -actin contents (clone AC-15; Ab, no. A1978; Sigma) was used as a house-keeping control (no differences between treatment groups, 15  $\mu$ g per sample).

#### 4.11. 5XFAD as an animal model of AD: pharmacological treatments

The 5XFAD is a double transgenic APP/PS1 that co-expresses five mutations of AD and presents robust oxidative levels [68]. 6-month-old female 5XFAD mice (n = 20) and wild type (Wt) mice (n = 20) were used to carry out the molecular analyses. The animals were randomly allocated into four experimental groups: Control 5XFAD and Wt, administered with vehicle (2-hydroxypropyl)- $\beta$ -cyclodextrin 1.8%, and treated 5XFAD and Wt administered with **LSL60101** diluted in vehicle (1 mg/kg/day). Treatment length was 4 weeks. Water consumption was controlled each week and the I<sub>2</sub>-IR

ligand concentration was adjusted accordingly to reach the precise dose. Animals had free access to food and water, and were kept under standard temperature conditions ( $22 \pm 2^\circ\text{C}$ ) and 12 h: 12 h light-dark cycles (300 lux/0 lux).

#### 4.12. Western blot analysis in 5xFAD and Wt mice

For subcellular fractionation, 150  $\mu\text{L}$  of buffer A (10 mM HEPES pH 7.9, 10 mM KCl, 0.1 mM EDTA pH 8, 0.1 mM EGTA pH 8, 1 mM DTT, 1 mM PMSF, protease inhibitors) were added to each sample and incubated on ice for 15 min. After this time, the samples were homogenized with a tissue homogenizer, 12.5  $\mu\text{L}$  Igepal 1% were added, and the each eppendorf was vortexed for 15 s. Following 30 s of full-speed centrifugation at  $4^\circ\text{C}$ , supernatants were collected (cytoplasmic fraction); 80  $\mu\text{L}$  of buffer C (20 mM HEPES pH 7.9, 0.4 M NaCl, 1 mM EDTA pH 8, 0.1 mM EGTA pH 8, 20% Glycerol 1 mM DTT, 1 mM PMSF, protease inhibitors) was added to each pellet and incubated under agitation at  $4^\circ\text{C}$  for 15 min. Subsequently, samples were centrifuged for 10 min at full speed at  $4^\circ\text{C}$ . Supernatants were collected (nuclear fraction).

For Western blot analysis, aliquots of 20  $\mu\text{g}$  of total hippocampal protein were used. Protein samples from mice ( $n = 3\text{--}5$  per group) were separated by Sodium dodecyl sulphate-polyacrylamide gel electrophoresis (SDS-PAGE) (8–12%) and transferred onto (Polyvinylidene difluoride) PVDF membranes (Millipore). Afterward, membranes were blocked in 5% non-fat milk in 0.1% Tris-buffered saline - Tween20 (TBS-T) for 1 h at room temperature, followed by overnight incubation at  $4^\circ\text{C}$  with the primary antibodies listed in Table S12.

Membranes were washed and incubated with the corresponding secondary antibodies for 1 h at room temperature. Immunoreactive proteins were viewed with a chemiluminescence-based detection kit, following the manufacturer's protocol (ECL Kit; Millipore) and digital images were acquired using a ChemiDoc XRS + System (Bio-Rad). Semi-quantitative analyses were carried out using ImageLab software (Bio-Rad), and results were expressed in Arbitrary Units (AU), considering control protein levels as 100%. Protein loading was routinely monitored by immunodetection of Glycerolaldehyde-3-phosphate dehydrogenase (GADPH) (Table S12).

#### 4.13. RNA extraction and gene expression determination in 5xFAD and Wt mice

Total RNA isolation was carried out using TRIzol<sup>®</sup> reagent according to manufacturer's instructions. The yield, purity, and quality of RNA were determined spectrophotometrically with a NanoDrop<sup>™</sup> ND-1000 (Thermo Scientific) apparatus and an Agilent 2100B Bioanalyzer (Agilent Technologies). RNAs with 260/280 ratios and RIN higher than 1.9 and 7.5, respectively, were selected. Reverse Transcription-Polymerase Chain Reaction (RT-PCR) was performed as follows: 2  $\mu\text{g}$  of messenger RNA (mRNA) was reverse-transcribed using the High Capacity cDNA Reverse Transcription Kit (Applied Biosystems). Real-time quantitative PCR (qPCR) from 24 mice of both strains ( $n = 4\text{--}6$  per group) was used to quantify mRNA expression of OS and inflammatory genes.

SYBR<sup>®</sup> Green real-time PCR was performed on a Step One Plus Detection System (Applied-Biosystems) employing SYBR<sup>®</sup> Green PCR Master Mix (Applied-Biosystems). Each reaction mixture contained 6.75  $\mu\text{L}$  of complementary DNA (cDNA) (which concentration was 2  $\mu\text{g}$ ), 0.75  $\mu\text{L}$  of each primer (which concentration was 100 nM), and 6.75  $\mu\text{L}$  of SYBR<sup>®</sup> Green PCR Master Mix (2X). Data were analysed utilizing the comparative Cycle threshold (Ct) method ( $\Delta\Delta\text{Ct}$ ), where the housekeeping gene level was used to

normalize differences in sample loading and preparation. The primers sequences used in this study are presented in Supplementary Table S10b. Normalization of expression levels was performed with  $\beta$ -actin for SYBR<sup>®</sup> Green-based real-time PCR. Each sample was analysed in duplicate, and the results represent the n-fold difference of the transcript levels among different groups.

#### 4.14. Statistical analysis for 5xFAD and Wt mice comparisons

The statistical analysis was conducted using the statistical software GraphPad Prism version 8. Data were expressed as the mean  $\pm$  Standard Error of the Mean (SEM). Means were compared with two-way ANOVAs, followed by Tukey-Kramer multiple comparisons post-hoc analysis. Statistical significance was considered when p-values were  $<0.05$ . The statistical outliers were carried out with Grubbs' test and subsequently removed from the analysis.

#### Declaration of competing interest

The authors declare that they have no known competing financial interests or personal relationships that could have appeared to influence the work reported in this paper.

#### Acknowledgment

This work was supported by Ministerio de Ciencia, Innovación y Universidades, Agencia Estatal de Investigación (Spain, PID2019-107991RB-I00, PID2019-106285RB), the Basque Government (IT1211/19) and Generalitat de Catalunya (GC) (2017SGR106). The project leading to these results has received funding from "la Caixa" Foundation (ID 100010434) under agreement CI18-00002. This activity has received funding from the European Institute of Innovation and Technology (EIT). This body of the European Union receives support from the European Union's Horizon 2020 research and innovation programme. C.G.-F, F.V., C.E., S.R.-A., A.B., and M.P. Financial support was provided for F.V. (University of Barcelona, APIF\_2017), S.R.-A. (Generalitat de Catalunya, 2018FI\_B\_00227), A.B. (Institute of Biomedicine UB\_2018), J.A.G.-S. is a member emeritus of the Institut d'Estudis Catalans (Barcelona, Catalonia). E.H.-H. is supported by a predoctoral scholarship (FPI/2102/2018; Consejería de Innovación, Investigación y Turismo del Gobierno de las Islas Baleares y del Fondo Social Europeo). M.R., T.D., and K.N. kindly acknowledge the project funded by the Ministry of Science and Technological Development of the Republic of Serbia, Contract No. 451-03-68/2020-14/200161, and HORIZON 2020-COST-Action CA18133 ERNEST: European Research Network on Signal Transduction. E. M. acknowledges funding to Severo Ochoa: CEX2019-917S. M.I.L, A.L.M. and J.B. gratefully acknowledge support from Xunta de Galicia (ED431C 2018/21 and ED431G 2019/02) and European Regional Development Fund (ERDF).

The authors thanks Dr. Rossend Obach and Dr. Ángel Menargues (LASA Laboratorios and later Ipsen Pharma SA, Barcelona, Spain) for initially providing the compound **LSL60101**.

#### Appendix A. Supplementary data

Supplementary data to this article can be found online at <https://doi.org/10.1016/j.ejmech.2021.113540>.

#### References

- [1] P. Bousquet, J. Feldman, J. Schwartz, Central cardiovascular effects of alpha adrenergic drugs: differences between catecholamines and imidazolines,

- J. Pharmacol. Exp. Therapeut. 230 (1984) 232–236.
- [2] P. Bousquet, A. Hudson, J.A. García-Sevilla, J.X. Li, Imidazoline receptor system: the past, the present, and the future, *Pharmacol. Rev.* 72 (2020) 50–79.
- [3] J.X. Li, Imidazoline I<sub>2</sub> receptors: an update, *Pharmacol. Ther.* 178 (2017) 48–56.
- [4] J. García-Sevilla, P.V. Escribá, M. Sastre, C. Walzer, X. Busquets, G. Jaquet, D.J. Reis, J. Guimón, Immunodetection and quantitation of imidazoline receptor proteins in platelets of patients with major depression and in brains of suicide victims, *Arch. Gen. Psychiatr.* 53 (1996) 803–810.
- [5] J.A. Lowry, J.T. Brown, Significance of the imidazoline receptors in toxicology, *Clin. Toxicol.* 52 (2014) 454–469.
- [6] J.X. Li, Y. Zhang, Imidazoline I<sub>2</sub> receptors: target for new analgesics? *Eur. J. Pharmacol.* 658 (2011) 49–56.
- [7] S. Regunathan, D.L. Feinstein, D.J. Reis, Anti-proliferative and anti-inflammatory actions of imidazoline agents. Are imidazoline receptors involved? *Ann. N. Y. Acad. Sci.* 881 (1999) 410–419.
- [8] K.L. Smith, D.S. Jessop, D.P. Finn, Modulation of stress by imidazoline binding sites: implications for psychiatric disorders, *Stress* 12 (2009) 97–114.
- [9] J.J. Meana, F. Barturen, I. Martín, J.A. García-Sevilla, Evidence of increased non-adrenoreceptor [<sup>3</sup>H]idazoxan binding sites in the frontal cortex of depressed suicide victims, *Biol. Psychiatr.* 34 (1993) 498–501.
- [10] J. Ruiz, I. Martín, L.F. Callado, J.J. Meana, F. Barturen, J.A. García-Sevilla, Non-adrenoreceptor [<sup>3</sup>H]idazoxan binding sites (I<sub>2</sub>-imidazoline sites) are increased in postmortem brain from patients with Alzheimer's disease, *Neurosci. Lett.* 160 (1993) 109–112.
- [11] C. Gargalidis-Moudanos, N. Pizzinat, F. Javoy-Agud, A. Remaury, A. Parini, I<sub>2</sub>-imidazoline binding sites and monoamine oxidase activity in human post-mortem brain from patients with Parkinson's disease, *Neurochem. Int.* 30 (1997) 31–36.
- [12] L.F. Callado, J.I. Martín-Gómez, J. Ruiz, J.M. Garibi, J.J. Meana, Imidazoline I<sub>2</sub> receptors density increases with the malignancy of human gliomas, *J. Neurol. Neurosurg. Psychiatry* 75 (2004) 785–787.
- [13] C. Dardouville, I. Rozas, Imidazoline binding sites and their ligands: an overview of the different chemical structures, *Med. Res. Rev.* 24 (2004) 639–661.
- [14] G.M. Gilad, V.H. Gilad, Accelerated functional recovery and neuroprotection by agmatine after spinal cord ischemia in rats, *Neurosci. Lett.* 296 (2000) 97–100.
- [15] K. Maiese, L. Pek, S.B. Berger, D.J. Reis, Reduction in focal cerebral ischemia by agents acting at imidazole receptors, *J. Cerebr. Blood Flow Metabol.* 12 (1992) 53–63.
- [16] Z. Han, M.J. Xiao, B. Shao, R.Y. Zheng, G.Y. Yang, K. Jin, Attenuation of ischemia induced rat brain injury by 2-(2-benzofuranyl)-2-imidazoline, a high selectivity ligand for imidazoline I<sub>2</sub>(2)receptors, *Neurol. Res.* 31 (2009) 390–395.
- [17] S.X. Jiang, R.Y. Zheng, J.Q. Zheng, X.L. Li, Z. Han, S.T. Hou, Reversible inhibition of intracellular calcium influx through NMDA receptors by imidazoline (I)<sub>2</sub> receptor antagonists, *Eur. J. Pharmacol.* 629 (2010) 12–19.
- [18] L.C. Rovati, N. Brambilla, T. Blicharski, J. Connell, C. Vitalini, A. Bonazzi, G. Giacobelli, F. Girolami, M. D'Amato, Efficacy and safety of the first-in-class imidazoline-2 receptor ligand CR4056 in pain from knee osteoarthritis and disease phenotypes: a randomized, double-blind, placebo-controlled phase 2 trial, *Osteoarthritis Cartilage* 28 (2020) 22–30.
- [19] R.J. Tyacke, J.F.M. Myers, A.V. Venkataraman, I. Mick, S. Turton, J. Passchier, S.M. Husband, E.A. Rabiner, R.N. Gunn, P.S. Murphy, C.A. Parker, D.J. Nutt, Evaluation of [<sup>11</sup>C]-BU99008, a PET ligand for the imidazoline<sub>2</sub> binding site in human brain, *J. Nucl. Med.* 59 (2018) 1597–1602.
- [20] H. Wilson, G. Dervenoulas, G. Pagano, R.J. Tyacke, S. Polychronis, J. Myers, R.N. Gunn, E.A. Rabiner, D. Nutt, M. Politis, Imidazoline 2 binding sites reflecting astroglia pathology in Parkinson's disease: an in vivo [<sup>11</sup>C]-BU99008 PET study, *Brain* 10 (2019) 3116–3128.
- [21] S. Abás, A.M. Erdozain, B. Keller, S. Rodríguez-Arévalo, L.F. Callado, J.A. García-Sevilla, C. Escolano, Neuroprotective effects of a structurally new family of high affinity imidazoline I<sub>2</sub> receptors ligands, *ACS Chem. Neurosci.* 8 (2017) 737–742.
- [22] C. Grinán-Ferré, F. Vasilopoulou, S. Abás, S. Rodríguez-Arévalo, A. Bagán, F.X. Sureda, B. Pérez, L.F. Callado, J.A. García-Sevilla, M.J. García-Fuster, C. Escolano, M. Pallàs, Behavioral and cognitive improvement induced by novel imidazoline I<sub>2</sub> receptor ligands in female SAMP8 mice, *Neurotherapeutics* 16 (2019) 416–431.
- [23] S. Abás, S. Rodríguez-Arévalo, A. Bagán, C. Grinán-Ferré, F. Vasilopoulou, I. Brocos-Mosquera, C. Muguruza, B. Pérez, E. Molins, F.J. Luque, P. Pérez-Lozano, S. de Jonghe, D. Daelemans, L. Naesens, J. Brea, M.I. Loza, E. Hernández-Hernández, J.A. García-Sevilla, M.J. García-Fuster, M. Radan, T. Djikic, K. Nikolic, M. Pallàs, L.F. Callado, C. Escolano, Bicyclic  $\alpha$ -iminophosphonates as high affinity imidazoline I<sub>2</sub> receptor ligands for Alzheimer's disease, *J. Med. Chem.* 7 (2020) 3610–3633.
- [24] D.A. Ruggiero, S. Regunathan, H. Wang, T.A. Milner, D.J. Reis, Immunocytochemical localization of an imidazoline receptor protein in the central nervous system, *Brain Res.* 780 (1998) 270–293.
- [25] J.A. García-Sevilla, P.V. Escribá, C. Walzer, C. Bouras, J. Guimón, Imidazoline receptor proteins in brains of patients with Alzheimer's disease, *Neurosci. Lett.* 247 (1998) 95–98.
- [26] D.S. Albers, M.F. Beal, Mitochondrial dysfunction and oxidative stress in aging and neurodegenerative diseases, *J. Neural. Transm. Suppl.* 5 (2000) 133–154.
- [27] J.P. Bolaños, M.A. Moro, I. Lizasoain, A. Almeida, Mitochondrial and reactive oxygen and nitrogen species in neurological disorders and stroke: therapeutic implications, *Adv. Drug Deliv. Rev.* 61 (2009) 1299–1315.
- [28] Z. Liu, T. Zhou, A.C. Ziegler, P. Dimitrion, L. Zuo, Oxidative stress in neurodegenerative diseases: from molecular mechanisms to clinical applications, *Oxid. Med. Cell Longev.* 2017 (2017) 1–11.
- [29] M. Johnstone, A.J. Geraing, K.M. Miller, A central role for astrocytes in the inflammatory response to beta-amyloid: chemokines, cytokines and reactive oxygen species are produced, *J. Neuroimmunol.* 93 (1999) 182–193.
- [30] D.J. Bonda, X. Wang, G. Perry, A. Nunomura, M. Tabaton, X. Zhu, M.A. Smith, Oxidative stress in Alzheimer disease: a possibility for prevention, *Neuropharmacology* 59 (2010) 290–294.
- [31] L.A. Lione, D.J. Nutt, A.L. Hudson, Characterisation and localisation of [<sup>3</sup>H]-2-(2-benzofuranyl)-2-imidazoline binding in rat brain: a selective ligand for imidazoline I<sub>2</sub> receptors, *Eur. J. Pharmacol.* 353 (1998) 123–135.
- [32] F. Vasilopoulou, C. Grinán-Ferré, S. Rodríguez-Arévalo, A. Bagán, S. Abás, C. Escolano, M. Pallàs, I<sub>2</sub> imidazoline receptor modulation protects aged SAMP8 mice against cognitive decline by suppressing the calcineurin pathway, *GeroScience* 43 (2021) 965–983.
- [33] J.A. García-Sevilla, J.J. Meana, F. Barturen, F.A. Gejjo, A. Menargues, R. Obach, F. Pla, Benzofuranylimidazole Derivatives and Therapeutical Compositions Containing the Same, 1994. US5354769(A), October 11.
- [34] R. Alemany, G. Olmos, P.V. Escribá, A. Menargues, R. Obach, J.A. García-Sevilla, LSL60101, a selective ligand for imidazoline I<sub>2</sub> receptors, on glial fibrillary acidic protein concentration, *Eur. J. Pharmacol.* 280 (1995) 205–210.
- [35] M.A. Boronat, G. Olmos, J.A. García-Sevilla, Attenuation of tolerance to opioid-induced antinociception and protection against morphine-induced decrease of neurofilament proteins by idazoxan and other I<sub>2</sub>-imidazoline ligands, *Br. J. Pharmacol.* 125 (1998) 175–185.
- [36] A. Casanova, G. Olmos, J. Ribera, M.A. Boronat, J.E. Esquerda, J.A. García-Sevilla, Induction of reactive astrocytosis and prevention of motoneuron cell death by the I<sub>2</sub>-imidazoline receptor ligand LSL60101, *Br. J. Pharmacol.* 130 (2000) 1767–1776.
- [37] N. MacInnes, S.L. Handley, Characterization of the discriminable stimulus produced by 2-BFI: effects of imidazoline I<sub>2</sub>-site ligands, MAOs,  $\beta$ -carbolines, agmatine and ibogaine, *Br. J. Pharmacol.* 135 (2002) 1227–1234.
- [38] Pentacle, Version 1.0.6, MolecularDiscoveryLtd., Perugia, Italy, 2009.
- [39] A. Krüger, V. Gonçalves, C. Wrenger, T. Kronenberger, ADME Profiling in Drug Discovery and a New Path Paved on Silica, *Drug Discovery and Development - New Advances*, 2019.
- [40] ADMET Predictor, V. 9.5, Simulations Plus Inc., Lancaster, CA, USA. <https://www.simulations-plus.com>.
- [41] A. Daina, O. Michielin, V. Zoete, SwissADME: a free web tool to evaluate pharmacokinetics, drug-likeness and medicinal chemistry friendliness of small mol, *Sci. Rep.* 7 (2017) 1–13.
- [42] D.A. Thorn, X. An, Y. Zhang, M. Pignini, J. Li, Characterization of the hypothermic effects of imidazoline I<sub>2</sub> receptor agonists in rats, *Br. J. Pharmacol.* 166 (2012) 1936–1945.
- [43] E. Hernández-Hernández, M.J. García-Fuster, Evaluating the effects of 2-BFI and trazoline, two potent I<sub>2</sub>-imidazoline receptor agonists, on cognitive performance and affect in middle-aged rats, *Naunyn-Schmiedeberg's Arch. Pharmacol. Pharmacology* 394 (2021) 989–996.
- [44] J.A. Craven, E.L. Conway, Effects of alpha 2-adrenoceptor antagonists and imidazoline 2-receptor ligands on neuronal damage in global ischemia in the rat, *Clin. Exp. Pharmacol. Physiol.* 24 (1997) 204–207.
- [45] D.W. Marion, L.E. Penrod, S.F. Kelsey, W.D. Obrist, P.M. Kochanek, A.M. Palmer, S.R. Wisniewski, S.T. DeKosky, Treatment of traumatic brain injury with moderate hypothermia, *N. Engl. J. Med.* 336 (1997) 540–546.
- [46] C.M. Maier, K.V. Ahern, M.L. Cheng, J.E. Lee, M.A. Yenari, G.K. Steinberg, J.R. Kirsch, Optimal depth and duration of mild hypothermia in a focal model of transient cerebral ischemia: effects on neurologic outcome, infarct size, apoptosis, and inflammation, *Stroke* 29 (10) (1998) 2171–2180.
- [47] E. Hernández-Hernández, A. Miralles, S. Esteban, M.J. García-Fuster, Improved age-related deficits in cognitive performance and affective-like behavior following acute, but not repeated, 8-OH-DPAT treatments in rats: regulation of hippocampal FADD, *Neurobiol. Aging* 71 (2018) 115–126.
- [48] E. Hernández-Hernández, A. Miralles, S. Esteban, M.J. García-Fuster, Repeated treatment with the  $\alpha$ 2-adrenoceptor agonist UK-14304 improves cognitive performance in middle-age rats: role of hippocampal Fas-associated death domain, *J. Psychopharmacol.* 32 (2) (2018) 248–255.
- [49] E. Comi, M. Lanza, F. Ferrari, V. Mauri, G. Caselli, L.C. Rovati, Efficacy of CR4056, a first-in-class imidazoline-2 analgesic drug, in comparison with naproxen in two rat models of osteoarthritis, *J. Pain Res.* 10 (2017) 1033–1043.
- [50] N. Mirzaei, B.C. Mota, A.M. Birch, N. Davis, C. Romero-Molina, L. Katsouri, E.O.C. Palmer, A. Golbano, L.J. Riggall, I. Nagy, R. Tyacke, D.J. Nutt, M. Sastre, Imidazoline ligand BU224 reverses cognitive deficits, reduces microgliosis and enhances synaptic connectivity in a mouse model of Alzheimer's disease, *Br. J. Pharmacol.* 178 (3) (2021) 654–671.
- [51] J.A. García-Sevilla, P.V. Escribá, C. Walzer, C. Bouras, J. Guimón, Imidazoline receptor proteins in brains of patients with Alzheimer's disease, *Neurosci. Lett.* 247 (1998) 95–98.
- [52] B. Uttara, A.V. Singh, P. Zamboni, R.T. Mahajan, Oxidative stress and neurodegenerative diseases: a review of upstream and downstream antioxidant therapeutic options, *Curr. Neuropharmacol.* 7 (1) (2009) 65–74.
- [53] E. Birben, U.M. Sahiner, C. Sackesen, S. Erzurum, O. Kalayci, Oxidative stress and antioxidant defense, *World Allergy Organ. J.* 5 (1) (2012) 9–19.
- [54] J.S. Tian, Q.J. Zhai, Y. Zhao, R. Chen, L.D. Zhao, 2-(2-benzofuranyl)-2-imidazoline (2-BFI) improved the impairments in AD rat models by

- inhibiting oxidative stress, inflammation and apoptosis, *J. Integr. Neurosci.* 16 (4) (2017) 385–400.
- [55] D.H. Choi, J.H. Yun, J. Lee, Protective effect of the imidazoline I<sub>2</sub> receptor agonist 2-BFI on oxidative cytotoxicity in astrocytes, *Biochem. Biophys. Res. Commun.* 503 (4) (2018) 3011–3016.
- [56] F. Vasilopoulou, S. Rodríguez-Arévalo, A. Bagán, C. Escolano, C. Griñán-Ferré, M. Pallàs, Disease-modifying treatment with I2 imidazoline receptor ligand LSL60101 in an Alzheimer's disease mouse model: a Comparative study with donepezil, *Br. J. Pharmacol.* (2021) 1–17.
- [57] Y. Chen, C. Qin, J. Huang, X. Tang, C. Liu, K. Huang, J. Xu, G. Guo, A. Tong, L. Zhou, The role of astrocytes in oxidative stress of central nervous system: a mixed blessing, *Cell Prolif* 53 (3) (2020) e12781.
- [58] L.C. Miller, M.L. Tainter, Estimation of the ED<sub>50</sub> and its error by means of logarithmic-probit graph paper, *Proc. Soc. Exp. Bio. Med.* 57 (1944) 261–264.
- [59] M.A. Randhawa, Calculation of LD<sub>50</sub> values from the method of miller and tainter, 1944, *J. Ayub Med. Coll. Abbottabad* 21 (3) (2009) 184–185.
- [60] MarvinSketch 5.5.1.0, ChemAxon, Budapest, Hungary, 2011 software available at, <https://www.chemaxon.com>.
- [61] J.J.P. Stewart, Optimization of parameters for semiempirical methods I. Method, *J. Comput. Chem.* 10 (1989) 209–220.
- [62] J.J.P. Stewart, Optimization of parameters for semiempirical methods II. Applications, *J. Comput. Chem.* 10 (1989) 221–264.
- [63] W.J. Hehre, L. Radom, PvR. Schleyer, J. Pople, *AB Initio Molecular Orbital Theory*, Wiley, 1986.
- [64] M.J. Frisch, *Gaussian 98 (Revision A.7)*, 1998.
- [65] CambridgeSoft Corporation, *ChemBio3D Ultra, Version 13.0*, 2013. Cambridge, MA, USA.
- [66] A. Duran, M. Pastor, An advanced tool for computing and handling grid-independent descriptors, *User Manual (2011)*. Version 1.06.
- [67] N. Percie du Sert, A. Ahluwalia, S. Alam, M.T. Avey, M. Baker, W.J. Browne, A. Clark, I.C. Cuthill, U. Dirnagl, M. Emerson, P. Garner, S.T. Holgate, D.W. Howells, V. Hurst, N.A. Karp, S.E. Lazic, K. Lidster, C.J. MacCallum, M. Macleod, E.J. Pearl, O.H. Petersen, F. Rawle, P. Reynolds, K. Rooney, E.S. Sena, S.D. Silberberg, T. Steckler, H. Würbel, Reporting animal research: explanation and elaboration for the ARRIVE guidelines 2.0, *PLoS Biol.* 18 (7) (2020), <https://doi.org/10.1371/journal.pbio.3000411>.
- [68] H. Oakley, S.L. Cole, S. Logan, E. Maus, P. Shao, J. Craft, A. Guillozet-Bongaarts, M. Ohno, J. Disterhoft, L. Van Eldik, R. Berry, R. Vassar, Intraneuronal  $\beta$ -amyloid aggregates, neurodegeneration, and neuron loss in transgenic mice with five familial Alzheimer's disease mutations: potential factors in amyloid plaque formation, *J. Neurosci.* 26 (2006) 10129–10140.





